Leslie M. Golden

Laboratory Experiments in Physics for Modern Astronomy

With Comprehensive Development of the Physical Principles

With 175 Illustrations

Springer

Laboratory Experiments in Physics for Modern Astronomy

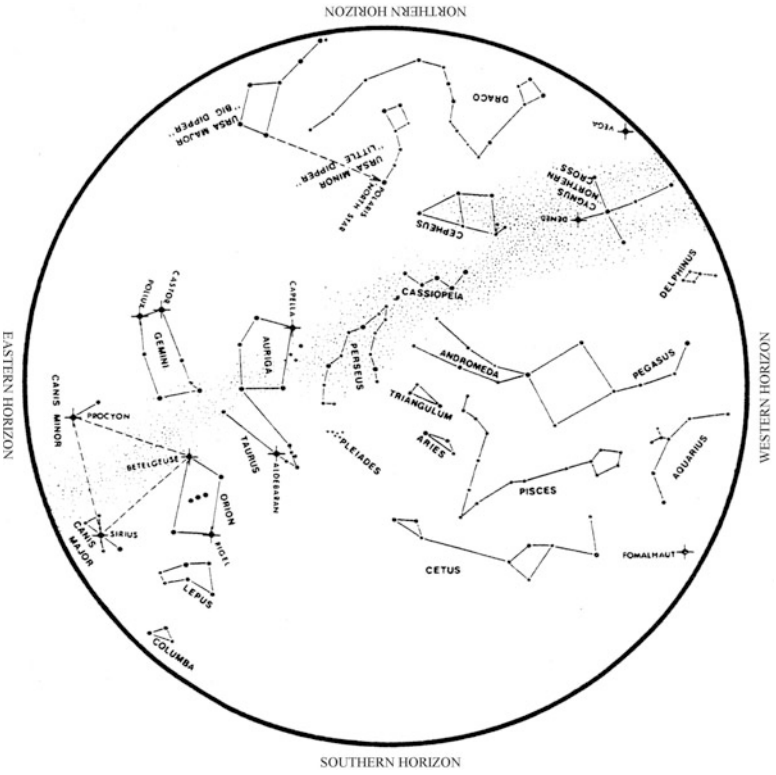

The night sky in December

Leslie M. Golden

Laboratory Experiments in Physics for Modern Astronomy

With Comprehensive Development of the Physical Principles

Springer

Leslie M. Golden
934 Forest Avenue
Oak Park, Illinois 60302
USA

ISBN 978-1-4614-3310-1 ISBN 978-1-4614-3311-8 (ebook)
DOI 10.1007/978-1-4614-3311-8
Springer New York Heidelberg Dordrecht London

Library of Congress Control Number: 2012935691

Cover illustration: This Hubble Space Telescope photograph shows a pair of colliding galaxies, NGC 6050 and IC 1179 (also referred to as NGC 6050A and NGC 6050B), which reside in the Hercules cluster of galaxies about 450 million light-years away. It was one of the fifty-nine new high-resolution images of colliding galaxies NASA released on April 24, 2008, to commemorate the eighteenth birthday of the Hubble Space Telescope. Many of the objects were compiled by astronomer Halton Arp in his Atlas of Peculiar Galaxies of 1966, which built on earlier work by B.A. Vorontsov-Velyaminov; this image was catalogued as Arp 272. The sensitive cameras of the HST revealed that the peculiar shapes observed by Arp resulted from comparatively low resolution images of these gravitationally-interacting objects. Part J of Experiment #1 examines the impending collision of our own Milky Way galaxy with the Andromeda galaxy, two additional spiral galaxies. Credits: NASA, ESA, the Hubble Heritage Team (STScI/AURA)-ESA/Hubble Collaboration and K. Noll (STScI).

Printed on acid-free paper

Springer is part of Springer Science+Business Media (www.springer.com)

To my parents, Anne K. and Irving R. Golden; my beloved pets Duffy, Tweetie, Byron, Cicero, Skipper, Emerson, Newton, Maxwell, and Enrico; the family of birds in my window at my apartment in Oakland, the fluffy white dog on Broadway near my apartment in Oakland, Onion the dog, the Ohio pit bulls Axle and Rusty, the two West Virginia pit bull mixes, and the other needy, stray, and abandoned dogs and feral cats and kittens, squirrels, rabbits, birds, mice, opossum, and other wildlife, farm and zoo animals, flying and crawling insects, and trees, bushes, plants, and grasses, all residents of the Earth, that I have loved, saved, and tried to save.

Cicero

Foreword

I have composed these laboratory experiments to introduce the physics of astronomical inquiry for use in 200 and 300 level courses in physics and astronomy departments. When competing with laboratory courses, particularly in biology and chemistry, astronomy courses have been at a disadvantage. Astronomical exercises, using actual data, often involve tedious calculations. In my experience, the student learns little about astronomy and, far from discovering its beauty, becomes disenchanted with the field. If the instructor chooses to assign standard introductory physics experiments, then he not only fails to inculcate much of the beauty of astronomy, but he must also justify their relevance to a course in astronomy. Computer-based simulations, with their sophisticated graphics and often accurate renditions, provide the glamour of the field but present little if any of the physics behind the phenomena.

This book presents experiments which will teach physics relevant to astronomy. The astronomer, as instructor, frequently faces this need when his college or university has no astronomy department and any astronomy course is taught in the physics department. This book resolves this problem. The physicist, as instructor, will find this intellectually appealing when faced with teaching a laboratory astronomy course.

From these experiments, the student will acquire important analytical tools, learn physics appropriate to astronomy, and experience instrument calibration and the direct gathering and analysis of data. Philosophically, the student will hopefully gain an understanding that rational inquiry leads to an understanding of natural processes. Experiments that can be performed in one laboratory session as well as month-long and semester-long observation projects are included.

The length of explanatory material in these experiments distinguishes this book from other laboratory manuals. This was needed for two reasons. First, my experience has been that graduate student teaching assistants may not be fully versed in all the subject matter. The explanatory material provides the necessary background for them. Second, the breadth of subjects cannot be found in any single source and I wanted the book to be self-contained. Although introductory physics texts certainly cover such subjects as heat capacity, blackbody radiation, the Bohr atom, and polarization of electromagnetic waves, one must refer to electrical engineering or

radio astronomy texts to explain radio antenna beam patterns and electrical skin depth, books in radar astronomy to explain range-Doppler mapping, astronomy texts to discuss Kirchhoff's Laws, optics manufacturer's instructions for the specifications of reticulated eyepieces, books on the history of science or astronomy for the various historical discussions, in particular the comparison of the Ptolemaic and Copernican theories presented in the experiment on the orbit of Venus, and the technical literature itself to explain diffuse reflection from planetary surfaces, for some examples. All the requisite explanatory material has been comprehensively presented here for the ease of the instructor, as well as the education of the student.

Several features aid the learning process. Except for the first two experiments, all are arranged in the same way, introduction, theory, procedure and observations, and calculations and analysis. All data are recorded and all calculations are performed on the data sheets. These are following by discussion questions to test the student's understanding and to introduce additional, associated concepts.

Other pedagogical features include the frequent presentation of graphical representations of equations. This will aid the student in obtaining intuition into phenomena. I provide examples or exercises, particularly in the first two chapters, that illustrate the application of the techniques to other areas of study. In this way, the techniques become part of the student's intellectual arsenal rather than simply a tool for doing science. I liberally include references to the history of astronomy to show the fruitful result of the development of rational inquiry less than 500 years ago. I also take the liberty of injecting humor. Not only does this refresh the student, but it's also a nod to the joyful times spent with colleagues. The extraterrestrial is a blatant advertisement for a subject that has captured the public attention and led to private funding for state-of-the-art telescope facilities in times of ever-decreasing federal support for astronomy. The book contains occasional references to the search for extraterrestrial intelligent life.

The data recording and analysis are performed on worksheets and the student is frequently asked to enter the results in tables. Although some may quibble with the "recipe" nature of this presentation, it serves useful purposes. First, it guides the student along in the data reduction process. Inadvertent errors early in the data reduction, which will propagate to the end result, are thereby avoided. The student is forced to be neat and well organized! Hopefully, the habits will become ingrained. Third, it facilitates grading whether performed by the instructor or teaching assistants. It also encourages standardized grading between teaching assistants, simplifying the task for those who may speak English as a second language.

The experiments have been designed to enable completion in one laboratory session of 2–3 h. Those experiments which would have required a greater amount of time have been broken up into two parts.

I should comment upon the units used. I believe it would be confusing to the student, for example, to use MKS (SI) units in measuring distances along an optical bench. It would also be confusing, for example, to use cgs units in discussing the orbits of the Galilean satellites. Accordingly, I use that system in a given context which I believe is most appropriate. The values of the mathematical constants in Appendix I are provided in both sets of units.

First, I present experiments on mathematical tools and graphing techniques, which should be part of every college student's intellectual equipment but which are often not. Facility in these techniques is achieved by usage in the subsequent experiments. Typically, the student should read the various experiments before coming to the laboratory and perform the data reduction in the week following. Experiments 1 and 2 would be more amenable to a different format. The experiments should be read before class, but the exercises should be done in the laboratory class itself. The student will find this congenial, with the rush of the first 2 weeks of class sometimes being overwhelming.

Inclusion of a section in the first experiment dealing with the collision of the Milky Way and M31 was written for several reasons. First, of course, it provides a good example of some of the techniques. It demonstrates that the various techniques do not stand alone, but that often more than one is needed in a given analysis. Third, the discovery of the decreased time scale for the collision of the Milky Way and M31 received widespread coverage in 2009 and it is frequently discussed during the course in the context of galactic cannibalism. I also wanted to use it as a demonstration of the value of mathematical physics, that seemingly intractable problems can be solved by the application of physics – here the conservation of energy and velocity of propagation of pressure waves in a medium. Finally, the result of the calculation is sufficiently intriguing that the student may well discuss it with his roommate or friends, engendering interest in astronomy.

The experiments on telescope optics are fairly comprehensive, and therefore performed in two laboratory sessions. Four experiments which can be conducted over a major portion of a semester, observations of the Galilean satellites, observations of Venus, microwave observations of the Moon, and determination of local geographic latitude from observations of lengths of Sun-cast shadows, will give the student a feel for observations. In addition, a numerical experiment on Kepler's laws is provided which utilizes ephemeris data. The geographic latitude experiment includes an introduction to the celestial sphere and the derivation of the zenith angle equation.

The experiments on the Galilean satellites, Kepler's laws, and the orbit of Venus will provide a short introduction to the history of astronomy. Throughout, the names and birth and death dates are provided for notable contributors. In particular, the Venus experiment compares the Ptolemaic and Copernican theories of the solar system.

The familiar laws of reflection are put into context in the real world by an experiment on diffuse reflection from the Moon and terrestrial planets. Specular reflection, scattering, polarization, and the electromagnetic wave are introduced in this context. These labs, by introducing the concept of models, also provide an introduction to the art of doing science. The formation of impact craters is discussed in the context of the conservation of energy as well as mathematical models. Pure physics experiments study blackbody radiation and spectral lines by way of the Bohr atom. This knowledge is combined into an experiment on Kirchhoff's Laws. I include a study quantifying the changing color of the Sun with zenith angle in the blackbody radiation experiment.

The subjects of radio and radar astronomy, areas which are normally not studied in laboratory courses in astronomy, are presented. They give the student a feeling for

the challenges of remote sensing of planetary surfaces and introduce the universal wave equation, circular motion, the Doppler shift, single slit diffraction, electrical skin depth, heat conduction, radiative transfer, and microwave radiometry. Because of the lack of student familiarity with these subjects, as well as the same circumstance with most teaching assistants in physics, these two experiments are divided into two parts. The first part of the radar experiment analyzes the radar echo from the planet Mercury. The second part of the radar experiment studies rotating simulated planetary or asteroid surfaces. The first part of the radio astronomy experiment deals with calibration of the radiometers. In the second part of the radio astronomy experiment, the student measures radiation coming from heated soil samples.

We have worked with vendors to develop affordable systems for use in the experiments on radar and radio astronomy. Indeed, several companies have produced "toy" and hobbyist radar guns. We have worked with one to provide a system which retains all frequencies produced in the echo and to allow that echo to be analyzed in a personal computer. Because microwave radiometers for radio astronomy, particularly those with Dicke switches and internal noise calibration, are expensive, colleges and universities with electrical engineering or astronomy departments are encouraged to have them produced locally. For those without such departments, a vendor is provided. Realizing that acquisition of such equipment may not be feasible, the instructor may utilize an alternative to the radio astronomy experiments in which only the sensing of the subsurface temperatures among different soil samples is performed. The two experiments become a single experiment in heat conduction rather than heat conduction and radiative transfer.

The radio astronomy experiments introduce the concepts of emissivity and the Rayleigh-Jeans approximation. I wanted to place these experiments in Part 2 dealing with the solar system. Because the subject of Experiment #17, which follows them in Part 3, is blackbody radiation, the instructor may wish to perform this experiment before the radio astronomy experiments.

From these various experiments, the student will acquire important analytical tools, learn physics appropriate to astronomy, and experience instrument calibration and the direct gathering and analysis of data. Some of the "art" of doing science, notably the role of judgment, is presented in the experiment on the Galilean satellites.

Experiments that can be performed in one laboratory session as well as month-long and semester-long observation projects are included. With a field trip to a nearby observatory or a planetarium and observation of a possible lunar or solar eclipse, the student will experience much of the excitement of astronomy while being sugar-fed that most powerful analytical tool, mathematical physics.

An Instructor's Guide includes solutions to the discussion questions that appear at the end of each experiment, information about equipment and equipment vendors, and other matters. It can be accessed online at http://www.springer.com/materials/book/978-1-4614-3310-1, below the title "Additional Information." Access is password protected.

In the preface to the student that follows, I write that the goal of this book is to show that everything in astronomy is based on physics, that mathematics is our friend, specifically those mathematics in mathematical physics, and that the study

of the electro-magnetic radiation from celestial objects enables us to understand their nature. To improve this book, I would greatly appreciate any suggestions and advice from colleagues to achieve those ends, as well as other ideas you may have. Please send your comments to drlesgo@aol.com.

Leslie M. Golden

Preface to the Student

Human beings arrive at truth in four ways: Faith, authority, revelation, and observation. All other animals rely only upon authority, by observing adults, and observation, by, for example, tasting fruit or experiencing the changing of the seasons. Very few species other than Man, although they, too, may experience territorialism, practice genocide or wage organized war. This is perhaps a commentary on the truth-finding role of faith, authority, and revelation in our consciousness.

The Role of Rational Inquiry

As tempting as it might be, these four methods cannot be organized historically. All four have existed since man obtained consciousness and remain practiced today. Similarly, they cannot be organized culturally. Native American populations, Chinese, the Maya and Incas, African tribes, Alaskan Indians, residents of the sub-continent, Pacific island inhabitant, and other civilizations developed religions, leaders, god-figures, and rational science. When anthropologists study previously unknown tribes, they find all four methods of obtaining truth in operation. Hope and prayer, shaman and village elders, miracles, and planning for the seasons, for examples, manifest the four methods.

In Western civilization, a tradition of rational inquiry and literacy of the Greeks was displaced by the revelation-inspired ignorance of the Dark Ages. Noteworthy was the nearly universal illiteracy during that 1,000-year period, when revelation-truth was communicated through art, notably religious paintings, drawings, and stained glass. The development of advanced seaworthy ships during the Age of Exploration and the consequent encounter with other civilizations with their own religions, the availability of books after the invention of the printing press, and the courage, insight, and brilliance of those who wondered about nature led to an outbreak of intellectual freedom known as the Renaissance, literally "re-birth."

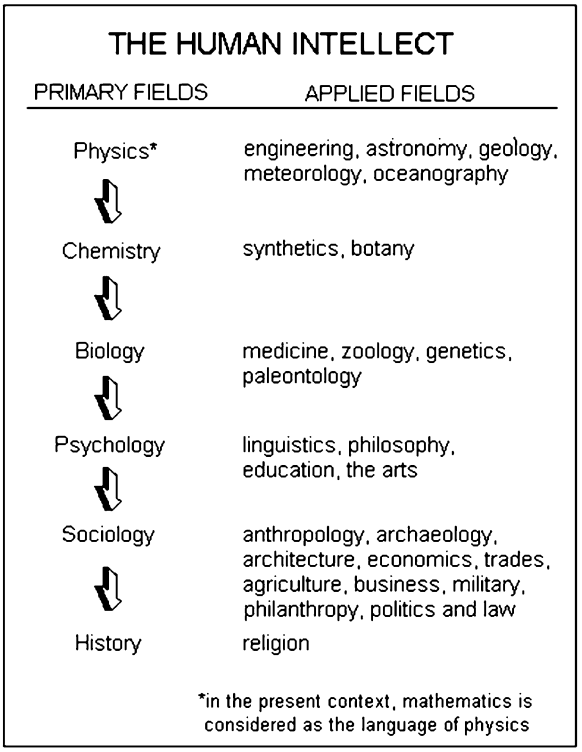

Leading the scientific Renaissance was the emphasis upon observation as the means of reaching truth. The observations of Tycho Brahe (1546–1601), codified by Johannes Kepler (1571–1630) into the laws which bear his name, the insistence of Galileo Galilei (1564–1642) upon the power of observation, and Sir Isaac Newton's (1643–1727) synthesis of Kepler's Laws with the Universal Law of Gravitation which he discovered occurred in rapid succession. Although Hans Lippershey (1570–1619) built the first telescope, it was Galileo's observations of the imperfective appearances of the surfaces of the Moon and Sun, the phases of Venus, and the orbiting satellites of Jupiter which displayed the intellectual value of direct observation to Europeans. In a well-studied era in the history of science, many of these scholars and their followers faced intellectual and physical hardship as they threatened the role of revelation.

As laws of nature were discovered, new mathematics was developed to allow their analysis and to provide the ability for prediction. In this way, Rene Descartes (1596–1650), Newton, and Gottfried Wilhelm Leibniz (1646–1716) developed the calculus, Newton to analyze the motions of the planets. He realized that the state of any system can be determined at any time if the rate of change of that system could be written down and an initial state provided. Following the formulation of the laws

of electricity and magnetism by Michael Faraday (1791–1867), Charles-Augustin de Coulomb (1736–1806), and others, their unification by Sir James Clerk Maxwell (1831–1879), including the strange magnetic force which counter intuitively occurs at right angles to the direction of motion, required the development of vector algebra. In the twentieth century, the discovery of general relativity by Albert Einstein (1879–1955) provided an application for tensor algebra. Today, inscrutable facts about the universe such as the existence of dark energy, the incredible relative weakness of the gravitational force, and the only mildly-satisfactory Standard Model for sub-atomic particles provides the impetus for the development of string theory.

Through it all, alone among all the sciences, stands the first science, astronomy. The Renaissance pioneers of modern science were stimulated by astronomical observations. The calculus was developed to explain the motions of the planets. Galileo turned his telescope to the skies.

Uncommon for a laboratory book, I accordingly and happily include small bits on the history of astronomy. These include some perspective on figures of the Renaissance as well as on modern researchers such as Maarten Schmidt.

In this book, I try to show the unequalled power of observations in reaching truth. Study of the complete scientific method is best done in philosophy of science classes, and accordingly I do not dwell on other of its aspects, classification of observations, formulation of hypothesis, prediction, and self-correction.

Astronomy as Physics

Displaying unashamedly a personal bias, I will state that physics provides the foundation of all human inquiry, whether the construct is direct or applied. The only limitation is appreciating these connections analytically is our limited intellect. In this way, chemistry is based on physics, biology is based on chemistry, and psychology is based on biology. Sociology is mass psychology and history can be considered psychology with the added dimension of time. Engineering, astronomy, geology, meteorology, and oceanography can be considered applied physics. Similarly, synthetics and botany can be considered applied chemistry; medicine, zoology, genetics, and paleontology can be considered applied biology; linguistics, philosophy, education, and the arts can be considered applied psychology; anthropology, archaeology, architecture, economics, the trades, agriculture, business, the military, philanthropy, and politics and law can be considered applied sociology; and religion can be considered applied history. Any inability to analytically derive the direct connection to physics results from our limited intelligence. (Unlike us, Hari Seldon in Isaac Asimov's *Foundation* series had the intellect to predict history from mass psychology).

The connection of physics to astronomy is direct and the two fields have much in common. Both rely totally (except when emotions get in the way of researchers with opposing views) on the scientific method, most notably the power of observation. Both use the construct of mathematics to interpret these observations and to make predictions.

The one manner in which they differ is the role of the experiment. In physics, most of the experiments are performed in a laboratory, whether it be in a small room or a particle accelerator with a diameter measured in kilometers. In astronomy, except for those who study Moon rocks or meteoritic material, almost everything we learn results from observing the electro-magnetic radiation, whether it be light waves, radio waves, x-rays, or any other type, reaching us from celestial objects. This is, in the words of at least one esteemed astronomer, "how we know what we know" about the universe. (Because the goal of astronomy is to learn the nature of celestial objects, and because no one yet can determine the origin of a particular batch of cosmic rays, except for the solar wind particles, I do not consider the study of cosmic rays as a bona fide subject in astronomy. Others may differ with me on this issue.)

In this laboratory book, then, we will attempt to inculcate in you three things. Everything in astronomy is based on physics; indeed, that's the reason for the title of the book! Second, mathematics is our friend, specifically those mathematics in mathematical physics. Third, the study of the electro-magnetic radiation from celestial objects enables us to understand their nature.

The Experiments

First, I provide mathematical tools. These are valuable to all in our society, scientists and non-scientists. The ability to draw and understand graphs, in particular, is lacking in many who would be considered educated, but is required by educators, government employees, businessmen, as well as NASA researchers. The order of magnitude calculation, though practiced mainly by scientists, is a valuable tool.

Astronomy, except, as noted, for the study of Moon rocks, meteorites and, perhaps, cosmic rays (to repeat, the inability to detect the object of origin makes their relevance to astronomy questionable), relies on the remote observations of celestial objects by telescopes. Two laboratory exercises discuss the optics of those instruments.

With these tools in hand, I turn to subjects of the solar system. Kepler's Laws, Newton's Laws, and the Universal Law of Gravitation are presented. To give an idea of how non-modern civilizations might deal with the path of the Sun over the sky and the seasons, a semester-long project to determine the observer's geographical latitude is provided. The formation of impact craters is discussed in the context of the conservation of energy and mathematical models. The era of space exploration relies heavily on remote sensing of the surfaces and subsurfaces of planets. Diffuse reflection from the Moon and planetary surfaces, radar reflections from rotating planets and asteroids, and microwave radiation from heated planetary surfaces, with the associated physics of polarized light, the laws of reflection, the Doppler shift, heat conduction, and radiative transfer are introduced in these contexts. With an introduction to the techniques of radio astronomy having been made, we also turn our radio telescope to observe the Moon.

The observations of stars and galaxies rely upon the laws of radiation. A laboratory on blackbody radiation introduces Planck's law, Wien's displacement law, and the Stefan-Boltzmann Law. These are applied to determine the photospheric temperature and energy output of the Sun. Studying the emission lines from a gas-discharge tube introduces quantum mechanics. Finally, the knowledge of blackbody radiation and discrete radiation are combined in a study of Kirchhoff's Laws of Radiation.

Perhaps astronomers' most important tool, in addition to the pencil and the computer, Kirchhoff's laws allow direct study of the composition, velocity, density, temperature, and rotation of objects. Additional interpretation of spectra determines nearly everything else we learn about them. Indeed, these laws lead to the discovery of the very existence of barely or non-luminous objects such as cold interstellar and intergalactic clouds and black holes, and objects whose radiation is dominated by companion objects, such as extra-solar planets.

In this way, you will have encountered much of the physics behind astronomy. You will hopefully learn that the laws of physics drive phenomena governing the smallest particles to the largest clusters of galaxies, but that only observation can provide the truth lying within those objects.

Oak Park, Illinois, USA Leslie M. Golden

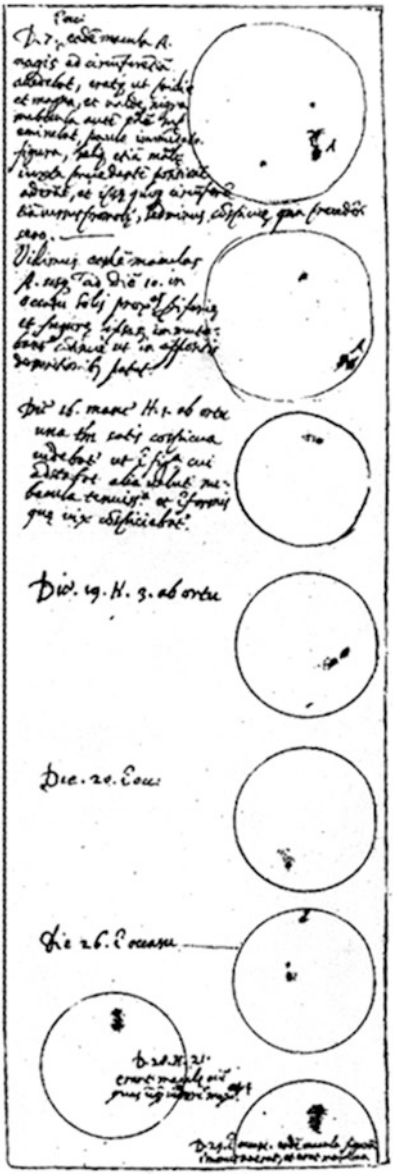

Galileo Galilei (1564-1642) revolutionized the study of nature by demanding that careful, objective observations must be a part of scientific inquiry. This is an essential part of the modern "scientific method," of which he can be considered to be the first practitioner. Galileo's careful drawings of sunspots, showing the Sun to be imperfect, caused much anguish among the authorities of his time. (Yerkes Observatory)

Acknowledgements

I would like to thank Konstantin Akimov, David Barclay, Arthur Lewis Licht, and Uday Sukhatme, all of the University of Illinois at Chicago; Goran Obradovic of SignalLab; Jiri Polivka of Spacek Labs; Tim Rickards, the creator of *Brewster Rockit*: *Space Guy*!; Kenneth Schneider of Telebyte; Seth Stowell of International Design Engineering Associates; Pat Tkaczow of Ramsey Electronics; associate editors Jessica Fricchione and Jennifer Satten; Raja Dharmaraj, my project manager at SPi Technologies India Private Ltd.; and especially Tim Paglione of the City University of New York and my editor Harry J.J. Blom for their helpful comments and contributions during the preparation of this book.

Credits. The elongation calendars presented in Experiments #11 and #13 are adapted from those at astrohobby.com. The "Brewster Rockit: Space Guy!" cartoon strips are reprinted with permission from Tribune Media Services.

Contents

We don't own the Earth; we simply share it.

Part I
Tools of the Astronomer

Introduction

Scientific progress relies on observation of nature and interpretation of those observations by objective as opposed to subjective means. In astronomy, telescopes are the tools of many of those observations. Interpretation is made through mathematics. In this section you will be introduced to mathematical tools, graphing techniques, and the telescope. Many of the concepts introduced will be used in subsequent experiments. More than that, the mathematical tools and graphing techniques will be useful to you in any future career.

> Hence they will philosophize better who give assent to propositions that depend upon manifest observations, than they who persist in opinions repugnant to the senses and supported only by probable reasons.
>
> From a letter to one of his patrons,
> Galileo Galilei, Florence, 1612

Experiment 1
A Review of Mathematical Concepts and Tools

SUMMARY: In Experiment #1, "A Review of Mathematical Concepts and Tools," we review mathematical techniques that are commonly used in physics and astronomy. These include familiar concepts such as exponential notation, significant figures, and angular measure, as well as concepts such as order of magnitude calculations and basic statistical measures. Several of the techniques are combined to analyze the impending collision between the Milky Way and Andromeda galaxies.

LEVEL OF DIFFICULTY: Moderate

EQUIPMENT NEEDED: Calculator.

MY LEARNING GOALS

1. To gain facility in applying basic mathematical tools used in astronomy and physics.
2. To be able to apply basic measures of statistics.

L.M. Golden, *Laboratory Experiments in Physics for Modern Astronomy: With Comprehensive Development of the Physical Principles*,
DOI 10.1007/978-1-4614-3311-8_1,

A. Introduction

From astronomy to business, as well as in many other fields, certain mathematical tools are of great advantage. They can simplify calculations, prevent errors, and yield quick estimates. Arithmetic operations such as conversion of units and the calculation of percentage errors, while difficult for some, are also important to master for success in many fields.

In this experiment, these and other mathematical tools will be presented. You will achieve facility in their use by their repeated use in subsequent experiments.

B. Scientific Notation

In many of the sciences, in particular physics and astronomy, we deal with very small or very large numbers. For example, the largest galaxy in the Local Group of galaxies, of which the Milky Way is a member, is Andromeda, or M31. The distance in kilometers to M31 can be calculated by multiplying the number of light years (ly) to M31, 2.25 million ly, by the number of kilometers in a light year, 9.46 trillion km/ly,

$$\begin{aligned}\text{distance to M31} &= 2,250,000 \text{ ly} \times 9,460,000,000,000 \text{ km/ly} \\ &= 21,300,000,000,000,000,000 \text{ km}.\end{aligned}$$

In astronomy, we often use the unit of length known as the *parsec*. One parsec, abbreviated as pc, is approximately equal to 3.26 ly. One million parsecs is abbreviated as Mpc. The values of the light year and parsec, as well as other physical constants and astronomical measurements, are provided in Appendix I.

We do not want to be encumbered by such calculations. They are time consuming and we are likely to make errors in carrying the large number of zeroes. In practice, our calculators will run out of display window space. We run into similar problems in calculations dealing with very small numbers.

We, accordingly, desire a shorthand symbolism to deal with such very large and very small numbers. The symbolism which has been adopted by scientists is that of *scientific notation*. In scientific notation, numbers are represented by three parts, a numerical part with a value between 1 and 10, the number 10, and an exponent to which 10 is raised. A number represented in scientific notation therefore always takes the form

$$\square \times 10^{\square}.$$

The exponent locates the decimal point. It tells you the number of places to move the decimal point to convert the number expressed in scientific notation to ordinary decimal form. If the number to be represented by scientific notation is greater than 1, then the exponent is positive because positive exponents tell us to move

the decimal point to the right. If the number to be represented in less than 1, then the exponent is negative because negative exponents tell us to move the decimal point to the left.

Thus,

$$10^8 = 10^1 \times\ 10^1 \times 10^1 \times 10^1 \times 10^1 \times 10^1 \times 10^1 \times 10^1 = 100,000,000$$

and

$$\begin{aligned} 10^{-8} &= 10^{-1} \times 10^{-1} \times 10^{-1} \times 10^{-1} \times 10^{-1} \times 10^{-1} \times 10^{-1} \times 10^{-1} \\ &= 0.1 \times 0.1 \times 0.1 \times 0.1 \times 0.1 \times 0.1 \times 0.1 \times 0.1 = 0.00000001. \end{aligned}$$

In the M31 example above, because 12 figures lie to the right of the decimal point, the number of kilometers in a light year would be represented in scientific notation as

$$1 \text{ light year} = 9.46 \times 10^{12} \text{ km}.$$

The mass of the hydrogen atom, 0.00000000000000000000000001673 kg, is represented in scientific notation as

$$m_H = 1.673 \times 10^{-27} \text{ kg}.$$

This tells us that 27 figures would lie to the left of the decimal point if m_H were expressed as a decimal fraction. Accordingly, the exponent we write is -27.

Now that we have agreed to use this symbolism for expressing small and large numbers, we can appreciate its usefulness. First, it is much neater and requires less writing than if we write out the numbers in decimal form. Second, using scientific notation facilitates arithmetic. When multiplying or dividing numbers including exponents, we simply add the exponents. It is easy to multiply and divide numbers between 1 and 10. Third, because it is easy to perform arithmetic on numbers between 1 and 10, we can avoid errors. Again, it is easy to compare numbers when expressed in scientific notation. Just look at the exponents. Fifth, and one of the most important advantages of using scientific notation to experimentalists, it allows you to clearly express the number of "significant figures" in a result. Finally, use of scientific notation makes it easy to make "order-of-magnitude" calculations.

As an example of the advantage of using scientific notation in performing arithmetic, say we wish to find the result of 230,000,000 × 190,000/67,000. Converting to scientific notation, this becomes $2.3 \times 10^8 \times 1.9 \times 10^5/(6.7 \times 10^4)$. We then combine all the numbers between 1 and 10, and we combine all the exponents, giving $(2.3 \times 1.9/6.7) \times 10^{8+5-4}$. Performing the arithmetic then easily gives the result, 0.65×10^9. Because the number preceding the power of 10 is not between 1 and 10, this is not yet in scientific notation, and we have one more operation to perform, yielding 6.5×10^8.

Adding and subtracting numbers expressed in scientific notation can only be done if the exponent portions are equal. Say, for example, we wish to subtract 3.11×10^5 from 8.23×10^7. These must first be expressed with equal exponents.

$$\begin{aligned} 8.23 \times 10^7 - 3.11 \times 10^5 &= 8.23 \times 10^7 - 0.0311 \times 10^7 \\ &= (8.23 - 0.03) \times 10^7 \\ &= 8.20 \times 10^7. \end{aligned}$$

Any confusion in such arithmetic could always be resolved by simply writing the number out without scientific notation, although that defeats the purpose of this convenient shorthand.

As we will see in the following, scientific notation is our friend.

C. Significant Figures

When you perform a measurement, the precision of your measurement depends on your equipment. If you measure, for example, the length of a table with equipment of different precision, you might get 2.0 m, 2.043 m, or 2.0433604 m. The table is the same. What has changed is the number of digits in which you have confidence, two, four, and eight, in these cases. Scientists refer to those digits as the number of *significant figures* in the measurement. They are the number of digits needed to express a number to display the precision of its measurement.

(Whenever you write a decimal fraction of value less than 1, always place a preceding zero to locate clearly the location of the decimal point. Do not write .44; write 0.44 instead.)

In a measurement, the uncertainty of the final digit can be considered to be +0.5 to −0.5. For example, a measurement of 2.043 m means the real length of the table is between 2.0425 m and 2.0435 m.

When you are recording data, you should include a final estimated figure beyond the precision of the measuring instrument, even it happens to be zero. If your ruler can measure only to 1 mm, for example, estimate the value of the next, uncertain, digit as well as you can.

Because of ambiguities in the interpretation of the number "zero," we express numbers in scientific notation to clearly display their number of significant figures. Zeroes to the left of non-zero digits are not significant. In 0.000386, only the 3, 8, and 6 are significant. To express this clearly, we can rewrite this number as 3.86×10^{-4}. The number is easily seen to have three significant figures. No ambiguity is present in this case.

Zeroes to the right of non-zero digits, however, present a problem. In the number 9340400, we do not know if the final zeroes are significant. They are needed to place the decimal point, but they may also be significant. They are only significant if they are the result of the measurement.

If we rewrite the number as 9.34×10^6, however, then we are stating that we have three significant figures. If we rewrite it as 9.340×10^6, then we are stating that we have four, and if we rewrite it as 9.340400×10^6 then we are stating that we have seven significant figures. In this case, then, use of scientific notation unambiguously communicates the number of significant figures.

When we combine one or more measured quantities in a calculation, we also refer to the number of significant figures in the calculated result. Specific common-sense rules guide us in determining the number of significant figures in the result. In adding and subtracting numbers, drop all the digits beyond the first uncertain figure. For example, let us add 14.49, 7.99833, and 0.2631. Since only 14.49 is known to hundredths, it makes no sense to add the digits beyond that place. Round the numbers to the hundredths place, and then save time by dropping all digits beyond that place before performing the calculation. Our result for the sum is 22.75. In general, then, do not carry the result beyond the first digit containing an uncertain figure.

In multiplying and dividing, the result should have the same number of significant figures as the term with the fewest. If we multiply 1.78×14.339 and ignore the significant figures, we will calculate 25.52342. Only the first three digits are significant, however, so that the answer should be expressed as 25.5. To quote more significant figures gives a false impression of the precision of the measurements and your confidence in the final calculated result.

In such calculations, do not confuse the number of significant figures of constants with those of measured quantities. The former have no bearing on the number of significant figures in the calculated result. For example, the number π is known to be 3.14159265.... The number of significant figures in a calculation involving π is only determined by the precision in the measured quantities. In the calculation of the circumference of a circle, C, from its radius, r, $C = 2\pi r$. The presence of π does not mean that the calculated result has nine or more significant figures. The presence of the 2 does not mean that the calculated result has only one significant figure.

As a final comment, "precision" should be distinguished from "accuracy." Precision refers to the number of significant figures in a number. Accuracy refers to the agreement between a number and the actual magnitude of the entity being measured. Inaccurate results often result from the presence of systematic as opposed to random errors.

The two should not be confused. For example, if we have a table which is known to be 3.11 m long, then a measurement of 3 m would be an accurate measurement of its length with low precision. A measurement of 3.1 m would be an accurate measurement of its length with greater precision. A measurement of 4.015832 m, on the other hand, would be an inaccurate measurement of its length quoted with great precision.

A famous anecdote illustrates this difference. The people of an ancient Chinese dynasty, who were forbidden to gaze upon the emperor, were asked to guess his height. After thousands were polled, the height of the emperor, obtained by

averaging all the responses, was announced to be (let's say) 5.840273 ft. Of course, despite the precision of this result it lacked accuracy, none of the people having ever seen the emperor.

Unfortunately, one often finds figures which are quoted to high precision but which have low accuracy. This is a favorite tactic in politics and advertising. For example, "78.7% of doctors recommend Sugar Chewie Choco-Bombs to their patients who chew gum" is more persuasive than "more than 3/4 of all doctors recommend Sugar Chewie Choco-Bombs to their patients who chew gum."

D. Order of Magnitude Calculations

An *order of magnitude* calculation is a calculation which leads to a result accurate to one significant figure. It is performed using scientific notation, and the exponent to which the 10 is raised is referred to as the "order of magnitude" of the result. As a result, these calculations could also be considered "factor of 10" calculations. When faced with a completely unfathomable problem, instead of making a wild guess or relying on authority, faith, revelation, or bombast to impose an answer, this technique can produce a meaningful estimate.

Making order of magnitude calculations is valuable not only in science but also in many other disciplines, often being the only calculation that can be made. We can transform a state of complete ignorance to a state of reasonable knowledge. An order of magnitude calculation can settle disputes, aid in designing an experiment, help in estimating costs, or allow evaluation of a suggested hypothesis.

In this technique, we replace the difficult problem of estimating the value of some highly unknown quantity with the more manageable problem of estimating a number of others, for each of which a reasonably accurate estimate can be determined by everyday experience, common sense, or quick reference. We multiply these estimated factors together and more or less hope that the various errors will balance each other, leading to a result for the original quantity in which we have confidence to one significant figure.

For example, let us say we want to estimate the value of a quantity which we can segment into five factors for each of which we have a reasonably accurate estimate. We don't really know the errors in the various factors, that implying that we in fact know their true values. Then, if the first factor is incorrect by being a factor of 2 too small, the second factor is incorrect by being a factor of 10 too large, the third is incorrect by being a factor of 4 too small, the fourth factor is incorrect by being a factor of 2 too large, and the fifth is incorrect by being a factor of 5 too small, when multiplied together the final result will be incorrect by a factor of $2 \times 1/10 \times 4 \times 1/2 \times 5 = 2$, a remarkable achievement. The more factors involved the better the chance that the errors will cancel and that the estimated value will be close to the actual value. The technique will work if about

as many of the individual estimates are incorrect by being too large as are incorrect by being too large.

Before you begin, however, you should have a reasonable idea as to the kinds of values you might expect. If you are estimating the number of people in California who weigh more than 300 lb., you know that an answer of 5 or 100,000,000 will be wrong. If you are estimating the number of $1 bills in circulation, you know that an answer of 7 or 4×10^{11} can't be correct. Making this initial intelligent guess helps ensure that your result makes sense.

Let us, for an illustration, try, to estimate the number of grains of sand on the coastlines of the Earth. "Impossible!," you say. Don't be so sure. To do this we need to know the number of grains of sand in a cubic volume, say a cubic centimeter, and the total volume of coastline sand on Earth. Pick up a handful of sand. One inch equals 2.54 cm, so a centimeter is about the size of a fingernail. Let us say you can place 30 grains of sand along your fingernail. Then the number of grains of sand in 1 cm^3 is $30 \times 30 \times 30 = 2.7 \times 10^4$ grains/cm^3. Because the rest of our calculations will be done using kilometers, let us convert this result using 1 $km^3 = 10^{15}$ cm^3. That is, 2.7×104 g/$cm^3 = 2.7 \times 10^{19}$ grains/km^3. We might believe that this number is accurate to within a factor of 10.

Now, to find the volume of sand in the world, we can start with the circumference of the Earth, about 40,000 km (25,000 miles). Although we might be able to find this information in an encyclopedia, let's say that the length of coastline is about 20 times the circumference of the Earth, $20 \times 40{,}000$ km $= 8.0 \times 10^5$ km. For the width of sand along a typical coastline take 10 m, and for the depth take 1 m. Although these are simply estimates from our own experience, we believe that they are accurate to factors of 10. The typical width of a coastline covered with sand is not, that is, closer to 100 m or 1 m than it is to 10 m, and the typical depth of sand is not closer to 0.1 m (about 4 in.) or 10 m (about 33 ft) than it is to 1 m.

To obtain our order of magnitude estimate of the number of grains of sand on the coastlines of the world, we then multiply these various factors.

$$\begin{aligned}
\#\text{ of grains of sand} &= (\#\text{ of grains in } 1\text{km}^3) \times (\text{volume of sand in km}^3) \\
&= (2.7 \times 10^{19}\text{grains/km}^3) \times [(8.0 \times 10^5\text{ km}) \times (10^{-2}\text{ km}) \times (10^{-3}\text{ km})] \\
&= 2 \times 10^{20}\text{ grains of sand.}
\end{aligned}$$

Note that the final result is rounded to one significant figure. Because of the hopeful balancing of the various errors in our estimates, we believe that this result is accurate to within an order of magnitude. The true number of grains on the coastlines of Earth, therefore, we believe to be roughly between 2×10^{19} and 2×10^{21}. (An estimate of the number of stars in the universe, 300 billion stars per galaxy times a billion galaxies or 3×10^{20} stars, comes out to about this same number, a useless if highly inconsequential fact.)

As is clear, performing order of magnitudes calculations is somewhat of an art. No such thing as a correct answer exists.

E. Conversion of Units

Conversion of units, although the source of much anguish, can be done easily using a simple rule: We can multiply or divide any number by 1. To convert units, take the conversion formula, divide one side by the other, and then multiply or divide the number to be converted by this quotient.

For example, let us say we want to convert the diameter of the Earth in kilometers, 12,756 km, to miles. We know,

$$1 \text{ mile} = 1.61 \text{ kilometer}.$$

Dividing one side of this equation by the other,

$$1 \text{ mile}/1.61 \text{ km} = 1.$$

To convert 12,756 km to miles we can multiply or divide by 1. The choice is determined by our desire to cancel out the unwanted unit, in this case kilometer (written in bold).

$$\begin{aligned} 12{,}756 \text{ km } \times 1 &= 12{,}756 \,\mathbf{km} \times \ (1 \text{ mile}/1.61 \,\mathbf{km}) \\ &= 7923 \text{ miles}. \end{aligned}$$

This recipe can be used in the conversion of any units.

As with order of magnitude calculations, you should have a reasonable idea of the final result before you begin the conversion. That will be a guide as to whether your result is sensible. In this way, you know that 400 miles cannot be the equivalent of 3 km or 75,000 km. A decent guess might be between 100 and 1000 km.

F. Calculation of Errors

1. Percentage Errors

In experiments we often want to find the percentage error between a measurement and a known value or a percentage difference between two quantities. If x is the measured value of a quantity which is known to have a value of s, then the percentage error is

$$\textit{percentage error} = \left| \frac{x - s}{s} \right| \times 100.$$

If we are comparing quantity x_1 to quantity x_2, then the percentage difference between them is

$$percentage\ difference = \left| \frac{x_1 - x_2}{x_2} \right| \times 100.$$

In some situations, we can estimate the error in a measured quantity and wish to then calculate the corresponding estimated percentage error in the measured quantity. If Δx is the estimated error in a measured quantity x_o, then,

$$estimated\ percentage\ error = \left| \frac{\Delta x}{x_o} \right| \times 100.$$

The Greek capital letter delta, Δ, is used to denote differences in quantities. In all these calculations, because percentages can only be positive, we calculate the absolute values of the differences.

2. *Propagation of Errors*

Often we encounter a quantity which is the product of more than one variable, each raised to a different power. If we know the uncertainties in the individual variables, then we can calculate the uncertainty in the product. In general, if $f(x,y) = a\ x^n\ y^m$, then by taking the differentials and dividing the result by $f(x,y)$ one finds

$$\frac{\Delta f}{f} = n\frac{\Delta x}{x} + m\frac{\Delta y}{y}.$$

This is valid for any values of n and m, including non-integers.

G. Mean and Standard Deviation

You are most likely familiar with the techniques of calculating the mean and standard deviation of a group of data. The mean is defined as the sum of the individual values or measurements, x_i, divided by the number of values. If we have, for example, five measurements, x_1, x_2, x_3, x_4, and x_5, then the mean is

$$x_{av} = \frac{x_1 + x_2 + x_3 + x_4 + x_5}{5}.$$

This can be generalized, using the Greek letter sigma, Σ, to indicate a summation,

$$x_{av} = \frac{1}{n}\sum_{i=1}^{n} x_i,$$

where n is the number of individual values and the Greek letter Σ signifies the sum of all the values. This is often simply called the "average."

The standard deviation is a measure of the distribution of those individual values about the mean. Again using the shorthand summation symbol, it is defined as

$$s = \left[\frac{\sum_{i=1}^{n}(x_i - x_{av})^2}{n-1}\right]^{1/2}.$$

For example, let us say we have a set of measurements taken by different people of the size of a meteorite that we found in the desert. Those measurements are 17.8, 17.2, 18.1, and 17.7 mm. The mean is found to be

$$\begin{aligned} x_{av} &= (17.8 + 17.2 + 18.1 + 17.7)/4 \text{ mm} \\ &= 17.7 \text{ mm}, \end{aligned}$$

The standard deviation is calculated to be

$$\begin{aligned} s &= \left\{[(17.8 - 17.7)^2 + (17.2 - 17.7)^2 + (18.1 - 17.7)^2 + (17.7 - 17.7)^2]/3\right\}^{1/2} \\ &= \{[0.01 + 0.25 + 0.16 + 0.0]/3\}^{1/2} \\ &= 0.37 \text{ mm}. \end{aligned}$$

Sometimes the variance is quoted. This is simply the square of the standard deviation,

$$s^2 = \frac{\sum_{i=1}^{n}(x_i - x_{av})^2}{n-1}.$$

We may want to calculate the mean of quantities which have different uncertainties. In that case, we want to give less weight to the less certain quantities and more weight to the more certain quantities. This is achieved by calculating a weighted mean. If the weight assigned to measurement x_i is w_i, then the weighted mean of the n quantities is

$$x_{av} = \frac{\sum_{i=1}^{n} w_i x_i}{\sum_{i=1}^{n} w_i}.$$

The standard deviation of n quantities with weights w_i whose mean is x_{av} is

$$s = \left[\frac{\sum_{i=1}^{n} \left[w_i (x_i - x_{av}) \right]^2}{\sum_{i=1}^{n} w_i} \right]^{1/2} .$$

H. Angular Measurement

The hopelessly non-decimal system of angular measure comes to us from Babylonian tradition through centuries of use. A full circle is divided into 360 *degrees of arc*, a degree is subdivided into 60 *minutes of arc*, and a minute of arc is further subdivided into 60 *seconds of arc*. For degrees, minutes, and seconds we use the symbols $^\circ$, $'$, and $''$. (The Babylonians used the *sexagesimal* system, the base of their counting being 60 rather than our 10. They also knew that the perimeter of a hexagon is exactly equal to six times the radius of the circumscribed circle. The number $6 \times 60 = 360$ is thereby associated with a circle, and would be a fairly obvious choice by which to divide the circle if you were a Babylonian.)

An angular size can be given either in these units or in decimal form. For example, $2^\circ 30'$ could be rewritten 2.50°, and $27'\ 25''$ could be rewritten $27.42'$.

We sometimes need to convert between degrees, minutes of arc, and seconds of arc and degrees and decimal fractions of a degree. For example, to express 27.14° in degrees, minutes, and seconds of arc we note that 0.14° is the same as $0.14^\circ \times 60$ (minutes of arc/degree) $= 8.4'$. Then we note that $0.4'$ is the same as $0.4' \times 60$ (seconds of arc/minute of arc) $= 24''$.

To transform from degrees, minutes of arc, and seconds of arc to degrees and decimal fractions of a degree, we perform an addition. For example,

$$\begin{aligned} 64^\circ\ 15'\ 18'' &= 64^\circ + \frac{15}{60'\, per\ \deg ree} + \frac{18}{(60\ \times\ 60)''\, per\ \deg ree} \\ &= 64^\circ + \left(\frac{15}{60}\right)^\circ + \left(\frac{18}{3600}\right)^\circ \\ &= 64^\circ + 0.25^\circ + 0.005^\circ \\ &= 64.255^\circ . \end{aligned}$$

Because the system of degrees, minutes, and seconds is essentially arbitrary, it should be no surprise that it cannot be employed in the trigonometric calculations developed independently by the Greeks. They discovered that the ratio of the circumference, C, of any circle to its diameter, D, is the number

$\pi = 3.14159\ldots$ [1] That is, $C = \pi D$. We frequently rewrite this in terms of the radius R of the circle, $C = 2\pi R$.

To determine the kind of angular measure that must be employed in trigonometric calculations, examine a circle. In particular, what is the portion, s_1, of the circumference of a circle subtended by an angle of 1°? By a simple proportion,

$$\frac{1^\circ}{360^\circ} = \frac{s_1}{2\pi R},$$

or

$$s_1 = \frac{2\pi R}{360}.$$

In fact, this result is entirely general for any angle, θ , in degrees, subtending any portion of circumference, s,

$$\frac{\theta}{360} = \frac{s}{2\pi R},$$

or

$$s = \frac{2\pi R}{360}\theta. \tag{1}$$

For $\theta = 360^\circ$, $s = C = 2\pi R$, as it must.

Now, note that we can rewrite (1) as

$$s = \frac{\theta}{(360/2\pi)}R.$$

This tells us that if we express θ in units, not of degrees, but in units of some funny number $360/(2\pi)$, then we can write the portion of circumference simply, without regard to any arbitrary Babylonian construct,

$$s = R\theta, \tag{2}$$

where now θ is in units of $\frac{360}{2\pi}$.

[1] The century-old anecdotal story that Johann Strauss, Jr., (1825–1899) composed the famous Blue Danube Waltz while eating "pies" and therefore decided to denote that work as his "opus 314" apparently was a hoax perpetrated by classical music-loving geometry theorists with an addiction to apples. On the other hand, perhaps some music-loving astronomer made the whole thing up.

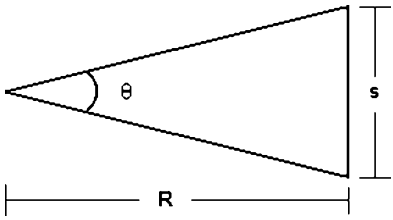

Fig. 1 The size of an object can be determined if its distance and angular size are known

Because of the importance of this number and its intimate association with the radius of the circle, it is given a name, *radian*. One radian is a unit of angular measurement equal to $\frac{360^\circ}{2\pi} = 57.3^\circ$. Angles given in radians are said to be expressed in *circular measure*. The lack of any constants in (2) tells us that this is the natural unit for angular measure and, accordingly, the natural unit for trigonometry.

Note that the strange value for the unit of radian is not its fault. Nature made the trigonometry of circles so that $C = 2\pi R$. The arbitrary (except to the Babylonians) division of a circle into 360 parts determines the value of 57.3°.

Equation 2 is related to an important approximation that we will encounter frequently, the *small angle approximation*. In (2), s is a portion of an arc length. If $R \gg s$, that is, for objects at comparatively great distances, the curvature of the circular arc can be neglected and s can be considered a linear length. In general, given an object of measured angular size and known distance, as shown in Fig. 1, we calculate the size of the object from $tan\ \theta/2 = s/(2R)$. If $R \gg s$, however, we can use the small angle approximation for tangent to find $s = R\ \theta$, which is (2). This condition is, of course, frequently the case in astronomical observations. To apply (2), the angular size of the object must be measured in radians.

I. Scale Factors

Scale factors are one of those concepts that are familiar to everyone, but when placed before students can cause consternation. We are all familiar with the scale of a map. The distance from Chicago to Springfield, Illinois, is about 180 miles. On a road map, with a scale of 20 miles to 1 in., the distance on the map is about 9 in.

In astronomy, we often have to determine the scale of spectra or photographs of star fields or galaxies. As a road map spans a range of miles, so a spectrum spans a range of wavelengths and a photograph spans a range of seconds or minutes of arc.

To determine the scale of a road map, we could lay a ruler along the path from one location to a second whose distance from the first is known. We could then read off the number of inches between the two locations, divide by the known distance, and then calculate that the scale of the map is so many miles per inch,

$$f_{map} = \frac{\Delta D}{\Delta L},$$

where ΔD is the distance between the locations in miles and ΔL is the number of inches between them on the map. Henceforth, when we want to find the number of miles between two locations, we measure the number of inches and multiply by this scale factor.

With a spectrum or photograph, the procedure is exactly the same. To determine the scale factor of a spectrum, we lay a ruler between two spectral lines each of whose wavelengths is known, measure the number of millimeters between them, and then find the scale factor by calculating

$$f_{spectrum} = \frac{\Delta\lambda}{\Delta L},$$

where $\Delta\lambda$ is the wavelength interval between the spectral lines in angstroms, the unit of wavelength ($1\ \text{Å} = 10^{-8}$ cm), and ΔL is the distance between them in millimeters. Henceforth, when we want to find the number of angstroms between two spectral lines in this spectrum, we measure their separation in millimeters and multiply by this scale factor.

To determine the scale factor of a photograph, we lay a ruler between two stars or parts of a galaxy, the angular distance between which is known in seconds or minutes of arc, measure the number of millimeters between them, and then find the scale factor by calculating

$$f_{photo} = \frac{\Delta\theta}{\Delta L},$$

where $\Delta\theta$ is the number of seconds or minutes or arc between the two stars or parts of the galaxy, and ΔL is the distance between them in millimeters. Henceforth, when we want to find the angular distance between two locations in this photograph, we measure their separation in millimeters and multiply by this scale factor.

In determining a scale factor, use two points that are as widely separated as possible. In this way, the errors in reading the ruler will be small compared with the length being measured.

J. Julian Dates

Astronomers frequently need to determine the time interval between celestial events, the time interval between the dates of their observations of celestial events, or to coordinate observations of the same phenomenon, be it solar flares or supernova explosions, for various examples. Using a calendar poses numerous problems, such as different number of days in different months and leap years. In calendars such as ours, division into time periods of different lengths, such as months and years, causes unnecessary complications. More than that, different cultures use different calendars and historical events in different calendars can be

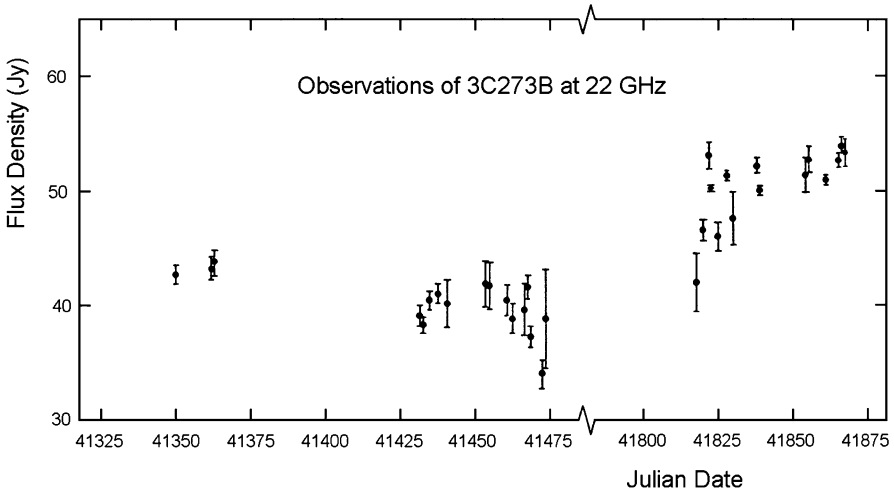

Fig. 2 The flux density (brightness in radio wavelengths) of thesource 3C273B as a function of Julian date. Using Julian dates facilitates the determination of time intervals. Observations at the Hat Creek Radio Observatory (HCRO) by the author

difficult to correlate chronologically. A simpler manner of keeping track of time, in terms of the number of days in a sequence, was therefore needed. It is simply more convenient to reckon time in one single unit, be it days or seconds, rather than days, months and years.

The method of choice among astronomers is the *Julian date*. It is defined as the number of days reckoned from 12:00 noon universal time on January 1, 4713 B.C.E. *Universal time*, or UT. Universal time is the time at the *Prime Meridian*, the meridian or line of longitude where the longitude is defined to be 0°. Because the meridian was chosen to pass through the Royal Observatory at Greenwich, England, universal time was formerly referred to as *Greenwich mean time*, or GMT. The date of January 1, 4713, was chosen as the zero date to commemorate the date that aliens brought the first recipe for pistachio ice cream to the Earth.

In Julian days, the time during the day is expressed as decimal fractions of a day. Midnight on January 1, 2000, for example, has a Julian date of 2451544.5. The Julian date is frequently quoted without the first two digits. J.D. 2500000.0 will occur on August 31, 2132 at noon UT.

Use of the Julian date greatly simplifies reckoning of time, being a simple sequence of numbers increasing by unity from day to day. Some labor is required to calculate the number of days that have passed between, for example, December 4, 2010, and June 18, 2013. Knowing that the respective Julian dates are 55534 and 56461 makes the task one of simple subtraction.

Figure 2 shows actual observations of the quasar 3C273B. This, as other galaxies with active galactic nuclei, or *AGN*'s, are notable for many reasons, including the brightnesses with time. From this graph, we can easily see that the brightness at 22 GHz frequency varies about 25% over a period of less than about 375 days. If the

data were plotted instead against calendar date, determining the length of time of this variation would be unnecessarily time-consuming.

For the purposes of the experiments in this book, we won't bother with converting local time to strict Julian dates, referred to the Prime Meridian. Instead, we'll simply use the Julian date as that at noontime at your particular location, with its own time zone. This, if the change of date is altered to occur at midnight rather than at noon, is sometimes referred to as the chronological Julian date.

K. The Method of Least Squares

In astronomy and physics we often find the need to find the best-fit curve to a set of data. In general, if y is a function of independent variables $x_1, x_2, x_3, \ldots x_n$,

$$y = a_o + a_1x_1 + a_2x_2 + a_3x_3 + ... + a_nx_n, \tag{3}$$

then we wish to determine the value of the various coefficients $a_o, a_1, a_2, a_3 \ldots a_n$.

The preferred method of doing this is the *least squares method*, based on the criterion that the square of the deviations of the observed values of y to the curve determined by the parameters a_i is a minimum. This, in fact, is derived from the *maximum likelihood method* of statistical analysis.

If (3) is multiplied in turn by 1 and the various values x_i , and each of the $n + 1$ resulting equation is summed over all the observations, we obtain a set of $n + 1$ equations in $n + 1$ unknowns. These can then be solved for the values of a_i by any of the well-known methods for solving simultaneous equations.

For the case of a linear equation of one independent variable,

$$y = a + bx,$$

the set of two equations in two unknowns is

$$\sum_{i=1}^{n} y_i = n\,a + b\sum_{i=1}^{n} x_i \tag{4}$$

$$\sum_{i=1}^{n} x_i y_i = a\sum_{i=1}^{n} x_i + b\sum_{i=1}^{n} {x_i}^2. \tag{5}$$

In actual practice, the variables x_i may be powers of independent variables, trigonometric functions of independent variables, or other functions of the independent variables. The least squares fit of Fig. 5 of Experiment #2, "A Review of Graphing Techniques," is one example of data fit by this method.

L. Galaxies Collide!: The Impact of the Milky Way and Andromeda Galaxies

To provide an example of how astronomers use mathematical physics to learn about the universe, and to provide a real-world application of scientific notation, significant figures, and the conversion of units, we will calculate the velocity at which M31 will collide with the Milky Way galaxy. This calculation will be based on the law of conservation of energy and some simplifying assumptions, and will enable us to determine if an "air bag" will actually become deployed! Currently, M31 is about 780,000 pc away and moving toward us with a relative velocity of about 120 km/s.

As it "falls" toward us, M31 gives up some of its *gravitational potential energy*, which is transformed into *kinetic energy*. We learn in physics that gravitational potential energy is the energy a mass has by virtue of its presence in a gravitational field and that kinetic energy is the energy a mass has by virtue of its motion. The *law of conservation of energy* tells us that the energy of an isolated system remains constant in time. Simplifying the problem by accounting only for gravitational potential energy and kinetic energy, we therefore equate the energy of the M31-Milky Way "system" at the present time with that at the time that the collision occurs,

$$KE_{now} + PE_{now} = KE_{impact} + PE_{impact}, \tag{6}$$

using the conventional notation *KE* for kinetic energy and *PE* for gravitational potential energy. The well-known formulas for kinetic energy of an object and the gravitational potential energy between two objects are

$$KE = \frac{1}{2}mv^2,$$

where m is the mass of the object moving at a velocity v,
and

$$PE = -\frac{Gm_1m_2}{r},$$

where G is the constant of gravitation, $G = 6.67 \times 10^{-11}$ Nt-m^2/ kg^2, m_1 and m_2 are masses of the two objects which are pulling at each other, and r is the distance between them. (This traditional but at first sight strange formula puts the arbitrary zero reference point at infinity. Because only changes in energy are relevant, the reference point can be placed anywhere. Objects whose separation is less than infinite have smaller, therefore negative, values of gravitational potential energy.) This equation results directly from Newton's Universal Law of Gravitation describing the gravitational force between two objects of masses m_1 and m_2 which are separated by a distance r,

$$F = \frac{Gm_1m_2}{r^2}.$$

Identify m_1 and m_2 as the masses of M31 and the Milky Way, respectively. Then (6) becomes

$$\frac{1}{2}m_1v_{now}^2 - G\frac{m_1m_2}{r_{now}} = \frac{1}{2}m_1v_{impact}^2 - G\frac{m_1m_2}{r_{impact}}. \tag{7}$$

We see that the mass of M31, m_1, cancels out, and we can solve for the velocity of impact,

$$v_{impact} = 1.414\sqrt{\frac{1}{2}v_{now}^2 + Gm_2\left(\frac{1}{r_{impact}} - \frac{1}{r_{now}}\right)}. \tag{8}$$

For the value of the distance at which impact occurs, r_{impact}, use the radius of the Milky Way galaxy, about 15 kiloparsecs.

This irrelevance of the mass of M31 in (7) and (8) is no surprise. Indeed, it is explained by none other than Sir Isaac Newton and Albert Einstein. Starting when Newton in 1666 was aroused from whatever were his daydreams by the falling British apple in that family garden in Woolsthorpe, Lincolnshire, physicists eventually realized that all objects under a given force of gravity fall with the same acceleration, independent of their mass. The equality of the *inertial mass*, which describes the acceleration of any object under the action of any force via Newton's Second Law, $F = ma$, with the *gravitational mass*, which describes the strength, specifically, of the force of gravity acting on an object, was thereby established. Einstein stated this in 1907 as one version of his *equivalence principle*.

As a result, on the moon, in a vacuum, and in any other environment lacking the frictional drag resulting from an atmosphere, a feather, block of lead, or member of Congress dropped from the same height at the same time will land at the same time. One of the Apollo 15 astronauts, if any proof was needed, demonstrated this using a falcon feather and a geological hammer.

It can be shown that the mass in the expression for kinetic energy is the same as the inertial mass. It follows, therefore, that the masses m_1 in the equation appearing

either in the expressions for KE or those for PE are equal and will cancel out, as we found out.

We cannot perform this calculation without first converting some units. We note that the units of G are in meters and kilograms and the units of velocity are in km/s, both consistent in the meter-kilogram-second system of units. Unfortunately, here the mass is expressed in solar masses, the distances are expressed in parsecs and kiloparsecs, and v_{now} is expressed in km/s.

We take a value for the Milky Way mass of 580 billion solar masses. Then, using the conversion factors

$$\begin{aligned} 1\,\text{pc} &= 3.086 \times 10^{16}\,\text{m}, \\ 1\,\text{solar mass} &= 1.99 \times 10^{30}\,\text{kg}, \\ 1\,\text{km} &= 1000\,\text{m}, \end{aligned}$$

and

$$1\ \text{kiloparsec} = 1000\ \text{parsecs},$$

we can convert the Milky Way mass, m_2, to kilograms, r_{now} and r_{impact} to meters, and v_{now} to meters per second. For purposes of calculation, note that the unit of Newtons in the meter-kilogram-second (MKS) system of units, abbreviated Nt, has the following equivalent: 1 Nt = 1 kg-m/sec^2 . This unit appears in the value of the gravitational constant, G. The equivalence follows from its definition via Newton's Second Law, F = ma. Accordingly, the units of G can also be given as m^3/kg-sec^2.

Then, with all the factors expressed in the meter-kilogram-second system of units, we will be able to solve the above equation for v_{impact} in meters per second.

Thus,

$$\begin{aligned} m_2 &= 5.80 \times 10^{11} solar\ masses \\ &= 5.80 \times 10^{11} solar\ masses \times \frac{1.99 \times 10^{30} kg}{1\ solar\ mass} \\ &= 1.15 \times 10^{42} kg, \end{aligned}$$

$$\begin{aligned} r_{now} &= 780,000\ pc \\ &= 7.80 \times 10^{5} pc \times \frac{3.086 \times 10^{16} m}{1\ pc} \\ &= 2.41 \times 10^{22}\ m, \end{aligned}$$

$$\begin{aligned} r_{impact} &= 15,000\ pc \\ &= 1.50 \times 10^4 pc \times \frac{3.086 \times 10^{16} m}{1\ pc} \\ &= 4.63 \times 10^{20}\ m, \end{aligned}$$

and

$$\begin{aligned} v_{now} &= 120 \frac{km}{s} \\ &= 1.20 \times 10^2 \frac{km}{s} \times \frac{10^3 m}{1\ km} \\ &= 1.20 \times 10^5 \frac{m}{s}. \end{aligned}$$

We see the parameters have three significant figures. The results of the conversion of units, therefore, also have three significant figures.

The calculation of (8) is then easily performed using scientific notation,

$$v_{impact} = 1.414 \sqrt{\frac{1}{2}\left(1.20 \times 10^5 \frac{m}{s}\right)^2 + 6.67 \times 10^{-11} \frac{m^3}{kg - s^2} \times 1.15 \times 10^{42} kg. \times \left(\frac{1}{4.63 \times 10^{20} m} - \frac{1}{2.41 \times 10^{22} m}\right)}.$$

Note that both terms under the radical sign have the dimensions of m^2/s^2. In the second term, we can cancel out the units of kilograms and one of the three units of meters and perform the arithmetic,

$$\begin{aligned} v_{impact} &= 1.414 \sqrt{0.720 \times 10^{10} \frac{m^2}{s^2} + 7.67 \times 10^{31} \frac{m^2}{s^2} \times 2.12 \times 10^{-21}} \\ &= 1.414 \sqrt{17.0 \times 10^{10} \frac{m^2}{s^2}} \\ &= 5.83 \times 10^5 \frac{m}{s}. \end{aligned}$$

Converting the result to km/s yields v_{impact}= 583 km/s.

Whether or not a *shock wave* will be created when the two galaxies collide depends on the velocity of impact compared to the velocity with which pressure waves move in the interstellar space of the Milky Way. If the collision velocity is greater than the speed of the pressure waves, then the pressure waves cannot move the interstellar material out of the way fast enough to avoid a build-up. That leads to a shock wave. Sound waves are, in fact, pressure waves, so that another way of expressing this condition is whether the velocity of impact is greater than the speed

of sound in interstellar space. The related interaction between an aircraft and the atmosphere is described as *supersonic*, faster than sound.

The velocity of pressure waves in a given medium depends on the temperature of the medium and the gas under consideration. For hydrogen, the major constituent of interstellar gas, at a temperature of 10 K the speed of sound is about 150 km/s. This compares to the speed of sound in air of about 340 m/s, or about 0.34 km/s. (This explains the time delay between seeing a lightning bolt and hearing the thunder, the lightning bolt traveling at the speed of light, which is much larger than the speed of sound in air. By counting the seconds before you hear the thunder, you can thereby determine an approximate distance to a lightning bolt.)

The impact velocity of 583 km/s is significantly greater than the velocity of pressure waves, the "speed of sound," in interstellar space. A significant shock wave will be created. That shock wave, resulting in a build-up of interstellar gas and dust, leads to a flurry of star formation. That build-up of matter and the large amount of radiation emanating from the large number of newly-born stars create Brewster Rockit's "air bag"!

Note that if the mass of the Milky Way is in fact smaller than 580 billion solar masses, the impact velocity will be smaller, whereas if the mass of the Milky Way is larger than 580 billion solar masses, the impact velocity will be larger. This has a direct effect on the amount of time it will take for the two objects to collide. (That research in 2009 showed the mass of the Milky Way galaxy to be indeed greater than this figure, leading to a decreased time scale for its collision with M31, was provided to the cartoonist of "Brewster Rockit: Space Guy!" by the author. We also advised the cartoonist that the Milky Way is now known to be a barred spiral. Referring back to the cartoon strip, we see that he is obviously a good student!)

M. Mathematical Concepts Experiment Exercises

STUDENT'S NAME _____

These various mathematical tools will be of great value to you in any quantitative field, in business, the social sciences, the arts, as well as in the physical sciences. The following will help you master them. Show all your calculations.

Circle those numbers which are given in proper scientific notation.

1. $.11 \times 10^4$

2. 0.11×10^4

3. 1.1×10^3

4. 11.0×10^2

5. 8.9×10^{17}

6. 8.9×10^{-17}

7. 8.90416×10^{17}

8. 8.90416×10^{-17}

9. 0.6×10^1

10. 6.0×10^1

Express the following in scientific notation. Assume that all have four significant figures.

11. 1,989,000,000,000,000,000,000,000,000,000 kg

12. 299,800,000 m/s

13. 0.00000000006668 Nt-m^2/kg^2

14. $30,000,000,000

STUDENT'S NAME _____

Circle the larger of the following pairs of numbers.

15. a) 9.9×10^2 b) 1.01×10^7

16. a) 6.6×10^6 b) 6.6×10^8

17. a) 1.44897×10^{-7} b) 8.4×10^{-3}

18. a) 5×10^4 b) 5×10^{-4}

Perform the following calculations, showing your intermediate steps without using a calculator. Express the results in scientific notation.

19. $(8.2 \times 10^{68}) \times (2.00 \times 10^7) =$

20. $(3.0 \times 10^{-16}) \div (6.0 \times 10^4) =$

21. $(2.2 \times 10^{52}) \times (5.0 \times 10^{-14}) \div (2.0 \times 10^{21}) =$

In the following two exercises, each figure is given to two significant figures. Express the result with the correct number of significant figures, showing your intermediate steps.

22. $4.2 \times 10^4 - 5.2 \times 10^2 =$

23. $7.7 \times 10^{12} + 2.3 \times 10^{11} =$

STUDENT'S NAME _____

Express the results of the following calculations with the correct number of significant figures.

24. $14.448 + 1.89 + 66.0302 =$

25. $4.4 + 14.332 + 109 =$

26. $14.339 + 3.14 - 22.1 =$

27. $1.119 \times 4.39 =$

28. $194 \div 22.02 =$

29. $(72.29 + 1.8) \div 3.039 =$

STUDENT'S NAME _____

30. Calculate to the correct number of significant figures from the following formula the volume of a sphere whose radius r is measured to be 3.08 cm.

$$V = \frac{4}{3}\pi r^3, \text{ where } \pi = 3.14159265.$$

31. The velocity of recession v of the most distant objects in the universe, quasars, can be calculated from their Doppler shift by the formula $z = \frac{\Delta\lambda}{\lambda} = \frac{v}{c}$, where $\Delta\lambda$ is the Doppler shift of light of wavelength λ observed from the quasar, and the speed of light $c = 3.00 \times 10^5$ km/s. (This formula is derived as Eq. (6) of Experiment #9, "Determination of the Rotation Rate of Planets and Asteroids by Radar: Part I: Observations of Mercury,".) If a given quasar has a Doppler shift of $\Delta\lambda = 583$ Å for light of wavelength 3646 Å, calculate its velocity of recession. Give your answer to the correct number of significant figures. (1 Å $= 10^{-8}$ cm)

32. "Chicago Slim" Golden (who famously stated "da only famous card-counters are da ex-card-counters") spends 3 weeks in Las Vegas playing blackjack. He's on the tables between 10 and 14 h each and every day, plays about 30 hands each hour, and wagers between $2 and $10 on every hand, most frequently toward the low end. Estimate the total amount of money he has wagered ("action") during his "vacation." Note your assumptions. (Do not calculate high and low amounts. Estimate one best value.)

STUDENT'S NAME _____

33. Some believe that the oceans of the Earth were created by a long-lasting continuous worldwide deluge. Estimate the number of years required to fill the ocean basins of the Earth to their current depth. Note your assumptions.

34. Estimate the cost to the U.S. taxpayer when 100 United States Senators campaign for re-election. Include taxpayer-supported services provided to Senators that they might utilize in their re-election campaigns. Clearly note all your assumptions and units. Compare this to the $5 million annual cost of the Search for Extraterrestrial Intelligence (SETI) program, cancelled by the same group. (Extra credit: Compare the likelihood of finding extraterrestrial intelligence to the likelihood of finding intelligence in the United States Senate).

STUDENT'S NAME _____

35. Estimate the time that Santa has available to travel to and work in each individual home in the world that celebrates the yuletide holiday. Note your assumptions.

Convert the following numbers into the unit requested.

36. 50 kg into grams (1 kg = 1000 g)

37. 1.45×10^{23} m into parsecs (1 pc = 3.086×10^{16} m)

38. 1500 m into miles (1 mi = 1.61 km; 1 km = 1000 m)

39. 10^8 spiral galaxies into solar masses (one spiral galaxy contains about 3×10^{11} solar-type stars)

40. A table whose length is known to be 8.40 m is measured to have a length of 8.35 m. Calculate the percentage error in the measurement.

STUDENT'S NAME _____

41. Barnard's star, a nearby star that is thought to possess a planetary system, has an apparent visual magnitude of 9.54^{m}. A student astronomer measures its apparent magnitude at 9.36^{m}. What is the percentage error in the measurement?

42. These are the average heights of a group of extraterrestrial visitors. Find their mean and standard deviation. 17.8 m, 19.2 m, 16.3 m, 17.2 m, 16.9 m

43. Convert 27.14° into degrees, minutes, and seconds of arc.

44. Convert $41^{\circ}50'$ into degrees and decimal fraction of a degree.

STUDENT'S NAME _____

45. Convert $7°10' 56''$ into degrees and decimal fraction of a degree.

46. A galaxy is known to be at a distance of 150 Mpc (1 Mpc $= 10^6$ pc). It subtends an angle of $25''$ of arc. Calculate its diameter in parsecs. Compare this to the diameter of the Milky Way galaxy, about 30,000 pc, or 30 kpc.

47. Using a ruler calibrated in millimeters and the wavelengths in angstroms provided, determine the scale factor of the following portion of the solar spectrum in angstroms per millimeter (Å /mm).

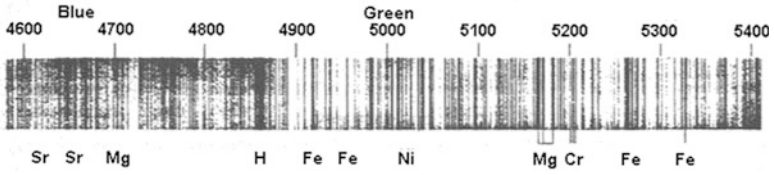

STUDENT'S NAME _____

48. The galaxy pictured in the drawing, similar to NGC 4303, an SBc galaxy in the Virgo cluster of galaxies, has an angular size of $11'$ of arc, about 1/3 the angular diameter of the moon. (NGC is the abbreviation for "New General Catalog.") Determine the scale factor of the drawing in minutes of arc per millimeter (min of arc/mm).

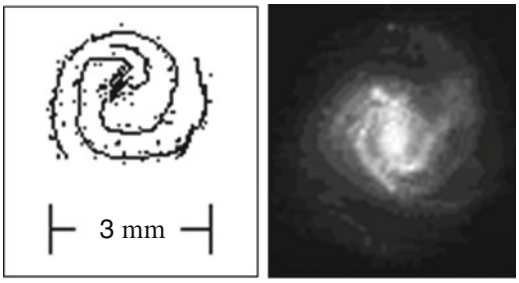

NGC 4303

49. In the sketch of a star field below, we are told that the scale factor is 47 seconds of arc per millimeter. Determine the angular distance between the stars labelled A and B. (Most photographs in astronomy, particularly for research purposes, are presented in the negative image, more easily analyzed than the positive image to which we are accustomed.)

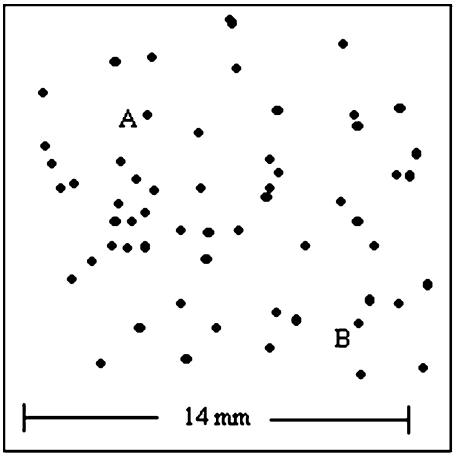

STUDENT'S NAME _____

50. The calculation to determine the velocity of impact of M31 and the Milky Way galaxy assumed that the mass of the Milky Way was 580 billion solar masses. Research in 2009 indicated that that Milky Way mass was larger, 710 billion solar masses, about equal to that of M31.

    a) Using (8), calculate the velocity of impact that would result if the Milky Way has a mass of 710 billion solar masses. Show all your calculations here, displaying all the units.

    b) In supersonic flight, the term *Mach number* (Ernst Mach, 1838–1916) refers to the ratio of the velocity of supersonic flight to the speed of sound in the medium. Calculate the Mach number describing the velocity of impact of M31 with a Milky Way of mass equal to 710 billion solar masses.

51. The Julian date corresponding to December 4, 2011, is 55899.

    a. How many days will have elapsed from December 4, 2011, until June 7, 2013? Show your calculations here.

    b. The Julian date corresponding to June 7, 2013, is 56450. Perform the same calculation using Julian dates.

Removing these DATA SHEETS from the book may damage the binding. You might consider entering the data and performing your calculations in the book, and then photocopying the DATA SHEETS for submission to your instructor for grading.

Experiment 2
A Review of Graphing Techniques

SUMMARY: In Experiment #2 "A Review of Graphing Techniques," we review the proper techniques for graphing data. This includes determination of slopes, interpolation, and extrapolation.

LEVEL OF DIFFICULTY: Low

EQUIPMENT NEEDED: Calculator.

MY LEARNING GOALS

1. To gain facility in constructing graphs.
2. To gain facility in analyzing graphical data so as to recognize the presence of underlying physical principles..

A. Introduction

When we perform an experiment, we usually vary one parameter of the experiment and measure the effect on another parameter. For example, we might vary the height of a ball above the ground and then measure the amount of time needed for it to fall to the ground.

L.M. Golden, *Laboratory Experiments in Physics for Modern Astronomy: With Comprehensive Development of the Physical Principles*,
DOI 10.1007/978-1-4614-3311-8_2,

The parameter whose values are varied by the experimenter is called the *independent variable*. The parameter whose value changes as a result is called the *dependent variable*. In most physical situations, more than one independent variable can affect the value of the dependent variable. For example, if we perform the falling ball experiment on Mars, Mercury, and the Earth, we will quickly discover that the gravity of the particular planet will also affect the time needed for the ball to fall to the ground.

Experimental results can be presented either in a table or graphically. In a table we provide the independent variable in the left-hand column and the dependent variable in the right-hand column. In a graph, we plot the independent variable along the x-axis and the dependent variable along the y-axis.

Graphing is a more visual means of presentation than displaying data in a table. You can easily discover relationships between variables and interpret data. You can, for example, determine if the dependent variable varies sensitively with changes in the independent variable or if it only slightly varies as the independent variable changes. You can see if the relationship is a straight-line or *linear* relationship, or one that is more complex. Because of its importance in interpreting experimental data, we must be experts in the techniques of graphing.

In many cases, if the data are believed to represent a physical law, we desire to determine a mathematical equation which represents the data. In this case, the independent variable will appear on the right hand side of the equation, and the dependent variable will appear on the left hand side of the equation.

An equation has several major advantages over the representation of data in a table or graphically. It is the simplest means of representation, it allows for all physically possible values of the variables, and it enables mathematical manipulation in order to, for example, allow predictions and testing of hypotheses, important elements of the scientific method.

Well-known graphical methods for determining the equation representing linearly-related data exist. In actual scientific practice, numerical rather than graphical methods are used, but for the purpose of many classroom laboratory experiments, and for quick analyses of real linearly-related scientific data, the graphical technique is not only simpler but also adequate.

In this experiment, we will master the techniques of graphing and the graphical determination of the equation representing linearly-related data.

B. Graphing Technique

The goal of presenting data in graphical form is clarity. Besides a few generally accepted rules, graphing technique is an art guided by common sense and clarity of presentation.

By convention, the independent variable values are plotted along the x-axis, also called the *abscissa* scale. The dependent variables are plotted along the

y-axis, also called the *ordinate* scale. If the values of the variables to be plotted are all positive, you need only provide the first quadrant of the Cartesian rectangular coordinate system on the graph paper, and the origin is placed near the lower left-hand corner of the paper. If both variables have both positive and negative values, then all four quadrants are needed and the origin will be placed somewhere near the center of the graph paper.

THE TITLE. The title should be short but informative in the format of "_____ as a Function of _____." Avoid using such terms as "vs.," "in regard to," "comparison of," "against," and so on. You should also avoid titles that are overly descriptive. If, for example, you were plotting the variations in brightness observed at the Hat Creek Radio Observatory from quasar 3C273B from December 4, 2010 to December 4, 2012, an appropriate title would be "Variations in Brightness of 3C273B as a Function of Time."

DRAW THE TWO SCALES AND PLACE TICK MARKS. Determine the range of the values for the abscissa and ordinate scales. Then use as much of the paper as you can to spread out the data and pick corresponding intervals for tick marks. Draw little lines at the tick marks and note the corresponding values. Note the following elements of good technique.

1. Choose sensible values for the intervals to ease your plotting of data. This is more important than using the entire sheet of paper. Use even numbers rather than odd numbers. Generally, intervals whose last digit is 1, 2, or 5 are best. Using other intervals makes it difficult to read numbers off the graph.
2. If the values are less than 1, always place a zero to mark the tens place. This prevents mistakes in placing the decimal point. Write, that is, 0.5 instead of .5, and −0.10 instead of −.10.
3. The intervals on the ordinate and abscissa scales need not be the same.
4. You need not write a number by every division of the graph paper.
5. You need not use the value zero. Many times, a value of zero is meaningless.
6. Avoid using the edge of the graph paper. This causes crowding of the scale titles and tick mark values and makes extrapolation (see the next section) difficult or impossible.
7. Put the titles of the axes outside and next to the axes, not at the edges of the graph paper.
8. Note the values of the abscissa and ordinate where the scales intersect.
9. To aid in setting up the scales, remember, you are free to orient the graph paper either with the long axis up and down, or with the long axis left to right.

SCALE TITLES. Outside the axes, write the name or algebraic symbol of the variables which are being plotted as independent and dependent variables, and the units of those variables. If they take on very large or very small numbers, you might want to economize writing by noting in parentheses below their name that the values being plotted are some factor of the actual data.

Here's an example of well-constructed abscissa and ordinate scales with their titles, for a graph of density of lunar soil as a function of depth, Fig. 1.

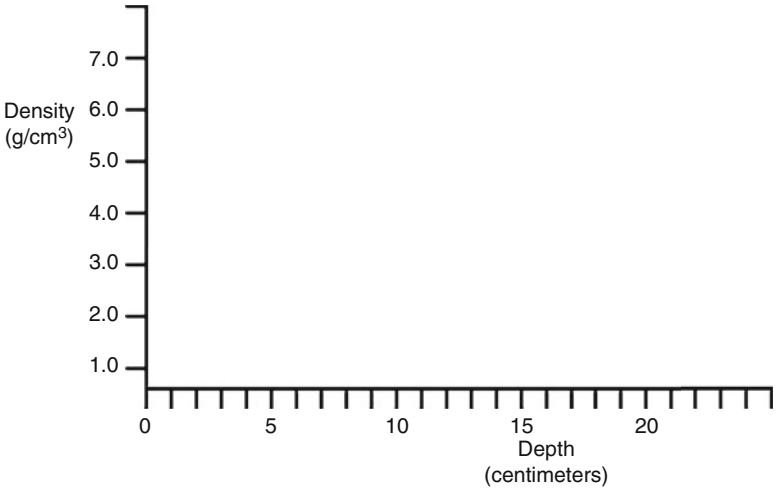

Fig. 1 Example of a graph with well-constructed abscissa and ordinate scales

PLOTTING DATA POINTS. Use symbols that make it easy to find the data points on the graph paper. Avoid tiny little dots. They are difficult to locate and will be obscured after drawing a line or curve through the data. Open or filled-in circles, circles with a dot in the center, little triangles, little squares, or a short vertical line crossed with a short horizontal line, either alone or encircled, are frequently used to locate data points. Do not write the coordinates of each point either on the graph or on the coordinate axes. Remember, our goal is clarity of presentation. If several sets of data are plotted on the same graph, use different symbols to distinguish them. A "key" should then be provided, identifying each group of data points.

If you are plotting experimental data and have an estimate of the possible range of values, *error bars* are placed above and below the plotted point to indicate the uncertainty. These are drawn as short horizontal lines above and below the data point joined by a vertical line that passes through the data point. The location of the short horizontal lines above and below the data point demonstrates the estimated range of values. If all the data have the same range of possible values, you can simply place one error bar within the borders of the graph to indicate its magnitude rather than superimposing them on each plotted data point.

Figure 2 is an example of appropriately plotted data for a hypothetical graph of "Number of Visible Nighttime Stars as a Function of Distance from Downtown Las Vegas, Nevada." The error bars would represent the variation of stars seen, let us say, from night to night or between those lucky students chosen to perform the observations.

FITTING A CURVE. In almost all real-life situations, random measurement error will ensure that not all the data points lie on a smooth curve. In the physical

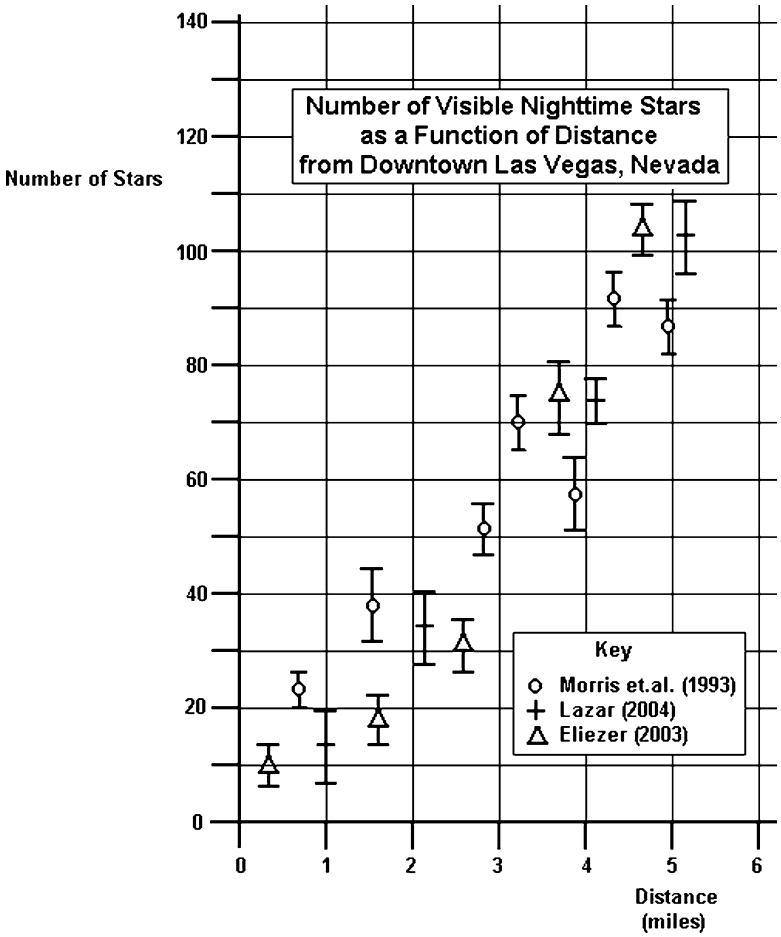

Fig. 2 An example of appropriately plotted data for a hypothetical graph of "number of visible nighttime stars as a function of distance from downtown Las Vegas, Nevada." The data are hypothetical (That's science-talk for "I made them up")

sciences, however, we believe that some physical law relates the values of the dependent to independent variables, so that indeed a smooth curve representing the mathematical form of that physical law should represent the data. Also, if additional error-free data were available between the points, we assume that all the points would lie on a smooth curve. With such considerations, when we try to fit data graphically, we do not draw a jagged line or a curve with many tiny wiggles so that each data point lies exactly on the curve. Rather, we try to draw the best smooth curve possible.

We draw the straight or curved line by eye in order of either increasing or decreasing values of the abscissa, paying attention to fit the general trend of the data

and not allowing any one or two data points to overly influence the form or position of the curve. Not all of the data points will fall on the curve. Do not draw the curve by simply connecting the first and last data points. Their uncertainty is as great as any other data points and they should not be overly weighted in determining the form or position of the curve. Numerical procedures exist to perform curve fitting rigorously, but usually drawing a good line by eye will yield a curve remarkably close to the curve which would be determined numerically.

Note that software programs that draw a smooth curve through data usually force the curve to pass through each data point. That does not usually represent physical reality. Whereas a curve that represents physical reality will pass close to data points that possess very small error bars, it can pass quite a distance from data points with large error bars. The commercial software programs will force the curve to pass through all data points, independent of their accuracy as represented by the size of the error bars.

If you are drawing a straight line with a ruler, place the ruler on its edge and rotate it until that edge represents the general trend of the data well. Then lay the ruler flat and draw the straight line along that edge. Unless you are using a transparent ruler, laying the ruler flat will hide the data points underneath it.

One of the few instances in which a curve should be forced through a point is when the dependent and independent variables are known to be directly proportional. In this case, the curve will also pass through the origin.

C. Analysis of Graphs

1. Slopes and Y-Intercepts of Straight-Line Graphs

Frequently you will be asked to determine the value of the *slope* of a straight line. The slope tells you the rate of increase or decrease of the dependent variable with changes in the independent variable. Pick two points on the straight line, widely separated to minimize the error resulting from the thickness of your pencil. Any two points will give the same result. Note that in general the two points will not be actual data points. Algebraically, we represent the coordinates of a point as (x,y). To distinguish different points we use subscripts. Thus, two points can be represented as (x_1, y_1) and (x_2, y_2).

To display your understanding of slope, on the graph paper draw a triangle composed of a horizontal line between the abscissa values of the two points, a vertical line between the ordinate values of the two points, and the segment of the straight line graph between the two points as the hypotenuse of the triangle. Then read off the coordinates of the two points on the line and calculate the slope. You may also want to write the values of the coordinates next to the points on the line. Always write the general formula for the slope,

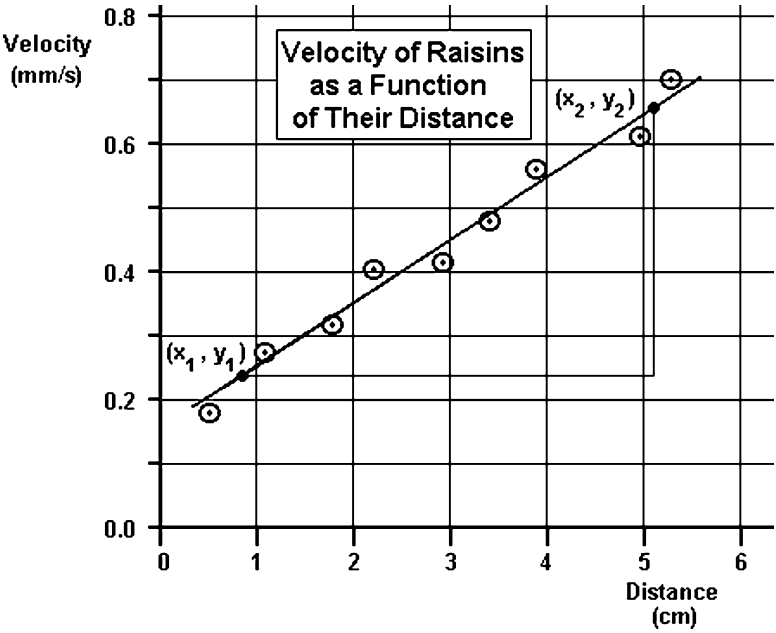

Fig. 3 Example of determining the slope of a straight line. The "raisin bread" model is often used to illustrate Hubble's law

$$m = \frac{y_2 - y_1}{x_2 - x_1},$$

and then substitute the values for the coordinates. This equation is often written

$$m = \frac{\Delta y}{\Delta x},$$

where Δ, the Greek letter delta, is used to designate the difference in two values.

Figure 3 presents the proper procedure for determining the slope of a straight line. The data are hypothetical, the expansion of a loaf of baking raisin bread often used to illustrate Hubble's law of expansion (see exercise #1 in Section E later). Here we can read the values of the two chosen points to be $y_2 = 0.65$ mm/s, $x_2 = 5.1$ cm, $y_1 = 0.24$ mm/s, and $x_1 = 0.85$ cm. The slope is calculated as

$$\begin{aligned} m &= \frac{0.65 - 0.24}{5.1 - 0.85} \frac{mm/s}{cm} \\ &= \frac{0.41}{4.2} \frac{mm/s}{cm} \\ &= 0.98 \frac{mm/s}{cm} \end{aligned}$$

The units are provided explicitly. Note that if the straight line is sloping downwards, then $y_2 - y_1 < 0$ and Eq. (2) shows that the slope will be negative in value.

The *y-intercept* is defined as the value of the ordinate for the value of $x = 0$. Accordingly, if you are asked to determine the value of the y-intercept your graph must extend to a value of $x = 0$. Reading off the value of ordinate where the line intercepts the y-axis will not give the value of the y-intercept if the independent variable scale does not include zero.

Slope also has meaning for curved line graphs. At every point on a curve, you can draw a straight line tangent to the curve. The slope of that straight line is then defined as the slope of the curve at that point.

You can determine the uncertainty in the slope and y-intercept of a straight line graphically. Draw the worst line which you think can still represent the data. If error bars accompany the data, use their extremities to guide you in drawing this line. Find its slope and y-intercept. Then the differences in these values of the slope and y-intercept from the best values you have previously determined are measures of their uncertainties. We write these uncertainties as plus or minus figures. For example, a slope of 0.018 with an uncertainty of 0.002 would be written

$$m = 0.018 \pm 0.002.$$

Again, numerical procedures exist to find these uncertainties, but in many cases the graphical approach yields comparable values.

2. Interpolation

Interpolation is the process of determining the value of a dependent variable within the range of values of independent variable in the experiment, but for a value of the independent variable for which the value of the dependent variable has not been directly measured. You find the value graphically by reading the value off the best-fit straight line or curve.

3. Extrapolation

Extrapolation is the process of determining the value of a dependent variable for a value of the independent variable beyond the range of the experimental data. You find the value graphically beyond the data points. If the graph is a straight line, simply extend the straight line with a straight edge and read the value off the graph. If the graph is curved, sketch or use a French curve to draw an extension of the curve through the value of the independent variable of interest. Then read the value off the graph.

4. Error Estimates from Graphical Representation of Data

Although the method of least squares discussed in Sect. K of Experiment #1, "A Review of Mathematical Concepts and Tools," can provide a measure of the goodness of fit, a graphical method also exists based on the same principles. If the best-fit straight line to a set of n data is given by $y = a + b\,x$, and the n data points are $\{x_i\,, y_i\}$, the mean of the square of the deviations from the best-fit straight line is given by

$$\sigma^2 = \frac{1}{n}\sum_{i=1}^{n}[y_i - (a + bx_i)]^2. \tag{1}$$

The square root of this is then a measure of the goodness of the fit. This method is easily generalized to data which are not linearly related.

D. Examples of Well-Constructed Graphs

1. Alien Beacons

Figure 4 is an example of a well-constructed graph. Radio astronomer Ronald Bracewell (1921–2007) of Stanford University has suggested that technically-advanced civilizations might send unmanned probes throughout the galaxy searching for other life. Once they would detect such life, they would go into orbit around that planet, observe, and signal back to the home planet the location and the nature of inhabitants of that planet.

If, of course, those being observed found the Bracewell Probe they might consider destroying it. To avoid this, the advanced civilization could program the probes to communicate with other nearby probes if life was discovered. They could be programmed to send signals back to their home planet communicating the distance of each from the newly-discovered planet by, for example, sending pulses whose period depends on the distance from that planet, Table 1.

Let us say that we on Earth have been detected by such an advanced civilization. Those probes might be signalling back our location by using data similar to that given in the table. The closer the probe to us, the shorter would be the pulse. That's their "road map" to Earth, and its water and interesting, perhaps succulent, life forms.

We plot those data. The axes are drawn with intervals that are sensible and which enable utilization of most of the graph paper. Tick marks are drawn from the intervals that are labeled, but not all of the major divisions on the graph paper are chosen to be labeled. The axes are drawn within the margins of the graph paper and the names of the independent and dependent variables and their units are adjacent. The title is clearly written in the proper form. Data points are clearly visible. Error

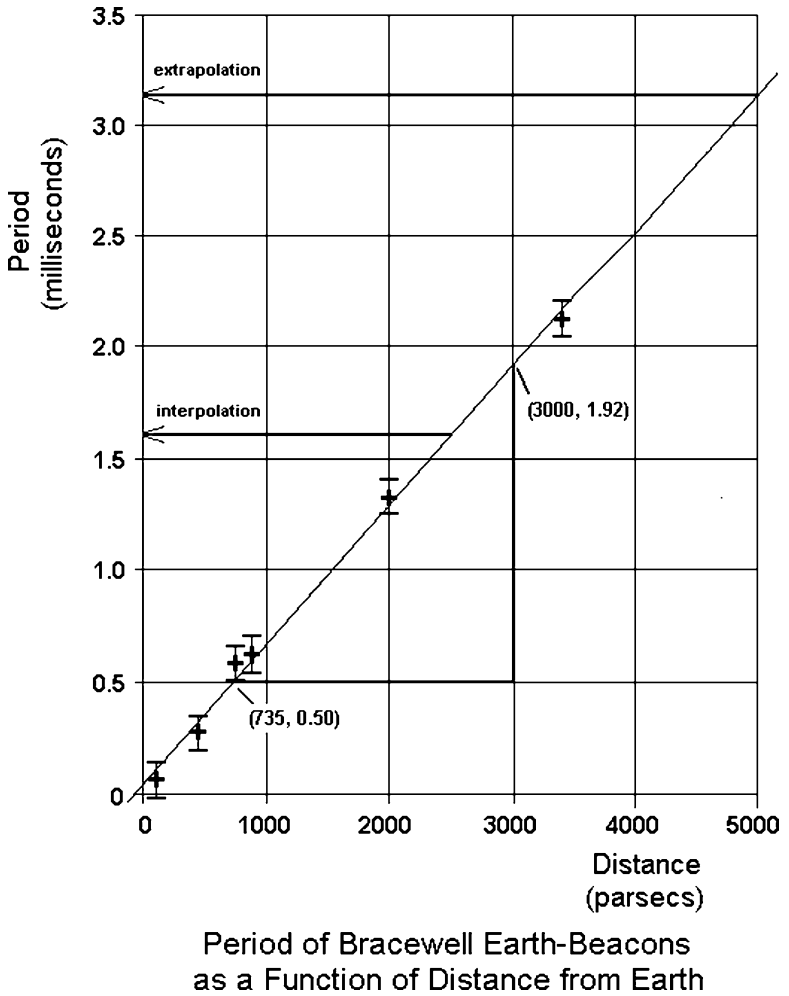

Fig. 4 Bracewell probes may now be signalling our presence to extraterrestrial intelligence civilizations. This hypothetical (again) graph displays the attributes of a well-constructed graph

Table 1 Bracewell probe monitoring of earthlings

Distance from Bracewell probe-beacon to earth (pc)	Time delay between pulses transmitted to home planet (ms)
104	0.068 ± 0.05
450	0.282 ± 0.05
740	0.581 ± 0.05
890	0.620 ± 0.05
2000	1.329 ± 0.05
3400	2.128 ± 0.05

bars provide a measure of the uncertainty in the time delay measurements. The errors here are taken, for illustration, as plus or minus 0.05 ms.

The analysis of the graph is aided by constructions on the graph itself. A straight line is fit by eye to the data. (Note that it is not a perfect straight line. This results from experimental error in the measurements of the time between pulses by the aliens and the position of the Bracewell probes having been changed over the eons by the gravitational pulls of passing stars.) The slope is determined by drawing a triangle near the extremities of the line and the coordinates to be used are written on the graph paper. The line is extended through the ordinate axis to aid in determining the value of the y-intercept. Arrows locate the positions of the abscissa for which interpolated and extrapolated values of the ordinate are to be determined. The slope is

$$\begin{aligned} m &= \frac{\Delta y}{\Delta x} \\ &= \frac{1.92 - 0.50}{3000 - 735} \quad \frac{ms}{pc} \\ &= 6.27 \times 10^{-4} \quad \frac{ms}{pc}, \end{aligned}$$

carried to three significant figures. Its units are provided explicitly. The y-intercept is read off the graph to be 0.03 milliseconds. The time delay at 2500 pc is read by interpolation to be 1.61 milliseconds and the time delay at 5000 pc is read by extrapolation to be 3.14 milliseconds.

If we were asked to determine the uncertainties in these values of the slope and y-intercept, an additional line would be drawn through the data which is the worst fit that to our eye would still represent the data. Its slope and y-intercept would be determined and the absolute value of the differences in these values from those determined by the best-fit straight line would be the uncertainties.

2. *The Microwave Phase Effect of the Planet Mercury*

In the actual practice of physics and astronomy, a straight line does not generally represent data. In the following graph, a more general situation is found. The error bars vary widely and the best fit to the data is highly non-linear. Such guidelines as the title of the graph, the choice of intervals for the axes, the titles of axes, and the presentation of data with error bars hold no matter the form of the graph, Fig. 5.

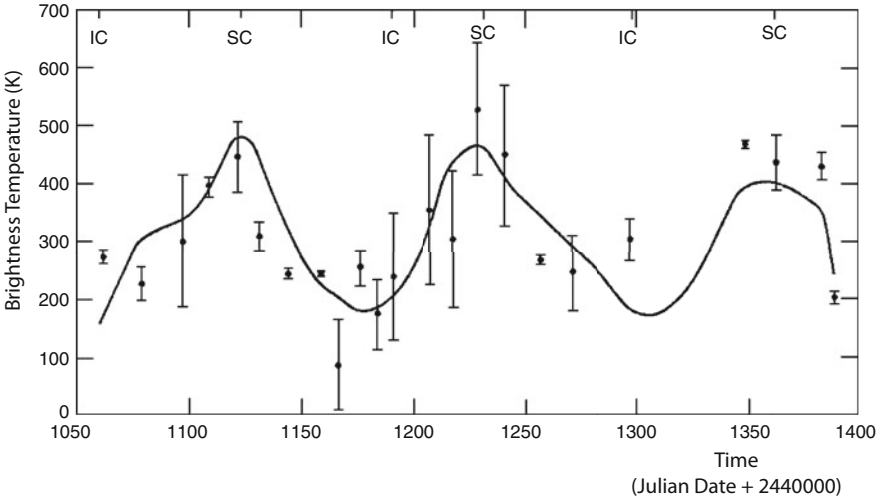

Fig. 5 Brightness temperature of the planet Mercury as a function of time. This example of a well-constructed graph displays the phase effect of Mercury at microwave wavelengths. The curve is the best fit mathematical model to the data, taken at the Hat Creek, California, radio observatory of the University of California, Berkeley, at 22 GHz (1.35 cm wavelength). The physics which is the basis of the model calculations is described in Experiments #14 and #15, "Thermal Radiation from a Planetary Subsurface: Part I: Calibration and Initial Measurements," and "Thermal Radiation from a Planetary Subsurface: Part II: Soil Sample Measurements,". "IC" and "SC" refer to the dates of inferior and superior conjunction of Mercury during the observations. Observations by the author

STUDENT'S NAME _____

E. Graphing Techniques Experiment Exercises

For the first two sets of data, construct a graph and draw the best straight-line curve. Find the slope and y-intercept, and determine their uncertainties. Show all your calculations on the DATA SHEET.

1. Leading to one of the most important discoveries in modern astronomy, if not the greatest, Edwin Hubble (1889–1953) in the 1920s used the new 100-in. telescope on Mt. Wilson to analyze the light coming from a special type of star in distant "nebulae," the early name given to galaxies. These fuzzy cloud-like objects had been observed by human beings for thousands of years (benefitting from skies free from smog and light pollution) and in more modern times catalogued by, among others, Charles Messier (1730–1817) in the famous Messier catalog of 1784. Hubble determined the distances of these galaxies from the period-luminosity relationship for Cepheid variable stars discovered by Henrietta Leavitt (1868–1921) and combined them with Vesto Slipher's (1875–1969) measurements of the redshifts determined for the galaxies from their spectra. Working with Milton L. Humason (1891–1972), Hubble discovered that the distances and redshifts were proportional, although with considerable scatter (the cause of which is now well-understood), and in 1929 Hubble and Humason announced their empirical Redshift Distance Law of galaxies, now commonly known as Hubble's law.

   The proportionality means that the further a galaxy is from Earth, the faster it is moving away. More generally, realizing that the Earth does not occupy a special place in the universe, the greater the distance between any two galaxies, the greater their relative speed of separation. This discovery was the first observational support for the Big Bang theory of the beginning to the universe and an expanding universe, thereby providing support for the general theory of relativity which predicted the expansion. It was indeed a momentous discovery.

   The data of Table 2 are similar to those used by Hubble and Humason. The slope of the line that you will determine is referred to as the "Hubble constant," a measure of the expansion rate of the universe.

STUDENT'S NAME _____

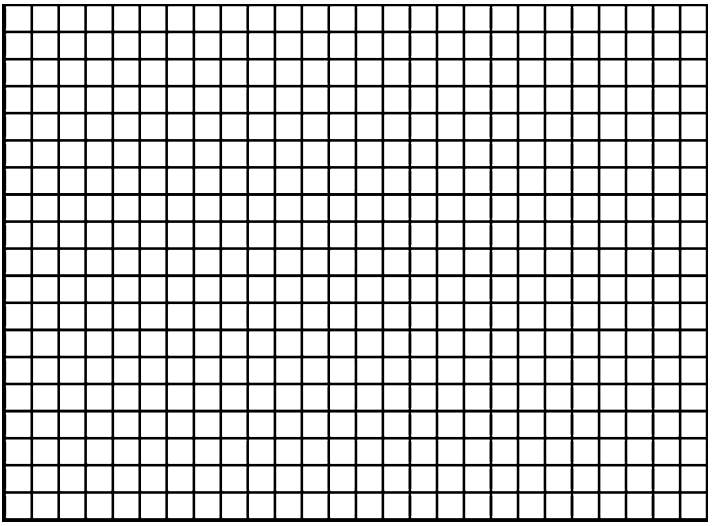

Table 2 Velocity of recession of galaxies

Distance of galaxy (Mpc)	Velocity of recession from earth (km/s)
41	1050
142	14,613
360	23,700
880	39,000
1100	61,000

Best straight line:

y-intercept = _____
Calculation of slope:

Worst straight line that still represents the data:

y-intercept = _____
Calculation of slope:

Calculation of uncertainty in y-intercept:

Calculation of uncertainty in slope:

STUDENT'S NAME _____

2. Graph the data of Table 3, the determination of apparent magnitudes of stars from their photographic images.

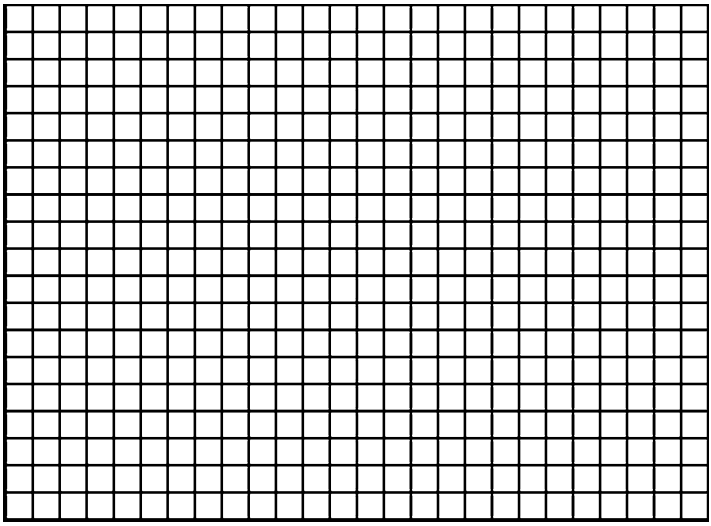

Table 3 Photography of stars

Size of photographic image (mm)	Apparent magnitude of stars (magnitudes)
3.20	12.5
2.60	12.9
2.50	13.2
2.65	13.4
2.15	14.0
1.75	14.2

Best straight line:

y-intercept = _____
Calculation of slope:

Worst straight line that still represents the data:

y-intercept = _____
Calculation of slope:

STUDENT'S NAME _____

Calculation of uncertainty in y-intercept:

Calculation of uncertainty in slope:

STUDENT'S NAME _____

3. Graph the data of Table 4, the acceleration of gravity above the surface of the Earth. These data do not follow a linear relationship.

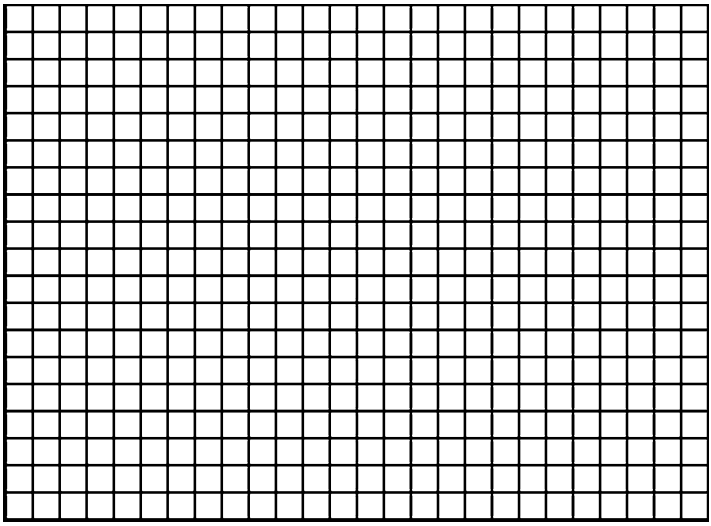

Table 4 Acceleration due to gravity

Height above earth (km)	Acceleration due to earth gravity (m/s^2)
0	9.80
1000	7.32
2000	5.68
3000	4.53
4000	3.70
5000	3.08
6000	2.60
7000	2.23
8000	1.93
9000	1.69
10,000	1.49

a) Draw the best smooth curve through the data.

b) Determine the slope at 2000 km above the surface of the Earth.

STUDENT'S NAME _____

c) Determine the slope at 6000 km above the surface of the Earth.

d) Interpolate graphically to find what the acceleration of an object due to the Earth's gravity would be at a distance of 8500 km above the surface of the Earth.

ANSWER: _____

e) Extrapolate by extending the curve and estimate the acceleration of an object due to the Earth at the distance of 14,000 km above the surface of the Earth.

ANSWER: _____

Removing these DATA SHEETS from the book may damage the binding. You might consider entering the data and performing your calculations in the book, and then photocopying the DATA SHEETS for submission to your instructor for grading.

If you used graph paper other than that provided, attach those graphs to these DATA SHEETS.

Experiment 3
The Optics of Telescopes:
Part I. Image Size and Brightness

SUMMARY: In Experiment #3 "The Optics of Telescopes: Part I. Image Size and Brightness," you will study telescope optics by aligning various types of light sources and lenses on a platform. In this experiment, we study those characteristics which determine image size and image brightness.

LEVEL OF DIFFICULTY: Moderate

EQUIPMENT NEEDED: Optical bench, frosted light bulb; unfrosted light bulb; converging (double-convex) lenses of various focal lengths; black pieces of cardboard; photometer; light baffles.

MY LEARNING GOALS

1. To be able to describe how an astronomical telescope gathers light from celestial objects and makes it available for our analysis
2. To be able to describe how the size and brightness of the image depends on the characteristics of the telescope.

L.M. Golden, *Laboratory Experiments in Physics for Modern Astronomy: With Comprehensive Development of the Physical Principles*,
DOI 10.1007/978-1-4614-3311-8_3,

A. Introduction

A telescope is a device for gathering light from a distant object and for magnifying the resulting image. In its simplest form, a telescope is composed of a converging lens to collect light, the *objective*, and a screen placed at the focus of the lens on which to view the image that the lens creates. Instead of a screen, astronomical telescopes have an eyepiece placed close to the focus which enables the image to be magnified. As seen in Fig. 1, an eyepiece is simply another converging lens. Tubing is placed around the entire assembly to keep out stray light.

In astronomical research for most of the twentieth century, the eyepiece might be replaced by a photographic plate, which was a high quality photosensitive emulsion on glass manufactured specifically for astronomical use by Eastman Kodak Corporation. This enabled time exposures so that objects too dim for the eye to detect could be detected and a permanent record of the image could be created. In modern telescopes more sophisticated detection and recording devices such as photometers, spectrographs, and charged-coupled detectors are used. In all cases, the physics of the light-gathering aspects of the telescope remains the same.

In this experiment and in Experiment #4, "The Optics of Telescopes: Part II. Magnification and Chromatic Aberration," we will investigate the optics of refracting telescopes by ray tracing and by using several lenses, eyepieces, filters, and sources of light. We will investigate (1) the increase of image size with focal length of the objective, (2). the effect of focal length and aperture on the brightness of an image, (3) the variation of magnification with focal lengths of the objective and eyepiece, and (4) the phenomena of chromatic aberration and its variation with the focal length of the objective lens.

B. Theory

1. Telescope Characteristics

The important characteristics of a telescope are its *collecting area*, *focal length*, *resolving power*, and *magnifying power*. The collecting area is approximately equal

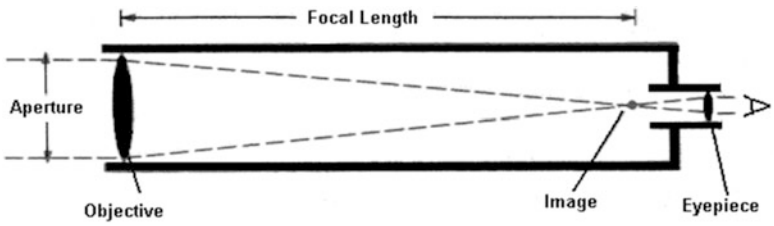

Fig. 1 Two lenses encased in tubing constitute a simple refracting telescope

to the cross-sectional area of the objective lens. In most types of telescope designs, part of the lens is blocked from viewing the sky, and in these cases the collecting area is slightly less than the cross-sectional area of the lens.

The focal length is the distance from the center of the *objective lens* along its axis of symmetry, or *optical axis*, to the location of the focused image of the distant object. An extended object forms an image on a plane perpendicular to the optical axis at the focal point called the *focal plane*. The resolving power or resolution is a measure of the smallest detail that the telescope can distinguish, either two small adjacent objects or fine details in an extended object.

An extended object viewed through a telescope appears larger, and therefore closer, than when viewed by the unaided eye. More precisely, the magnifying power, or power, of a telescope is the ratio of the angular size of the image as viewed through the telescope to the angular size of the object viewed by the unaided eye. For example, an eyepiece that makes an object which is 1 minute of arc in angular size appear to be 100 minutes of arc in angular size when seen through the telescope is said to yield 100 power. (Binoculars are rated by two numbers, such as 7×35. The first number is the magnifying power and the second is the diameter of the objective lens, or *aperture*, in millimeters.)

2. Telescope Relationships

Geometrical optics and the physics of waves provide mathematical relationships between these characteristics of a telescope and the diameter and focal length of the objective lens and the focal length of the eyepiece.

If D is the diameter of the aperture, then the collecting area is approximately the area of a circle of diameter D,

$$A = \pi \frac{D^2}{4}, \tag{1}$$

where blockage of the incoming light beam has been neglected.

Study of the phenomenon of diffraction of waves and the optics of image formation provides the Rayleigh criterion (Lord Rayleigh, 1842–1919) for the angular resolution of two images as

$$\Delta\theta = 1.22 \frac{\lambda}{D} \text{ radians.}$$

This applies to any kind of wave, including sound waves and ocean waves as well as the electro-magnetic waves such as visible light that astronomers employ to observe celestial objects.

If we express λ in angstroms (Å) and D in centimeters, then $\Delta\theta$ in seconds of arc is

$$\Delta\theta = 0.00251\frac{\lambda}{D}. \tag{2}$$

At optical wavelengths, this relationship can be approximated by *12*/*D* seconds of arc, where *D* is measured in centimeters. For example, a 10-cm aperture at a wavelength of 5000 Å yields a resolving power of about 1.2 seconds of arc.

Equation 2 quantifies the ability to distinguish two separate objects, for example, the two stars in a binary pair, as well as the ability to observe details on a single object. These could be, for examples, craters on the Moon, gas filaments in a remnant of a supernova explosion, or agricultural artifacts such as rectangular patterns of crop fields on a planet being searched for evidence of intelligent life.

The magnifying power, m, of a telescope with objective focal length f_o and eyepiece focal length f_e can be shown by the geometry of the telescope and trigonometry to be

$$m = \frac{\textit{telescope image size}}{\textit{unaided image size}}$$

$$= \frac{f_o}{f_e}. \tag{3}$$

From (3), it would appear that any telescope can be made to provide any magnifying power simply by using an eyepiece of sufficiently short focal length.

In practice, three effects limit the magnifying power that can be achieved. First, atmosphere turbulence limits air quality, or *seeing*, to 1/4 of arc at the best sites in the world, and more typically 1 second of arc. Increasing magnification to enable seeing detail below these sizes magnifies turbulence and causes the image to shimmer wildly. Second, as magnification is increased, the image gets increasingly faint as the same amount of light is spread out over an increasingly large area. Finally, the physics of light waves, as expressed by the Rayleigh criterion, provides a fundamental limit to the resolution of details. A telescope of aperture *D* cannot resolve details smaller than the limit given in (2). Magnification beyond this limit just magnifies a fuzzy image.

As a result of these limitations, the maximum useful magnifying power for most telescopes on most nights is about 20 power per centimeter of aperture.

3. *Properties of an Image*

The important properties of an image are its *size* and its *brightness*. The size of an image is determined by the focal length of the objective lens: The larger the focal length, the larger the image of a given object. For an object of angular size α seconds of arc and a lens of focal length f_o, the image size s is given by

$$s = \frac{\alpha f_o}{206265}, \tag{4}$$

where 206,265 is the number of seconds of arc in a radian, and the image size and focal length are measured in the same units, for example, centimeters. The Moon, 30 minute of arc in angular size, observed through a telescope with 100 cm focal length, will accordingly have an image size of

$$s = (30\ \text{min}\ \textit{of arc}) \times \frac{(60\ \text{sec}\ \textit{of arc})}{1\ \text{min}\ \textit{of arc}} \times 100\ \textit{cm} \times \frac{1}{206265\ \text{sec}\ \textit{of arc}}$$
$$= 0.87\ \textit{cm}.$$

The small size of this image may surprise you. The advantage of the telescope, as shown in Fig. 1, is the close proximity of an eyepiece to a bright image, allowing magnification of the image.

The brightness of the image depends on two factors. First, the greater the collecting area, the more light is collected to be concentrated in producing the image. Accordingly, the brightness of the image is proportional to the square of the lens diameter, or *aperture*. Second, increasing the size of the image spreads out this light, reducing its brightness. For a given eyepiece, the larger the focal length of the objective, the greater the size of the image, as expressed in (4). The brightness is therefore inversely proportional to the square of the focal length. Mathematically, then, the brightness, b, of a source of intrinsic brightness, B, is related to the aperture, D, and focal length, f_o, of the telescope by, omitting constants,

$$b \cong B\left(\frac{D}{f_o}\right)^2. \tag{5}$$

(In photography, the ratio $\frac{f_o}{D}$ is called the "f-number" of the lens. An f-number of $\frac{f}{1.4}$ means that $\frac{f_o}{D} = 1.4$. A lens with a small f-number, that is, a large diameter and a short focal length, is referred to as "fast." As can be seen from (5), such a lens forms an image whose brightness is large, so that the time required to chemically form an image on photographic paper is small.)

4. *Ray Tracing*

In one of the following experiments, you will have to predict the size and position of the image created by a lens. This is done by a graphical technique called *ray tracing*.

Ray tracing utilizes three characteristics of so-called *thin* lenses: (1) rays parallel to the optical axis pass through the focal point of the lens, (2) parallel rays which are not parallel to the optical axis focus at an off-axis point in the focal plane, and (3) rays pass through the center of the lens undeviated.

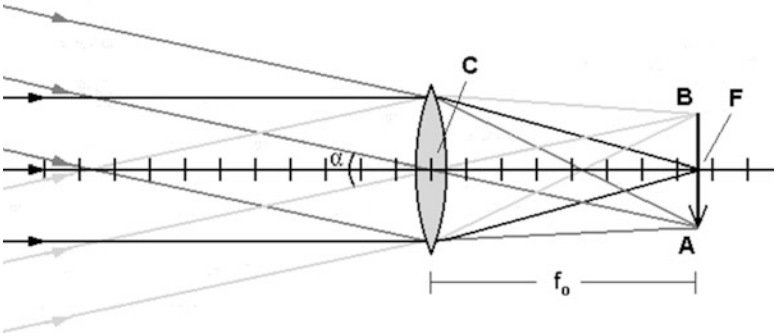

Fig. 2 Ray tracing with a converging thin lens of an object $\alpha = 20°$ in angular size. The object is considered to be at infinity, so that the rays from the top of the object are parallel, coming to focus at point *A* in the focal plane, the rays from the bottom of the object are parallel, coming to focus at point *B* in the focal plane, and the rays from the center of the object are parallel, coming to focus at point *F* in the focal plane. The image size can be shown by such a diagram to be proportional to the angular size of the object and the focal length of the lens. The rays are bent or "refracted" at each interface with the air, but for purposes of illustration they are frequently displayed as simply being bent in the center of the lens

General discussions of ray tracing in physics courses deal with objects which are not far from the lens. In the case of telescopes, we are interested in very distant objects. In this case, every point object, or the individual points of an extended object, generates a group of parallel rays of light which are observed by the telescope.

Ray tracing follows these steps for the converging lenses used as objectives in refracting telescopes, Fig. 2:

1. Draw a horizontal straight line to represent the optical axis of the lens, place equally spaced markings along it to an appropriate scale, and draw a vertical line at one of the markings near the left end of the optical axis to represent the position, *C*, of the lens. You may also want to draw the curved boundaries of the lens for illustrative purposes.
2. Mark the focal point, *F*, of the lens on the optical axis at an arbitrary distance to the right of the lens.
3. Draw three rays parallel to the optical axis, one passing through the top of the lens, bent downward at the lens so as to pass through the focal point, one through the center, and one through the bottom of the lens, bent upwards at the lens so as to pass through the focal point. These rays represent the light from the center of the object being viewed.
4. Measure an angle equal to one-half the angular size of the object. At that angle draw additional three parallel rays passing downward through the lens. These will come to focus at an off-axis point, B, on the focal plane below the optical axis.
5. Repeat step 4 using three parallel rays passing upward through the lens from the same angle. These will come to focus at an off-axis point, *A*, on the focal plane above the optical axis. The resulting image, of linear size *s*, will be inverted

compared to the appearance of the object viewed with the unaided eye. (In binoculars, prisms are included to yield an erect rather than inverted image.)

As an example of the usefulness of ray tracing, the formula of (4) can be easily derived. In Fig. 2, by similar triangles, we see that the angle ∠ BCA = α. In the triangle ΔABC, then, we have $tan\ \alpha/2 = (s/2)/f_o$. For small angles, $tan\ \alpha/2 = \alpha/2$, so that $s = \alpha f_o$, with α expressed in radians. Because there are 206,265 seconds of arc in a radian, this becomes $s = \alpha f_o/206{,}265$, with α now expressed in seconds of arc. This is Eq. (4).

The important subject of *chromatic aberration* is discussed in Experiment #4, "The Optics of Telescopes: Part II. Magnification and Chromatic Aberration".

C. Procedure and Observations

1. Equipment

In optics experiments, the source of light, lenses, mirrors, eyepieces, and other optical components are set on a straight, metallic track about a meter in length called an optical bench. The components are placed in frames which are clamped onto the optical bench by leaf springs or set screws, and the frames are positioned along the bench at locations marked by a graduated scale. When you are placing the components on the bench, make sure that each lies along the optical axis by turning on the source of light and then adjusting the height of each frame so that the light passes through the center of the component. Figure 3 shows a simple optical bench. A light source passes through a lens and the image is formed on a piece of cardboard.

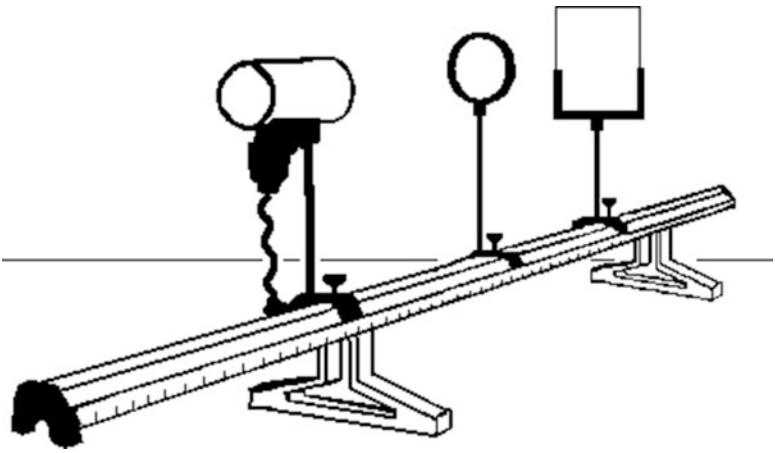

Fig. 3 The three pieces of equipment on this optical bench are held in place by clamps at positions along a graduated scale

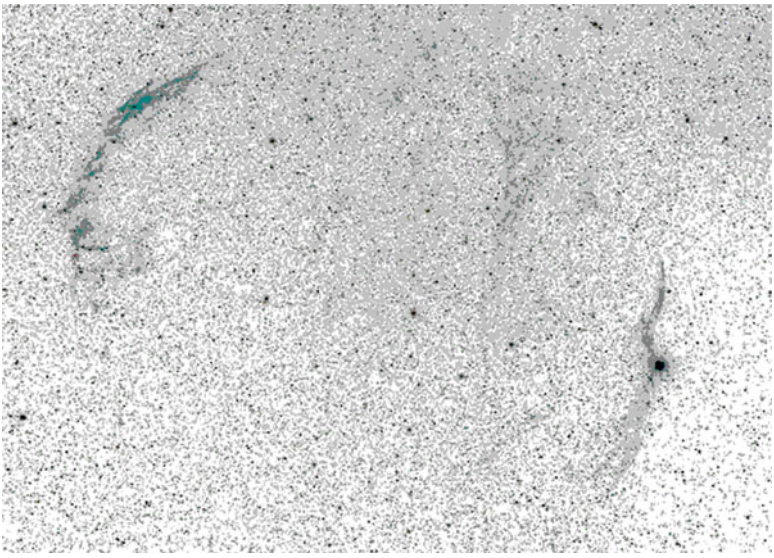

Fig. 4 The Vela supernova remnant, part of the Gum Nebula. Stretching over 40° in the sky in the southern constellations of Vela and Puppis, the Gum Nebula is itself a supernova remnant, the result of a star that exploded about one million years ago. It continues to expand, at the rate of 20 km/s. The Vela supernova remnant is estimated to be 11,000 years old and stretches about 5° over the sky. The Vela pulsar is located at its center. In astronomy, visual images are often presented in the negative, to better view asteroids, stars, galaxies, and gas clouds, such as this object, as dark objects against a light background. The many *little black dots* in this photo are images of stars in the region of the Vela constellation, a small portion of the our Milky Way galaxy

2. *Image Size: Effect of Objective Focal Length*

First demonstrate the effect of focal length on the image size by ray tracing. Draw two configurations on the DATA SHEET, one for a lens with a focal length of 2 cm and one for a lens with a focal length of 4 cm. Assume the object being observed is 40° wide, the angular size of the nearby Gum Nebula *supernova remnant*. This is a gas cloud created one million years ago by the explosion of a massive star in the constellation Vela. Inside of the nebula is another supernova remnant, the Vela supernova remnant, estimated to be 11,000 years old, Fig. 4. On your drawings, use ray tracing to determine the extent of the image of the Gum Nebula created by each of the two lenses. Measure the heights, s, of the images to the nearest 0.1 mm if possible and enter the results on the DATA SHEET.

We will now observe the unfrosted light bulb. Place it at the far end of the optical bench, simulating a location at astronomical distances. Place a converging lens well down the bench from the bulb and place a screen consisting of a piece of black cardboard on the side of the lens opposite the light bulb. Move the image screen back and forth until a clear image of the light bulb filament appears on it, assuring that it is located at the focus. This configuration is shown in Fig. 3. Measure the

distance of the lens from the image screen, the focal length f_o of the lens, and the size of the image, s, on the image screen. You can use any dimension of the image as a measure of its size, but for consistency measure the height. Enter these values on the DATA SHEET to the nearest 0.1 mm.

Repeat this procedure for several more lenses of different focal lengths to determine the focal lengths of the lenses and the sizes of the images.

3. Image Brightness: Effect of Collecting Area and Focal Length

Place a frosted light bulb at the far end of the optical bench, simulating a location at astronomical distances, and put the black blinder over it. The blinder is simply a piece of black cardboard with a small hole punched in it to create a "point source" for us to observe.

Place a converging lens well down the bench from the light bulb and place a screen on the side of the lens opposite the light bulb. Move the image screen back and forth until the image of the frosted light bulb is as small as possible.

Now, replace the image screen with a photometer. Position the photometer so that its aperture is as close to the position of the screen as possible. Make sure the beam of light from the frosted light bulb passes into the photometer sensor. Then move the photometer slowly about that position and secure it on the optical bench at the location yielding the highest reading.

We have in this way accurately determined the position of the focal plane of the lens. Measure to the nearest 0.1 mm if possible the distance from the lens to the image screen, the focal length f_o of the lens, and enter the value on the DATA SHEET.

Now place a baffle in front of the lens so that only a portion of it can be illuminated by the point source. The baffle is simply another piece of black cardboard with a circular hole cut out from its center. The diameter of the circular hole should be smaller than the diameter of the lens. Measure the diameter of the hole you've cut out of the baffle, D. Enter it and the intensity reading of the photometer in the top row of Table 3 of the DATA SHEET.

Repeat the intensity reading with baffles with circular holes of different diameters. Then repeat the entire procedure for two additional lenses. Enter all your results in Table 3 of the DATA SHEET.

D. Calculations and Analysis

1. Image Size: Effect of Objective Focal Length

From the ray tracing, divide the heights, s, of the images by the focal lengths f_o of the two hypothetical lenses. Enter the results in Table 1 of the DATA SHEET.

You should find similar values for s/f_o from the two tracings.

The ratio s/f_o is the angular size α of the light bulb filament in radians as seen from the lens. Multiply s/f_o by 206,265 seconds of arc/radian to get the angular size of the light bulb filament in seconds of arc. Perform these calculations on the DATA SHEET and enter the results in Table 1 of the DATA SHEET.

Construct a graph of observed image size in centimeters as a function of focal length in centimeters and find its slope. By (4), this slope should be $\alpha/206{,}265$, the angular size of the light bulb filament in radians. Compare the slope to the value you calculated directly above for α. Perform these calculations on the DATA SHEET. Determine the y-intercept. It should be close to zero.

Perform the same calculations for the image sizes determined using the actual lenses on the optical bench. Enter the results in Table 2 of the DATA SHEET. Perform all your calculations on the DATA SHEET.

2. *Image Brightness: Effect of Collecting Area and Focal Length*

From the values of D and f_o calculate $(D/f_o)^2$, the square of the ratio of the baffle diameters to the focal lengths of the various lenses. Show your calculations on the DATA SHEET. Enter the results in Table 3 of the DATA SHEET.

Construct a graph of the image brightnesses you entered on the DATA SHEET as a function of $(D/f_o)^2$. Fit a straight line to the data and determine the y-intercept. As seen from (5), it should be close to zero.

E. Telescope Optics Experiment I Data Sheets

1. Image Size

STUDENT'S NAME _____

RAY TRACING

a. Ray tracing of Gum Nebula with lens of focal length $f_o = 2$ cm. The straight line represents the optical axis.

_____

b. Ray tracing of Gum Nebula with lens of focal length $f_o = 4$ cm. The straight line represents the optical axis.

_____

Table 1 Ray tracing

Lens	Focal length f_o (cm)	Image height s (cm)	$\alpha = s/f_o$ (radians)	$\alpha = 206{,}265\ s/f_o$ (sec of arc)
1	2			
2	4			

Are the two values of s/f_o equal? _____ If not, how can you explain the difference?

Seconds of arc:

STUDENT'S NAME _____

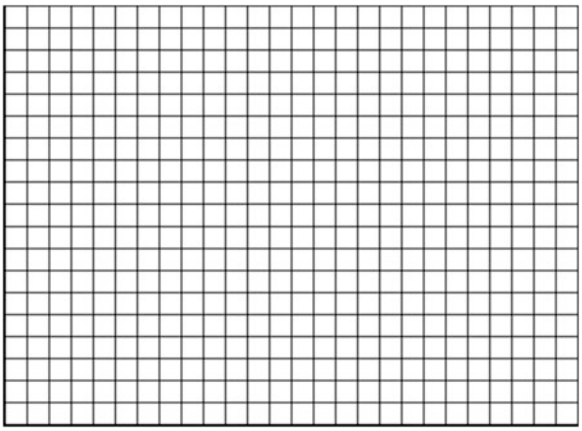

Calculation of the slope of the graph of image size in centimeters as a function of the focal length in centimeters:

Calculation of percentage difference between the slope and α in radians from above:

Value of y-intercept of the graph: of image size as a function of focal length _____

Is the value of the y-intercept close to zero? If not, provide an explanation of the difference.

STUDENT'S NAME _____

OPTICAL BENCH OBSERVATIONS: IMAGE OF LIGHT BULB

Table 2 Light bulb image

Lens	Focal length f_o (cm)	Image height s (cm)	$\alpha = s/f_o$ (radians)	$\alpha = 206{,}265\ s/f_o$ (sec of arc)
1				
2				
3				
4				
5				

Calculation of the angular size of the light bulb in seconds of arc:

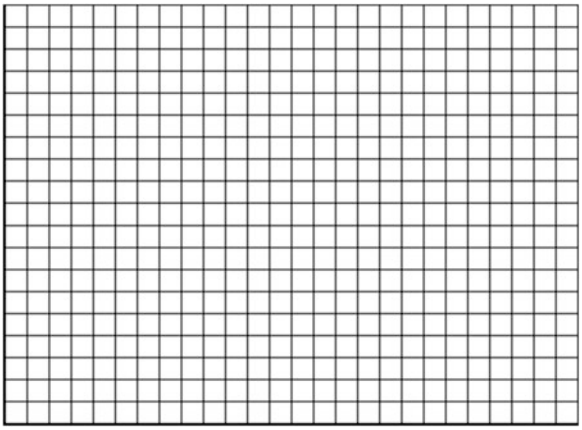

Calculation of the slope of the graph of image size in centimeters as a function of the focal length in centimeters:

Calculation of percentage difference between the slope and $\alpha/206{,}265 =$ in radians from above:

Value of y-intercept of the graph: of image size as a function of focal length _____

Is the value of the y-intercept close to zero? If not, provide an explanation of the difference.

2. *Image Brightness*

STUDENT'S NAME _____

Lens 1: f_o = _____ cm

Lens 2: f_o = _____ cm

Lens 3: f_o = _____ cm

Table 3 Image brightness

Lens	Baffle	D (cm)	$(D/f_o)^2$	Intensity
1	1			
1	2			
1	3			
2	1			
2	2			
2	3			
3	1			
3	2			
3	3			

Show your calculations of $(D/f_o)^2$ here.

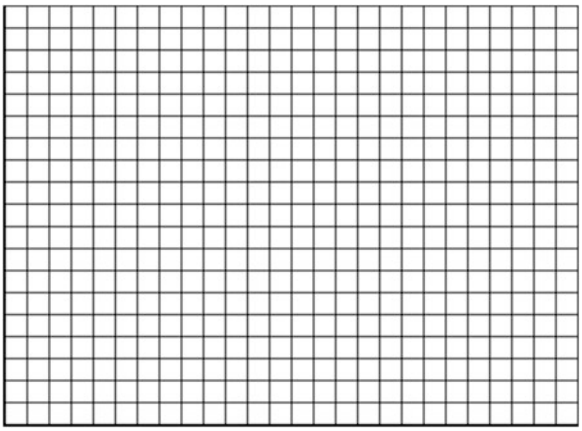

STUDENT'S NAME _____

Value of y-intercept = _____

Is the value of the y-intercept close to zero? If not, provide an explanation of the difference.

STUDENT'S NAME _____

F. Telescope Optics Experiment I Discussion Questions

In the following, write the formula that has led you to your answer.

1. In the image brightness part of the experiment, describe the variation of intensity reading with $(D/f_o)^2$.

2. We want to observe the smallest craters we possibly can on the Moon. All other specifications of the telescope the same, would we want to use a telescope with a focal length of 50 cm or one with a focal length of 100 cm? Why? Show the calculations that lead you to your answer.

3. Which of the above focal length telescopes would we use to observe the distant planet Pluto? Why? Show the calculations that lead you to your answer.

4. The Rayleigh criterion (Lord Rayleigh, 1842–1919) for resolution of two images is $\Delta\theta = 1.2\frac{\lambda}{D}$ radians, where λ and D are given in the same unit, for example, centimeters. Show that, if we express λ in angstroms (Å) and we express D in centimeters, then $\Delta\theta$ in seconds of arc is given by (2).

STUDENT'S NAME _____

5. This is a drawing, from memory, of a being from another planet that I encountered while camping near Roswell, New Mexico. He (she, it) introduced himself as "XyTk@2." Let's talk about the superior sensory adaptations of XyTk@2. Use (2) to calculate your answers. Show all your calculations here.

a. If the pupil of the eyeball of XyTk@2 is 10 cm in diameter, what is the smallest object he could resolve in sunlight of 6500 Å wavelength?

b. If the antennae of XyTk@2 can be spread to 0.5 m separation, what is the smallest object he could resolve using a 70-cm wavelength radar?

STUDENT'S NAME _____

c. If the ears of XyTk@2 are 80 cm apart, what is the smallest separation between two sound speakers radiating at 3000 Hz that he could resolve? Assume the speed of sound on his planet is 1000 m/s. (The speed of sound at sea level on the Earth is about 340 m/s.)

d. What general statement can you make about the ability to resolve an image and the wavelength of observation?

6. Many organisms exist on XyTk@2's planet that like to eat members of his species. The most voracious one, the all-consuming IRS1040, is about 4 m in size and can run at a speed of 30 m/s while making loud, strange gurgling sounds at all radio and sound wavelengths. XyTk@2 needs 10 s to hide in his home once he discovers an IRS1040 creature approaching him.

   a. What angular resolution must XyTk@2 have in any sensory device to detect it in time to hide? Use (2) to calculate your answer.

   b. Which sensory device or devices would enable XyTk@2 to detect an approaching IRS1040 in time to hide? Compare the resolving power of the sensory device to your answer of part a).

STUDENT'S NAME _____

7. Based on your answers to part a), b), and c) of question #5, and your answer to question #6, what is the most likely description of XyTk@2's home planet that has led to XyTk@2's evolution of these sensory adaptations? More than one description may be correct. Explain your answer in terms of the ability of members of XyTk@2's species to detect the presence of their predators.

    1. Very distant from a dim red star, with a thick atmosphere.
    2. Very close to a dim red star, with a thick atmosphere.
    3. Very distant from a dim red star, with a thin atmosphere.
    4. Very close to a dim red star, with a thin atmosphere.
    5. An atmosphere with constant radio-noise generating thunderstorms.
    6. A planetary surface with tall, smooth rock columns left over from an age of volcanic activity.

ANSWER: _____

8. On another camping trip to Roswell, I saw a fellow who had apparently been dating a relative of XyTk@2, and he told me that the members of the alien species referred to themselves as "VisiGhots" or "Ghots," for short. Assume that the pupil of the alien is again 10 cm in diameter. Assume the pupils of the human being are 5 mm in diameter and that his eyes are separated by 12 cm. Show all your calculations here.

STUDENT'S NAME _____

a. Compare the brightnesses of the image of a given object as seen by the two beings by calculating their ratio. Assume the focal lengths of the eyeballs of the two beings are the same.

b. Compare the angular resolutions obtainable by the two beings by calculating their ratio.

9. The "log telescope" depicted in the cartoon is about 12 in. in diameter. What angular resolution would it provide if observing light of 5000 Å wavelength? Show all your calculations here.

STUDENT'S NAME _____

Removing these DATA SHEETS from the book may damage the binding. You might consider entering the data and performing your calculations in the book, and then photocopying the DATA SHEETS for submission to your instructor for grading.

If you used graph paper other than that provided, attach those graphs to these DATA SHEETS.

Experiment 4
The Optics of Telescopes: Part II. Magnification and Chromatic Aberration

SUMMARY: In Experiment #4, "The Optics of Telescopes: Part II. Magnification and Chromatic Aberration," we continue our study of telescope optics, in this experiment studying magnification and chromatic aberration using the optical bench, lenses, and color filters.

LEVEL OF DIFFICULTY: Moderate

EQUIPMENT NEEDED: Optical bench; unfrosted light bulb; converging (double-convex) lenses of various focal lengths; black pieces of cardboard, photometer; light baffles; eyepieces of various focal lengths; color filters.

MY LEARNING GOALS

1. To be able to predict how different eyepieces in an astronomical telescope magnifies the image.
2. To be able to describe why light of different wavelengths have different focal points.

L.M. Golden, *Laboratory Experiments in Physics for Modern Astronomy: With Comprehensive Development of the Physical Principles*,
DOI 10.1007/978-1-4614-3311-8_4,

A. Introduction

We continue with our study of the properties of telescopes with an examination of the magnification of telescopes and the phenomenon of chromatic aberration. The equipment setup is the same as in Experiment #3, "The Optics of Telescopes: Part I. Image Size and Brightness".

B. THEORY: Chromatic Aberration

The type of telescope built with lenses, as shown in Fig. 1 of Experiment #3, "The Optics of Telescopes: Part I. Image Size and Brightness," is called a *refracting telescope* or *refractor*. The light rays from the celestial object are refracted, or bent, by the objective lens to the focus. (Binoculars are essentially twin refracting telescopes, mounted together.) The focal length of a lens depends in part on the material out of which the lens is constructed, being inversely proportional to $n-1$, where n is the *index of refraction* of the material. It is defined in such a way that light passing through materials of comparatively high values of n is refracted at comparatively large angles.

The value of n for a given material, however, varies with wavelength. For most glass materials, n is about 1.5 for visible wavelengths. It increases slightly in value from the long wavelengths of red light to the short wavelengths of violet light, Fig. 1. Accordingly, because the violet light is bent through a larger angle than the red light, the focal length will decrease slightly as we observe light through this range of colors, Fig. 2. That is, each wavelength has its own slightly different focal length. This effect, *chromatic aberration*, known since construction of the earliest telescopes, is largely corrected in modern refracting telescopes by using a compound lens, two lenses of different types of glass cemented together.

Reflecting telescopes, or *reflectors*, utilize mirrors to collect and focus the light. Because the light does not then pass through glass or other refractive substance, no chromatic aberration occurs. This is one reason that modern telescopes are reflectors rather than refractors.

C. Procedure and Observations

1. Magnification: Objective and Eyepiece Focal Lengths

The first part of the procedure is similar to that of Sect. C.2 in Experiment #3, "The Optics of Telescopes: Part I. Image Size and Brightness". Place the unfrosted light bulb at the far end of the optical bench, simulating a location at astronomical distances. Place a converging lens with the largest focal length available well down the bench from the light bulb and place a screen on the side of the lens opposite the light bulb. As in Experiment #3, "The Optics of Telescopes: Part I. Image

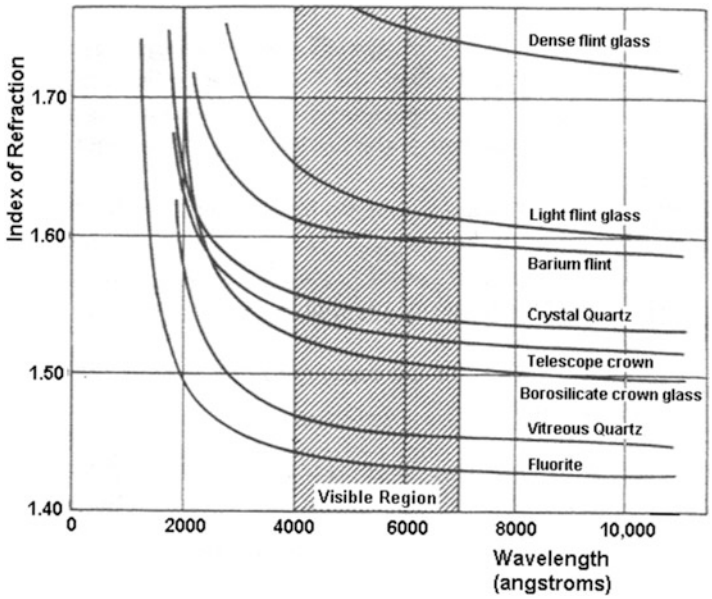

Fig. 1 The index of refraction for various glasses as a function of wavelength. The variation of n with wavelength results in such well-known phenomena as the dispersion of white light into colors by a prism, the creation of rainbows, and chromatic aberration in refracting telescopes

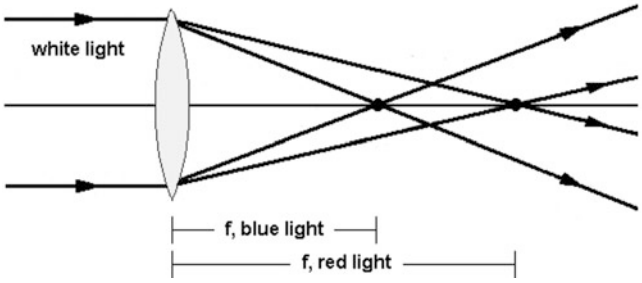

Fig. 2 The light passing through the objective lens of a refracting telescope experiences chromatic aberration if the lens is constructed of only one material

Size and Brightness," the screen is simply a piece of black cardboard on which to view the various images.

Move the image screen back and forth until a clear image of the light bulb filament appears on it, assuring that it is located at the focus. Measure to the nearest 0.1 mm if possible the distance from the lens to the image screen, the focal length f_o of the lens, and the size of the image, s, on the image screen. You can use any dimension of the image as a measure of its size, but for consistency measure the height. Enter these values on the DATA SHEET.

Table 1 Correspondence between wavelength and colors

Color	Approximate wavelength (Å)
Red	6300–7000
Orange	5900–6300
Yellow	5700–5900
Green	5000–5700
Blue	4500–5000
Violet	4000–4500

Now remove the image screen and replace it with an eyepiece. Move the eyepiece slowly away from the lens until an image of the light bulb filament is seen. Measure the distance, d, along the bench from the lens to the eyepiece. Enter its value in Table 2a of the DATA SHEET.

Repeat this procedure for several eyepieces. Then repeat the entire procedure for two lenses of smaller focal length. Enter their values for d in Table 2b and Table 2c of the DATA SHEET, respectively.

2. *Chromatic Aberration*

As in Sect. 2 of Experiment #3, "The Optics of Telescopes: Part I. Image Size and Brightness," place the unfrosted light bulb at the far end of the optical bench, simulating a location at astronomical distances. Place a converging lens with the largest focal length available well down the bench from the light bulb and place a screen on the side of the lens opposite the light bulb. Move the image screen back and forth until the image of the frosted light bulb is as small as possible, assuring that it is located at the focus.

Measure the distance to the nearest 0.1 mm if possible from the lens to the image screen, the focal length f_o of the lens, and enter this value on the DATA SHEET. Now place various color filters over the lens and move the image screen along the track until point images are again obtained. Enter these values, f, in Table 3a of the DATA SHEET. Also enter the approximate wavelength of the transmitted light using the values in Table 1.

Repeat this procedure for a lens with the smallest focal length available. Enter these values of f in Table 3b of the DATA SHEET.

D. Calculations and Analysis

1. *Magnification: Objective and Eyepiece Focal Lengths*

For each lens, calculate the angular size α of the object in radians by dividing s by f_o. Enter these values on the DATA SHEET to the nearest 0.1 mm.

Subtract f_o from this distance to find the focal length of the eyepiece, f_e. You can then calculate the angular size β of the magnified image in radians by dividing s by f_e. Also calculate the magnification, $m = \beta/\alpha$. Enter the results in Table 2a, etc., of the DATA SHEET.

Construct a graph of f_o/f_e as a function of magnification, m, on the graph paper provided. Fit a straight line to the data. As seen from Eq. (3), the slope of this line should be close to 1. Determine the slope and the percentage error in the slope. Perform all calculations on the DATA SHEET.

2. Chromatic Aberration

For each lens, calculate the values of $f - f_o$. Enter the results in Table 3a, etc., of the DATA SHEET.

For each lens, construct a graph of the difference $f - f_o$ as a function of wavelength. Plot both sets of data on the same graph, but use different symbols to distinguish them. Determine the slopes of the two curves. Perform all calculations on the DATA SHEET.

STUDENT'S NAME _____

E. Telescope Optics Experiment II Data Sheets

1. Magnification

Lens #1: f_o = _____ cm

s = _____ cm

$\alpha = s/f_o$ = _____ radians

Table 2a Magnification with lens #1

Eyepiece	d (cm)	$f_e = d - f_o$ (cm)	$\beta = s/f_e$ (radians)	$m = \beta/\alpha$
1.				
2.				
3.				

Lens #2: f_o = _____ cm

s = _____ cm

$\alpha = s/f_o$ = _____ radians

Table 2b Magnification with lens #2

Eyepiece	d (cm)	$f_e = d - f_o$ (cm)	$\beta = s/f_e$ (radians)	$m = \beta/\alpha$
1.				
2.				
3.				

Lens #3: f_o = _____ cm

s = _____ cm

$\alpha = s/f_o$ = _____ radians

Table 2c Magnification with lens #3

Eyepiece	d (cm)	$f_e = d - f_o$ (cm)	$\beta = s/f_e$ (radians)	$m = \beta/\alpha$
1.				
2.				
3.				

STUDENT'S NAME _____

Graph of f_o/f_e as a function of magnification

Calculation of slope:

Calculation of percentage error in slope:

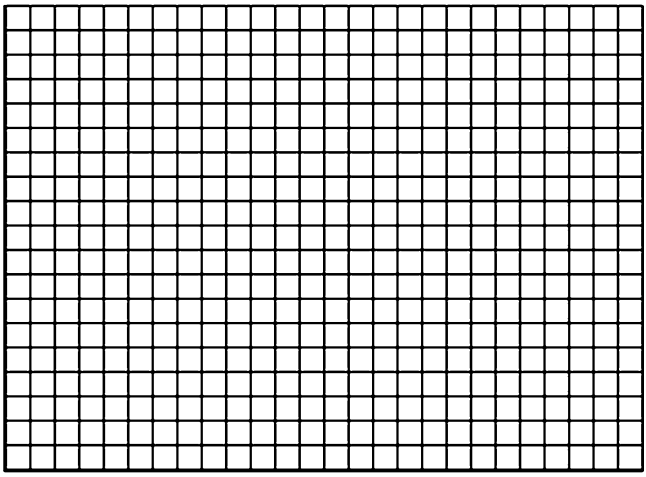

2. *Chromatic Aberration*

STUDENT'S NAME _____

Large focal length lens

focal length of lens for white light, f_o = _____ cm

Table 3a Chromaticaberration with large focal length lens

Filter color	Wavelength of filter (Å)	f (cm)	$f - f_o$ (cm)
1.			
2.			
3.			
4.			
5.			

Small focal length lens

focal length of lens for white light, f_o = _____ cm

Table 3b Chromatic aberration with small focal length lens

Filter color	Wavelength of filter (Å)	f (cm)	$f - f_o$ (cm)
1.			
2.			
3.			
4.			
5.			

Graph off$_o$ – f_e as a function of wavelength

Calculation of slope for lens #1:

STUDENT'S NAME _____

Calculation of slope for lens #2:

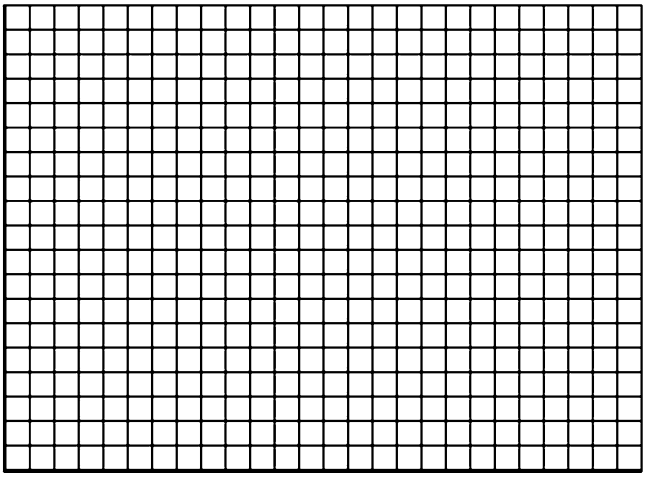

STUDENT'S NAME _____

F. Telescope Optics Experiment II Discussion Questions

In the following, write the formula that has led you to your answer.

1. Two binoculars have lenses with a 50 mm aperture, but one has a magnifying power of 5× and the other 10×.
   a. Which binoculars provides the larger image size to the user? Why?
   b. Which gives a brighter image? Why?
   c. Which would be easier to hold still and thus minimize the effect of unsteadiness in your hands (which is magnified as much as the image)? Why?

2. A telescope can be equipped with two eyepieces, one of focal length 5 cm and the other of focal length 1 cm.
   a. Which would give a better view of a distance galaxy? Why?
   b. Which would give a better view of the planet Mars? Why?

3. In the chromatic aberration part of the experiment, describe the shape of the graph of $f - f_o$ as a function of wavelength. How is it related to Fig. 2?

4. For the lens you used in studying chromatic aberration, what is the distance between the focal points for light of wavelength 3500 Å and light of wavelength 6500 Å? Show your calculations here.

STUDENT'S NAME _____

5. Referring to Fig. 2, at which region of the electro-magnetic spectrum would the effect of chromatic aberration be the least or greatest, the infrared region or the ultraviolet region. Explain your answers.

Removing these DATA SHEETS from the book may damage the binding. You might consider entering the data and performing your calculations in the book, and then photocopying the DATA SHEETS for submission to your instructor for grading.

If you used graph paper other than that provided, attach those graphs to these DATA SHEETS.

Part II
The Solar System

Introduction

As the closest of the astronomical objects, the planets, Moons, comets, and asteroids of the solar system were the first celestial objects to be studied during the rebirth of human rationalism called the Renaissance. Tycho Brahe, Galileo Galilei, Johannes Kepler, Sir Isaac Newton, and others observed the planets and the Moon and arrived at laws of nature, without reliance on the always unreliable "eyewitness testimony," faith, revelation, authority, or bombast. Some of the experiments involve observations carried out over a portion of a semester or an entire semester, all thereby providing insight into the experiences of these scientists.

The two-part experiments on reflection of light from planets and the Moon, determination by radar of the rotation rates of planets and asteroids, and thermal radiation from planetary subsurfaces present more recent techniques. These significantly complement the manned and unmanned space program, probably the greatest technological achievement of mankind, in providing knowledge of the solar system. Challenging experiments, they provide insight into the analysis techniques of real astronomical research.

Sunset and evening star,
And one clear call for me!
—Alfred Lord Tennyson (1809–1892)

Experiment 5
Earth: The Seasons and Local Latitude

SUMMARY: In Experiment #5, "Earth: The Seasons and Local Latitude," you will determine your latitude on the Earth by measuring the length of the shadow cast by a meter stick at noontime and comparing those measurements to those expected at various latitudes. Your measurements will be made over most of the semester.

LEVEL OF DIFFICULTY: Low

EQUIPMENT NEEDED: Meter stick.

MY LEARNING GOALS

1. To be able to describe how the tilt of the axis of the Earth creates the seasons.
2. To be able to predict the effect of geographical latitude on the seasons.
3. To be able to apply the geometry of the celestial sphere in locating objects in the sky.
4. To be able to apply the zenith angle equation in predicting diurnal events such as sunrise and sunset times.

L.M. Golden, *Laboratory Experiments in Physics for Modern Astronomy: With Comprehensive Development of the Physical Principles*,
DOI 10.1007/978-1-4614-3311-8_5,

A. Introduction

The seasons of the Earth result from the tilt of the rotational axis of the Earth and its revolution about the Sun. As shown in Fig. 1, the rotational axis of the Earth is tilted by 23.4° to the plane of the orbit of the Earth about the Sun. As a result, as the Earth revolves about the Sun in its yearly motion, the rays from the Sun at a given hour, for example, noontime, hit the Earth at different angles.

In the northern hemisphere, the angle at a given hour as measured from the zenith is relatively small during the summer and is relatively large during the winter. In the autumn and spring, the angle is intermediate in value. The direct rays of summer provide the most energy per unit area and are therefore the most effective in heating the surface of the Earth. The slanting rays of winter provide the least energy per unit area and are the least effective in heating the surface. Such variations result in the seasons. (Two other effects of the changing angle also contribute, the shorter winter days compared to summer days and the longer path through the atmosphere that the slanted rays of the Sun traverse during winter compared to summer, causing greater absorption of energy in the atmosphere during the winter than during the summer.)

The amount of seasonal variation of the angle of the rays of the Sun depends on the geographical latitude, l. At the equator, $l = 0°$, the Sun never gets lower than 23.4° in the sky at noontime. At the poles, $l = 90°$ north and $l = 90°$ south, the Sun never rises for the 6 months between the dates of the autumnal equinox (about September 21) and the vernal equinox (about March 21). In fact, for all northern latitudes greater than $l = 67.5°$ north and all southern latitudes greater than $l = 67.5°$ south, the Sun does not rise for at least one complete day during the winter.

In this experiment, we will measure the variation of the angle of the rays of the Sun indirectly, by measuring the length of the shadow cast by a meter stick or pole of known length. We will then use those measurements to determine our geographical latitude. Figure 2a, for example, shows the length of shadow, L, cast by a pole of length, H, at noontime at position P on the surface of the Earth.

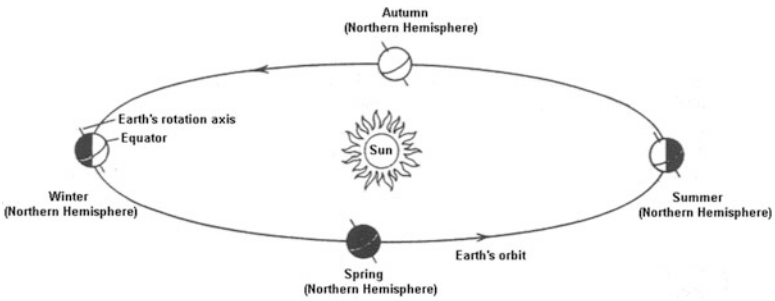

Fig. 1 The rays of light from the Sun are incident upon different geographical latitudes on the Earth at different angles as the Earth makes its annual revolution about the Sun. This causes the seasons

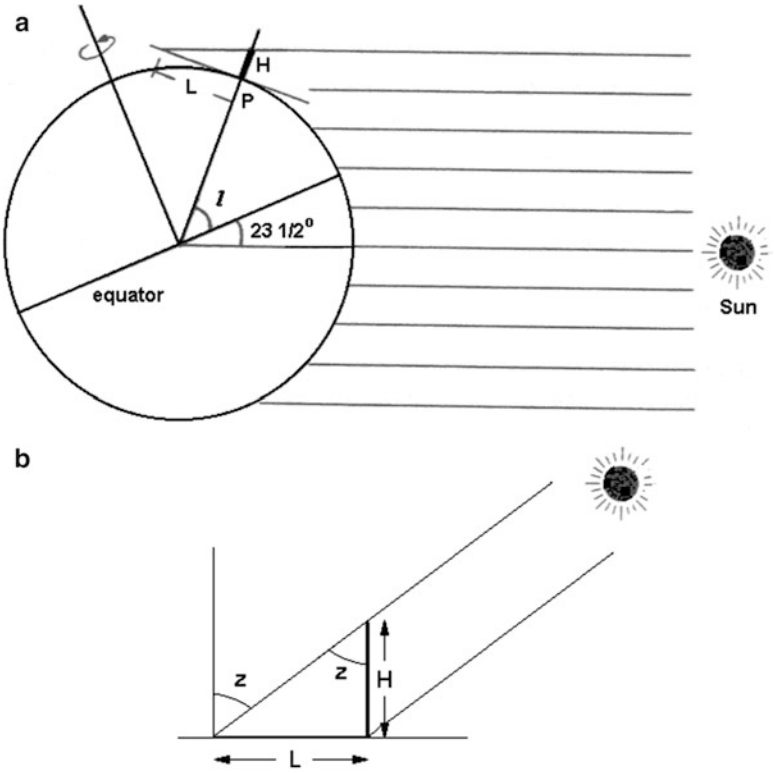

Fig. 2 (**a**) The length of shadow cast by a stick of length H, at a given time of day, depends on the day of the year and geographical latitude. The configuration shown is that of the date of the winter solstice (about December 21), when the Sun is lowest in the sky and the day is shortest in the northern hemisphere. (**b**) Closeup of the geometry explicity showing the dependence of the length of the shadow on the zenith angle, z

B. Theory: The Celestial Sphere and Zenith Angle Equation

Although instruments of high precision allow us to determine the angle of the Sun from the zenith, we will use a simple and ancient technique to do so. As can be seen in Fig. 2, the length of shadow, L, cast by a stick of height H placed perpendicular to the ground depends on the angle the Sun makes with the zenith. Besides the time of day, this angle depends on the date of the year and the geographical latitude, l, of the observer. We will accordingly use the length of the shadow as an indicator of the angle of the Sun from the zenith.

The length of the shadow cast by the Sun as a function of the geographical latitude is a special case of the more general *zenith angle equation*, which relates to the position in the sky of any celestial object. To examine that general case, consider the celestial sphere, defined in spherical geometry by Fig. 3. The center

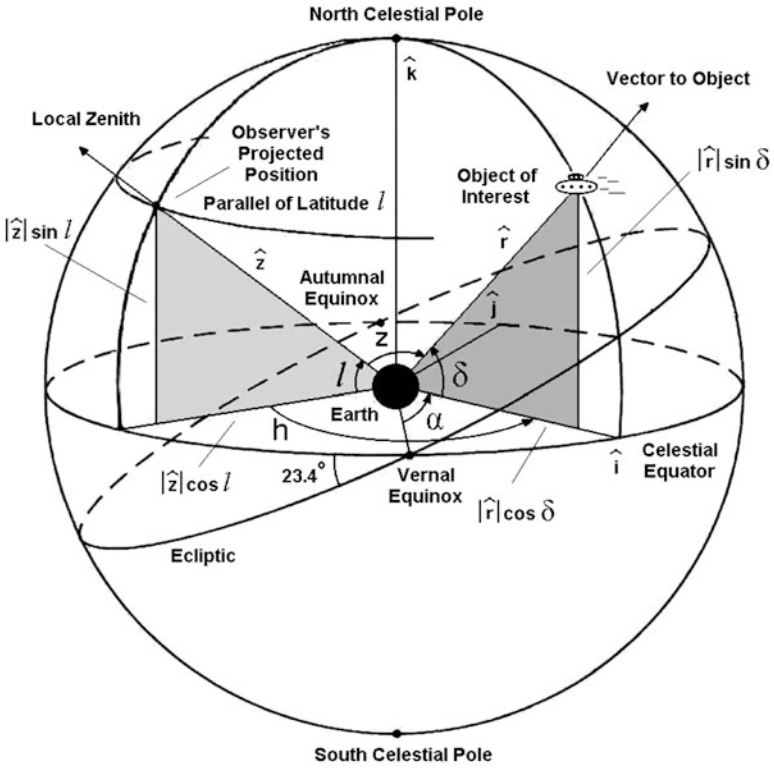

Fig. 3 The celestial sphere and its spherical geometry is used to define astronomical coordinate systems and thereby position measurements

of the celestial sphere is the center of the Earth, and great circles represent the equator and the ecliptic.

Two additional great circles locate the object of interest and the observer. Both are perpendicular to the great circle of the equator and therefore pass through the north and south celestial poles. The object is imagined to be located on a great circle at an angle h, the hour angle, from that of the observer, which itself passes through the local zenith. The portion of this latter great circle visible from horizon to horizon of the observer is called the meridian. In other words, the meridian in the context of an observation could be defined as the locus of points in the sky for which the hour angle of the object of interest is zero.

In the coordinate system used in astronomy, the position of an object is given by its right ascension and declination. The latter is the angle δ measured upwards or downwards to the object from the celestial equator. The former, denoted by α in Fig. 3, is the angle measured eastwards along the celestial equator from the reference point of the vernal equinox. (A common error among the uninitiated is to consider the vernal equinox as a moment in time. In fact, as shown in Fig. 4, it is a position in the sky, defined by the intersection of the ecliptic and celestial equator.

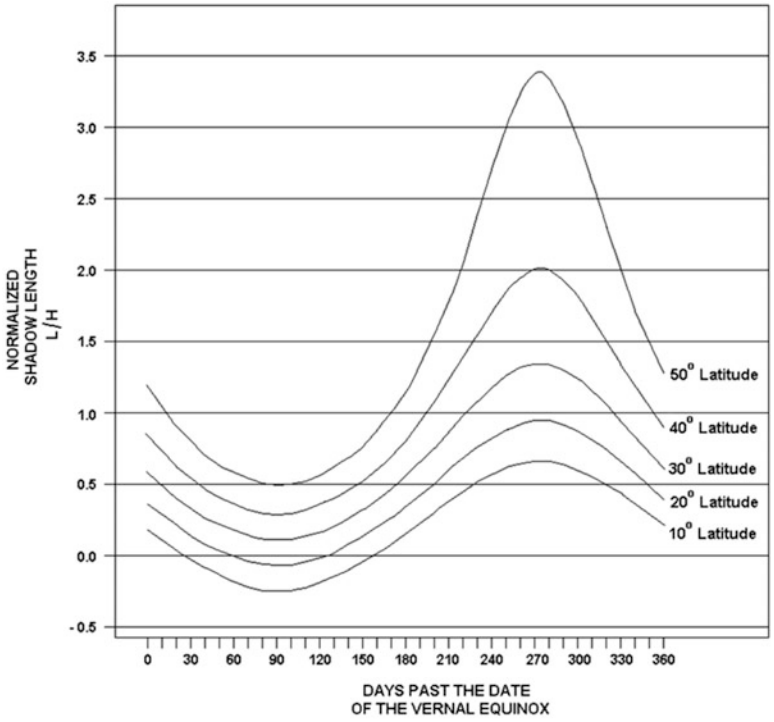

Fig. 4 Normalized shadow length as a function of time for values of the geographical latitude l from 10° to 50°. The graph is reproduced with a larger scale on the DATA SHEET for analysis of your observations

The associated moment in time is that at which the Sun is located in the sky at the position of the vernal equinox.)

Distant objects such as stars have fixed positions in the sky. As a result, as the Earth rotates, the hour angle of the object changes. For solar system objects, whose positions are not fixed in the sky, the additional complication of their motion exists. That is, if the Earth were suddenly to stop rotating, the stars and galaxies would keep their same position in the sky whereas the planets, Sun, and Moon would continue to move, creating some major problems for astrologers. That, of course, would be the least of our worries.

With the celestial sphere defined, to determine the value of z we employ a sly trick. We instead find the value of $\cos z$, from which we can then, of course, find z. You will remember from vector algebra that the dot product of two vectors $\bar{a}$ and $\bar{b}$ is defined as

$$\overline{a} \bullet \overline{b} = |\overline{a}| \left|\overline{b}\right| \cos\theta,$$

where the angle between the two vectors is θ. If we, therefore, can find two vectors in the celestial sphere between which the angle is z, we need only create the dot product of those vectors, and *voila, cos z* would appear.

What two vectors define the zenith angle? The zenith angle is defined as the angle between the local overhead point, or zenith, and the object of interest. First, we define a coordinate system within the celestial sphere. Because we're interested in a given celestial object, it makes sense to define that coordinate system based on a plane passing through the object as well as the two celestial poles. If it passes through the object of interest, then its intersection with the celestial sphere will be a portion of a great circle, on which we can perform trigonometry. If it passes through the object of interest, then, as we will soon see, we need only worry about two components of the two vectors.

The relevant portion of that plane is the darkly-shaded triangle in Fig. 2. As also shown in Fig. 3, the unit vectors of that coordinate system are $\hat{i}$, $\hat{j}$, and $\hat{k}$. In terms of that coordinate system, the unit vector in the direction of the object of interest, $\hat{r}$, is expressed as,

$$\hat{r} = \cos\,\delta\,\hat{i} + \sin\,\delta\,\hat{k}.$$

The unit vector in the direction of the local zenith, $\hat{z}$, is first projected onto the $\hat{k}$ direction and onto the equatorial plane, shown in the lightly-shaded triangle in Fig. 3, and then the component in the equatorial plane is projected onto the $\hat{i}$and $\hat{j}$directions by use of the hour angle, h. This yields components,

$$\hat{z} = \cos\;l\;\cos h\,\hat{i} + \cos\,l\;\sin h\,\hat{j} + \sin\,l\,\hat{k}.$$

Because a unit vector has a magnitude, by definition, of unity, showing $|\,\hat{r}\,|$ and $|\,\hat{z}\,|$ explicitly in Fig. 3 is not needed. We do this solely to identify the origin of their components.

With the unit vectors $\hat{r}$ and $\hat{z}$ now defined, we perform their dot product to find the cosine of the zenith angle,

$$\hat{r}\cdot\hat{z} = \cos\;z$$

$$\cos z = \sin l\;\sin\delta + \cos\;l\;\cos\delta\;\cos h. \tag{1}$$

(Note that the *j*th component is irrelevant, a result of our choice of the plane defining our coordinate system passing through the object of interest.)

This is the world-famous formula for the zenith angle. It has wide applications. It is used by engineers and architects to determine the shadow imprint of buildings, meteorologists to determine the rising and setting time of the Sun, Moon, and planets, and astronomers to determine where to point their telescopes to observe a given object. Astrologers never heard of it. In particular, in the alt-az telescope mount, short for "altitude-azimuth," the altitude angle is $90^\circ - z$, measured from the horizon upwards rather than from the zenith downwards.

Let's apply (1) to determine the length of the day, the time between sunrise and sunset. Sunrise and sunset would be defined as $z = 90^\circ$ so that $cos\ z = 0$. Then solving (1) for $cos\ h$,

$$\cos\ h = -\tan\ l\ \tan\ \delta. \tag{2}$$

Using the declination of the Sun on the given day and your latitude, you can now determine the hour angles at which the Sun rises and sets. Although (2) does not appear to have two solutions, being not, for example, a quadratic, recall that the trigonometric functions have an ambiguity in the four quadrants. In particular, positive values of cosine of the same absolute value occur in the first and fourth quadrants and negative values of the same absolute value occur in the third and fourth quadrants.

Let us calculate the length of the day on which the Earth passes through the vernal equinox. Then the declination of the Sun is zero, so that (2) becomes simply $cos\ h = 0$, independent of the latitude. The solutions for h are, of course, $\pm\ 90^\circ$. With the correspondence of 15 degrees of arc to 1 h of time for a rotating Earth, we see that the day is 12 h long, 6 h from sunrise to noon and 6 h from noon to sunset. This is what we experience on the Earth at all latitudes on the date of the vernal equinox.

Note that by "noon" we mean "astronomical noon," defined as $h = 0$, the Sun appearing on the meridian. Because of the manner in which time zones are defined, the times of sunrise and sunset published in your newspaper will generally not agree with the astronomical times calculated from (1). Time zones extend over 15° of longitude, but the Sun is directly overhead only at a specific longitude, obviously not within the entire time zone. The times of sunrise and sunset that appear in the newspaper, in short, are adjusted for the actual longitude of location of your city. (In addition, during the day the Sun itself has moved and its declination has changed, if only slightly. The calculation above has used a single value for the declination, zero, during the entire day. Greater accuracy results by using the declinations of the Sun at sunrise and sunset. The error in the length of the day introduced by such an approximation is typically a few minutes of time, small enough not to offend any self-respecting rooster.)

The equation relevant to our experiment is a special case of (1). We will observe the Sun directly overhead, that is, along the meridian. Accordingly, (2) becomes

$$\cos\ z = \sin\ l\ \sin\ \delta + \cos\ \ l\ \cos\ \delta,$$

which by a familiar trigonometric identity becomes

$$\cos\ z = \cos\ (l - \delta).$$

From Fig. 2b, we see that $tan\ z = L/H$. Therefore,

$$L = H\ \tan\ (l - \delta). \tag{3}$$

That's the variation of the length of shadow L of a vertical pole measuring stick of height H, when the Sun passes through the prime meridian, as a function of the declination of the Sun, δ, and geographical latitude, l.

To determine the value of δ at a given time on a given date, we could look it up. We know, however, that it varies sinusoidally with the date as the Earth orbits the Sun. Accordingly, we can be clever and simply write

$$\delta = i \ \sin 2\pi \frac{t - t_o}{365.25},$$

where i is the inclination of the axis of the Earth to its orbit, 23.45°, and t_o is the date of the vernal equinox, about March 21, when $\delta = 0$. The quantity $t - t_o$ is then the number of days of the measurement reckoned from the vernal equinox. From (3), then, we get

$$L = H \ \tan \left(l - i \ \sin \frac{2\pi(t - t_o)}{365.25} \right). \tag{4}$$

This is now the variation of the length of shadow, L, of a vertical pole measuring stick of height, H, when the Sun passes through the prime meridian, as a function of the date, t, and geographical latitude, l.

Note in (4) that roughly 90 days past the vernal equinox, the summer solstice, the sine factor will be equal to 1 and L will be minimum, and that roughly 270 days past the vernal equinox, the winter solstice, the sine factor will be equal to -1 and L will be maximum. This agrees with our experience and gives us confidence in the above equation, if we needed further assurance. In such equations as this one, we state that L is a function of t, and the parameter of the equation is the geographical latitude, l.

C. Procedure and Observations

In this experiment, we will measure the length of the shadow cast by a measuring stick at noontime over a period of months, plot its variation, and by comparison with predicted variations for several latitudes determine our geographical latitude. The longer the measuring stick you can find the better. The fuzziness of the end of the shadow is then small with respect to the total length of the shadow and reduces uncertainty in the measurements. A long pole, a 3-m stick, or a yardstick are preferred to a 1-ft ruler.

Two precautions must be observed to get useful measurements of the length of the shadow cast by your measuring stick. First, the measurement must be made when the Sun passes through the *meridian*, that is, on the imaginary circle passing from the north pole, through the point directly overhead, to the south pole.

Unfortunately, a clock can only be taken as an approximate guide for the passage of the Sun through the meridian for two reasons. First, if daylight savings is in effect, then

passage of the Sun through the meridian will occur around 1:00 p.m. rather than 12:00 noon. Second, all the clocks within a given time zone will read the same, but the passage of the Sun through the meridian will occur at different times depending on your geographical longitude. Without access to a table of local astronomical time for your longitude, a simple way to determine passage of the Sun through the meridian is to wait until the shadow of your measuring stick is aligned exactly north–south. (This is one of the principles of the sundial.) Knowing that the shadow will be the shortest during the day when the Sun passes through the meridian can also be used as an aid.

The second precaution you must take is to ensure that the measuring stick is exactly perpendicular to the ground. For this, you can use a plumb bob, a weight attached to a string. Hold the string above the ground so that the weight points to the center of the Earth, and therefore perpendicular to the ground. Then line up your measuring stick parallel to the string. Alternatively, if little or no wind is present, you can simply grab one end of the measuring stick and lower it slowly until it touches the ground. It should then be perpendicular to the ground. To get reduce the measurement uncertainties, you should repeat the measurement of the shadow several times and average the results.

In Table 2 of the DATA SHEET enter the date of your observation and the length of the shadow cast as close to noontime as possible. Because we will deal with the ratio L/H in our analysis, you need not use the same length pole for all observations. Doing this, however, might avoid some confusion. In case you use measuring sticks of different lengths, enter in Table 2 of the DATA SHEET the length of the measuring stick or sticks. Enter all lengths in centimeters.

D. Calculations and Analysis

In Table 2 of the DATA SHEET enter the number of days the date of your observations are past the date of the vernal equinox. Use Table 1 or the Days-of-the-Year tables of Appendix III to determine that figure. Divide the length of the

Table 1 Days past the date of the vernal equinox (March 21)

Date	Days
April 1	10
May 1	40
June 1	71
July 1	101
August 1	132
September 1	163
October 1	193
November 1	224
December 1	254
January 1	285
February 1	316
March 1	344

shadow cast divided by the height of the measuring stick and enter the result in Table 2 of the DATA SHEET.

The variation of the length of shadow L of a vertical measuring stick of height H, when the Sun passes through the meridian, as a function of the date, t, and geographical latitude, l, is given by (4).

For the analysis, we will plot the theoretical predictions of this equation for various values of geographical latitude, a "family of curves parameterized by l." We will plot our experimental data and then determine our geographical latitude by seeing where our data lie in comparison to the theoretical curves.

Because different students may use measuring sticks of different heights, we will deal with the ratio L/H, which is independent of the particular measuring stick used and which is, from (4),

$$\frac{L}{H} = \tan\left(l - i\ \sin\frac{2(t - t_o)}{365}\right). \tag{5}$$

In Fig. 4, values of L/H from (5) are given as a function of $t - t_o$, the number of days past the vernal equinox, for values of the geographical latitude, l, from 10° to 50°. Positive (negative) value means that the shadow points northward (southward) for northern latitudes. This sense is reversed for southern latitudes. Figure 4 is reproduced, enlarged, on the DATA SHEET for your analysis.

Plot your values from the DATA SHEET for the ratio L/H as a function of $t - t_o$ on Fig. 4 as reproduced on the DATA SHEET. You will find that your data probably does not lie along any given curve. If your measurements have been careful, however, your data should lie entirely between two adjacent curves.

STUDENT'S NAME _____

E. Seasons and Local Latitude Experiment Data Sheets

Table 2 Shadow measurements

Date	Days past vernal equinox	Shadow length, H (cm)	Length of measuring stick used, L (cm)	L/H
1.				
2.				
3.				
4.				
5.				
6.				
7.				
8.				
9.				
10.				
11.				
12.				
13.				
14.				
15.				
16.				
17.				
18.				
19.				
20.				
21.				
22.				
23.				
24.				
25.				

(continued)

Table 2 (continued)

Date	Days past vernal equinox	Shadow length, H (cm)	Length of measuring stick used, L (cm)	L/H
26.				
27.				
28.				
29.				
30.				
31.				
32.				
33.				
34.				
35.				
36.				
37.				
38.				
39.				
40.				

STUDENT'S NAME _____

Graph your values for L/H as a function of the number of days past the vernal equinox on the figure below.

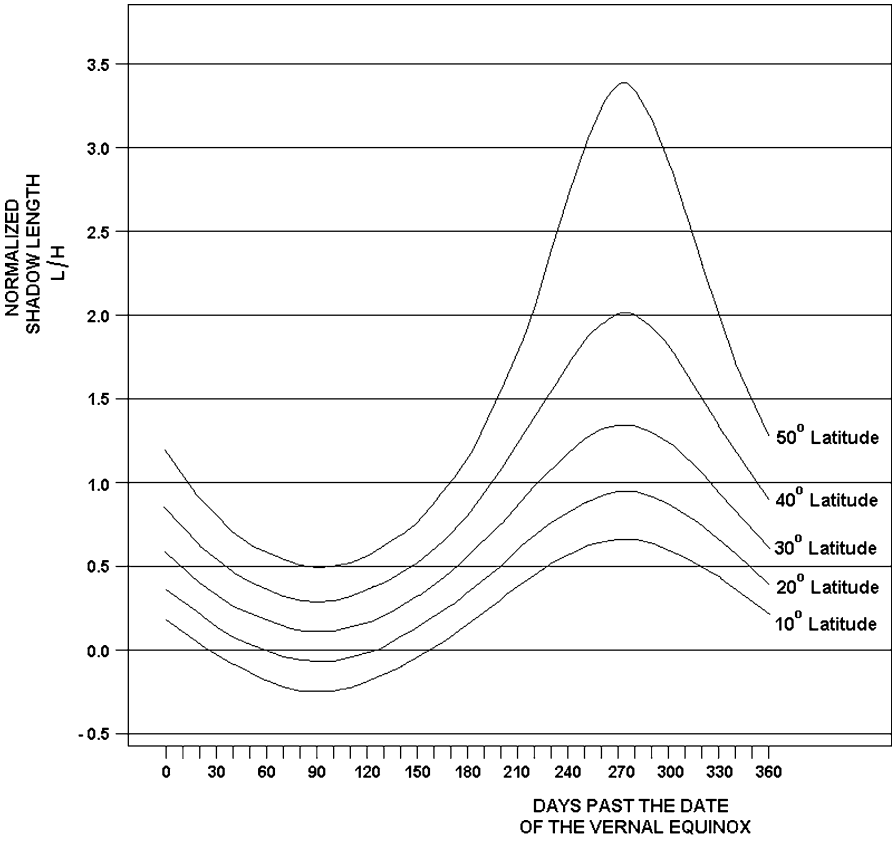

STUDENT'S NAME _____

Estimate your geographical latitude by the location of your plotted data between two of the family of curves.

Experimental value for geographical latitude = _____.

What error in this number would you estimate from the range of values in your plotted data and your judgment as to their position within the two curves?

Estimated error in geographical latitude = _____.

On a globe or in an atlas, look up the location of your city and find its geographical latitude.

Actual geographical latitude = _____.

Compare the experimentally determined geographical latitude and your actual latitude. Calculate the percentage error in your result. Show all your calculations here.

Compare this calculated percentage error to the estimated error that you noted above in question #2.

F. Seasons and Local Latitude Experiment Discussion Questions

1. Discuss the sources of error in your determination of your local latitude.
   a. In which direction, larger or smaller latitude, would you expect to err if your measurements were not taken exactly at noon? Why?

   b. In which direction, larger or smaller latitude, would you expect to err if your pole was not held exactly vertical, but was tilted in turn to the north, to the east, to the south, or to the west? Why?

STUDENT'S NAME _____

2. Using (2), showing your calculations here, calculate the length of the day at your latitude at,
   a. The winter solstice, for which the declination of the Sun is -23.4°
   b. The summer solstice, for which the declination of the Sun is 23.4° .
   c. Calculate the length of the day at a latitude of 25° at the winter solstice.
   d. Based on your results for part a. and part c., why are those people who travel from the northern states to live in Florida during the winter called "snowbirds" or "sunbirds"?

3. Again using (2), and showing all calculations here,
   a. Calculate the zenith angle of the Sun at noontime at your latitude at the winter solstice.
   b. Calculate the zenith angle of the Sun at noontime at your latitude at the summer solstice.

STUDENT'S NAME _____

c. On the figure below, draw lines approximately at the two zenith angles calculated in parts a) and b) to show the relative elevations of the Sun at the winter and summer solstices at noontime at your latitude.

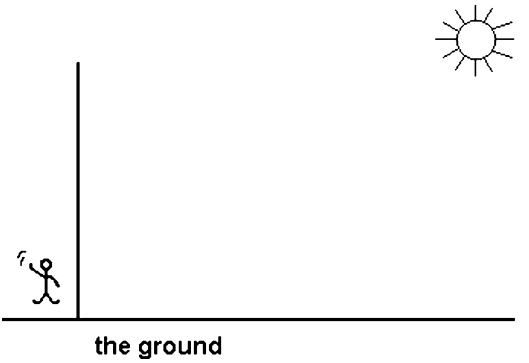

Removing these DATA SHEETS from the book may damage the binding. You might consider entering the data and performing your calculations in the book, and then photocopying the DATA SHEETS for submission to your instructor for grading.

Experiment 6
The Surface Roughness of the Moon. Reflection and Scattering from a Planetary Surface: Part I. Surface Materials

SUMMARY: In Experiment #6, "The Surface Roughness of the Moon. Reflection and Scattering from a Planetary Surface: Part I. Surface Materials," which provides a taste of how astronomers really perform their research, we study the reflection of light from simulated planetary surfaces. A bright light shines parallel beams of light onto sand boxes filled with common Earth soils and rocks. A photometer which can be rotated on a stand measures the amount of light being reflected into different angles from the vertical. With the use of a polarizing filter, we also measure the amount of polarized light reflected from each of the soil samples. In Experiment #7, "The Surface Roughness of the Moon. Reflection and Scattering from a Planetary Surface: Part II. Beads and Surface Coverage," we will measure the sizes of the particles of each sample and determine if the amount of polarization depends upon those sizes.

LEVEL OF DIFFICULTY: Moderate to High. This challenging experiment requires moderate skill in making careful measurements.

EQUIPMENT NEEDED: Sand boxes filled with pebbles, pea gravel, and rocks; photometer mounted on rotatable stand; plumb bob; light baffles; 500-Watt halogen lamp; polarizing filters.

MY LEARNING GOALS

1. To be able to describe the physics of reflection and how planetary surfaces composed of various materials reflect visible light.
2. To be able to describe the difference between specular and diffuse reflection.
3. To be able to predict how various materials polarize light upon reflection.
4. To be able to describe how astronomers use mathematics to analyze data in testing hypotheses.

L.M. Golden, *Laboratory Experiments in Physics for Modern Astronomy: With Comprehensive Development of the Physical Principles*,
DOI 10.1007/978-1-4614-3311-8_6,

A. Introduction

Look upwards at the Moon on the night of a full or near-full Moon. We see by reflected sunlight the entire lunar disk. At its other phases, we see varying portions of the lunar disk. Why is there such a *phase effect*? Why, in particular, can the Moon appear "full"? As we will see in this experiment, the Moon exhibits a phase effect because the lunar surface is rough, not smooth.

The lunar phases are shown in Fig. 1, a view of the Earth-Moon system looking downward on the solar system from interplanetary space. The inner circles show the Moon as illuminated by the Sun, the side of the Moon facing the Sun in full sunlight and the side of the Moon facing away from the Sun in shadow. The outer circles display the appearance of the lunar disk from the Earth as the Moon revolves about the Earth in its monthly orbit. This is what we refer to as the phase effect.

The structure and composition of the surface of moons and planets can be analyzed by their reflected sunlight. These include the Moon, Mercury, asteroids, the Galilean satellites, and even the rings of Saturn. Mars can also be studied, but its atmosphere reduces the effectiveness of the technique. The atmosphere both scatters light out of the incoming radiation, rendering it diffuse rather than the collimated rays needed, and scatters the light which is being reflected back to the observer. If we ever get to explore other solar systems, one of the primary techniques will be to study the reflected light from its worlds.

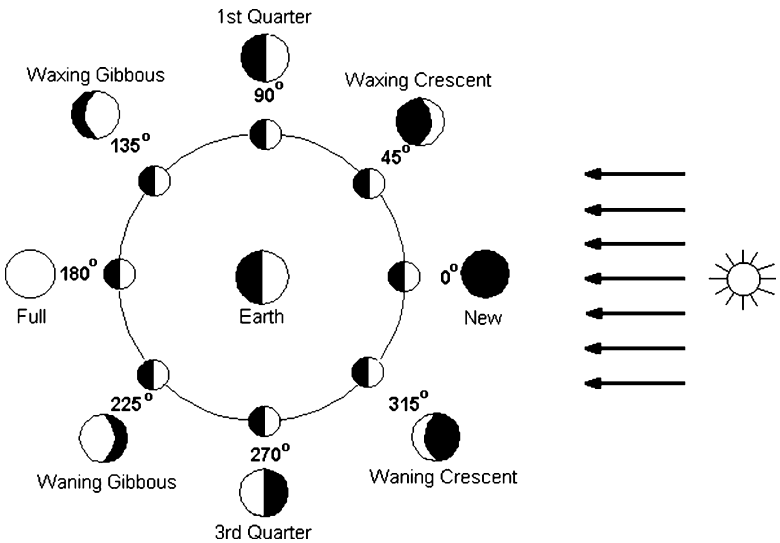

Fig. 1 The phases of the Moon result from its rough surface reflecting sunlight as the Moon revolves about the Earth in its monthly orbit. The *inner disks* show the half of the Moon illuminated by the Sun. The *outer disks* show the appearances of the Moon from the Earth at the various phases noted

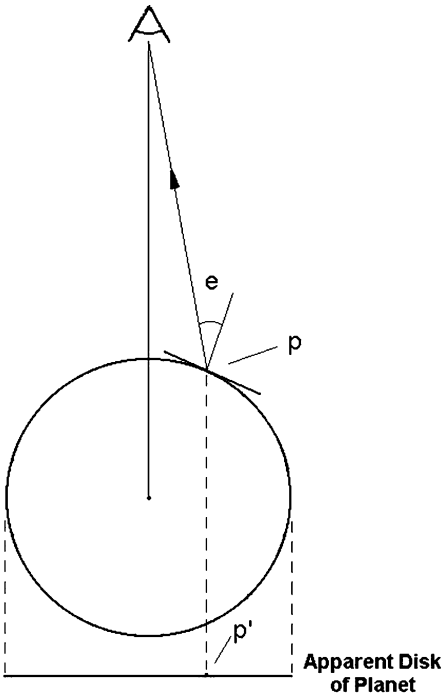

Fig. 2 Observing the intensity of light from different portions of the apparent disk of a planet or the Moon (point P') enables us to determine the ability of the surface material at a corresponding location (point P) to reflect light in a given direction, given by the angle of observation, *e*

Astronomers can determine the roughness of the Moon or planetary surface from the Earth. This is done by observing the intensity of light emanating from different portions of the apparent disk of the object. As can be seen from Fig. 2, by observing the radiation at different angles from the sub-Earth point, you determine the ability of the surface material to reflect radiation in that direction. This, of course, requires the ability that the telescope can resolve the disk of the Moon or planet.

In Experiments #6, "The Surface Roughness of the Moon. Reflection and Scattering from a Planetary Surface: Part I. Surface Materials," and Experiments #7, "The Surface Roughness of the Moon. Reflection and Scattering from a Planetary Surface: Part II. Beads and Surface Coverage," we will study reflection and scattering from simulated planetary surface materials. We will use our results to reach some conclusions about the material on the lunar surface and, in Experiment "The Surface Roughness of the Moon: Reflection and Scattering from a Planetary Surface," the amount of surface covered by the small glass beads discovered by the Apollo astronauts during their excursions over the lunar surface.

B. Theory

1. *Reflection*

The story of reflection and scattering is told in two parts. First, we discuss the radiation that falls on the surface, the *incident* radiation. Figure 3 shows the familiar geometry that explains how the slanting rays of winter result in less energy from the Sun heating the surface of the Earth. We examine a beam of sunlight of width L. Its "depth" into the paper is a constant d. In (a), the rays are incident from directly overhead. In (b), the rays hit the surface at the *angle of incidence*, i. Let the amount of energy in the beam be S_o. Then the intensity of light per unit area hitting the surface from directly overhead is

$$E(0) = \frac{S_o}{dL}. \tag{1}$$

where *E(0)* refers to the intensity at an angle of incidence $i = 0$.

Because of the slant of the rays, the same energy with which the directly overhead rays illuminate an area of size $d\ x\ L$ would illuminate a larger area of size $d\ x\ s$, where $s = \frac{L}{\cos i}$, Fig. 3b. The resulting intensity of the sunlight illuminating the surface with an angle of incidence i is therefore, in comparison to (1),

$$E(i) = \frac{S_o}{d\,\frac{L}{\cos\ i}},$$

or

$$E(i) = \frac{S_o \cos\ i}{dL}.$$

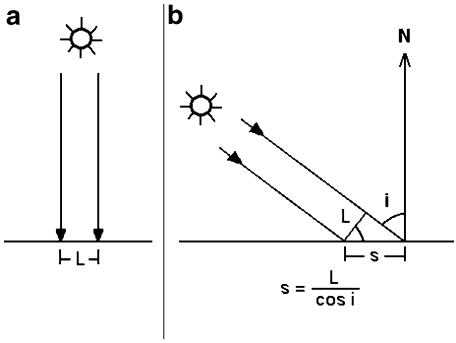

Fig. 3 The radiation incident onto a surface is spread out as the inverse of the cosine of the angle of incidence, i. This "foreshortening" is the major cause of the seasons. It also enables us to understand reflection from the idealization referred to as a Lambert surface

By (1) we can rewrite this as

$$E(i) = E(0)\ \cos\ i. \tag{2}$$

That's the familiar cosine reduction of the amount of solar energy hitting the surface in winter because of "foreshortening," but it holds for any situation in which we are comparing rays incident from directly overhead to rays incident at a slant.

Now, this is purely a geometrical effect, having nothing to do with the nature of the surface material. That kind of information is obtained by studying the light reflected from the surface.

Two idealized cases for reflection exist. If the surface is smooth compared to the wavelength of the incident radiation, then the reflection obeys the *laws of reflection* of geometrical optics, Fig. 4. These state that the angle of reflection is equal to the angle of incidence and that the incident ray, the reflected ray, and the normal to the surface all lie in the same plane. For any angle of incidence, the light is reflected into a single angle of observation. The phenomenon in which light is reflected according to the familiar laws of reflection is referred to as *specular reflection*. (This is derived from the Latin word "speculum," meaning mirror). Aside from calm bodies of water, purely specular reflection results mainly from man-made objects. That, for example, governs the *geometric optics* which describe reflections within telescopes, as discussed in Experiments #3 and #4, "The Optics of Telescopes: Part I. Image Size and Brightness" and "The Optics of Telescopes: Part II. Magnification and Chromatic Aberration".

This type of reflection would be observed from a sphere whose surface was covered with smooth glass. If such an object were in the sky, it would reflect sunlight back to us only from a small portion of its surface. If the lunar surface, for a real-life example, were smooth compared to the wavelengths of light, and if the Sun were a point object in the sky, then we would only see a point on the Moon, Fig. 5, and no phase effect would occur. Here, two configurations during the waning gibbous phase of the Moon are shown. As is seen, that point would be located at the center of the portion of the Moon illuminated by the Sun and visible from the Earth, the so-called "sub-Earth point."

(In fact, because the Sun is about 30 minutes of arc in angular size as seen from the Earth or Moon, and not a point in the sky, the angular region we would see by reflection from a fictional smooth moon would have greater extent than a point. Using the geometry of the Earth-Moon system, the size of this illuminated region can be found to be less than 10 seconds of arc. Because the images of stars as seen through our atmosphere are a few seconds of arc in size, this would appear to be a large, bright star. Venus, on the other hand, as described in Experiment #11, "The Orbit of Venus," is about 60 seconds of arc in size when it is closest to the Earth. The Moon, if a perfect reflector, would accordingly be only about 1/10th of this size.)

Naturally-occurring surfaces, such as those of the Moon and terrestrial planets, are rough. They can be sandy, boulder-strewn, or mountainous. Such surfaces do

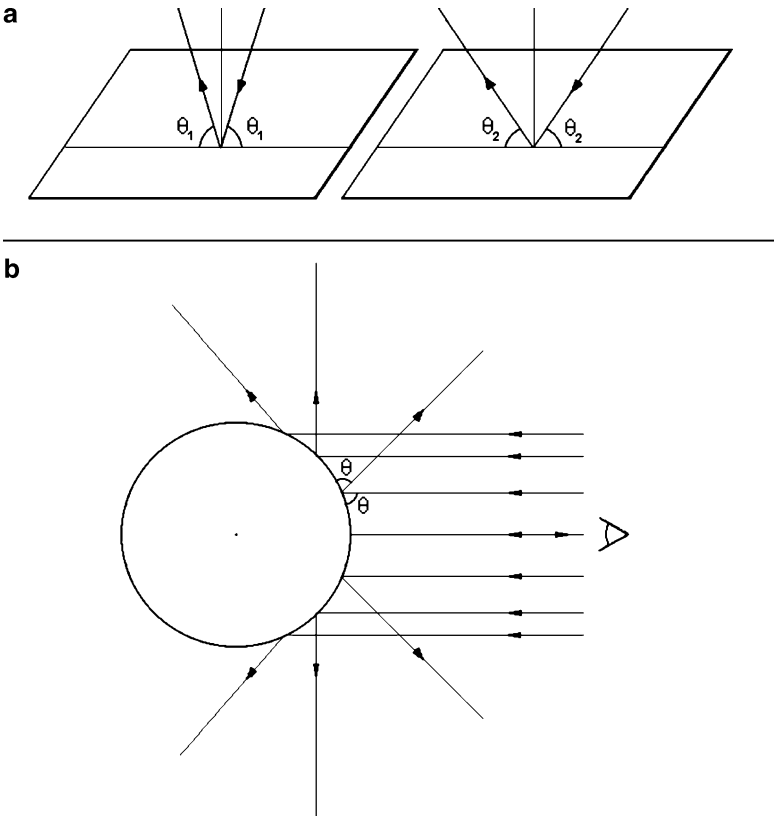

Fig. 4 Specular reflection. (**a**) The light reflected from a surface which is smooth on scales of the wavelengths of light obeys the laws of reflection. (**b**) A smooth sphere will reflect light in only one direction, determined by the laws of reflection applied to a plane tangent to the sphere at the point at which the ray of light is incident on the sphere

not produce specular reflection; the laws of reflection shown in Fig. 4 do not apply. This roughness enables us to see phases of the Moon rather than a point of light.

In the case of such natural-occurring surfaces, individual rays from a beam of light are reflected in different directions from small smooth spots, again according to the laws of reflection. Such light, reflected off of a rough surface, is referred to as *quasi-specular reflection* or sometimes as *diffuse reflection*.

The second idealization for a reflecting surface is a *Lambert* surface (Johann Lambert, 1728–1777). A Lambert surface is an ideal diffuser in that it scatters light incident at any angle with an equal intensity in all directions, Fig. 6. The light is said to be scattered *isotropically*. No matter the direction of observation, from directly above or to the side, a photometer reading will be the same. Surfaces which approximate a Lambert surface are more common in nature than those which produce specular reflection.

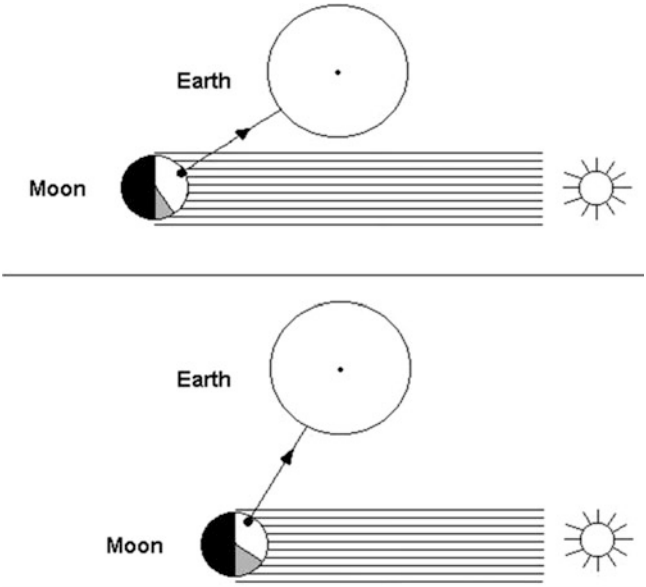

Fig. 5 If the Moon were a smooth surface, no phases would be observed. Only a bright patch of light less than 10 s of arc in diameter at the sub-Earth point would be visible from the Earth

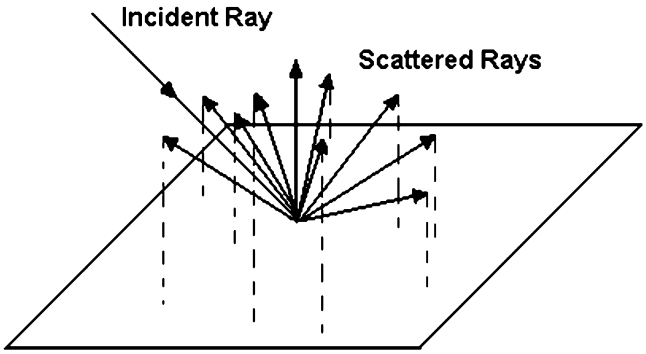

Fig. 6 The scattering of the light incident on a Lambert surface is isotropic

2. Scattering

We have now introduced the term *scattering*. The definition of scattering off of a planetary surface is a little less definite than the definition of scattering, for example, by a gas, atoms, molecules, or imperfections in a crystal. For these, the type of scattering is defined by the relative sizes of the wavelength of light and the scattering particles.

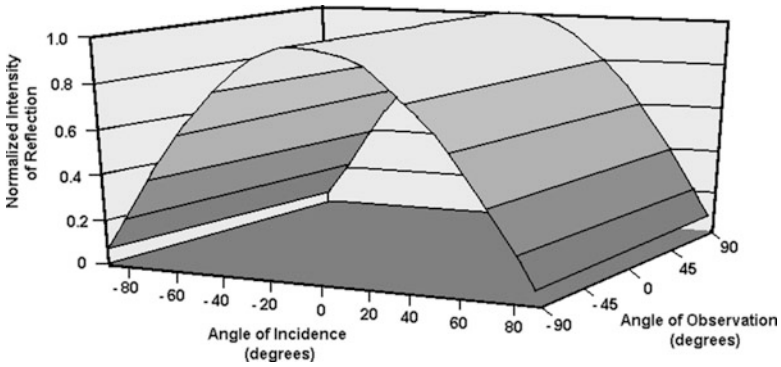

Fig. 7 A two-dimensional representationn of a three-dimensional graph of reflection from a Lambert surface. For a given angle of incidence, the reflection into any angle of observation is constant for this idealized surface. The variation with angle of incidence is purely geometrical, resulting from the same effect of slanting of incident rays that is the major cause of the seasons

When discussing light interacting with a surface, some physicists and astronomers simply distinguish specular reflection and the pure diffuse reflection occurring with a Lambert surface. Commonly, the term scattering in this context refers to those processes in which radiation is reflected into angles other than those predicted by the laws of reflection that govern specular reflections. Quasi-specular reflections as well as reflections from a Lambert surface would thus be considered the result of scattering whereas unscattered reflections are referred to as specular reflections. For objects large compared to the wavelength, geometric optics well describe their interaction with light, and the interaction is not described as scattering.

Here, we will employ the following terminology. We will refer to the light being *observed* by the photometer as reflected light. We will reserve the term "scattering" for the sometimes complicated combination of multiple interacting *processes* of reflection, refraction, and absorption that occur on the top layer of the surface and within the subsurface layers of facets that produce the reflected light.

The light reflected from a Lambert surface brightness must and does, of course, follow the purely geometrical effect of (2). In other words, the light reflected from a Lambert surface depends on the angle of incidence, but is independent of the angle of observation. Figure 7 shows this dependence in three dimensions. For comparison, you will be asked in an exercise to provide the corresponding graph for the intensity of reflected light for specular reflection.

The lunar surface, in fact, approximates a Lambert surface, with notable differences. Perhaps the most striking occurs at a perfect full Moon, when the subsolar point on the Moon is observed. This results from the presence of small glass beads and which is the subject of Experiment #7, "The Surface Roughness of the Moon: Reflection and Scattering from a Planetary Surface: Part II. Beads and Surface Coverage".

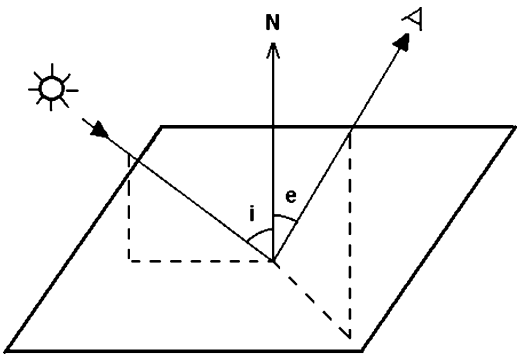

Fig. 8 In general, light emanating from a rough surface does not obey the laws of reflection of specular reflection. The angle *i* and the angle *e* are not equal, and the plane of incidence is not co-planar with the plane of emission. The angle of incidence, *i*, and the angle of observation, *e*, are defined with respect to the normal to the surface at the point of incidence

3. Geometry of the Reflection

The simple geometry of Fig. 4 is not adequate to represent quasi-specular reflection or the diffuse reflection of Fig. 6. Instead, we must refer to a three-dimensional geometry such as in Fig. 8. The light can be reflected into any angle measured from the vertical as well as in the azimuthal direction. As mentioned above, on the Moon or a planetary surface, this occurs by a combination of interactions. The incident light can undergo specular reflection at the top layer of the surface, or can penetrate into the surface and undergo absorption and refraction, or can reflect off one or more surfaces below the top layer.

Partially because of the possible confusion between the terms reflection and scattering referred to earlier, the angle of observation is sometimes referred to as the "emittance angle." Hence it is labeled "*e*" in Fig. 8.

In this experiment we will simplify matters greatly by using light incident directly from above. The incident angle, *i*, that is, will be zero. With that simplification, we can construct a graph of the appearance of these various types of reflections.

Figure 9 shows the graph of amount of reflected light as a function of the angle of observation, *e*, for this case of $i = 0$. The intensity values have all been normalized to their value at $e = 0$ for ease of comparison. For the idealization of specular reflection, the light will be reflected back directly upwards. For reflection from a Lambert idealized surface, the amount of reflected light is the same for every angle. (Note that the straight line corresponds to the locus of points forming a straight line on the topmost portion of the three-dimensional graph of Fig. 7.) For intermediate cases, the reflected light is maximum near $e = 0$ but has a finite value for other angles. For all but specular reflection, the reflection will also occur at azimuthal

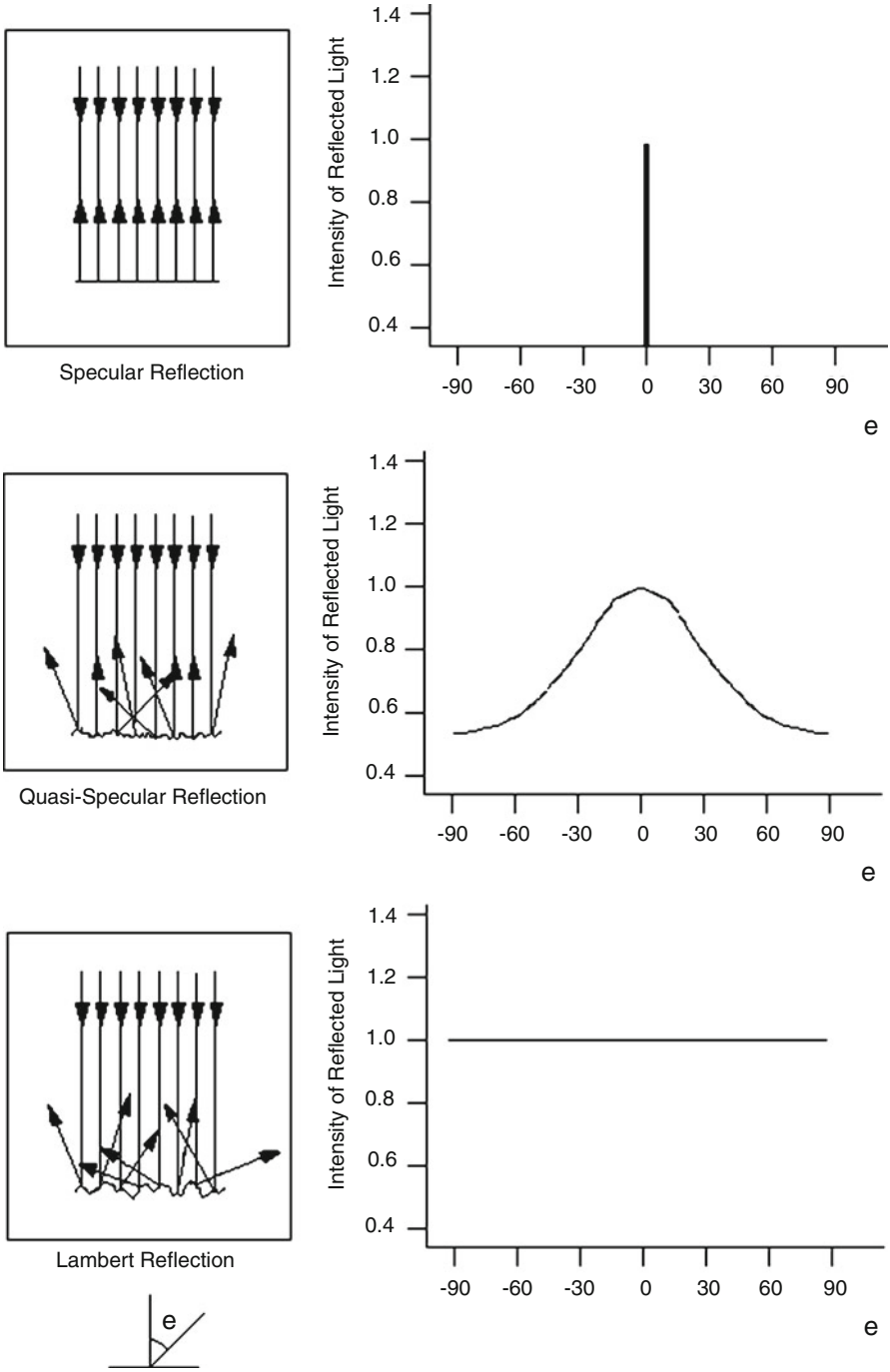

Fig. 9 Depending on the roughness of the Moon or planetary surface, the intensity of reflected light as a function of the angle of observation will vary from a sharp function to a flat curve. Most natural materials produce intermediate shapes such as shown for the case "quasi-specular reflection"

angles. Most natural materials reflect by neither of the idealizations of specular reflection nor a Lambert surface but according to such intermediate cases.

The reflective properties of a surface depend not only on the roughness of the surface, a result of the size and shape of the particles, but also the composition and darkness of the surface material, the presence of slopes, and the physical structure such as the amount of void space among the particles. We all know, for example, that dark coal reflects light poorly whereas a wall painted white reflects light well. In this experiment we will study only the effect that surface roughness has on reflection. Accordingly, all the soil sample materials are painted with the same white paint. This will also ensure a strong reflection easily detected by the photometer.

In this experiment, we will study the reflection and scattering characteristics of various soil samples. By comparison to observations of the Moon, we can get an idea of the type of material on its surface.

4. The Polarization of Light

In one of the greatest achievements in the history of science, physicist Sir James Clerk Maxwell (1831–1879) combined the forces of electricity and magnetism into the electro-magnetic force by writing the famous Maxwell's equations. The importance of this synthesis is comparable to that of Newton's Universal Law of Gravitation. He was then able to show that those equations implied the existence of electromagnetic waves, Fig. 10, and showed that these waves travel through space at the speed of light. The result is evident everywhere in our world. From television to computers, automobile motors to satellite communications, and electric shavers to cell phones, all work because of the application of Maxwell's discovery. Because of this and his other contributions, particularly in the kinetic theory of gases, he is considered with Sir Isaac Newton and Albert Einstein as one of the three greatest physicists of all time.

Light is an electromagnetic wave, as are γ-rays, x-rays, ultraviolet rays, infrared rays, and radio waves. Because the electric and magnetic fields are perpendicular to the direction of motion of the waves, they are an example of a *transverse* wave. Water waves and the waves you create on a jump rope are also transverse waves.

Looking at Fig. 10, one wonders whether nature prefers one orientation of the wave over another. That is, does nature prefer the diagram be rotated by some angle about the direction of motion? In fact, most natural sources of electromagnetic waves emit electromagnetic waves of all orientations. No preferred orientation exists; on average, half of the electrical and magnetic vibrations are each in perpendicular planes. When electromagnetic waves interact with matter, however, a preferred orientation frequently is created. These interactions include the familiar transmission, reflection, refraction (bending), and scattering phenomena. This results in a phenomenon that is familiar, the *polarization* of light.

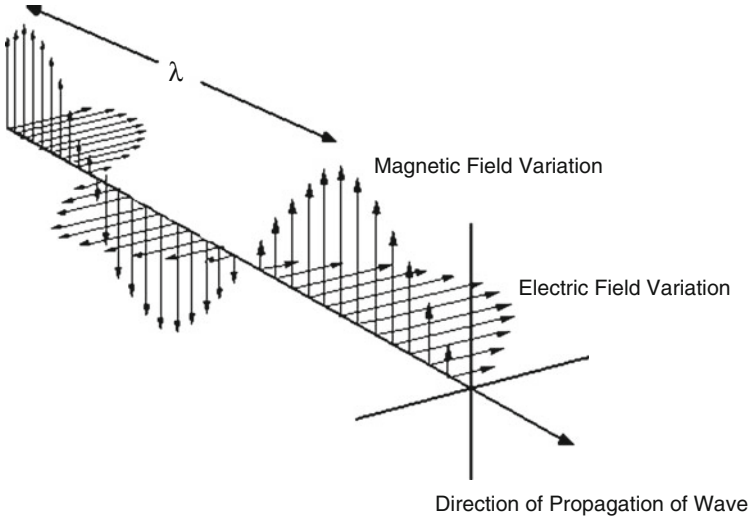

Fig. 10 An electromagnetic wave carries energy through space in its electrical and magnetic fields. As many waves, it is sinusoidal, with the magnetic and electrical variations perpendicular to each other as well as to the direction of motion, or propagation. The wave travels at the speed of light, and the electrical and magnetic components, as shown, have the same wavelength, λ, and frequency. These are attributes of all electromagnetic waves, from the shortest wavelength gamma-rays, to the longest wavelength radio waves. If we consider the drawing as representing one polarization of the wave, the other polarization would be visualized by rotating the wave 90° clockwise (or counterclockwise) about the direction of motion

Polarization resulting from reflection is well known. The glare from the sea and the blinding sunlight reflecting off of the hood of a car result when reflection polarizes the incident sunlight, so that a large fraction has one preferred orientation. Polarized sunglasses reduce the glare by filtering out those rays. If the light is 100% polarized, then the all of the electrical vibrations of the light waves occur in a single plane and all of the magnetic vibrations of the light waves occur in another plane, perpendicular to that of the electrical vibrations as shown in Fig. 10.

The light reflected from the idealized Lambert surface, however, by definition will not be polarized, even if the incident light itself is polarized. Any polarization that might result from a single reflection would get randomized by the complex interactions that occur within the surface layer. In fact, "Lambert's law" is a definition of "diffuse reflection": Incident light of any polarization and angle of incidence that is diffusely reflected will be isotropic and unpolarized.

Depending on the nature of the surface, scattering of sunlight from the particles of a planetary surface can result in partial polarization of the reflected light. In the experiment, we will also study the extent to which the light reflecting off of the various soil samples becomes polarized.

C. Procedure and Observations

1. Equipment

Three types of soil are placed in separate shallow sand boxes. We use sand, pebbles or pea gravel, and stones. A 500-Watt halogen lamp is mounted several feet (see below) above the table on which the sand boxes will be placed, Fig. 11. To prevent the light entering the photometers of the other experimenters in the lab, baffles are placed to the sides of the halogen lamp. The result resembles stage lights such as used in the theatre.

A photometer on a stand is positioned about 1 ft above the sand box and displaced about 1 ft from the plumb line from the lamp to the sand box. The photometer is able to pivot looking downwards from the vertical to an angle of $\beta = 65°$ from the vertical. Attached to the photometer are baffles to limit the field of view and a sleeve into which a polarizing filter can be inserted. From the geometry of Fig. 11, we can see that the angles β and e are equal.

We know that the lunar surface is composed of a mixture of different types of soil materials, differing in size, shape, and composition. By using sand, pebbles or pea gravel, and stones in the experiment we are attempting to simulate one of the characteristics of the lunar material, the particle size. Astronomers and physicists routinely develop a *model* to simulate natural phenomena, either mathematically or in the laboratory. Because we are not modeling the composition of the soil

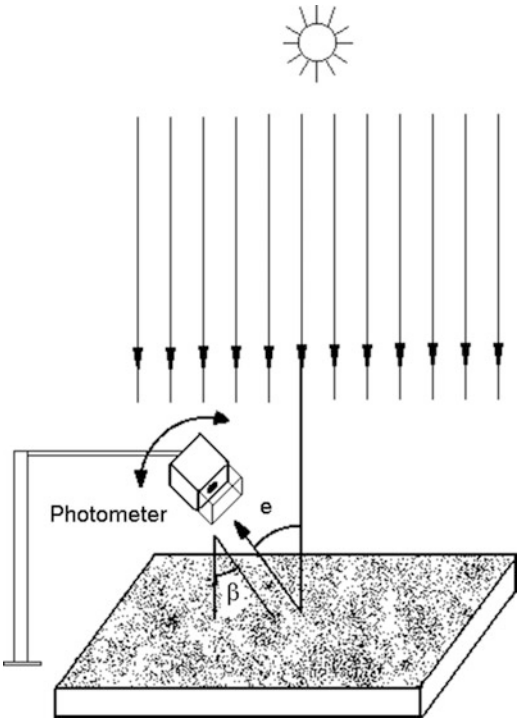

Fig. 11 The experimental apparatus. A lightbulb provides the "sunlight" and a photometer, which can rotate in orientation, measures the reflected light at different angles. A sand box is filled with various soil samples to simulate different types of planetary surfaces. Because in this experiment the incident angle i is zero, the angles β and e are equal

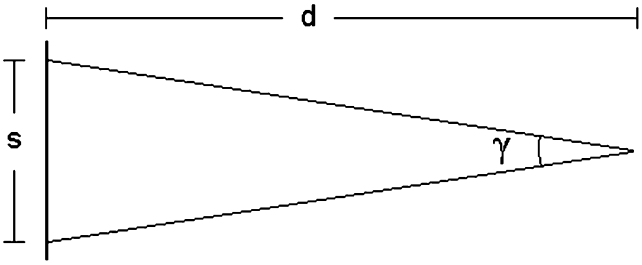

Fig. 12 Using the small angle approximation, we can determine how far to place the light bulb from the sand box surface to ensure that approximately parallel rays of light are incident upon it over a large portion of the surface

materials, only the particle size, and because we want to ensure a large reflection, the materials are all painted white.

The light source that we use to simulate sunlight must have two properties. First, it must illuminate the soil sample bed uniformly over the surface that will be viewed by the photometer. Second, the rays should be parallel, as the Earth receives light from the distant Sun. Uniform illumination can be achieved using a diffuser, such as a piece of frosted glass or a piece of plexiglas which is lightly sanded. Parallel rays can be achieved using a piece of polarizing sheet or a collimating lens.

Neither of these is adequate for our purposes. Polarizing sheets produces polarized light, whereas sunlight is unpolarized and indeed part of the experiment is to detect how unpolarized light becomes polarized when scattered. A collimating lens or short focal length condenser lens, on the other hand, does not provide a wide enough beam to illuminate all of the surface area of the soil sample bed that will be viewed by the photometer at large angles.

Instead of those strategies, we can satisfy both the requirements of both a uniformly illuminated surface and parallel rays requirements geometrically if we place the light bulb at a sufficiently far distance. Figure 12 shows the geometry. We would like angle γ to be close to zero. Because

$$\sin\frac{\gamma}{2} = \frac{s/2}{d}, \tag{3}$$

where s is the width and length of the area to be illuminated and d is the distance to the light bulb, this would mean that the light bulb would have to be at a great distance from the sphere. In practice, let us consider a value of $\gamma = 20^\circ$ as tolerable. Then we can use the small angle formula, Eq. (2) of Experiment #1, "A Review of Mathematical Concepts and Tools," to rewrite (3) as,

$$d \sim \frac{s}{\gamma}.$$

Remembering to express γ in radians by dividing our 20° by $360/2\pi = 57.3^\circ$/rad, we find $d = 5.7$ ft would illuminate a 2-ft square area of the sand box. The lamp should be placed at least this far above the surface of the sand box. Use a plumb

bob to orient the lamp so that the rays of light are perpendicular upon the surface of the sand box

2. *Observations*

Place the sand box of sand under the lamp. Rotate the photometer so that it makes a 5° angle with the vertical. Enter the photometer reading in the second column of Table 1a of the DATA SHEET. Place the polarizing filter into the sleeve to measure polarized light and repeat the measurement. We will refer to that orientation as "horizontal" polarization. Enter the photometer reading in the third column of Table 1a of the DATA SHEET. Remove the polarizing filter, rotate it 90° so that it will now measure the other sense of polarized light, insert the rotated filter back into the sleeve, and repeat the measurement. Enter the photometer reading in the third column of Table 1a of the DATA SHEET. We will refer to that orientation as "vertical" polarization. Carefully note which orientation of the polarizing filter you have used in each measurement for future reference in the experiment.

Rotate the photometer 10° so that it now makes an angle of 15° with the vertical. Repeat the three measurements and enter the results on the DATA SHEET. Make sure that the measurements with the polarizing filter are consistently entered according to their orientation as "horizontal" or "vertical." Continue rotating the photometer by 10° and making the three measurements until you have reached the maximum 65° angle we will employ. On completion, you will have made measurements at 5°, 15°, 25°, 35°, 45°, 55°, and 65°.

Repeat the same series of measurements with the sand boxes containing pebbles or pea gravel and stones. Enter all results in Tables 1b and 1c, respectively, of the DATA SHEET.

D. Calculations and Analysis

1. *Degree of Polarization*

From the measurements of total reflection intensity, "horizontal" polarization intensity, and "vertical" polarization intensity for each soil sample entered on Tables 1a, 1b, and 1c, calculate a "degree of polarization" in percent by the following formula,

$$D = \frac{I_H - I_V}{I_T} \times 100, \tag{4}$$

where the subscripts refer to horizontal, vertical, and total. The values of D will range from −100%, for the case in which all the reflection has been "vertically"

polarized, through zero, for the case in which no polarization has occurred, to +100%, for the case in which all the reflection has been "horizontally" polarized.

Perform all calculations on the DATA SHEET and enter your results in the right-hand column of Tables 1a, 1b, and 1c for the three soil samples of sand, pebbles or pea gravel, and stones, respectively.

2. *Geometrical Correction Factor*

Before additional analysis of the measurements is made, they must be corrected for a geometrical effect. (These corrections were not needed in the calculation of the degree of polarization, because the correction factors we will find would cancel out in (4).) As can be seen from Fig. 13, as the photometer is rotated at increasingly larger angles from the vertical, reflections from increasingly larger areas of the surface are being received. If A_0 is the area from which reflection is received when the photometer is pointed directly downwards, then the area from which reflection is received when the photometer is pointed at an angle e from the vertical has increased by a factor equal to its increased length. This would bias those observations and a correction is required.

To determine the correction factor, examine Fig. 13b, c. The angle from which reflection is received by the photometer is labeled α_o. If the distance from the photometer support to the beginning of the reception area is x and the distant to the far extent of the reception area is s, then the total linear extent of the footprint of the photometer is $l = s - x$. That's what we need to determine. The width w of the footprint remains the same, where in general $A = lw$.

From the geometry of Fig. 13c

$$L = s - x$$

$$= H\left[\tan(\beta + \frac{\alpha_o}{2}) - \tan(\beta - \frac{\alpha_o}{2})\right].$$

Using trigonometric identities, this can be shown to be identical to

$$L = H\frac{2\ \sin\alpha_o}{\cos\ \alpha_o + \cos 2\beta}. \tag{5}$$

We don't know the value of α_o, but we know it is small. Now that we've separated α_o from β, which is not necessarily small, we can therefore simplify (5) by the small angle approximations to the sine and cosine,

$$L = H\frac{2\alpha_o}{1 + \cos 2\beta}. \tag{6}$$

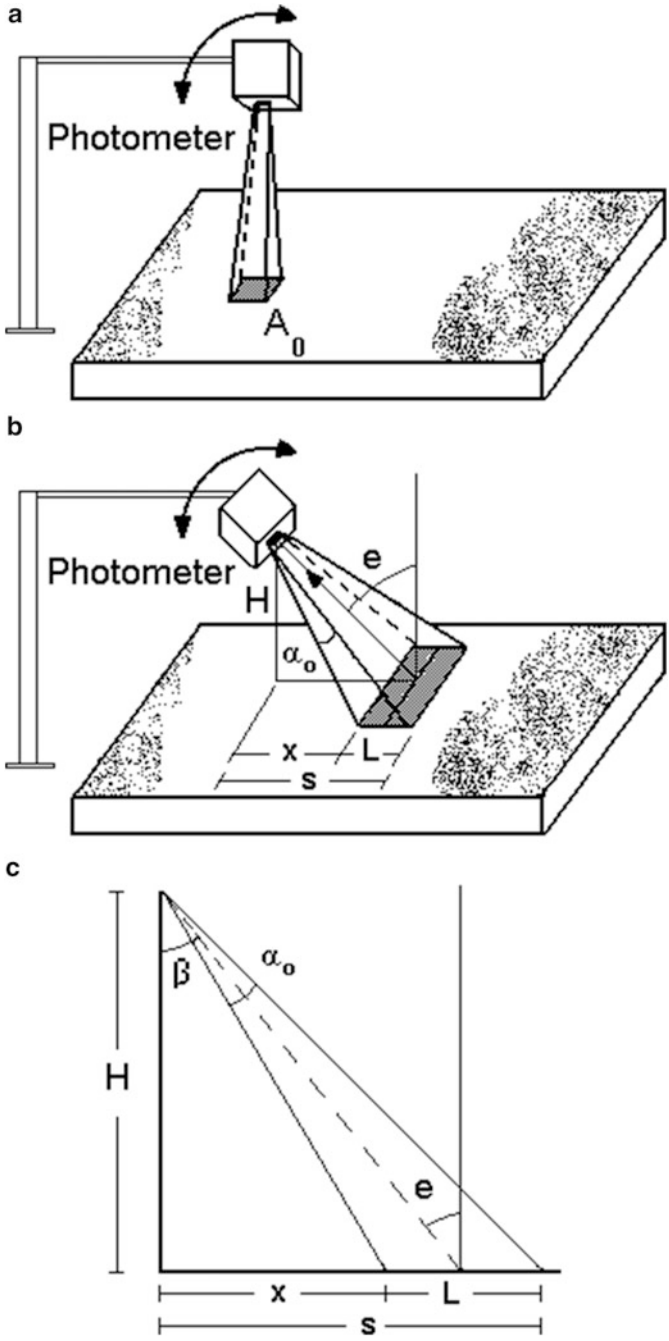

Fig. 13 The measurements must be corrected for the slanted region on the surface from which the reflected light is received. The photometer receives reflected light in an angle α_o. That angle is spread out over a distance L which changes as the photometer is rotated. (**a**) A three-dimensional schematic with the photometer viewing the surface from directly overhead. (**b**) A three-dimensional schematic with the photometer viewing the surface at an oblique view. (**c**) The geometry for determination of the correction factor in which, for clarity, the photometer is shown in a side view. Note that angle β is equal to the angle of observation, e

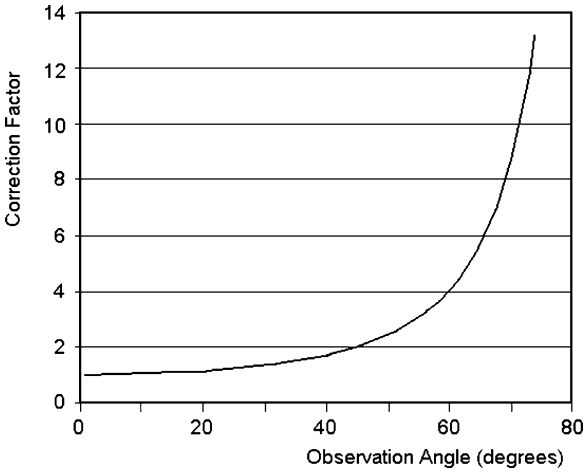

Fig. 14 The correction factor for viewing the surface of the sand box at a slant becomes appreciable for angles greater than about 40°

To check, if $\beta = 0$, then $L = H\alpha_o$, and if $\beta = 90°$, then $L = \infty$. This is exactly the behavior we expect. A measurement taken with the photometer pointed directly downwards would not need to be corrected whereas one at 90° would be seeing an "infinite" amount of area.

To put (6) into a form that can be used for any values of H and α_o,

$$f \equiv \frac{L}{\alpha_o H} = \frac{2}{1 + \cos 2\beta}. \tag{7}$$

This is the correction factor we will use, dividing the observations by the values of f as a function of the observation angle, β. As its graph, Fig. 14, shows, the correction becomes appreciable for observation angles great than about 40°, an effect you can observe by shining a flashlight beam against a wall. (It is interesting to note that this is the same formula employed in using "side-looking" radar to map the surface of planets from orbiting satellites as well as in airplane-borne radar for agricultural and geological applications on Earth.)

Note that this is not the same as the *cos i* effect resulting from foreshortening, (2). That refers to parallel rays incident on a surface at an angle of incidence i. This correction refers to the finite field of view of a detector placed near the surface of interest and oriented at an angle of observation e (as angle α_o approaches zero, then angle β can be identified with the angle of observation, e). The *cos i* factor is irrelevant to the experiment, the angle of incidence being a constant 0°.

On the DATA SHEET, calculate the values of f from (7) or by reading the value off of Fig. 14 corresponding to the values of the angles of observation, β. Enter those values in Tables 2a, 2b, and 2c of the DATA SHEET. Correct the values for total reflection, "horizontal" polarization, and "vertical" polarization entered in Tables 1a, 1b, and 1c by dividing by those factors. Enter the results in Tables 2a, 2b, and 2c.

3. *Analysis*

Construct three graphs, one for each of the soil materials. On each, plot both the total reflection and the degree of polarization as a function of the angle of observation. To distinguish the two sets of data, use the left hand vertical scale to provide the tick marks and scale for the total reflection and the right-hand vertical scale to provide the tick marks and scale (from −100 to +100) for the degree of polarization results. Draw smooth lines through the data points. Continue the smooth curve carefully, graphically extrapolating to 0° angle of observation.

From the graph of total reflection intensity as a function of the angle of observation for each soil sample, read the values at 0° and 50° and enter them on the DATA SHEET as I_0 and I_{50}. Calculate the ratio $C = \frac{I_{50}}{I_o}$ for each soil sample on the DATA SHEET and enter the results in Table 3. We have thereby defined a "coefficient of roughness." It can vary from a value of zero for specular reflection to unity for reflection from a Lambert surface. Quasi-specular reflection will result in an intermediate value.

In Experiment #7, "The Surface Roughness of the Moon: Reflection and Scattering from a Planetary Surface: Part II. Beads and Surface Coverage," we will determine the sizes of the sand particles, pebbles or pea gravel, and stones. We will then construct a graph of the coefficients of roughness as a function of particle size.

STUDENT'S NAME _____

E. Surface Roughness Experiment I Data Sheets

Table 1a Photometer intensity readings at various angles of observation (material: sand)

θ	Total reflection	"Horizontal" polarization	"Vertical" polarization	Degree of polarization
5°				
15°				
25°				
35°				
45°				
55°				
65°				

Table 1b Photometer intensity readings at various angles of observation (material: pebbles or pea gravel)

θ	Total reflection	"Horizontal" polarization	"Vertical" polarization	Degree of polarization
5°				
15°				
25°				
35°				
45°				
55°				
65°				

Table 1c Photometer intensity readings at various angles of observation (material: stones)

θ	Total reflection	"Horizontal" polarization	"Vertical" polarization	Degree of polarization
5°				
15°				
25°				
35°				
45°				
55°				
65°				

STUDENT'S NAME _____

Table 2a Corrected readings at various angles of observation (material: sand)

θ	Geometrical correction factor f	Corrected total reflection	Corrected "horizontal" polarization	Corrected "vertical" polarization
5°				
15°				
25°				
35°				
45°				
55°				
65°				

Table 2b Corrected readings at various angles of observation (material: pebbles or pea gravel)

θ	Geometrical correction factor f	Corrected total reflection	Corrected "horizontal" polarization	Corrected "vertical" polarization
5°				
15°				
25°				
35°				
45°				
55°				
65°				

Table 2c Corrected readings at various angles of observation (material: stones)

θ	Geometrical correction factor f	Corrected total reflection	Corrected "horizontal" polarization	Corrected "vertical" polarization
5°				
15°				
25°				
35°				
45°				
55°				
65°				

STUDENT'S NAME _____

Table 3 Coefficients of roughness

Soil sample	I_0	I_{50}	$C = I_{50}/I_0$
Sand			
Pebbles or Pea Gravel			
Stones			

F. Surface Roughness Experiment Discussion Questions

1. Compare the curves of total intensity as a function of angle of observation between sand, pea gravel, and stone soil samples. Refer to the graphs to provide your answer.

   a. Are the total intensities greater for any type? Explain the difference in terms of the sizes of these particles and the reflection and scattering of the incident light.

   b. Do you expect this kind of result? Why or why not?

2. Compare the curves of degree of polarization as a function of angle of observation between sand, pea gravel, and stone soil samples. Refer to the graphs to provide your answer.

   a. Are the total intensities greater for any type? Explain the difference in terms of the sizes of these particles and the reflection and scattering of the incident light.

   b. Do you expect this kind of result? Why or why not?

STUDENT'S NAME _____

3. Because the Moon has different terrain, some rocky, some lava-covered, and some a mixture, the curve for the Moon of intensity of reflected radiation as a function of angle of observation is not smooth as are those of Fig. 9. Assume you are observing the Moon from the Earth near full Moon.

   a. Which type of material, large, round boulders or rough lava fields with much void space, would cause a dip or enhancement in this curve at an angle of observation of zero degrees (that is, the sub-Earth point)? Which would occur and which of the materials would be the cause? Why?

   b. Similarly, which type of material would cause a dip or enhancement in this curve at an angle of observation of 45° degrees? Which would occur and which of the materials would be the cause? Why?

4. Look at the Moon with binoculars or a small telescope when it is close to being full. The *mare* or lava plains are darker than the other regions because of the intrinsic darkness of the material. If all the material on the Moon were the same intrinsic darkness, what would be the relative brightness of the mare now?

STUDENT'S NAME _____

5. To restrict ourselves to the one variable of particle size we painted all the soil sample particles white. Based on the graphs of the intensity of reflected light as a function of angle of observation that you have determined, draw what you think the reflection curves for each of the three soil samples would have been if we had painted the soil sample particles gray. To enable comparison, place all three on the graph to the left below. Do the same if we had painted the soil sample particles black, again placing all three on the graph to the right below. Provide tick marks and identify the values of the intervals between appropriate tick marks on the axes.

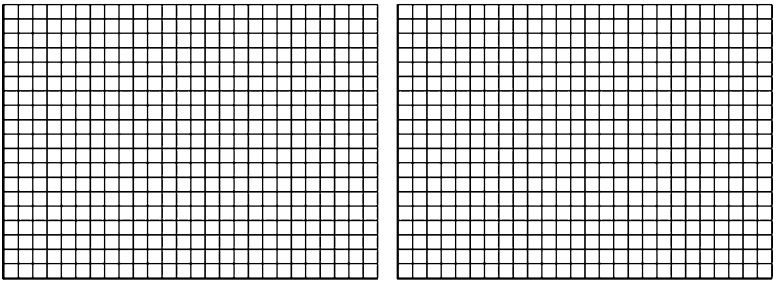

Removing these DATA SHEETS from the book may damage the binding. You might consider entering the data and performing your calculations in the book, and then photocopying the DATA SHEETS for submission to your instructor for grading.

If you used graph paper other than that provided, attach those graphs to these DATA SHEETS.

Experiment 7
The Surface Roughness of the Moon. Reflection and Scattering from a Planetary Surface: Part II. Beads and Surface Coverage

SUMMARY: In the second part of our study of the reflection of light from a planetary surface we study how the small glassy beads found on the lunar surface by Apollo astronauts effect the reflective properties of the surface and the polarization of the reflected light. We place successively larger numbers of materials simulating the beads below the illuminating light bulb and, as in Experiment #6, "The Surface Roughness of the Moon: Reflection and Scattering from a Planetary Surface: Part I. Surface Materials," measure the reflected light.

LEVEL OF DIFFICULTY: Moderate to High. This challenging experiment requires moderate skill in making careful measurements.

EQUIPMENT NEEDED: Sand boxes filled with sand; photometer mounted on rotatable stand; plumb bob; light baffles; 500-Watt halogen lamp; polarizing filters; micrometer; small spherical beads, such as plastic pearls, ball bearings of various sizes, or particles of silica gel.

1. To be able to predict how planetary surfaces covered with various amounts of highly reflecting materiall will cause various degress of increased polarization of the reflected light.
2. To be able to describe how astronomers construct mathematical models of reflecting surfaces.

MY LEARNING GOALS

L.M. Golden, *Laboratory Experiments in Physics for Modern Astronomy: With Comprehensive Development of the Physical Principles*,
DOI 10.1007/978-1-4614-3311-8_7,

A. Introduction

In Part I of this experiment we measured the reflected intensity from sand, pebbles or pea gravel, and stones. We measured the total intensity and the intensity in the two polarized components. In this part of the experiment, we will examine the effect on the reflections on the presence of small spherical beads and the particle size. We will then use these results to derive an estimate of the fraction of the lunar surface covered by small glass beads.

B. Theory: Glass Beads on the Lunar Surface

As noted in Experiment #6, "The Surface Roughness of the Moon: Reflection and Scattering from a Planetary Surface: Part I. Surface Materials," the lunar surface approximates a Lambert surface, with notable differences. Perhaps the most striking occurs at a perfect full Moon, when the subsolar point on the Moon is observed. On the Earth, we never see the perfectly full Moon. When the alignment required for that occurs, we in fact see a lunar eclipse. The Apollo astronauts, however, were easily able to observe the amount of reflection at the exact subsolar point. They found, remarkably, that the exact subsolar point is about 30% brighter than the sub-Earth point during any full Moon as observable from the Earth.

Looking down at the lunar surface, they saw small objects of various colors, green and orange, depending on their chemical composition. (Black ones are also seen, the crystallization products of the orange glasses.) These small glass beads possess various shapes, described as spheres, teardrops, and flakes. Although the sizes vary, a typical dimension is 0.03 mm. Created on the surface of the Moon and, presumably, planetary surfaces by meteoroid impact-caused shock melting and rapid cooling and as cooling products of volcanic eruptions, these small glass beads reflect the direct rays of the Sun by specular reflection, significantly increasing the amount of reflected light. We will study that effect in Experiment #7, "The Surface Roughness of the Moon: Reflection and Scattering from a Planetary Surface: Part II. Beads and Surface Coverage". It will enable us to get an estimate of the fraction of the lunar surface that is on the average covered by these beads.

These glass particles are not insignificant trace constituents of the lunar surface. The impact-generated glasses are ubiquitous, found everywhere, on the lunar surface. Samples from the rays of the major impact crater Copernicus, for example, are composed of 70–90% of these glass particles. Those of volcanic origin constitute major fractions of the soil material near those features. (Some of these beads, more remarkably, contain small amounts of water!)

C. Procedure and Observations

1. *Particle Sizes*

We also want to measure the particle sizes. With a micrometer, measure the sizes of the grains of sand, pebbles or pea gravel, and stones. Express all results in millimeters. Measure at least five of each object, and calculate the average. In measuring the stones, because they are not circular, measure the largest and smallest diameters and take the average for each of the stones you measure. If the sand particles you are using are too small to accurately measure, lay a number of them down side to side and then use a ruler to measure the length of the sand line you have created. Divide by the number of sand particles to get an average size. Perform your calculations on the DATA SHEETS. Enter your results in Table 1 of the DATA SHEET.

Similarly measure the sizes of the various materials you use to simulate the glass beads. Perform your calculations on the DATA SHEETS. Enter your results in Table 2 of the DATA SHEET.

2. *Glass Bead Enhancement*

Let us examine the full Moon effect observed by the Apollo astronauts. Put the sand box containing sand under the lamp and photometer. Move the photometer down next to the lamp so that its view of the surface is not obscured by the photometer. Use a plumb bob to orient the lamp so that the rays of light are perpendicular upon the surface of the sand box. Enter the photometer readings of total intensity and intensity in the two polarizations in the first row of Tables 3a, 3b, and 3c.

The small glass beads found on the lunar surface are about 0.03 mm in size. Such material is not readily available, but we can simulate the effect with plastic pearls, ball bearings of various sizes, and the particles of silica gel used commercially as desiccants. Choose three sizes of particles for use. Use the smallest group of particles you can locate, hopefully about 1 mm in size. The largest group of particles you use should be at least about 1 cm (about 3/8 of an inch). That will give us a range of an order of magnitude in "bead" size. All particles should be painted white to maximize the maximum reflections.

Place some of the group of the largest beads that you have available onto the surface of the sand. Cover about 10% of the surface centered under the photometer field with them. Count the number of beads that you have placed on the surface and enter the result in Table 4. Repeat the three measurements of total intensity and intensity in the two polarizations. Enter the photometer readings of total intensity and the intensity in the two polarizations in the second row of Table 3a of the DATA SHEET.

A simple geometric argument can provide a fairly accurate estimate of the number of beads needed to attain the 10% coverage. If the area of the sand box

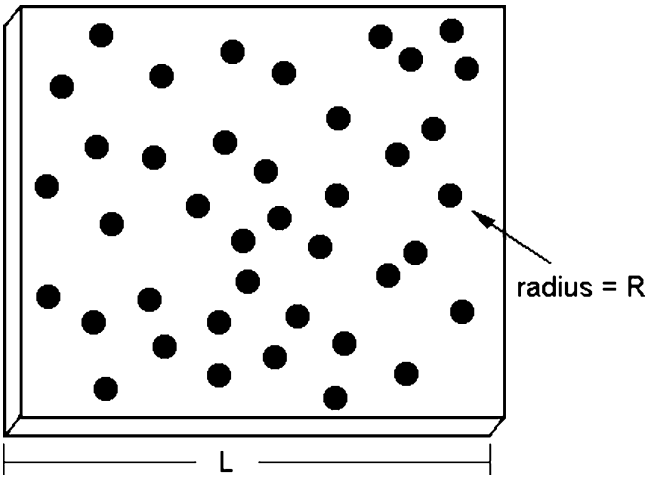

Fig. 1 To calculate the number of beads needed to cover 10% of the surface of the sand box, we can employ the geometry shown

that the baffled light bulb illuminates is a square of side L and if the bead has a radius R, as determined in the next section, then the coverage resulting from placing N beads on the surface will be,

$$\%\ Covered = N\ \frac{\pi R^2}{L^2} \times 100,$$

as shown in Fig. 1. For the desired coverage of 10%, this provides

$$N = \frac{L^2}{10\ \pi R^2}. \tag{1}$$

For example, if the length of the illuminated square sides is have a length of 25 cm and the radius of the beads size is 1 cm, then $N = 20$ beads are needed to obtain the 10% coverage initially desired.

With the lights in the laboratory dimmed, turn on the light bulb and measure the length of the side of the area that is illuminated. Calculate the values of N needed for each of the bead sizes. Perform these calculations on the DATA SHEET.

Cover an additional 10% of the surface with these beads by doubling the number of beads you have placed on the surface. Repeat the three measurements of total intensity and intensity in the two polarizations. Continue adding beads and making measurements until you have covered about 70% of the surface. Enter these photometer readings of total intensity and the intensity in the two polarizations in the third through eighth rows of Table 3a of the DATA SHEET.

Remove the large beads from the surface. Place beads of intermediate size on the surface, again covering about 10% of the surface centered under the photometer

field with the smallest beads you have available. Count the number of beads that you have placed on the surface and enter the result in Table 4. Repeat the sequence of measurements that you made with the largest beads. Enter the photometer readings of total intensity and the intensity in the two polarizations in Table 3b of the DATA SHEET.

Remove those intermediate-sized beads and cover about 10% of the surface centered under the photometer field with the smallest beads you have available. Count the number of beads you have placed on the surface to achieve this 10% coverage and enter the result in Table 4. Repeat the sequence of measurements. As with the large and intermediate-sized beads, enter the photometer readings of total intensity and intensity in the two polarizations for the various levels of coverage. Enter these readings in Table 3c of the DATA SHEET.

D. Calculations and Analysis

1. Coefficients of Roughness

In Experiment #6, "The Surface Roughness of the Moon: Reflection and Scattering from a Planetary Surface: Part I. Surface Materials," we calculated coefficients of roughness from the curves of total reflected intensity as a function of angle of observation. These values were entered in Table 3a, etc. Using the results for the sizes of the sand, pea gravel, and stones, construct a graph of those coefficients of roughness, C, as a function of particle size. Draw a smooth curve through the three data points. Because of the large number of graphs we will be constructing, we will enumerate the graphs. They are all found on the DATA SHEET following Table 7. This is Graph 1 on the DATA SHEET.

2. Bead Reflection Enhancement

We placed three sizes of beads on the surface to cover, in turn, 10–70% of it. Calculate the degree of polarization by Eq. (4) of Experiment #6, "The Surface Roughness of the Moon: Reflection and Scattering from a Planetary Surface: Part I. Surface Materials," and enter the respective results in the right-hand column of Tables 3a, 3b, and 3c.

Construct a graph of the degree of polarization as a function of bead surface coverage for each bead size. Because only seven data points have been produced for each bead size, you should be able to plot these values on the same graph. Clearly distinguish which points represent the results for each bead size by using different symbols. Those frequently used include a filled-in circle, a cross (+), a triangle, or a dot in the center of a circle. This is Graph 2 on the DATA SHEET. If plotting all three on the same graph makes it overly cluttered, then graph each separately. Draw

a smooth line between each set of seven data points. These graphs indicate how the degrees of polarization vary with the presence of the different sized beads.

In addition to creating polarized reflected light, the beads should also increase the amount of reflected light compared to the amount reflected from the surface with no beads. You have provided the latter results in the first rows of Tables 3a, 3b, and 3c. Calculate the percentage increases in reflected intensity for each bead size in total intensity and the two polarization components. Perform your calculation on the DATA SHEET and enter your results in Tables 5a, 5b, and 5c, which correspond to the three sizes of beads used. Henceforth, we will refer to these percentage increases as "enhanced" intensities, either enhanced total intensities or enhanced intensities in the two polarizations.

Construct a graph of percentage increases in the intensities from Table 5a, etc., as a function of bead surface coverage for each bead size. On each of the three graphs, graph the enhanced total intensity as well as the enhanced intensities in the two polarizations. As with the graph of the degree of polarization, because only seven data points have been produced for each bead size, you should be able to plot these values on the same graph. Clearly distinguish which points represent the results for the enhanced total and enhanced intensities in the two polarization components by using different symbols. This is Graph #3 on the DATA SHEET. If plotting the enhanced total intensity and the enhanced intensities in the two polarization components on the same graph makes it overly cluttered, then graph each separately. Draw a smooth line between each set of seven data points. These graphs indicate how the intensities of reflected light increase with the presence of the beads.

3. Bead Surface Coverage on the Lunar Surface

The presence of small glass beads on the lunar surface are considered the cause of the 30% enhanced reflection observed by the Apollo astronauts at the subsolar point over that observed on Earth from the sub-Earth point during any full Moon. Our experimental data enable us to estimate the percentage coverage of the lunar surface by such beads.

To do this, we construct additional graphs of the data for enhanced total intensity corresponding to the various percentages of bead coverage. For ease of comparison and plotting, copy the data from Table 5 into Table 6. This will provide a summary of the measurements for each bead side. Copy the measurements in the second column of Table 5a into the second column of Table 6, the measurements in the second column of Table 5b into the third column of Table 6, and the measurements in the second column of Table 5c into the last column of Table 6. Calculate the logarithms to base 10 of the square of the bead sizes and enter those results in the third row of Table 6 of the DATA SHEET.

Construct a graph of the enhanced total intensity from Table 6 as a function of the logarithm of the square of the bead size. Four graphs are provided. Plot the data for 10% and 20% bead surface coverage on Graph 4a, the data for 30% and 40%

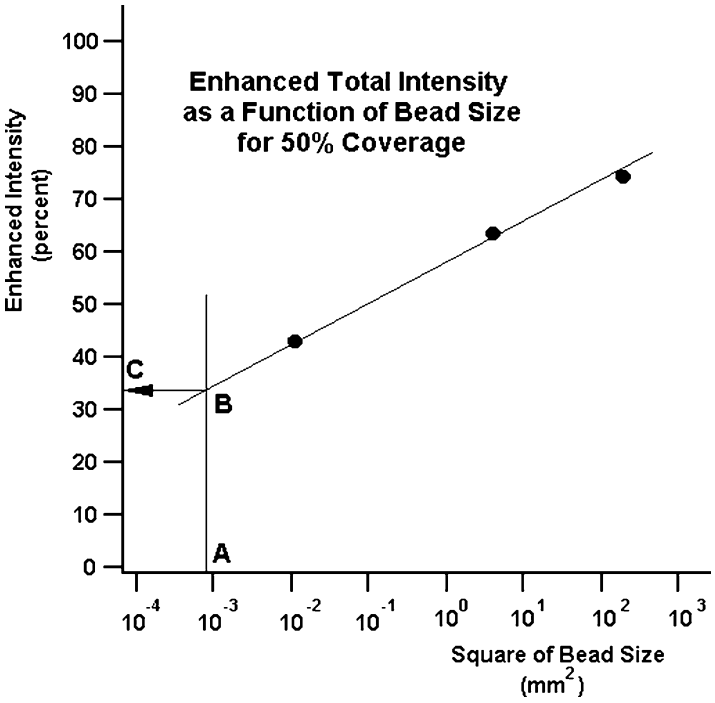

Fig. 2 Hypothetical results for enhanced total intensity as a function of bead size for bead coverage of 50%. The analysis allows determination of the enhanced intensity expected from 50% coverage of the 0.03 mm-sized glass beads found on the lunar surface. This datum is used in Figure 3

bead coverage on Graph 4b, the data for 50% and 60% bead coverage on Graph 4c, and the data for 70% bead coverage on Graph 4d. These all appear on the DATA SHEET. We use the square of the bead size because that is a measure of the area of the bead from which the incident light will be reflected. We use the logarithm because the range of abscissa will be several orders of magnitude. Although this is much smaller than the smallest bead size, extend the abscissa scale down to 1×10^{-4} mm^2, the square of 0.01 mm. Construct the graph with an abscissa range from 1×10^{-4} to 10^3 mm^2.

Plot three points corresponding to the three bead sizes. Draw a smooth curve through those three points and extrapolate the curve through 9×10^{-4} mm^2. This corresponds to the 0.03 mm size of the glass beads that the Apollo astronauts discovered on the lunar surface. On these four graphs, we plot only the total enhanced intensity. That is what the astronauts estimated while on the lunar surface.

Figure 2 shows the expected appearance of your graph. Each of the four graphs should look generally like this hypothetical example.

Draw a vertical line at the abscissa position of 9×10^{-4} mm^2, labeled point A in the hypothetical graph. This corresponds to the 0.03 mm size of the lunar glass beads. That vertical line will intercept the curve you have drawn, at point B in the

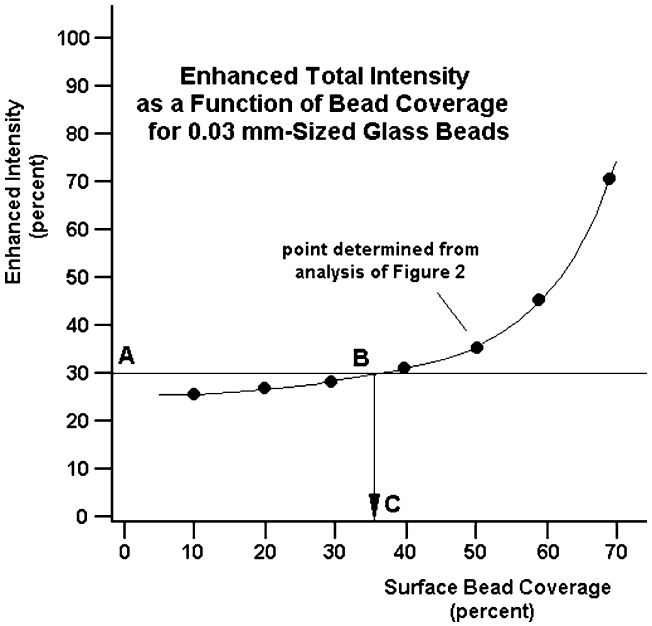

Fig. 3 Hypothetical results for enhanced total intensity as a function of surface bead coverage for 0.03 mm-sized glass beads. Knowing that reflection from the subsolar point is enhanced by 30% by the presence of these beads, we can determine the percentage of the actual lunar surface covered by them

hypothetical graph. Draw a horizontal line from point A to the ordinate axis, intersecting the ordinate axis at point C. Read the value off the ordinate axis and enter it into Table 7. These graphs, based on hypothetical data, would have told us that with a 50% coverage, the size of the glass beads found on the lunar surface will enhance the total intensity of the reflected light by about 35%. This example is provided to guide you only; do not take it as an indication of what your actual results will be.

After the construction of these graphs for each percentage of coverage, from 10% to 70%, you will have seven data points for the total intensity enhancement. Next, we will construct a graph of these seven points. It is a graph of the enhanced total intensity as a function of the percentage of coverage, but now for the 0.03 mm size glass beads. Note, that we wouldn't have to perform these graphing chores if we in fact had 0.03 mm glass beads available. This is Graph 5 on the DATA SHEET.

Your result will look something like Fig. 3. Draw a smooth curve through the points. Now, similar to the exercise with Fig. 2, we know that the enhanced reflection from the lunar surface is about 30%. Draw a horizontal line from the ordinate scale at the 30% enhancement level, point A. That line will intercept the curve, at point B. Draw a vertical line from point B to where it intercepts the abscissa axis, at point C. That yields the percentage of the surface that is covered

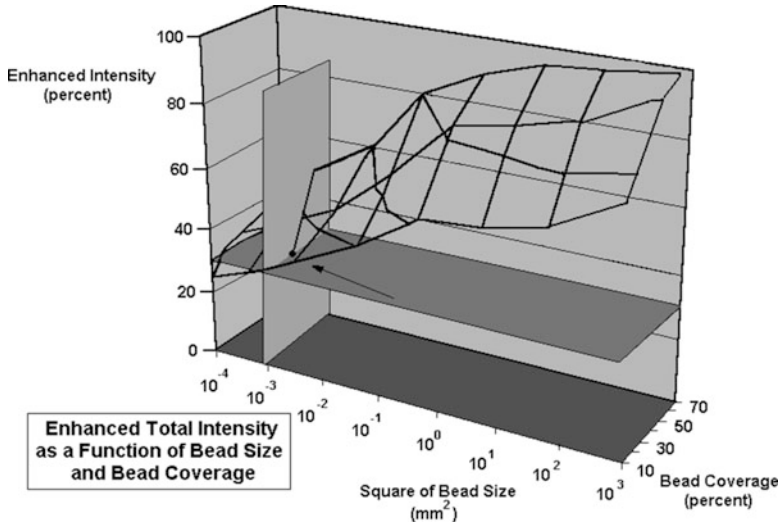

Fig. 4 The analysis described in the text to determine the surface coverage of 0.03 mm-sized glass beams to yield a 30% subsolar enhanced reflection from the Moon can be performed using a two-dimensional representation of a three-dimensional graph. The measurements will define an irregularly-shaped plane in the 3-d space. The intersection of that plane with a vertical plane located at 9×10^{-4} mm^2 and a horizontal plane located at 30% will define a point. The mutual intersection point is shown by the *arrow*. The value of that point on the "bead coverage" abscissa scale is the percentage coverage of the 0.03 mm-sized beads on the lunar surface. The hypothetical data shown here would yield a result of about 34%. This determination is highly dependent on the model and various assumptions

with 0.03 mm size beads to provide the 30% enhancement level observed by the Apollo astronauts. Enter that result for the enhanced total intensity on the DATA SHEET. For example, in the hypothetical example, we have found that on the average 36% of the lunar surface is covered by the 0.03 mm-sized beads.

To provide some insight into this analysis, note that we could have performed the analysis with a two-dimensional representation of a three-dimensional graph. (The results would likely have been less precise). We would plot the enhanced intensities as a function of both the bead size and percentage of coverage and then construct intersecting planes corresponding to the 0.03 mm size of the glass beads found on the Moon and the 30% enhancement observed at the subsolar point. Figure 4 displays an example of how this analysis would be performed. In practice, astronomers would perform the analysis numerically by a least squares fit.

STUDENT'S NAME _____

E. Surface Roughness Experiment II Data Sheets

Table 1 Particle sizes of soil sample material

	Sand	Pebbles or pea gravel	Stones: large diameter	Stones: small diameter	All stones: average diameter
Soil sample	Particle size (mm)	Particle size (mm)	Particle size (mm)	Particle size (mm)	Particle size (mm)
1					
2					
3					
4					
5					
Average					

Calculation of average particle size

Sand:

Pebbles or Pea Gravel:

Stones:

STUDENT'S NAME _____

Table 2 Bead particle sizes

Bead	Large size	Intermediate size	Small size
Particle size (mm)			
1			
2			
3			
4			
5			
Average			

Calculation of average bead size

Large:

Intermediate:

Small:

STUDENT'S NAME _____

Table 3a Photometer intensity readings at 0° angle of observation (material: sand with large beads)

Soil sample coverage	Total reflection	"Horizontal" polarization	"Vertical" polarization	Degree of polarization
Without beads				
10% bead coverage				
20% bead coverage				
30% bead coverage				
40% bead coverage				
50% bead coverage				
60% bead coverage				
70% bead coverage				

Table 3b Photometer intensity readings at 0° angle of observation (material: sand with intermediate size beads)

Soil sample coverage	Total reflection	"Horizontal" polarization	"Vertical" polarization	Degree of polarization
Without beads				
10% bead coverage				
20% bead coverage				
30% bead coverage				
40% bead coverage				
50% bead coverage				
60% bead coverage				
70% bead coverage				

STUDENT'S NAME _____

Table 3c Photometer intensity readings at 0° angle of observation (material: sand with Intermediate-Sized beads)

Soil sample coverage	Total reflection	"Horizontal" polarization	"Vertical" polarization	Degree of polarization
Without beads				
10% bead coverage				
20% bead coverage				
30% bead coverage				
40% bead coverage				
50% bead coverage				
60% bead coverage				
70% bead coverage				

STUDENT'S NAME _____

Table 4 Number of beads of different sizes (needed to cover 10% of experimental surface)

Beads	Number, N, to cover 10% of surface
Large	
Intermediate size	
Small	

Calculate the number N of beads needed from (1) here.

Size of Illuminated area L = _____

N for large beads:

N_{large} = _____

N for intermediate-sized beads:

$N_{intermediate}$ = _____

N for small beads:

N_{small} = _____

STUDENT'S NAME _____

Table 5a Analysis of bead photometer intensity readings (ratio of intensities with and without beads on surface) (material: sand with large beads

Soil sample coverage	% increase total intensity	% increase "horizontal" polarizations	% increase "vertical" polarizations
Without beads			
10% bead coverage			
20% bead coverage			
30% bead coverage			
40% bead coverage			
50% bead coverage			
60% bead coverage			
70% bead coverage			

Calculations of % Increases; Large Beads

STUDENT'S NAME _____

Table 5b Analysis of bead photometer intensity readings (ratio of intensities with and without beads on surface) (material: sand with Intermediate-Sized beads)

Soil sample coverage	% increase total intensity	% increase "horizontal" polarizations	% increase "vertical" polarizations
Without beads			
10% bead coverage			
20% bead coverage			
30% bead coverage			
40% bead coverage			
50% bead coverage			
60% bead coverage			
70% bead coverage			

Calculations of % Increases; Intermediate Size Beads

STUDENT'S NAME _____

Table 5c Analysis of bead photometer intensity readings (ratio of intensities with and without beads on surface) (material: sand with small beads)

Soil sample	% increase total intensity	% increase "horizontal" polarizations	% increase "vertical" polarizations
Soil sample coverage			
10% bead coverage			
20% bead coverage			
30% bead coverage			
40% bead coverage			
50% bead coverage			
60% bead coverage			
70% bead coverage			

Calculations of % Increases; Intermediate-Sized Beads

STUDENT'S NAME _____

Table 6 Summary of enhanced total intensity measurements from Table 5

Bead	Small	Intermediate	Large
Bead size (mm)			
Bead size squared (mm^2)			
Log (bead size squared)			
Soil sample coverage			
10% bead coverage			
20% bead coverage			
30% bead coverage			
40% bead coverage			
50% bead coverage			
60% bead coverage			
70% bead coverage			

Table 7 Enhanced total intensity results for extrapolated 0.03 mm size beads

Soil sample coverage	Intensity
10% bead coverage	
20% bead coverage	
30% bead coverage	
40% bead coverage	
50% bead coverage	
60% bead coverage	
70% bead coverage	

STUDENT'S NAME _____

Graph 1 Coefficients of roughness as a function of particle size

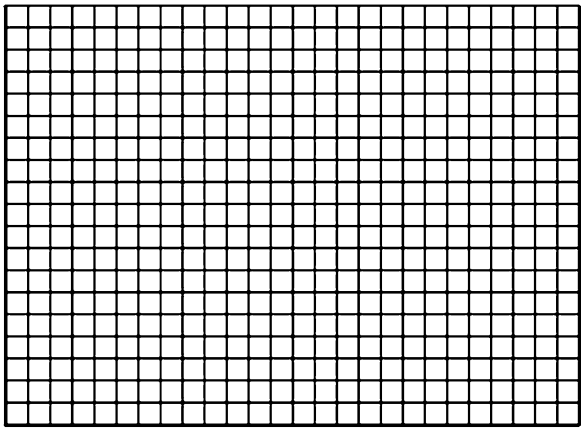

Graph 2 Degree of polarization as a function of bead coverage

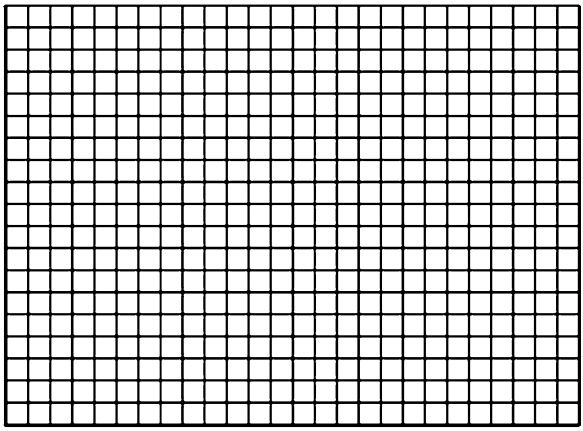

Graph 3a Increases in enhanced intensities as a function of bead coverage for small beads

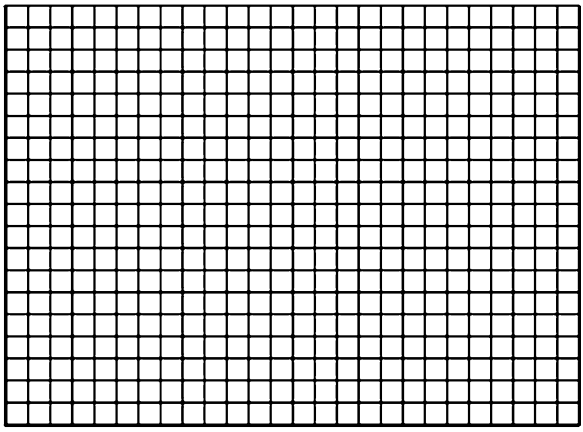

STUDENT'S NAME _____

Graph 3b Increases in enhanced intensities as a function of bead coverage for intermediate-sized beads

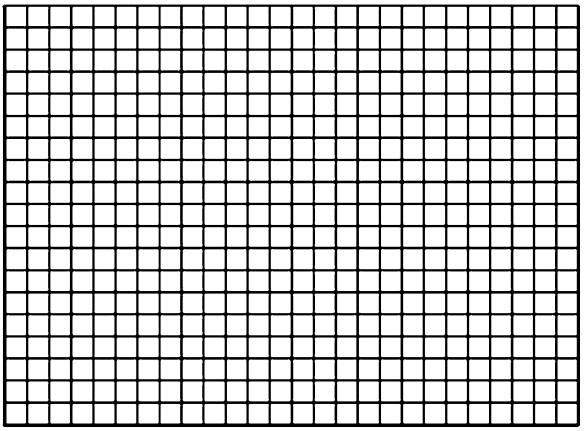

Graph 3c Increases in enhanced intensities as a function of bead coverage for large beads

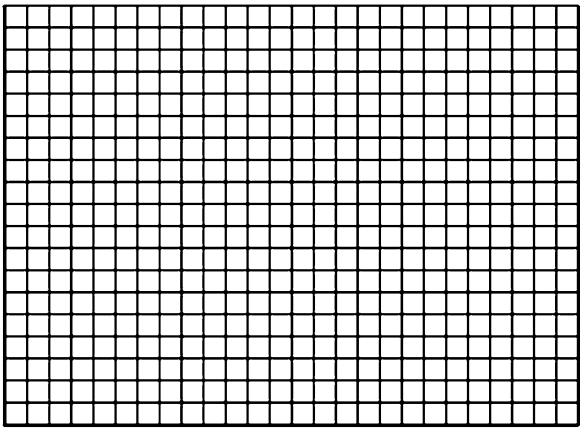

STUDENT'S NAME _____

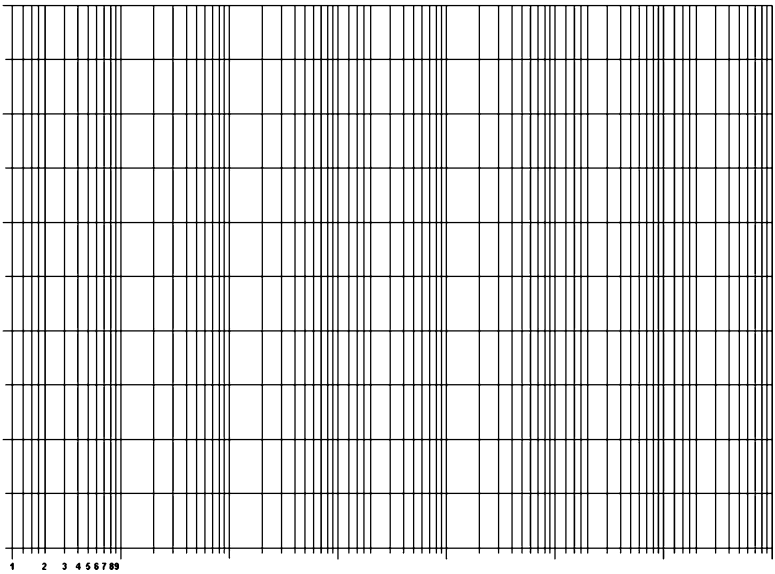

Graph 4a Enhanced intensities as a function of square of the bead size for 10% and 20% coverage

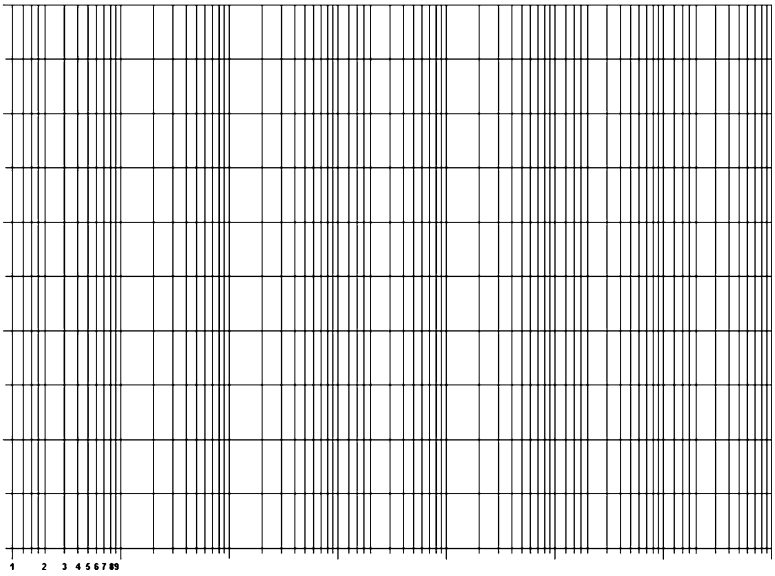

Graph 4b Enhanced intensities as a function of square of the bead size for 30% and 40% coverage

STUDENT'S NAME _____

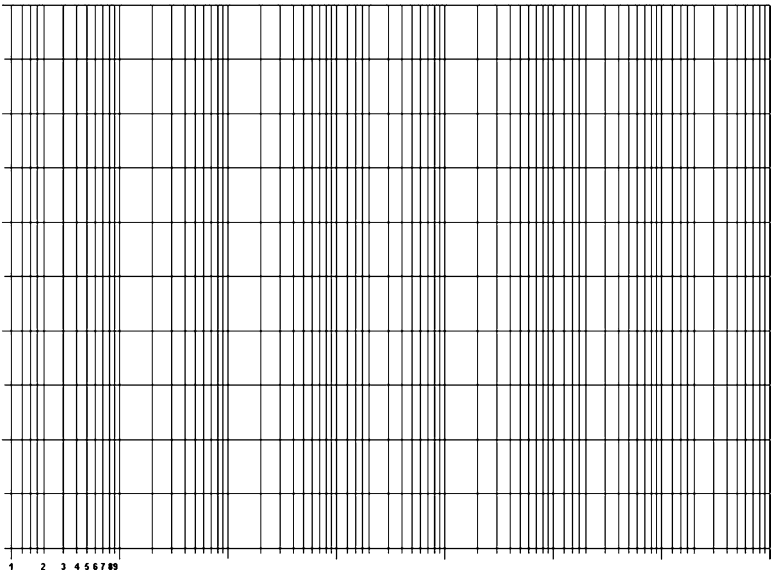

Graph 4c Enhanced intensities as a function of square of the bead size for 50% and 60% coverage

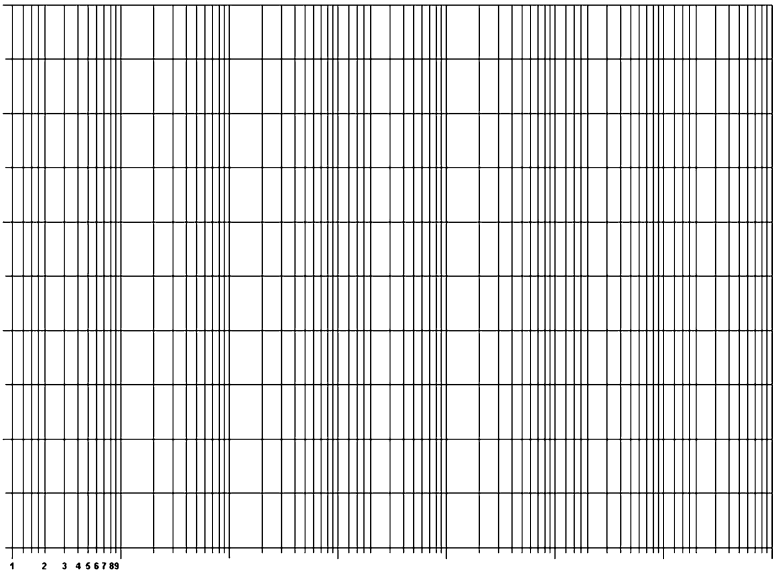

Graph 4d Enhanced intensities as a function of square of the bead size for 70% coverage

STUDENT'S NAME _____

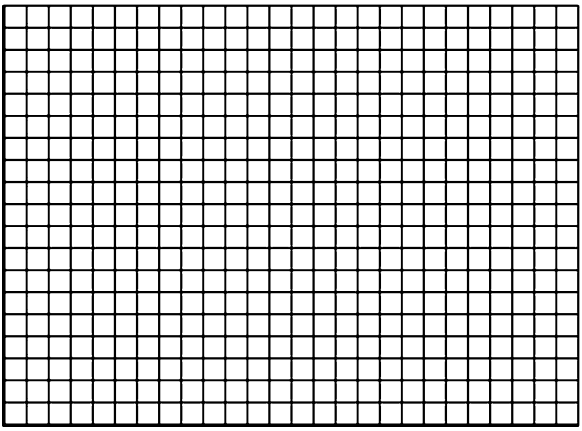

Graph 5 Enhanced intensities as a function of bead coverage for 0.03 mm size beads

F. Surface Roughness Experiment Discussion Questions

1. The surface of the Moon is close to being a Lambert surface, with the exception of enhanced reflectivity at the subsolar point and enhanced reflectivity near the limb. Accordingly, if we calculate the coefficient of roughness was calculated for the Moon, it would be close to 1.0. (We ignore the enhanced reflections resulting from the presence of the glass beads.) Based on the graph you constructed from the calculated values of C for sand, pebbles or pea gravel, and stones, what would material would you consider as being the dominant constituent of the lunar surface, or would a combination of materials be indicated? Explain your answer.

2. The enhanced reflections from the 0.03 mm-sized glass beads on the Moon result from specular reflection. By examining the percentage increases for the total intensity compared to those for the two polarized components on the graphs you constructed from the data of Table 5, what can you say about the type of radiation that results from specular reflection of unpolarized light? Explain your answer.

STUDENT'S NAME _____

3. Experiments #6 and #7, "The Surface Roughness of the Moon: Reflection and Scattering from a Planetary Surface: Part I. Surface Materials," and "The Surface Roughness of the Moon: Reflection and Scattering from a Planetary Surface: Part II. Beads and Surface Coverage," introduced a model for the reflection of light from the Moon and planetary surfaces. Of the various characteristics of the surface soil, only the roughness was considered. That was explicitly stated. In Experiment #7, "The Surface Roughness of the Moon: Reflection and Scattering from a Planetary Surface: Part II. Beads and Surface Coverage," we used that model to determine the percentage of coverage of the lunar surface with 0.03 mm glass beads needed to provide an enhanced 30% subsolar reflection.

   a. Discuss the assumptions made in this analysis that were not explicitly stated.

   b. Which of the assumptions do you think are most likely to affect the accuracy of this determination of the glass bead coverage on the Moon?

4. Assume that you are observing the Moon at the infrared wavelength of 1 mm. Construct a smooth graph of the intensity of reflected light as a function of the angle of observation that you would expect for each of the three soil sample materials whose average particle sizes you calculated on the DATA SHEET. Refer to the discussion of scattering in Sect. B.1 of Experiment #6, "The Surface Roughness of the Moon: Reflection and Scattering from a Planetary Surface: Part I. Surface Materials," Fig. 9 of Experiment #6, "The Surface Roughness of the Moon: Reflection and Scattering from a Planetary Surface: Part I. Surface Materials," and the determination of average particle sizes that you tabulated in Table 1 in providing your graphical answer. On all the graphs in this and the next two questions, provide tick marks and identify the values of the intervals between appropriate tick marks on the axes.

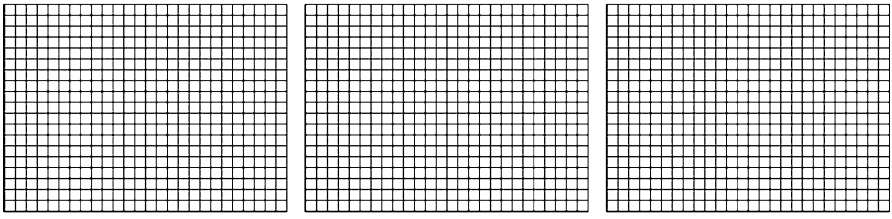

STUDENT'S NAME _____

5. Repeat question #4 for observations at the microwave radio wavelength of 5 cm.

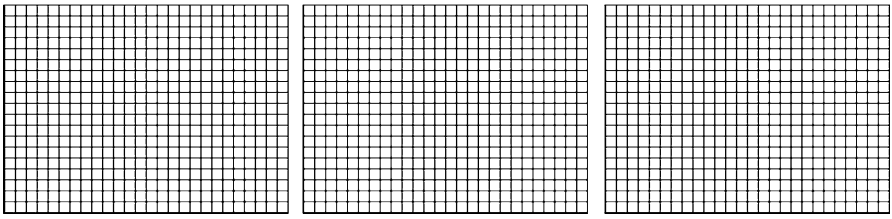

6. Repeat question #4 for observations at the FM radio wavelength of 1 m.

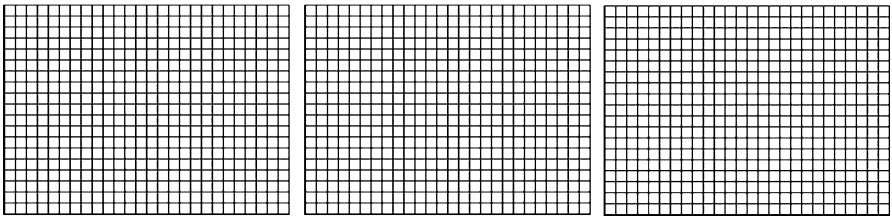

7. Using Fig. 1 of Experiment #6, "The Surface Roughness of the Moon: Reflection and Scattering from a Planetary Surface: Part I. Surface Materials," as a guide, show the appearances of the Moon as seen from the Earth as it revolves around the Earth if the Moon were a perfectly spherical mirror.

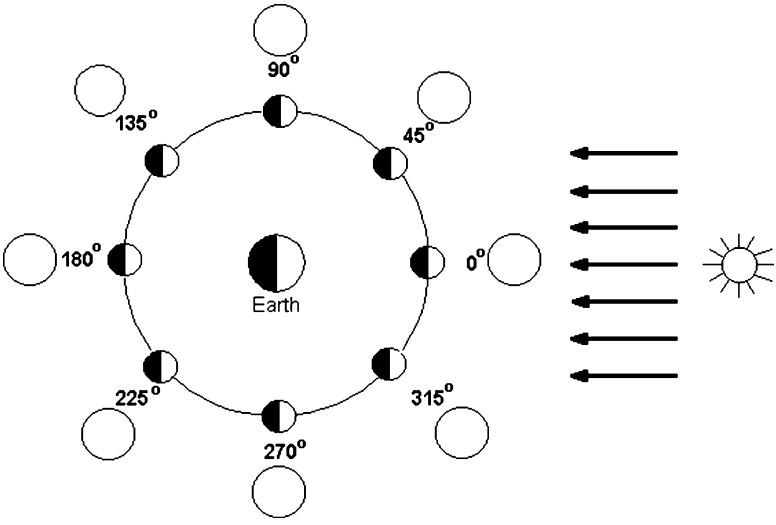

STUDENT'S NAME _____

8. Similarly, show the appearances of the Moon as seen from the Earth as it revolves around the Earth if the Moon was painted a non-reflecting black color.

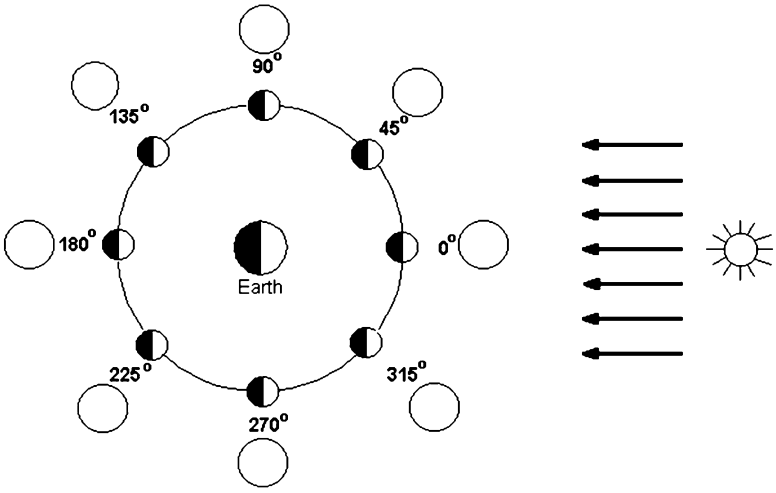

9. Figure 7 of Experiment #6, "The Surface Roughness of the Moon. Reflection and Scattering from a Planetary Surface: Part I. Surface Materials," presented the three-dimensional graph representing reflection from a Lambert surface. Below is the same graph "paper," but it is blank. Draw the graph that represents specular reflection.

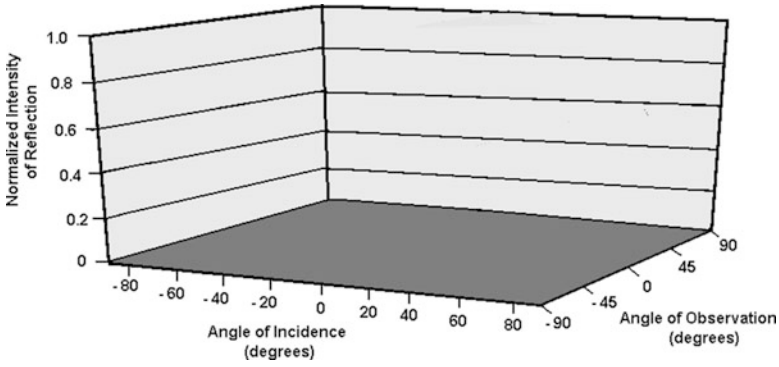

Removing these DATA SHEETS from the book may damage the binding. You might consider entering the data and performing your calculations in the book, and then photocopying the DATA SHEETS for submission to your instructor for grading.

If you used graph paper other than that provided, attach those graphs to these DATA SHEETS.

Experiment 8
The Formation of Impact Craters

SUMMARY: In Experiment #8, "The Formation of Impact Craters," we study how the kinetic energy of impacting objects form craters on the surfaces of Moons and planets. We drop projectiles onto various soil samples and measure the diameter of the crater and the height of the crater rims and then compare those measurements with the kinetic energy of the projectiles upon impact.

LEVEL OF DIFFICULTY: Low.

EQUIPMENT NEEDED: Sand boxes filled with dry fine sand, wet fine sand, and coarse sand; platform with graduated scale; baseball-sized objects such as tennis balls, baseballs, and wood and metal spheres; pole; straight edge; ruler; meter stick; mass-measuring scale; moderate-sized drinking glass or container.

MY LEARNING GOALS

1. To be able to describe the physics governing the creation of the various features of an impact crater.
2. To be able to describe the conversion of kinetic energy of impact projectiles into various modes of energy within impact craters.
3. To be able to predict how soil structure influences the resulting morphology of the impact crater.

L.M. Golden, *Laboratory Experiments in Physics for Modern Astronomy: With Comprehensive Development of the Physical Principles*,
DOI 10.1007/978-1-4614-3311-8_8,

A. Introduction

The existence of craters on the surfaces of the Moon, planets, and their Moons has been known since 1610 when Galileo observed such features on the Moon. Indeed, that observation is one of those historic events that showed that the celestial objects were not perfect, not of divine origin, and that brought rationality into the study of natural phenomena. Figure 1 shows the famous Copernicus crater on the near side of the Moon, essentially the same as how Galileo saw it with his telescope but with greater resolution.

Craters are made in two ways, one by interior agents and the other by exterior agents. The former are created by volcanic eruptions. In these, the magma material is ejected and forms a shield of elevated material. A *caldera*, a crater created when the underlying lava withdraws and the surface subsides, often appears at the center. The Olympus Mons volcano on Mars, 700 km wide and 25 km (82,000 ft) high, displays such features. That the entire structure is above the level of the surrounding plains is one major means of establishing craters to be of volcanic origin, as shown in Fig. 2.

Fig. 1 Copernicus crater, one of the most prominent features on the near side of the Moon, is about 93 km wide and 3.8 km deep. It was formed about 800 million years ago by the impact of an object several kilometers in diameter. Ejecta created the prominent rim as well as the radial material, the so-called rays. The Apollo 12 astronauts collected samples from one of the rays coming from Copernicus. Note that all of the craters in the photo, no matter their size, are circular in shape, indicating origins by hypervelocity impacts. Knowing the latitude of Copernicus on the Moon and the position of the Sun enables determination of the height of the crater rim by measurement of the length of its shadow in comparison to the known diameter of the crater and use of the zenith angle equation

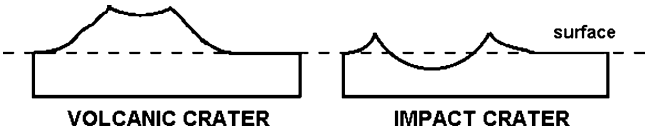

Fig. 2 Craters created by volcanic processes and impact events can be distinguished by their profiles. All of the former are elevated above the surrounding undisturbed surface. The bowl of impact craters will generally lie below the level of the surrounding surface. In some craters observed on the Moon and planets, the impact released fluid magma from below the surface and this volcanic material flooded the crater so that the bowl is in fact level with the surface

The majority of craters are created by the impact of exterior agents, meteoroids, from microscopic to many kilometers in size, and comets. In general, these objects when considered as creators of impact craters are referred to as *impactors*. Unless the angle of impact is very shallow, the craters so-formed are nearly circular. They often have a central peak, the result of the surface material being forced downwards into the subsurface and then pushed outwards by the increased pressure they experience by the compressed subsurface material.

These two types of craters have many features in common, which has historically led to debate on their origin. Both types of craters have ray systems. In volcanic craters, long trails of molten lava as well as explosively ejected rocks radiate from the crater. In impact craters, in comparison, ejected material forms streaks of material as well as trains of secondary or tertiary craters as fragmented material skips along the surface. Again, both types of craters are often seen aligned with others, but for different reasons. As compared to the trains of secondary and tertiary impact craters, volcanic craters can be found aligned on planets on which active molten interiors lead to continental drift. Volcanoes appear along the fault lines created by colliding plates. In addition, as the continents glide over the underlying mantle over geological time-scales, "hot spots" create a string of volcanoes. A well-known example is the Hawaiian Islands. A string of craters resulting from vulcanism can also be created by subsistence. An example of this is the system associated with crater Davy photographed by the Apollo 14 astronauts. When the lava that upwelled through linear faults in the surfaces cooled and the subsurface molten lava receded, the domes collapsed creating caldera-like features. Erosional processes such as settling under the force of gravity, impacts of subsequent smaller meteoroids, dust storms, or, on Earth, weathering, causes slumping of the material of the inner and outer slopes of the crater rims of both impact and volcanic craters.

In this experiment, we will simulate the creation of meteorite craters by dropping objects of various masses from various heights onto sand boxes containing different types of soil material. We will then compare the energy of impact of the object with the shape of the resulting crater. In this way we have in effect calibrated the impact process and can now examine other craters and determine the energy of the impactors which created them from the shape of the craters. We will also study whether excavation of the crater or ejection of its material dominates as the mode of crater formation and the effect of the density of the surface material on the crater shape.

B. Theory

1. Impact Energy

Analysis of photographs taken of the surfaces of the Moon, Mars, Mercury, and the moons of various planets along with laboratory hypervelocity impact studies inspired by such explorations, particularly those of the Moon, have led to an understanding of the process of impact crater formation. The theory is based on the conservation of energy.

The kinetic energy of the impacting projectile is transferred upon impact to the planetary or moon surface by pushing and lifting forces, heat transfer, and creation of sound and seismic waves, converting the energy into many forms. The projectile provides kinetic energy to the material of the crater, excavating it from the crater interior and expelling it as ejecta, forming the crater rim, the blanket of ejected material beyond the rim, and the rays of material beyond the ejecta blanket; internal energy to some of the material, deforming, fragmenting, pulverizing, melting, or vaporizing it; and kinetic energy of compression and rarefaction of subsurface material as sound or seismic waves. Of these various manifestations of the conversion of energy, the most easily measured in existing craters are the diameter of the crater and the height of the crater rim.

An estimate of the impact velocity that occurs on planets and moons in the solar system can be found by examining Kepler's laws, or simply taking the known orbital data which are consistent with Kepler's laws. For the Earth, for example, we know that the semi-major axis is $a = 1$ A.U. $= 1.50 \times 10^{11}$ m, and that the orbital period is $P = 356.3$ days. The velocity of the Earth in its orbit is therefore, after converting days to seconds, $2\pi a/P = 30$ km/s. This will be the velocity of objects in orbit at the distance of the Earth. As the object falls to the surface, it will gain an additional kinetic energy. The actual velocity upon impact will depend on the nature of the orbit of the impactor, which determines the angle at which it intercepts the Earth in its orbit. Roughly, the impact velocity of objects hitting the surfaces of objects in the solar system range from 5 to 50 km/s.

These high velocities explain the finding that nearly all impact craters are circular. In 1893, geologist G.K. Gilbert (1843–1918) was the first to suggest that the craters on the Moon resulted from large meteor impacts in the famous article in the *Bulletin of the Philosophical Society* entitled "The Moon's Face, A Study of the Origin of its Features." A major problem that opponents found with Gilbert's theory was the circular shape of lunar craters. Any objects impacting the lunar surface at an angle other than the exact vertical would have been expected, they claimed, to create oblong craters.

Realizing that the high velocity of impact leads to the creation of shock waves resolves this problem. The velocity of the impacting objects in so-called hypervelocity impacts is greater than the speed of sound of the surface material. The material, that is, cannot move aside out of the path of the speeding projectile and a shock wave is created in which the projectile, be it a meteoroid or comet, explodes

on impact at a depth which can be shown to be several projectile diameters below the surface. Instead of boring through the material and creating an oblong crater, the explosion creates a spherical shock wave resulting in a circular crater at the point of impact. Gilbert was right. Non-uniform geology of the surface material, not the angle of impact, causes any lack of circularity.

In our experiment, our projectiles (thankfully) do not attain these velocities. We can calculate the kinetic energy of the projectile on impact by conservation of energy. If the projectile has a mass m and is dropped at rest from a height H, then, with the surface of the soil sample as the reference for the gravitational potential energy, we have

$$\frac{1}{2}mv_i^2 = mgH, \tag{1}$$

where v_i is the velocity of impact, the height H is measured from the surface, and the acceleration of gravity g $= 9.8$ m/s^2. Falling from a height of 3 m, (1) provides the impact velocity as $v_i = \sqrt{2gH} = 7.7$ m/s. This is a factor of 4000 less than the velocity of actual solar system objects impacting the Earth and the Moon. In order to obtain a circular crater, in our experiment setup we therefore drop the projectile from directly above the sand box.

In our case, the conservation of energy is simplified. We do get conversion of the kinetic energy of the projectile into internal energy, but not in sufficient amounts to melt or vaporize the material. Waves are created in the subsurface material, but they contain much less energy than in hypervelocity impact events. As a result, a significantly larger amount of the kinetic energy of the impacting projectile results in excavation of the crater and creation of the crater rims and ejecta blanket than in the case of impacts on planetary and moon surfaces. The smaller the kinetic energy of the impacting projectile, the greater the relative amounts of energy converted to excavation and creation of the crater rim and ejecta blanket compared to conversion to internal energy.

2. *Mathematical Model of Crater Formation*

By ignoring all effects except excavation and ejection of material, we can create some simplified mathematical models of the process. In excavation, an amount of mass is dislodged from the surface essentially by a pushing force. For simplicity of the model, we take this pushing action to be free of heat gain or loss, that is, *adiabatic*. Because it is reasonable to assume that the depth of the crater will scale with the diameter of the crater, this amount of mass can be taken to be proportional to the density of the material and the cube of the diameter of the crater, D. The pushing force does work on the material in the crater, providing it kinetic energy until it comes to rest. The energy of impact E leading to the displacement of mass through the pushing force is thereby proportional to D^3.

In ejection, the material is provided kinetic energy which is converted into gravitational potential energy as the material is lifted and then is converted back to kinetic energy as the material falls back down to the surface. It is again reasonable to assume that the height to which the material is lifted to enable it to be ejected from the crater is proportional to the diameter of the crater. Matter, for example, must be ejected great distances to be ejected from large craters. In this case, then, we can model the amount of energy provided for ejection by mgH. The mass is proportional to the density of the material and D^3 and h is proportional to D, so that the total amount of energy converted in ejection is proportional to the density of the material and D^4.

Of course, both processes are active. In actual crater formation, large amounts of energy are converted to internal energy and waves as well.

Based on this simplified model of our laboratory experiment, we can write

$$D = a\,E^{1/3} + bE^{1/4}. \tag{2}$$

The coefficients a and b depend on various factors, including the density of the material.

If we were preparing a research paper, we would determine the values of these coefficients by a least-squares regression and thereby evaluate the relative importance of the two processes. By evaluating the coefficients a and b in this way we could determine which process, if either, dominates in the laboratory in the creation of the crater. Here we can try to take a short cut. We rewrite (2) as

$$D = a\,E^{1/3}\left(1 + k_1/E^{1/12}\right),$$

where $k_1 = b/a$. Taking the logarithm of both sides, we find

$$\log D = \log a + \frac{1}{3}\log E + \log\left(1 + k_1/E^{1/12}\right). \tag{3}$$

This tells us that the extent to which a plot of *log D* as a function of *log E* differs from a straight line with a slope of 1/3 indicates the importance of the ejection process in the energy balance. Now, for reasonable values of value of k_1, the third term will become small for large values of E. Rewriting (2) in this form will therefore not greatly aid us in discriminating between the two models. Instead we choose the less sophisticated procedure of simply graphing *log D* as a function of *log E,*

$$\log D = \log c_1 + n\ \log E, \tag{4}$$

and seeing if the slope n is closer to 1/3 or 1/4. We will then be able to write the *D (E)* relationship as

$$D(E) = c_1\,E^n. \tag{5}$$

Although we cannot determine the relative amounts of kinetic energy of the projectile that are converted to these modes compared to the internal energy and wave modes, we might expect that the relative importance would be similar in crater formation on moons and planetary surfaces. Whatever their relative importance, the total amount of energy converted to these modes is a lower limit to the total energy of the impacting projectile, other energies being converted into these internal energy and wave modes.

Similarly, we can study the relative importance of these two processes in the creation of the crater rim. Instead of (2), we have the corresponding equation for the height of the crater rim, h,

$$h = c\,E^{1/3} + d\,E^{1/4}.$$

As with the crater diameter analysis, we will graph $log\ h$ as a function of $log\ E$,

$$\log\ h = \log\ c_2 + m\ \log\ E, \tag{6}$$

and see if the slope m is closer to 1/3 or 1/4. We will then be able to write the relationship as

$$h(E) = c_2\,E^m. \tag{7}$$

It is altogether possible that the two processes differ in importance in creation of the crater bowl itself and the crater rim. After all, it makes sense that formation of the crater bowl would be dominated by the pushing force of excavation whereas formation of the crater rim would be dominated by the lifting force of ejection. You will examine such considerations in this experiment.

The density of the surface material will also affect the morphology of the resulting crater. The force created by the shock wave or, in our experiment, the subsonic impact, depends only on the impacting body. The more dense the affected volume of surface material the more inertia it will present to being dislodged. Simply by $F = ma$, the resulting acceleration of the ejected crater material will be inversely proportional to its mass.

We therefore examine the crater morphology resulting from the projectiles dropped into three different soil samples of different densities. These are dry fine sand, wet fine sand, and coarse sand.

3. *Measurable Crater Parameters*

Although we can readily determine the energy of impact of the falling object, we need to be able to identify that energy with some characteristic of the shape of the resulting crater. Of the many characteristics of the crater morphology, we can

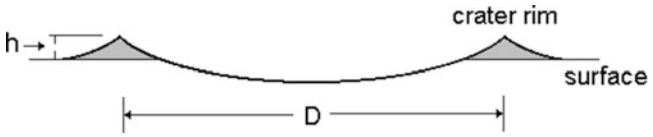

Fig. 3 We will relate the diameter of the crater and the height of the crater rim to the kinetic energy of the projectile upon impact

identify its depth, profile, diameter or radius, height of the crater rim, and maximum distance of ejected material. As on the planets and moons themselves, the most easily measured of these in our laboratory are the diameter of the crater and the maximum height of the crater rim, Fig. 3.

C. Procedure and Observations

Because in our experiment a shock wave is not created with the resultant vaporization of the projectile and violent ejection of surface material, we must choose projectiles with particular properties so that their kinetic energy is the only variable that determines the crater morphology. Our projectiles must, first, excavate substantially more material than simply the size of the projectile. Otherwise, our crater will simply be the size of the projectile. That means that the projectile must be substantially massive and must be dropped from a sufficiently large height. Following $E = mgH$, these conditions will ensure the projectiles obtain a large enough kinetic energy to excavate substantial material. To prevent the size of the projectile itself from influencing the results, it should be the much smaller than the dimensions, particularly depth, of the sand box. The density of the projectile material should be sufficiently great that air resistance does not slow the projectile in its fall, reducing its kinetic energy. Finally, to provide a wide range in the value of the impact kinetic energy, the projectiles should vary widely in mass and a wide range of heights from which they are dropped should be used.

If we vary the height of the drop from about 1/3 m, about 1 ft, to 3 m, we will have a range of about a factor of 10 in the drop height. If the masses of the projectiles vary by another factor of 10, we will have a sufficient range of a factor of one hundred for the projectile kinetic energies. If your laboratory does not have space for 3-m high platforms, a maximum height of 1 m will still provide an order of magnitude range in projectile kinetic energies.

Baseball-sized object such as tennis balls, cloth baseballs, league baseballs, or machined wood, aluminum, steel, or lead balls, all of the same size, will provide these attributes. Measure the diameter of each of the projectiles and enter the result in centimeters in Table 1 of the DATA SHEET. The diameters should be very nearly the same. Weigh each of the projectiles and enter the masses in grams in Table 1.

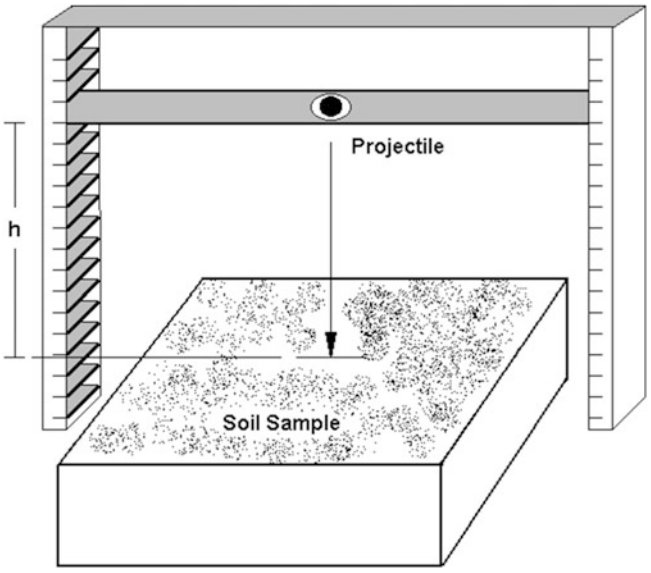

Fig. 4 The projectile is dropped from a hole in a platform that fits into slats attached to a graduated scale. Target sand boxes contain various soil samples. The height of the drop can be varied by moving the platform to slots at different heights

To determine the density of the three soil samples, we will compare the mass of a sample of given volume to that of water. Weigh a moderate-sized drinking glass or other container, and enter the result, m_c, in Table 2 of the DATA SHEET. Fill the glass with water, measure its mass using the scale, and enter the result, $m_c + m_w$, in Table 2. Similarly, fill the glass with each soil sample, measure their masses using the scale, and enter the results, $m_c + m_1$, $m_c + m_2$, and $m_c + m_3$, in Table 2.

We use an assembly such as depicted in Fig. 4 to provide accurate measurements of the height of the projectile drop. Beginning at a height of about 1/3 m, drop one of the projectiles onto the sand box containing the dry fine sand. If the excavation is simply the size of the projectile, the datum is not of value and you should drop the projectile from a greater height. Enter the type and mass of the projectile in columns 2 and 3 of Table 3a of the DATA SHEET and the height of the drop, H, in column 4 of Table 3a of the DATA SHEET. Note that the height of the drop must be reckoned to the layer of the soil sample not the base of the platform.

We now measure the diameter of the crater and the height of the crater rim. To measure the diameter of the crater, simply lay a pole, straight edge, or meter stick across the top of the crater rim and passing over the center of the crater. Do this twice, orienting the pole, straight edge, or meter stick along two different position angles along the circumference of the crater. Enter your results in columns 5 and 6 in Table 3a of the DATA SHEET. Your use of either a pole, straight edge, or meter stick depends on the actual diameter of the crater created.

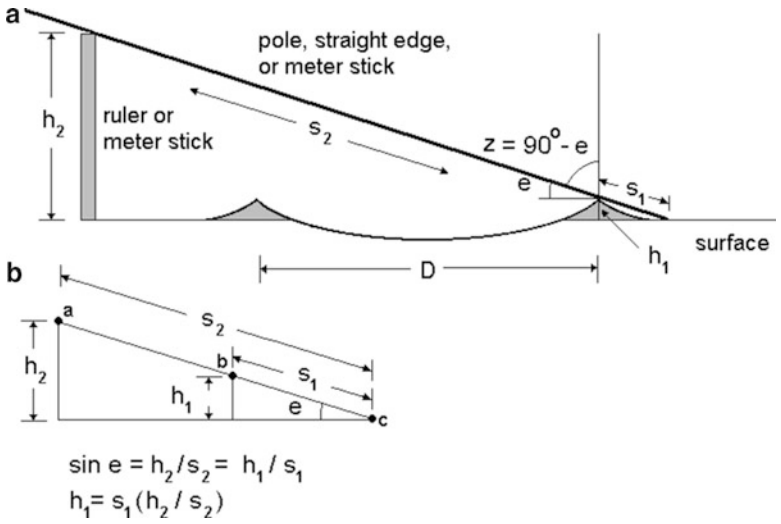

Fig. 5 The height of the crater rim, h_1, can be determined using similar triangles. As shown in part (**a**), the distance s_2 from the surface to the top of a ruler or meter stick is the length of the hypotenuse of the larger of two similar triangles. Part (**b**) displays the similar triangles. The elevation angle, e, is the complement of the zenith angle, z. If we identify s_2 as being measured along the path of a beam of light from the Sun which casts a shadow, this procedure simulates the technique by which heights of mountains and crater rims are determined on the moons and planets of the solar system

To measure the height of the crater rim, we could simply hold a meter stick perpendicular to the sand box. If the height is small, however, this technique could suffer from significant random errors. We could, alternatively, simulate the technique used to measure the heights of craters on the Moon, Mercury, and Mars, in which the length of the shadow cast by the Sun is measured. Here we would correspondingly measure the shadow that the crater rim casts when illuminated by a lamp with a narrow beam. This, too, however, may be subject to significant random errors. Instead, it is simpler to use a straight edge and the geometry of similar triangles.

The technique is illustrated in Fig. 5. Carefully place one end of a pole, straight edge, or meter stick so that it touches the surface of the sand box containing the dry fine sand at a point several inches beyond the crater rim. This is point *c* in Fig. 5b. With the elevated tip of the pole, straight edge, or meter stick pointing generally in the diametrically-opposed direction, rotate it slowly downward until it just touches the top of the crater rim. That point is point *b* in Fig. 5b. While you hold the pole, straight edge, or meter stick at that position, your lab partner should now move a ruler or meter stick, whichever is more appropriate depending on the height of the crater rim, under the far end of the pole, straight edge, or meter stick until it just makes contact. That point is point *a* in Fig. 5b. This completes a right triangle which is similar to the right triangle formed with the height of the crater rim as one side, as shown in Fig. 5.

The pole, straight edge, or meter stick and the surface of the sand box define an angle whose sine is proportional to the height of the crater rim. Measure the

distance, s_2, from point a to point c and enter the result in column 2 of Table 3b of the DATA SHEET. Measure the distance, s_1, from point b to point c and enter the result in column 5 of Table 3b of the DATA SHEET.

By lowering the pole or straight edge in the diametrically-opposed direction, as noted, you will obtain the largest possible values of s_1 and s_2, thereby reducing the percentage error in their measurements.

Lay the pole, straight edge, or meter stick across the crater rim at a second position along the circumference of the crater and repeat the measurements of s_1 and s_2. Enter those values in columns 3 and 6, respectively, of Table 3b of the DATA SHEET.

Remove the projectile from the sand box and smooth out the surface with a straight edge, raise the platform, and drop the projectile again from a greater height. Repeat the measurements at four or five heights and enter the results in Tables 3a and 3b.

Repeat this sequence of drops from various heights for the other projectiles, dropping them over the sand box containing dry fine sand. You need not use the same heights for each projectile, although you might find that convenient. Enter all results in Tables 3a and 3b.

Then repeat the sequence of measurements for each projectile dropped from different heights for the sand box filled with wet fine sand and the sand box filled with coarse sand. Enter these measurements in Tables 4a, etc., and 5a, etc., respectively, of the DATA SHEET.

As mentioned, using the lengths of shadows cast by the Sun is one method that is used to measure the heights of mountains and crater rims on the Moon, Mars, Mercury, and moons of other planets. Knowing the hour angle and declination of the Sun as observed from the object whose height is desired, and its latitude, the zenith angle equation, Eq. (2) of Experiment #5, "Earth: The Seasons and Local Latitude," is calculated. Then the trigonometry of Fig. 5 can provide the height of the crater or mountain.

D. Calculations and Analysis

The data entered in Table 2 of the DATA SHEET enable us to determine the densities of the three soil sample materials. Subtract the mass of the container, m_c, from the mass of the container holding the water, $m_c + m_w$, to obtain the mass of the water alone, m_w. Enter the result in column 6 of Table 2. Similarly, subtract the mass of the container, m_c, from the masses of the containers holding the three soil samples, $m_c + m_1, m_c + m_2, and\, m_c + m_3$, to obtain the masses of the three soil samples alone. Because we know that the density of water is 1 g/cc, the ratio of the masses of the soil samples to that of the water will yield the densities of the three soil samples, ρ_1, ρ_2, and ρ_3 . Perform those calculations and enter the results in columns 10 through 12 of Table 2 of the DATA SHEET. Show all your calculations on the DATA SHEET.

Calculate the average values of the two measurements each of crater diameter, D, length s_1, and length s_2 entered in columns 5 and 6 of Tables 3a, 4a, and 5a of the DATA SHEET for the three soil samples, respectively. Enter the results for the average crater

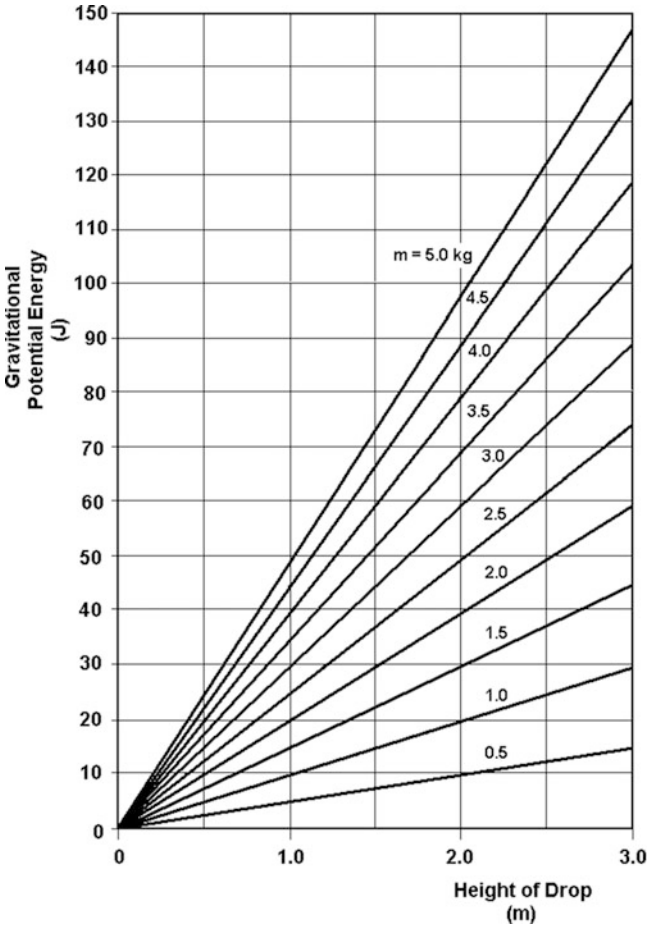

Fig. 6 The gravitational potential energy, mgH, of an object of mass m dropped from a height H is shown as a function of H, with m as a parameter. The *lines* represent the case for masses from 0.5 to 5.0 kg. The values for other heights or masses can be interpolated. Alternatively, (1) can be used directly. For purposes of entering the data in the tables of the DATA SHEET, 1 J = 107 ergs

diameter in column 7 of Tables 3a, 4a, and 5a. Enter the results for s_{2av} and s_{1av} in columns 4 and 7, respectively, of Tables 3b, 4b, and 5b of the DATA SHEET.

From the values of s_{1av}, h_2, and s_{2av} calculate the heights of the various crater rims by $h_1 = s_{1av}\, h_2 // s_{2av}$ and enter the results in column 8 of Tables 3b, 4b, and 5b for the three soil samples, respectively. Show all your calculations on the DATA SHEET.

From the values of m and H of each projectile as entered in Tables 3a, 4a, and 5a dropped onto the three soil samples, respectively, we can determine the energy of the projectile on impact. You can either calculate the kinetic energy of impact from (1) or use Fig. 6, which graphs mgH for various values of mass of the impacting

object and the height from which it is dropped. Enter the results in column 2 of Tables 6, 7, and 8 for the three soil samples, respectively. Show all your calculations on the DATA SHEET.

Henceforth, we will designate h, without the subscript, as the height of the crater rim. To graph $log\ D$ and $log\ h$ as a function of $log\ E$, you can either use the log-log graph paper that is provided on the DATA SHEET or you can use rectangular coordinate graph paper, in which case you will have to calculate the logarithms of D, h, and E. If you or your instructor chooses the latter, then calculate the logarithms of D, h, and E and enter the results in columns 3, 4, and 5 of Tables 6, 7, and 8 for the three soil samples, respectively.

Construct a graph of $log\ D$ as a function of $log\ E$ on your rectangular coordinate graph paper or on the log-log graph paper provided on the DATA SHEET. Use different symbols for each soil sample and draw a smooth curve through each set of data. Label the curves accordingly. If a straight line approximates the smooth curve well, determine its slope and y-intercept and then express the results as in (5). Show all your calculations on the DATA SHEET.

Similarly, construct a graph of $log\ h$ as a function of $log\ E$ on the graph provided on the DATA SHEET and, if a straight line approximates the smooth curve well, determine its slope and y-intercept and then express the results as in (7). Show all your calculations on the DATA SHEET.

With the slopes and y-intercepts determined, construct graphs of their values as a function of the density of the soil sample material. Using the graph paper provided on the DATA SHEET, plot the results for the y-intercepts using the left-hand ordinate scale and the results for the slopes using the right-hand ordinate scale. Construct two such graphs, one for the y-intercepts and slopes of the $log\ D - log\ E$ equation and one for the y-intercepts and slopes of the $log\ h - log\ E$ equation.

STUDENT'S NAME _____

E. Formation of Impact Craters Experiment Data Sheet

Length of ruler or meter stick, h_2 = _____ cm

Table 1 Projectile data

Projectile type	Diameter (cm)	Mass, m (g)

Table 2 Soil sample density measurements

m_C (g)	$m_C + m_W$ (g)	$m_C + m_1$ (g)	$m_C + m_2$ (g)	$m_C + m_3$ (g)	m_W (g)	m_1 (g)	m_2 (g)	m_3 (g)	$\rho_1 = m_1/m_W$ (g/cc)	$\rho_2 = m_2/m_W$ (g/cc)	$\rho_3 = m_3/m_W$ (g/cc)

Calculations of density of soil sample material:

STUDENT'S NAME _____

Table 3a Projectile impact for dry fine sand: crater diameter

Expt. number	Projectile type	Mass m (g)	Height of drop, H (cm)	Measurement #1 of crater diameter, D (cm)	Measurement #2 of crater diameter, D (cm)	Average, D_{av} (cm)
1						
2						
3						
4						
5						
6						
7						
8						
9						
10						
11						
12						
13						
14						
15						

STUDENT'S NAME _____

Table 3b Projectile impact for dry fine sand: height of crater rim

Expt. number	Measurement #1 of length s_2 (cm)	Measurement #2 of length s_2 (cm)	Average length s_{2av} (cm)	Measurement #1 of length s_1 (cm)	Measurement #2 of length s_1 (cm)	Average length s_{1av} (cm)	Crater rim height $h_1 = s_{1av}h_2/s_{2av}$
1							
2							
3							
4							
5							
6							
7							
8							
9							
10							
11							
12							
13							
14							
15							

STUDENT'S NAME _____

Table 4a Projectile impact for wet fine sand: crater diameter

Expt. number	Projectile type	Mass m (g)	Height of drop, H (cm)	Measurement #1 of crater diameter, D (cm)	Measurement #2 of crater diameter, D (cm)	Average, D_{av} (cm)
1						
2						
3						
4						
5						
6						
7						
8						
9						
10						
11						
12						
13						
14						
15						

STUDENT'S NAME _____

Table 4b Projectile impact for wet fine sand: height of crater rim

Expt. number	Measurement #1 of length s_2 (cm)	Measurement #2 of length s_2 (cm)	Average length s_{2av} (cm)	Measurement #1 of length s_1 (cm)	Measurement #2 of length s_1 (cm)	Average length s_{1av} (cm)	Crater rim height $h_1 = s_{1av}\, h_2/s_{2av}$
1							
2							
3							
4							
5							
6							
7							
8							
9							
10							
11							
12							
13							
14							
15							

STUDENT'S NAME _____

Table 5a Projectile impact for coarse sand: crater diameter

Expt. number	Projectile type	Mass, m (g)	Height of drop, H (cm)	Measurement #1 of crater diameter, D (cm)	Measurement #2 of crater diameter, D (cm)	Average, D_{av} (cm)
1						
2						
3						
4						
5						
6						
7						
8						
9						
10						
11						
12						
13						
14						
15						

STUDENT'S NAME _____

Table 5b Projectile impact for coarse sand: height of crater rim

Expt. number	Measurement #1 of length s_2 (cm)	Measurement #2 of length s_2 (cm)	Average length s_{2av} (cm)	Measurement #1 of length s_1 (cm)	Measurement #2 of length s_1 (cm)	Average length s_{1av} (cm)	Crater rim height $h_1 = s_{1av}$ h_2/s_{2av}
1							
2							
3							
4							
5							
6							
7							
8							
9							
10							
11							
12							
13							
14							
15							

STUDENT'S NAME _____

Calculations of height of crater rim for dry fine sand:

Calculations of height of crater rim for wet fine sand:

Calculations of height of crater rim for coarse sand:

STUDENT'S NAME _____

You need only fill in columns 3, 4, and 5 of Tables 6 through 8 if you choose to plot the data on rectangular coordinate graph paper. If you use the log-log graph paper provided below, then only fill in column 1 of these tables.

Table 6 Logarithmic data for dry fine sand

Experiment number	Impact energy, E = mgH (ergs)	log D[a]	log h[a]	log E[a]
1				
2				
3				
4				
5				
6				
7				
8				
9				
10				
11				
12				
13				
14				
15				

[a]You need fill in these columns only if you're using rectangular graph paper

Calculations of impact energy for dry fine sand:

STUDENT'S NAME _____

Table 7 Logarithmic data for wet fine sand

Experiment number	Impact energy, E = mgH (ergs)	log D[a]	log h[a]	log E[a]
1				
2				
3				
4				
5				
6				
7				
8				
9				
10				
11				
12				
13				
14				
15				

[a]You need fill in these columns only if you're using rectangular graph paper

Calculations of impact energy for wet fine sand:

STUDENT'S NAME _____

Table 8 Logarithmic data for coarse sand

Experiment number	Impact energy, E = mgH (ergs)	log D[a]	log h[a]	log E[a]
1				
2				
3				
4				
5				
6				
7				
8				
9				
10				
11				
12				
13				
14				
15				

[a]You need fill in these columns only if you're using rectangular graph paper

Calculations of impact energy for coarse sand:

STUDENT'S NAME _____

Whether you use rectangular graph paper or the log-log sheet below, label the axes and plot the crater diameter as a function of impact energy. If you use your own rectangular graph paper, graph the data of Tables 6 through 8 for the three soil samples, respectively. If you use the log-log graph paper below, graph the values of Tables 3a through 5a for the three soil samples, respectively. Use different symbols for each type of soil. Draw a smooth curve through each set of data and label the corresponding curves accordingly. If the curves are close to a straight line, determine the slopes and y-intercepts, and write the result in the form of (5). Show all your calculations here.

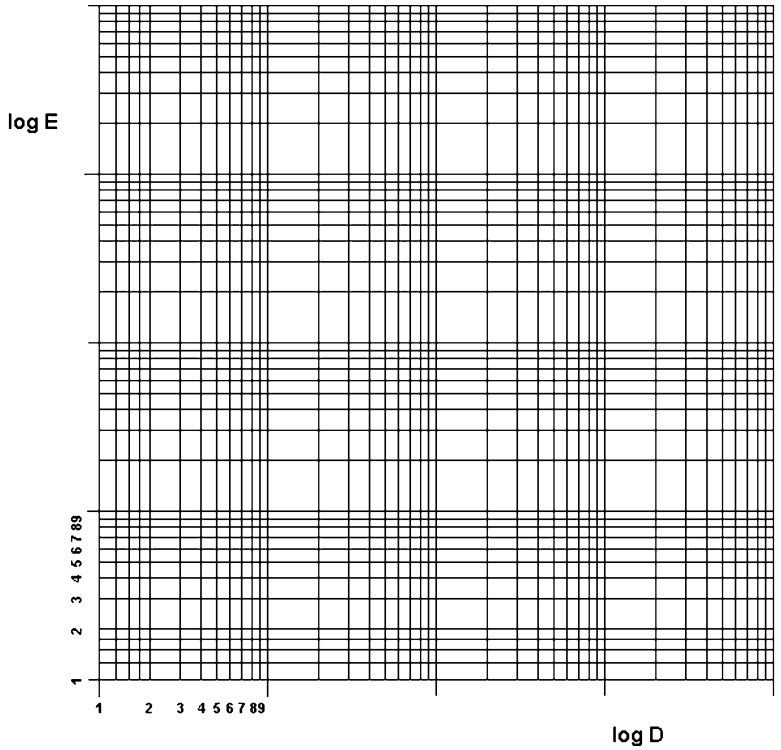

Log of crater diameter, D, as a function of impact kinetic energy of projectile, E

Dry fine sand, calculation of slope:

Slope = _____

y-intercept = _____

Equation: _____

STUDENT'S NAME _____

Wet fine sand, calculation of slope:

Slope = _____

y-intercept = _____

Equation: _____

Coarse sand, calculation of slope:

Slope = _____

y-intercept = _____

Equation: _____

STUDENT'S NAME _____

Whether you use rectangular graph paper or the log-log sheet below, label the axes and plot the height of the crater rim as a function of impact energy. If you use your own rectangular graph paper, graph the data of Tables 6 through 8 for the three soil samples, respectively. If you use the log-log graph paper below, graph the values of Tables 3b through 5b for the three soil samples, respectively. Use different symbols for each type of soil. Draw a smooth curve through each set of data and label the corresponding curves accordingly. If the curves are close to a straight line, determine the slopes and *y*-intercepts, and write the result in the form of (7). Show all your calculations here.

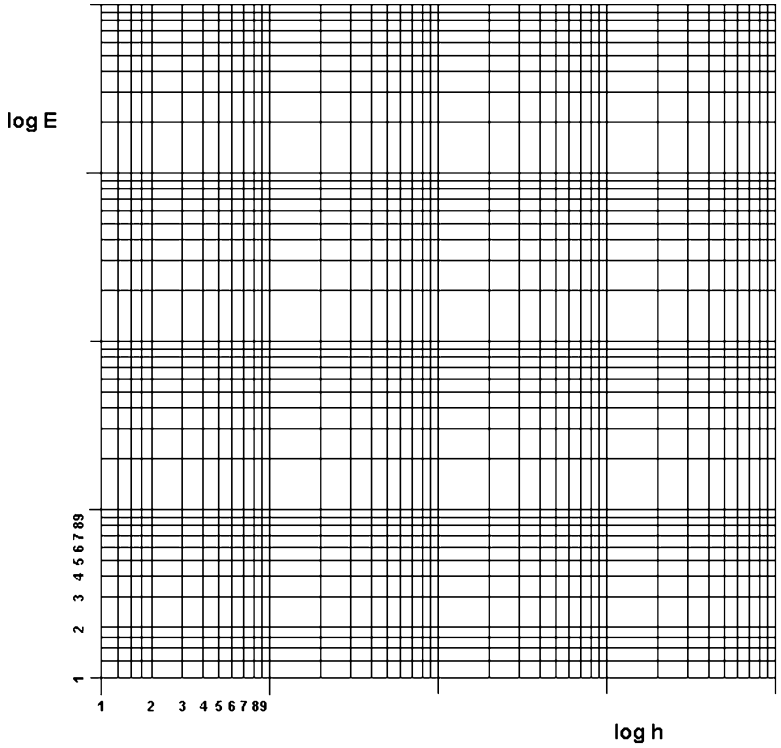

Log of height of crater rim, *h*, as a function of impact kinetic energy of projectile, *E*

Dry fine sand, calculation of slope:

Slope = _____

y-intercept = _____

Equation: _____

STUDENT'S NAME _____

Wet fine sand, calculation of slope:

Slope = _____

y-intercept = _____

Equation: _____

Coarse sand, calculation of slope:

Slope = _____

y-intercept = _____

Equation: _____

STUDENT'S NAME _____

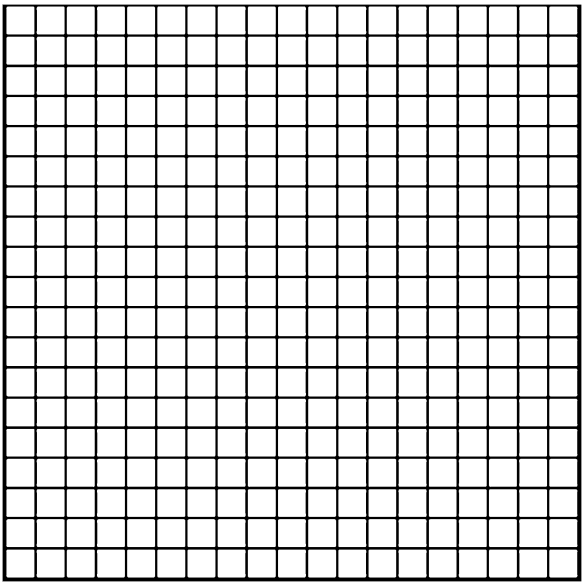

Graph of *y*-intercept and slope of the equations of *log D* as a function of *log E* for the three soil samples as a function of the density of the soil samples. Use different symbols to represent the two variables.

Describe and explain any systematic variation that you find.

STUDENT'S NAME _____

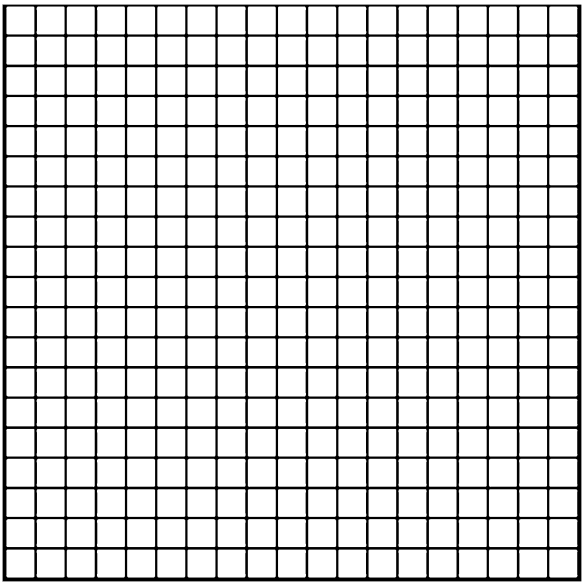

Graph of *y*-intercept and slope of the equations of *log h* as a function of *log E* for the three soil samples as a function of the density of the soil samples. Use the left ordinate scale for the *y*-intercept and the right ordinate scale for the slope. Use different symbols to represent the two variables.

Describe and explain any systematic variation that you find.

STUDENT'S NAME _____

F. Formation of Impact Craters Experiment Discussion Questions

1. Copernicus crater on the Moon is about 93 km wide.

   a. Using the results you found for the dependence of crater diameter as a function of impactor energy for the dry fine sand, determine the energy of the impactor that formed this lunar feature. Show your calculations here.

   b. Assuming that the impactor had a velocity of 10, 20, and 30 km/s, calculate the diameter of the impactor. Assume that the impactor was spherical and that it had a density of typical stony meteorites, about 3.0 g/cm^3 . Show your calculations here.

      10 km/s:

      20 km/s:

      30 km/s:

2. The rim of Copernicus crater is about 1 km in height. It varies around the rim because of slumping of the rim from gravitational forces and erosion by other meteoroids over geologic time, one of the processes referred to as *crater degradation*.

   a. Using the results you found for the dependence of crater rim height as a function of impactor energy for the dry fine sand, determine the energy of the impactor that formed this lunar feature. Show all your calculations here.

STUDENT'S NAME _____

b. Assuming that the impactor had a velocity of 10, 20, and 30 km/s, calculate the diameter of the impactor for each case. Assume that the impactor was spherical and that it had a density of typical stony meteorites, about 3.0 g/cm^3 . Show your calculations here.

10 km/s:

20 km/s:

30 km/s:

3. The energy estimated for the impactor that created Copernicus crater has been estimated as about 1×10^{23} J. (This is one million times greater than the energy of the explosion of Mt. St. Helens in 1980.) Our results above should be substantially smaller.

a. Calculate the ratio of the energy found in question #1a and 1×10^{23} J.

b. Explain the difference between these energies.

4. Compare the results you obtained for the energy of the impactor in questions (1) and (2). If they differ, offer suggestions as to why in terms of the procedure used in the experiment and possible errors of measurement as well as the mathematical model.

5. The 1.2 km-diameter Barringer Meteor Crater near Winslow, Arizona, was formed about 25,000 years ago by the impact of a large meteoroid. The mass of the meteoroid has been estimated at 300,000 t, or about 2.7×10^8 kg.

STUDENT'S NAME _____

a) Assuming all of the impact kinetic energy was converted to excavating the crater, what diameter is predicted by your results for the fine sand? Assume the meteoroid velocity upon impact was 11 km/s. Show your calculations here.

b) If this disagrees substantially with the known diameter, explain the discrepancy.

STUDENT'S NAME _____

6. We obtained curves for three types of soil materials.
   a) Compare the results obtained for the slope and y-intercept for each soil material.

   b) If significant differences appear, explain them in terms of the densities of the three soil materials.

7. Secondary impact craters are often seen to be elliptical in shape. Why are they not circular as are their parent craters?

8. From kinematics, we know that the time needed for an object to fall a distance H from rest can be found from $H = \frac{1}{2} g t^2$. In the below, show all your calculations.
   a) For a mass of 1 kg dropped from a height of 3 m, determine from Fig. 6 the amount of energy stored in gravitational potential energy and then calculate the amount of power generated by that mass when it falls the 3 m. Recall 1 Watt = 1 Joule/second.

   b) How many seconds would that power keep a 100-Watt light bulb burning?

   c) Derive the general formula to calculate the amount of power generated when an object of mass m falls a distance H. It should be independent of t.

STUDENT'S NAME _____

d) The "surface" gravity on the planet Jupiter is 2.53 times greater than that on Earth. Using the general formula you derived in part (c), by what factor would the power generated increase for the same mass dropped from the same height on Jupiter?

9. You are asked to design an experiment to study hypervelocity impacts in the laboratory. In addition to the equipment used in the current experiment, what type of equipment would be needed?

STUDENT'S NAME _____

10. With all the potable water on the Earth having been polluted with pesticides and urban runoff, you're the geology/hydrology officer on a spacecraft whose mission is to discover water on alien worlds. You've discovered a heavily-cratered planet and have determined the distributions of the diameters of meteorite impact craters in three regions, shown below.

    a. Which region is the most likely to possess the most amounts of water? _____

    b. Why?

    c. What are the major assumptions you have made that allow you to compare these three regions?

Region 1

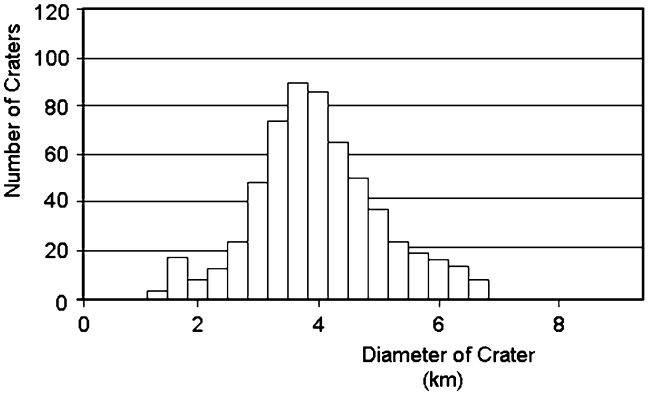

Region 2

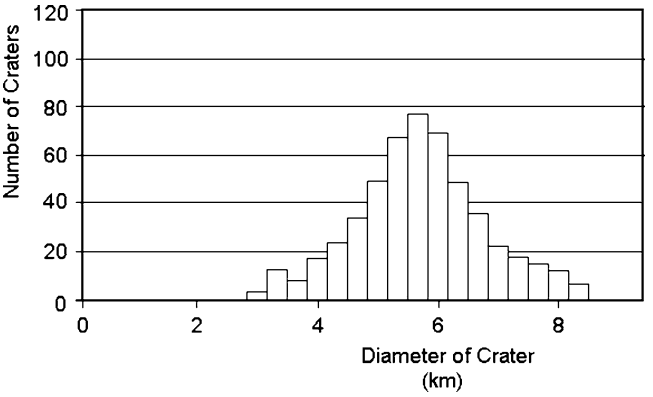

Region 3

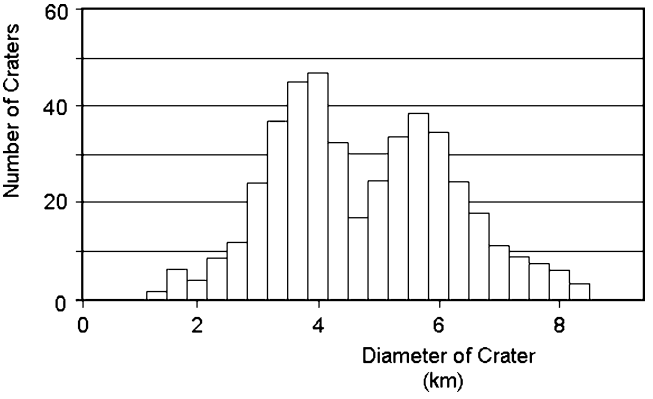

Removing these DATA SHEETS from the book may damage the binding. You might consider entering the data and performing your calculations in the book, and then photocopying the DATA SHEETS for submission to your instructor for grading.

If you used graph paper other than that provided, attach those graphs to these DATA SHEETS.

Experiment 9
Determination of the Rotation Rate of Planets and Asteroids by Radar: Part I. Observations of Mercury

SUMMARY: In Experiment #9, "Determination of the Rotation Rate of Planets and Asteroids by Radar: Part I. Observations of Mercury," and Experiment #10, "Determination of the Rotation Rate of Planets and Asteroids by Radar: Part II. Observations of Simulated Planets," we examine how radar systems provide information on the rotation rate and surface topography of planets and asteroids. In Experiment #9, "Determination of the Rotation Rate of Planets and Asteroids by Radar: Part I. Observations of Mercury," we analyze radar echoes obtained from the planet Mercury. In Experiment #10, "Determination of the Rotation Rate of Planets and Asteroids by Radar: Part II. Observations of Simulated Planets," we calibrate a radar transmitter and microwave receiver and then determine the rotation rate of simulated planets and asteroids by bounding radar signals off of them.

LEVEL OF DIFFICULTY: Low

EQUIPMENT NEEDED: Straight-edge.

MY LEARNING GOALS

1. To be able to describe how the Doppler-shift of electro-magnetic radiation enables astronomers to determine their velocity relative to the Earth.
2. To be able to describe how how range-doppler radar provides resolution of planetary surfaces.
3. To be able to predict the effect of smooth and mountainous regions on a planetary surface on the appearance of the echo of range-doppler radar.

L.M. Golden, *Laboratory Experiments in Physics for Modern Astronomy: With Comprehensive Development of the Physical Principles*,
DOI 10.1007/978-1-4614-3311-8_9,

A. Introduction

Ever since man looked at the Moon with a discerning eye, it became clear that the Moon keeps the same side pointed to the Earth. The man in the Moon, so to speak, always looks right at us. The time it takes for the Moon to revolve about the Earth, the orbital period, is approximately the same as the time it takes for the Moon to rotate on its axis, the rotation period, both about 28 days. This *synchronous rotation* results from a tidal interaction between the Earth and the Moon.

Accordingly, the planet Mercury, because of its proximity to the Sun, was thought to also experience a tidal interaction that would lead to synchronous rotation. Its rotation period was thought to be the same as its orbital period, about 88 days, and it would keep the same face pointed to the Sun. Because of this proximity, features on Mercury can only be observed well when it is at its greatest distance from the Sun in the sky, the so-called configurations of *eastern elongation* and *western elongation*. Those difficult visual observations seemed to confirm the synchronous rotation.

In 1965, however, astronomers Gordon Pettengill and Richard Dyce, using the powerful radar system associated with the newly completed 1000-ft radio telescope at Arecibo, Puerto Rico, bounced radar waves off of Mercury. They made the momentous discovery that the rotation period was actually about 59 days, two-thirds of the orbital period. That discovery was subsequently explained theoretically.

Venus and asteroids are similarly susceptible to radar measurements of their rotation periods. Radar has also been used to study Mars, the Galilean satellites of Jupiter, the rings of Saturn, and Titan, the largest moon of Saturn. In this experiment, we will analyze actual observations of radar echoes from Mercury. In Experiment #10, "Determination of the Rotation Rate of Planets and Asteroids by Radar: Part II. Observations of Simulated Planets," we will use a radar system to study radar echoes from rotating spheres covered with various types of material.

B. Theory

1. Red Shifts and Blue Shifts

The technique is based on the Doppler shift principle. In Fig. 1, our extraterrestrial with superior sensory adaptations, XyTk@2, is observing a wave approaching him from a stationary source. In 1 s, XyTk@2 sees ten waves go by. The frequency of the wave emitted by the source is accordingly 10 cycles per second, $f = 10$ Hz, where we use the unit of Hertz, abbreviated Hz, for cycles per second. The time interval between emission of waves is the same as the time for the one cycle of the wave to move by, the *period*, P. Then it must be that $f = 1/P$.

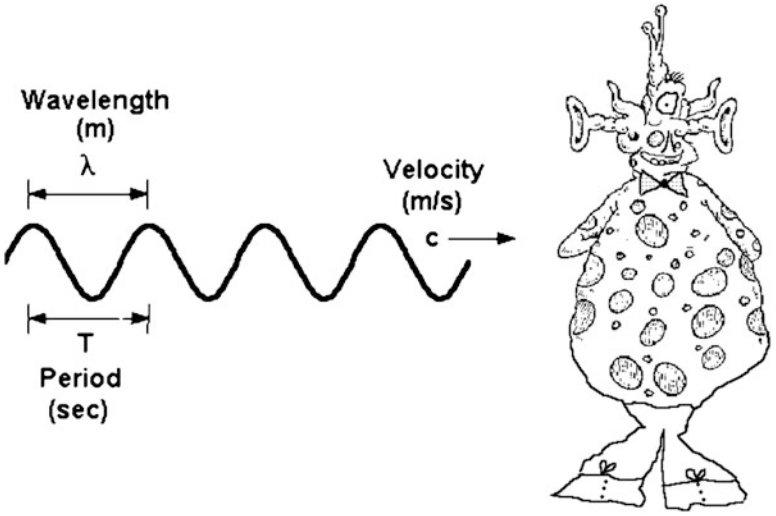

Fig. 1 The universal wave equation relates the frequency and wavelength of any wave. A change or "shift" in the magnitude of the frequency and wavelength occurs if the source of the waves and the observer are in relative motion

The wave is moving, let us say, at a velocity of 20 m/s to the right, $c = 20$ m/s. Because ten wave crests pass by in 1 s traveling at 20 m/s, the distance from wave crest to wave crest must be 2 m. That is one measure of what we mean by the *wavelength*. If the wave were traveling at 30 m/s, then the wavelength would have to have been 3 m. This can be generalized in the well-known relationship between frequency and wavelength of any kind of wave, the *universal wave equation*,

$$\lambda = \frac{c}{f}. \tag{1}$$

Let's suppose that the source of the waves begins to move toward XyTk@2 at 10 m/s. Now XyTk@2 would see an additional ten waves each second; that is, $f = 20$ Hz. Because the speed of the wave being emitted remains the same, the wavelength as observed by XyTk@2 becomes, from (1), 1 m; that is, $\lambda = 1$ m. The wavelength from the source moving toward XyTk@2 has been shortened. Similarly, if the source of the radiation began to move away from XyTk@2, fewer waves would be seen in a second, the frequency would decrease, and the wavelength would increase.

This is the Doppler effect. To derive the formula which expresses the mathematics behind the Doppler effect, we want to relate the wavelength and frequency of the wave observed when the source is at rest to those observed when it is moving. By the universal wave equation, (1), we have

$$\lambda_1 = \frac{c}{f_1} \tag{2}$$

and

$$\lambda_2 = \frac{c}{f_2}, \tag{3}$$

where the subscript 2 refers to the situation in which the source is moving toward the observer and the subscript 1 refers to that in which the source is stationary. According to special theory of relativity, the speed of light, c, is constant no matter the relative motion of the source and the observer.

Now, look at the crest of a wave after it was emitted by the source moving toward XyTk@2. In an amount of time Δt, the crest of the wave has moved a distance $d_w = c\,\Delta t$, where the subscript w refers to the crest of the wave. The source itself has moved a distance equal to $d_s = v\,\Delta t$. If at that instance the source emits a second wave, then the distance between its crest and the crest of the previously emitted wave is

$$\begin{aligned}\lambda_2 &= d_w - d_s \\ &= c\Delta t - v\Delta t.\end{aligned}$$

As we reasoned, the distance between wave crests, that is, the wavelength, has decreased.

We used an arbitrary time interval to examine the two waves, Δt. Let's identify that time interval as the period, the amount of time between emission of successive waves. Because the frequency f of the wave is the number of waves emitted per second, we realize that $1/f$ is in fact equal to the period P. In words, the distance between the two wave crests has been decreased by the distance the source moved in one period. We find then that the decreased wavelength is given by

$$\lambda_2 = \frac{c - v}{f_1}$$

This equation, with either (2) or (3), gives us a system of two equations in two unknowns. Using (2), we can substitute for f_1,

$$\lambda_2 = \frac{c - v}{c/\lambda_1},$$

or

$$\lambda_2 = \lambda_1\left(1 - \frac{v}{c}\right). \tag{4}$$

(If we had used (3) instead, we would have obtained the corresponding relationship between f_1 and f_2, which could then be converted back into (4).)

The negative sign tells us that for objects moving toward the observer, the wavelength decreases. This is referred to as a *blue shift*.

If we had performed the derivation with the object moving away from XyKt@2, we would have found that the sign is reversed and he would experience an increased wavelength given by

$$\lambda_2 = \lambda_1\left(1 + \frac{v}{c}\right). \tag{5}$$

Here, the wavelength increases, a so-called *red shift*.

Because the velocity v is a vector, it can take either positive or negative values depending on the direction of the motion of the source. As a result, the latter equation suffices for both approaching and receding cases.

By convention, the wavelength of the radiation from an object at rest is referred to as λ_o, so that the wavelength observed from a moving object is usually written as

$$\lambda = \lambda_o\left(1 + \frac{v}{c}\right).$$

In astronomy, the Doppler formula is usually given in terms of the change in the wavelength relative to the *rest wavelength*. Denoting the rest wavelength as λ_o, $\Delta\lambda = \lambda - \lambda_o$. From the above equation we therefore define a parameter z as

$$z \equiv \frac{\Delta\lambda}{\lambda_o} = \frac{v}{c}. \tag{6}$$

This is the familiar formula for the Doppler shift in terms of the velocity of motion of the emitting object relative to the speed of light.

To summarize, if the object is moving away from us, the wavelength increases so that $\Delta\lambda > 0$, the velocity is positive, and the object is said to have a *red shift*. If the object is moving toward us, the wavelength decreases so that $\Delta\lambda < 0$, the velocity is negative, and the object is said to have a *blue shift*. Because most astronomical objects for which Doppler shifts are measured have red shifts, the parameter z is actually referred to as the *redshift*.

For cases in which $v \ll c$, this is a good approximation. For values of v close to c, the more general expression derived from Einstein's theory of special relativity must be used. That is the formula from which the large values of redshift quoted for distant objects such as quasars are derived.

2. *Doppler Shifts for Rotating Objects*

In Fig. 2, we look down upon a rotating planet or asteroid. One side of the object is rotating toward the observer and one side is rotating away from the observer. Any radiation emitted from the side rotating toward the observer will be blue-shifted, and any radiation emitted from the side rotating away from the observer will be

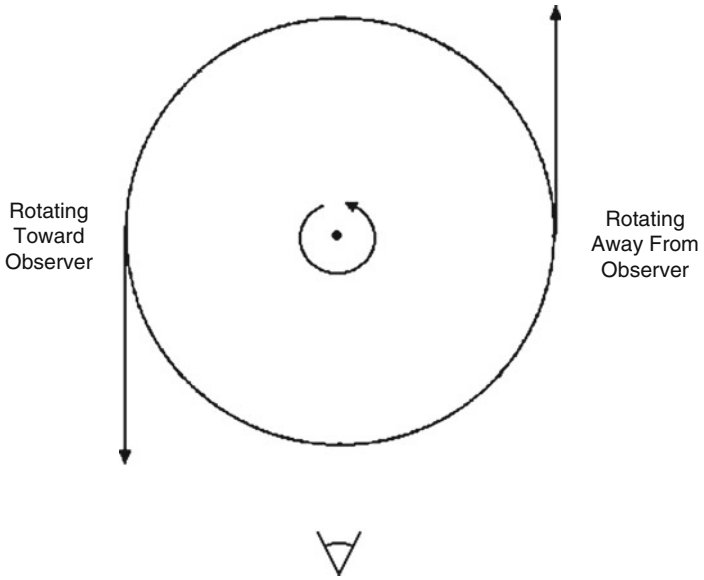

Fig. 2 The *top* view of a rotating planet or asteroid shows that the Doppler shifts of the radar echo are positive on one side and negative on the other side of the sub-observer point

red-shifted. The further from the center of the visible disk, the greater the magnitude of the wavelength shift.

As a result, when a radar signal of wavelength $\lambda_o$is reflected off of a rotating object, the echo is spread out over a band of wavelengths centered at λ_o. At the blue end of the band, the shift is given by (4). At the red end of the band, the shift is given by (5). The total wavelength *bandwidth* of the radar echo would therefore seem to be,

$$BW_\lambda = \frac{2v}{c}\lambda_o.$$

Now, this is not quite the correct answer for the radar echo wavelength bandwidth. Because this is an echo, the wavelength shifts are twice that produced by a source which is simply emitting. The wavelength is altered when the transmitted radar pulse impinges on the surface element as well as when it is reflected back to Earth. You can understand this by remembering that the Doppler shift occurs when objects are in relative motion. The element of surface receives a radar signal from the Earth as it moves at a given velocity, v. The wavelength it sees is accordingly Doppler shifted from the wavelength emitted by the radar. It reflects back that Doppler shifted wavelength, but the radar receiver on the Earth sees the surface element in motion with the same velocity v and receives a wave that is further Doppler shifted. The result is a Doppler shift that is twice as large as if the planet was not rotating.

Accordingly, we have to multiply by a factor of two to obtain the observed bandwidth of the echo. The total wavelength bandwidth of the radar echo is therefore

$$BW_\lambda = \frac{4v}{c}\lambda_o, \tag{7}$$

where the velocity v is that at the equator.

Observations of radar echoes are made using a multi-channel detector, or *spectrum analyzer*. These detect the frequency bandwidth rather than the wavelength bandwidth. From (1), by differentiating λ as a function of f,

$$\frac{BW_\lambda}{BW_f} = \left|\frac{\Delta\lambda}{\Delta f}\right| = \frac{c}{f_o^2}.$$

With (7), the total frequency bandwidth of the radar echo is therefore

$$BW_f = \frac{4v}{\lambda_o}. \tag{8}$$

This yields the velocity of the edge of the equator in terms of the frequency bandwidth of the echo,

$$v = \frac{\lambda_o}{4}BW_f. \tag{9}$$

This relationship will be utilized in Experiment #10, "Determination of the Rotation Rate of Planets and Asteroids by Radar: Part II. Observations of Simulated Planets".

We can relate this easily to the rotation period of the planet or asteroid. From the equations of circular motion, we know that the velocity of an object in circular motion is equal to the circumference of the circle divided by the time required to traverse the circumference,

$$v = \frac{2\pi R}{P}. \tag{10}$$

Here the "circle" is the equator of the planet or asteroid and R is its radius. Combining (9) and (10), we can determine the period of rotation from observations of the bandwidth,

$$P = \frac{8\pi R}{\lambda_o}\frac{1}{BW_f}. \tag{11}$$

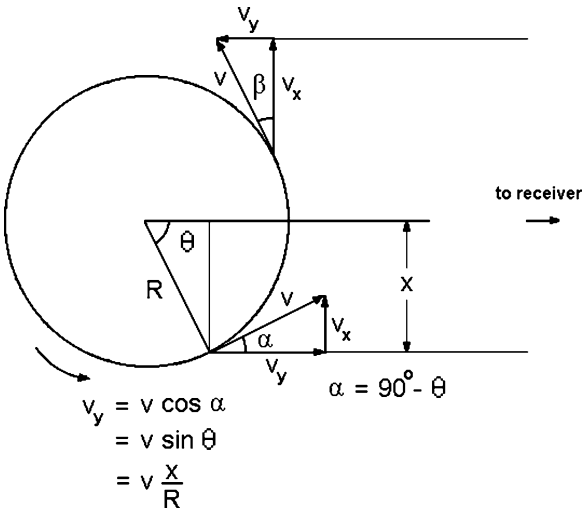

Fig. 3 The velocity of a given portion of a planetary surface along the direction of the line-of-sight, designated as v_y , varies with its angular position, θ. This is a *top* view of a planet rotating with its axis of rotation perpendicular to the line-of-sight

The larger the frequency bandwidth of the echo return, the smaller the period, that is, the more quickly the object is rotating.

Equation 10 can also be rearranged to yield the rotation period P,

$$P = \frac{2\pi R}{v}. \tag{12}$$

The bandwidth of the radar echo is measured and yields, by (9), the velocity of the edge of the disk. Knowing the radius of the planet or asteroid, that value of bandwidth yields the rotation period, P, by (11).

Not all locations on the sphere move with the velocity v found in (10). The geometry of Fig. 3 shows that the closer the point on the planetary surface is to the sub-Earth point, the lower the velocity in the line-of-sight. This is the component of velocity which determines the amount of Doppler shift. In general, the velocity in the line of sight is given by

$$v_y = v\,\frac{x}{R}, \tag{13}$$

where v is the rotational velocity of the planet as given in (10), and x/R is the fractional part of the radius of the planet from the sub-Earth point toward the edge of the visible planetary disk, as shown in Fig. 3.

Although we've performed this derivation for a position at the equator, the relationship of (13) holds at any planetary latitude. The effective radius of the "circle" at a latitude l is $R(l) = R \cos l$; it decreases in size from R at the equator to zero at the pole. The velocity of rotation of an element of the planetary surface, however, also decreases with latitude, as $v \cos l$. This follows from (10),

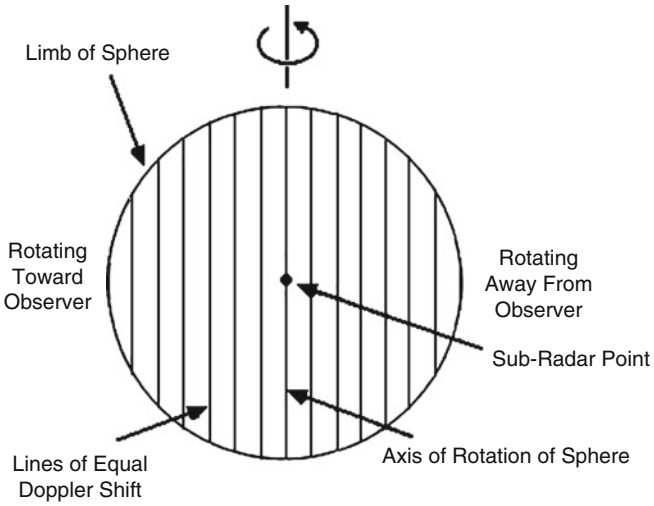

Fig. 4 Because of the rotation of the planet, strips of surface of given velocities in the line-of-sight produce the same range of Doppler shifts

$$v(l) = \frac{2\pi R(l)}{P} = \frac{2\pi R \cos l}{P} = v \cos l.$$

As a result, generalizing (13) for any latitude l,

$$v_y(l) = v(l)\frac{x}{R(l)}$$

$$= v \cos l \frac{x}{R \cos l}.$$

The two factors of cos l cancel out, so that v_y depends only on x, the distance from the center of the apparent disk of the planet to the location of interest, and not the latitude.

If strips of the planetary disk are characterized in this way by representative values of v_y, we can draw a figure such as Fig. 4. By studying the radar echo with different Doppler shifts we can resolve at least strips of the planetary surface, without the need for telescopes possessing high angular resolution. The smaller the bandwidth of the impinging radar and the faster the planet rotates, the greater the resolution in strips over the surface.

3. *Range-Doppler Radar Mapping*

The surface of a planet or asteroid can also be resolved in distance. A natural reference point is the intersection of a line drawn between the radar site and the

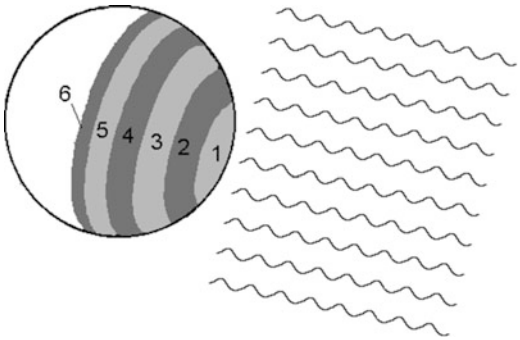

Fig. 5 The radar signal impinges on annular regions at greater distances from the sub-radar point at increasingly larger times. The corresponding echoes also take an increasingly longer time to return to Earth for reception

center of the planet with the surface of the object being studied. This intersection is referred to as the sub-radar point. For distant objects such as the Moon, planets, and asteroids, it is located simply at the center of the visible disk of the object as seen from the Earth.

As we see in Fig. 5, portions of the surface at increasingly greater distance from the sub-radar point become illuminated at increasingly later times. Region 1 is illuminated before region 2, and so on, region 6 being the last to be illuminated. Their radar echoes similarly are received at Earth from the surface at differing times. Consequently, if the radar receiver samples the radar echo in small time intervals, the radar echo from the various annular regions concentric with the sub-radar point can be detected and analyzed separately. This is referred to as *gated* reception. For a given sampling time interval, the smaller the duration of the radar pulse and the larger the planet the greater the resolution in distance over the surface.

With the ability to resolve strips of surface from the Doppler-shifted frequency and annular regions from the gated echo, the surface of the planet or asteroid can be resolved into areas. This is referred to as *delay-Doppler* mapping or *range-Doppler mapping,* Fig. 6. It allows significant resolution of a planetary surface without the need for telescopes possessing high angular resolution.

Most of the echo arises from reflection from areas on the planet that are perpendicular to the impinging radar beam. For a smooth or nearly smooth surface, these areas are located at and near the sub-radar point. If the surface is not perfectly smooth, material on the surface with sizes comparable to the wavelength of the radar will also create an echo because some of their facets will be perpendicular to the incident radar. In this way, for example, a radar with a wavelength of 1 cm will be partially reflected by pebbles distant from the sub-radar point. A radar with a wavelength of 70 cm (about 2.3 ft), such as the Arecibo radar, will be partially reflected by small boulders distant from the sub-radar point.

The range-Doppler technique has two shortcomings. An ambiguity exists between the northern and southern hemispheres, it being impossible without further

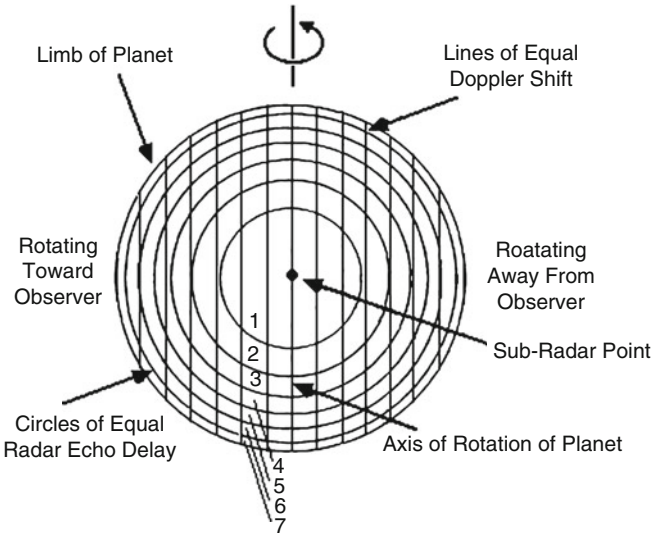

Fig. 6 Range-Doppler mapping allows resolution of the surface of a rotating planet or asteroid

information to distinguish the radar echo coming from regions symmetrically placed north and south of the equator. Second, the resolution differs over the disk of the planet or asteroid. Near the poles, the areas whose echoes are received are relatively small, and centralized. Near the equator, where the lines of equal Doppler shift become tangent to the circles of equal echo delay, the areas whose echoes are received are relatively large, and elongated. Additional information is needed to somewhat reduce these problems. Astronomers must compensate for the different surface areas from which the echo is received when they analyze their data.

4. Radar Systems

In Experiment #10, "Determination of the Rotation Rate of Planets and Asteroids by Radar: Part II. Observations of Simulated Planets," we will observe the radar echo from rotating spheres covered with various materials, a simulation of the surfaces of planets and asteroids. The use of radar in planetary studies and in our experiment is more complex than in its commercial use to simply detect relative speeds. In general, the radar beam at a microwave frequency, f_1 is emitted by a radio antenna and impinges on, or "illuminates," a target, in our case spheres simulating the planets. The target reflects the radar beam that impinged on it back at a microwave Doppler-shifted frequency, f_2 to an antenna which collects the radar echo and the signal is processed by a radio receiver. In that receiver, the transmitted signal and the echo are combined or "mixed" in such a way as to produce two new signals, one signal at a frequency equal to the sum of f_1 and f_2 and the other signal at

a frequency equal to the difference of f_1 and f_2. The former is discarded electronically and the latter, which is at the low audio frequencies from 0 Hz to about 20 kHz, is processed to yield the relative speed. In commercial radar, that audio signal is displayed as a digital readout.

A complication exists in planetary studies and in our simulation experiment. The echo consists not of a signal with a single Doppler-shifted frequency, but a signal spread out over a finite bandwidth of frequencies composed of different Doppler-shifted signals reflected from different regions of the rotating surfaces. The receiver must therefore mix all the frequencies in the bandwidth down to audio frequencies and the strength of each such part of the echo must be measured separately. This measurement is performed by a *spectrum analyzer*.

The spectrum analysis can be done either electronically or by computer software. We will use the latter. The audio bandwidth is sent to the input of a computer sound card and the software produces a display of the echo strength as a function of frequency, the spectrum of the echo. This then allows us to discriminate visually between echoes of different Doppler shifts originating from different regions of the surface of the spheres.

C. Procedure and Observations: Radar Observations of Mercury

Here we will analyze radar observations of the planet Mercury. Our own radar observations will be performed in Experiment #10, "Determination of the Rotation Rate of Planets and Asteroids by Radar: Part II. Observations of Simulated Planets".

Figure 7 shows actual radar echoes from Mercury, obtained using the Arecibo radar telescope and published in 1967 by Rolf Dyce, Gordon Pettengill, and Irwin Shapiro. The radar had a wavelength of 70 cm, the pulses were 100 μs (1 microsecond $= 10^{-6}$ s), and the average transmitted pulse had a peak strength of 2 MW, equivalent to about 20,000 light bulbs. Each successive graph in the sequence shows the echoes with an increasing radar delay, the signals coming from annular regions increasingly distant from the sub-Earth point. You can see the decreasing strength of the echoes for the reflections near the limb. There, much of the 70 cm radar beam is reflected out into space, not back toward the Earth. That any echo occurs results from the roughness of the surface.

From (10), we can calculate the speed of rotation at the equator of Mercury. With a radius $R = 2{,}440$ km and a rotation period $P = 59$ days, we find $v = 3$ m/s.

In practice, observational complexities occur. The echo is not smooth. This results from only partially from the physical effect of interest, the varying roughness of the surface over the disk. This is also caused by differing sizes of areas from which the echo is received and the difficulty in observing faint echoes from distant objects in the presence of noise in the radio receiver. In analyzing their data, astronomers calculate the compensations needed for those two effects as well as the contribution to the Doppler shifts from the motions of Earth and Mercury in their orbits.

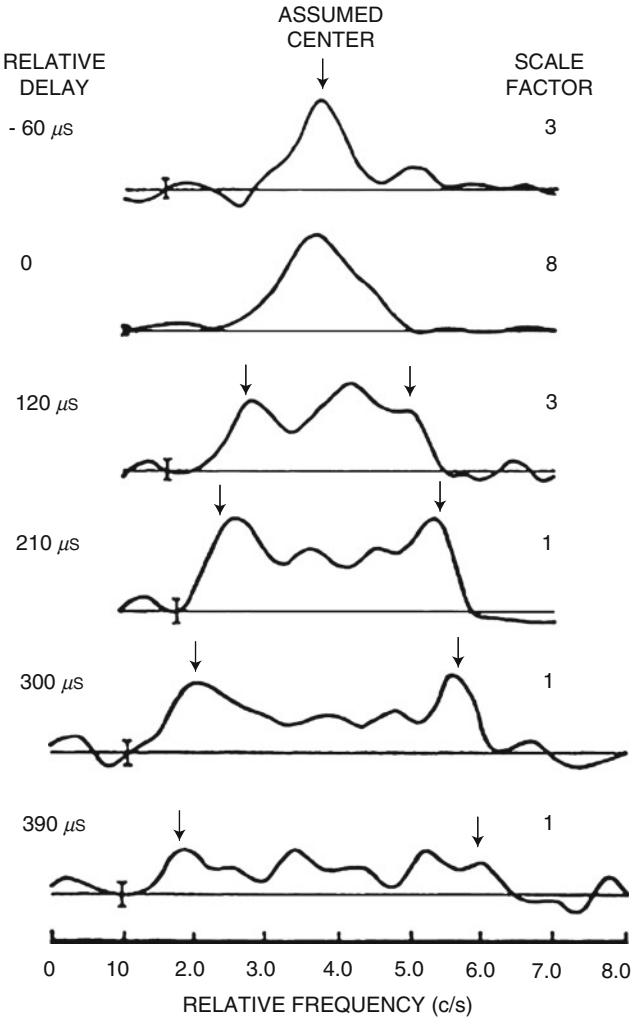

Fig. 7 The 1967 radar observations of Mercury at a wavelength of 70 cm

As can be seen from the notation inside Fig. 7, the graphs display the echo from nearly distinct annular regions. Although the pulses were 100 μs long, the echoes in the graphs are separated by 90 μs. Accordingly, we can sum up the contributions to the echo represented in each graph to determine approximately the total amount of energy in the echo. The result will be used in Experiment #10, "Determination of the Rotation Rate of Planets and Asteroids by Radar: Part II. Observations of Simulated Planets".

Figure 7 is reproduced enlarged on the DATA SHEET. On it, draw thin vertical lines from bottom to top at the locations of the abscissa tick marks. Also draw thin vertical lines from bottom to top at the midway points between the tick marks. Draw an additional vertical line at the location of the sub-Earth point.

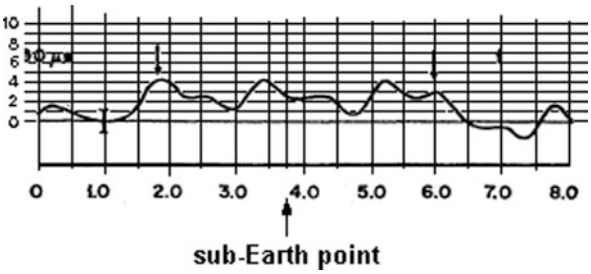

Fig. 8 To analyze the data of Fig. 7, draw grid lines such as shown here

We also need to draw horizontal lines on the five graphs. Each graph has a baseline. On each graph, draw thin horizontal lines vertically spaced by 1/4 cm, about 0.1 of an inch, above the baseline. Label those horizontal from 0 to 10. They will represent arbitrary levels of echo intensity.

As a result you will have a series of grid lines superimposed on each graph. Your results should look like Fig. 8, the radar echo of Fig. 7 at a delay of 390 μs.

D. Calculations and Analysis

At each abscissa point on the enlarged radar observations graph on the DATA SHEET, estimate the ordinate values of the radar echo for each delay. You should be able to do this to the nearest 0.1 of a unit. For example, in Fig. 8, at the abscissa location of 0.5 c/s (or Hz), the height of the curve is about 0.8 units. Enter any values less than zero, such observations resulting from the noise in the Arecibo radar system, as zero. Enter your results in Table 1 of the DATA SHEET.

In performing this exercise, be careful to align the data correctly in c/s in Table 1 of the DATA SHEET. You will note that the bottom two graphs corresponding to relative delays of 300 μs and 390 μs have greater range in abscissa values than the others.

The top three graphs in Fig. 7 have larger scale factors than the rest. The data were presented in this way by the researchers for ease of presentation. For our analysis, however, we must adjust the data in those top three graphs before adding the columns together to get the total radar echo. Multiply the values that you entered into Table 1 from the graphs corresponding to relative delays of −60 μs, 0 μs, and 120 μs by the factors 3, 8, and 3, respectively, and enter the results in the respective rows of Table 2 of the DATA SHEET. For the other graphs, simply copy the entries of Table 1 into Table 2.

After you have corrected those three lines of data, add the numbers in each column to get the total radar echo at that frequency displacement. Enter those sums in the bottom row of Table 2 of the DATA SHEET.

Construct a graph of the resulting totals, plotting intensity in our arbitrary units as ordinate against frequency displacement as abscissa. Draw a smooth curve between the data points. This is the total radar echo from Mercury represented by the observations of Fig. 7, summed over all the echo delay intervals.

STUDENT'S NAME _____

E. Rotation Rate by Radar Experiment I Data Sheets

Radar observations of Mercury

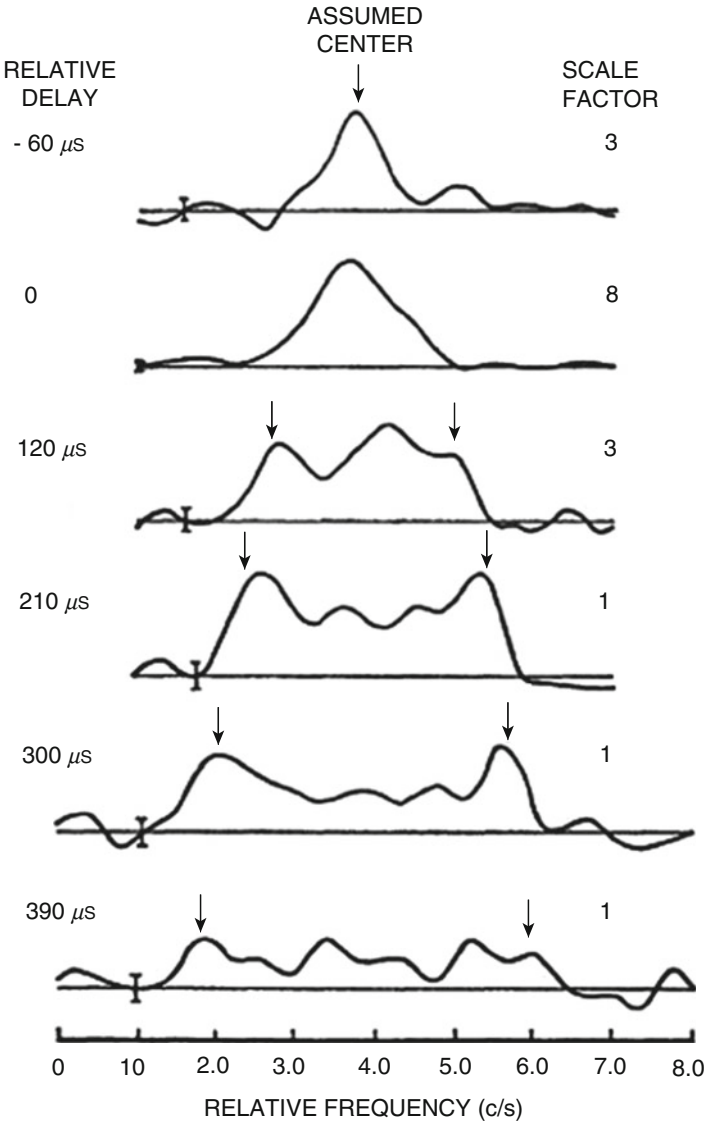

STUDENT'S NAME _____

Table 1 Mercury radar echo

Graph	0.0	0.5	1.0	1.5	2.0	2.5	3.0	3.5	Sub-Earth	4.0	4.5	5.0	5.5	6.0	6.5	7.0	7.5	8.0
−60 μs	0	0															0	0
0 μs	0	0															0	0
120 μs	0	0															0	0
210 μs	0	0															0	0
300 μs																		
390 μs																		

Table 2 Adjusted mercury radar echo data

Graph	0.0	0.5	1.0	1.5	2.0	2.5	3.0	3.5	Sub-Earth	4.0	4.5	5.0	5.5	6.0	6.5	7.0	7.5	8.0
−60 μs × 3	0	0															0	0
0 μs × 8	0	0															0	0
120 μs × 3	0	0															0	0
210 μs	0	0															0	0
300 μs																		
390 μs																		
SUM																		

STUDENT'S NAME _____

Graph of total Mercury radar echo

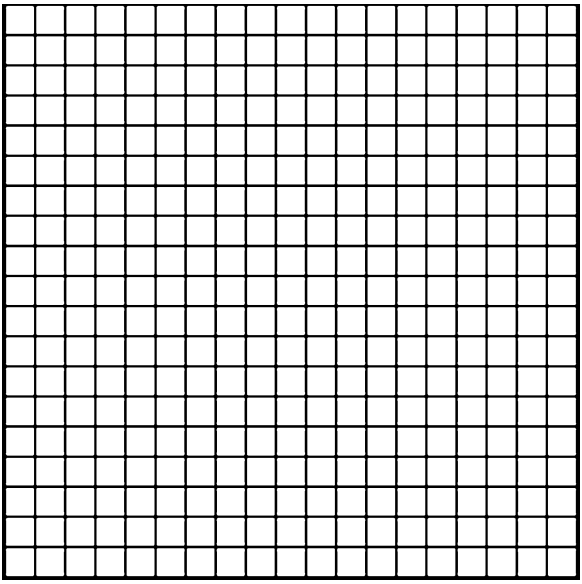

STUDENT'S NAME _____

F. Rotation Rate by Radar Experiment I Discussion Questions

1. In deriving the equation for the Doppler shift, we wrote (4). As the speed of the source approaches the speed of the wave, the wavelength gets smaller and smaller and the waves "bunch up." Assume we are dealing with sound waves. Describe the common experience you hear when a source of sound actually moves as fast or faster than the speed of sound, about 1000 ft/s at ground level.

2. Mercury spins on its axis once every 58.6 days. Its diameter is 4879 km. From (10), calculate the velocity of a point at its equator. Show your calculations here.

3. Perform the same calculation for the Earth as you did for Mercury in question #2. The diameter of the Earth at the equator is 12,756 km.

4. Figure 7 provides observations of the radar echo of Mercury at a frequency of 430 MHz, equivalent to a wavelength of 70 cm. From the frequency bandwidth of the radar echo shown in Fig. 7, calculate the inferred velocity of a point on the equator of Mercury. Show your calculations here. Note: It may differ from the result of question #2.

5. Calculate the percentage difference between the results for the velocity on the equator of Mercury that you calculated from question #2 and question #4. Show your calculations here. How can you explain any difference? Is that difference in the direction you would expect?

STUDENT'S NAME _____

6. You have prepared a graph showing the total radar echo from all annular regions of Mercury as a function of frequency displacement from the frequency of the radar signal of 430 MHz. From that graph, sketch what the graph of the total radar echo would look like for a planet similar in topography and diameter to Mercury but rotating twice as fast as Mercury.

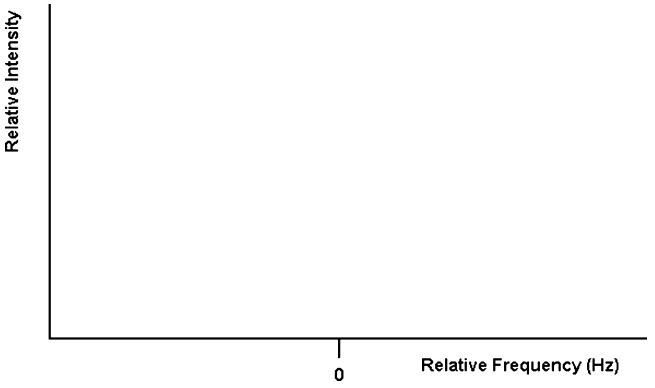

Is the total amount of energy in the echo changed? Why or why not?

7. We have assumed in the experiment that the planet rotates about an axis perpendicular to our line-of-sight. Assume such a planet was tilted toward the Earth by a substantial angle. How would the radar echo change? Explain your answer by a diagram.

STUDENT'S NAME _____

8. Similarly, assume the planet of question #6 was tilted toward the Earth by a 90° angle so that its axis of rotation points directly at the Earth. How would the radar echo change now? Explain your answer by a diagram.

9. The graphs of the radar echoes from Mercury have wiggles in them. Suggest some causes for the wiggles.

10. Here are the gated radar echoes from a hypothetical observation. Seven features are identified. The range-Doppler map of the planet provides the corresponding locations whose radar echo created the features. (Because of north–south hemisphere ambiguity, we are assuming that all features are present on the northern hemisphere.) Provide the location on the range-Doppler map corresponding to the lettered features in Table 3.

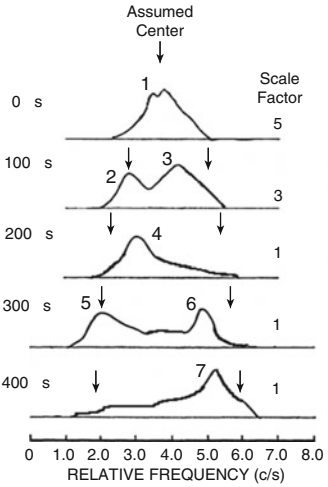

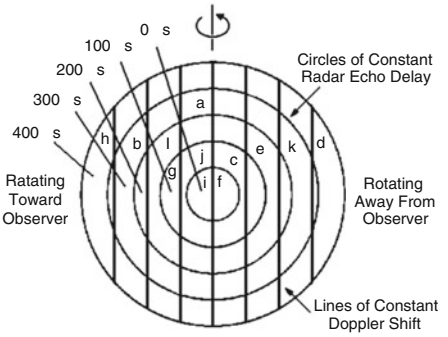

STUDENT'S NAME _____

Table 3 Correspondences for question #10

Feature	Location
1	
2	
3	
4	
5	
6	
7	

11. Diffuse and specular reflection, phenomena of optics that we studied in Experiment #6, "The Surface Roughness of the Moon: Reflection and Scattering from a Planetary Surface: Part I. Surface Materials," and #7, Experiment "The Surface Roughness of the Moon: Reflection and Scattering from a Planetary Surface: Part II. Beads and Surface Coverage," occur for all types of waves. Recall that a condition for specular reflection is the surface being smooth compared to the wavelength of the incident radiation.

    a. Describe the total radar echo from Mercury in terms of specular or diffuse reflection.

    b. The Moon at visible wavelengths is close to a Lambert surface. The surface of Mercury is similar to that of the Moon, would you expect the surface of Mercury to be close to a Lambert surface at 70-cm wavelength? Explain your answer.

Removing these DATA SHEETS from the book may damage the binding. You might consider entering the data and performing your calculations in the book, and then photocopying the DATA SHEETS for submission to your instructor for grading.

If you used graph paper other than that provided, attach that graph to these DATA SHEETS.

Experiment 10
Determination of the Rotation Rate of Planets and Asteroids by Radar: Part II. Observations of Simulated Planets

SUMMARY: Just like ET, we use a spinning turntable to great advantage in Experiment #10, "Determination of the Rotation Rate of Planets and Asteroids by Radar: Part II. Observations of Simulated Planets". We place spheres covered by different types of material to simulate rotating planets and asteroids, and then bounce radar signals off of them. As we learned in Experiment #9, "Determination of the Rotation Rate of Planets and Asteroids by Radar: Part I. Observations of Mercury," the characteristics of the radar echo enables us to determine the rotation rate of the simulated planets, roughness of their surfaces, and the presence of topographic features.

LEVEL OF DIFFICULTY: Moderate to High

EQUIPMENT NEEDED: Radar system; 1-foot and 2-foot radar support stands; spectrum analyzer or spectrum analyzer software; personal computer; electric household fan; two sets of spheres of packaging Styrofoam or other light-weight non-metallic material; vinyl record turntable adjustable to 33 1/3 and 78 rpm; 1/4-inch diameter wooden dowel; 4-foot diameter circular disk of aluminum foil-covered cardboard or wood; large pieces of cardboard; staples, nails, paper clips, aluminum foil; wire, string, or Velcro; planimeter (optional); safety goggles.

MY LEARNING GOALS

1. To be able to describe how the Doppler effect is applied to rotating planets to determine their rotation rates.
2. To be able to predict the effect of planetary surface roughness on the rotation rates of planets determined by radar.

L.M. Golden, *Laboratory Experiments in Physics for Modern Astronomy: With Comprehensive Development of the Physical Principles*,
DOI 10.1007/978-1-4614-3311-8_10, © Springer Science+Business Media New York 2013

A. Introduction

In Experiment #9, "Determination of the Rotation Rate of Planets and Asteroids by Radar: Part I. Observations of Mercury," we introduced the theory of radar range-Doppler mapping and analyzed a radar echo from the planet Mercury. Here, we will use an actual radar system to bounce microwave radar off simulated rotating planets and asteroids. The rotation is achieved by placing the simulated planets onto the turntable of a record player. Use of a spectrum analyzer, spectrum analyzer software, or a suitable oscilloscope then enables us to determine the rotation speed of our simulated planets and the effect on the echo of different surface materials.

B. Theory

1. *Our Rotating Planets*

Our planets will be spheres covered with various thin metallic materials of different sizes. These thin materials are not transparent to radar. It may be surprising, but even a single sheet of aluminum foil strongly reflects the microwave signals. It is found and can be shown theoretically that the echo reflected off metals, because they are good conductors of electrical currents, originate from a shallow, thin layer. The depth of the effective layer from which the echo radiates is accordingly called the *skin depth* and it varies only slightly among different metals. At the microwave frequencies of this experiment, the skin depth can be shown to be about 1 μm (1×10^{-6} m), Fig. 1. This is much smaller than the thickness of a piece of aluminum foil.

We simulate rotating planets by placing these spheres onto an elongated spindle of the turntable of a record player. The turntable can be spun at 33 1/3 rpm (revolutions per minute) and 78 rpm, corresponding to 0.56 rps (revolutions per second) and 1.30 rps, respectively.

By definition, the rotation rate, s, in revolutions per second is related to the period of rotation of the turntable, P, and therefore that of the spheres, by

$$s = \frac{1}{P}, \tag{1}$$

where the period, P, is given in seconds. (We use s for "spin" rate to enable us to avoid using f, for revolution frequency, which could cause confusion with the use of f for the frequency of electro-magnetic radiation).

The velocity of the equator of a sphere of radius R can be found by noting that in a length of time equal to the period, the equator traverses a distance of $2\pi R$. Accordingly, by combining (1) with Eq. (10) of Experiment 9, "Determination of

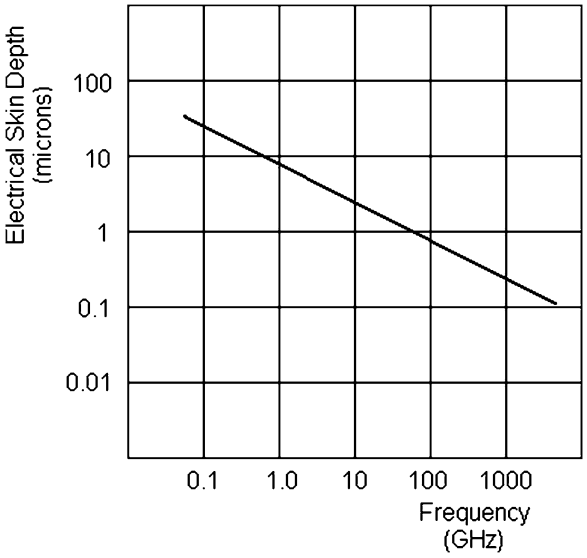

Fig. 1 Electrical skin depth as a function of frequency. The skin depth is inversely proportional to the square root of both the frequency of the radiation and the conductivity of the metal. Better conductors have more shallow skin depths. The straight line (on the log-log graph) closely represents the behavior of most metals, little difference between their skin depth variation with frequency existing. Intuitively, the variation makes sense – the smaller the wavelength the more shallow the skin depth. 1 μm = 1×10^{-6} m

the Rotation Rate of Planets and Asteroids by Radar: Part I. Observations of Mercury," the velocity of the edge is given by

$$v = 2\pi Rs. \tag{2}$$

When using radar to explore the planets and asteroids, gated delay allows resolution of the surface in annular regions and the Doppler effect allows resolution of the surface in strips of frequency displacement. With Mercury, for example, we found the echo was delayed up to 450 μs (microseconds) in time from the sub-radar point to the limb, a result of the 2440 km radius of the planet. Because of those delays, we had to sum up the contributions to the echo from the various delays to obtain the total amount of energy reflected.

Here, however, we are dealing with spheres of diameters measured in feet. The corresponding delay, given by $t = R/c$, where R is the radius of the sphere, is only about 3×10^{-9} s., that is, 0.003 μs. As a result, we obtain no resolution in delay. In the laboratory, therefore, instead of the resolution of the surface displayed in Fig. 6 of Experiment #9, "Determination of the Rotation Rate of Planets and Asteroids by Radar: Part I. Observations of Mercury," we have only that of its Fig. 4. Because our

simulated planet is small and the speed of light large, we obtain an echo from the entire hemisphere containing all the reflected energy.

2. *Radar System Conversion of Microwave to Audio Frequencies*

The transmitted signals and therefore reflected signals in radar systems are at microwave wavelengths, 2.6 GHz (11.5 cm) in the system we will be using. To facilitate the actual analysis of radar echoes in radar systems, however, the microwave echoes are first converted to audio frequencies, those frequencies less than about 20 kHz, by a process called *mixing*. In this process, the reflected signals are combined electronically with the transmitted signals to produce signals at a frequency equal to the difference between those of the reflected and transmitted signals. The resulting frequencies, referred to as *intermediate frequencies* or IF, are at audio frequencies.

The audio frequencies produced can be easily calculated. The total radar Doppler shift coming from a moving object, following the argument leading to Eq. (8) of Experiment #9, "Determination of the Rotation Rate of Planets and Asteroids by Radar: Part I. Observations of Mercury," is $\Delta f = 2\ v/c\ f_o$, where v is the velocity of the moving object, c is the speed of light, and f_o is the frequency of the transmitted signal. The IF frequency is defined as $f_{IF} = f_o - f_{reflected}$, where $f_{reflected}$ is the frequency of the reflected signal. We know, however, that $f_{reflected} = f_o \pm \Delta f$, where the plus and minus signs refer to a receding (red-shifted) or approaching (blue-shifted) object, respectively. Simply, then, we find

$$f_{IF} = f_o - (f_o \pm \Delta f),$$

or,

$$f_{IF} = \pm\ 2v/c f_o \tag{3}$$

C. Procedure and Observations

1. *Simulated Planet Surface Material*

The simulated planets consist of a sphere onto which various metallic materials are embedded. We will use spheres of two different sizes. Depending on the material available, they can be constructed out of various low-density materials such as the packaging material commonly, but incorrectly, referred to as Styrofoam (which is

in fact a building material), exercise or beach balls of pliable plastic filled with expanding foam, foam rubber, or plastic Earth globes covered with a layer of foam rubber. Exercise balls, in particular, range in size from 1 to 3 ft in diameter.

Packaging Styrofoam is a poor reflector of radar and is suggested as the preferred alternative. If you cannot obtain spheres made of packaging Styrofoam, you can construct then by gluing pieces of packaging Styrofoam together and then forming the composite into a spherical shape using a heat gun. Using a blade to sculpt the material will tend to rip it apart.

Alternatively, you can create the larger spheres in particular by stuffing spherical objects. For this, slice open beach balls, exercise balls, or similar balls of pliable plastic, stuff them with pieces of packaging Styrofoam and then tape the balls closed.

We will utilize six different spheres, three "small-size" and three "large-size" spheres. Depending on the material you have available and the size of your laboratory, you can use 1-ft, 2-ft, 3-ft, or 4-ft diameter spheres. Because we will be comparing echoes from the various spheres, it is best to use the same technique and materials to construct all of the three spheres of a given size.

Onto them are placed various metallic objects. We use metallic objects to ensure a strong radar echo. Although rocks, sand, soils, and baseballs all reflect radar, they are not metallic and echoes from them are not as strong as those from metallic objects. (Although they are not metals, the atoms and molecules of non-metallic materials oscillate when an electromagnetic wave is incident upon them and those oscillations create the reflected electromagnetic wave we detect as an echo).

Three types of metallic objects are embedded into spheres of each size. Ordinary staples will simulate the roughness of sand. Nails and paper clips simulate the roughness of pebbles. Crumpled-up pieces of aluminum foil, stapled onto the spheres, simulate rocks. Sand, pebbles, and rocks are created by various geological processes, for example, water and wind erosion of rocks, erosion of mountains, and volcanic eruptions. Of course, all three types of objects are present on the surfaces of planets and asteroids. With our microwave radar, the presence of these "peebles" and "rocks" will create a rough surface so that we can obtain a radar echo from the surface even at an appreciable distant from the sub-radar point.

With a micrometer or ruler, measure the widths of the metal portion of the staples, paper clips, and nails. Obtain several measurements of the scale of the roughness of the crumpled-up pieces of aluminum foil. Enter the results on DATA SHEET.

2. Record Player Turntable: The Planetary Rotation

We simulate rotating planets by putting these spheres onto a rotating platform, the turntable of a vinyl record player, Fig. 2. The spheres are placed onto the elongated spindle of the turntable of the record player. A 1/8-in. hole is created through the sphere from top to bottom into which the elongated spindle of the turntable of a record player can be inserted. To create the elongated spindle, a hole can be drilled

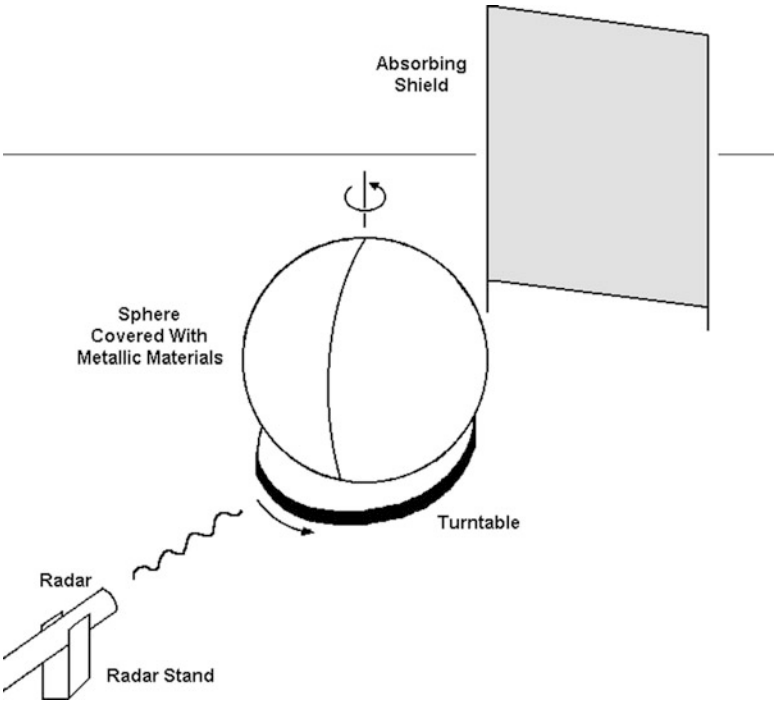

Fig. 2 The experimental setup. Spheres with imbedded metallic material are mounted on an elongated spindle of a record turntable. To ensure that spillover is not a problem, an absorbing piece of cardboard is placed behind the turntable

through the center of a 1/4-in. diameter wooden dowel which is then placed over the existing turntable spindle.

Depending on the rotation speed of the turntable, the surfaces of the spheres attain various velocities. From (2), when the turntable is run at 78 rpm, equivalent to 1.30 rps, the surfaces of 1-ft, 2-ft, 3-ft, and 4-ft diameter spheres attain velocities of 1.3, 2.5, 3.7, and 5.0 m/s (or 16.3 ft/s), respectively. When the turntable is run at 33 1/3 rpm, the corresponding velocities are 0.5, 1.1, 1.6, and 2.1 m/s (or 7.0 ft/s), respectively. If your laboratory has equipment with a platform that can rotate twice as rapidly, it can be used instead of the 33 1/3 rpm rate. The 5.0 m/s speed corresponds to 18 km/h (or 11 miles/h). (I think that my colleague, ET the Extraterrestrial, who used a similar turntable to communicate to his friends in their spaceship, would approve and maybe use this experiment in his astronomy classes once he retires from his movie career.)

NOTE: At these velocities, the metallic objects embedded in the spheres can pose a danger. Make sure that the staples, nails, and paper clips are inserted securely into the spheres. Whenever the turntables are turned on, wear safety goggles.

Such velocities for the edge of the sphere are adequate for our experiment by serving two purposes. First, with the S-band radar of 11.5-cm wavelength that we will be using, they produce a radar echo, found from (8) of Experiment #9, "Determination of the Rotation Rate of Planets and Asteroids by Radar: Part I. Observations of Mercury," with up to a 175 Hz bandwidth for a 4-ft diameter sphere spinning at 78 rpm, well resolved with the 1–5 Hz resolution that can be obtained with a spectrum analyzer or spectrum analyzer software. A 1-ft diameter sphere spinning at 33 1/3 rpm produces an 18 Hz bandwidth, still easily resolved.

Second, we will then be able to distinguish radar echoes from the rotating spheres from any signals bouncing off of individuals walking about in the laboratory. Although a typical walking gait speed for adults is about 1.3 m/s, those moving about the laboratory would be walking appreciably more slowly.

Individuals in the laboratory pose little problem for other reasons. Clothing and flesh are poor microwave reflectors whereas the metallic materials which have been placed on the rotating spheres are excellent microwave reflectors. Also, the other students in the laboratory will be much further from your receiver than the rotating sphere. Because the intensity of the echo radiation decreases proportionally to the inverse square of the distance, their echoes will be that much fainter. We will also be placing the radar system sufficiently close to the rotating spheres to minimize reception from other sources.

As illustrated in Fig. 3 of Experiment #9, "Determination of the Rotation Rate of Planets and Asteroids by Radar: Part I. Observations of Mercury," echoes reflected from portions of the rotating spheres that are not at the edge of the visible disk as viewed from the radar receiver have a smaller velocity in the line-of-sight than echoes reflected from the limb. For the reasons mentioned, however, echoes from walking students should not interfere even with these portions of the radar echo.

Two practical difficulties arise with the use of a turntable. The turntable spindle itself does not rotate. The elongated spindle is created simply to prevent the spheres from wobbling as they rotate on the turntable. Various techniques of securing the spheres to the turntable, however, can be employed. A piece of wire or string can be tightly wound around the base of the turntable and then wrapped over the top of the sphere. Alternatively, after removing or compressing a small portion of the sphere, causing a slight flattening, Velcro can be glued onto the flattened portion and on corresponding places on the turntable adjacent to, and surrounding, the spindle. Of course, these techniques can be used in combination. To prevent any small bias which may affect the experimental results, whichever techniques are chosen should be employed on all the spheres of a given size.

The second practical difficulty concerns free rotation of the spheres. The rotation of the spheres may be encumbered by the armature assembly of the turntable. To prevent this, either the armature can be removed or the spheres can be elevated above the armature by placing them on top of a packaging Strofoam platform of relatively small dimensions. This sits directly on the turntable and is secured to it by one or more of the above techniques. The spheres would then be secured to the platform rather than the turntable.

3. The Radar System

Radar systems of high power used by professional astronomers are expensive, but inexpensive low-power systems are adequate to receive echoes from a distance of several meters to hundreds of meters. The radar system we will use, the Lab-RAD ("Radar Analysis and Display") radar system, was designed specifically for use by students of Laboratory Experiments in Physics for Modern Astronomy by engineers at International Design Engineering Associates (I. D. E. A.) in Lexington, Massachusetts (www.labRAD.co, ideaseth@verizon.net, 1-781-862-1238).

Radar systems are designated historically by names corresponding to their frequency ranges and corresponding wavelength ranges as shown in Table 1. Sports radar guns used to determine the speed of thrown baseballs, for example, operate in Ka-band and government agencies interested in generating revenue by measuring automobile speeds operate in X-band. The Lab-RAD operates in S-band, at 2.6 GHz, or 11.5-cm wavelength, approximately 4.5 in. The internal antenna is 1.1 in. long, a quarter-wave antenna common in electronics.

The results obtained with the system are sensitive to the precise location of the quarter-wave antenna within its housing. You should not expect to get the same exact results using different systems even if you observe the same rotating sphere.

The Lab-RAD requires a standard 12-V DC, 200 milliamperes (mA), power supply and emits a beam sufficiently powerful to detect echoes from objects the size of moderately-large automobiles at a distance of about 200 m. This range is more than sufficient to receive echoes in the laboratory from our rotating spheres even if they're covered with material that reflects microwaves poorly. If your laboratory does not have DC power supplies available, the Lab-RAD can utilize various types of battery packs. These include eight or, preferably, nine alkaline "D" cell batteries, two 6-V or one 12-V lantern battery, or a 12-V NiCad pack such as used in video cameras or cellular telephones. Retailers such as Radio Shack sell inexpensive battery holders appropriate to any of the battery types selected by your instructor. Note that after the radar is turned on, it emits a continuous stream of signals until it is turned off.

Table 1 Standard names of the radar frequency bands

Band name	Frequency (GHz)	Wavelength (cm)
L band	1–2	30.0–15.0
S band	2–4	15.0–7.5
C band	4–8	7.5–3.8
X band	8–12	3.8–2.5
Ku band	12–18	2.5–1.7
K band	18–27	1.7–1.1
Ka band	27–40	1.1–0.75
V band	40–75	0.75–0.40
W band	75–110	0.40–0.27

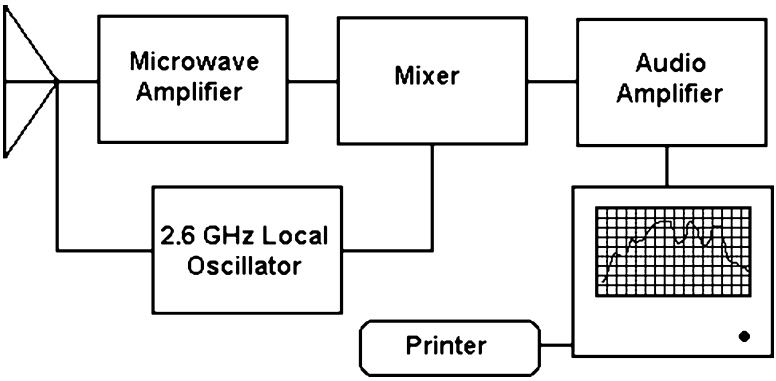

Fig. 3 Simplified schematic of the Lab-RAD radar system. The 2.6 GHz signal is sent both to the antenna for transmission as the radar beam and to the mixer. The mixed signal, at audio frequencies, is sent to the computer by a cable and a spectrum analyzer, spectrum analyzer software, or a suitable oscilloscope displays the spectrum of the echo. The power supplies attached to the amplifiers and local oscillator are not shown

As seen from (3), mixing in the Lab-RAD between the transmitted microwaves signal and the microwave signal reflected from our spheres produces an IF audio signal up to about 87 Hz, a total bandwidth of about 175 Hz, for a 4-ft diameter sphere spinning at 78 rpm. Although this mixing, as noted, is the normal operating mode for all radar systems, the manufacturer has configured the output of the Lab-RAD for our use to include a modified phone jack and a standard 3.5 mm stereo phone plug cable. One plug goes into the phone jack and the other plug goes into either the input of spectrum analyzer hardware, an appropriate oscilloscope, or the sound card jack of your computer, as described in the next section. The IF signal is then available for display and analysis, as shown in Fig. 3.

For reasons describe in the next section, the Lab-RAD translates the radar echo in frequency so that it is centered at 1 kHz. As a result, your echo will be centered, not about the physically-meaningful 0 Hz, that is, DC, but about 1 kHz. The bandwidth of the echo is unaltered.

4. Spectrum Analyzer Software

Spectral analysis enables us to measure the intensity of the radar echoes from our simulated planets simultaneously over a range of frequencies. This can be performed either by spectrum analyzer hardware or by simulating the hardware by spectrum analyzer software. Unless already available in your laboratory, the former instruments, costing from thousands to tens of thousands of dollars, are not feasible for our use. Some models of the familiar oscilloscope, however, do have spectrum

analysis capability that can process signals from 0 Hz to higher frequencies. Among these, the Tektronix TDS 210 series oscilloscopes are relatively inexpensive and process signals from DC to about 10 MHz, much greater than our needs. Their output can be stored on a Secure Digital (SD) memory card or sent directly to a computer through standard serial (RS-232) connectors to display graphs of the intensity of the echo as a function of frequency and for analysis, printing, and storage.

Spectrum analyzer software also enables us to measure the intensity of the radar echo from our simulated planets simultaneously over a range of frequencies. Once the audio signal is input into your computer sound card from the Lab-RAD, the spectrum analyzer software will display graphs of the intensity of the echo as a function of frequency. The data are stored on your computer by the software for analysis. The programs allow different total bandwidths to be displayed, and we can choose 20 Hz, which is greater than the 18 Hz bandwidth we will obtain from a 1-ft diameter sphere spinning at 33 1/3 rpm, up to 200 Hz, which is greater than the 175 Hz bandwidth we will obtain from a 4-ft diameter sphere spinning at 78 rpm. The modified Sigview FFT ("Fast Fourier Transform") Spectrum Analyzer software that we recommend for possible use was designed specifically for use by students of Laboratory Experiments in Physics for Modern Astronomy by engineers at SignalLab (Europe) (http://www.sigview.com; Mr. Goran Obradovic, info@sigview.com).

Unlike spectrum analyzer hardware and appropriate oscilloscopes, which have a flat frequency response upwards from 0 Hz, if you use spectrum analyzer software the response of your computer to the radar echo is limited by the frequency response of the computer sound card. Because these are designed to respond approximately to the range of human hearing, from 20 to 20,000 Hz, the response of computer sound cards below frequencies of 40–50 Hz is less than at higher frequencies (see, for example, http://jimmyauw.com/2006/08/09/sound-card-comparison/). This means that significant portions of the radar echo, particularly from near the subradar point, would normally not be detected.

To compensate for this, the Lab-RAD translates the radar echo in frequency so that it is centered at 1 kHz. As a result, your echo will be centered, not about the physically-meaningful 0 Hz but about 1 kHz. The bandwidth of the echo will be the same.

The range of frequencies detectable by spectrum analyzer software and the minimum frequency detectable, and therefore the frequency resolution, depend on the sampling rate of the sound card in your computer and the duration of the echo sampled. As we show in Appendix IV, the entire range of echo frequencies in our experiment is detectable. For the rotation speeds of the turntable, the frequency resolution and therefore minimum frequency detectable is approximately 1 Hz.

Different spectral analyzer software programs provide the measure of intensity in different ways. Some provide the actual power in the echo, in Watts per Hertz. In that case, the total power in the echo can be obtained by simple addition of the contributions in each frequency interval. Others provide the decibel measure of the power. The decibel level is a dimensionless measure related to the power by

$$P_{dB} = 10 \log \frac{P}{P_o}, \tag{4}$$

where P is the power in Watts per Hertz and P_o is its reference level. If the spectral analysis software you are using provides the echo strength in decibels, you must convert it to actual power before adding the contributions from different frequency intervals by calculating P_o times the antilog of $P_{dB}/10$, that is,

$$P = 10^{\frac{P_{dB}}{10}} P_o. \tag{5}$$

In addition to its various mathematical advantages, animal perception, for example, of sound and light, is closer to logarithmic than linear. Decibel notation is widely used in engineering.

5. *Calibration of the Radar System and Background Noise*

The first time you use the radar, you should perform a simple experiment to ensure that it can detect a band of frequencies present in the echo. Place a simple electric household fan a few feet in front of the radar. You might want to wrap aluminum foil around the blades of the fan, removing the protective cover if necessary, to obtain a stronger echo, but an echo will be obtained even from a fan with plastic blades. Rotate the fan so that it makes about a 45° angle with the line-of-sight to the radar. Then turn on the fan and the radar. The spectrum analyzer computer screen display should show a finite width of frequencies in the echo. The width of the display should change both as you change the rotational speed of the fan and as you change its orientation with respect to the radar.

Effective use of the radar requires determination of three factors. We must calibrate the scale by determining a value of Doppler shift for a known velocity, determinate the magnitude of background interference and system noise, and determine the appropriate amplification, or *gain*, of the amplitude of the echo signal. Concerning the first factor, unlike the calibration when receiving echoes from objects moving with a single speed, such as automobiles, we have an easily calibrated situation. The sub-radar point will provide the largest echo, and has a zero relative velocity with respect to the radar. The other parts of the echo received from the rotating sphere are essentially symmetric in frequency, the only asymmetries arising from differences in roughness from the placement of the metallic objects on the surface.

Potentially strong microwave signals in the laboratory are produced by fluorescent lights and power mains and electrical lines operating at 60 Hz. Because we want to determine the total energy in the radar echo, we must measure these spurious sources of noise as well as the noise in the system itself. To do so, we simply measure the output with the radar not firing.

Make sure that none of the other experimenters in the laboratory are firing their radar transmitters. You might say, “Measuring noise levels, please do not use your radar.” Once you are assured of no interference, point the radar at a 5-ft square piece of cardboard, standing upright, in front of which your spheres will be placed. Make sure no fluorescent lights are in the line-of-sight. Then start the spectrum

analyzer, spectrum analyzer software, or suitable oscilloscope and print out a copy of the computer screen image of the echo. That will be a record of the level of noise produced not only by the background in the laboratory but also by the system itself.

Concerning the third factor, in general the appropriate setting of gain depends on the desire to amplify signals above the noise while operating in the stable range of the electronics. In single frequency radar systems such as radar guns, the gain setting governs the amplification of a signal at a single audio frequency after it has been digitized for LED readout. It does not govern the amplification of the radio frequency echo itself. Instead of digitization, the Lab-RAD system sends the band of frequencies in the radio frequency echo directly to the spectrum analyzer or to the computer for display by the spectrum analyzer software. Accordingly, no need exists for a gain setting in the Lab-RAD. Your spectrum analyzer software may allow you to change the vertical scale of the display.

The magnitude of the echo received depends on several factors, the size of the reflecting object, its distance, and how it disperses in frequency the transmitted beam on reflection. The latter depends on the surface characteristics of the object and whether or not it rotates. Unlike the use of radar to detect, for example, automobile speeds, the Lab-RAD radar system detects portions of relatively small objects, segments of the surfaces of the rotating spheres, each moving at different speeds. The relatively small size of the reflecting regions will reduce the magnitude of the echo in each frequency interval compared to the magnitude of an echo reflected from a non-rotating object. In addition, our spheres are not completely covered with metallic material. These factors will reduce the magnitude of the echo compared to the outdoor scenario. On the other hand, our rotating spheres are relatively close to the radar system and we will place them so that they intercept and therefore reflect most of the transmitted radar beam. These two factors will increase the magnitude of the echo. As a result of these various considerations, easily detectable signals are created in our laboratory.

6. *Positioning the Radar System*

We must ensure that the radar system is located at such a distance that the radar beam fully illuminates the hemisphere of the sphere facing the radar. If it does not, then we will not be receiving echoes with the largest redshifts and blueshifts and will not be able to accurately determine the rotational velocity of our spheres. As well, we don't want the transmitted radar signal to spill over the edges of the spheres. This not only wastes some of the energy, decreasing the amount of energy to be reflected and then detected by our receiver, but it also leads to interference problems for your own laboratory setup and for those of other students in the laboratory.

Figure 4 shows the relevant geometry. The radar beam has a finite angular size, θ. As the radar system is moved away from the target, a larger and larger portion of

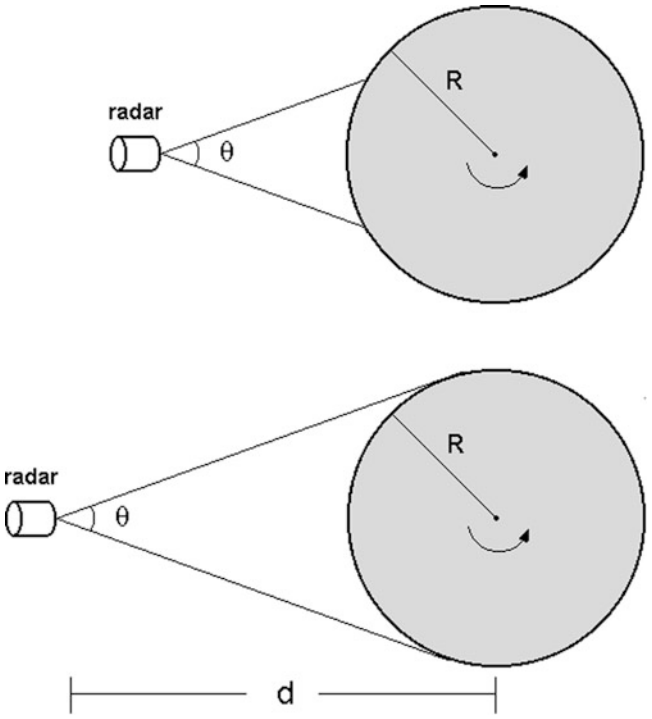

Fig. 4 In this *top* view, the radar is moved successively further away from the reflecting rotating target until the target is fully illuminated. At this distance, d, the bandwidth of the echo will be its largest, and will not increase with further distance

its surface is illuminated. At the same time, assuming the entire transmitted beam is intercepted by the target, the intensity of the echo decreases as $1/d^2$.

In fact, Fig. 4 oversimplifies the nature of the radar beam in both transmission and reception. As we will see in Experiment #15, "Thermal Radiation from a Planetary Subsurface: Part II. Soil Sample Measurements," the beam is actually a single slit diffraction pattern with a main lobe and side-lobes. As a result, our determination of the distance of the radar from the sphere for full illumination is not as perfectly well defined as Fig. 4 would imply.

In this simplified model of the beam, full illumination of the target will occur at a distance, d, given by $tan\ \theta/2 = R/d$, where R is the radius of the target, Fig. 4.

We can imagine two ways of determining the position necessary for full illumination. First, we could move the radar increasingly far from a flat disk whose radius is that of the sphere that will be used to simulate the planets until the radar spills over the side of the target. As we move the radar away from the target disk to a distance d, the echo signal from the target disk will decrease as $1/d^2$. Once we get sufficiently far from the target disk that the radar beam spills over the edge of the disk, then the amount of transmitted radiation to be reflected will decrease additionally by the ratio $\pi R^2/\pi r^2$, where R is the radius of the target disk and r is the

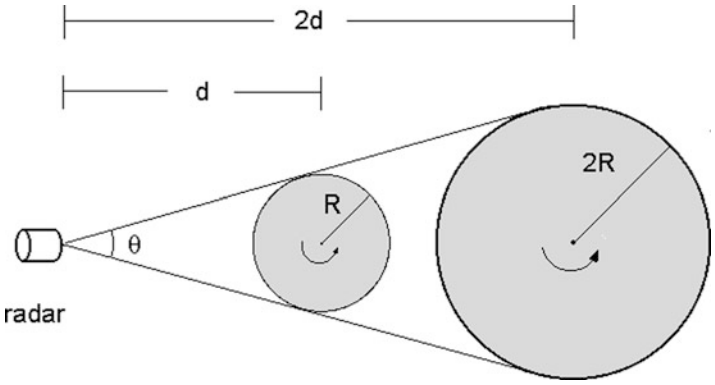

Fig. 5 By similar triangles, the distance, d, for the radar to fully illuminate a 4-ft diameter sphere will be twice that to fully illuminate a 2-ft diameter sphere, if those are the sizes of spheres you will be using

radius of the transmitted beam when it has reached the target disk. Only that fraction of the beam will now be reflected. The beam size r when it has reached the target disk, however, is related by $tan\ \theta = r/d$ to the distance, d, of the transmitter to the target. Accordingly, once the distance is sufficiently great, the strength of the echo will decrease by another factor of $1/d^2$ so that the total diminution will go as $1/d^4$.

Unfortunately, this change of dependence on d, while strong, is not strong enough to be a reliable basis for determining the distance d at which the full sphere would be illuminated. One of several problems is that the echo from the outer parts of the target disk would be observed in the side-lobes of the radar antenna, masking the effect.

The second technique, and the one we will use, observes the increasing width of the echo received as the radar is moved from the actual target sphere. As you move the radar away to increasingly greater distances from the target sphere the bandwidth of the radar echo will increase until the entire surface is illuminated. If you move the radar to greater distances the intensity of the echo will decrease at all Doppler shifts as $1/d^2$ but the bandwidth of the echo will not increase. That will tell you that you have illuminated the entire hemisphere of the sphere visible from the radar.

We will use one of the small-size spheres. Using, for example, the 1-ft diameter sphere allows us to determine the full-illumination distance with measurements twice as close to the sphere than if we had used a 2-ft diameter sphere, as shown in Fig. 5. This would provide a four-fold increase in echo intensity, providing more accurate results. From similar triangles, we see that the full-illumination distance for a 2-ft diameter sphere will simply be twice the value determined using a 1-ft diameter sphere, as shown in Fig. 5. Other ratios in distance apply, of course, if you are using small-size and large-size spheres whose diameters are not in that ratio. We will spin the small-size sphere at the smallest rotation rate available. This will result

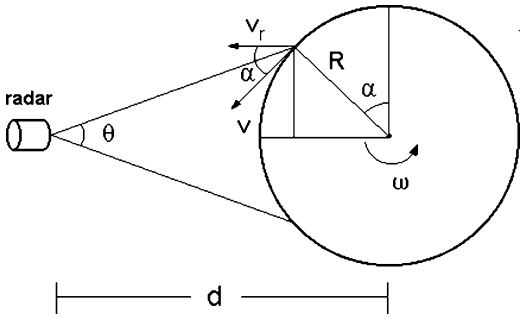

Fig. 6 The bandwidth of the echo as seen from the radar is approximately proportional to the distance of the radar from the target

in a spread of the echo energy over a relatively small bandwidth, producing the highest intensity of the echo over the echo bandwidth that we can achieve.

The dependence of the bandwidth of the echo on distance is approximately linear. As shown in Fig. 6, the component of the rotational velocity toward the radar is $v_r = R\omega \cos \alpha$, where R is the radius of the sphere and α is the angle measured as shown. We can express $\tan \theta/2$ in terms of this geometry as $R \cos \alpha/(d\text{-}R \sin \alpha)$. Neglecting $R \sin \alpha$ compared to d, this simplifies to $\tan \theta/2 = R/d \cos \alpha$. We therefore find that $v_r \approx \omega d \tan \theta/2$, so that v_r is proportional to d. In other words, as the radar is moved further from the target the width of the Doppler-shifted echo will increase linearly with d until full illumination is achieved. This is easily observed.

Place the small-size sphere covered with crumpled-up aluminum foil on the elongated spindle of the turntable. This highly reflecting material will provide the largest echo. Place a 5-ft square piece of cardboard upright behind the sphere. Place the radar system about 1 foot from the target on the 1-ft radar stand and point it directly at the center of the sphere. Measure the distance and enter it in Table 2 of the DATA SHEET in centimeters.

To avoid stray signals from the other radar systems in the laboratory, including the radar transmissions themselves, their echoes, and reflections of these transmissions and echoes, it is best that none of the other experimenters in the laboratory are firing their radar transmitters while you make your observations. You might say, "Observing, please do not use your radar." Once you are assured of no interference, and if no other students have informed you that they are currently observing, turn on the radar. Put on your safety goggles, turn on the rotating turntable, spinning it at 33 1/3 rpm, the lowest rotation rate available, and start the spectrum analyzer software.

If you are displaying the echo on a computer, print out a copy of the computer screen image. You will notice on the computer screen a finite width of the echo signal. Enter in Table 2 of the DATA SHEET the frequency, f_1, at which the signal is detectable at the low frequency end and the frequency, f_2, at which the signal is detectable at the high frequency end of the bandwidth. Also enter the value of frequency, f_o, for which the intensity is greatest.

Move the radar system successively at slightly greater distances further from the target and repeat the observations. Obtain a printout of each computer screen. As you move the radar antenna further and further away from the target, the values of f_1 should decrease and the values of f_2 should increase. The values of f_o should

remain the same. Continue moving the radar system further from the target until no significant change in the values of f_1 or f_2 occurs. Then turn off the radar system and the turntable. Enter that distance on the DATA SHEET in centimeters. The computer printout of this particular computer screen, for the crumpled-up aluminum stapled onto the small-size sphere, will be used for the analysis of the following section. Identify that printout by writing "aluminum foil, small-size sphere, 33 1/3 rpm" on it along with your name and that of your lab partner.

With the radar transmitter at this position you will totally illuminate the small-size spheres simulating the planets and asteroids with little or no spillover. Multiply that distance by the appropriate ratio to determine the distance from the large-size sphere at which full illumination will occur and enter that result on the DATA SHEET. Even with this precaution, place the 5-ft square piece of cardboard upright behind the turntable platform to ensure that spillover is not a problem.

From the geometry of Fig. 6, full illumination of the sphere will occur for $\tan \theta/2 = R/d$. The width of the illuminating beam will depend on your construction of the housing portion of the RG7 radar. With a beam, for illustration, of about 60°, the distance, d, from a 1-ft diameter sphere for full illumination will be about 0.9 ft or 0.3 m. The corresponding distance from a 2-ft diameter sphere will be about 1.7 ft or 0.5 m.

7. *Observations of Simulated Planets*

Keep the radar system located at the distance you have just determined and keep the small-size sphere with the crumpled-up aluminum foil on the extended spindle of the turntable. Set the turntable to 78 rpm and turn it on. Every time you turn on the turntable, put on your safety goggles.

As in the previous section, we want to avoid stray signals from the other radar systems in the laboratory. Accordingly, it is best that none of the other experimenters in the laboratory are firing their radar transmitters while you make your observations. You might say, "Observing, please do not use your radar." Once you are assured of no interference, and if no other students have informed you that they are currently observing, turn on the radar. If you are displaying the echo on a computer, print out a copy of the computer screen image. Then turn off the turntable and radar. Identify that printout by writing "aluminum foil, small-size sphere, 78 rpm" on it along with your name and that of your lab partner.

Remove the sphere with the crumpled-up aluminum foil and place the small-size sphere with the imbedded staples on the extended spindle of the turntable. Reset the turntable speed to 33 1/3 rpm, turn it on, and turn on the radar. If you are displaying the echo on a computer, print out a copy of the computer screen image. As before, identify the printout by writing the material, sphere size, and speed of the turntable on it along with your name and that of you lab partner. Repeat the procedure with the turntable speed at 78 rpm. Turn off the turntable and the radar.

Remove the sphere with the imbedded staples and place the small-size sphere with the imbedded nails and paper clips on the extended spindle of the turntable. Repeat the sequence of observations. If you are displaying the echo on a computer, print out a copy of the computer screen image for both rotation speeds. Turn off the turntable and the radar.

Now move the radar system to the appropriate distance from the turntable, twice if, for example, you are using 1-ft diameter and 2-ft diameter spheres. We will now obtain the radar echo from the three large-size spheres. Place the radar system on the 2-ft radar stand. With the radar system pointed directly at the center of the spheres, repeat the pairs of observations for the crumpled-up aluminum foil, imbedded staples, and imbedded nails and paper clips at both rotation speeds. In each case, if you are displaying the echo on a computer, print out a copy of the computer screen image. When you have completed the observations, you will have 12 printouts of the computer screen, radar echoes for six spheres rotated at 78 and 33 1/3 rpm.

D. Calculations and Analysis

1. The Soil Samples

You obtained several measures of the roughness of the aluminum foil. Average those values and enter the result on the DATA SHEET.

2. System Calibration

Using the printout of the computer screen of background and system noise, estimate the intensities in 5 Hz intervals. If this is not convenient with the spectral analyzer software you are using, choose a more appropriate interval. Enter the range of frequencies in the channel and the noise results in Table 3 of the DATA SHEET. Add up the intensities and enter the value, I_N , in the bottom row of Table 3 of the DATA SHEET. If the spectral analyzer software you are using provides results in decibels, convert those values to measures of power using (5). An additional column is provided in Table 3 to display the results of those conversions.

3. Echo Intensities

Using the printout of the computer screen of the sets of echoes obtained with the small-size and large-size spheres, we will estimate the intensity in 1 Hz intervals above the level of background and system noise as entered in Table 3. If this

frequency interval is not convenient with the printout obtained with the spectrum analyzer software you are using, choose a more appropriate interval.

Enter the range of frequencies in each frequency channel in column 2 of Table 4a of the DATA SHEET. Using the printout of the computer screen of the six sets of echoes received from the small-size spheres, estimate the values of the raw intensities of the echoes in Table 4a of the DATA SHEET.

If the spectral analysis software you are using provides results in decibels, convert those values to measures of intensity using (5). If this was needed, enter the results of those conversions in Table 4b. For bookkeeping purposes, also copy the values of the range of frequencies in each frequency channel from column 2 of Table 4a into column 2 of Table 4b.

We can now estimate the level of intensity above the background and system noise. To get these estimates, at each frequency interval on each computer screen printout draw a horizontal line representing the level of intensity of the background and system noise that you entered in Table 3 of the DATA SHEET. Your result will look like Fig. 7.

Now subtract the values of background and system noise from the values of raw intensity entered in Table 4a (or Table 4b if conversion was necessary). To most effectively avoid errors, this can be done graphically using the computer printouts. Alternatively, you can subtract the values entered in Table 3 from those entered in Table 4a (or Table 4b). Enter those results in Table 4c. If the result of any subtraction is less than zero, enter zero for the result. For bookkeeping purposes, also copy the values of the range of frequencies in each frequency channel from column 2 of Table 4a into column 2 of Table 4c.

Add up the contributions to the intensities from each frequency interval. Enter the result in the bottom row of Table 4c on the DATA SHEET. This is a measure of the intensity of the total radar echo, corrected for the background and system noise. Summarize those values in Table 6 of the DATA SHEET.

Note that if you have a planimeter available in your laboratory, you can determine the corrected intensity of the total radar echo directly, without the calculations, by measuring the area between the echo curve and the background and noise levels on your computer screen printouts corresponding to Fig. 7.

Using the printout of the computer screen of the six sets of echoes obtained with the large-size spheres, perform these same calculations. Enter the raw data in Table 5a, the converted data from decibels, if needed, in Table 5b, and the difference between the raw data and the background and system noise in Table 5c. Add up the contributions to the intensities from each frequency interval. Enter the result in the bottom row of Table 5c on the DATA SHEET. This is a measure of the total radar echo, corrected for the background and system noise. Summarize those values in Table 6 of the DATA SHEET.

Construct a graph of the echo energy as a function of the particle size of the three "soil samples." Use the graph paper provided on the DATA SHEET. Clearly distinguish the 12 data points as to rotation rate of the turntable, sphere diameter, and nature of the material on the surface by drawing a line connecting the data for a given sphere diameter and using a different symbol for the two rotation rates.

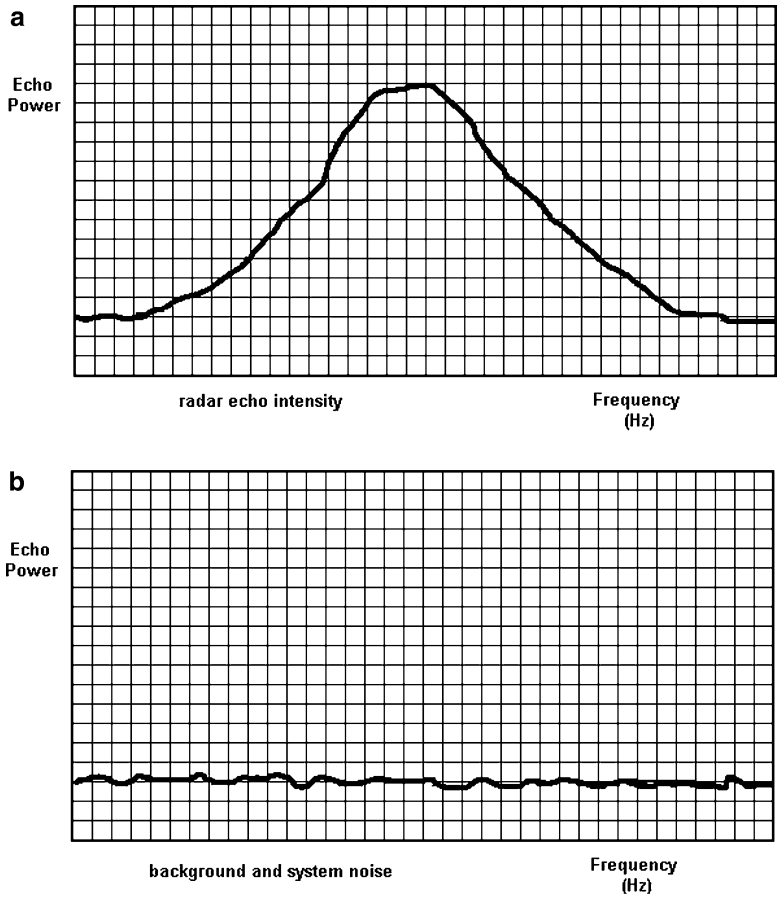

Fig. 7 (**a**) Spectrum analyzer software provides the echo strength as a function of frequency. (**b**) The intensity of the echo in each frequency interval must be reduced by the intensity of background and system noise, observed separately without the radar transmitting a signal toward the spheres. If the result that you calculate is negative, consider the intensity of the echo to be zero

4. Rotational Velocities

From (2) and knowledge of the radii of the spheres, calculate the rotational velocities in m/s of the spheres at rotation rates of 33 1/3 and 78 rpm. Show your calculations on the DATA SHEET and enter the results in Table 7 of the DATA SHEET. Copy the results into the third column of Table 8. Note that the velocities do not depend on the nature of the soil material so that each result will be copied into three rows.

From the printout of each of the computer screens, estimate the minimum and maximum frequencies at which an echo was received. Enter those results in Table 8

of the DATA SHEET, calculate their differences, the echo bandwidth $f_2 - f_1$, and enter those results in Table 8. Equation 9 of Experiment #9, "Determination of the Rotation Rate of Planets and Asteroids by Radar: Part I. Observations of Mercury," provides the period of rotation of the planet in terms of the observed radar echo bandwidth,

$$v = \frac{\lambda_o}{4} BW_f, \tag{6}$$

where BW_f is identified here as $f_2 - f_1$. From the echo bandwidths tabulated in Table 8, calculate the value of the rotational velocities and enter them in the final column of Table 8 of the DATA SHEET. Perform all your calculations on the DATA SHEET.

Using the results of columns 3 and 7 in Table 8, construct a graph comparing the two rotational velocities. Use the graph paper provided on the DATA SHEET. Clearly distinguish the 12 data points as to rotation rate of the turntable, sphere diameter, and nature of the material on the surface by using different symbols for the data points.

STUDENT'S NAME _____

E. Rotation Rate by Radar Experiment II Data Sheets

1. Soil Material

Thickness of staples: _____ mm
Thickness of paper clips: _____ mm
Thickness of nails: _____ mm
Scale of crumpled-up aluminum foil folds: _____ mm
_____ mm
_____ mm
_____ mm

Calculation of average value of crumpled-up aluminum folds

Average value of aluminum foil folds: _____mm

2. System Calibration

Table 2 Positioning the radar

Measurement number	Distance (cm)	Maximum frequency, f_1	Minimum frequency, f_2	Frequency of maximum echo, f_o

Distance from small-size spheres for full illumination: _____ cm
Distance from large-size spheres for full illumination: _____ cm

STUDENT'S NAME _____

Table 3 Background and system noise levels

Channel number	Channel range (Hz)	Intensity	(Converted from dB)	Channel number	Channel range (Hz)	Intensity	(Converted from dB)
1				21			
2				22			
3				23			
4				24			
5				25			
6				26			
7				27			
8				28			
9				29			
10				30			
11				31			
12				32			
13				33			
14				34			
15				35			
16				36			
17				37			
18				38			
19				39			
20				40			

STUDENT'S NAME _____

3. Echo Intensities

Table 4a Raw echo intensities from small-size diameter rotating spheres

Channel number	Channel range (Hz)	Intensity 33 1/3 rpm "sand"	Intensity 33 1/3 rpm "pebbles"	Intensity 33 1/3 rpm "rocks"	Intensity 78 rpm "sand"	Intensity 78 rpm "pebbles"	Intensity 78 rpm "rocks"
1							
2							
3							
4							
5							
6							
7							
8							
9							
10							
11							
12							
13							
14							
15							
16							
17							
18							
19							
20							

STUDENT'S NAME _____

Table 4b Intensities converted from dB (if needed) small-size diameter rotating spheres

Channel number	Channel range (Hz)	Intensity 33 1/3 rpm "sand"	Intensity 33 1/3 rpm "pebbles"	Intensity 33 1/3 rpm "rocks"	Intensity 78 rpm "sand"	Intensity 78 rpm "pebbles"	Intensity 78 rpm "rocks"
1							
2							
3							
4							
5							
6							
7							
8							
9							
10							
11							
12							
13							
14							
15							
16							
17							
18							
19							
20							

STUDENT'S NAME _____

Table 4c Intensities corrected for background and system noise small-size diameter rotating spheres

Channel number	Channel range (Hz)	Intensity 33 1/ rpm "sand"	Intensity 33 1/ rpm "pebbles"	Intensity 33 1/ rpm "rocks"	Intensity 78 rpm "sand"	Intensity 78 rpm "pebbles"	Intensity 78 rpm "rocks"
1							
2							
3							
4							
5							
6							
7							
8							
9							
10							
11							
12							
13							
14							
15							
16							
17							
18							
19							
20							
TOTAL							

STUDENT'S NAME _____

Table 5a Raw echo intensities from large-size diameter rotating spheres

Channel number	Channel range (Hz)	Intensity 33 1/ rpm "sand"	Intensity 33 1/ rpm "pebbles"	Intensity 33 1/ rpm "rocks"	Intensity 78 rpm "sand"	Intensity 78 rpm "pebbles"	Intensity 78 rpm "rocks"
1							
2							
3							
4							
5							
6							
7							
8							
9							
10							
11							
12							
13							
14							
15							
16							
17							
18							
19							
20							
21							
22							
23							
24							
25							
26							

(continued)

STUDENT'S NAME _____

Table 5a (continued)

Channel number	Channel range (Hz)	Intensity 33 1/ rpm "sand"	Intensity 33 1/ rpm "pebbles"	Intensity 33 1/ rpm "rocks"	Intensity 78 rpm "sand"	Intensity 78 rpm "pebbles"	Intensity 78 rpm "rocks"
27							
28							
29							
30							
31							
32							
33							
34							
35							
36							
37							
38							
39							
40							

STUDENT'S NAME _____

Table 5b Intensities converted from dB (if needed) large-size diameter rotating spheres

Channel number	Channel range (Hz)	Intensity 33 1/ rpm "sand"	Intensity 33 1/ rpm "pebbles"	Intensity 33 1/ rpm "rocks"	Intensity 78 rpm "sand"	Intensity 78 rpm "pebbles"	Intensity 78 rpm "rocks"
1							
2							
3							
4							
5							
6							
7							
8							
9							
10							
11							
12							
13							
14							
15							
16							
17							
18							
19							
20							
21							
22							
23							
24							
25							
26							

(continued)

STUDENT'S NAME _____

Table 5b (continued)

Channel number	Channel range (Hz)	Intensity 33 1/ rpm "sand"	Intensity 33 1/ rpm "pebbles"	Intensity 33 1/ rpm "rocks"	Intensity 78 rpm "sand"	Intensity 78 rpm "pebbles"	Intensity 78 rpm "rocks"
27							
28							
29							
30							
31							
32							
33							
34							
35							
36							
37							
38							
39							
40							

STUDENT'S NAME _____

Table 5c Intensities corrected for background and system noise large-size diameter rotating spheres

Channel number	Channel range (Hz)	Intensity 33 1/ rpm "sand"	Intensity 33 1/ rpm "pebbles"	Intensity 33 1/ rpm "rocks"	Intensity 78 rpm "sand"	Intensity 78 rpm "pebbles"	Intensity 78 rpm "rocks"
1							
2							
3							
4							
5							
6							
7							
8							
9							
10							
11							
12							
13							
14							
15							
16							
17							
18							
19							
20							
21							
22							
23							
24							
25							

(continued)

STUDENT'S NAME _____

Table 5c (continued)

Channel number	Channel range (Hz)	Intensity 33 1/ rpm "sand"	Intensity 33 1/ rpm "pebbles"	Intensity 33 1/ rpm "rocks"	Intensity 78 rpm "sand"	Intensity 78 rpm "pebbles"	Intensity 78 rpm "rocks"
26							
27							
28							
29							
30							
31							
32							
33							
34							
35							
36							
37							
38							
39							
40							
TOTAL							

STUDENT'S NAME _____

Table 6 Corrected echo energies

Simulated planet	Rotation rate (rpm)	Corrected echo energy
small-size sphere: "sand"	33 1/3	
small-size sphere: "pebbles"	33 1/3	
small-size sphere: "rocks"	33 1/3	
small-size sphere: "sand"	78	
small-size sphere: "pebbles"	78	
small-size sphere: "rocks"	78	
large-size sphere: "sand"	33 1/3	
large-size sphere: "pebbles"	33 1/3	
large-size sphere: "rocks"	33 1/3	
large-size sphere: "sand"	78	
large-size sphere: "pebbles"	78	
large-size sphere: "rocks"	78	

Graph of corrected echo energy as a function of soil sample particle size

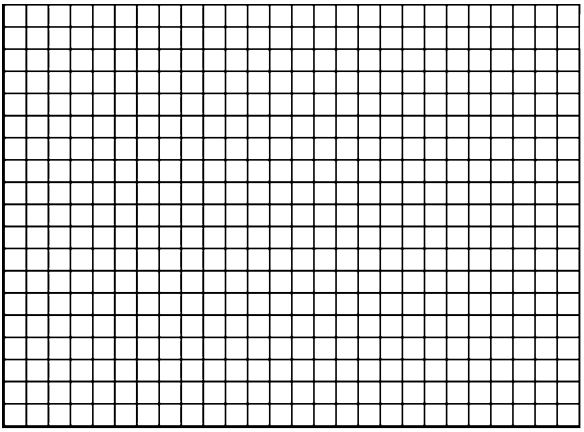

STUDENT'S NAME _____

Description of graphical results

Is there a dependence of total energy on particle size? Would you expect such a dependence? Why or why not?

Is there a dependence of total energy on the diameter of the spheres? Would you expect such a dependence? Why or why not?

Is there a dependence of total energy on rotation rates of the turntable? Would you expect such a dependence? Why or why not?

4. Rotational Velocities

Table 7 Rotational velocities of the turntable edge

Simulated planet	33 1/3 rpm	78 rpm
small-size sphere		
large-size sphere		

Calculation of rotational velocities

Rotational velocity of small-size sphere at 33 1/3 rpm:

Rotational velocity of small-size sphere at 78 rpm:

Rotational velocity of large-size sphere at 33 1/3 rpm:

Rotational velocity of large-size sphere at 78 rpm:

STUDENT'S NAME _____

Table 8 Rotational velocities from echo

Simulated planet	Rotation rate (rpm)	Corresponding rotational velocity = v_1 (m/s)	Minimum frequency f_1 (Hz)	Maximum frequency f_2 (Hz)	Echo bandwidth $f_2 - f_1$ (Hz)	Deduced rotational velocity v_2 (m/s)
small-size sphere: "sand"	33 1/3					
small-size sphere: "pebbles"	33 1/3					
small-size sphere: "rocks"	33 1/3					
small-size sphere: "sand"	78					
small-size sphere: "pebbles"	78					
small-size sphere: "rocks"	78					
large-size sphere: "sand"	33 1/3					
large-size sphere: "pebbles"	33 1/3					
large-size sphere: "rocks"	33 1/3					
large-size sphere: "sand"	78					
large-size sphere: "pebbles"	78					
large-size sphere: "rocks"	78					

STUDENT'S NAME _____

Calculation of deduced rotational velocity from (6)

small-size sphere: "sand" 33 1/3 rpm:

small-size sphere: "pebbles" 33 1/3 rpm:

small-size sphere: "rocks" 33 1/3 rpm:

small-size sphere: "sand" 78 rpm:

small-size sphere: "pebbles" 78 rpm:

small-size sphere: "rocks" 78 rpm:

large-size sphere: "sand" 33 1/3 rpm:

large-size sphere: "pebbles" 33 1/3 rpm:

large-size sphere: "rocks" 33 1/3 rpm:

large-size sphere: "sand" 78 rpm:

large-size sphere: "pebbles" 78 rpm:

large-size sphere: "rocks" 78 rpm:

STUDENT'S NAME _____

Comparison of the rotational velocities determined by the turntable rotation rate (ordinate) and the echo bandwidth (abscissa):

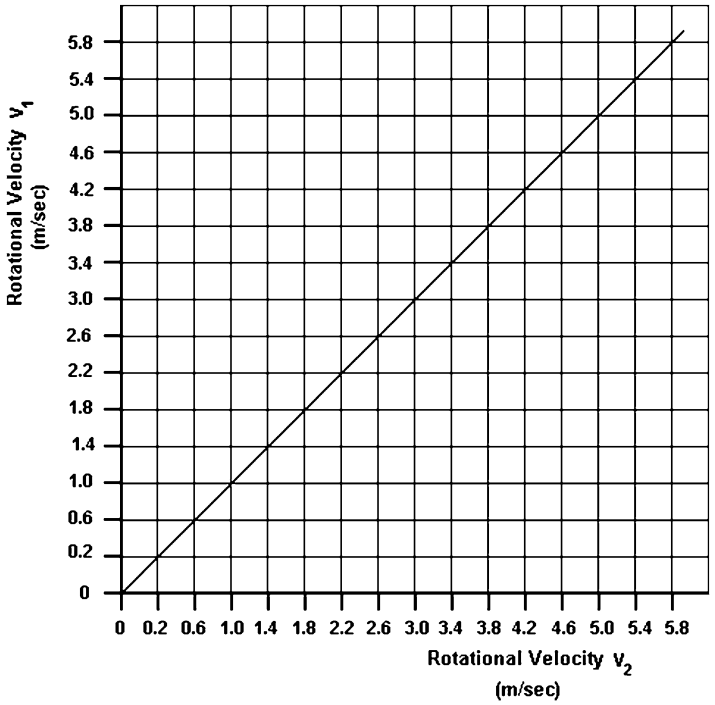

If the radar echo produced exactly the expected values, the points you plot should fall along the straight line. In general they do not. For data points representing which rotation rates, sphere diameters, and material is the difference significant?

Provide explanations of any differences.

STUDENT'S NAME _____

F. Rotation Rate by Radar Experiment II Discussion Questions

1. Let's say we are trying to determine the rotation rate of a spherical asteroid and that at the moment of observation an extremely high chain of mountains appears at the edge of the disk. How would that affect the period of rotation determined by the radar? Show which equations of Experiment #9, "Determination of the Rotation Rate of Planets and Asteroids by Radar: Part I. Observations of Mercury" you use to reach your conclusion.

2. Below is a simplified drawing of a radar echo. For the same planet, assume that the edge of the planet moving toward us has a chain of high mountains and that the edge of the planet moving away from us has a deep and wide chasm along the equator, of greater extent than the vast Valles Marineris on Mars. Draw the appearance of the radar echo that would now be observed.

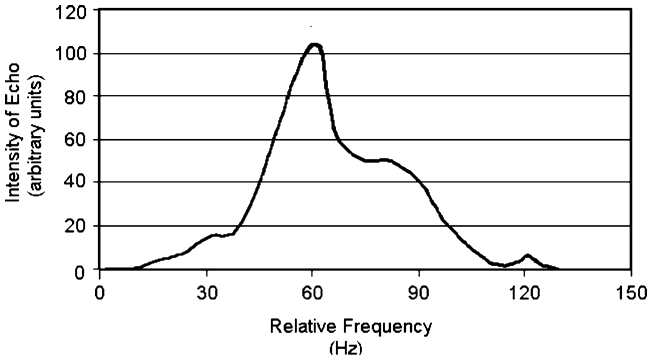

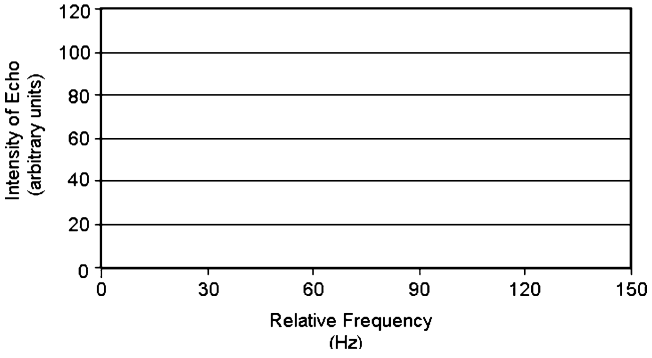

Explain your answer.

STUDENT'S NAME _____

3. Here are simplified drawings of total radar echoes from four hypothetical planets. Two are covered with ice, and therefore smooth on a scale of our radar wavelength, and two have rough surfaces. Two are twice as large as the other two. They all rotate at the same velocity. Which radar echo, 1, 2, 3, and 4, comes from which planet?

   a. smooth surface and large diameter planet _____

   b. smooth surface and small diameter planet _____

   c. rough surface and large diameter planet _____

   d. rough surface and small diameter planet _____

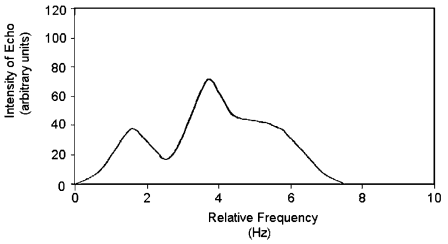

(1)

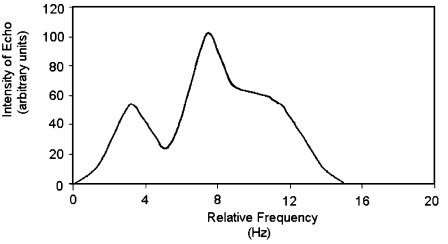

(2)

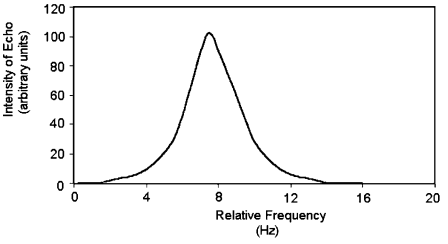

(3)

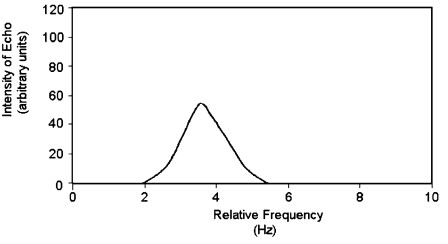

(4)

Explain your answers.

STUDENT'S NAME _____

4. Radar is not useful to determine the rotation rate of the cloud-enshrouded planets of Jupiter and Saturn. The planets are sufficiently distant that the strength of the echoes would be very weak and the thick atmospheres would absorb the incident radar signals. Assume that these problems don't exist. Based on your knowledge of these two planets, provide at least two other reasons that radar can't be used to determine their rotation rates.

5. In Experiment #9, "Determination of the Rotation Rate of Planets and Asteroids by Radar: Part I. Observations of Mercury," we calculated that the velocity at the equator of Mercury resulting from its rotation is about 3 m/s. Assume this yields a radar echo bandwidth of 10 Hz.

   a. Calculate the velocity at the equator of the Earth resulting from the rotation of the Earth.

   b. If XyTk@2 were observing the Earth using radar at the same frequency, what would be the bandwidth of the radar echo he would determine? Show all your calculations here.

STUDENT'S NAME _____

6. Asteroids in an assemblage would continually affect each other by gravity and collisions. As a result, the distribution of their rotation speeds might be expected to be described by the same unimodal shaped curve that governs the speed of molecules in a gas, the Maxwellian distribution. Let's say astronomers obtain the radar echoes of hundreds of asteroids and the distribution of their total radar bandwidths is not unimodal but rather bimodal as shown. Assume the asteroids in the sample to be the same shape and the same size, so that the observed bandwidths of the radar echo are simply proportional to the rotation speed. Provide two or more possible explanations of these (hypothetical) results.

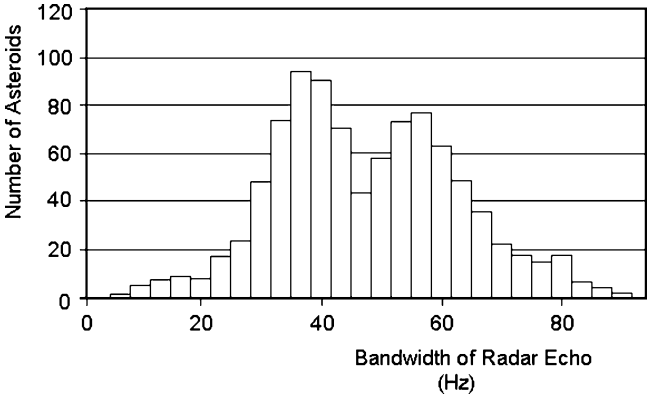

STUDENT'S NAME _____

7. Let's say that XyTk@2 was observing the Earth with the radar of question #5 at the time that San Francisco was at the sub-radar point. Sketch the appearance of the resulting radar echo, summed over all delays. Use the result of question #5b and Eq. (8) of Experiment #9, "Determination of the Rotation Rate of Planets and Asteroids by Radar: Part I. Observations of Mercury," to provide the range on the abscissa axis.

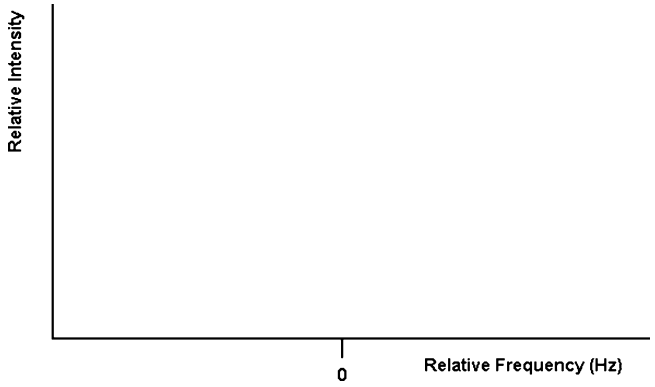

8. In Sect. E of Experiment #9, "Determination of the Rotation Rate of Planets and Asteroids by Radar: Part I. Observations of Mercury," you provided a graph of the total radar echo of the planet Mercury at a wavelength of 70 cm. As discussed there, the velocity of the limb of Mercury resulting from its rotation is 3 m/s. In the present experiment, the velocity at the surface of a 2-ft diameter sphere is similar, 2.5 m/s when rotated at 78 rpm. Answer the following if your experiment employed a sphere with a diameter close to two feet.

   a. Compare the graph of the total radar echo of the planet Mercury with those for the 2-ft diameter spheres rotated at 78 rpm covered with each of the three surface materials. Does the graph of the total radar echo of Mercury resemble any of our three total radar echoes?

   b. Do you expect a resemblance? Why or why not?

9. In Experiment #17, "Blackbody Radiation," you will study Wien's displacement law. This tells us that many warm objects radiate the maximum of their radiation at a wavelength inversely proportional to the temperature of the object,

$$\lambda_{\max} = \frac{0.3}{T},$$

   where $\lambda_{\max}$ is given in cm and T is given in K.

STUDENT'S NAME _____

a. If the temperature of the laboratory is 25°C, what is the value of λ_{max} of the radiation it is emitting? Show your calculations here.

b. Our radar emits at a wavelength of 11.5 cm. Will the radiation being emitted by the room create a substantial problem with our experimental results? Show your calculations here.

c. At what room temperature would a problem with our experiment occur? Show your calculations here.

10. Diffuse and specular reflection, phenomena of optics that we studied in Experiment #6 and #7, "The Surface Roughness of the Moon: Reflection and Scattering from a Planetary Surface: Part I. Surface Materials," and "The Surface Roughness of the Moon: Reflection and Scattering from a Planetary Surface: Part II. Beads and Surface Coverage," occur for all types of waves. Recall that a condition for specular reflection is the surface being smooth compared to the wavelength of the incident radiation.

a. For which of the surface materials with which we covered our spheres would you expect to see a radar echo that would be close to specular reflection?

b. Do the printouts of the computer screens of those echoes indicate specular reflection? If not, provide an explanation.

c. What kind of material could we place on the surface of our rotating spheres to obtain radar echoes that would produce specular reflection at our 11.5-cm wavelength?

STUDENT'S NAME _____

Removing these DATA SHEETS from the book may damage the binding. You might consider entering the data and performing your calculations in the book, and then photocopying the DATA SHEETS for submission to your instructor for grading.

Attach the printouts of the computer screens to these DATA SHEETS or your photocopies.

Experiment 11
The Orbit of Venus

SUMMARY: In Experiment #11, "The Orbit of Venus," we employ a reticulated eyepiece attached to a modest telescope to observe the planet Venus as it orbits the Sun. Holding the telescope fixed in position, you will determine the field of view of the telescope by tracking a bright star. This will enable you to determine the angular size of Venus at various times. Graphing that data will enable determination of its orbital period.

LEVEL OF DIFFICULTY: Low

EQUIPMENT NEEDED: Binoculars or small telescope; reticulated eyepiece.

MY LEARNING GOALS

1. To be able to describe the differences between the Ptolemaic and Copernican models of the solar system, particularly their relative complexities.
2. To be able to recognize the use of authority rather than reason to reach truth.
3. To be able to predict the appearance of interior planets through a telescope depending on their location in their orbit relative to the Earth.
4. To be able to apply the physics of circular motion to derive the orbital period of a planet.

L.M. Golden, *Laboratory Experiments in Physics for Modern Astronomy: With Comprehensive Development of the Physical Principles*,
DOI 10.1007/978-1-4614-3311-8_11,

A. Introduction

When Galileo Galilei (1564–1642) pointed the telescope he had built (after hearing of the invention of such instruments by a Dutch optician, Hans Lippershey (1570–1619)) to the skies, he made four momentous discoveries about the solar system. He found spots on the Sun, craters on the Moon, and satellites revolving around Jupiter, and he discovered that Venus, the brightest object in the sky when visible, displays phases like the Moon. The first two discoveries showed that the objects of the solar system were imperfect, contrary to accepted belief. The last two provided observational proof of the theory of Nicolaus Copernicus (1473–1543) that the Sun, not the Earth, was the center of the solar system. He saw that the satellites of Jupiter revolve about Jupiter. The phases of Venus showed that it revolves about the Sun. At least one object was thereby shown to orbit the Sun. Some of Galileo's observations of sunspots are reproduced on the back cover of this book.

More precisely, Galileo observed that different portions of the surface of Venus were in sunlight, displaying its *phases*, as it changed its size and angular distance from the Sun with time. He saw that when Venus was nearly fully illuminated it was small in size but close to the Sun in the sky, that when Venus was half-illuminated it was intermediate in size but far from the Sun, and that when Venus was nearly dark it was large in size and, again, close to the Sun. This clearly indicated that Venus was in orbit about the Sun.

In this experiment, we shall observe Venus. By measurement of its angular size and observation of its phases, we will be able to plot Venus in its orbit and demonstrate that its oribt is *heliocentri*c, that is, Sun-centered, rather than *geocentric*, or Earth-centered. Using that graph, we will be able to determine the length of the year on Venus, the time it takes for Venus to complete one orbit about the Sun, its *orbital period*.

More specifically, we will observe Venus and determine its distance by observing it through a telescope to which is attached a reticulated eyepiece. The apparent angular size measured through the telescope, θ_{app}, will be converted to the true angular size of Venus, θ_{true}, at the time of the observation. The angular size of Venus at the known distance of closest approach, θ_o, then allows us to calculate its distance. Performing this operation over several months, and being aware of its changing phases, will allow us to establish that Venus has a heliocentric orbit, to map out its orbit, and to calculate its orbital period.

B. Theory: Interpretations of the Orbit of Venus

1. The Ptolemaic System

For more than 1500 years, the strange movement of Venus observed in the sky as well as the movements of the Sun, Moon, and the other planets known to

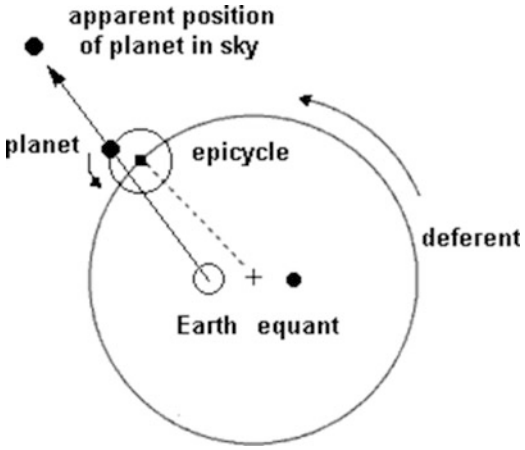

Fig. 1 In the Ptolemaic system of the universe, the Sun, Moon, and planets are postulated to reside on circles, the epicycles, which themselves rotate and move along a second circle, the deferent

antiquity, Mercury, Mars, Jupiter, and Saturn, was explained in terms of a model that was geocentric. The Earth, after all, was considered to be the center of the universe.

A complicated, purely geometric model was used to explain both the motions of these objects, the variations in the speed and direction of their motion as seen from the Earth, and the changes in the apparent distances of the planets from the Earth. The system of epicycles ("on the circle" in Greek) and eccentric, that is, non-concentric, circles that was devised is called *Ptolemaic* after the Greek astronomer, mathematician, geographer, and astrologer Ptolemy (Claudius Ptolemaeus, ca. 90–ca. 168), a Roman citizen who lived in Egypt, but wrote in the Greek language. It is so named although the system had been developed by earlier Greek astronomers, including the originator, Apollonius of Perga (ca. 262 B.C.E.–ca. 190 B.C.E.), and, most notably, Hipparchus (second century B.C.E.) of Rhodes. Indeed, Hipparchus used the system extensively nearly 500 years before Ptolemy synthesized and extended it to explain his geocentric theory in his major work in astronomy, the *Almagest*.

As shown in Fig. 1, the Ptolemaic system was, in fact, not purely geocentric, the center of the system being slightly displaced in space from Earth. The motion of the planet was actually centered about a point halfway between the Earth and another point, called the *equant*. That midway point was the center of the so-called *deferent* circle. Circles called *epicycles*, on which the object was located, both rotated in uniform circular motion and revolved along the deferent in uniform circular motion. Each of the seven objects required a different equant and a different deferent, in addition to their own epicycle. The deferents, to add additional complexity, were eccentric as opposed to concentric.

The model was accepted as the correct cosmological model by European and Islamic astronomers and was endorsed by Aristotle and powerful political forces. Because of its influence, the Ptolemaic system is sometimes considered as synonymous to the geocentric model and, indeed, similar ideas were held in ancient China. It was gradually replaced by the heliocentric model of Nicolaus Copernicus

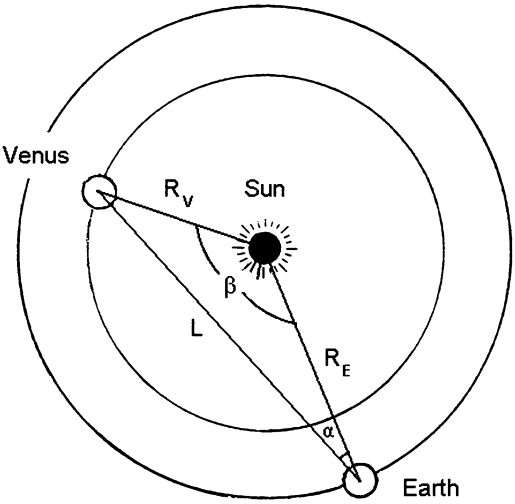

Fig. 2 The phase angle, α, of Venus as observed from the Earth can be calculated at any position in its orbit by application of the law of cosines. The angle β is the difference in heliocentric longitudes of the two planets. In this configuration, Venus is an evening star

(1473–1543), Galileo Galilei (1564–1642), and Johannes Kepler (1571–1630). This model was provided a rational basis by the mathematical physics of Sir Isaac Newton, marking the beginning of the modern age of scientific inquiry. The heliocentric theory, in fact, had been proposed by Greek astronomers, notably Aristarchus of Samos, 310–230 B.C.E., but was rejected in favor of Aristotle's support of geocentric, Earth-centered theories.

2. *The Simplicity of the Heliocentric Model*

With the planets orbiting the Sun, however, we can explain their movement in the sky, in particular that of Venus, in terms of simple geometry. Figure 2 shows Venus and Earth at arbitrary locations along their orbits, assumed for simplicity to be perfectly circular.

By the law of cosines, that generalization of the Pythagorean Theorem for non-right triangles, we can determine the value of the side of the triangle L,

$$L^2 = {R_V}^2 + {R_E}^2 - 2R_V R_E \cos\beta.$$

The angle β is the difference between the angles that the two planets make with the Sun. This can be calculated easily, knowing that the Earth and Venus complete an orbit in 365.2 days and 224.7 days, respectively. The date of reference, t_o, is arbitrary. Defining it here as the date of inferior conjunction β is given as

$$\beta = 2\pi(t - t_o)\left[\frac{1}{365.2} - \frac{1}{224.7}\right]. \tag{1}$$

Accurate values of those angles, without the simplifying assumption of perfectly circular orbits, are tabulated in astronomical tables for each planet as its

heliocentric longitude. The zero degree reference for heliocentric longitude is the location of the vernal equinox.

Once the value of L as a function of t is known, a second application of the law of cosines provides the phase angle, α, the angular distance between the Sun and Venus as observed from the Earth,

$$R_V{}^2 = L^2 + R_E^2 - 2L\,R_E \cos\ \alpha,$$

from which

$$\cos\alpha = \frac{R_V{}^2 - L^2 - R_E{}^2}{-2L\,R_E}.$$

The inverse cosine then provides the phase angle α as a function of t.

A simple application of the law of cosines, then, explains the strange motion of Venus in the sky. Hundreds of years of complex adjustments of the geometry of the Ptolemaic system compared to the simplicity of the heliocentric model is an example of the quasi-principle in science known as *Occam's Razor* (William of Ockham, ca. 1285–ca. 1349): The simplest explanation is usually the correct explanation. This has wide application in any field of rational inquiry.

3. *The Configurations of the Interior Planets*

The aspect of Venus as seen from the Earth has a cycle of about 584 days, its *synodic period*. During this period, the various positions of Venus in its orbit correspond to geometric relationships, or *configurations*, with respect to the Earth. The more unique configurations are given names, Fig. 3. *Inferior conjunction* is the configuration in which Venus lies directly between the Earth and the Sun. In *superior conjunction*, Venus lies directly on the far side of the Sun. In *western elongation*, Venus is as far to the west as it can be seen, a morning star. In *eastern elongation*, Venus is as far to the east as it can be seen, an evening star. The planet Mercury, also interior to the Earth in the solar system, exhibits similar configurations.

Note that when Venus is at elongation, a line drawn from the Earth to Venus will be tangent to the orbit of Venus. In other words, at elongation Venus lies at the right angle of a right triangle formed by the Sun, Earth, and Venus. This was the basis for Copernicus' determination of the distance to Venus in terms of the distance of the Earth from the Sun, the *astronomical unit*, abbreviated A.U. , Fig. 4.

When Venus is at large angular distances from the much brighter Sun, it can be observed. After being difficult to see for about one month because of its proximity to the Sun near inferior conjunction, Fig. 5, Venus can be observed west of the Sun for about 6–7 months. It is then difficult to see for the next 5–6 months near superior conjunction, and then becomes visible east of the Sun for the next 6–7 months. It alternates being an evening and morning star, being visible in the few hours before the Sun sets or in the few hours before it rises.

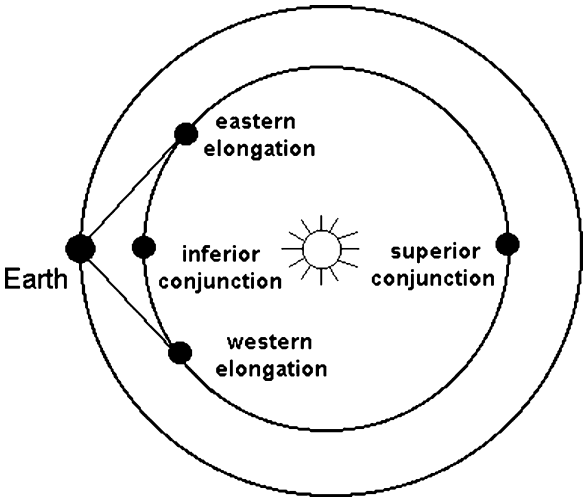

Fig. 3 The standard terminology of conjunctions and elongations applies to the two interior planets, Mercury and Venus

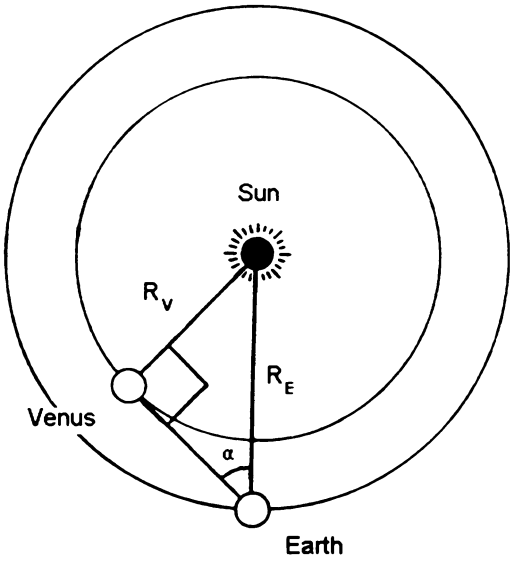

Fig. 4 At elongation, the distance from Venus to the Sun can be determined by trigonometry. Measurement of the angle α allows its calculation by $R_V = R_E \sin \alpha$. This was the basis for Copernicus' determination of the distance to Venus in terms of the distance of the Earth from the Sun, the A.U. The configuration shown is eastern elongation, at which Venus is an evening star. Venus appears in its half phase, half of its visible disk being illuminated by the Sun

4. Determination of the Distance of Venus

We can determine the distance of Venus from the Earth from its angular size by a simple proportion. From the sketch of the appearance of Venus, we can then determine the location of Venus in its orbit.

At its closest approach to Earth, the angular diameter of Venus is 60.3 seconds of arc. This occurs at inferior conjunction, when Venus and the Earth are aligned on

the same side of the Sun, Fig. 8. At this time, Venus is at a distance 1.0000 A.U.–0.7233 A.U. = 0.2767 A.U. from the Earth.

In Fig. 6, an object of linear size, D, is located at a distance, d. These are related by

$$\tan\frac{\theta}{2} = \frac{D/2}{d}. \tag{1}$$

If $d >> D$, then θ is small. For small angles, $\sin \theta/2 \approx \theta/2$ and $\cos \theta/2 \approx 1$, so that

$$\tan\frac{\theta}{2} = \frac{\sin\frac{\theta}{2}}{\cos\frac{\theta}{2}} \approx \frac{\theta}{2}.$$

Accordingly (1) becomes

$$\frac{\theta}{2} = \frac{D/2}{d},$$

or, as was stated equivalently in (2) of Experiment #1, "A Review of Mathematical Concepts and Tools,"

$$\theta = \frac{D}{d}.$$

Now, as shown in Fig. 7, if D is the diameter of Venus, d_1 and d_2 are its distances from the Earth at two different times, and θ_1 and θ_2 are its observed angular sizes at those times, then

$$\frac{d_1}{d_2} = \frac{\theta_2}{\theta_1}.$$

In particular, if L = 0.2767 A.U. is the distance of closest approach of Venus to Earth, and θ_o = 60.3″ is the angular diameter of Venus at that time, then for any other measured angular diameter, θ, the distance d of Venus in A.U. is given by

$$\frac{d}{L} = \frac{\theta_o}{\theta},$$

where θ is measured in seconds of arc, or

$$d = L\frac{\theta_o}{\theta}.$$

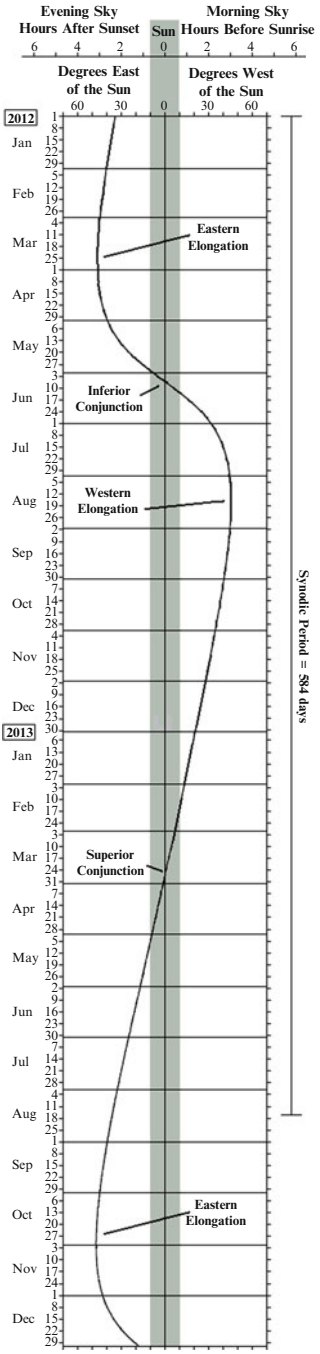

Fig. 5 The phase plot, or elongation calendar, for Venus for 2012 and 2013. The planet is easily observed as the brightest "star" in the sky over much of the year. The elongations in subsequent years can be determined knowing that the synodic period of Venus is 584 days

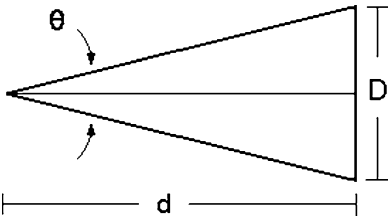

Fig. 6 Small angle approximation geometry

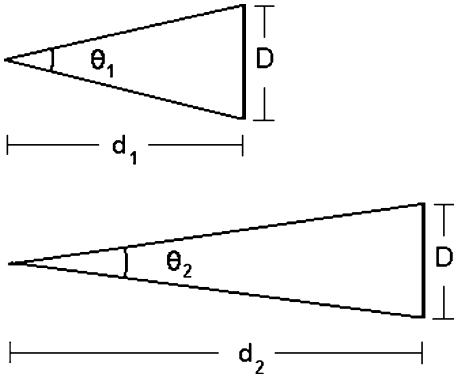

Fig. 7 The angular diameter, θ, of an object whose size, D, is small compared to its distance from the observer, d, is approximately inversely proportional to its distance. Accordingly, $d_1/d_2 = \theta_2/\theta_1$

Using the above known values,

$$d = 0.2767 \times \frac{60.3''}{\theta}\text{A.U.}$$
$$= \frac{16.7''}{\theta}\text{A.U.} \quad (2)$$

For each measurement of θ in seconds of arc we can then find the distance to Venus in A.U.

5. *Determination of the Orbital Period by Kepler's Second Law*

To determine the orbital period, we need not observe Venus over its entire orbit. We can, instead, take advantage of *Kepler's Second Law*, which will be discussed in Experiment #12, "Kepler's Laws of Planetary Motion," and the near circularity of the orbit of Venus. Kepler's Second Law states that the radius vector from the focus of the elliptical orbit, the Sun, to the location of Venus in its orbit sweeps out equal areas in equal times. With the good approximation that the orbit of Venus is

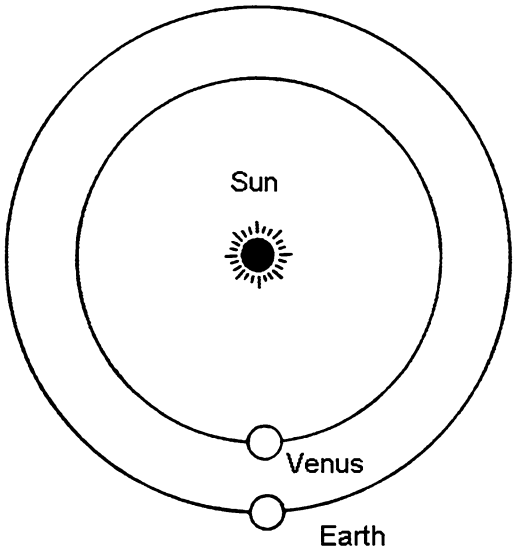

Fig. 8 The configuration of the Sun, Venus, and the Earth referred to as inferior conjunction. See also Fig. 3

circular, we therefore know that the length of time for it to traverse an angular distance of 360° and complete an orbit about the Sun, the orbital period, P, is related to the time interval between two observations separated by an angular distance $\Delta\theta$ by a simple proportion,

$$\frac{P}{360^{\circ}} = \frac{\Delta t}{\Delta\theta},$$

where Δt is the amount of time for Venus to traverse an angular distance $\Delta\theta$ in its orbit, measured in degrees. The period then follows as

$$P = 360^{\circ}\frac{\Delta t}{\Delta\theta}. \tag{3}$$

C. Procedure and Observations

1. Observing Venus

The days in which Venus is not obscured by the Sun and can be observed are displayed in the phase plot, frequently referred to as an *elongation calendar*, Fig. 5. This shows the *phase angle* of Venus as a function of date. The *synodic period* is the time for the completion of a full cycle of the phases, 584 days for Venus. Accordingly, although this phase plot displays the phases of Venus only for 2011 and 2012,

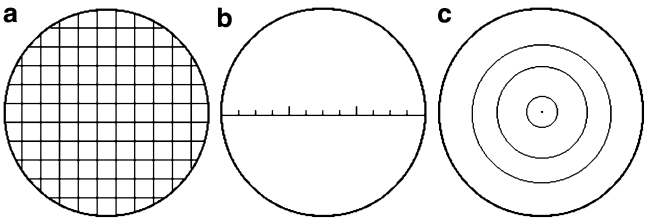

Fig. 9 An eyepiece with a grid (**a**) either etched or composed of fine wire allows measurement of the apparent size of an object, the angular separation between double-star components, or, in our case, the angular separation between Jupiter and the Galilean satellites. An eyepiece with a linear scale (**b**) or a "bull's eye" of concentric circles (**c**) can also be used

the same pattern repeats at 584-day intervals. (In fact, because the number of days in five synodic periods is the same as the number of days in eight Earth years, a total of about 2920 days, the phase plot/Earth calendar association repeats every 8 years.)

Use the phase plot as a guide to your observing. The Earth rotates on its axis a full 360° in 24 h, or 15° every hour. If we somewhat subjectively say that the Sun obscures Venus when it is within 10° of the planet in the sky, then this corresponds to about 40 min of time before sunrise or after sunset. We see that Venus is not obscured, by this 10° definition, the vast majority of time in its synodic cycle. If, however, you prefer a dark sky and want to observe Venus at least 2 h before sunrise or after sunset, corresponding to 30° in the sky, then the phase plot shows that you are restricted to observations during the 5 months bracketing eastern elongation and the 5 months bracketing western elongation. The Sun is within 30° in the sky of Venus during 7 months around superior conjunction and 1 1/2 months around inferior conjunction.

2. *Reticulated Eyepieces for Observations*

We will need a telescope with a reticulated eyepiece for angular size measurements of Venus and polar graph paper on which to draw its orbit.. These eyepieces come in various forms. As shown in Fig. 9, they will typically have a grid, linear scale, or concentric circles in a "bull's eye" configuration either etched on, or composed of fine wire emplaced in, the glass located in the focal plane of the eyepiece. These scales allow measurement of the apparent size of an object, the angular separation between double-star components, or, in Experiment #13, "The Galilean Satellites of Jupiter," the angular separation between Jupiter and the Galilean satellites. (It also helps astronomy professors point out objects to inexperienced observers at public demonstrations or stargazing parties.)

The Meade 12 mm focal length Illuminated Reticle Astrometric Eyepiece is an illuminated reticle device suitable for our purposes. As shown in Fig. 10, it possesses

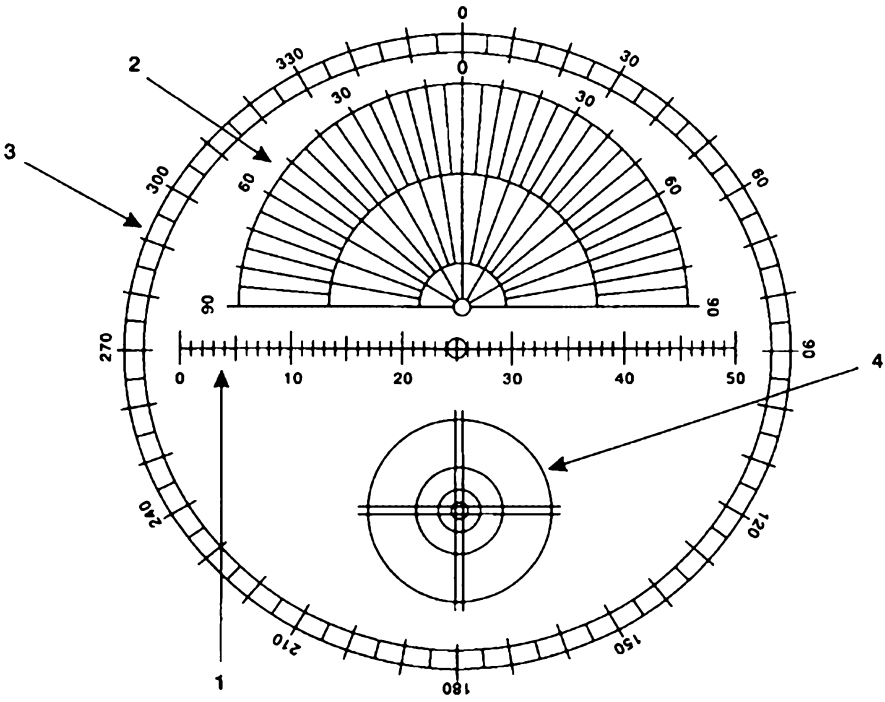

Fig. 10 The Meade 12 mm focal length Illuminated Reticle Astrometric Eyepiece is an illuminated reticle device suitable for our purposes. It possesses four reticle scales etched onto the glass: (1) A linear scale, (2) a semicircular position-angle scale, similar to a protractor, (3) a 360° position-angle scale, and (4) four concentric circles with the inner circles having diameters of 1/2, 1/4, and 1/10 that of the outermost circle, all bisected by a double cross-hair. The eyepiece can be rotated in its housing in the telescope to align its linear scale in a given direction. We will use this feature in Experiment #13, "The Galilean Satellites of Jupiter," to align the linear scale with the line in the sky between Jupiter and the Galilean satellites

four reticle scales etched onto the glass: (1) A linear scale, (2) a semicircular position-angle scale, similar to a protractor, (3) a 360° position-angle scale, and (4) four concentric circles with the inner circles having diameters of 1/2, 1/4, and 1/10 that of the outermost circle, all bisected by a double cross-hair. Either the first or the fourth scales can be used to measure the angular size of an object or the angular separation between two objects. A red light illuminates the reticle scales for ease of measurement. As with all eyepieces, it can be rotated in its housing in the telescope. This will allow us in Experiment #13, "The Galilean Satellites of Jupiter," to align the linear scale with the line in the sky between Jupiter and the Galilean satellites.

Reticulated eyepieces are also available from the major hobby telescope manufacturers and manufacturers of medical microscopes. Celestron Telescopes refers to them as "microguide eyepieces" (part #94171). Orion telescopes refers to them as "illuminated reticule eyepieces" (part #12355). American Optical manufactures eyepieces for medical applications. Most of these have linear graduated scales placed on the eyepieces.

3. Calibration of the Telescope Field of View

When Venus is visible, observe it through the telescope to which is attached a reticulated eyepiece. Carefully sketch the appearance of Venus, indicating the changing size of the disk and distinguishing the portion illuminated by sunlight from the portion which is dark.

We want to determine the angular size of Venus. We must clearly distinguish the angular size of the magnified image of Venus as seen through the telescope, the *apparent* angular size, from the angular size of Venus as seen with the unaided eye, the *true* angular size. We measure the former, but for this experiment we require the latter. The two are related by the magnification of the telescope.

Measurement of the apparent angular sizes of astronomical objects as seen through a telescope is not trivial. In some professional telescopes, a device known as a *filar micrometer* is placed at the focal plane of the eyepiece. The linear size of the object of interest as measured by the micrometer together with the known focal length of the eyepiece then yields the apparent angular size. Unfortunately, filar micrometers are expensive and are generally found only at astronomical observatories.

In the absence of such a device we can calibrate the telescope, that is, determine by alternative means the apparent angular size of its field of view. Knowing the number of grid spacings in the reticulated eyepiece, we can then determine the angular distance between grid lines. This will allow fairly precise measurements of the apparent angular size of objects such as Venus.

We will use *star crossing*, or *star tracking*, to perform this calibration. The telescope is so positioned that a bright star appears at the left edge of the field of view. The telescope is then locked in place and, as the Earth rotates under the star, the star moves through the field of view. The amount of time required for the star to traverse the field of view along a diameter to the opposite side, knowing that the Earth rotates 360° in 24 h, or 15′ per minute, allows calculation of the angular size of the field of view. For example, if the star traverses the field of view in 5 min then the angular size of the field of view is $15'/\text{min} \times 5\ \text{min} = 75'$. If the reticulated eyepiece has 10 grid spacings, then the angular distance between grid spacings is $75'/10 = 7.5'$.

Actually, this is true only for a star on the celestial equator. To understand this, consider a time exposure photograph of the night sky. As the Earth rotates for a given period of time through a given angle, stars near the celestial equator traverse a comparatively large arc length in the sky whereas stars far from the celestial equator traverse a comparatively small arc length in the sky. For example, as the Earth rotates the North Star does not move at all. Astronomers refer to the angular position of an object north or south of the celestial equator as its *declination*, δ. The position of an object along the celestial equator is referred to as its *right ascension*. From the geometry of the sphere, it can be shown that, for a given interval of right ascension, the arc length at declination δ is reduced by the factor $\cos \delta$ from its value at the celestial equator, at which location by definition $\delta = 0$.

Now imagine you are looking through a telescope first at a star at a low declination and then at a star at a relatively high declination. The field of view of the telescope is of course the same, but the star at the higher declination requires more time to pass through that field of view than does the star at the lower declination. It can be shown that the ratio of these time intervals is again *cos* δ.

The technique to determine the apparent angular size of the field of view of a telescope can then be summarized mathematically as follows. If you observe that a star at declination δ takes Δt minutes to traverse the field of view, then the apparent angular size of the field of view is

$$\theta_{field} = 15 \cos\delta \, \Delta t \text{ minutes of arc.}$$

This is the technique we will use in this experiment to calibrate the telescope, that is, determine the angular size of its field of view.

The angular distance, θ_{grid}, between grid lines of the reticulated eyepiece of the telescope is then found by dividing this apparent angular size of the field of view by the number of grid spacings, N, in the eyepiece,

$$\Delta\theta_{grid} = 15 \cos\delta \, \frac{\Delta t}{N} \text{minutes of arc.}$$

Knowing this angular distance between grid lines enables us to determine the apparent angular size of Venus.

In this technique, you need not in fact wait for the star to traverse the entire field of view. You can time the star as it traverses adjacent grid lines or several grid lines. It is best to use the entire field of view, however, because then we minimize the effects of timing errors and the fuzziness of the star image. Because of errors in the timing of the motion of the star and blurriness in its image resulting from poor seeing, you should do this star tracking experiment twice and average the results.

A list of the 25 brightest stars is provided in Table 1. Use the brightest star which is visible at the time of the year that you are performing the experiment to calibrate the reticulated eyepiece.

(We might consider using *visual binary* stars, double stars which are physically associated, in orbit about each other, to perform this calibration. Many stars, about 5–10% of all stars, are in binary pairs, so that a double star can often be found in the sky near to where you are observing. This technique, however, requires that you know the separation of the stars at the time of your observation. Unfortunately, the angular separation provided in catalogs is the maximum angular separation whereas the separation changes with time as the two stars orbit each other. In addition, on the night of your observations you should, but might not, have a bright pair of stars in the sky available with an angular separation in the sky significantly greater than the *seeing*, the amount that a stellar image is smeared out by the atmosphere. We therefore choose to use the star tracking procedure to calibrate the telescope.)

Table 1 The brightest stars

	Star	Name	Position (2000.0)		Apparent magnitude	Spectral type	Absolute magnitude	Distance
			R.A.	*Dec.*	(V)			D (pc)
1.	α CMa A	Sirius	06 45 08.9	−16 42 58	−1.46	Al V	1.4	2.6
2.	α Car	Canopus	06 23 57.1	−52 41 44	−0.72	F0 la	−8.5	360
3.	α Boo	Arcturus	14 15 39.6	+19 10 57	−0.04	K2 IIIp	−0.2	280
4.	α Cen A	Rigil Kentaurus	14 39 36.7	−60 50 02	0.00	G2 V	+4.4	1.3
5.	α Lyr	Vega	18 36 56.2	+38 47 01	0.03	A0 V	+0.5	8.1
6.	α Aur	Capella	05 16 41.3	+45 59 53	0.08	G8 III	+0.3	13
7.	β Ori A	Rigel	05 14 32.2	−08 12 06	0.12	B8 la	−7.1	280
8.	α CMi A	Procyon	07 39 18.1	+05 13 30	0.38	F5 IV	+2.6	3.5
9.	α Ori	Betelgeuse	05 55 10.2	+07 24 26	0.50	M2 lab	−5.6	95
10.	α Eri	Achernar	01 37 42.9	−57 14 12	0.46	B5 IV	−1.6	26
11.	β Cen AB	Hadar	14 03 49.4	−60 22 22	0.61	B1 II	−5.1	140
12.	α Aql	Altair	19 50 46.8	+08 52 06	0.77	A7 IV-V	+2.2	5.1
13.	α Tau A	Aldebaran	04 35 55.2	+16 30 33	0.85	K5 III	−0.3	21
14.	α Vir	Spica	13 25 11.5	−11 09 41	0.98	B1 V	−3.5	79
15.	α Sco A	Antares	16 29 24.3	−26 25 55	0.96	M1 Ib	4.7	100
16.	α PsA	Formalhaut	22 57 38.9	−29 37 20	1.16	A3 V	+2.0	6.7
17.	β Gem	Pollux	07 45 18.9	+28 01 34	1.14	K0 III	+0.2	11
18.	α Cyg	Deneb	20 41 25.8	+45 16 49	1.25	A2 la	−7.5	560
19.	β Cru	Beta Crucis	12 47 43.2	−59 41 19	1.25	B0 III	−5.0	130
20.	α Leo A	Regulus	10 08 22.2	+11 58 02	1.35	B7 V	−0.6	26
21.	α Cru A	Acrux	12 26 35.9	−63 05 56	1.41	B1 IV	−3.9	110
22.	ε CMa A	Adhara	06 58 37.5	−28 58 20	1.50	B2 II	−4.4	150
23.	λ Sco	Shaula	17 33 36.4	−37 06 14	1.63	B2 IV	−3.0	84
24.	γ Ori	Bellatrix	05 25 07.8	+06 20 59	1.64	B2 III	−3.6	110
25.	β Tau	Elnath	05 26 17.5	+28 36 27	1.65	B7 III	−1.6	40

4. *The Observations*

To calibrate the grid spacing of the reticulated eyepiece, perform two star crossing calibration experiments. Enter on the DATA SHEET the name of the star you are using and its declination from Table 1. Enter in Table 4 of the DATA SHEET the beginning and ending time in seconds of each trial and the number of grid spacings, *N*, traversed during each of the two star trail time intervals. The number of grid spacings traversed need not be exactly the same for both trials.

On various days over two to three months measure the apparent angular diameter of Venus by counting the number of grid spacings, *n*, on the reticulated eyepiece within which its image appears. Estimate the apparent angular diameter to the nearest 0.1 of a grid spacing if possible. Be sure to measure the entire disk

Table 2 Heliocentric longitude of the Earth, λ, for days reckoned from the vernal equinox, March 21

Days	λ	Days	λ	Days	λ
0	0	125	123	250	246
5	5	130	128	255	251
10	10	135	133	260	256
15	15	140	138	265	261
20	20	145	143	270	266
25	25	150	148	275	271
30	30	155	153	280	276
35	35	160	158	285	281
40	39	165	163	290	286
45	44	170	168	295	291
50	49	175	173	300	296
55	54	180	177	305	301
60	59	185	182	310	306
65	64	190	187	315	311
70	69	195	192	320	315
75	74	200	197	325	320
80	79	205	202	330	325
85	84	210	207	335	330
90	89	215	212	340	335
95	94	220	217	345	340
100	99	225	222	350	345
105	104	230	227	355	350
110	108	235	232	360	355
115	113	240	237	365	360
120	118	245	242		

of Venus, not simply the portion illuminated by sunlight. At those phases when more than half of Venus is in sunlight, you can measure the apparent angular radius diameter directly, from which you can calculate the apparent angular diameter. At the other phases, you will have to estimate the portion of Venus that is in darkness.

Enter the calendar date, the time in military time, and the number of grid spacings, *n*, in Table 4 of the DATA SHEET. Draw a sketch of the appearance of Venus in column 7 of Table 4 of the DATA SHEET. Each sketch should show a circular disk. Try to represent the phase of Venus by shading the part of the disk that is not illuminated by the Sun. Include lines representing the eyepiece grid on the sketch.

In the analysis below, we will be drawing arcs at the distance from the Earth determined for Venus on polar graph paper. The arcs so created, however, do not uniquely define the orbit of Venus. As you will see, many circles could be drawn passing through all of them. To determine the orbit, one trick involves observing Venus at its half phase, either as a morning or evening star. At that configuration, we know that the triangle formed by Earth, Sun, and Venus is a right triangle with

its 90° angle at Venus, as shown in Fig. 4. Knowing the distance from the Earth to Venus at that half phase will provide a point on the orbit of Venus. Your observations, therefore, should include one or more taken on days as close to the half phase as possible. Those dates correspond to the dates of the configuration of elongation, provided on the phase plot of Fig. 5.

D. Calculations and Analysis

1. *Calibration of the Telescope Field of View*

Calculate the star crossing time for each of the two trials by subtracting the beginning time from the ending time. Enter the results in Table 4 of the DATA SHEET. Divide each by the respective number of grid spacings traversed and then calculate the mean of these two quotients. Calculate $cos\ \delta$, $15\ cos\ \delta\ \Delta t$, and $\Delta\theta_{grid}$, the angular distance between grid lines in minutes of arc. Show these calculations on the DATA SHEET and enter the results in Table 4 of the DATA SHEET.

2. *Telescope Magnification*

The true angular size of Venus, θ_{true}, is calculated by dividing the apparent angular size by the magnification of the telescope. As given by Eq. (3) of Experiment #3, "The Optics of Telescopes: Part I. Image Size and Brightness,"

$$m = \frac{\theta_{app}}{\theta_{true}}$$

$$= \frac{f_o}{f_e},$$

where f_o is the focal length of the objective and f_e is the focal length of the eyepiece. Enter the two focal lengths on the DATA SHEET and calculate the magnification m.

3. *The Orbit of Venus*

For each observation, calculate the apparent angular size of Jupiter, θ_{app}, by multiplying n by the angular distance between grid spacings, $\Delta\theta_{grid}$. Then calculate the true angular as $\theta_{true} = \theta_{app}/m$. The distance from the Earth to Venus at the time

of the observation is then found from (3). Show these calculations on the DATA SHEET and enter the results in Table 4 of the DATA SHEET.

Demonstration of the heliocentric nature of the orbit of Venus and determination of its orbital period will be made using polar graph paper. A polar graph is reproduced on the DATA SHEET. We assume for simplicity that the orbit of the Earth is circular, represented by the circular perimeter of the graph.

Determine the scale of the graph by measuring its radius. Enter that result on the DATA SHEET below the graph.

The radial coordinate on the polar graph is the distance from the Sun. The angular coordinate is the heliocentric longitude, λ, of the Earth. By definition, $\lambda = 0$ occurs on the date of the vernal equinox, March 21. Because the year is 365.2 days long, the Earth moves about 1° of heliocentric longitude each day. The correspondence is not exact, however, and you must refer to Table 2 to accurately plot the heliocentric longitude of the Earth on a given date reckoned from the date of the vernal equinox.

For each observation, locate Earth in its orbit. You may want to refer to the Days-of-the-Year Table in Appendix III to facilitate your determination of the number of days past March 21, which you need to find the heliocentric longitude for the days of your observations. Plot the successive data points around the graph in a counterclockwise direction, the direction of motion of the planets about the Sun as viewed looking down on the solar system.

From each location of the Earth, use a compass to draw an arc with a radius equal to the distance determined by (3), converted to centimeters according to the scale factor of the graph. Extend the arc from the outer circle representing the orbit of the Earth to about half the distance to the center, which is the graphical location of the position of the Sun. In this way, the arc will be certain to intersect the orbit of Venus that you will determine.

A circular arc centered on the Earth will intersect the orbit of Venus in two locations. As shown in Fig. 11, if Venus is east of the Sun, it will be an evening star. If Venus is to the west of the Sun, it will be a morning star. The appearance of Venus differs between the two positions. When east of the Sun, the illuminated portion of the visible disk of Venus is to the west. When west of the Sun, the illuminated portion of the visible disk of Venus is to the east.

Knowing this allows you to determine which of the two possible crossings represents the position of Venus on the date of observation. At that position on your graph draw a small circle to represent Venus, shading in the hemisphere of Venus that is in shadow as in Fig. 11.

Repeat this for every observation. Figure 12 presents a hypothetical example of the results you might get after four observations made during the fall.

The actual position of Venus along the various arcs requires determination of its distance from the Sun. This can be determined from the observation of Venus at elongation. As shown in Fig. 12, the angle between the radius vector from the Sun to Venus and the line between the Earth and Venus is a right angle. That uniquely determines the position of Venus along the arc that was drawn.

Once that position has been determined, use a compass to draw a circle with a radius equal to the distance of the Sun to Venus, R_V. That is the orbit of Venus,

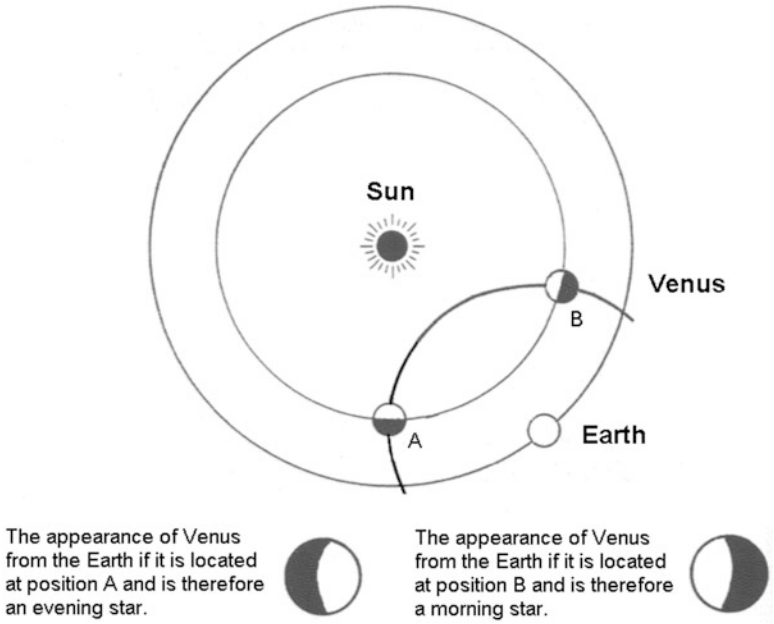

Fig. 11 When determining the angular diameter of Venus, allowance must be made for the portion of the disk which is not illuminated by the Sun. Whether Venus is a morning or evening star enables you to determine its position relative to the Sun and the Earth

assumed circular. Mark the intersection of that circle with the various other arcs to note the location of Venus at the time of the various other observations.

Measure the length of R_V and convert it to A.U. using the scale factor of the graph. Calculate the percentage error between R_V and the known value of 0.7233 A. U. on the DATA SHEET.

Galileo recognized that Venus had a heliocentric orbit by observing how the appearance of its phases changed as the visible disk varied in size. Make a horizontal sketch on the DATA SHEET of the various phases of Venus that you observed and the angular size θ_{app} that you determined, both as entered in Table 4, arranged in either monotonically increasing or monotonically decreasing order of θ_{app}.

4. The Orbital Period

We can now determine the orbital period of Venus. Choose a pair of observations from Table 4 of the DATA SHEET. In Table 5 of the DATA SHEET, enter the date and time of the two observations and, from the table of Julian dates in Appendix II, the corresponding Julian dates. Enter the Julian dates to the nearest hour, expressing

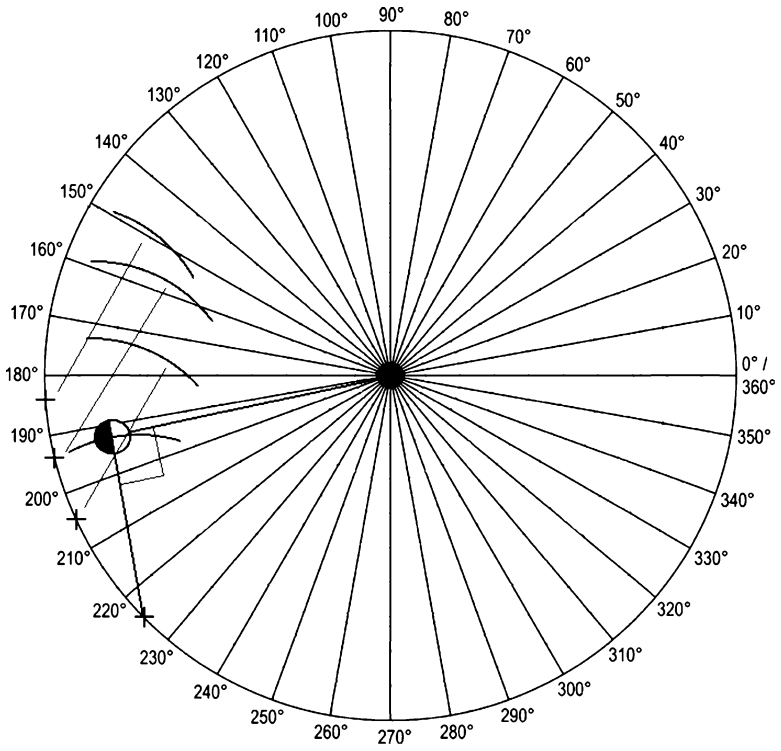

Fig. 12 Hypothetical results for mapping out the orbit of Venus. At each observation, the angular diameter of Venus allows determination of the distance of Venus from the Earth, placing it somewhere along an arc. The *narrow lines* indicate which arc is associated with each position of the Earth at the time of the observation. At elongation, when Venus is at half phase, the right triangle allows us to determine the actual radial position of Venus from the Sun. Assuming a circular orbit, that allows us to draw a circle through the other arcs, in that way locating the position of Venus at the various times of observation. The angular coordinate is the heliocentric longitude of the Earth, whose zero angle position is the date of the vernal equinox, March 21. This example, therefore, displays hypothetical observations taken in September, October, and November

each hour as 0.04 of a day. For example, if an observation were made at 2 p.m. on December 4, 2012, it would be entered as J.D. 55265.08 on the DATA SHEET.

Although each sector of the polar graph paper is 10° in angular width, you should be able to estimate the actual position to 1°–2°. This can be done between any pair of observations of the position. The greater the separation, however, the smaller will be the errors in the values of θ_2 and θ_1 compared to the value of $\theta_2 - \theta_1$.

On the polar graph, extend radii to the perimeter at the dates of these two observations and read off the corresponding heliocentric longitudes, λ. Try to estimate the value of λ to the nearest degree. Enter the values of the heliocentric longitudes in Table 5 of the DATA SHEET.

Repeat this for several pairs of observations. Use those with widely separated dates to minimize the errors introduced by your reading of the heliocentric longitude.

If Venus traverses an angular distance $\Delta\theta$ in its orbit during a length of time Δt days, then we can calculate the period of its orbit P by (3). Enter your results for the orbital period as determined by each pair of observations in Table 5 of the DATA SHEET. Average these to provide the best estimate of the orbital period and enter your result on the DATA SHEET. Show all your calculations on the DATA SHEET.

STUDENT'S NAME _____

E. Venus Experiment Data Sheets

1. Calibration of the Telescope Eyepiece

Name of the star selected: _____

Declination of the star, δ = _____

Table 3 Star tracking calibration of eyepiece

Trial	Start time	End time	N	$\Delta t/N$ (sec)	Mean $\Delta t/N$ (sec)	δ of star	cos δ	$\Delta\theta_{grid} = 15' \cos\delta\, \Delta t/N$ (min of arc)
1								
2								

First timing:

Time for star to cross field of view, Δt_1 = _____ seconds

Second timing:

Time for star to cross field of view, Δt_2 = _____ seconds

$\Delta t_1/N_1$ = _____ seconds

$\Delta t_2/N_2$ = _____ seconds

Mean $\Delta t/N$ = _____ seconds

Mean $\Delta t/N$ = _____ minutes of time

cos δ = _____

Angular distance between grid or scale spacings,

$\Delta\theta_{grid} = 15'\ \cos\ \delta\ \frac{\Delta t}{N}$ = _____ minutes of arc

2. Telescope Magnification

Focal length of objective, f_o = _____

Focal length of eyepiece, f_e = _____

Telescope magnification, $m = f_o/f_e$ = _____

Table 4 Observations of Venus

Observation	Date	Time	n	$\theta_{app} = n\,\Delta\theta_{grid}$ (sec of arc)	$\theta_{true} = \theta_{app}/m$ (sec of arc)	Distance, d (A.U.)	Sketch
1							
2							
3							
4							
5							
6							
7							
8							
9							
10							
11							
12							
13							
14							
15							
16							
17							
18							
19							
20							
21							
22							
23							
24							
25							

STUDENT'S NAME _____

Table 5 Determination of orbital period of Venus

Sets of observations	Date	Time	J.D.	Heliocentric longitude, λ	Δ(J.D.)	Δ λ	Period
Observation 1							
Observation 2							
Observation 1							
Observation 2							
Observation 1							
Observation 2							
Observation 1							
Observation 2							
Observation 1							
Observation 2							
Observation 1							
Observation 2							
Observation 1							
Observation 2							
Observation 1							
Observation 2							

Perform your calculations of θ_{app}, θ_{true}, and the distance here.

STUDENT'S NAME _____

Calculation of Period

Set #1:

Set #2:

Set #3:

Set #4:

Set #5:

Set #6:

Set #7:

Set #8:

Calculation of average value for period:

STUDENT'S NAME _____

Polar graph paper for plotting positions of Earth and Venus. The circle corresponds to 1 A.U.

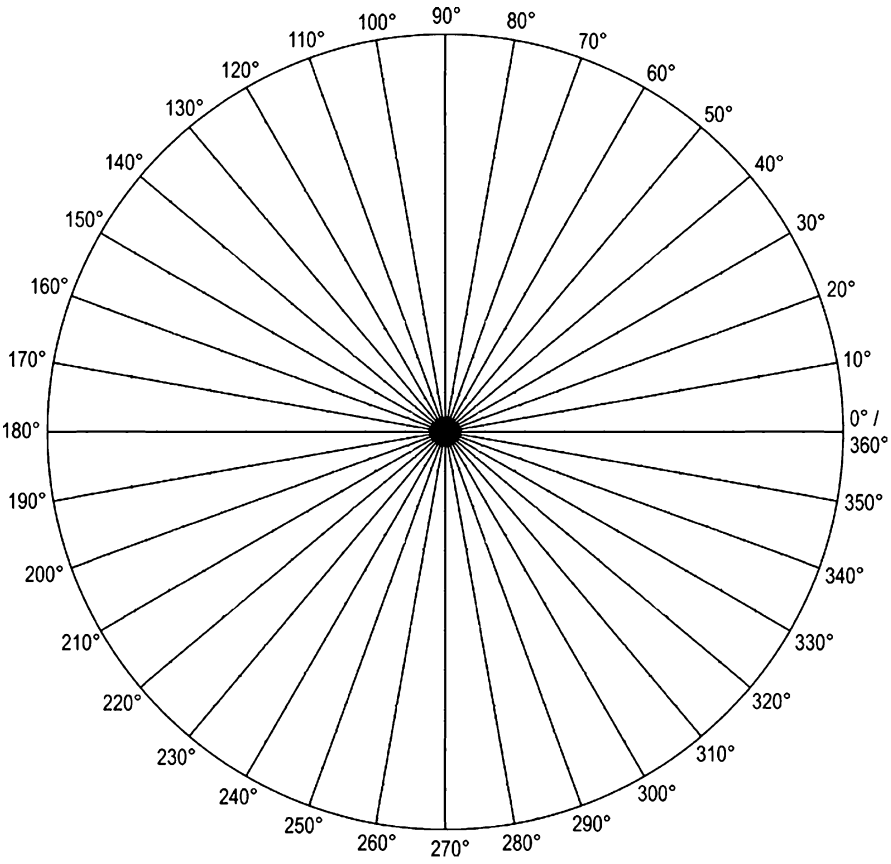

Scale factor: 1 A.U. = _____ cm

STUDENT'S NAME _____

Conversion of R_V to A.U.:

Calculation of the percentage error between R_V and 0.7233 A.U. :

From Table 5, show the correspondence between the appearance of the visible disk of Venus and its apparent angular size.

Phases:

θ_{app} :

F. Venus Experiment Discussion Questions

1. In honor of the 50th anniversary of the landing of Apollo 11 on the Moon, Brewster Skywalker has enrolled in an astronomy class for the fall semester of 2019.
   a) Referring to the phase plot, what month will Venus be near either eastern or western elongation in the fall of 2019? Show your calculations below.

   b) Will it be an evening or morning star?

STUDENT'S NAME _____

2. "Crop circles" are geometric patterns, more than 10,000 by some count, cut out of agricultural fields in many countries, 90% in southern England. Here are several suggested origins.

   1) They are road signs placed by extraterrestrial intelligent space travelers to guide fellow extraterrestrials to sources of water and delectable food.
   2) They are logic games developed by highly intelligent prairie dogs.
   3) They were carved out as a hoax by tractors driven by troublesome farmer youth with too much time on their hands.
   4) They are patterns of beetle infestation caused by artistically-inclined beetles with a sense of humor who got A's in geometry.

   a) Under each possibility, list some of the assumptions that would be required for the explanation to be viable.

   b) Using Occam's Razor, what is the most likely origin of these features?

Answer: _____

STUDENT'S NAME _____

3. "Lucky" Eddie Malvolio got into a horrible car accident but came out of it with only minor bruises. Here are several suggested explanations.

   1) When he went to heaven, his relatives told him, "We're not ready for you yet," and pushed him back to Earth.

   2) He was wearing a seat belt.

   3) The Lord greeted him at the Pearly Gates and said to him, "My computer is down and so you shall be My messenger to the Earthlings of the Earth and for this I shall grant you eternal life," and brought him back to life.

   4) He was just lucky.

      a) Under each possibility, list some of the assumptions that would be required for the explanation to be viable.

      b) Using Occam's Razor, what is the most likely explanation of Lucky Eddie's luck?

   Answer: _____

STUDENT'S NAME _____

4. The orbital period of Venus is known to be 224.7 days. Calculate the percentage error in the value you determined. Show your calculations here.

5. Other than errors in measuring the angular size of the disk of Venus, what are the sources of error in this determination?

6. The same technique could be applied to determine the orbital period of Mercury. What is the major difficulty with such a determination? Make a sketch of the inner planets of the solar system to explain your answer.

7. The planets interior to the Earth, Mercury and Venus, exhibit phases as they go around the Sun. The planets exterior to the Earth do not. Why not? Make a sketch of the solar system to explain your answer.

STUDENT'S NAME _____

8. Depending on the epoch of your observations, Venus may have been close to one or more of the configurations referred to as eastern elongation, inferior conjunction, western elongation, or superior conjunction. From your graph, estimate the dates for any of these configurations that may have occurred during your observations.

   a. date of eastern elongation:

   b. date of inferior conjunction:

   c. date of western elongation:

   d. date of superior conjunction:

9. At which of the configurations is the distance to Venus the smallest, and therefore the angular diameter as viewed from the Earth the greatest?

10. At which of the configurations is the distance to Venus the greatest, and therefore the angular diameter as viewed from the Earth the smallest?

11. On your graph of the orbit of Venus, draw a line from the position of the Earth on the first date of your observation tangent to the orbit of Venus. Let θ be the angle between this line and the line between the Earth and the Sun. Measure θ using a protractor and find its sine.

    $\theta =$

    $\sin \theta =$

    What is the significance of $\sin \theta$?

12. Calculate the percentage error between this value and the known semi-major axis of Venus, 0.7233 A.U.

Removing these DATA SHEETS from the book may damage the binding. You might consider entering the data and performing your calculations in the book, and then photocopying the DATA SHEETS for submission to your instructor for grading.

If you used graph paper other than that provided, attach those graphs to these DATA SHEETS.

Experiment 12
Kepler's Laws of Planetary Motion

SUMMARY: In Experiment #12, "Kepler's Laws of Planetary Motion," you will study Kepler's Laws of Planetary Motion as applied to the planets Mercury and Mars. Using published astronomical position data, you will create graphs of their orbits on polar graph paper. Using those orbits, you will then test Kepler's Second Law, the equal area law, and Third Law, the period-semimajor axis relationship.

LEVEL OF DIFFICULTY: Low

EQUIPMENT NEEDED: Ruler; planimeter (optional).

1. To be able to describe Kepler's three laws of planetary motion.
2. To be able to apply the mathematics of Kepler's Third Law to determine the orbital period of planets from their distance from the sun.
3. To be able to describe the effect of comet jets on their orbits.

MY LEARNING GOALS

L.M. Golden, *Laboratory Experiments in Physics for Modern Astronomy: With Comprehensive Development of the Physical Principles*,
DOI 10.1007/978-1-4614-3311-8_12, © Springer Science+Business Media New York 2013

A. Introduction

A burst of scientific activity in Europe in the sixteenth and seventeenth centuries accompanying the Renaissance yielded an understanding of planetary motions that survived unchallenged until Einstein's development of the General Theory of Relativity in the early twentieth century. Even today, the results of the Renaissance investigations, in particular those of Sir Isaac Newton, remain the basis of our understanding of how the planets revolve about the Sun.

The observational data that yielded these discoveries were obtained by the Danish astronomer Tycho Brahe (1546–1601). After his death, his young assistant Johannes Kepler (1571–1630) utilized the data to derive an accurate description of the orbit of Mars. Kepler, in contrast to earlier scientists who had tried to fit the orbit of Mars to a circle, showed that the orbit of Mars was an ellipse with the Sun at one focus. With such a realization, Kepler was able to show that all of the planets have elliptical orbits with the Sun at one focus. This is now known as Kepler's First Law of Planetary Motion.

The historical, scientific, religious, and philosophical importance of this cannot be overstated. The perfection of a circle was shown to no longer describe the orbits of the planets. In this experiment, we will determine the orbits of Mercury and Mars about the Sun and study if they agree with Kepler's findings. We will also study comets and how the non-gravitational effect of their jets alters their orbits.

B. Theory

1. Kepler's Laws

Rather than their staying at one distance from the Sun, Kepler's First Law showed that the distances of planets from the Sun change over their orbit. In particular, following the terms *perigee* and *apogee* for an ellipse in general, the location in its orbit at which an object gets closest to the Sun is called the *perihelion* of the orbit and the location in its orbit at which an object gets furthest from the Sun is called the *aphelion* of the orbit.

The shape of an elliptical orbit is quantified by providing its eccentricity, defined as the distance between the two foci divided by the major axis. For those solar system objects with close to circular orbits, such as most of the planets, because both foci are inside the Sun this is impossible to calculate. Instead, an equivalent means of calculating the eccentricity is used. Noting that $2f + 2p = 2a$, where f is the distance from the center of the orbit to a focus, p is the perihelion distance of the object in its orbit, and a is the semi-major axis, we see that $e = 2f/2a$ can be expressed as

$$e = 1 - \frac{p}{a}. \tag{1}$$

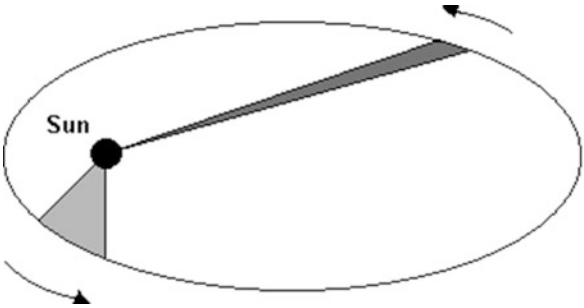

Fig. 1 Kepler's first and second laws. The orbit of any object about the Sun is an ellipse with the Sun at one focus. In equal periods of time, the area swept out by a line from the Sun to the planet is a constant

This is the expression we will use in our analysis of the orbits of Mercury and Mars.

Kepler also determined the speeds of the planets in their orbits and the sizes of the orbits. He found that the further a planet is from the Sun in its orbit, the slower it moves. More precisely, he expressed this geometrically by stating that a line drawn from the Sun to the planet sweeps out equal areas of the orbit in equal times, as shown in Fig. 1. If you consider such a line as the height of a triangle with the distance traveled along the orbit during a small time period the base of the triangle, then you can understand that the equal area in equal times requirement demands that the further the planet is from the Sun (the height of the triangle), the less distance the planet must move in a given period of time (the base of the triangle) and hence the slower its motion must be. This geometrical statement has become known as Kepler's Second Law of Planetary Motion.

Because an ellipse cannot be described by a single radius, Kepler studied the length of the semi-major axes of the elliptical orbits as a measure of their size. The semi-major axis of an ellipse is one-half the major axis, the line connecting the aphelion and perihelion points. It can be considered the longest "diameter" of the ellipse.

Kepler discovered that the magnitude of the semi-major axis of a planet was related to the amount of time needed for the planet to complete an orbit about the Sun, the period of the orbit, or orbital period. Mathematically, he found that the cube of the semi-major axis is proportional to the square of the period. This is Kepler's Third Law of Planetary Motion.

If the period, P, is measured in years, and a, the semi-major axis, is measured in astronomical units, then Kepler's Third Law is stated mathematically in a simple form,

$$P^2 = a^3. \tag{2}$$

Nothing magical exists in this simple form of Kepler's Third Law. It is simply the result of our choice of units for P and a. Because 1 A.U. is defined as the distance from the Earth to the Sun, and because our orbital period is the year, for this equation to hold for the Earth, $1^2 = 1^3$ without the complication of any constants.

In common language, Kepler's three laws tell us that the planets in their orbits are not always at the same distance from the Sun, that the velocity of the planets along their orbits depends on their distance from the Sun, and that the greater the average distance between a planet and the Sun during its orbit the greater is its period.

Kepler's Laws, however, are descriptive, telling us how the planets move but without any explanation, and it might be wondered if fundamental laws of nature are hidden within them. This was indeed shown to be the case by Sir Isaac Newton (1642–1727), arguably the greatest scientist of all time. His Newton's Laws of Motion and Universal Law of Gravitation can be used to mathematically derive Kepler's Laws of Planetary Motion.

Kepler's Laws were the first mathematical formulations to correctly describe nature, and therefore can be considered as the beginning of the field of mathematical physics. The repercussions of this development, both philosophically and practically, are fundamental: It both revolutionized our way of thinking about nature, that its behavior can be expressed by the human construct known as mathematics, and also made our modern technological world possible.

2. *Comets and Kepler's Second Law*

Kepler's Laws assume the existence of only one force, the gravitational force. We know, however, that other forces act on objects in orbit about the Sun. The other objects in the solar system exert a gravitational force, the solar wind particles and radiation exerts pressure on objects, and collisions with dust particles exert a drag frictional force, for a few examples.

Comets, however, feel an additional force, a rocket-like thrust arising from the ejection of gas and dust through surface vents from beneath their surfaces. When a comet gets close to the Sun, the surface ice on the side of the comet facing the Sun sublimes or is melted, creating these pathways for the material below to escape. It does so explosively. The so-called *jets* were directly observed in 1986 by Soviet, Japanese, and European spacecraft flying by Halley's comet on its return to the inner solar system as part of its 76-year orbital travels. The European Giotto spacecraft got as close as 600 km from the nucleus of the comet. As with any jet propulsion, Newton's third law tells us that the force the comet nucleus exerts on the gas molecules and dust particles to eject them is equal to a force in the opposite direction that the particles exert on the comet nucleus. The components of that force lead to both a rotation of the comet nucleus and an acceleration or deceleration along its orbit.

We can estimate the acceleration and deceleration of the comet that results from this force. The material ejected is evaporated ammonia, methane, and water vapor, and dust. Ammonia (NH_3), methane (CH_4), and water (H_2O) molecules are composed of 17, 16, and 18 nucleons, respectively, and a dust molecule, for example, SiO_2 or FeO, is composed of 60 nucleons and 72 nucleons, respectively. For a rough estimate, then, say a typical ejected molecule is composed of 50 nucleons. With a mass of the proton of 1.67×10^{-24} g and an estimated loss of 10^{30} molecules per

second when the comet is close enough to the Sun to have an active set of jets, we multiply these factors together to find a mass loss of about 8×10^4 kg/s.

To find the effective acceleration and deceleration we remember that linear momentum is defined as $p = mv$ so that the acceleration is given by

$$a = \frac{1}{m}\frac{dp}{dt}.$$

To calculate this we need to know the velocity with which the molecules are ejected from an initial rest state. This has been estimated from the 1986 flyby studies of Halley's comet to be about 1 km/s. From conservation of linear momentum, the change in the acceleration of the comet is then

$$a_c = \frac{1}{m_c}\frac{dp_e}{dt} \tag{3}$$

where dp_e is the change in momentum, $p_e = m_e\, v$, of a mass m_e of material ejected from the comet in the time dt moving at a velocity, v, and m_c is the mass of the comet. Comet nuclei vary in mass from 10^{12} to 10^{16} kg, similar to the masses of small asteroids. Use $m_c = 10^{14}$ kg as a typical value, close to the 2.2×10^{14} kg value ascribed to Halley's Comet. Substituting the values for mass loss, ejection velocity, and comet mass in (3), we find the acceleration or deceleration to be about 8×10^{-7} m/s^2.

We can compare this to the acceleration resulting from the gravitational force of the Sun, Gm_{sun}/r^2, where m_{Sun} is the mass of the Sun. Taking as an example $r = 1$ A.U., or 1.5×10^{11} m, we find 6×10^{-3} m/s^2. As expected, the acceleration resulting from the gravitational force is much greater than that resulting from the jet force, but it is only about four orders of magnitude greater for the particular illustrative numbers we've used. Although the effect may be small, it is, however, detectable. I. In fact, observations of the trajectories of some comets before the Halley flybys of 1986 led astronomers to hypothesize that the jets existed.

When the comet is near the Sun, the jet effect results in a slight deceleration at approach, that is, before perihelion, and a slight acceleration when the comet recedes, that is, past perihelion. These effects almost exactly balance, so that the overall effect on the period of the comet is negligible. The only net effect results from the receding comet having a slightly lower mass than when it was approaching, a result of the mass ejection.

C. Procedure and Observations

In this experiment, we shall use observational data published in the *Astronomical Almanac* and its predecessor the *American Ephemeris and Nautical Almanac*, the authoritative annual compilation of celestial phenomena, to test Kepler's Laws. Of the planets which orbit the Sun in a relatively small amount of time, only Mercury and Mars have sizable orbital eccentricities; that is, only they have appreciably

elliptical orbits. Venus, the Earth, and Jupiter, by comparison, have nearly circular orbits. We will accordingly examine only the orbits of Mercury and Mars.

We will graph the orbit of these two planets and find that they are elliptical in shape. We will then test Kepler's First, Second, and Third Laws.

On the two polar graph papers on the DATA SHEET, plot the orbits of Mercury and Mars about the Sun using the data from the *Ephemeris*. The angular coordinate is the *longitude* and the length coordinate is the *radius vector* as provided in the *Ephemeris*. The longitudes are *heliocentric*, relative to the Sun.

Represent the position of the Sun at the center of the graph paper. On each graph, note the scale you are using, for example, 10 cm = 1 A.U., by definition the size of the semi-major axis of the Earth, and draw a line at the bottom of the graph paper whose length according to this scale represents 1 A.U. Choose your scale to use a reasonably large portion of the graph paper.

For Mercury, we will use the data reproduced from the *Ephemeris* for 1969, the year man first landed on the Moon. That historic date, marking one of the greatest events in the history of mankind, was July 20. For Mars, data is reproduced from the *Ephemeris* for 1994 and 1995, 1994 being the year that extraterrestrial intelligent civilizations were first detected in our galaxy and communication was established with them, successfully persuading them, in return for a 1956 mint-condition Mickey Mantle baseball card, not to attack Earth and destroy all sources of its overly loud rock music. (That would have been one of the greatest events in the history of mankind.) Write the corresponding Julian Date (J.D.) as provided in the Ephemeris next to each data point in the orbit.

D. Calculations and Analysis

1. Kepler's First Law

Mark the locations of aphelion and perihelion in each orbit. On each graph, draw a straight line from the perihelion position on the orbit to the Sun and through the Sun to the diametrically-opposite point on the orbit. That line is the major axis. Measure the distance from Sun to the perihelion point and the length of the major axis, both in centimeters. Enter the results in Table 1 of the DATA SHEET. Calculate the eccentricity of the orbit according to (1), and enter that result in Table 1 of the DATA SHEET. The accepted values for the eccentricity of the orbits of Mercury and Mars are 0.206 and 0.093, respectively. Calculate the percentage error between these values and the values you have determined.

2. Kepler's Second Law

To test Kepler's Second Law, we need to measure the areas swept out by a line from the Sun to the planet for equal time intervals in the orbit. In the graph of the orbit for each

planet, draw a line from the Sun to a position on the orbit. Then draw a second line from the Sun to a position on the orbit a certain time interval later, perhaps a week for Mercury and a month for Mars. The deciding consideration is to provide a large enough area to reduce the error resulting from the measurement technique we shall use.

To determine the area, the simplest procedure is to use a planimeter. If your laboratory does not have these, a square grid is superimposed on the graph paper to enable determination of areas by counting the number of squares and fractional squares. Count the number of squares within the triangular-shaped sector determined by the two "radii" and the path swept out by the orbit. First count the number of full squares and then estimate the sum of the areas of partial squares. Enter your results as "full" and "partial" in Table 2 and Table 3 of the DATA SHEET for Mercury and Mars, respectively. Add them and enter the total result in these tables. Also enter the Julian dates corresponding to the two points along the orbit defining the area.

Repeat this procedure and calculate an average value for the area.

Do this a total of five times for different triangular-shaped sectors along the orbit, labeling each sector as #1, #2, and so on. For at least two of the measurements, use a time interval equal to two, three, or more times as long as the first time interval. Use of larger areas will help reduce the percentage errors in the area determination and will allow us to graph the results with a large range of ordinates and abscissas. For each triangular-shaped sector determine the area twice and average the results. Enter your results for the areas and the Julian dates of the points along the orbit defining the area in Tables 2 and 3 of the DATA SHEET for Mercury and Mars, respectively.

Calculate the time interval for the radius vector to sweep out the areas by subtracting the two values of Julian dates defining the areas.

For each planet, construct a graph of the average area as a function of the time interval using the graph paper supplied on the DATA SHEET. For each planet, calculate the slope of the curve on the DATA SHEET.

3. *Kepler's Third Law*

To test Kepler's Third Law, we need to determine the length of the semi-major axis of the orbit of each planet. For each, carefully measure the length in centimeters of the largest "diameter" of the orbit, the major axis. Repeat the measurement and then calculate the average value. One-half of this value is the length of the semi-major axis in centimeters. Enter your results and perform your calculations on the DATA SHEET.

To use the simple form of (1) for Kepler's Third Law, we must convert the units of the semi-major axes for Mars and Mercury from centimeters to A.U. To do this, divide the values obtained for the semi-major axis of each planet by the scale factor, the number of centimeters you have chosen to represent 1 A.U. when you plotted each orbit. Enter your results for a and a^3 on the DATA SHEET.

The period of the orbit is the time needed for the planet to go around the Sun. You can determine the period from the table of positions reproduced from the

Ephemeris by subtracting the values of the Julian dates (J.D.) on successive appearances of the planet at the same heliocentric longitude. Divide this difference by 365.2 days/year to find the period in years, $P = \Delta(\text{J.D.})/365.2$. Enter your results for P and P^2 on the DATA SHEET.

On a piece of graph paper, plot P^2 as a function of a^3. For a third data point, use the values for the Earth. Because P is measured in years and a is measured in A.U., these values are simply $P^2 = 1$ and $a^3 = 1$. Fit a straight line to these three points. Estimate the value of the y-intercept and enter it on the DATA SHEET. Calculate the slope on the DATA SHEET. The y-intercept should be close to 0, and the slope should be close to 1.

MERCURY, 1969

HELIOCENTRIC POSITIONS FOR 0h EPHEMERIS TIME
MEAN EQUINOX AND ECLIPTIC OF DATE

Date	Julian Date	Longitude	Latitude	Radius Vector	Date	Julian Date	Longitude	Latitude	Radius Vector
	244					244			
Jan. 0	0221·5	328 56 08·9	−6 52 38·5	0·396 0530	Feb. 15	0267·5	201 46 07·4	+3 06 16·0	0·419 7758
1	0222·5	332 50 32·7	6 46 17·5	·390 4748	16	0268·5	205 07 12·5	2 43 51·1	·424 4562
2	0223·5	336 51 40·5	6 37 48·3	·384 7987	17	0269·5	208 23 52·7	2 21 22·4	·428 9289
3	0224·5	340 59 54·9	6 27 02·2	·379 0498	18	0270·5	211 36 28·9	1 58 54·0	·433 1836
4	0225·5	345 15 38·0	6 13 50·6	·373 2558	19	0271·5	214 45 21·1	1 36 29·3	·437 2109
5	0226·5	349 39 11·2	−5 58 05·1	0·367 4479	20	0272·5	217 50 48·3	+1 14 11·5	0·441 0029
6	0227·5	354 10 54·8	5 39 38·2	·361 6597	21	0273·5	220 53 08·6	0 52 03·1	·444 5524
7	0228·5	358 51 07·2	5 18 23·0	·355 9284	22	0274·5	223 52 39·5	0 30 06·5	·447 8534
8	0229·5	3 40 04·1	4 54 14·3	·350 2947	23	0275·5	226 49 37·5	+0 08 23·5	·450 9004
9	0230·5	8 37 58·1	4 27 09·1	·344 8019	24	0276·5	229 44 18·7	−0 13 04·0	·453 6885
10	0231·5	13 44 57·2	−3 57 06·8	0·339 4964	25	0277·5	232 36 58·2	−0 34 14·6	0·456 2140
11	0232·5	19 01 04·4	3 24 10·5	·334 4273	26	0278·5	235 27 50·9	0 55 06·8	·458 4730
12	0233·5	24 26 15·7	2 48 27·5	·329 6455	27	0279·5	238 17 10·9	1 15 39·3	·460 4626
13	0234·5	30 00 20·0	2 10 09·8	·325 2031	28	0280·5	241 05 12·1	1 35 51·2	·462 1804
14	0235·5	35 42 57·1	1 29 35·0	·321 1523	Mar. 1	0281·5	243 52 07·7	1 55 41·2	·463 6242
15	0236·5	41 33 37·5	−0 47 06·3	0·317 5441	2	0282·5	246 38 11·0	−2 15 08·3	0·464 7922
16	0237·5	47 31 41·1	−0 03 12·9	·314 4272	3	0283·5	249 23 34·5	2 34 11·4	·465 6828
17	0238·5	53 36 17·3	+0 41 30·6	·311 8457	4	0284·5	252 08 30·9	2 52 49·6	·466 2952
18	0239·5	59 46 25·0	1 26 25·1	·309 8382	5	0285·5	254 53 12·6	3 11 01·7	·466 6287
19	0240·5	66 00 53·3	2 10 48·3	·308 4358	6	0286·5	257 37 51·8	3 28 46·8	·466 6829
20	0241·5	72 18 22·8	+2 53 56·3	0·307 6607	7	0287·5	260 22 40·7	−3 46 03·5	0·466 4580
21	0242·5	78 37 27·5	3 35 05·7	·307 5257	8	0288·5	263 07 51·6	4 02 50·6	·465 9537
22	0243·5	84 56 37·7	4 13 35·8	·308 0328	9	0289·5	265 53 36·7	4 19 06·9	·465 1712
23	0244·5	91 14 22·2	4 48 50·6	·309 1739	10	0290·5	268 40 08·3	4 34 50·8	·464 1110
24	0245·5	97 29 11·9	5 20 20·2	·310 9305	11	0291·5	271 27 38·8	4 50 00·7	·462 7742
25	0246·5	103 39 42·1	+5 47 42·3	0·313 2750	12	0292·5	274 16 21·1	−5 04 34·9	0·461 1626
26	0247·5	109 44 35·7	6 10 42·3	·316 1722	13	0293·5	277 06 27·9	5 18 31·5	·459 2785
27	0248·5	115 42 44·9	6 29 13·7	·319 5797	14	0294·5	279 58 12·4	5 31 48·3	·457 1239
28	0249·5	121 33 12·4	6 43 17·3	·323 4505	15	0295·5	282 51 48·3	5 44 22·9	·454 7015
29	0250·5	127 15 12·9	6 52 59·9	·327 7347	16	0296·5	285 47 29·4	5 56 12·8	·452 0150
30	0251·5	132 48 12·0	+6 58 33·7	0·332 3804	17	0297·5	288 45 30·2	−6 07 15·1	0·449 0680
31	0252·5	138 11 47·1	7 00 14·8	·337 3350	18	0298·5	291 46 05·4	6 17 26·6	·445 8650
Feb. 1	0253·5	143 25 45·2	6 58 21·5	·342 5473	19	0299·5	294 49 30·6	6 26 44·0	·442 4114
2	0254·5	148 30 02·6	6 53 14·0	·347 9673	20	0300·5	297 56 01·7	6 35 03·2	·438 7129
3	0255·5	153 24 43·4	6 45 12·7	·353 5473	21	0301·5	301 05 55·3	6 42 20·2	·434 7762
4	0256·5	158 09 58·0	+6 34 37·9	0·359 2427	22	0302·5	304 19 28·7	−6 48 30·4	0·430 6090
5	0257·5	162 46 01·7	6 21 49·2	·365 0116	23	0303·5	307 36 59·8	6 53 28·7	·426 2200
6	0258·5	167 13 13·9	6 07 04·9	·370 8157	24	0304·5	310 58 47·4	6 57 09·6	·421 6189
7	0259·5	171 31 56·6	5 50 42·0	·376 6194	25	0305·5	314 25 10·7	6 59 27·1	·416 8172
8	0260·5	175 42 34·0	5 32 55·9	·382 3908	26	0306·5	317 56 30·0	7 00 15·0	·411 8272
9	0261·5	179 45 31·2	+5 14 00·7	0·388 1008	27	0307·5	321 33 05·9	−6 59 26·1	0·406 6632
10	0262·5	183 41 14·0	4 54 08·6	·393 7230	28	0308·5	325 15 19·8	6 56 53·2	·401 3413
11	0263·5	187 30 08·5	4 33 30·6	·399 2338	29	0309·5	329 03 33·6	6 52 28·4	·395 8795
12	0264·5	191 12 40·3	4 12 16·5	·404 6124	30	0310·5	332 58 09·8	6 46 03·6	·390 2978
13	0265·5	194 49 14·5	3 50 34·7	·409 8398	31	0311·5	336 59 30·7	6 37 30·2	·384 6190
14	0266·5	198 20 15·7	+3 28 32·4	0·414 8992	Apr. 1	0312·5	341 07 58·8	−6 26 39·7	0·378 8682
15	0267·5	201 46 07·4	+3 06 16·0	0·419 7758	2	0313·5	345 23 56·4	−6 13 23·4	0·373 0735

MERCURY, 1969

HELIOCENTRIC POSITIONS FOR 0h EPHEMERIS TIME
MEAN EQUINOX AND ECLIPTIC OF DATE

Date	Julian Date	Longitude	Latitude	Radius Vector
	244	° ′ ″	° ′ ″	
Apr. 1	0312·5	341 07 58·8	−6 26 39·7	0·378 8682
2	0313·5	345 23 56·4	6 13 23·4	·373 0735
3	0314·5	349 47 44·8	5 57 33·0	·367 2657
4	0315·5	354 19 44·1	5 39 00·8	·361 4788
5	0316·5	359 00 12·7	5 17 40·3	·355 7500
6	0317·5	3 49 26·3	−4 53 26·1	0·350 1201
7	0318·5	8 47 37·3	4 26 15·3	·344 6324
8	0319·5	13 54 53·7	3 56 07·5	·339 3337
9	0320·5	19 11 17·9	3 23 05·8	·334 2729
10	0321·5	24 36 46·2	2 47 17·7	·329 5010
11	0322·5	30 11 06·9	−2 08 55·5	0·325 0702
12	0323·5	35 53 59·6	1 28 16·7	·321 0327
13	0324·5	41 44 54·5	0 45 44·9	·317 4394
14	0325·5	47 43 11·1	−0 01 49·4	·314 3387
15	0326·5	53 47 58·6	+0 42 55·0	·311 7749
16	0327·5	59 58 15·5	+1 27 49·2	0·309 7860
17	0328·5	66 12 50·6	2 12 10·7	·308 4031
18	0329·5	72 30 24·2	2 55 15·6	·307 6479
19	0330·5	78 49 30·3	3 36 20·6	·307 5331
20	0331·5	85 08 39·0	4 14 45·1	·308 0602
21	0332·5	91 26 19·2	+4 49 53·3	0·309 2210
22	0333·5	97 41 01·9	5 21 15·4	·310 9965
23	0334·5	103 51 22·5	5 48 29·5	·313 3590
24	0335·5	109 56 04·3	6 11 21·2	·316 2726
25	0336·5	115 53 59·6	6 29 44·2	·319 6953
26	0337·5	121 44 11·8	+6 43 39·4	0·323 5798
27	0338·5	127 25 55·6	6 53 14·0	·327 8761
28	0339·5	132 58 37·3	6 58 40·3	·332 5322
29	0340·5	138 21 54·2	7 00 14·4	·337 4957
30	0341·5	143 35 34·1	6 58 14·8	·342 7151
May 1	0342·5	148 39 33·3	+6 53 01·5	0·348 1407
2	0343·5	153 33 56·2	6 44 55·1	·353 7249
3	0344·5	158 18 53·2	6 34 15·9	·359 4230
4	0345·5	162 54 39·9	6 21 23·3	·365 1936
5	0346·5	167 21 35·7	6 06 35·7	·370 9980
6	0347·5	171 40 02·8	+5 50 10·0	0·376 8010
7	0348·5	175 50 25·4	5 32 21·6	·382 5709
8	0349·5	179 53 08·6	5 13 24·3	·388 2785
9	0350·5	183 48 38·3	4 53 30·7	·393 8974
10	0351·5	187 37 20·4	4 32 51·5	·399 4043
11	0352·5	191 19 40·6	+4 11 36·4	0·404 7784
12	0353·5	194 56 04·1	3 49 53·8	·410 0006
13	0354·5	198 26 55·2	3 27 50·9	·415 0546
14	0355·5	201 52 37·7	3 05 34·3	·419 9251
15	0356·5	205 13 34·2	2 43 09·2	·424 5991
16	0357·5	208 30 06·5	+2 20 40·4	0·429 0651
17	0358·5	211 42 35·5	+1 58 12·0	0·433 3126

Date	Julian Date	Longitude	Latitude	Radius Vector
	244	° ′ ″	° ′ ″	
May 17	0358·5	211 42 35·5	+1 58 12·0	0·433 3126
18	0359·5	214 51 21·0	1 35 47·5	·437 3325
19	0360·5	217 56 42·1	1 13 30·0	·441 1170
20	0361·5	220 58 56·9	0 51 21·9	·444 6589
21	0362·5	223 58 22·8	0 29 25·6	·447 9521
22	0363·5	226 55 16·4	+0 07 43·1	0·450 9910
23	0364·5	229 49 53·5	−0 13 43·9	·453 7712
24	0365·5	232 42 29·6	0 34 53·9	·456 2884
25	0366·5	235 33 19·2	0 55 45·5	·458 5389
26	0367·5	238 22 36·6	1 16 17·4	·460 5200
27	0368·5	241 10 35·5	−1 36 28·6	0·462 2291
28	0369·5	243 57 29·4	1 56 17·9	·463 6643
29	0370·5	246 43 31·2	2 15 44·3	·464 8235
30	0371·5	249 28 53·8	2 34 46·7	·465 7058
31	0372·5	252 13 49·6	2 53 24·1	·466 3095
June 1	0373·5	254 58 31·1	−3 11 35·4	0·466 6343
2	0374·5	257 43 10·4	3 29 19·6	·466 6800
3	0375·5	260 27 59·9	3 46 35·4	·466 4465
4	0376·5	263 13 11·7	4 03 21·6	·465 9337
5	0377·5	265 58 58·0	4 19 36·9	·465 1425
6	0378·5	268 45 31·3	−4 35 19·7	0·464 0739
7	0379·5	271 33 03·9	4 50 28·6	·462 7286
8	0380·5	274 21 48·7	5 05 01·6	·461 1087
9	0381·5	277 11 58·3	5 18 57·0	·459 2161
10	0382·5	280 03 46·1	5 32 12·5	·457 0532
11	0383·5	282 57 25·7	−5 44 45·8	0·454 6228
12	0384·5	285 53 10·9	5 56 34·2	·451 9283
13	0385·5	288 51 16·2	6 07 35·0	·448 9734
14	0386·5	291 51 56·5	6 17 44·9	·445 7629
15	0387·5	294 55 27·2	6 27 00·5	·442 3018
16	0388·5	298 02 04·3	−6 35 17·8	0·438 5959
17	0389·5	301 12 04·4	6 42 32·8	·434 6522
18	0390·5	304 25 44·8	6 48 40·8	·430 4782
19	0391·5	307 43 23·6	6 53 36·8	·426 0826
20	0392·5	311 05 19·3	6 57 15·2	·421 4755
21	0393·5	314 31 51·4	−6 59 30·1	0·416 6679
22	0394·5	318 03 20·0	7 00 15·0	·411 6725
23	0395·5	321 40 05·9	6 59 23·0	·406 5037
24	0396·5	325 22 30·5	6 56 46·7	·401 1773
25	0397·5	329 10 55·7	6 52 18·3	·395 7118
26	0398·5	333 05 43·8	−6 45 49·6	0·390 1271
27	0399·5	337 07 17·3	6 37 12·1	·384 4461
28	0400·5	341 15 58·8	6 26 17·2	·378 6939
29	0401·5	345 32 10·3	6 12 56·3	·372 8985
30	0402·5	349 56 13·2	5 57 01·0	·367 0911
July 1	0403·5	354 28 27·6	−5 38 23·8	0·361 3056
2	0404·5	359 09 11·8	−5 16 57·9	0·355 5797

MERCURY, 1969

HELIOCENTRIC POSITIONS FOR 0h EPHEMERIS TIME
MEAN EQUINOX AND ECLIPTIC OF DATE

Date	Julian Date	Longitude	Latitude	Radius Vector
	244	° ′ ″	° ′ ″	
July 1	0403·5	354 28 27·6	−5 38 23·8	0·361 3056
2	0404·5	359 09 11·8	5 16 57·9	·355 5797
3	0405·5	3 58 41·4	4 52 38·4	·349 9536
4	0406·5	8 57 08·7	4 25 22·1	·344 4713
5	0407·5	14 04 41·4	3 55 08·9	·339 1795
6	0408·5	19 21 22·0	−3 22 02·1	0·334 1269
7	0409·5	24 47 06·3	2 46 09·1	·329 3649
8	0410·5	30 21 42·4	2 07 42·4	·324 9456
9	0411·5	36 04 49·9	1 26 59·8	·320 9209
10	0412·5	41 55 58·3	0 44 25·1	·317 3420
11	0413·5	47 54 27·2	−0 00 27·6	0·314 2570
12	0414·5	53 59 25·1	+0 44 17·7	·311 7102
13	0415·5	60 09 50·4	1 29 11·4	·309 7394
14	0416·5	66 24 31·6	2 13 31·2	·308 3752
15	0417·5	72 42 08·7	2 56 33·0	·307 6393
16	0418·5	79 01 15·8	+3 37 33·6	0·307 5438
17	0419·5	85 20 22·6	4 15 52·5	·308 0903
18	0420·5	91 37 58·2	4 50 54·1	·309 2698
19	0421·5	97 52 33·6	5 22 09·0	·311 0634
20	0422·5	104 02 44·6	5 49 15·2	·313 4429
21	0423·5	110 07 14·6	+6 11 58·7	0·316 3723
22	0424·5	116 04 56·4	6 30 13·5	·319 8095
23	0425·5	121 54 53·4	6 44 00·7	·323 7069
24	0426·5	127 36 21·0	6 53 27·5	·328 0146
25	0427·5	133 08 45·6	6 58 46·5	·332 6805
26	0428·5	138 31 45·1	+7 00 13·8	0·337 6521
27	0429·5	143 45 07·3	6 58 08·0	·342 8781
28	0430·5	148 48 48·9	6 52 49·2	·348 3088
29	0431·5	153 42 54·3	6 44 37·8	·353 8969
30	0432·5	158 27 34·4	6 33 54·3	·359 5975
31	0433·5	163 03 04·7	+6 20 57·9	0·365 3693
Aug. 1	0434·5	167 29 44·9	6 06 07·1	·371 1739
2	0435·5	171 47 57·0	5 49 38·6	·376 9762
3	0436·5	175 58 05·3	5 31 47·9	·382 7444
4	0437·5	180 00 35·1	5 12 48·8	·388 4494
5	0438·5	183 55 52·2	+4 52 53·6	0·394 0651
6	0439·5	187 44 22·5	4 32 13·1	·399 5683
7	0440·5	191 26 31·6	4 10 57·0	·404 9379
8	0441·5	195 02 44·8	3 49 13·7	·410 1551
9	0442·5	198 33 26·3	3 27 10·4	·415 2035
10	0443·5	201 58 59·9	+3 04 53·3	0·420 0681
11	0444·5	205 19 48·2	2 42 28·0	·424 7360
12	0445·5	208 36 13·0	2 19 59·2	·429 1954
13	0446·5	211 48 35·0	1 57 30·9	·433 4361
14	0447·5	214 57 14·2	1 35 06·5	·437 4491
15	0448·5	218 02 29·5	+1 12 49·2	0·441 2262
16	0449·5	221 04 39·1	−0 50 41·4	0·444 7607

Date	Julian Date	Longitude	Latitude	Radius Vector
	244	° ′ ″	° ′ ″	
Aug. 16	0449·5	221 04 39·1	+0 50 41·4	0·444 7607
17	0450·5	224 04 00·2	0 28 45·6	·448 0401
18	0451·5	227 00 49·5	+0 07 03·5	·451 0773
19	0452·5	229 55 22·9	−0 14 23·1	·453 8494
20	0453·5	232 47 55·6	0 35 32·5	·456 3586
21	0454·5	235 38 42·4	−0 56 23·6	0·458 6010
22	0455·5	238 27 57·3	1 16 54·9	·460 5740
23	0456·5	241 15 54·1	1 37 05·5	·462 2750
24	0457·5	244 02 46·3	1 56 54·1	·463 7018
25	0458·5	246 48 46·9	2 16 19·8	·464 8529
26	0459·5	249 34 08·5	−2 35 21·4	0·465 7264
27	0460·5	252 19 03·7	2 53 58·0	·466 3219
28	0461·5	255 03 45·0	3 12 08·5	·466 6384
29	0462·5	257 48 24·6	3 29 51·8	·466 6756
30	0463·5	260 33 14·7	3 47 06·8	·466 4336
31	0464·5	263 18 27·4	−4 03 52·1	0·465 9123
Sept. 1	0465·5	266 04 15·0	4 20 06·4	·465 1128
2	0466·5	268 50 50·0	4 35 48·2	·464 0358
3	0467·5	271 38 24·7	4 50 56·0	·462 6821
4	0468·5	274 27 11·8	5 05 27·9	·461 0540
5	0469·5	277 17 24·3	−5 19 22·1	0·459 1534
6	0470·5	280 09 15·3	5 32 36·3	·456 9824
7	0471·5	283 02 58·5	5 45 08·3	·454 5440
8	0472·5	285 58 47·8	5 56 55·3	·451 8414
9	0473·5	288 56 57·7	6 07 54·5	·448 8788
10	0474·5	291 57 42·9	−6 18 02·8	0·445 6606
11	0475·5	295 01 19·1	6 27 16·7	·442 1919
12	0476·5	298 08 02·1	6 35 32·2	·438 4788
13	0477·5	301 18 08·7	6 42 45·2	·434 5278
14	0478·5	304 31 56·1	6 48 51·1	·430 3469
15	0479·5	307 49 42·4	−6 53 44·7	0·425 9448
16	0480·5	311 11 46·3	6 57 20·6	·421 3314
17	0481·5	314 38 27·1	6 59 32·8	·416 5179
18	0482·5	318 10 05·1	7 00 14·9	·411 5171
19	0483·5	321 47 01·0	6 59 19·8	·406 3433
20	0484·5	325 29 36·3	−6 56 40·2	0·401 0124
21	0485·5	329 18 12·8	6 52 08·2	·395 5428
22	0486·5	333 13 12·9	6 45 35·7	·389 9548
23	0487·5	337 14 59·2	6 36 54·1	·384 2712
24	0488·5	341 23 54·1	6 25 54·8	·378 5171
25	0489·5	345 40 19·7	−6 12 29·3	0·372 7209
26	0490·5	350 04 37·3	5 56 29·2	·366 9135
27	0491·5	354 37 07·1	5 37 46·9	·361 1294
28	0492·5	359 18 07·2	5 16 15·8	·355 4057
29	0493·5	4 07 53·0	4 51 50·8	·349 7833
30	0494·5	9 06 36·9	−4 24 29·1	0·344 3061
Oct. 1	0495·5	14 14 26·4	−3 54 10·5	0·339 0208

MERCURY, 1969

HELIOCENTRIC POSITIONS FOR 0h EPHEMERIS TIME
MEAN EQUINOX AND ECLIPTIC OF DATE

Date	Julian Date	Longitude	Latitude	Radius Vector
	244	° ′ ″	° ′ ″	
Oct. 1	0495·5	14 14 26·4	−3 54 10·5	0·339 0208
2	0496·5	19 31 23·8	3 20 58·4	·333 9763
3	0497·5	24 57 24·6	2 45 00·5	·329 2239
4	0498·5	30 32 16·8	2 06 29·4	·324 8157
5	0499·5	36 15 39·5	1 25 43·0	·320 8039
6	0500·5	42 07 02·2	−0 43 05·2	0·317 2394
7	0501·5	48 05 43·8	+0 00 54·2	·314 1704
8	0502·5	54 10 52·8	0 45 40·4	·311 6404
9	0503·5	60 21 27·2	1 30 33·8	·309 6877
10	0504·5	66 36 15·0	2 14 51·8	·308 3424
11	0505·5	72 53 56·3	+2 57 50·5	0·307 6260
12	0506·5	79 13 04·8	3 38 46·8	·307 5503
13	0507·5	85 32 10·3	4 17 00·2	·308 1163
14	0508·5	91 49 41·9	4 51 55·3	·309 3149
15	0509·5	98 04 10·5	5 23 02·8	·311 1268
16	0510·5	104 14 12·3	+5 50 01·0	0·313 5237
17	0511·5	110 18 30·8	6 12 36·4	·316 4695
18	0512·5	116 15 59·2	6 30 42·9	·319 9216
19	0513·5	122 05 41·4	6 44 21·9	·323 8323
20	0514·5	127 46 52·8	6 53 41·0	·328 1518
21	0515·5	133 19 00·5	+6 58 52·6	0·332 8277
22	0516·5	138 41 42·5	7 00 13·0	·337 8080
23	0517·5	143 54 46·9	6 58 01·0	·343 0411
24	0518·5	148 58 10·8	6 52 36·5	·348 4774
25	0519·5	153 51 58·8	6 44 20·2	·354 0696
26	0520·5	158 36 21·8	+6 33 32·3	0·359 7733
27	0521·5	163 11 35·6	6 20 32·1	·365 5466
28	0522·5	167 37 59·9	6 05 38·0	·371 3518
29	0523·5	171 55 56·8	5 49 06·8	·377 1535
30	0524·5	176 05 50·7	5 31 13·8	·382 9203
31	0525·5	180 08 06·9	+5 12 12·7	0·388 6231
Nov. 1	0526·5	184 03 11·1	4 52 16·0	·394 2357
2	0527·5	187 51 29·3	4 31 34·3	·399 7351
3	0528·5	191 33 27·1	4 10 17·2	·405 1003
4	0529·5	195 09 29·7	3 48 33·2	·410 3127
5	0530·5	198 40 01·4	+3 26 29·3	0·415 3558
6	0531·5	202 05 25·9	3 04 11·9	·420 2148
7	0532·5	205 26 05·8	2 41 46·5	·424 8764
8	0533·5	208 42 22·7	2 19 17·6	·429 3294
9	0534·5	211 54 37·6	1 56 49·3	·433 5634
10	0535·5	215 03 10·1	+1 34 25·2	0·437 5692
11	0536·5	218 08 19·4	1 12 08·1	·441 3391
12	0537·5	221 10 23·5	0 50 00·7	·444 8660
13	0538·5	224 09 39·7	0 28 05·2	·448 1439
14	0539·5	227 06 24·5	+0 06 23·6	·451 1672
15	0540·5	230 00 53·9	−0 15 02·5	0·453 9315
16	0541·5	232 53 23·0	−0 36 11·4	0·456 4325

Date	Julian Date	Longitude	Latitude	Radius Vector
	244	° ′ ″	° ′ ″	
Nov. 16	0541·5	232 53 23·0	−0 36 11·4	0·456 4325
17	0542·5	235 44 06·7	0 57 01·8	·458 6669
18	0543·5	238 33 18·9	1 17 32·5	·460 6317
19	0544·5	241 21 13·5	1 37 42·4	·462 3243
20	0545·5	244 08 03·8	1 57 30·3	·463 7427
21	0546·5	246 54 02·9	−2 16 55·2	0·464 8851
22	0547·5	249 39 23·4	2 35 56·1	·465 7503
23	0548·5	252 24 18·0	2 54 31·9	·466 3371
24	0549·5	255 08 59·0	3 12 41·6	·466 6451
25	0550·5	257 53 38·6	3 30 24·1	·466 6738
26	0551·5	260 38 29·1	−3 47 38·1	0·466 4232
27	0552·5	263 23 42·6	4 04 22·5	·465 8933
28	0553·5	266 09 31·5	4 20 35·8	·465 0853
29	0554·5	268 56 08·0	4 36 16·6	·463 9997
30	0555·5	271 43 44·6	4 51 23·3	·462 6377
Dec. 1	0556·5	274 32 34·1	−5 05 54·1	0·461 0011
2	0557·5	277 22 49·3	5 19 47·1	·459 0920
3	0558·5	280 14 43·5	5 33 00·0	·456 9126
4	0559·5	283 08 30·2	5 45 30·6	·454 4659
5	0560·5	286 04 23·6	5 57 16·2	·451 7553
6	0561·5	289 02 37·9	−6 08 14·0	0·448 7848
7	0562·5	292 03 28·1	6 18 20·6	·445 5587
8	0563·5	295 07 09·6	6 27 32·7	·442 0822
9	0564·5	298 13 58·6	6 35 46·4	·438 3614
10	0565·5	301 24 11·6	6 42 57·4	·434 4033
11	0566·5	304 38 06·0	−6 49 01·2	0·430 2152
12	0567·5	307 55 59·9	6 53 52·5	·425 8063
13	0568·5	311 18 11·9	6 57 25·9	·421 1864
14	0569·5	314 45 01·5	6 59 35·5	·416 3668
15	0570·5	318 16 49·0	7 00 14·7	·411 3602
16	0571·5	321 53 55·0	−6 59 16·5	0·406 1811
17	0572·5	325 36 41·0	6 56 33·6	·400 8455
18	0573·5	329 25 29·0	6 51 58·1	·395 3718
19	0574·5	333 20 41·3	6 45 21·7	·389 7804
20	0575·5	337 22 40·4	6 36 36·0	·384 0939
21	0576·5	341 31 48·9	−6 25 32·4	0·378 3379
22	0577·5	345 48 28·8	6 12 02·2	·372 5404
23	0578·5	350 13 01·4	5 55 57·2	·366 7331
24	0579·5	354 45 46·7	5 37 09·8	·360 9500
25	0580·5	359 27 02·9	5 15 33·4	·355 2286
26	0581·5	4 17 05·4	−4 51 03·1	0·349 6097
27	0582·5	9 16 06·2	4 23 35·9	·344 1374
28	0583·5	14 24 12·8	3 53 11·9	·338 8584
29	0584·5	19 41 27·3	3 19 54·5	·333 8218
30	0585·5	25 07 45·0	2 43 51·7	·329 0790
31	0586·5	30 42 53·7	−2 05 16·0	0·324 6821
32	0587·5	36 26 32·2	−1 24 25·7	0·320 6831

MARS, 1994

HELIOCENTRIC POSITIONS FOR 0^h DYNAMICAL TIME
MEAN EQUINOX AND ECLIPTIC OF DATE

Date	Longitude	Latitude	Radius Vector	Date	Longitude	Latitude	Radius Vector
	° ′ ″	° ′ ″			° ′ ″	° ′ ″	
Jan. 0	277 37 41.4	− 1 22 38.7	1.439 8844	July 3	31 18 19.8	− 0 34 41.9	1.434 1026
4	279 58 21.5	1 25 36.3	.435 4925	7	33 39 12.2	0 30 21.0	.438 4592
8	282 19 53.0	1 28 26.4	.431 2203	11	35 59 12.7	0 25 58.6	.442 9303
12	284 42 14.9	1 31 08.4	.427 0758	15	38 18 20.6	0 21 35.3	.447 5077
16	287 05 26.2	1 33 41.9	.423 0668	19	40 36 35.1	0 17 11.5	.452 1835
20	289 29 25.4	− 1 36 06.4	1.419 2012	23	42 53 55.8	− 0 12 47.9	1.456 9493
24	291 54 11.2	1 38 21.5	.415 4864	27	45 10 22.2	0 08 24.7	.461 7970
28	294 19 42.1	1 40 26.7	.411 9300	31	47 25 54.0	− 0 04 02.5	.466 7184
Feb. 1	296 45 56.4	1 42 21.7	.408 5389	Aug. 4	49 40 31.0	+ 0 00 18.3	.471 7055
5	299 12 52.2	1 44 06.1	.405 3203	8	51 54 13.2	0 04 37.3	.476 7502
9	301 40 27.6	− 1 45 39.4	1.402 2808	12	54 07 00.5	+ 0 08 54.1	1.481 8443
13	304 08 40.6	1 47 01.4	.399 4267	16	56 18 53.0	0 13 08.3	.486 9802
17	306 37 28.8	1 48 11.7	.396 7642	20	58 29 51.0	0 17 19.7	.492 1498
21	309 06 50.1	1 49 10.1	.394 2989	24	60 39 54.7	0 21 27.8	.497 3456
25	311 36 42.0	1 49 56.2	.392 0363	28	62 49 04.4	0 25 32.4	.502 5598
Mar. 1	314 07 02.0	− 1 50 29.9	1.389 9813	Sept. 1	64 57 20.6	+ 0 29 33.1	1.507 7851
5	316 37 47.3	1 50 50.9	.388 1384	5	67 04 43.7	0 33 29.7	.513 0140
9	319 08 55.4	1 50 59.2	.386 5118	9	69 11 14.4	0 37 22.0	.518 2395
13	321 40 23.3	1 50 54.7	.385 1051	13	71 16 53.3	0 41 09.7	.523 4545
17	324 12 08.2	1 50 37.1	.383 9215	17	73 21 41.0	0 44 52.6	.528 6520
21	326 44 07.1	− 1 50 06.6	1.382 9637	21	75 25 38.3	+ 0 48 30.4	1.533 8255
25	329 16 17.0	1 49 23.1	.382 2338	25	77 28 45.9	0 52 03.1	.538 9682
29	331 48 35.0	1 48 26.7	.381 7337	29	79 31 04.8	0 55 30.3	.544 0740
Apr. 2	334 20 57.9	1 47 17.6	.381 4643	Oct. 3	81 32 35.7	0 58 52.1	.549 1365
6	336 53 22.6	1 45 55.7	.381 4263	7	83 33 19.5	1 02 08.1	.554 1497
10	339 25 46.0	− 1 44 21.4	1.381 6199	11	85 33 17.3	+ 1 05 18.4	1.559 1078
14	341 58 05.1	1 42 34.9	.382 0446	15	87 32 30.0	1 08 22.7	.564 0051
18	344 30 16.8	1 40 36.3	.382 6994	19	89 30 58.5	1 11 21.0	.568 8361
22	347 02 18.0	1 38 26.1	.383 5828	23	91 28 44.0	1 14 13.2	.573 5955
26	349 34 05.7	1 36 04.6	.384 6929	27	93 25 47.5	1 16 59.2	.578 2781
30	352 05 37.0	− 1 33 32.1	1.386 0271	31	95 22 10.0	+ 1 19 38.9	1.582 8790
May 4	354 36 49.0	1 30 49.1	.387 5823	Nov. 4	97 17 52.7	1 22 12.3	.587 3934
8	357 07 38.8	1 27 56.0	.389 3552	8	99 12 56.6	1 24 39.2	.591 8167
12	359 38 03.9	1 24 53.2	.391 3417	12	101 07 22.9	1 26 59.7	.596 1443
16	2 08 01.4	1 21 41.3	.393 5375	16	103 01 12.7	1 29 13.7	.600 3722
20	4 37 28.9	− 1 18 20.8	1.395 9377	20	104 54 27.2	+ 1 31 21.3	1.604 4961
24	7 06 23.9	1 14 52.1	.398 5372	24	106 47 07.5	1 33 22.2	.608 5122
28	9 34 44.2	1 11 15.8	.401 3303	28	108 39 14.8	1 35 16.6	.612 4166
June 1	12 02 27.5	1 07 32.6	.404 3110	Dec. 2	110 30 50.3	1 37 04.4	.616 2058
5	14 29 31.7	1 03 42.9	.407 4731	6	112 21 55.1	1 38 45.7	.619 8762
9	16 55 54.8	− 0 59 47.3	1.410 8100	10	114 12 30.5	+ 1 40 20.3	1.623 4247
13	19 21 35.2	0 55 46.3	.414 3149	14	116 02 37.6	1 41 48.4	.626 8481
17	21 46 31.0	0 51 40.7	.417 9806	18	117 52 17.6	1 43 09.8	.630 1433
21	24 10 40.7	0 47 30.8	.421 7999	22	119 41 31.7	1 44 24.7	.633 3076
25	26 34 02.9	0 43 17.4	.425 7651	26	121 30 21.2	1 45 33.0	.636 3383
29	28 56 36.3	− 0 39 00.9	1.429 8686	30	123 18 47.2	+ 1 46 34.8	1.639 2328
July 3	31 18 19.8	− 0 34 41.9	1.434 1026	34	125 06 50.9	+ 1 47 30.0	1.641 9888

MARS, 1995

HELIOCENTRIC POSITIONS FOR 0^h DYNAMICAL TIME
MEAN EQUINOX AND ECLIPTIC OF DATE

Date	Longitude	Latitude	Radius Vector	Date	Longitude	Latitude	Radius Vector
	° ′ ″	° ′ ″			° ′ ″	° ′ ″	
Jan. −1	123 18 47.2	+ 1 46 34.8	1.639 2328	July 2	205 09 11.2	+ 0 45 49.0	1.608 6413
3	125 06 50.9	1 47 30.0	.641 9888	6	207 01 46.6	0 42 28.9	.604 6286
7	126 54 33.5	1 48 18.7	.644 6039	10	208 54 56.1	0 39 05.0	.600 5080
11	128 41 56.2	1 49 01.0	.647 0761	14	210 48 41.0	0 35 37.5	.596 2833
15	130 29 00.3	1 49 36.7	.649 4033	18	212 43 02.4	0 32 06.5	.591 9586
19	132 15 46.9	+ 1 50 06.0	1.651 5838	22	214 38 01.5	+ 0 28 32.2	1.587 5383
23	134 02 17.2	1 50 28.9	.653 6158	26	216 33 39.4	0 24 54.7	.583 0267
27	135 48 32.4	1 50 45.4	.655 4976	30	218 29 57.3	0 21 14.3	.578 4284
31	137 34 33.8	1 50 55.5	.657 2280	Aug. 3	220 26 56.2	0 17 31.1	.573 7483
Feb. 4	139 20 22.5	1 50 59.3	.658 8055	7	222 24 37.3	0 13 45.4	.568 9913
8	141 05 59.7	+ 1 50 56.8	1.660 2288	11	224 23 01.6	+ 0 09 57.3	1.564 1626
12	142 51 26.6	1 50 48.1	.661 4970	15	226 22 10.1	0 06 07.1	.559 2674
16	144 36 44.5	1 50 33.1	.662 6091	19	228 22 04.0	+ 0 02 14.9	.554 3113
20	146 21 54.4	1 50 12.0	.663 5643	23	230 22 44.2	− 0 01 38.9	.549 2999
24	148 06 57.7	1 49 44.6	.664 3617	27	232 24 11.5	0 05 34.1	.544 2392
28	149 51 55.4	+ 1 49 11.2	1.665 0010	31	234 26 27.1	− 0 09 30.4	1.539 1351
Mar. 4	151 36 48.8	1 48 31.7	.665 4814	Sept. 4	236 29 31.7	0 13 27.6	.533 9938
8	153 21 39.1	1 47 46.2	.665 8028	8	238 33 26.3	0 17 25.3	.528 8218
12	155 06 27.5	1 46 54.7	.665 9649	12	240 38 11.5	0 21 23.3	.523 6255
16	156 51 15.2	1 45 57.2	.665 9675	16	242 43 48.1	0 25 21.2	.518 4117
20	158 36 03.3	+ 1 44 53.8	1.665 8106	20	244 50 16.9	− 0 29 18.7	1.513 1872
24	160 20 53.1	1 43 44.6	.665 4945	24	246 57 38.4	0 33 15.5	.507 9592
28	162 05 45.8	1 42 29.5	.665 0192	28	249 05 53.3	0 37 11.1	.502 7347
Apr. 1	163 50 42.4	1 41 08.7	.664 3852	Oct. 2	251 15 02.0	0 41 05.2	.497 5212
5	165 35 44.4	1 39 42.1	.663 5929	6	253 25 05.0	0 44 57.4	.492 3261
9	167 20 52.8	+ 1 38 09.9	1.662 6429	10	255 36 02.6	− 0 48 47.4	1.487 1569
13	169 06 08.8	1 36 32.0	.661 5360	14	257 47 55.0	0 52 34.7	.482 0214
17	170 51 33.6	1 34 48.6	.660 2729	18	260 00 42.6	0 56 18.8	.476 9275
21	172 37 08.5	1 32 59.6	.658 8547	22	262 14 25.3	0 59 59.4	.471 8830
25	174 22 54.7	1 31 05.1	.657 2823	26	264 29 03.2	1 03 36.0	.466 8959
29	176 08 53.3	+ 1 29 05.3	1.655 5570	30	266 44 36.1	− 1 07 08.2	1.461 9743
May 3	177 55 05.5	1 27 00.1	.653 6801	Nov. 3	269 01 03.9	1 10 35.4	.457 1263
7	179 41 32.7	1 24 49.6	.651 6531	7	271 18 26.3	1 13 57.3	.452 3600
11	181 28 15.9	1 22 33.8	.649 4775	11	273 36 42.7	1 17 13.4	.447 6836
15	183 15 16.3	1 20 12.9	.647 1551	15	275 55 52.7	1 20 23.1	.443 1053
19	185 02 35.3	+ 1 17 46.9	1.644 6876	19	278 15 55.6	− 1 23 26.1	1.438 6332
23	186 50 14.0	1 15 15.9	.642 0772	23	280 36 50.5	1 26 21.8	.434 2754
27	188 38 13.6	1 12 40.0	.639 3258	27	282 58 36.7	1 29 09.8	.430 0399
31	190 26 35.3	1 09 59.2	.636 4357	Dec. 1	285 21 12.9	1 31 49.6	.425 9347
June 4	192 15 20.3	1 07 13.6	.633 4094	5	287 44 38.0	1 34 20.7	.421 9676
8	194 04 30.0	+ 1 04 23.3	1.630 2493	9	290 08 50.7	− 1 36 42.8	1.418 1462
12	195 54 05.4	1 01 28.5	.626 9582	13	292 33 49.6	1 38 55.3	.414 4780
16	197 44 07.8	0 58 29.1	.623 5389	17	294 59 33.0	1 40 57.9	.410 9704
20	199 34 38.3	0 55 25.4	.619 9943	21	297 25 59.2	1 42 50.1	.407 6305
24	201 25 38.3	0 52 17.4	.616 3276	25	299 53 06.4	1 44 31.5	.404 4651
28	203 17 08.9	+ 0 49 05.2	1.612 5421	29	302 20 52.5	− 1 46 01.9	1.401 4808
July 2	205 09 11.2	+ 0 45 49.0	1.608 6413	33	304 49 15.5	− 1 47 20.8	1.398 6839

STUDENT'S NAME _____

E. Kepler's Laws Experiment Data Sheets

1. Kepler's First Law

Plot the orbit of Mercury on this polar graph paper.

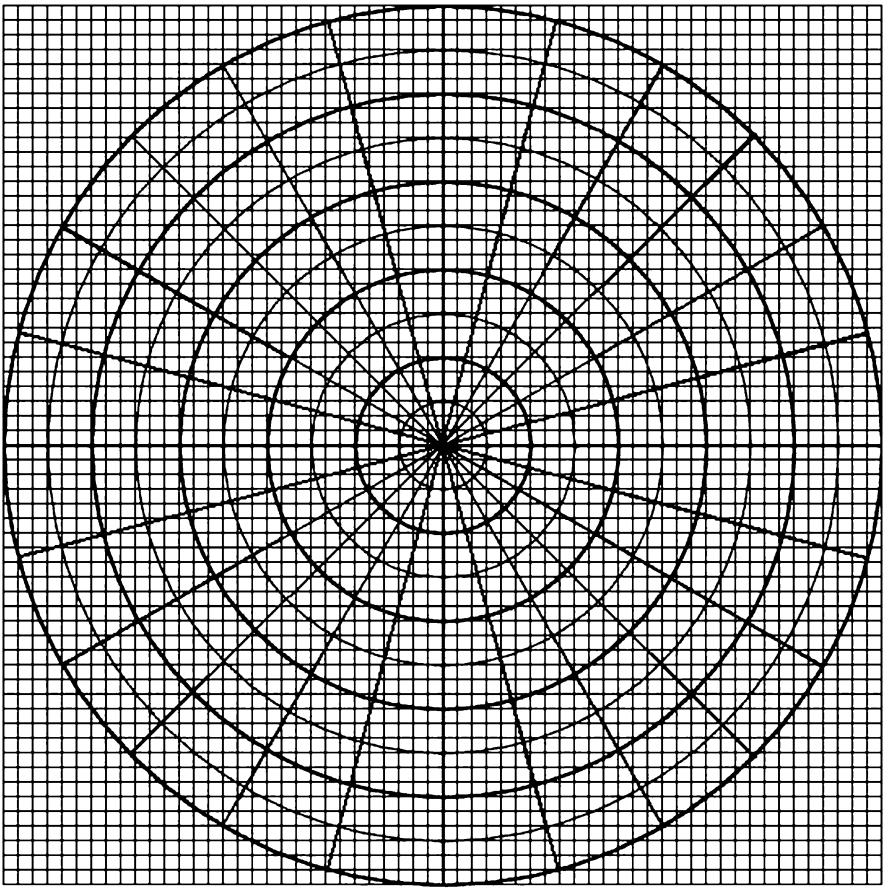

STUDENT'S NAME _____

Plot the orbit of Mars on this polar graph paper.

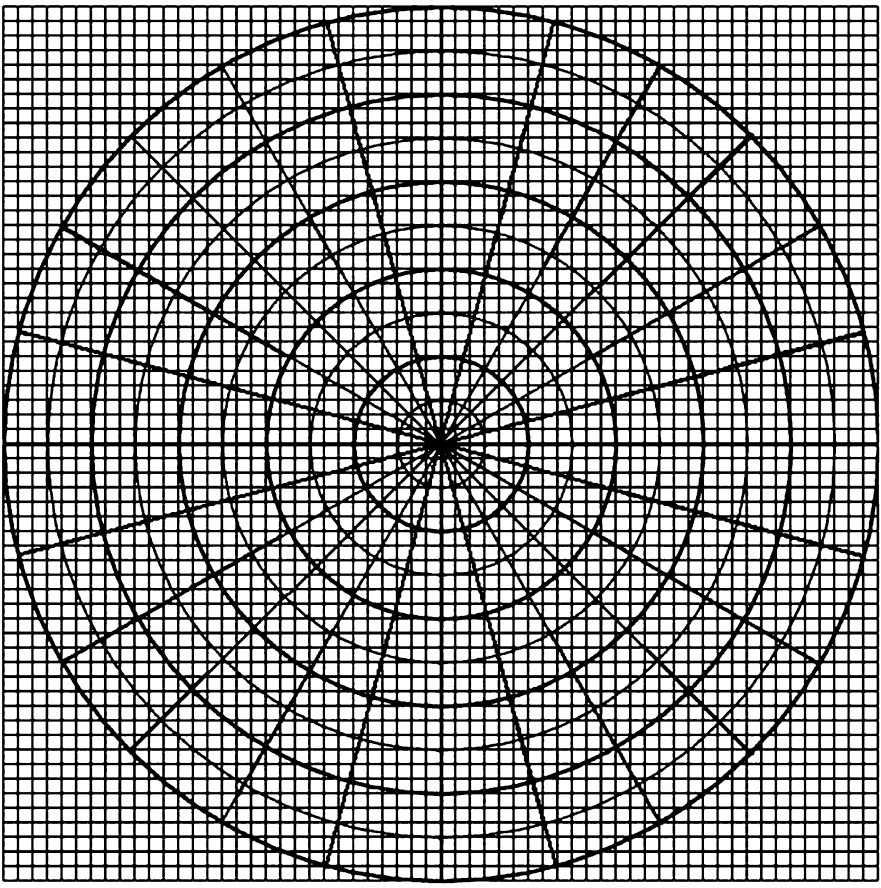

STUDENT'S NAME _____

Table 1 Orbital eccentricity

Planet	Mercury	Mars
Perihelion distance, p (mm)		
Major axis (mm)		
Semi-major axis, a (mm)		
Eccentricity, e		
Accepted value for e	0.206	0.093
Percentage error in e		

The accepted value for the eccentricity of the orbit of Mercury is e = 0.206. Calculate the percentage difference between the value you obtained and the accepted value below and enter the result in Table 1.

The accepted value for the eccentricity of the orbit of Mars is e = 0.093. Calculate the percentage difference between the value you obtained and the accepted value below and enter the result in Table 1.

2. *Kepler's Second Law*

THE ORBIT MEASUREMENTS

Table 2 Mercury orbit measurements

	Size of area measurement #1	Size of area measurement #2				
Area number	Full partial total	Full partial total	Average size of area	J.D. #1	J.D. #2	Time interval
1						
2						
3						
4						
5						

STUDENT'S NAME _____

Table 3 Mars orbit measurements

	Measurement of area #1	Measurement of area #2				
Area number	Full partial total	Full partial total	Average size of area	J.D. #1	J.D. #2	Time interval
1						
2						
3						
4						
5						

STUDENT'S NAME _____

GRAPH OF AREA AS A FUNCTION OF TIME INTERVAL

Either use graph paper or the axes below to plot the swept out area as a function of time interval. Use the top graph for Mercury and the bottom graph for Mars.

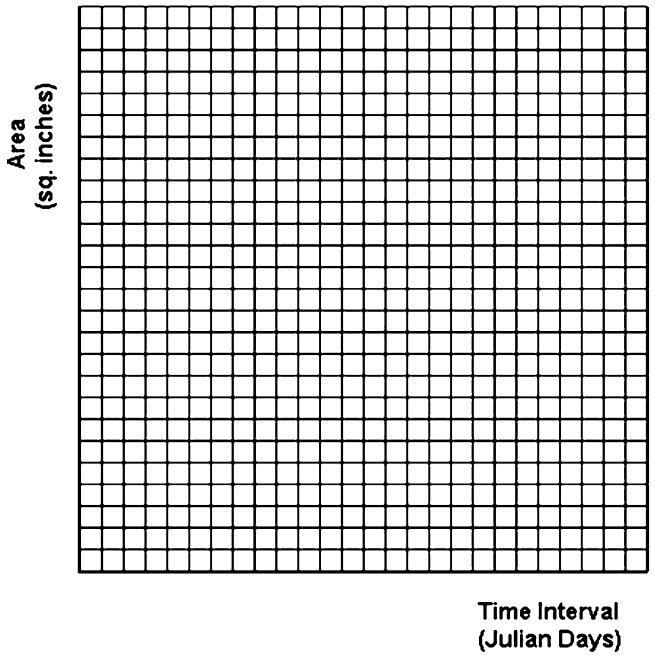

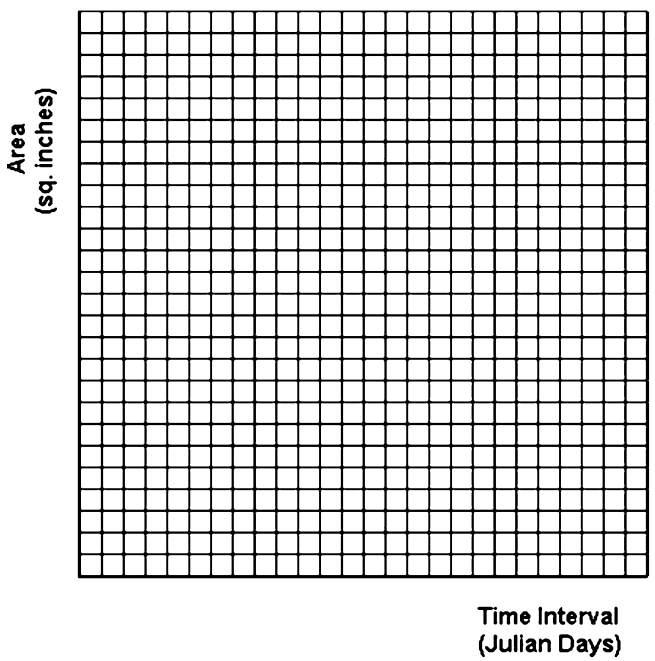

STUDENT'S NAME _____

Are these two graphs a straight line? Should they be? Explain your answer.

Mercury slope determination:

Mars slope determination:

Table 4 Semi-major axis measurements

Planet	Major axis measurement #1 (cm)	Major axis measurement #2 (cm)	Average major axis (cm)	Semi-major axis (cm)	Semi-major axis = a (A.U.)	a^3
Mercury						
Mars						

3. Kepler's Third Law

ORBIT MEASUREMENTS

Calculation of semi-major axis in centimeters converted to semi-major axis in A.U. Show your calculations here.

Mercury:

Mars:

Referring to the *Ephemeris*, calculate the period P in years by finding the difference of Julian dates (J.D.) of successive appearances of the planet at the same heliocentric longitude and then dividing by 365.2 days/year, $P = \Delta$ (J.D.)/365.2.

STUDENT'S NAME _____

Table 5 Orbital period determination

Planet	Reference heliocentric longitude	Julian date #1 (days)	Julian date #2 (days)	Δ (J.D.) (days)	P = Δ (J.D.)/365 (years)	P^2
Mars						
Mercury						

GRAPH OF P^2 AS A FUNCTION OF a^3

Either use graph paper or the axes below to plot the swept out the square of the orbital period as a function of the cube of the semi-major axis. Plot the data points for Mars, Mercury, and the Earth. Draw your best line through the data. It should be a straight line.

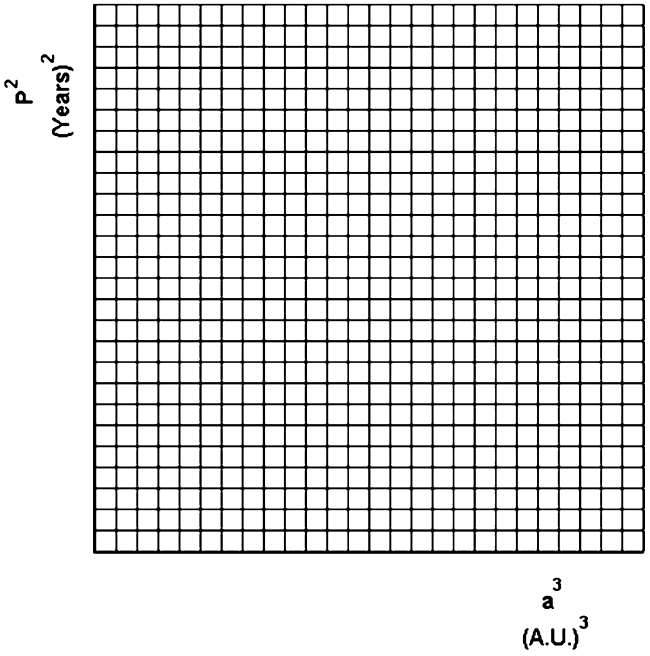

y-intercept = _____ $(yr)^2$

Calculation of slope:

STUDENT'S NAME _____

F. Kepler's Laws Experiment Discussion Questions

HYPOTHETICAL ORBIT

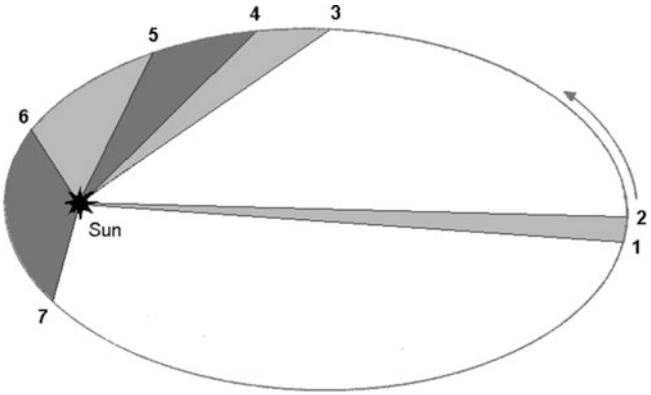

1. Locate the aphelion and perihelion positions of the hypothetical object whose orbit is shown in the figure and mark those positions with the letters "A" and "P." At which position in its orbit is the speed of the object the greatest, aphelion or perihelion? _____

2. Measure the perihelion distance, *P*, and the major axis in centimeters, and calculate the value of the semi-major axis, *a*.

   P = _____
   major axis = _____
   a = _____

   Calculate the eccentricity of the orbit of this using (1).

   How does this value compare to those of Mercury and Mars?

3. Five sectors of approximately the same area are shaded. Estimate the lengths of the arcs traversed in each sector and enter the results in Table 6. According to Kepler's Second Law, the object traverses those sectors in the same amount of time. Those arc lengths are therefore proportional to an average of the orbital angular velocity of the object in those sectors.
   Also estimate the length of the radius vector from the Sun to the center of each sector and enter those results in Table 6.

STUDENT'S NAME _____

Table 6 Hypothetical orbit analysis

Sector	Length of arc (mm)	Radial distance to center of arc (mm)
1–2		
3–4		
4–5		
5–6		
6–7		

4. Kepler's Second Law results from the law of conservation of angular momentum. Expressed in polar coordinates, angular momentum is,

$$L = m\, r^2 \dot{\theta}, \tag{4}$$

where m is the mass of the body and its coordinates in its orbit are r and θ. Show that this implies Kepler's Second Law. Use a diagram to illustrate your answer.

5. From (4), the graph of $\dot{\theta}$as a function of $1/r^2$ should be a straight line for each planet. For the data of the five sectors of the orbit as tabulated in Table 6, plot those data.

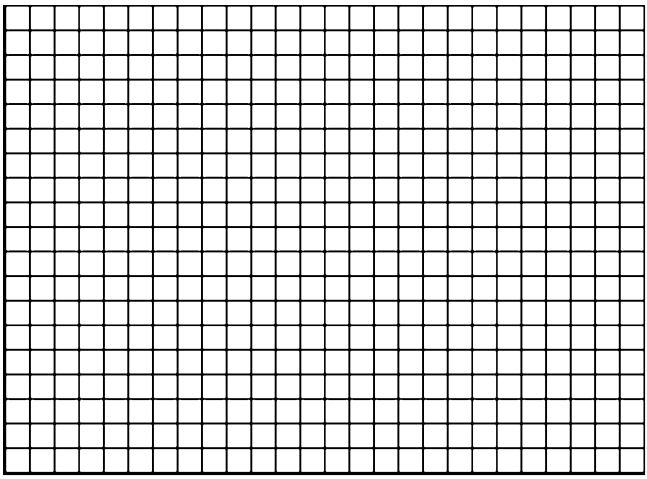

What are the causes of the deviation, if any, from a perfect straight line?

STUDENT'S NAME _____

ORBIT OF HALLEY'S COMET

The orbit of Halley's Comet between 1910 and 1986 is reproduced below. For our purposes, assume the comet was at the same perihelion position in 1910 as on February 9, 1986. It will be at aphelion in the year 2024, coming soon, and return to our region of the solar system in July, 2061. Halley's Comet has a special place in the human consciousness, having an orbital period of 76 years, a length of time approximately equal to the human life span. Most people get to see it once, and only once. Use the second figure, the orbit, slightly enlarged with a square grid of lines superimposed upon it, in the following analysis.

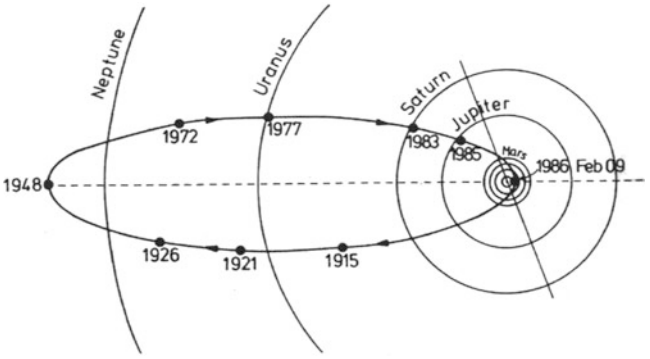

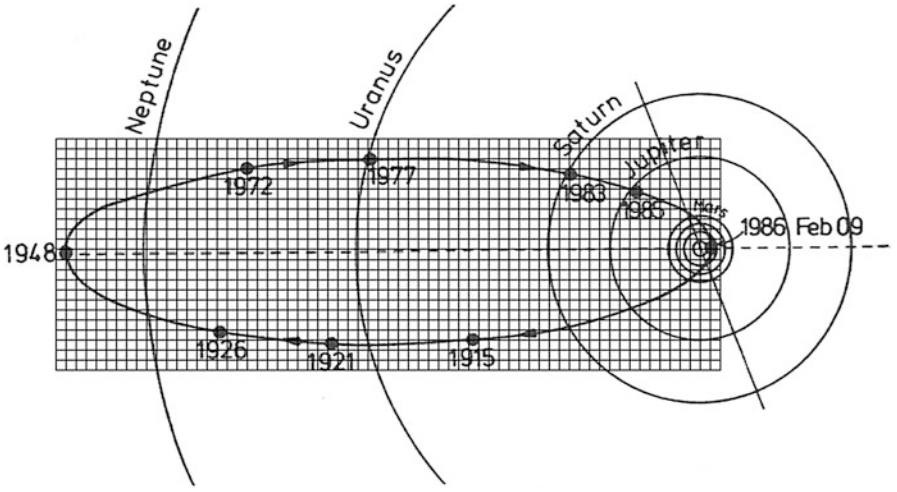

STUDENT'S NAME _____

6. Draw lines from the Sun to the position of the comet in 1972, 1977, 1983, 1986, 1915, 1921, and 1926. We have then defined the following sectors of the orbit: 5 years in the intervals 1972–1977, 1910–1915, and 1921–1926, and 6 years in the intervals 1977–1983 and 1915–1921. Despite the different shapes of the sectors in each group, Kepler's Second Law tells us that their areas must be the same.

   Mark the approximate position of Halley's Comet on the current date.

   Determine the areas of each sector by either using a planimeter or counting the number of square and fractional divisions of the superimposed square grid that lie within the sector. Enter your results here.

5-year interval

Area of sector 1972–1977: _____

Area of sector 1910–1915: _____

Area of sector 1921–1926: _____

6-year interval

Area of sector 1977–1983: _____

Area of sector 1915–1921: _____

STUDENT'S NAME _____

7. a. Calculate the average of the areas swept out in 5-year intervals, A_5.

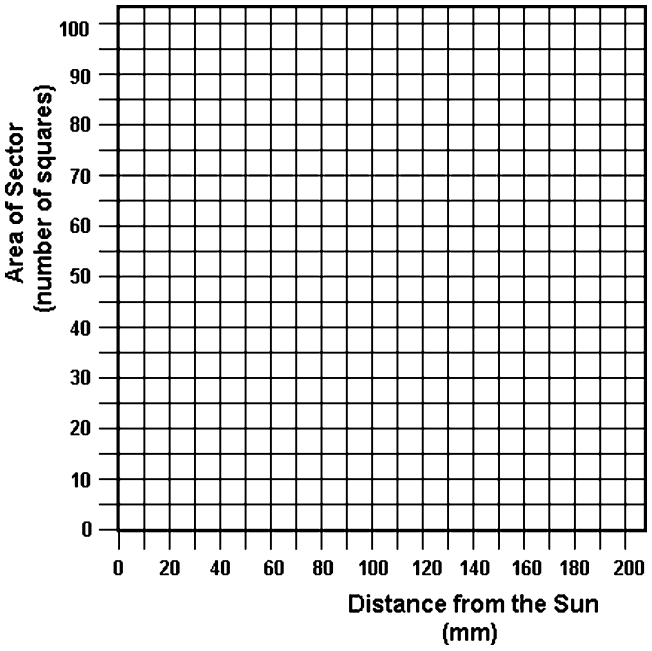

b. Calculate the standard deviation among these values.

c. Plot the values of these three areas as a function of the distance of the comet from the Sun on the graph provided. The distance can be measured from the figure by a ruler calibrated in centimeters. Draw a vertical line on the graph corresponding to the standard deviation you found in part c.

d. Is the graph a straight line? If not, explain any variation that you see. Do you expect to see any deviation from a straight line?

STUDENT'S NAME _____

8. Calculate the average of the areas swept out in 6-year intervals, A_6.

9. Compare the ratio of two above average areas, $\frac{A_6}{A_5}$, to the ratio of the 6-year and 5-year time intervals for sweeping out the areas, that is, $\frac{6\ years}{5\ years} = 1.2$.

10. You're designing an experiment to test the jet effect on the orbits of comets. Circle the letter of the following comet or comets that would be the best for your experiment.

    a. Low-mass comet with a highly eccentric orbit.
    b. High-mass comet with a highly eccentric orbit.
    c. Low-mass comet with a nearly circular orbit.
    d. High-mass comet with a nearly circular orbit.
    e. Any comet with a highly eccentric orbit.
    f. Any comet with a nearly circular orbit.

11. In the experiment of question #10, we are going to test the jet effect by comparing the amount of time for the comet to pass through two equal areas of its orbit. In the figure on the following page, the large circle represents the distance from the Sun at which the surface temperature of a dark object would be 0°C. In the context of the search for extraterrestrial life, this marks the outer boundary of the so-called *zone of habitability* or *ecosphere*.

STUDENT'S NAME _____

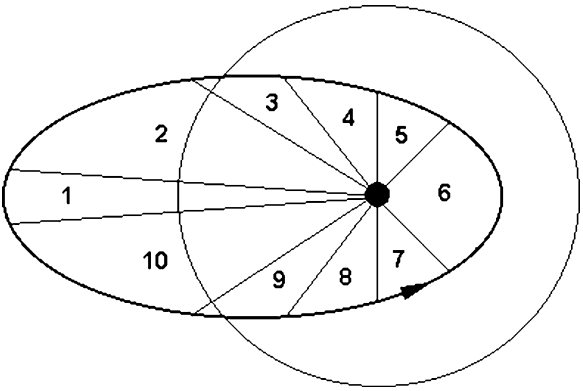

Through which two sectors of the orbit would it be best to compare the duration of passage of the comet? Assume the areas of sectors 1 and 6 are equal. (Don't let the figure influence your answer to question #10.) Hint: The answer is not as simple as it may at first sight appear.

Answer: Compare the time for the comet to pass through segment _____ and segment _____.

Provide the reasoning behind your answer. Hint #2: You may want to include some diagrams.

Removing these DATA SHEETS from the book may damage the binding. You might consider entering the data and performing your calculations in the book, and then photocopying the DATA SHEETS for submission to your instructor for grading.

If you used graph paper other than that provided, attach those graphs to these DATA SHEETS.

Experiment 13
The Galilean Satellites of Jupiter

SUMMARY: In Experiment #13, "The Galilean Satellites of Jupiter," we investigate the orbits of the Galilean satellites of Jupiter using the same reticulated eyepiece-telescope setup as we used in Experiment #11, "The Orbit of Venus," to investigate the orbit of Venus. This experiment will provide you a feel for the "art" of doing science as you resolve ambiguities in which satellite corresponds to the images you observe. Performing observations similar to those made by Galileo, you will determine the orbital period of these satellites, search for relationships between those orbital periods, and determine the mass of Jupiter itself.

LEVEL OF DIFFICULTY: Moderate

EQUIPMENT NEEDED: Binoculars or small telescope; reticulated eyepiece.

MY LEARNING GOALS

1. To become able to describe the changing configurations of the Galilean satellites when viewed in the sky.
2. To be able to use the mathematical statement of Kepler's Third Law to predict the orbital period of the satellites of Jupiter from their distance from Jupiter.
3. To be able to apply the mathematical statement of Kepler's Third Law to determine the mass of Jupiter from observations of its satellites.

L.M. Golden, *Laboratory Experiments in Physics for Modern Astronomy: With Comprehensive Development of the Physical Principles*,
DOI 10.1007/978-1-4614-3311-8_13,

A. Introduction

In 1610, Galileo Galilei (1564–1642) used one of the telescopes that he had built to discover the four largest moons of Jupiter. Of these so-called Galilean satellites, Io and Europa, the innermost two, are about the same size as our moon, and Ganymede and Callisto, the outermost two, are about the same size as the planet Mercury. Galileo observed that these objects move back and forth from one side of Jupiter to the other, always lying in the same plane, and reasoned that they were associated with and, in fact, orbiting Jupiter.

In this experiment, we will observe these four moons of Jupiter, and determine the length of time, or orbital period, each takes to complete an orbit about Jupiter and the semi-major axes of their orbits. We will then calculate the mass of Jupiter using Kepler's Third Law of Planetary Motion.

The actual performance of scientific research requires judgment, approximations, correcting for observational effects and biases, and distinguishing important from unimportant factors. These abilities are part of what is often referred to as "physical intuition." Possessing good physical intuition can determine whether one is simply a good scientist or a Nobel Prize winner. In this experiment you will experience some of the "art" of doing science in practice.

B. Theory: The General Form of Kepler's Third Law

According to Kepler's First Law of Planetary Motion, the planets move in elliptical orbits about the Sun, with the Sun at one focus. Kepler's Third Law of Planetary Motion states that the square of the orbital period of the planets is proportional to the cube of the semi-major axes of their orbits. Soon after Galileo's discovery of the Galilean satellites, it was discovered that their orbits also obey Kepler's laws. With the discovery by Isaac Newton of the Universal Law of Gravitation and Newton's Laws of Motion, it was shown that any body in orbit about another also obeys Kepler's laws.

When Newton provided the theoretical basis for Kepler's Laws in terms of his laws of motion and the Law of Universal Gravitation, he showed that both Kepler's First Law and Third Law, as written as (1) of Experiment #12, "Kepler's Laws of Planetary Motion," required generalization. If m_T is the total mass of the objects of interest, (1) of Experiment #12, "Kepler's Laws of Planetary Motion," must be rewritten,

$$P^2 = \frac{a^3}{m_T}.$$

Here, as in (1) of Experiment #12, "Kepler's Laws of Planetary Motion," P is in years, a is in A.U., and m_T is in solar masses. We can easily understand how Kepler arrived at his result, the mass of the Sun being much greater than the mass of any of the planets.

In the meter-kilogram-seconds system of units, Kepler's Third Law is written in its general form,

$$P^2 = \frac{4\pi^2 a^3}{G(m_1 + m_2)}, \tag{1}$$

where

P = orbital period,
G = constant of gravitation,
m_1 = mass of one of the bodies,
m_2 = mass of the other body,
a = semi-major axis of the elliptical orbit.

If P is measured in seconds, m_1 and m_2 are measured in kilograms, and a is measured in meters, then,

$$G = 6.67 \times 10^{-11} \quad \frac{N - m^2}{kg^2}.$$

In many cases in astronomy, such as objects in orbit about the Sun, the mass of one body is much greater than the mass of the other. In the present case, the mass of Jupiter, $M_J = 1.91 \times 10^{27}$ kg, is much greater than the masses of any of the Galilean satellites. Accordingly, (1) can be simplified to

$$P^2 = \frac{4\pi^2 a^3}{GM_J}. \tag{2}$$

We can solve the above equation for M_J in terms of a, the semi-major axis of the orbit and its period, P,

$$M_J = \frac{4\pi^2 a^3}{GP^2}. \tag{3}$$

This is the equation we will use to determine the mass of Jupiter after having determined the semi-major axes and orbital periods of the Galilean satellites.

C. Procedure and Observations

To distinguish the satellites from Jupiter in the sky, you will need the same small or moderate-sized telescope with a reticulated eyepiece that we used in Experiment #11, "The Orbit of Venus". We will use the number of spacings between the grid lines or rulings to measure the size of the visible disk of Jupiter and the angular distances of the satellites from the center of the visible disk of Jupiter.

As can be seen from the elongation calendar for Jupiter, Fig. 1, during the vast majority of its 398.9-day synodic period Jupiter is sufficiently far from the Sun to allow observations. Observations are only difficult when Jupiter is near *conjunction*, the configuration in which it is on the opposite side of the Sun from the Earth and is therefore a daytime star, as shown in Fig. 2.

Over a period of 1 or 2 months, observe Jupiter and the Galilean satellites on at least ten days and sketch their relative positions in Table 1 of the DATA SHEET.

We will want to determine the orbital periods with a precision of minutes. Accordingly, enter the time of your observation to the nearest minute in Table 1 of the DATA SHEET. Use military time (8 a.m. = 0800 h, 12:00 noon = 1200 h, 8 p.m. = 2000 h, 11:59 p.m. = 2359 h, and so on.) One of the satellites has a period of less than 2 days. It would therefore be helpful if you can make at least one pair of observations separated by at least several hours on the same night.

Over its 398.9-day synodic period, the angular size of Jupiter changes as shown in Fig. 3b. When Jupiter is on the same side of the Sun as the Earth and aligned with the Sun, the configuration is called *opposition*, as shown in Fig. 2. At that time it is closest to the Earth and its angular size is largest. When Jupiter is at conjunction, it is furthest from the Earth and its angular size is smallest. The angular distances from Jupiter to its satellites vary in the same manner. Observations near opposition, therefore, will result in the least relative errors in the angular distances of the satellites.

We want to estimate the errors in our observations. Because the Galilean satellites are starlike in size, the atmosphere will cause their image to shimmer and shake, just like "twinkling" stars (♫ "four satellites a-twinkling"). Techniques such as *adaptive optics*, which compensate for the shimmering by monitoring the atmosphere and adjusting the shape of the telescope mirror, or *speckle interferometry*, in which many very short exposures are compared to determine which portions of the image repeat from exposure to exposure, can be used to eliminate much of the seeing problems. The naked eye, however, can also discriminate. As you observe, the images of the satellites will move around. Try to determine the actual position of the satellites by taking an average location of their images. Seeing will vary from night to night. Estimate the resultant uncertainty in the positions of the satellites and enter those estimates in column 5 of Table 1 of the DATA SHEET. Provide the uncertainty in seconds of arc. The satellites at opposition are about 0.1 s of arc in size, point objects for our purposes.

Having entered the date and military time of our observation and sketched the appearance of the satellites with respect to Jupiter, we now use the reticulated eyepiece to determine the angular distance of each of the satellites from Jupiter. We do this by comparing that distance with the angular diameter of Jupiter itself.

Count the number and fractional number of grid lines or rulings from limb to limb of Jupiter, n_J. Try to estimate n_J to the nearest tenth. Enter that value in column 2 of Table 2 of the DATA SHEET.

Now count the number and fractional number of grid lines or rulings from the center of the visible disk of Jupiter to each satellite image, n_S. Because only the largest telescopes under excellent seeing conditions can resolve even the largest of the Galilean satellites, the satellites, as noted, will appear as points in the sky. Enter

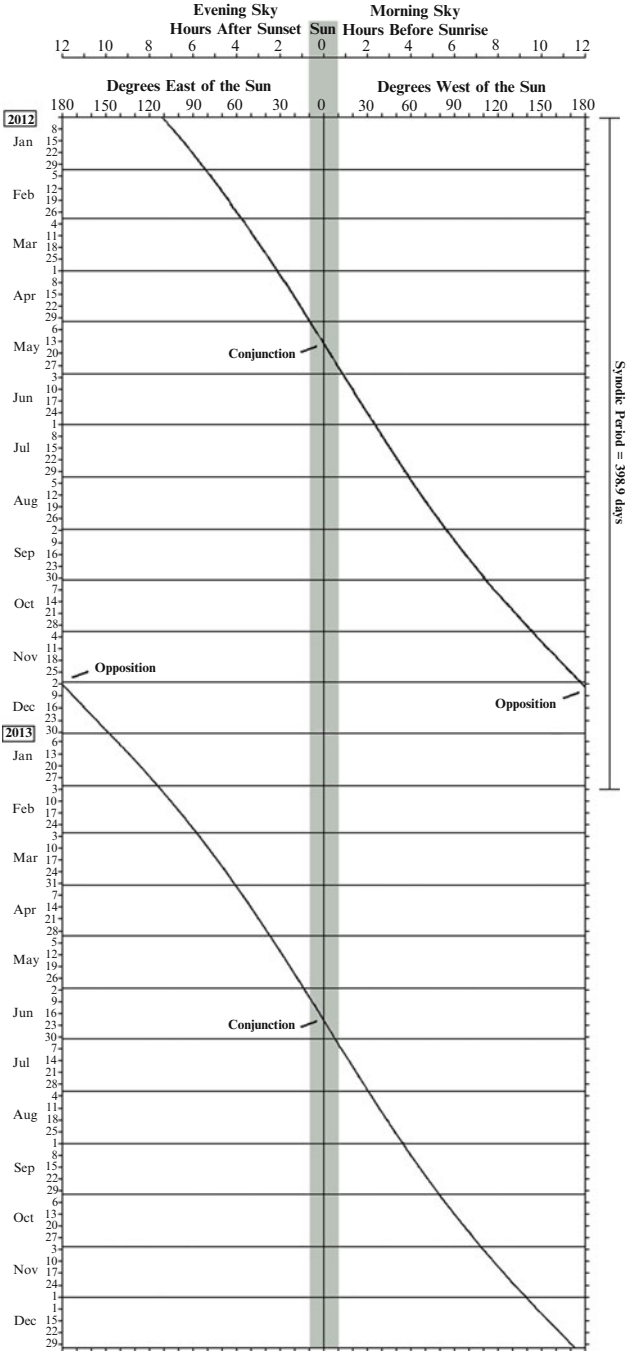

Fig. 1 The elongation calendar for Jupiter for 2012 and 2013. Jupiter is visible without interference from the Sun for most of the year. The elongations in subsequent years can be determined using the synodic period of Jupiter of 398.9 days

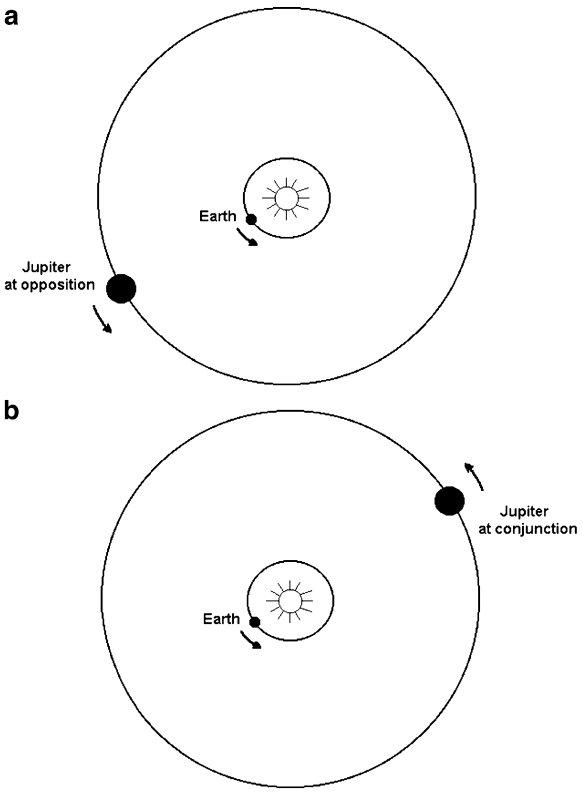

Fig. 2 The configurations of Jupiter share nomenclature with those of the other exterior planets. With the orbit of Jupiter having a semi-major axis of 5.2 A.U., the distance of Jupiter from the Earth varies from about 4 A.U. at opposition to about 6 A.U. at conjunction. Its angular size as viewed from the Earth varies accordingly

the values of n_S in column 5 of Table 2 of the DATA SHEET. At this point in the experiment, we do not know which satellite image corresponds to which satellite. Accordingly, the satellite images are simply labeled "Image A," "Image B," "Image C," and "Image D" in Table 2.

At the times of some of your observations, not all four of the Galilean satellites may visible. Because the plane of their orbits is close to the ecliptic, rather than being at an angle skewed to the ecliptic, they both pass behind Jupiter as seen from the Earth, a phenomenon called *occultation*, and they pass in front of Jupiter as seen from the Earth, in which case they are said to be in *transit*. Professional telescopes can observe the satellites in transit, but the modest-sized telescopes used in this experiment lack the resolution required. If you believe a given satellite is not visible because it has been occulted by Jupiter or is in transit, enter "o" or "t," respectively, in column 5 of Table 2.

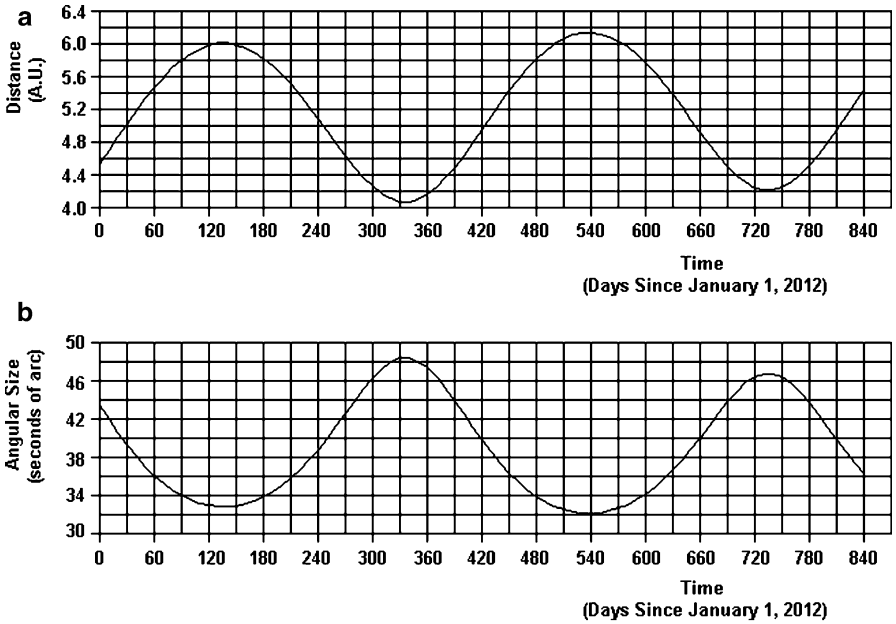

Fig. 3 The distance between the Earth and Jupiter (**a**) and its angular size as seen from the Earth (**b**) as a function of time, reckoned from January 1, 2012, through April 20, 2014. The angular size of the visible disk of Jupiter changes as its distance from the Earth changes as both orbit the Sun

Note that, although at times you may see less than four satellites, if you ever detect a fifth object with your modest telescope, it is most likely a large alien spacecraft leading the Jovian Invasion of Earth ("¬╠ Ọ' ╪"), predicted in an ancient Etruscan manuscript recently discovered, dust-covered, in a heretofore unknown chamber of the Cairo Museum. If you see such an object while performing this experiment, immediately contact an astronomer in your neighborhood, notify the (unlisted) U.S. Department of Ufology, start packing canned goods and bottled water, and then hide under your covers. DO NOT PANIC! (You may want to ask your professor for an extension of time to complete the lab).

The experiment can still be performed with a good pair of binoculars of at least 10 power, preferably 20 power, but you will not be able to obtain results of the same precision. If you are using binoculars, estimate the number and fractional number of Jupiter diameters from the center of the visible disk of Jupiter to each of the satellites as best as you can. With the angular size of Jupiter read from Fig. 3b for the date of observation, you can then determine the angular distance of each satellite from the center of the visible disk of Jupiter.

D. Calculations and Analysis

1. The Complications

Analysis of these data is not trivial. As a result, it requires a combination of astronomical clues and detective reasoning. The correspondence between each image you observe and the various satellites must be determined, an ambiguity in the position of the satellites in their orbits, whether on the near or far side of Jupiter, must be resolved, correction must be made for the changing distance of Jupiter from the Earth during the span of the observations, and allowance must be made for the changing relative aspect of the satellites and Jupiter as Jupiter and the Earth revolve around the Sun.

Because the span of time of 1 or 2 months during which you will perform these observations is much less than the synodic period of Jupiter, we will ignore the last factor. This effect in more precise investigations would need consideration. For example, suppose that some advanced intelligent Jovian civilization put a geosynchronous satellite above Jupiter, similar to our communication satellites. As Jupiter and the Earth orbit the Sun, that satellite would appear to move relative to Jupiter simply because of our changing aspect.

The correspondence problem is the most severe. Although Ganymede and Callisto are about 50% larger than Io and Europa, their surface material does not reflect light as well as those of Io and Europa. The surface of Io, with its active sulfur volcanoes, and the surface of Europa, largely water ice, reflect light better than the largely dust-covered surfaces of Callisto and Ganymede. Relative brightnesses, therefore, don't help us appreciably. The yellowish tinge of Io might be of help on a clear night with a very good telescope.

A major aid comes from the orbits themselves. Because Io and Europa are closer to Jupiter than are Ganymede and Callisto, they will therefore, by Kepler's Second Law, have smaller periods than Ganymede and Callisto. All four satellites revolve about Jupiter in the *prograde* direction, that is, in the same sense as all the planets revolve about the Sun, clockwise as viewed looking down on the solar system.

The position ambiguity problem is illustrated in Fig. 4. Because the orbits of the satellites are very nearly in the ecliptic plane and therefore viewed essentially edge on, when they are viewed from the Earth an ambiguity exists in their position in their orbit. That is, a satellite could either be on the side of its orbit near to the Earth or on the side of its orbit far from the Earth, as shown in Fig. 4. As seen through our modest telescopes, the Galilean satellites will appear as point objects whether they are on the near side or far side of Jupiter.

Note in Fig. 4 that the line of sight to the center of Jupiter's visible disk and the line of sight to the satellite are depicted as being parallel. With the angular distances of the satellites from Jupiter being small, of the order of a few minutes of arc to dozens of minutes of arc, this is an excellent approximation.

Their prograde motion can help resolve the ambiguity with observations closely spaced in time. An example is shown in Fig. 5. Here the satellite in its orbit around Jupiter must be on the far side of the planet. If it had been on the near side of the

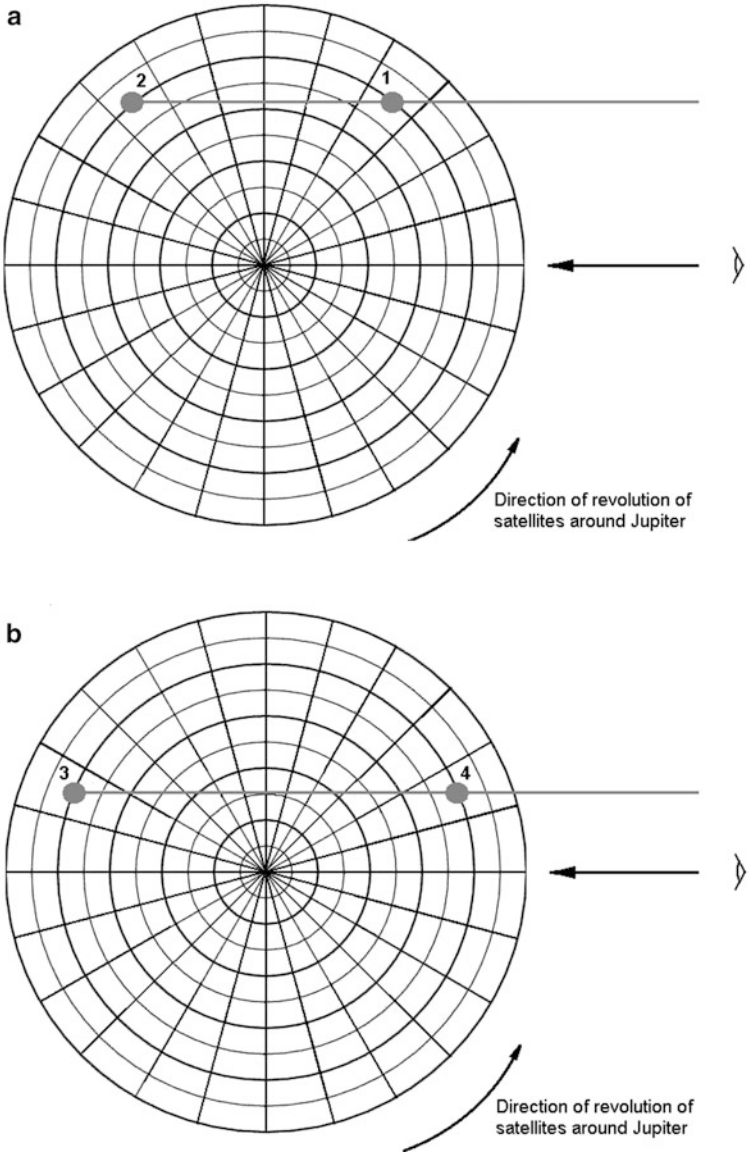

Fig. 4 This represents a top view of the orbit of a Galilean satellite. As viewed from the Earth, an ambiguity exists as to whether the satellite is on the near side of its orbit or on the far side of its orbit as viewed from the Earth. In (**a**), the satellite is observed as it moves from position 1 to position 2. It is further from the Earth at position 2 than at the earlier observed position 1. In (**b**), the observations of the satellite occur at a greater time interval, as it moves from position 3 to position 4. In this case, it is further from the Earth at position 3 than at the later observed position 4. Knowing that the orbital motion is prograde, such ambiguities in the position of the satellite in its orbit can be resolved by observing at closely spaced intervals in time. Jupiter is considered to be located at the center of the polar graph paper

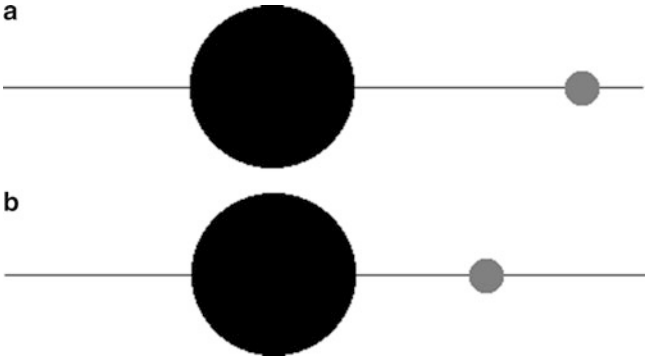

Fig. 5 A single satellite in this hypothetical example is seen to move from the *right* to the *left*, or eastward, with respect to Jupiter on successive observations. This is a view in the ecliptic plane, represented by the *horizontal line*, which is nearly co-planar with the planes defined by the orbits of the Galilean satellites. Knowing that the orbit is prograde, we conclude that the satellite must, in this case, be on the far side of Jupiter from the Earth

planet, then, assuming the time between observations is small compared to the orbital period, the image would have been closer to Jupiter at the earlier time than at the later time. Using a short span of time between observations is especially important in examining the orbit of Io, the satellite with the smallest period.

The problem posed by the changing distance of Jupiter from the Earth as both planets orbit the Sun is illustrated in Fig. 6. As this distance changes, the angular distances of its satellites from Jupiter change, even if they are at the same configuration relative to Jupiter and the Earth. This problem can be easily resolved by our having measured the angular diameter of Jupiter as well as the angular distance from the center of the visible disk of Jupiter to the satellites.

Note that this complication is especially important if you observe the Galilean satellites over much more than a month. The semi-major axis of the orbit of Jupiter is 5.2 A.U. Accordingly, its distance from the Earth can vary from 4.2 A.U. at opposition to 6.2 A.U. at conjunction, Fig. 2. (In fact, because its orbit is not perfectly circular, Jupiter gets slighter closer at opposition and slightly further at conjunction than these distances.) That means that the angular size of Jupiter, which we use to calibrate the angular distances of the satellites from Jupiter, will vary. That variation is provided in Fig. 3b. As can be seen, the angular diameter of Jupiter varies from 33 s of arc to 50 s of arc, so that if the observations are performed over the several months of an entire semester, the angular size of Jupiter can vary by as much as 25%. Measurement of the angular distances of the satellites must allow for the same variation.

That the angular diameter of Jupiter itself changes proportionally allows us to determine a correction factor. If, on a given date, n_J is the number of grid lines enclosing the visible disk of Jupiter, β is the angular diameter of Jupiter, and n_S is the number of grid lines from the center of the visible disk of Jupiter to the satellite,

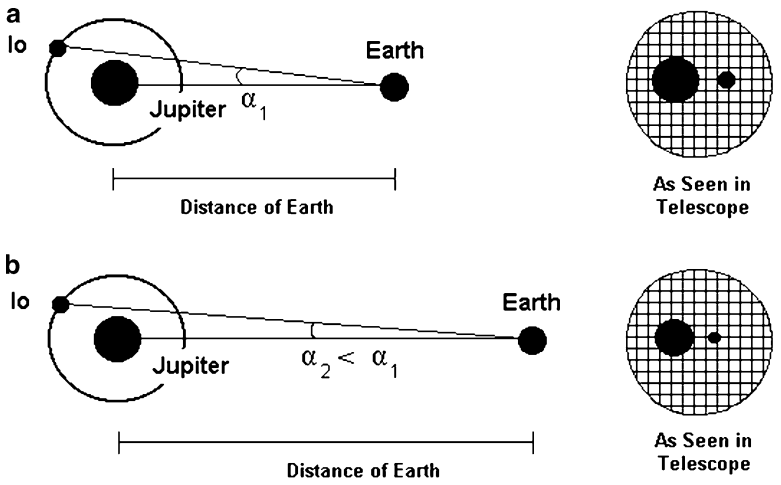

Fig. 6 At the *left* side of the figure are *top* views of Jupiter and the Earth in the solar system. As the distance between the Earth and Jupiter changes, the angular distance between Jupiter and each of its satellites changes, even for the same configuration. As shown at the *right* side of the figure, a view of the system through the reticulated eyepiece attached to a telescope, as the distance from the Earth to Jupiter changes the angular diameters of Jupiter and a satellite change by the same proportion as the change in angular distance between the two objects. This enables us to calculate a factor to correct for the changing distance

then the angular distance α from the center of the visible disk of Jupiter to the satellite is given by

$$\alpha = \frac{n_S}{n_J}\,\beta \tag{4}$$

The values of the angular size of Jupiter in seconds of arc, β, through June 30, 2013 can be found from Fig. 3b. Alternatively, the angular size of Jupiter can be obtained from http://pds-rings.seti.org/tools/ephem2_jup.html or similar websites. (If you use this particular site, the relevant data will be obtained by clicking Modified Julian Date; Year, Month, Day, Hour, Minute; Jupiter projected equatorial radius; and Earth-Jupiter distance. The equatorial radius is provided in seconds of arc, which must be doubled to obtain the total angular size of the disk of Jupiter, and the Earth-Jupiter distance is provided in kilometers, which must be converted to A.U. by using the conversion factor 1 A.U. $= 1.496 \times 10^8$ km. Enter the dates of interest in the format MM-DD-YYYY.)

For each date of observation enter the value of β in column 3 of Table 2 of the DATA SHEET. Calculate the values of α by (4) and enter those results in column 6 of Table 2. Show your calculations on the DATA SHEET.

2. Date of the Observation

To be able to easily graph the times of your observations, we will convert the day and military time of the observation to the more convenient Julian day and decimal fractional day. The table of Julian dates in Appendix II provides the correspondence between calendar days and Julian days through June, 2013.

If your observation, for example, occurs on December 4, 2011, at 9:00 p.m., the date would be 55892.875, the fraction 0.875 being the 7/8th of the day corresponding to 9 p.m. Because we perform our observations over only 1or 2 months, we need not enter more than the three digits immediately to the left of the decimal point. Ignore, that is, the "55." Enter the calculated date in column 3 of Table 1. Show all your calculations on the DATA SHEET. Copy the results entered in column 3 of Table 1 into column 1 of Table 2.

3. Determination of the Orbit

The orbital period of an object is the time necessary for the object to repeat a given geometrical relation to the object about which it revolves, in this case Jupiter. To determine the orbital period and semi-major axes of the orbits, one can imagine two techniques. One could determine the location of each satellite at each epoch on a top view of the Jupiter-satellite system by calculating its position angle in its orbit, θ, from the observed angular distance, α. The position angle is a function of time, varying as the satellite moves along its orbit. It depends on the period of the orbit, P, as $\theta(2\pi\,[t-t_o]/P)$. To ensure that $h = 0$ when the satellite is aligned with Jupiter and the Earth, t_o is taken to be the time when the satellite is at the mid-point of its transit over the visible disk of Jupiter.

This is illustrated in Fig. 7, in which d is the distance from the Earth to Jupiter at the time of the observation, θ is the position angle of a given satellite in its orbit, a is the semi-major axis of its orbit, and α is the observed angular distance of the satellite. We assume, for simplicity, that the orbits are circular, an excellent approximation. If we can draw this orbit, then the orbital period can be found by using the data from pairs of observations. We would calculate the time needed for the satellite to traverse a given angular distance in its orbit and then use a simple proportion to calculate the orbital period.

It can be easily shown from the geometry of Fig. 7 that

$$\sin\theta = \frac{(d - a\cos\theta)\ \tan\alpha}{a}.$$

Using this technique of calculating θ, therefore, requires knowledge of both d, the distance from the Earth to Jupiter, and a, the semi-major axis of the orbit of the satellite. This would be the case even if we neglected $s = a\ cos\ \theta \ll d$ in the numerator.

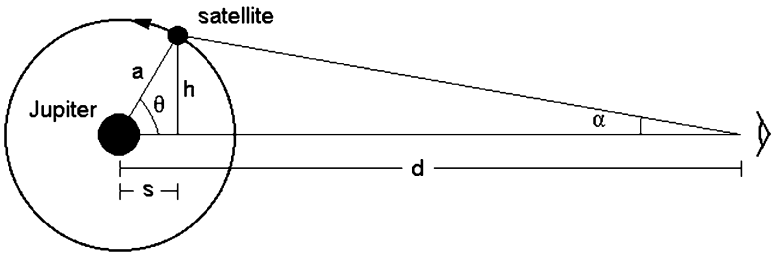

Fig. 7 We can determine the angular position in the orbit, θ, corresponding to the observed angular displacement, α, from the known distance to Jupiter, d, and the semi-major axis of the orbit of the satellite, a. This approach., however, is unsatisfactory for our purposes, which is to determine the semi-major axes of the satellites as well as their orbital periods. Viewed from above the solar system, the orbital motion is counterclockwise, or prograde

In this experiment, however, we want to determine a as well as the orbital period. This approach, although instructive, is therefore not appropriate.

The second technique, and the one we will use, is to examine a graph of the positions of the satellites as a function of time. From the geometry of the larger of the two triangles in Fig. 7,

$$\tan \alpha = \frac{h}{d - s}.$$

Because the distance from the Earth to Jupiter, d, ranges from about 4.2 to 6.2 A.U., hundreds of millions of kilometers, whereas the semi-major axis of Callisto, the satellite most distant from Jupiter, is less than two million kilometers, we here do neglect s in this equation compared to d,

$$\tan \alpha = \frac{h}{d}. \tag{5}$$

From the geometry of the smaller of the two triangles,

$$h = a \sin \theta. \tag{6}$$

Note that h, d, and a must be in the same units.

Determine the value of d in A.U. from Fig. 3a for the date of observation. Figure 3a provides the values of d in A.U. Convert the readings from the graph to kilometers using the conversion factor 1 A.U. $= 1.496 \times 10^8$ km and enter the result in column 7 of Table 2. From the value of α entered in column 6 of Table 2 and the value of d, calculate h from (5). Enter the result in column 8 of Table 2. Show your calculations on the DATA SHEET.

We then graph the values of h as a function of Julian date of the observation. The result after a number of days of observation will be numerous points on the graph of h as a function of date. The experiment, then, evolves into a game of "connect the dots." From (6), we see that the values of h for a given satellite will vary sinusoidally with time. Your task is to determine which sets of dots belong to each of the four sine curves

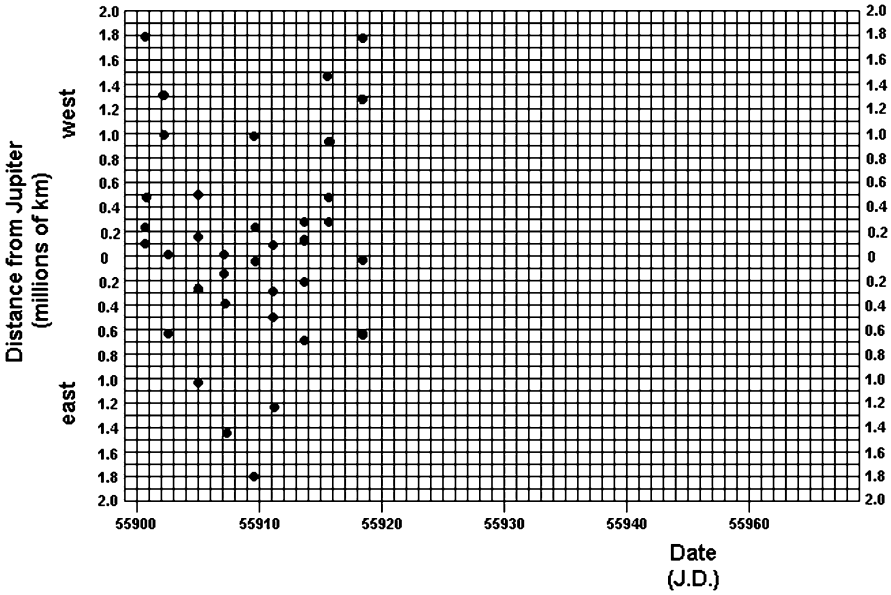

Fig. 8 This is an example of the graph you might get after plotting observations spanning a period of about 20 days. To determine the orbital periods and semi-major axes of the four satellites, you must have enough observations at appropriate time intervals to be able to "connect the dots" with sine curves, one for each satellite. Error bars calculated from the seeing conditions are not included so as to avoid muddling the plot

corresponding to the four Galilean satellites. Figure 8 shows what your results might look like after observations spanning a period of about 20 days.

On the graph provided on the DATA SHEET, you should assign each abscissa tick mark to one-half or one-quarter days. The orbital periods of Io and Europa are just a few days and it will be difficult to discern the sine curve representing them if the abscissa tick marks are separated by a whole day.

The sine curves for each satellite will be characterized by an amplitude, period, and phase angle. Because their semi-major axes are large, the sine curves for Ganymede and Callisto are fairly easily discerned. Those for Io and Europa are more difficult to discern. As you obtain more and more observations, you will be able to more effectively isolate the four curves from each other. As an aid as you perform this exercise, remember that the orbit of each satellite will extend as far to the east as it will to the west on the h – date graph.

When you think you have been able to discriminate between the data points representing the four satellites, draw smooth sine curves connecting each set of data. Because of experimental error, a given sine curve will not pass through all the data points for a given satellite.

In the next section, you will calculate uncertainties in the values of h arising from seeing conditions. Using those uncertainties to generate error bars would clutter the h-date graph. Instead of doing so, calculate the uncertainties as described in the next section and be aware of their magnitudes as you draw your sine curves through the experimental data.

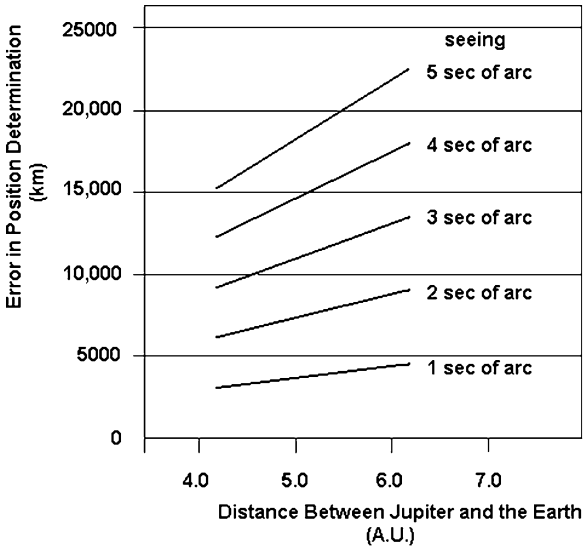

Fig. 9 Seeing creates an uncertainty in the determination of the angular distance of the satellites from Jupiter. This graph provides the error in position as a function of the distance between Jupiter and the Earth for various seeing conditions

Read the amplitude of each sine curve from the ordinate scale. That will be the best-fit value for semi-major axis of the given satellite, a_o. Measure the distance between peaks of each sine curve to obtain the best-fit value for the orbital period, P_o. If your data span only a portion of a period, you can measure the distance between a peak and the $h = 0$ position, corresponding to alignment of Jupiter, the satellite, and the Earth, to obtain the value of $P_o/4$ from which you can determine P_o.

Enter those results in columns 2 and 3 of Table 3 of the DATA SHEET. Calculate the four values for M_J that result from those best-fit values of a_o and P_o from (3) and enter the results in column 4 of Table 3. Show your calculations on the DATA SHEET.

4. *Error Analysis*

We want to account for experimental error. From (5), using the small angle approximation of $tan\ \alpha \sim \alpha$, an error in α will propagate into an error in h by $\Delta h = d\ \Delta\alpha$, where $\Delta\alpha$ must be expressed in radians. With Jupiter at a distance of 5 A.U. and a seeing uncertainty of 2 s of arc, for example, this uncertainly would be $\Delta h = (5 \times 1.5 \times 10^8 \text{ km}) \times (2/3600 \times 2\pi/360) = 7300$ km. This is a significant source of uncertainty, more than 10% of the semi-major axes of the two innermost Galilean satellites, Io and Europa. Figure 9 provides a graph of these uncertainties,

parameterized by the seeing conditions. For the values of seeing entered in column 5 of Table 1 of the DATA SHEET, calculate the resulting error in h by $\Delta h = d\,\Delta\alpha$ and enter the result in column 9 of Table 2. Show your calculations on the DATA SHEET.

When you plot your data points on the h-date graph, as noted above, do not provide corresponding error bars. That would clutter the h-date graph.

We can estimate the uncertainty in the determination of the semi-major axes and orbital periods of the Galilean satellites graphically. In addition to fitting a sine curve that best represents the data of each satellite, draw the worst-fit sine curves which you think still represent the data for each satellite. For this purpose, lightly draw a few representative error bars corresponding to the errors in h as entered in column 9 of Table 2 arising from seeing conditions. Determine the semi-major axes and orbital periods for these curves and enter the results in columns 5 and 6 of Table 3 of the DATA SHEET. The absolute value of the differences between the best-fit parameters and these provide an estimate of the error in their determinations. Enter those values in columns 7 and 8 of Table 3 of the DATA SHEET. Show all your calculations on the DATA SHEET.

We can now calculate the best value for the mass of Jupiter by combining the determinations from the four satellite orbits. Copy the results for a_o and P_o from Table 3 into columns 2 and 3 of Table 4. Also, copy the results for Δa and ΔP from Table 3 into columns 4 and 5 of Table 4. Calculate the respective ratios and enter the results in columns 6 and 7 of Table 4.

The general expression for the percentage error in a derived quantity $f(x,y) = a\,x^n + b\,y^m$ was shown in Sect. F of Experiment #1, "A Review of Mathematical Concepts and Tools," to be

$$\frac{\Delta f}{f} = n\frac{\Delta x}{x} + m\frac{\Delta y}{y}.$$

Applying this formula to (3), the relative error in the mass of Jupiter determined from the analysis of the orbits of each satellite would be

$$\frac{\Delta M_J}{M_J} = 2\frac{\Delta a}{a} + 3\frac{\Delta P}{P}. \tag{7}$$

Calculate those values and enter the results in column 8 of Table 4 of the DATA SHEET. Show all your calculations on the DATA SHEET.

With those relative errors, we can now calculate the weighted average of the four determinations of M_J, using the formula presented in Sect. G of Experiment #1, "A Review of Mathematical Concepts and Tools". For the weights, we use the reciprocal of the squares of the relative errors, $\Delta M_J / M_J$. In this way, the determinations which are highly uncertain will be given small weight whereas those that are highly certain will be given large weights. Calculate this weighted average on the DATA SHEET and enter the result. Then calculate the standard

deviation in this value, again using the weighted value formula presented in Sect. G of Experiment #1, "A Review of Mathematical Concepts and Tools". Enter the result on the DATA SHEET.

The accepted value for the mass of Jupiter is $M_J = 1.90 \times 10^{27}$ kg. On the DATA SHEET, compare the value for the weighted average you have calculated with this accepted value by calculating the percentage error.

The accepted semi-major axes and orbital periods for the satellites are provided in Table 5. Using your results from columns 2 and 3 of Table 3, calculate the absolute values of the differences between your best-fit values and the accepted values and enter the results in columns 4 and 5 of Table 5. Calculate the percentage errors in your determinations and enter the results in Table 5. Show your calculations on the DATA SHEET.

STUDENT'S NAME _____

E. Galilean Satellites Experiment Data Sheet

Sketch the configurations of Jupiter and the four Galilean satellites on each of the days of observation. Give the date of observation in Julian days and decimal days.

Table 1 Observed positions of the Galilean satellites

Observation date	Military time	Date (J.D.)	Drawing of relative positions	Estimated error in positions "seeing" (sec of arc)
1.				
2.				
3.				
4.				
5.				
6.				
7.				
8.				
9.				
10.				
11.				
12.				
13.				
14.				
15.				
16.				
17.				
18.				
19.				
20.				

STUDENT'S NAME _____

Calculation of data in J.D. from observation data and military time of the observation

STUDENT'S NAME _____

Table 2 Observations of Galilean satellites

Date (J.D.)	Number of grid lines enclosing Jupiter, n_J	Angular diameter of Jupiter, β (sec of arc)	Satellite image	Number of grid lines to image, n_S	Angular distance to satellite $\alpha = n_S/n_J$ β (sec of arc)	Earth distance to Jupiter, d (km)	Physical distance to satellite, h = d sin α (km)	Error in h resulting from seeing (km)
1.			Image A					
			Image B					
			Image C					
			Image D					
2.			Image A					
			Image B					
			Image C					
			Image D					
3.			Image A					
			Image B					
			Image C					
			Image D					
4.			Image A					
			Image B					
			Image C					
			Image D					
5.			Image A					
			Image B					
			Image C					
			Image D					
6.			Image A					
			Image B					
			Image C					
			Image D					

(continued)

STUDENT'S NAME _____

Table 2 (continued)

Date (J.D.)	Number of grid lines enclosing Jupiter, n_J	Angular diameter of Jupiter, β (sec of arc)	Satellite image	Number of grid lines to image, n_S	Angular distance to satellite $\alpha = n_S/n_J$ β (sec of arc)	Earth distance to Jupiter, d (km)	Physical distance to satellite, h = d sin α (km)	Error in h resulting from seeing (km)
7.			Image A					
			Image B					
			Image C					
			Image D					
8.			Image A					
			Image B					
			Image C					
			Image D					
9.			Image A					
			Image B					
			Image C					
			Image D					
10.			Image A					
			Image B					
			Image C					
			Image D					

STUDENT'S NAME _____

Table 2 Observations of Galilean satellites

Date (J.D.)	Number of grid lines enclosing Jupiter, n_J	Angular diameter of Jupiter, β (sec of arc)	Satellite image	Number of grid lines to image, n_S	Angular distance to satellite $\alpha = n_S/n_J$ β (sec of arc)	Earth distance to Jupiter, d (km)	Physical distance to satellite, $h = d \sin \alpha$ (km)	Error in h resulting from seeing (km)
11.			Image A					
			Image B					
			Image C					
			Image D					
12.			Image A					
			Image B					
			Image C					
			Image D					
13.			Image A					
			Image B					
			Image C					
			Image D					
14.			Image A					
			Image B					
			Image C					
			Image D					
15.			Image A					
			Image B					
			Image C					
			Image D					
16.			Image A					
			Image B					
			Image C					
			Image D					

(continued)

STUDENT'S NAME _____

Table 2 (continued)

Date (J.D.)	Number of grid lines enclosing Jupiter, n_J	Angular diameter of Jupiter, β (sec of arc)	Satellite image	Number of grid lines to image, n_S	Angular distance to satellite $\alpha = n_S/n_J$ β (sec of arc)	Earth distance to Jupiter, d (km)	Physical distance to satellite, $h = d \sin \alpha$ (km)	Error in h resulting from seeing (km)
17.			Image A					
			Image B					
			Image C					
			Image D					
18.			Image A					
			Image B					
			Image C					
			Image D					
19.			Image A					
			Image B					
			Image C					
			Image D					
20.			Image A					
			Image B					
			Image C					
			Image D					

STUDENT'S NAME _____

Calculation of angular distance from Jupiter to the satellites

Calculation of physical distance from Jupiter to the satellites

Calculation of error in h resulting from seeing

STUDENT'S NAME _____

The *h*-date graph for the Galilean satellites

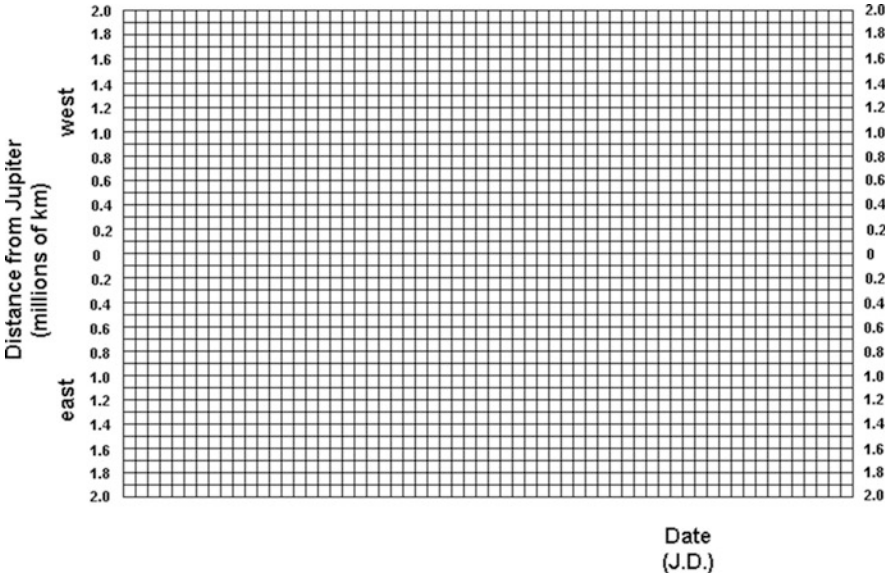

STUDENT'S NAME _____

Table 3 Mass of Jupiter and estimated errors in satellite parameters

Satellite	Best Fit value for $a = a_o$ (km)	Best Fit value for $P = P_o$ (days)	M_J (kg)	Worst Fit value for $a = a^*$ (km)	Worst Fit value for $P = P^*$ (days)	$\Delta a = \lvert a_o - a^* \rvert$ (km)	$\Delta P = \lvert P_o - P^* \rvert$ (days)
Io							
Europa							
Ganymede							
Callisto							

Calculation of the value of M_J

Io:

Europa:

Ganymede:

Callisto:

Calculation of the difference between accepted value for semi-major axes of satellites and best fit value

Io:

Europa:

Ganymede:

Callisto:

STUDENT'S NAME _____

Calculation of the difference between accepted value for orbital periods of satellites and best fit value

Io:

Europa:

Ganymede:

Callisto:

STUDENT'S NAME _____

Table 4 Calculation of errors in determination of M_j

Satellite	a_o (km)	P_o (days)	Δa (km)	ΔP (days)	$\Delta a/a_o$	$\Delta P/P_o$	$\Delta M_J/M_J$
Io							
Europa							
Ganymede							
Callisto							

Calculation of Relative Error, $\Delta M_J/M_J$

Io:

Europa:

Ganymede:

Callisto:

Calculation of weighted average value of M_J

Calculation of standard deviation in weighted average value of M_J

Calculation of the percentage error between accepted value for M_J and the weighted average value

STUDENT'S NAME _____

Table 5 Errors in semi-major axes and orbital periods

Satellite	Accepted value for a (km)	Accepted value for P (days)	$\lvert a-a_o \rvert$ (km)	$\lvert P-P_o \rvert$ (days)	Percentage error in a	Percentage error in P
Io	422,000	1.77				
Europa	671,000	3.55				
Ganymede	1,070,000	7.16				
Callisto	1,880,000	16.69				

Calculation of percentage errors in semi-major axes

Io:

Europa:

Ganymede:

Callisto:

Calculation of percentage errors in orbital periods

Io:

Europa:

Ganymede:

Callisto:

STUDENT'S NAME _____

F. Galilean Satellites Experiment Discussion Questions

1. To show your understanding of the nature of an ellipse, draw an ellipse of arbitrary size in the space below. Label the major axis, the semi-major axis, the position of the two foci, and the aphelion and perihelion points.

2. As seen looking downward on the plane of the solar system, in what direction (clockwise or counterclockwise) do the satellites orbit Jupiter?

3. How does this direction compare ("same" or "opposite") with

   a. the direction of rotation of Jupiter about its axis? _____
   b. the direction of revolution of Jupiter around the Sun? _____
   c. the direction of revolution of the Earth around the Sun? _____
   d. the direction of revolution of the Moon around the Earth? _____
   e. the direction of rotation of the Earth about its axis? _____
   f. the direction of rotation of the Sun on its axis? _____

4. At certain times in their orbits, the satellites disappear from view. How do you explain this?

5. An astronomy professor on Ganymede uses pirated copies of this laboratory book for his (her, its) own class. Our present Experiment #13, "The Galilean Satellites of Jupiter," has been altered to determine the orbital period and semi-major axis of our Moon, which are then used to determine the mass of the Earth. Because we have only one moon, the experiment is greatly simplified. A major difficulty, however, is present. Use a top view of the solar system to explain this difficulty.

STUDENT'S NAME _____

6. We have determined errors in the semi-major axes and orbital periods in two ways, by comparing the best-fit values to the worst-fit values and by comparing the best-fit values to the accepted values. The former are summarized in columns 4 and 5 of Table 4 and the latter are summarized in columns 4 and 5 of Table 5. Do the results of the two methods of determining the errors agree? If any disagreement is significant, provide possible explanations.

   Compare Δa and $|a - a_o|$

   Io:

   Europa:

   Ganymede:

   Callisto:

   Compare ΔP and $|P - P_o|$

   Io:

   Europa:

   Ganymede:

   Callisto:

   Provide explanations of any significant differences

STUDENT'S NAME _____

7. A regularity exists among the orbital periods of the Galilean satellites.

   a. Calculate the ratio of the accepted orbital periods of Europa, Ganymede, and Callisto to that of Io. Show your calculations here.

      Europa/Io:

      Ganymede/Io:

      Callisto/Io:

STUDENT'S NAME _____

b. You will notice a regularity. Describe it.

c. If the satellites are aligned on one side of Jupiter on a given date, how many days will be required for the innermost three satellites to again appear in the same configuration?

d. Explain your answer.

8. A hypothetical configuration of the Galilean satellites is shown. Assume for the point of the exercise that each satellite is at the apogee of its orbit. Vertical lines are overlaid for use in measuring the distances of the satellites from Jupiter. (The objects are not drawn to scale).

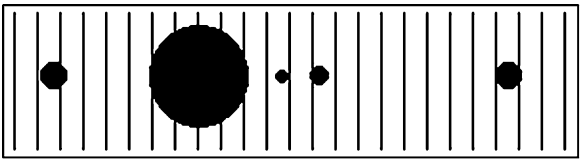

a. Make a drawing showing the locations of the satellites from both the top and side views 12 days later. Ignore any changing perspective resulting from Jupiter and the Earth revolving about the Sun. On the top view, indicate with arrows the direction of motion of each satellite about Jupiter. On the side view, that seen from the Earth, provide the satellite names. As an aid, create the top view first.

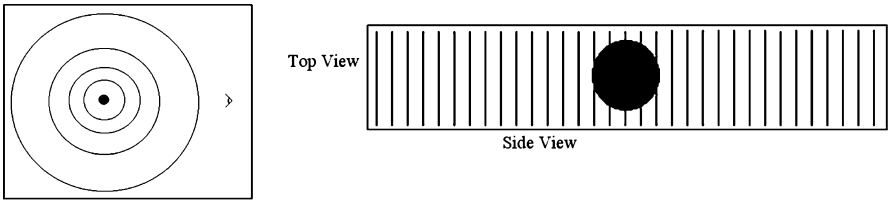

b. Which satellites, if any, may not be visible from the Earth? Why?

STUDENT'S NAME _____

9. One of the effects we neglected was the changing aspect of Jupiter and its satellites as the Earth and Jupiter revolve about the Sun in their orbits. Assume Jupiter is near opposition and that your observations span a significant amount of time, a month or more. How will these motions affect the values you find for the orbital periods? Draw a top view of the solar system displaying the orbit of the Earth and Jupiter and the orbit of the satellites about Jupiter to explain your answer.

10. As of 2011, Jupiter has 63 known satellites, including the four the Galilean satellites. Kepler's laws, of course, apply equally to all of them. Using Kepler's Third Law of Planetary Motions, use the known orbital periods of the orbits of these satellites to determine their semi-major axes. Express the results in both A.U. and the number of Jupiter radii, 71,500 km.

    a) Amalthea, orbital period of 12 h.

    b) Sinope, orbital period of 758 days.

11. The figure shows a top view of hypothetical planet Shvitz in orbit around its central star. The semi-major axis of the circular orbit is 0.3 A.U.

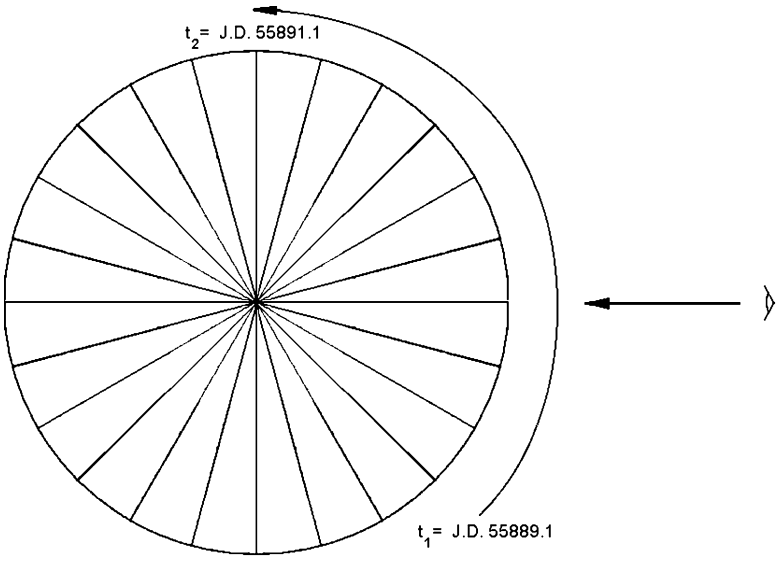

STUDENT'S NAME _____

a. On the *h*-date graph paper provided, draw the portion of the sinusoidal path that would be observed from an external observer between the two epochs noted.

b. Determine the orbital period of the object in days and convert it to years. Show all necessary calculations here.

c. From the expression for Kepler's Third Law given in (2) of Experiment #12, "Kepler's Laws of Planetary Motion," calculate the mass of the star in solar masses required to yield an object with such an orbit.

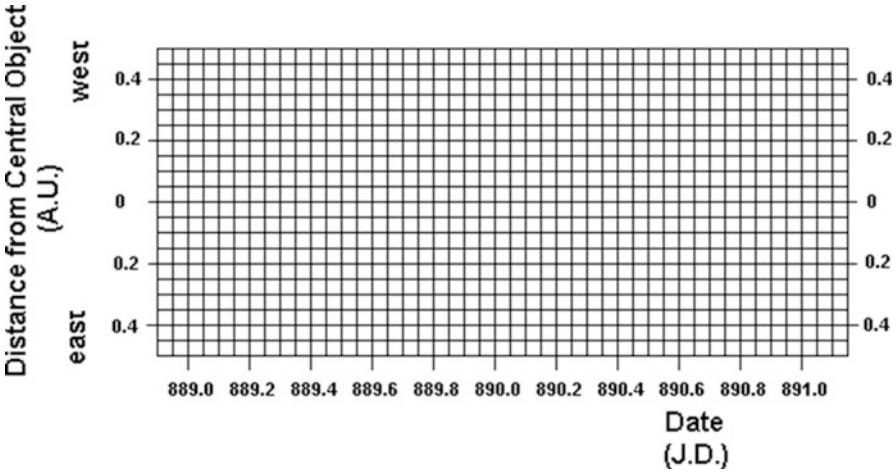

d. From Table 6 of the characteristics of main sequence stars, what would be the spectral classification of such a star and the associated surface temperature?

Type: _____

Surface temperature: _____

STUDENT'S NAME _____

e. Would this object be a suitable location for the evolution of life? Explain your answer.

Table 6 Characteristics of main sequence stars

Spectral type	Mass (solar masses)	Surface temperature (K)	Color of star
O	> 16	>28,000	Blue to violet
B	3.3–16	10,000–28,000	White to blue
A	1.7–3.3	7500–10,000	White
F	1.1–1.7	6000–7500	Yellow to white
G	0.8–1.1	5000–6000	Orange to yellow
K	0.4–0.8	3500–5000	Red to orange
M	< 0.4	2000–3500	Red

Removing these DATA SHEETS from the book may damage the binding. You might consider entering the data and performing your calculations in the book, and then photocopying the DATA SHEETS for submission to your instructor for grading.

Experiment 14
Thermal Radiation from a Planetary Subsurface: Part I. Calibration and Initial Measurements

SUMMARY: In Experiment #14, "Thermal Radiation from a Planetary Subsurface: Part I. Calibration and Initial Measurements," and Experiment #15, "Thermal Radiation from a Planetary Subsurface: Part II. Soil Sample Measurements," we demonstrate how astronomers determine the nature of planetary surfaces using remote sensing, in this case of microwave radio waves. You will place thermometers at various depths into several soil samples that simulate the materials of planetary surfaces and heat the surface with incandescent light bulbs. At the same time you will observe the radio radiation being emitted by the subsurface layers of the soils. Experiment #14 "Thermal Radiation from a Planetary Subsurface: Part I. Calibration and Initial Measurements," introduces these concepts and calibrates (an act that all astronomers perform) the 11 GHz radio receiver using an ice-water bath and a boiling-water bath and obtains a measure of its gain variability by measuring the radiation from soil samples at room temperature.

LEVEL OF DIFFICULTY: Moderate

EQUIPMENT NEEDED: Fragmented granite rock, coarse sand, water, and ice; 2.5 × 2.5 × 2-ft sand boxes; 2.5 × 2.5 × 1-ft water containers; Ku-band radiometer with horn antenna; digital thermometers; meter stick; micrometer; thin sheets of plastic bubble-wrap; plumb bob.

MY LEARNING GOALS

1. To be able to describe which types of electromagnetic radiation can be used to study the atmospheres and surfaces of planets.
2. To be able to describe how different surface materials change the appearance of a planet in terms of a phase effect.
3. To be able to predict mathematically the amount of solar energy available to solar system objects.
4. To recognize that the beam pattern of a radio telescope is the single slit diffraction pattern.

L.M. Golden, *Laboratory Experiments in Physics for Modern Astronomy: With Comprehensive Development of the Physical Principles*,
DOI 10.1007/978-1-4614-3311-8_14,

A. Introduction

In addition to the visible radiation which enables us to see the nighttime stars twinkling through our atmosphere, astronomers "see" objects in the universe at every other wavelength region of the electro-magnetic spectrum. Telescopes are built to detect the very shortest wavelengths from gamma rays and x-rays to the longest radio wavelengths.

The maximum radiation for objects whose temperatures are Earthlike occurs in the infrared range of wavelengths, slightly more than 7000 Å to about 1 mm (7×10^{-5} cm to 0.1 cm). (This follows from the relationship that is an excellent approximation to many real objects, the *Planck Blackbody Radiation Law*, the subject of Experiment #17, "Blackbody Radiation"). The radiation at many of these wavelengths, however, is absorbed by the gases in the atmospheres of planets and do not reach our Earth-bound detectors. For planets without atmospheres, the radiation at infrared wavelengths can provide information about the top few millimeters of the surface. The somewhat longer wavelength rays of *microwave* radiation, 1–100 cm, however, emanate from comparatively deeper subsurface layers and can penetrate through the atmospheres. Astronomers accordingly study planets with both infrared and microwave instruments in addition to optical telescopes.

In this experiment and Experiment #15, "Thermal Radiation from a Planetary Subsurface: Part II. Soil Sample Measurements," you will examine the physics and one of the techniques by which astronomers learn about the subsurface material of the terrestrial-like objects in the solar system, that is, the rocky planets and moons. In Experiment #14, "Thermal Radiation from a Planetary Subsurface: Part I. Calibration and Initial Measurements," you will become familiar with the microwave equipment by performing calibration and a "trial run" of soil samples at room temperature, determine estimates of random errors in the radiometer and temperature readings, and evaluate the variation of gain of the receiver with time. In Experiment #15, "Thermal Radiation from a Planetary Subsurface: Part II. Soil Sample Measurements," you will heat the soil samples and take measurements of the resulting enhanced radiation.

B. Theory

1. Planetary Heat Balance

As shown in Fig. 1, the radiation from the Sun or other parent star impinges upon the surface of a planet or moon. Some of that radiation is simply reflected back into space. The rest heats the surface and that heat is transferred downwards into the subsurface by the familiar processes of heat conduction and radiation. That

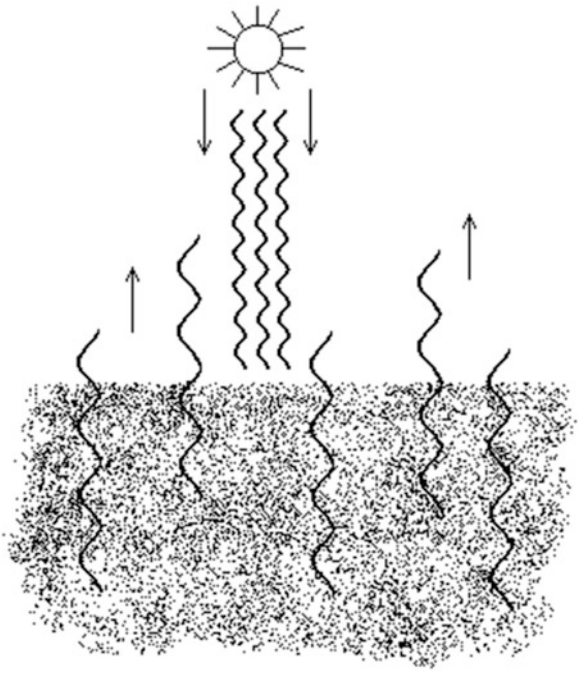

Fig. 1 The radiation from the Sun or other parent star heats the surface of a planet or moon. That heat is conducted and radiated downwards and the heated subsurface layers radiate blackbody radiation outwards. This radiation is observed in the microwave and infrared portions of the electromagnetic spectrum. That the wavelengths of sunlight are much smaller than the wavelengths of microwave and infrared radiation is indicated by the relative wave sizes (not to scale)

material, now warmed, emits radiation outwards. It is that radiation which is detected by the microwave or infrared detectors.

The amount of microwave or infrared radiation received, and how it varies with the amount of solar or stellar radiation illuminating the surface of the planet or moon, depends on the composition of the surface and subsurface material and its structure. Analysis of that radiation using the physics of heat conduction and radiative transfer enables astronomers to determine the chemical and physical properties of the soil.

Two extreme cases illustrate the technique. If, for one extreme, the material were a poor conductor of heat, then the subsurface would not be well heated and the majority of the microwave radiation we would detect would emanate from near the surface, independent of the ability of the subsurface material to radiate. The amount of radiation detected would be nearly proportional to the amount of surface illuminated by the Sun or parent star. It is as if the surface was a good reflector. Because of the similarity to the phases of the Moon and planets that are observed in visible light as their position relative to the Sun changes, such studies are frequently referred to as studies of the *phase effect*.

On the other hand, if the material were a good conductor of heat but a poor radiator of microwave or infrared radiation, then the subsurface layers would be warmed but would retain their warmth for long periods of time and radiation would be detected even when the surface was not illuminated. The amount would be constant, a nearly uniformly-warmed planetary disk independent of the phases. The

situation with real soil materials, of course, lies between these extremes, and detailed analysis of the microwave and infrared radiation enables astronomers to determine the conductive and radiative properties of the soil, from which they learn its composition and structure.

The actual physics underlying these concepts, the theory of heat conduction within a planetary surface and the radiation of energy back into space, is presented in Experiment #15, "Thermal Radiation from a Planetary Subsurface: Part II. Soil Sample Measurements".

2. *Insolation*

The radiation from a source spreads out into space according to the inverse square law. If, that is, S_o is the intensity of a source, then at a distance R the radiation has diminished according to

$$I = \frac{S_o}{4\pi R^2}. \tag{1}$$

The energy that the Earth receives from the Sun, for example, as we will study in Experiment #18, "The Surface Temperature and Energy Output of the Sun," is approximately 1368 W on every square meter of the surface of the Earth, or 1,368 W/m. This, I_{Sun}, is referred to as the *solar constant*. By (1), at the distance of Mars, as shown in Table 12 of Experiment #15, "Thermal Radiation from a Planetary Subsurface: Part II. Soil Sample Measurements," that radiation intensity is decreased by a factor of $(1.5)^2 = 2.25$. The "solar constant" at Mars is less than one-half of that at Earth.

Knowing the semi-major axes of the planets in their orbit about the Sun (Table 10 of Experiment #15, "Thermal Radiation from a Planetary Subsurface: Part II. Soil Sample Measurements,") we can calculate the "solar constants" for all the planets. These are presented in Fig. 2. (The solar constant for the Earth is defined as the energy received at its mean distance from the Sun, not at a distance equal to its semi-major axis. These two figures differ significantly only for Mercury and Pluto, with their highly eccentric orbits,)

3. *Radio Telescopes: Beam Patterns*

A microwave *radiometer*, a "meter" with which to measure the intensity of radio waves, detects the radiation from the soil samples. Radiometers consist of a low-noise radio receiver with a suitable antenna. Just like a radio or television collects radio waves from transmitting stations, the antenna collects the emitted microwave radiation from the object being study, here, our soil samples. The receiver converts

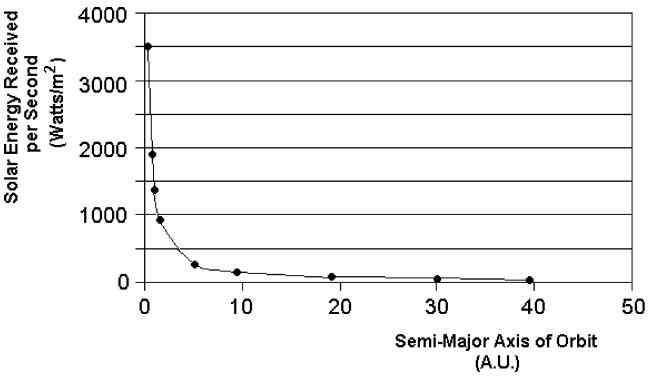

Fig. 2 The energy received per second from the Sun at given distances in the solar system decreases as the inverse square of the distance. The positions of the planets are represented by *dots*. At the Earth, the value for the energy received per second is 1368 W/m^2, the solar constant

the microwave signal into a proportional output voltage. When used to observe celestial objects, a radiometer functions as a *radio telescope*.

Although radio telescopes and optical telescopes both collect electro-magnetic radiation, the difference in the wavelengths they receive and the difference in the size of the collector, be it a mirror or an antenna, create significant differences in the portion of the sky that they detect. In general, radio telescope antennas receive radiation from a substantial solid angle in space, as shown in Fig. 3. If an object is present in a portion of the sky at which the antenna is pointed, then the antenna will receive radiation from that object. If multiple objects are within the solid angle viewed by the antenna, then the antenna will receive radiation from each. This, of course, is also the case in optical astronomy, but the distinction lies in the size of the field of view, square seconds or square minutes of arc view for optical telescopes compared to many square degrees for radio telescopes composed of a single antenna.[1]

As this implies, unlike optical telescopes, microwave antennas receive radiation from directions other than close to the direction to which they are pointed. Most of the radio radiation is received in the primary or *main lobe* or *main beam* aligned

[1] Radio telescope *interferometers* are composed of more than one antenna, or *element*, separated by substantial distances and connected electronically or by later computer analysis. Separating them by substantial distances effectively increases the diameter of the antenna; the interferometer simulates a larger antenna in its resolving power but without the corresponding collecting area. In this way, continental-wide spacings of up to the diameter of the Earth can be attained, a configuration referred to as *very-long baseline interferometer*, or *VLBI*. As a result, beam sizes not only of seconds of arc but of thousandths of seconds of arc can be obtained, much better than that of traditional optical telescopes. Future astronomers will hopefully be able to observe with telescopes consisting of elements located on both the Earth and the Moon. Optical interferometers have also been developed.

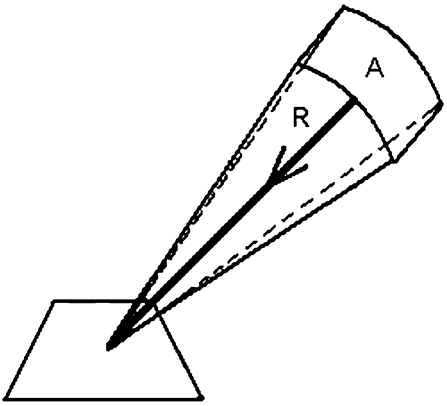

Fig. 3 Radio telescopes receive radiation from all objects located within a solid angle in the sky in the direction to which the telescope is pointing. This simplified figure does not display the lobe structure of the antenna power pattern. The surface of a sphere of radius R is $4\pi R^2$. Accordingly, a solid angle σ subtended by an area A has the value $\sigma = A/R^2$

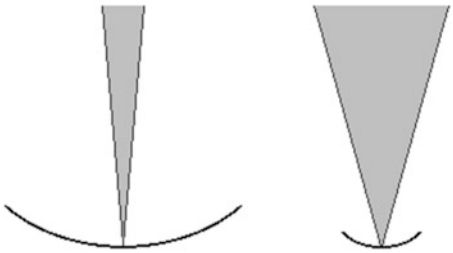

Fig. 4 Large antennas provide greater spatial resolution than small antennas. Their beam patterns have smaller lobes, proportional to λ/D. The side lobes of the beam patterns are not shown in this representation

with the axis of the antenna. The larger the antenna, the smaller the width of the main lobe, as shown in Fig. 4. Antennas, however, also receive radiation with much decreased sensitivity from other directions, in the *side lobes*.

Figure 5 shows the sensitivity pattern for one antenna design with the side lobes shown out to 60° from the axis of the antenna. As the graph shows, the main lobe is about 50° in angular diameter. At an angle of about 10° from the axis the sensitivity has been reduced to about 1% of that in the directly- forward direction.

Various terms describe an antenna pattern. The *beam width between first nulls*, or BWFN, is the difference between those angles at which the beam pattern first becomes zero with increasing angular distance from the maximum of the beam pattern. The *half power beam width,* or HPBW, is the angular distance between those angles for which the beam pattern is half of its maximum value. The level

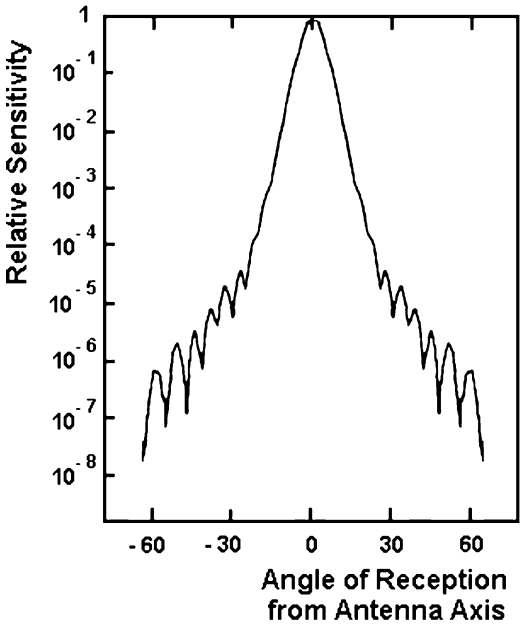

Fig. 5 A microwave antenna receives radiation from directions far from the axis of the antenna. For many, such as the antenna whose pattern is provided here, the sensitivity in the main lobe is greatly reduced for angles greater than 10–15° from the axis. It is even smaller in the side lobes. This graph shows the antenna power pattern with the abscissa representing the angle linearly. Antenna patterns are often also displayed in polar coordinates, as shown in Fig. 12

of sensitivity of the side lobes is often provided in decibels below that of the main lobe.

For those students who have studied optics, this pattern may remind you of the diffraction pattern of a single slit. Indeed, the physics and mathematics describing the beam of a radio antenna is the same as the physics and mathematics of a single slit diffraction pattern.

That mathematics provides the antenna pattern/diffraction pattern shown in Fig. 6.[2] As shown in Fig. 6, BWFN $= 2\ \lambda/D$ radians for an antenna that is equally sensitive to incoming radiation over its entire aperture. This is referred to as *uniform illumination*, a term borrowed from a uniformly-lit diffraction slit in visible light.

Although you may have thought of diffraction as an optical phenomenon, it occurs for all waves, in particular for that part of the electro-magnetic spectrum referred to as microwaves. (You can hear voices from around the corner of a building because sound or *acoustic waves*, too, undergo diffraction.) Instead of the slit being on the order of a micron ($1\ \mu = 10^{-6}$ m) in size and the wavelength being in the visible region of approximately 4000–7000 Å (0.4–0.7 μ), here the "slit" size is centimeters in size and the wavelength is in the microwave range of 1–100 cm. Shockingly enough, because for both the beamwidth is approximately λ/D, we find

[2] The diffraction pattern shows the electric field. In radiometry, the lobe structure is the antenna power pattern. If $E(\theta)$ is the electric field pattern, assumed cylindrically symmetrical, then the power pattern is $P(\theta) = E(\theta)\ E^*(\theta)$, where $E^*(\theta)$ is the complex conjugate of $E(\theta)$.

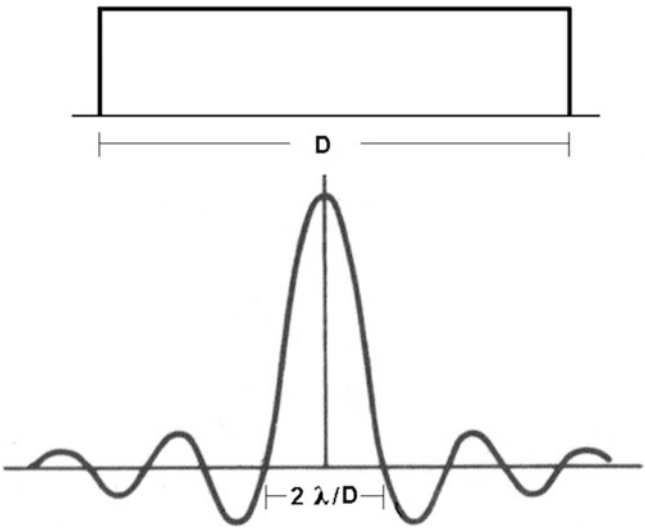

Fig. 6 A uniformly-illuminated square aperture (*top*) produces an electric field pattern (*bottom*) of the same form as a single slit diffraction pattern. The width of the beam between the first nulls, or BWFN, is equal to $2\ \lambda/D$ radians. The width of the beam at half-power, or HPBW, of the associated power pattern is approximately equal to λ/D radians. The maximum of the first side lobes of the power pattern is a factor of 20 less than the maximum of the main lobe

that $\lambda/D = (0.5\ \mu)/(1\ \mu) = 0.5$ radians for the beamwidth of the primary lobe of the pattern produced by the diffraction grating is of the same order of magnitude as $\lambda/D = (2.7\ \text{cm})/(8\ \text{cm}) = 0.32$ radians for the beamwidth of the primary lobe of the radio telescope we will be using in this experiment. In contrast, a 1-m diameter optical telescope will have a corresponding beamwidth, more often described by the corresponding resolving power (Eq. (2) of Experiment #3, "The Optics of Telescopes: Part I. Image Size and Brightness,") of $\lambda/D = (0.5\ \mu)/(10^6\ \mu) = 5 \times 10^{-7}$ radians, or about 0.1 seconds of arc. All these results, however, come from the same physics!

It is that difference in relative size of wavelength and the collector size that create the differences in field of view that are detected in the two types of telescopes. In optical astronomy, the wavelength of observation is many orders of magnitude smaller than the dimensions of the collecting lens or mirror; in radio astronomy, they are similar in size.

4. *Radio Telescopes: Bandwidths*

Another major difference between radio and optical astronomy is the range of wavelengths that can be simultaneously detected. Unlike optical astronomy, where the entire range of optical wavelengths can be reflected by a mirror and

therefore detected at the same time, in radio astronomy we are limited to only a small range or *bandwidth* of wavelengths.

This results from both the physics of wave propagation and technological considerations. Whether the receiver consists of a resonant cavity, as in a radio, or a waveguide, as in a radio telescope, only certain wavelengths can be selected out of the radiation gathered by the antenna. In addition, in many radio receivers the radiation collected by the antenna is mixed with a *local oscillator* signal in order to convert it to lower frequencies, referred to as *intermediate frequencies*, abbreviated *IF*, for contrast with the terminology of radio frequencies, or *RF*. These altered signals deliver the same astronomical information but suffer much less attenuation than the higher frequency signals in processing by the receiver. The center of the RF bandwidth that is detected depends upon the local oscillator frequency with which that incoming radiation is mixed. In this experiment, for example, the RF signals gathered by the antenna in the 1 GHz bandwidth of 10.7–11.7 GHz are mixed with a local oscillator frequency of 9.75 GHz so that a 1 GHz IF bandwidth of signals between 950 and 1950 MHz is actually detected by the receiver.

As a result of these considerations, a different receiver is required for each such separate bandwidth at which the sky is desired to be observed. Changing receivers is effectively tuning the radiometer to a different frequency, as one would tune a television or a radio. In some advanced radio telescopes, the incoming radiation is divided up and mixed with different local oscillators signals. These enable the creation of *multi-channel receivers*.

5. *Radio Telescopes: Radio Astronomy Targets*

It should be noted that radio telescopes don't simply provide the ability to observe a given object at a wavelength different from those of optical telescopes. Objects that are invisible in optical radiation, for example, the dust-shielded center of the Milky Way galaxy or the massive radio-emitting regions adjacent to active galaxies, are detectable in radio waves. Certain physical phenomena create radiation in the radio wavelength region and not in the optical region, for example, the famous *21-centimeter line* of neutral hydrogen and emission from interstellar molecules. Again, some physical phenomena create radiation in the radio wavelengths of greater intensity than in the optical region. As with infrared, x-ray, and gamma ray astronomy, radio astronomy provides new windows to the universe.

Unfortunately, this interest has not spread to amateur astronomers. With CCD detectors, amateur astronomers can obtain excellent visual images with small telescopes even in the suburbs of large cities. (The author's Near Earth Asteroid Reconnaissance Project utilizes this resource.) The proliferation of radio interference from military and commercial satellites, radar, microwave transmitters, and hand-held personal communication devices since the 1950s produces disturbingly large interference in radio frequencies. Except for the Sun, natural phenomena that would be of interest to amateurs produce signals that are weak in intensity and broadband,

requiring expensive equipment. In addition, more appeal attaches to the image of a bright star cluster or nebula than the pen recording or ammeter display of radio receiver static. It is interesting, nonetheless, to know that one of the first detections of radio astronomical extraterrestrial signals was made in 1937 by a radio engineer and amateur astronomer in his backyard, Grote Reber of Wheaton, Illinois. (He constructed a 31-ft diameter parabolic antenna for the purpose!)

C. Procedure and Observations

The experimental equipment has three components. They are the soil sample material which simulates the planetary or moon soil, incandescent light bulbs to simulate the Sun or a star (used in Experiment #15, "Thermal Radiation from a Planetary Subsurface: Part II. Soil Sample Measurements,") and a *microwave radiometer* to detect the radiation emanating from the subsurface layers of the sample material. As with a radio, a microwave radiometer consists of an antenna, a receiver, and a device to record the received signal. (In your radio, this device is a speaker; in the microwave radiometer it is a voltage meter or ammeter). Thermometers are placed under the microwave receiver at various depths of the sample material to measure the temperatures at those depths.

1. The Soil Samples

We utilize three types of readily available material, which are similar to material we expect may be present on the surfaces of planets and rocky moons. Granite is an igneous rock, largely composed of silicon dioxide, or quartz, formed when magma cools slowly upon ejection from volcanoes. We use fragmented granite to simulate the soils of volanic regions of the Moon, Venus, and Mars. Sand is composed of finely fragmented sandstone, a sedimentary rock composed mainly of broken-up granite, quartz, and feldspars, a group of common rock-forming igneous minerals, after it undergoes compression. Feldspars are aluminum silicates combined with other elements. We use sand to simulate dried river beds such as we believe are found on Mars. The third sample is this sand immersed in water to within 10 cm of its surface. Some believe that Mars has a permanent layer of ice beneath the surface, or *permafrost*, such as exists in the arctic region of Earth. This sample represents a soil that might exist if a permafrost layer melts, for example near the equator during Martian summer.

We will use coarse sand. If the sand were fine grained, the water in the third sample would seep upwards so that the effective depth of the wet sand would decrease with time. The early and late measurements would be taken of essentially different material.

Both granite and sandstone are composed mainly of the chemical elements oxygen and silicon. The chemical formula for quartz is SiO_2. These two elements together account for nearly 75% by mass of all the elements in the crust of the Earth and are the two most common elements in the crusts of the terrestrial planets. Being common, both granite and sand are excellent choices for our soil sample material

In addition, the ability of these substances to radiate when heated, as measured by their emissivities, differs widely. As shown in Table 1 of Experiment #15, "Thermal Radiation from a Planetary Subsurface: Part II. Soil Sample Measurements," the *emissivity* of granite is about 0.45 whereas that of sand varies from 0.76 to 0.90. (The relationship between emissivity and the amount of radiation provided by a heated object is discussed in Experiment #17, "Blackbody Radiation".) Astronomical studies have shown that the heat conduction within planetary soils includes a contribution from a radiative term. As a result, this difference in emissivity may have an effect in our experiments.

With a ruler, measure the diameter of a number of pieces of the granite rock. With a micrometer, measure the diameter of a number of grains of the coarse sand. Enter the results in Table 1 of the DATA SHEET.

2. *The Incandescent Light Bulbs and Sand Boxes*

In Experiment #15, "Thermal Radiation from a Planetary Subsurface: Part II. Soil Sample Measurements," we will heat the soil samples and measure the radiation they then emit. As shown in Fig. 7, sets of four 150-W incandescent light bulbs, one set for each sand box, are mounted on rigid stationary platforms to heat the soil samples. Here we will measure the radiation emitted from the soil samples at room temperature.

The soil samples are placed in sand box containers. Thermocouples or digital thermometers calibrated in the Celsius scale are located just below the surface of the samples and at five depths, 1, 3, 10, 25, and 60 cm, about 2 ft. We don't want to measure the temperature at the surface, but just below it, at a depth of about 0.5 cm, or 1/4 of an inch. The depth of the sand boxes should be slightly greater than the 60 cm depth at which the deepest thermometer will be placed. Even if the heat from the lamps would penetrate deeper than that in the 75 min during which the soil samples will be heated, the 2.7 cm-wavelength radiation from greater depths will not contribute significantly to the detected signal. Holes in the side of the sand box are drilled into which the thermometers or thermocouples are inserted. The sensors of the thermometers should be placed within the material, directly below the microwave radiometer. For their reading, they can be pulled out of the sand box.

As shown in Fig. 7, the soil samples containers sit on platforms mounted on casters. They can be rolled back and forth from below the light bulb assembly to below a stationary microwave receiver. To ensure no bias occurs in either heating the soil samples or measuring their emission, care must be taken to ensure that each soil sample box is located at the same location directly under the center of the two

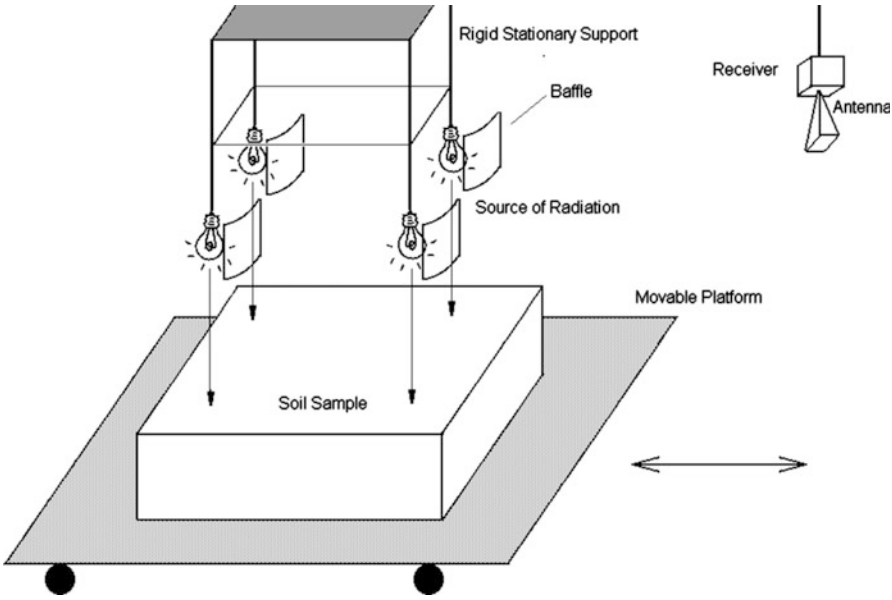

Fig. 7 The soil sample sand boxes sit on a platform which can be rolled into position under the antenna or remain under a suspended rigid light bulb assembly of four incandescent light bulbs. A separate assembly heats each of the three soil samples. These will be used in Experiment #15, "Thermal Radiation from a Planetary Subsurface: Part II. Soil Sample Measurements"

assemblies. To accomplish this positioning under the radiometer, a plumb bob is attached to the side of the antenna, as shown in Fig. 8. This can be done with a simple piece of tape. Each time an assembly is rolled into position below the radiometer, attach the plumb bob. It should hang directly over the center of the sand box. After positioning the sand box correctly, remove the plumb bob to prevent it radiating a spurious signal into the antenna.

When calibration measurements are being taken rather than measurements of the emission from the soil samples, the sand boxes should be placed sufficiently distant from the radiometer to ensure that no radiation enters the main lobe or close side lobes of the antenna. Care should also be taken to position the sand boxes distant from the antennae of other groups in the laboratory.

The sample of sand partially immersed in water requires a bit of care to prepare. Fill the sand box to within 10 cm of its surface with the coarse sand. Then pour in water until the top is moist, but not soaked. Then fill in the rest of the sand box with the sand. To ensure that this water is at room temperature, it should stand overnight in the laboratory.

The microwave radiometer we will use detects only one of the two linear polarizations of radiation. To prevent a bias in your measurements, the material in the sand boxes should be stirred to prevent any clumping of material in a given direction.

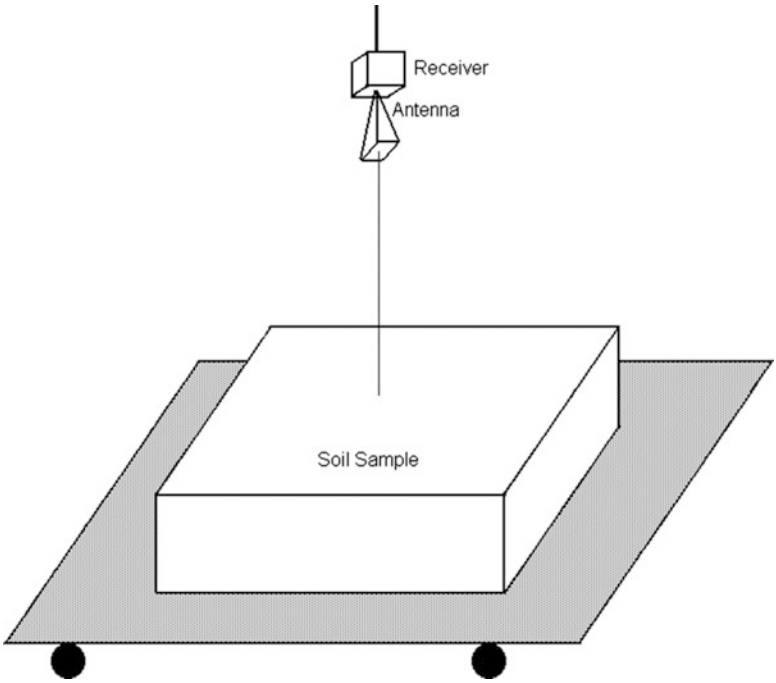

Fig. 8 A sand box is shown in position *under* the suspended antenna for measurement of the radiation emitted by the soil samples. A removable plumb bob can be hung from the side of the antenna to ensure that it is located directly over the *center* of the sand box so that the nearest side lobes see only the soil sample

The areal dimensions of the sand box depend upon the radiometer specifications. This is discussed in section "Radio Telescopes: Bandwidths" later.

3. *The Radiometer*

A microwave radiometer detects the radiation from the soil samples. As shown in Fig. 8, it is suspended over the soil samples for their measurement. The radiometer we will use, the model RTL-11H Portable Radio Telescope, was designed specifically for use by students of *Laboratory Experiments in Physics for Modern Astronomy* by microwave engineers at Spacek Labs in Santa Barbara, California. This is the same lab that has designed microwave systems for the Cassini spacecraft, CLOUDSAT satellite, TIROS-K satellites, and other space and Earth-based applications. The system can be obtained from the designers (email:jpolivka@spaceklabs.com) or, if your university has an electrical engineering department, its staff can put together the system with the specifications that will be described.

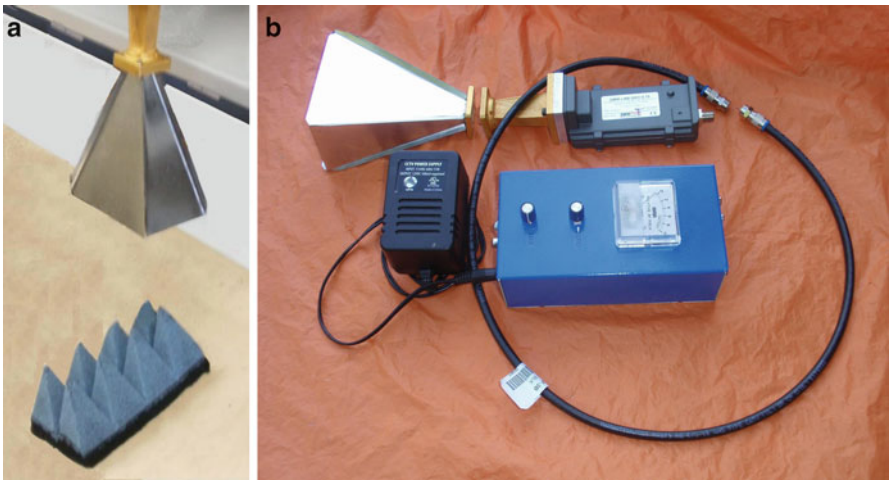

Fig. 9 (**a**) The Ku-band horn antenna is shown observing the radiation from a pyramidal microwave absorber. Photograph by Dr. J. Polivka, Spacek Labs. (**b**) The actual components of the RTL-11H are shown, clockwise from upper left: The horn antenna, the waveguide connecting the horn to the LNB and the LNB, the F/F cable (RG-6 designation) which connects the LNB to the IF Processor Box, the IF Processor Box, and the power supply. Screws are provided to connect the horn to the waveguide leading to the LNB. Photograph by the author

For the antenna, although either a horn antenna or a small parabolic dish, such as used by home microwave receivers, can be used, we have chosen the less expensive, compact horn antenna. Figure 9 shows that to be used in our system. Because we will design the setup of the equipment (see below) so that the beam will almost entirely view the soil sample box, the higher directivity of the parabolic dish is not needed. The horn antenna as designed by the Spacek engineers has dimensions of 6 cm by 10 cm and provides a 20 dB gain compared to an isotropic radiator. As shown by Eq. (4) of Experiment #10, "Determination of the Rotation Rate of Planets and Asteroids by Radar: Part II. Observations of Simulated Planets," a 20 dB gain is equivalent to a factor of $10^2 = 100$ increase in directional properties over a non-directional antenna.

The receiver we will use in the radiometer operates in Ku-band at 10.7–11.7 GHz, or 2.6–2.8 cm wavelength, slightly larger than 1 in. This is the band of television signals broadcast by the Astra 1KR satellite, launched in 1988. We use this receiver for several reasons. Being commercially produced, Ku-band receivers are inexpensive. Smaller wavelength (higher frequency) systems are more expensive. Longer wavelength (smaller frequency) systems have beam patterns which would require sand boxes holding our soil samples to be unwieldy large. In addition, many television systems, radar systems, and data and sensor transmission devices utilize frequencies below 10 GHz and their associated harmonics, thereby creating spurious, undesired signals.

Figure 10 shows the schematic of the receiver. It lacks two important components of sophisticated professional radio astronomy receivers. First, being

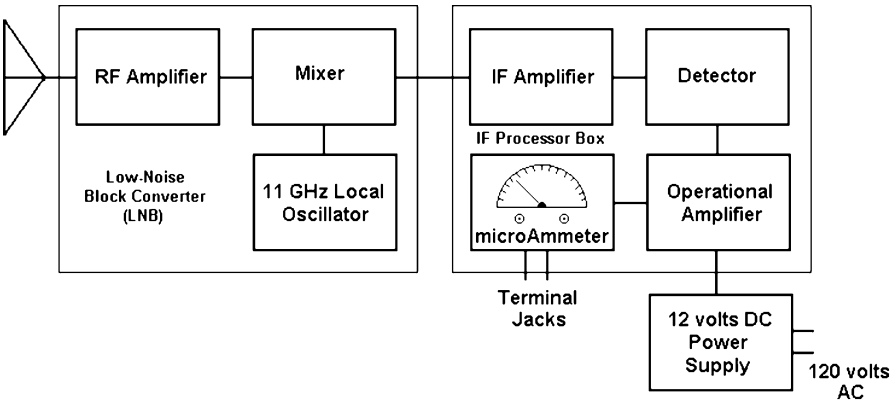

Fig. 10 The receiver for the RTL-11H system. This is a simple total power (non-switched between the signal and a reference) receiver. The intermediate-frequency (IF) signal from the LNB is sent via cable to the IF Processor Box where it is converted into a voltage in the detector and then amplified. The resulting voltage is displayed on a microammeter. An F/F cable connects the two boxes as well as delivering the power from the power supply back to the LNB. Terminal jacks allow connection to a digital voltmeter (DVM) or an analog-to-digital converter (ADC) for input into a personal computer if a digital record is desired. No internal loads are provided for calibration. This simplifies the system but we then require frequent calibration using external references of known temperatures and emissivities

a simple *total power* receiver, it does not employ *Dicke switch* systems, in which the receiver input is switched rapidly between the signals from the source of interest and a comparison noise source. (Such systems are also available from Spacek Labs at increased cost.) Such systems greatly reduce the effect of gain variations of the various components of the receiver so that the sensitivity of the system depends mainly on system noise, not gain variations. Second, professional receivers employ alternating observations of the celestial source and two objects of known temperature, such as *loads* or *noise diodes*, to calibrate the output of the radiometer.

For the sake of affordability and simplicity, our system lacks both these features. We accordingly require calibration that is not only frequently performed but which also uses external references of known temperatures and emissivities. This is discussed in section "Radio Telescopes: Radio Astronomy Targets" later.

The radiometer has only moderate *gain*, or amplification, stability, with a maximum drift of 10 K/min. Terminal jacks allow connection to a digital voltmeter (DVM) or an analog-to-digital converter (ADC) for input into a personal computer if a digital record is desired. Although the schematic displays a microammeter, its output terminals provide a DC output in millivolts. Accordingly, we will refer to the output of the system as millivolts. As noted above, the radiometer detects only one of the two linear polarizations of radio waves.

As will be discussed in section "Radio Telescopes: Bandwidths" below, we will place the system at a height of 1.3 m, 4 ft, above the sand box. The cable connecting the

Fig. 11 The RTL-11 Portable Radio Telescope utilizes the same Ku-band receiver as that designed for our purposes, but uses the more directional 32-cm (1-ft) diameter parabolic antenna

LNB to the IF Processing Box, as shown in Fig. 10, is about 3 ft long. Accordingly, the IF Processing Box itself will be placed on a platform above the sand box.

In using this system indoors, you should try to minimize the amount of fluorescent lights which are turned on. The many 150-W light bulbs used to heat the soil samples should create enough light in the laboratory that no fluorescent lights are needed. Although fluorescent bulbs generate visible light by the recombination of ionized atoms, the many free electrons generate microwave noise of intensity equivalent to that of a blackbody heated to a temperature of about 10,000 K. The fluorescent bulbs, of course, are in the ceiling and do not directly radiate into the horn antenna of the RTL-11H. That noise, however, can be reflected into the antenna by metal, people, and the calibration water baths and soil samples themselves.

A system similar to the RTL-11H and also designed by the Spacek Labs engineers, the RTL-11 Portable Radio Telescope, uses the same receiver but a larger parabolic dish antenna, Fig. 11. With a diameter of 32 cm, slightly larger than 1 ft, it provides a 5° main lobe and maximum side lobes 18 dB lower (a factor of about 60) than the main lobe. Although this system is less expensive than the RTL-11H, the necessity to locate the antenna at significant heights above the soil sample, because of the greater distance from large compared to small antennas at which the beam pattern forms, may make this system unsuitable for an indoor laboratory environment. In addition, the side lobes, being much stronger than those of the RTL-11H, may receive significant emission from people in the laboratory, including their hands. These are the concerns which led us to adopt the RTL-11H for use

in this experiment and in Experiment #15, "Thermal Radiation from a Planetary Subsurface: Part II. Soil Sample Measurements".

4. Sand Box Dimensions

Knowing the specifications of our receiver and the wavelength of observation, we can determine the appropriate dimensions of the sand box holding our soil samples. With uniform illumination over its aperture, the horn antenna at 2.7 cm-wavelength provides HPBWs in the two directions, given by λ/D, of $\theta_1 = (2.7\text{ cm})/(6\text{ cm}) = 25.8°$ by $\theta_2 = (2.7\text{ cm})/(10\text{ cm}) = 15.5°$. The first side lobe can be calculated to be depressed below the maximum of the main lobe by 13 dB, equivalent to a factor of $10^{1.3} = 20$. Because, furthermore, the angular extent of the first side lobe is much smaller than that of the main lobe, as shown in Figs. 5 and 6, the error incurred by the side lobe viewing an object at ambient temperature, such as the table or floor on which the sand boxes sit, is less than 5%.

As in Experiment #10, "Determination of the Rotation Rate of Planets and Asteroids by Radar: Part II. Observations of Simulated Planets," the microwave radiation gathered by the antenna is mixed with radiation provided by a local oscillator. Because the receiver will be close to the soil sample in the laboratory, some of that radiation could be reflected by the soil sample and detected by the radiometer. To minimize this effect, the Spacek engineers suggest that the antenna and LNB portion of the receiver should be placed at least 1 m above the soil samples. We will place the system at a height of 1.3 m, 4 ft, above the sand box.

We can now determine the required size of the sand box. Figure 12 shows the geometry for a simplified antenna pattern. The required sand box size is accordingly, $L = 2D \tan \theta/2$. With the radiometer placed 1.3 m above the soil samples, the dimensions of sand boxes required to intercept the entire main lobe of the antenna beam are calculated to be about 60 cm by 34 cm, or about 24 in. by 14 in.

With either the RTL-11 or the RTL-11H radiometer, we should use somewhat larger square sand boxes for several reasons. We want to ensure that the main lobe of the antenna beam pattern falls entirely on the soil sample and that a minimum amount of radiation from other objects in the laboratory gets into the side lobes. The large angular extent of the beam pattern and anticipated imprecision in positioning the antenna directly over the center of the sand box create these concerns. A larger size will also allow much of the radiation coming from the incandescent light bulbs to fall on the surface of the soil samples and will prevent a significant loss of heat by conduction through the sides of the sand box walls. The latter consideration is especially important if the RTL-11 system with its large side lobes is being used. We also prefer to use square sand boxes. Because the narrow part of the aperture of the horn generates a larger beam in the perpendicular direction than does the wide dimension, the large side of a rectangular sand box should be oriented perpendicular to the long dimension of the horn, as shown in Fig. 8. The confusion

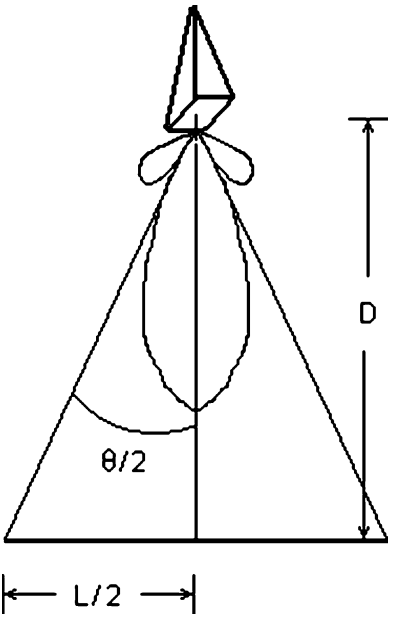

Fig. 12 With the distance of the radiometer above the sand box determined and the angular size of the main beam known, the size of the sand box required to intercept the entire main beam can be calculated. A somewhat larger sand box should be used to reduce the amount of stray radiation received from other objects in the laboratory in the side lobes. This simplified view of the antenna power pattern is plotted using polar coordinates

that can easily result from this suggests using a square sand box of the dimension corresponding to the smaller of the horn dimensions.

With such considerations, two and one-half foot square sand boxes are employed. Such dimensions will minimize the amount of stray radiation received in both the main lobe and the side lobes from any objects in the laboratory other than the calibration and soil samples.

As noted above, the depth of the sand boxes should be slightly greater than 60 cm, about 2 ft. The resulting 2.5 × 2.5 × 2-ft dimensions of the sand boxes is equivalent to 12.5 ft^3 of soil sample material.

5. *Radiometer Calibration: Use of Water Baths*

As in all quantitative astronomical observations, we must first calibrate our instrument, here the microwave radiometer. This has two aspects. First, we want to calibrate the radiometer scale. Instead of using internal loads as is done in professional radio astronomy, in the laboratory we can use a simple technique. We take a substance which is an excellent radiator of microwaves, that is, having an emissivity close to unity, and measure its radiation at widely-separated temperatures. Second, we want to monitor the changes of the gain of the total power receiver with time, which arise from numerous factors including time-varying voltage of the power supply and time-varying ambient temperature.

Assuming a linear dependence of the voltage output of the radiometer on the temperature of the test object, we can determine the calibration scale by taking two measurements. This is the same as determining the slope and *y*-intercept of the straight line relating the voltage reading and the temperature of the object. Subsequent voltage readings of our soil samples can then be converted to the effective temperature of the soil samples either numerically or graphically. Because we will be performing this calibration frequently, we will use the numerical approach. (The various constants in the Rayleigh-Jeans approximation, discussed in Experiment #17, "Blackbody Radiation," are common to all measurements, and therefore need not be included explicitly in this mathematical procedure.)

Several objects can serve the purpose of being a calibration target. They should have two characteristics. First, their actual physical temperature should be known or measureable accurately. Second, the emissivity of the material at Ku-band should be close to 1.0, which means that it emits the maximum amount of radiation given its temperature and reflects very little radiation at these frequencies.

Both a thick layer of wet newspapers, with its dark ink, and charcoal grilling briquets have emissivities close to 1.0 and are suggested by the Spacek Labs engineers. To avoid the mess with those samples, we can use *microwave absorbers*. A suitable microwave absorber for our purposes is a commercially-produced piece of dark foam material with 2–3 in. diameter cones extending upwards from the surface, a foam *pyramidal absorber*, as shown in Fig. 8. For all three materials, we could use the ambient temperature for one measurement and heat them to a high temperature in an oven or with a heat gun and then measure its temperature with a thermometer or infrared thermocouple placed just inside the surface of the material for the second measurement. This technique, suggested by Spacek engineers, however has two problems. First, the material will quickly cool, so that the measured temperature and the actual temperature when observed by the radiometer will differ. Second, folds in the newspaper, void spaces among the briquets, and tears in the material of the foam leads to different portions of the samples cooling differentially so that the temperature over the entire sample will vary. These materials, therefore, are not preferred as calibration targets.

Instead we will use containers of water. The first will be an ice-water bath, whose temperature is accurately known to be $T = 273.2$ K. The second will be a boiling-water bath, whose temperature is accurately known to be $T = 373.2$ K.

Using water also has two problems. The first problem concerns steam coming from the boiling-water bath. Not only will the water vapor enter the antenna, but it also radiates at microwave wavelengths, a process that will be discussed in Experiment #17, "Blackbody Radiation". To eliminate this problem, we place a thin sheet of plastic over the boiling-water bath.

Because the emissivity of plastic is not 1.0, its use causes two subsididary problems. First, of course, we have effectively changed the emissivity of the water by covering it with plastic. To correct for this, we will also observe an ambient-temperature water bath, both uncovered and covered with the plastic sheet. Second, the plastic will reflect some of the microwaves bouncing around the laboratory, from the walls, electrical circuits, and people, into the antenna. To

minimize this problem, we will use not a flat plastic sheet but a thin sheet of plastic bubble-wrap to create a rough, less reflective surface.

Water not having an emissivity equal to 1.0, but rather about 0.97, poses a second problem for its use in calibration. It will reflect about 3% of the radiation that impinges on it. This will not be a severe problem with the rough surfaces of the ice-water bath and the two baths covered with the thin sheet of plastic bubble-wrap. To minimize it with the uncovered ambient-temperature water bath, gently stir the container of water immediately prior to its measurement. Our calibration measurements will be corrected for the non-unity emissivity of water.

The water containers should have the same areal dimensions as the soil sample box, 2.5 × 2.5 ft. A depth of 1 ft is sufficient for the calibration. This amounts to about 47 gal of water for each of the three containers. Because of the weight of this amount of water, the three water containers are also seated on a platform mounted on casters for rolling into position under the antenna. One container of water should stand overnight in the laboratory to enable it to reach room temperature.

6. *Radiometer Calibration: The Procedure*

In this experiment we will measure the signal from unheated soil samples, which we will refer to as "nighttime" observations. With all the samples at room temperature, this will enable us to gain experience in using the radiometer, determine the random errors in the temperature measurements and the magnitude of gain variations, and discover if any systematic differences in the signals from the three soil samples exist, either among them or with depth. In Experiment #15, "Thermal Radiation from a Planetary Subsurface: Part II. Soil Sample Measurements," we will use this experience to measure the signal from the heated soil samples. Throughout the experiment, try to keep your hands from under the antenna. Your body emits radiation at the 11 GHz frequency of the experiment.

We want to prevent spurious signals being received by the radiometer. As noted above, when the following calibration measurements are being taken, the sand boxes of soil samples, even though they are at room temperature, should be placed sufficiently distant from the antenna to ensure that no radiation from them enters the main lobe or close side lobes of the antenna. Similarly, when soil sample measurements are being taken in the next section of the experiment, the water baths should be placed sufficiently distant from the antenna. Care should also be taken to position the sand boxes distant from the antennae of other groups in the laboratory.

First, we must set the zero and gain settings of the microammeter. Because all the measured signals will be greater than the signal received from the ice-water bath, we use an observation of the ice-water bath to establish the zero of the microammeter. Attach the plumb bob to the antenna and roll the ice-water bath into position below the antenna. Adjust the position of the water container until its center is directly under the plumb bob. Remove the plumb bob. Read the signal from this bath and set the zero of the microammeter to read about one-fifth of the

total scale. This is a reading of 10 divisions if the microammeter scale has a total of 50 divisions. Enter the position of this zero setting on the DATA SHEET.

We now use the signal received from the boiling-water bath to set the gain of the microammeter. Roll the ice-water bath from below the antenna and roll the boiling-water bath into position under it, again using the plumb bob to center it under the antenna. The boiling-water bath should be covered by a thin sheet of plastic bubble-wrap. Read the signal from the boiling-water bath, and adjust the gain of the microammeter so that it reads about three-quarters of the microammeter scale. Enter the position of this gain setting on the DATA SHEET. For consistency between observations, use the same zero and gain settings throughout the experiment.

Also enter the microammeter reading obtained with the boiling-water bath in column 2 of Table 2 of the DATA SHEET. If you are using an analog-to-digital converter to record the data, enter that result in Table 2.

With the zero and gain settings now set, roll the boiling-water bath from under the antenna, roll the ice-water bath into position using the plumb bob, and reread the signal from the ice-water bath. Enter the result in column 1 of Table 2 of the DATA SHEET. If you are using an analog-to-digital converter to record the data, enter that reading in Table 2.

We now measure the signal from the ambient-temperature water bath, both with and without an overlaid thin sheet of plastic bubble-wrap, in order to determine a correction factor for the emissivity of the plastic sheet. Use different thin sheets of bubble-wrap plastic for the ambient-temperature water bath and the hot-water bath measurements. Roll the ice-water bath from below the antenna and roll the ambient-temperature water bath into position under it. Remember to gently stir the uncovered ambient-temperature water bath to create a rough, less reflective surface. Enter these microammeter readings in columns 3 and 4 of Table 2 of the DATA SHEET. If you are using an analog-to-digital converter to record the data, enter those results in Table 2.

7. "Nighttime" Soil Sample Measurements

We will perform some "trial runs" of the observations that we will perform repeatedly in Experiment #15, "Thermal Radiation from a Planetary Subsurface: Part II. Soil Sample Measurements". There we will measure the soil temperatures and signals emitted by the heated soil samples. Here we measure the unheated, "nighttime" soil temperatures and signals. As noted above, to prevent a bias in your measurements resulting from the measurement of only one of the two linear polarizations of radiation by the radiometer, the material in the sand boxes should be stirred to prevent any clumping of material in a given direction. In all these measurements, use the plumb bob suspended from the antenna to ensure that the antenna is positioned directly above the center of the sand boxes.

We measure the signals from each of the sand boxes in turn. Roll the sand box containing the granite soil sample into position under the antenna. Attach the plumb bob to the antenna and adjust the position of the sand box until its center is directly

under the plumb bob. Remove the plumb bob. Enter the beginning time of the observation in Table 3 of the DATA SHEET. Read the signal and enter the result in Table 3 of the DATA SHEET. Then roll the sand box away from the antenna.

Repeat these measurements using the soil sample box containing sand and the soil sample box containing sand partially immersed in water. Enter the results in Table 3 of the DATA SHEET.

To obtain a measure of the gain stability of the receiver of the RTL-11H radiometer, repeat these measurements a total of four times, separated by 5-min intervals. Enter all results in Table 3 of the DATA SHEET. Enter the ending time of the observation in Table 3 of the DATA SHEET.

These "nighttime" signals may not be exactly the same, varying with characteristics of the materials such as their emissivities and surface roughnesses, which are related to the sizes of their constituent particles.

8. "Nighttime" Temperature Measurements

For each of the soil samples, obtain the thermometer readings at each depth. Enter the results in columns 2, 3, and 4 of Table 4 of the DATA SHEET in degrees K. All the temperatures should be the same, close to room temperature, about 74°F, equivalent to 23°C or 296 K. Their variation will provide one measure of the random statistical random errors we will expect in the measurements of Experiment #15, "Thermal Radiation from a Planetary Subsurface: Part II. Soil Sample Measurements".

D. Calculations and Analysis

1. The Soil Sample

Calculate the mean values of the sizes of the granite, rocks, and coarse sand that you entered in Table 1 of the DATA SHEET. Also calculate the standard deviations of these two mean values. Show all your calculations on the DATA SHEET. Enter the results in Table 1 of the DATA SHEET.

2. Radiometer Calibration

Divide the output of the radiometer received from the "Ambient Water Bath Without Plastic Sheet" from column 3 of Table 2, by the output received from the "Ambient Water Bath With Plastic Sheet" from column 4 of Table 2. Enter the result, the correction factor, f_s, in column 5 of Table 2.

Multiply the value of the boiling-water bath output in column 2 of Table 2 by the correction factor, f_s. Enter the result in column 6 of Table 2. This is now the value of the boiling-water bath output corrected for the emissivity of the plastic sheet.

We now determine the calibration equation, which will allow us to convert the microammeter reading from the radiometer to temperatures,

$$T = a + bV.$$

where V is the microammeter reading and T is the temperature of the soil sample at 11 GHz. Calculate the coefficients a and b of the calibration equation, using

$$T_i = a + b\ V_i$$
$$T_b = a + b\ V_b,$$

where the temperature of the ice-water bath is $T_i = 273.2$ K, the temperature of the boiling-water bath is $T_b = 373.2$ K, and V_i and V_b are the microammeter readings when observing the ice-water bath and (corrected) boiling-water bath, respectively. The solution of these two equations in two unknowns is easily shown to be

$$a = T_b - (T_b - T_i)/(V_b - V_i)V_b \tag{2}$$

$$b = (T_b - T_i)/(V_b - V_i). \tag{3}$$

Using the data in Table 2, solve for the values of a and b. Show all your calculations on the DATA SHEET.

A correction for the non-unity value of the emissivity of water must be made to these data. To correct for a representative value of emissivity of 0.97, it is easily shown that we must multiply the values of a and b, and therefore the calibrated temperatures, by an additional factor $f_e = 1.03$. We therefore arrive at the corrected calibration equation,

$$T = f_e(a + b\ V). \tag{4}$$

3. *Soil Sample Observations and Gain Variations*

With this corrected calibration equation, convert the values of soil sample output from column 4 of Table 3 of the DATA SHEET to calibrated soil sample output. Enter those values in column 5 of Table 3. Show all your calculations on the DATA SHEET.

For each soil sample, calculate the mean and standard deviation among the four calibrated temperatures that you have entered in column 5 of Table 3. Show your calculations on the DATA SHEET and enter the results in columns 6 and 7 of Table 3 of the DATA SHEET.

To determine if the mean calibrated temperatures vary with physical characteristics of the soil sample, namely the surface roughness, construct a graph of the mean calibrated intensity as a function of particle size. Use the graph paper on the DATA SHEET or your own graph paper. Use the standard deviations from Table 1 for the size of error bars along the abscissa scale and the standard deviations from column 7 of Table 3 for the size of error bars along the ordinate scale. You will have two points on the graph, one corresponding to the granite and one corresponding to the dry sand.

To evaluate the magnitude of gain variations of the receiver of the RTL-11H radiometer, construct a graph of the four measurements for each soil sample of the calibrated output as a function of time. Use the graph paper on the DATA SHEET or your own graph paper. For the first datum in each set of four, use the beginning time as entered in column 2 of Table 3 for the abscissa value. For the last datum in each set of four, use the ending time as entered in column 3 of Table 3 for the abscissa value. For the second and third data, use an interpolated time. Use different symbols for the three soil samples. For the zero of the abscissa scale, use a time equal to the nearest whole hour before the first observation. Show error bars corresponding to the standard deviations you have entered in column 7 of Table 3 of the DATA SHEET.

Draw a best-fit straight line through each of the three sets of four data points corresponding to the three soil samples and determine the y-intercept and slope of the three straight lines. These slopes are measures of the gain variation in the receiver of the RTL-11H radiometer over the period of about an hour in which we made the observations. Perform all your calculations on the DATA SHEET.

We can also use these results to get an estimate of the uncertainty in the measurement of the signals. In general, we need to calculate the squares of the deviations of the data points from the best-fit straight line. This is done using Eq. (1) of Experiment #2, "A Review of Graphing Techniques". Perform the calculation on the DATA SHEET for each of the three sets of four data points corresponding to the three soil samples. (If the straight line that you drew through the data of the various soil samples is perfectly flat, then the standard deviation you entered in column 7 of Table 3 will be close in value to this result, depending on how closely the y-intercept you determined equals the mean value entered in column 6 of Table 3.)

The average of these three square deviations provides our estimate of the random errors in the measurement of the radiation intensity. Calculate that average and then calculate the square root to obtain the error estimate, σ_I. Perform all your calculations on the DATA SHEET.

4. "Nighttime" Temperature Measurements

In Table 4 of the DATA SHEET, you entered the values of temperature at six depths for each soil sample. Calculate the mean values and standard deviations at each of

the six depths of the three values of temperatures measured for the three soil samples. Enter the results in Table 4 of the DATA SHEET.

Construct a graph on the graph paper provided on the DATA SHEET or on a piece of your own graph paper of these six mean temperatures as a function of depth and draw a best-fit straight line to the data. Construct error bars based on the values of the standard deviations entered in Table 4. Because all temperatures should be about the same, room temperature, the line should have zero slope indicating no dependence on depth.

Calculate the mean value, $<T>_{room}$, and standard deviation, σ_{room}, of all 18 temperature measurements. This is a measure of the statistical uncertainty in the measurement of the subsurface temperatures. Show all your calculations on the DATA SHEET.

STUDENT'S NAME _____

E. Planetary Subsurface Experiment I Data Sheet

1. Soil Samples

Table 1 Size of soil material

Sample	Granite	Coarse sand
1		
2		
3		
4		
5		
6		
7		
8		
9		
10		
Mean value		
Standard deviation		

Calculation of mean particle size, granite:

Calculation of standard deviation, granite:

Calculation of mean particle size, sand:

Calculation of standard deviation, sand:

2. Calibration Data

STUDENT'S NAME _____

Zero setting of the radiometer: _____
Gain setting of the radiometer: _____

Table 2 Calibration data and measured "nighttime" readings

Ice-water bath output, V_i (millivolts)	Boiling water bath output, V'_b (millivolts)	Ambient water bath without plastic sheet, V_1 (millivolts)	Ambient water bath with plastic sheet, V_2 (millivolts)	$f_s = V_1/V_2$	Corrected boiling water bath output, $V_b = f_s V'_b$ (millivolts)

Determination of calibration equation. Show your calculations here.

y-intercept, a = _____ slope, b = _____

3. "Nighttime" Soil Sample Observations

STUDENT'S NAME _____

Table 3 Observed and calibrated outputs

Sample/observation	Beginning time	Ending time	Output (millivolts)	Calibrated output (K)	Mean value	Standard deviation
Granite Obs. #1						
Granite Obs. #2						
Granite Obs. #3						
Granite Obs. #4						
Sand Obs. #1						
Sand Obs. #2						
Sand Obs. #3						
Sand Obs. #4						
Sand in water Obs. #1						
Sand in water Obs. #2						
Sand in water Obs. #3						
Sand in water Obs. #4						

STUDENT'S NAME _____

Calibrated Outputs

Show your calculations of the calibrated outputs calculated from (4), $T = f_e(a + bV)$, for each of the four measurements of each soil sample.

Granite:

Sand:

Sand partially immersed in water:

Mean values and standard deviations

Show your calculations here of the means and standard deviations of the calibrated outputs for each soil sample.

Granite:

Mean value of granite calibrated outputs (K) = _____
Standard deviation of granite calibrated outputs (K) = _____

Sand:

Mean value of sand calibrated outputs (K) = _____
Standard deviation of sand calibrated outputs (K) = _____

Sand partially immersed in water:

Mean value of sand partially immersed in water calibrated outputs (K) = _____
Standard deviation of sand partially immersed in water calibrated outputs (K) = _____

STUDENT'S NAME _____

Graph of the mean calibrated intensity as a function of particle size

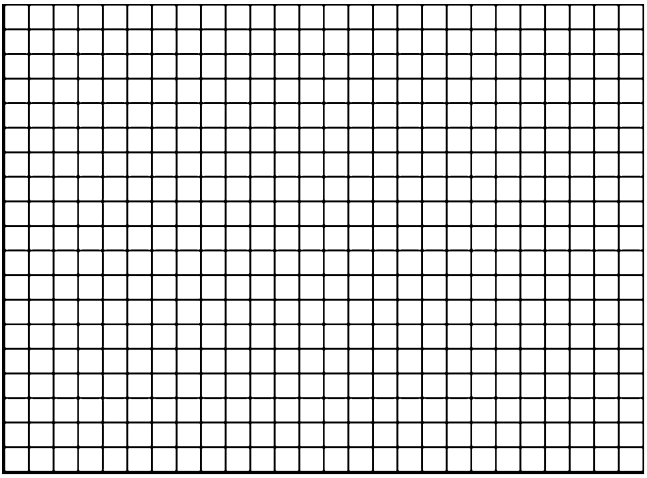

Graph of the mean calibrated intensity as a function of particle size.

Do you find a variation?

Do you expect to find a variation? Explain your answer.

Graph of the four measurements of the calibrated output as a function of time

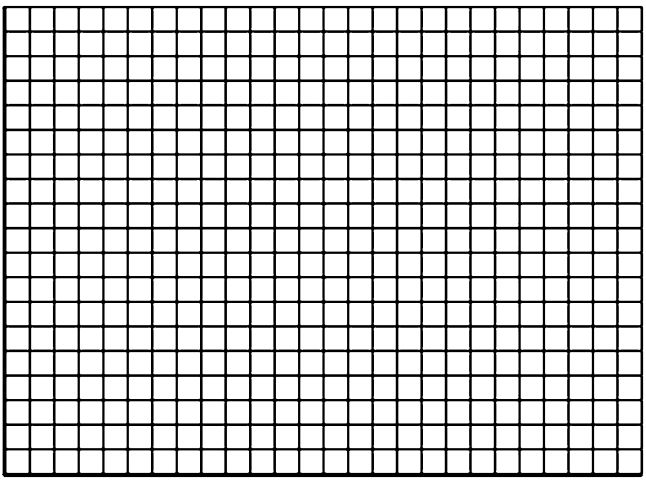

STUDENT'S NAME _____

Use different symbols for the three soil samples.

Calculation of the y-intercept and slope of the line for each soil sample.

Granite:

y-intercept = _____ K
slope = _____ K/minute

Sand:

y-intercept = _____ K
slope = _____ K/minute

Sand partially immersed in water:

y-intercept = _____ K
slope = _____ K/minute

STUDENT'S NAME _____

Calculation of the squares of the deviations of the data from the best-fit curve

Granite:

Sand:

Sand partially immersed in water:

Calculation of the average of those three squares of the deviations and its square root

Uncertainty, σ_I = _____

4. "Nighttime" Temperature Measurements

Table 4 "Nighttime" temperatures

Depth (cm)	Granite (K)	Sand (K)	Sand immersed in water (K)	Mean value (K)	Standard deviation (K)
0.5					
1					
3					
10					
25					
60					

Do you find a variation of temperature with depth?

STUDENT’S NAME _____

Do you expect one? Explain your answer.

Calculation of mean temperature and standard deviation

Show your calculations here of the means and standard deviations of the temperatures at each depth.

Calculation of mean temperature and standard deviation, 0.5 cm:

$< T > =$ _____
$\sigma =$ _____

STUDENT'S NAME _____

Calculation of mean temperature and standard deviation, 1 cm:

$< T > =$ _____
$\sigma =$ _____

Calculation of mean temperature and standard deviation, 3 cm:

$< T > =$ _____
$\sigma =$ _____

Calculation of mean temperature and standard deviation, 10 cm:

$< T > =$ _____
$\sigma =$ _____

Calculation of mean temperature and standard deviation, 25 cm:

$< T > =$ _____
$\sigma =$ _____

Calculation of mean temperature and standard deviation, 60 cm:

$< T > =$ _____
$\sigma =$ _____

Calculation of the mean temperature and standard deviation of all 18 measurement. Show your calculations here.

$< T >_{\text{room}} =$ _____
$\sigma_{\text{T-room}} =$ _____

STUDENT’S NAME _____

Graph of mean values of temperatures as a function of depth for “nighttime” observations

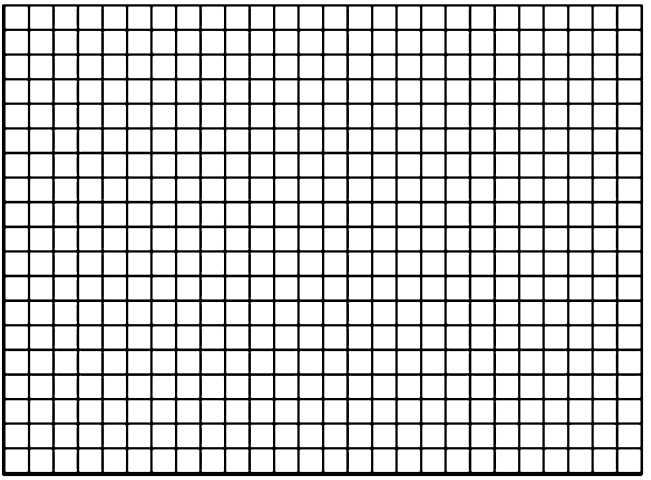

STUDENT'S NAME _____

F. Planetary Subsurface Experiment I Discussion Questions

1. For the "nighttime" measurements of intensity, compare the intensities received from each of the soil samples on your graph. Do they agree within their standard deviation or are do they differ significantly? If they differ significantly, how can you explain that?

2. The temperature of the ice bath is 273.2 K. The temperature of your body is about 98.6°F, or 310 K. If you were using a microwave antenna that had very poor directional characteristics, so that a side lobe received radiation from the entire surface of your hand at 100% efficiency, what temperature would the calibrated microwave radiometer detect rather than 273.2 K? Assume that your hand is placed next to the ice water bath container, that the main lobe of the antenna pattern has 100% efficiency, and that the main lobe obtains radiation from the entire surface of an ice water bath which is 80 cm on a side.

   a. What additional parameter must be estimated to enable you to make this calculation? Provide a value for that parameter here.

   b. Perform the calculation.

   c. Calculate the percentage error that would result from the presence of the strong side lobe.

3. You have created a graph of the mean calibrated intensities as a function of particle size.

   a. Does it show a variation with particle size?

STUDENT'S NAME _____

b. If so, which type of particle is associated with the greatest mean value of intensity?

c. The color of granite rock can be pinkish or gray depending on its composition. The sand that you used may be dark or light. As you will learn in Experiment #17, "Blackbody Radiation," dark-colored objects generally have greater values of emissivity than light-colored objects. Depending on the color of the material that you used, did this effect increase or decrease any difference between the two values of mean calibrated intensities?

Removing these DATA SHEETS from the book may damage the binding. You might consider entering the data and performing your calculations in the book, and then photocopying the DATA SHEETS for submission to your instructor for grading.

If you used graph paper other than that provided, attach those graphs to these DATA SHEETS.

Experiment 15
Thermal Radiation from a Planetary Subsurface: Part II. Soil Sample Measurements

SUMMARY: In Experiment #15, "Thermal Radiation from a Planetary Subsurface: Part II. Soil Sample Measurements," you will continue the investigations of Experiment #14, "Thermal Radiation from a Planetary Subsurface: Part I. Calibration and Initial Measurements". Here, incandescent light bulbs shine upon the surface of the soil samples, simulating the Sun, while thermometers record the changing temperatures at various depths with time. You will use a microwave receiver operating at 11 GHz to detect the radiation being emitted by the subsurface layers and compare the results among the various soil samples.

LEVEL OF DIFFICULTY: Moderate

EQUIPMENT NEEDED: Fragmented granite rock, coarse sand, water, and ice; 2.5 × 2.5 × 2-ft sand boxes; 2.5 × 2.5 × 1-ft water containers; Ku-band radiometer with horn antenna; digital thermometers; meter stick; thin sheets of plastic bubble-wrap; heating coils; plumb bob; 150-W incandescent bulbs and socket assembly, light baffles.

MY LEARNING GOALS

1. To be able to describe how mathematics represents the physical process of heat conduction.
2. To be able to describe how concepts of radiative transfer allows us to understand the nature of subsurface materials.
3. To be able to describe how the microwave radiation from a planet depends on the nature of its subsurface material.

L.M. Golden, *Laboratory Experiments in Physics for Modern Astronomy: With Comprehensive Development of the Physical Principles*,
DOI 10.1007/978-1-4614-3311-8_15,

A. Introduction

In Experiment #14, "Thermal Radiation from a Planetary Subsurface: Part I. Calibration and Initial Measurements," we were introduced to the heating of a surface by a source such as the Sun or a star, the conduction of heat from the surface to subsurface layers, and the outward-directed radiation that results from those warmed subsurface layers. We calibrated the microwave radiometers used for the experiment and measured the radiation received when the soil samples are all at room temperature. In this experiment, we will turn on the source of the heat, incandescent light bulbs, and perform the same measurements. We will discover how the radiation changes with the various materials and with the length of time of exposure to the energy source.

This experiment requires almost constant recording of data. Instead of two or three students working together, groups of four students should be assigned to each station. Two should record the temperature measurements and two should record the measurements from the microwave radiometer. Halfway through the laboratory class period, the roles can be interchanged so that each student will get experience in each mode and so that the first pairs can share the techniques in data acquisition that they have acquired with the second pairs.

B. Theory

Let us say we have a source of energy of intensity S_o shining upon a surface, given in energy per second per unit area. In the case of the Sun, this incident energy is called the *insolation*. The heated surface radiates energy depending on its temperature and physical characteristics of the material of which it is composed. The dependence on temperature is given by *Planck's Radiation Law*, an idealized description of materials radiating with perfect efficiency which is the subject of Experiment #17, "Blackbody Radiation".

Real materials don't radiate with perfect efficiency, however, and that lack of perfection is incorporated by a dimensionless factor of value less than unity called the *emissivity*, ε, a characteristic of the surface material. The emissivity of crushed or fragmented rocky materials is typically 0.7–0.9. Some very dark-colored materials have an emissivity close to 1. Light-colored materials have lower values of emissivity. Emissivities for some common materials are provided in Table 1. (In general, emissivity varies with the temperature of the sample and the wavelength of the radiation being observed).

Once the surface is heated, the energy that is not radiated outward from the surface propagates downward by the process of *heat conduction*. This is one of the three familiar modes of heat transfer, along with convention and radiation.

The *equation of heat conduction*, a special case of the *diffusion equation*, follows from the law of conservation of energy. It is known empirically (Fourier's Law;

Table 1 Emissivities of some materials

Material	Emissivity
Aluminum foil	0.04
Basalt	0.72
Granite	0.45
Graphite powder	0.97
Gravel	0.28
Gypsum ($CaSO_4 \cdot 2H_2O$)	0.085
Ice (rough or smooth)	0.966–0.985
Limestone	0.96
Sand	0.76–0.90
Soil (dry)	0.92
Soil (saturated with water)	0.95
Water	0.95–0.98

Jean Baptiste Joseph Fourier, 1768–1830) that the rate of flow of heat across a surface is proportional to the gradient of the temperature across that surface; that is, in time Δt the amount of heat flowing across a surface of area A is,

$$\Delta Q = -k_{th} \frac{dT}{dx} A \, \Delta t,$$

where in one dimension the gradient is the ordinary spatial derivative and where the constant of proportionality k_{th} is the *thermal conductivity* of the material, having the dimensions of Watts/m-K. This represents the common experience that the greater the temperature variation the greater the amount of heat that flows in a given interval of time. The negative sign represents heat flowing from the warmer to the colder region.

From conservation of energy, absent any other sources of energy, this flow of heat of ΔQ across the surface into the material of thickness Δx and the resulting temperature rise leads to an equal increase ΔQ in the internal energy in the material manifested by a change over time in its temperature, ΔT,

$$\Delta Q = c_p \rho \, \Delta T \, A \, \Delta x,$$

where the *specific heat capacity*, c_p, is a characteristic of the material describing the temperature response of the material to the introduction of heat and ρ is its density. The increase in internal energy in the material over a given time period is accounted for entirely by the flow of heat across the boundary in that time period.

By using the integral calculus to sum over finite time periods and a finite distance, the heat conduction equation relating these two phenomena can be derived. The resulting distribution of temperature as a function of t and x depends, therefore, on the thermal conductivity, the specific heat capacity, and the density of the material. It provides the rate of change of temperature at all locations in the medium. An example of the solution of the heat conduction equation along a bar in which these properties have been given uniform values is provided graphically in Fig. 1.

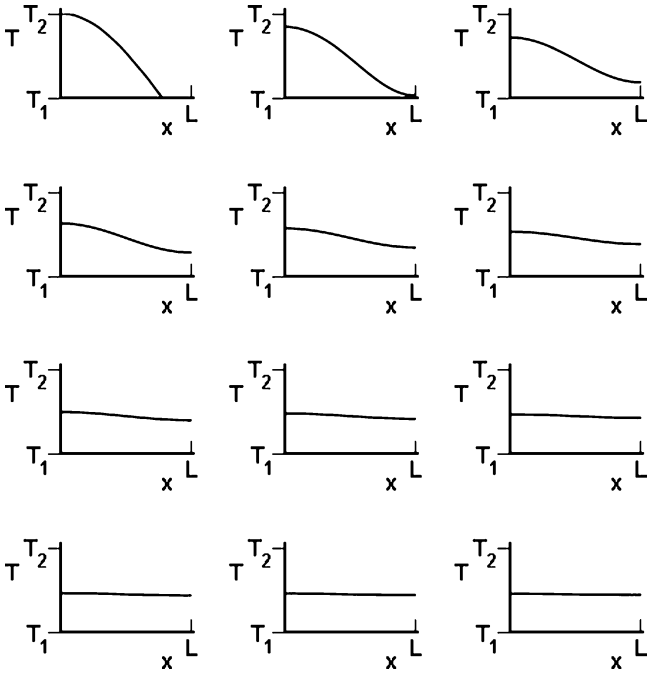

Fig. 1 The solution of the heat conduction equation in one dimension for initial temperatures varying as shown from T_1 to T_2 along a uniform bar of length L. The time interval between each frame is constant, but of arbitrary size

The result in one dimension is

$$\frac{dT}{dt} = \frac{k}{\rho c_p} \frac{d^2T}{dx^2}, \tag{1}$$

where $k/(\rho c_p)$ is referred to as the *thermal diffusivity*. From (1), the thermal diffusivity thereby characterizes the transient heat flow through a material. Because materials with large values of thermal diffusivity have relatively large values of dT/dt, they relatively quickly change their temperature in the presence of temperature gradients. This makes sense. They have large thermal conductivities and low capacity to absorb energy without experiencing an increase in temperature. As a result, when heated they reach thermal equilibrium with their surroundings relatively quickly.

From (1), we can interpret the appearance of Fig. 1. Examine the curvature of the temperature profile, that is, the change with depth of the gradient, $d^2T/dx^2 = d/dx\ (dT/dx)$, at a given time. Where the curvature is negative, such as near $x = 0$, the temperature gradient decreases with depth. Equation (1) shows that the rate of change of the temperatures at those depths is negative, so that the temperature is decreasing with time. That is shown by the subsequent graphs. On the other hand, at depths at which the curvature is positive, so that the temperature

gradient increases with depth, the rate of change of the temperatures is positive. This indicates that the temperature is increasing at those depths.

At the extremes, if the material has a thermal diffusivity of zero, then the temperatures at any depth will not change with time as the insolation varies. The material is a perfect insulator. If the material has a large thermal diffusivity, then the temperatures will change rapidly with time as the insolation varies.

In deriving this equation, we have assumed that k, ρ, and c_p are constants. In fact, thermophysical studies of the Moon, lunar rocks, and the planet Mercury have shown that k is a function of temperature and depth in a planetary surface, ρ is a function of depth, and c_p is a function of temperature. In Particular, the thermal conductivity depends not only on actual physical contact between soil particles but also on a transfer of energy between particles by radiation. This radiative contribution has been found from studies of lunar soils to have a T^3 dependence. As a result, at high temperature it can provide a greater contribution to the thermal conductivity than the actual physical contact. The thermal conductivity has an additional contribution on planets with atmospheres, where energy is transferred between soil particles by collisions with gas molecules. Accordingly, we see that energy transport by condition in planetary surface can in fact occur by all three familiar modes, conduction, convection, and radiation. In general, solution of the heat conduction equation for planetary subsurfaces must therefore be performed numerically.

Examining equation (1), we see that a characteristic depths can be determined from deimensional analysis. The resulting diffusion coefficient or diffusion depth is given by

$$D(t) = \sqrt{\frac{k}{\rho c_p}}\, t. \tag{2}$$

It is reasonable to consider this as the depth to which a temperature change has occurred as a function of time.

Table 2 provides the thermal diffusivities of some materials. The values range five orders of magnitudes among natural materials. These values are not determined by simply combining the factors of k, ρ, and c_p. Instead they are determined directly in laboratory studies as a function of temperature. The values provided are representative.

Once the subsurface layers are warmed by heat conduction to a temperature T, they radiate as blackbodies. That energy propagates outwards through the material by the process of *radiative transfer*. In this, the heated material not only radiates as a blackbody but also absorbs some radiation impinging upon it from the lower levels, as shown in Fig. 2. This process depends only on the density of the material and its electrical absorption coefficient, k_{elec},

$$\frac{dI}{dx} = \rho k_{elec}[B(v,T) - I],$$

where typical values for k_{elec} are 0.05 cm^2/g and $B(v,T)$ is the formula for Planck's Radiation Law, Eq. (1) of Experiment #17, "Blackbody Radiation". The Planck curve for an idealized object at 6000 K, close to the effective temperature of the Sun, is shown in Fig. 1 of Experiment #17, "Blackbody Radiation".

Table 2 Thermal diffusivities of some materials

Substance	Thermal diffusivity (m^2/s)
Wood (yellow pine)	8.2×10^{-8}
Water	1.4×10^{-7}
Silicon dioxide (polycrystalline)	8.3×10^{-7}
Sandstone	1.2×10^{-6}
Quartz	1.4×10^{-6}
Air (1 atm, 300 K)	2.2×10^{-5}
Water vapor (1 atm, 400 K)	2.3×10^{-5}
Iron	2.3×10^{-5}
Aluminum	8.4×10^{-5}
Copper	1.1×10^{-4}
Pyrolytic graphite flow parallel to layers	1.2×10^{-3}

Pyrolytic graphite is a synthetic material whose thermal properties make it useful in the manufacture of such items as heat sinks, rocket nozzles, and heating elements

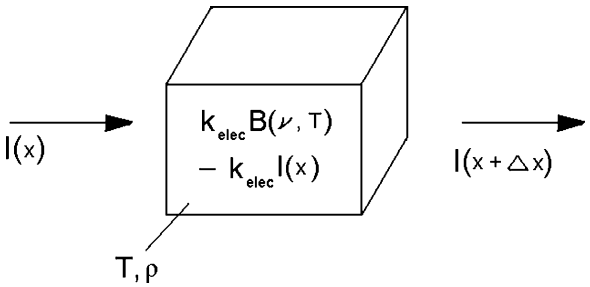

Fig. 2 In the process of radiative transfer in a planetary surface, a volume element of material of density ρ and electrical absorption coefficient k_{elec} both absorbs incoming radiation and emits additional radiation according to its temperature

The intensity of radiation we receive thereby depends on these many characteristics of the soil material and its temperature. That is why astronomers find such studies to be of great value. The values of characteristics for some materials are provided in Table 3. The density ρ of water is by definition 1 g/cm^3. The porous igneous rock, pumice, has a smaller density than this, depending on its porosity, and actually floats in water.

In the microwave region of the electromagnetic spectrum at which these types of studies are made and at which we are performing our experiment, $B(\nu,T)$ is approximately proportional to T with fair to excellent precision. For a body at Earth-like temperatures of 300 K, the approximation is very good for $\lambda > 2.5$ mm. In our experiment at a wavelength of about 2.7 cm, the approximation is excellent.

This is not only a good approximation, but it is also very convenient. The measurement by a microwave radiometer of the emitted radiation is then directly proportional to the temperature of the emitting body. For us, the calibration of the

Table 3 Thermal properties of common materials

Material	Density (kg/m^3)	Specific heat (J/kg-K)	Thermal conductivity (W/m-K)
Water	1000	4186	0.58
Pumice	641	200	0.5–2.5
Solid rock (granite)	2691	790	2–7
Sand	1602	835	0.30
Wet sand	1922	1931	2.20
Dry soil	1249	800	1.5
Wet soil	1602	1480	2–4
Air, 300 K	1.3	1100	0.024

microwave radiometer in Experiment #14, "Thermal Radiation from a Planetary Subsurface: Part I. Calibration and Initial Measurements," by reference to the known temperatures of an ice-water bath and a boiling-water bath means that our measurements of the heated soil materials we are about to perform can be directly converted to temperature. For real materials, $B(v,T)$ is also proportional to the emissivity, e, of the material.

C. Procedure and Observations

1. The Incandescent Light Bulbs

As shown in Fig. 7 of Experiment #14, "Thermal Radiation from a Planetary Subsurface: Part I. Calibration and Initial Measurements," sets of four 150-W incandescent light bulbs are mounted on rigid stationary platforms, one set for each sand box. They simulate the radiation coming from the Sun or any other star about which planets are located. The light bulbs are closely spaced to ensure heating of the soil samples directly below them. The heights of the light bulb assembly can be adjusted. Your laboratory may choose to use infrared lamps as the source of radiation.

Although the light bulbs will be turned off when measurements of the radiation from the soil samples are actually being made, they will still be hot and radiating energy, heating the antenna and receiver. Accordingly, they are shielded from the microwave radiometer by baffles, such as pieces of styrofoam, to prevent radiation from the light bulbs from entering the antenna. Styrofoam itself has a sizable emissivity of 0.60, but because it will be seen in the side lobes of the antenna it will not contribute substantial amounts of radiation. Gypsum, the component of dry wall, with an emissivity of 0.085, is also suitable, although its greater density may create a problem in mounting.

When a sand box is rolled into position under the radiometer, the light bulbs should be turned off. After measurements are made of the signals from the sand box

and the soil temperatures, the sand box is rolled back under the light bulb assembly and the light bulbs are turned back on.

On the Earth, the surface is heated by sunlight for hours as the Sun passes through the sky. We, in the laboratory, lack this time luxury but we need to have significant amounts of energy reaching the surfaces of the soil samples in no more than 1 h in order to provide measurable effects. This requires the light bulbs to be placed relatively close to the surface of the soil samples, no more than 15 cm above the surface. Using a meter stick, check to see that the light bulbs assemblies for the three soil samples are located so that the light bulbs are 15 cm above the surfaces of each of the soil samples. To enable valid comparison of the results among the three soil samples, the light bulb assemblies should be the same heights above each sand box.

2. *Radiometer Calibration*

In Experiment #14, "Thermal Radiation from a Planetary Subsurface: Part I. Calibration and Initial Measurements," we measured the signals from unheated soil samples, which we referred to as "nighttime" observations. Here, we will use this experience to measure the signals from heated soil samples.

As discussed in Experiment #14, "Thermal Radiation from a Planetary Subsurface: Part I. Calibration and Initial Measurements," in these indoor observations, you should try to minimize the amount of fluorescent lights which are turned on. The many 150-W light bulbs used to heat the soil samples should create enough light in the laboratory that no fluorescent lights are needed. Although fluorescent bulbs generate visible light by the recombination of ionized atoms, the many free electrons generate microwave noise of intensity equivalent to that of a blackbody heated to a temperature of about 10,000 K. The fluorescent bulbs, of course, are in the ceiling and do not directly radiate into the horn antenna of the RTL-11H. That noise, however, can be reflected into the antenna by metal, people, and the calibration water baths and soil samples themselves.

The gain variations expected with the RTL-11H radiometer requires that we calibrate the system by measuring the signals from the ice-water bath and boiling-water bath frequently. In Experiment #14, "Thermal Radiation from a Planetary Subsurface: Part I. Calibration and Initial Measurements," we calibrated the system only once. Here, the measurements of the soil temperatures will delay the time between measurements of the signals from the soil samples. Accordingly, it is prudent at first to calibrate the system before measuring the signals from each soil sample. If during your observations you find that the signals from the ice-water bath and boiling-water bath do not change rapidly over a few minutes, then you can reduce the frequency of your calibration measurements and perform the calibration before each set of observations of the three soil samples.

Measuring the signals from the ambient-temperature water bath, to determine the emissivity of the thin sheet of plastic bubble-wrap, need only be performed

once. In all these calibration measurements, use the plumb bob suspended from the antenna to ensure that the antenna is positioned directly above the center of the water containers. Use different thin sheets of plastic bubble-wrap for the ambient-temperature water bath and the hot-water bath.

First, as in Experiment #14, "Thermal Radiation from a Planetary Subsurface: Part I. Calibration and Initial Measurements," we must set the zero and gain settings of the microammeter. Because all the measured signals will be greater than the signal received from the ice-water bath, we use an observation of the ice-water bath to establish the zero of the microammeter. Attach the plumb bob to the antenna and adjust the position of the water container until its center is directly under the plumb bob. Remove the plumb bob. Read the signal from this bath, and set the zero of the microammeter to read about one-fifth of the total scale. This is a reading of 10 divisions if the microammeter scale has a total of 50 divisions. Enter the position of this zero setting on the DATA SHEET.

We now use the signal received from the boiling-water bath to set the gain of the microammeter. Roll the ice-water bath from below the antenna and roll the boiling-water bath into position under it, again using the plumb bob to center it under the antenna. The boiling-water bath should be covered by a thin sheet of plastic bubble-wrap. Read the signal from the boiling-water bath, and adjust the gain of the microammeter so that it reads about three-quarters of the microammeter scale. Enter the position of this gain setting on the DATA SHEET. For consistency between observations, use the same zero and gain settings throughout the experiment. These settings should be very close to those obtained in Experiment #14, "Thermal Radiation from a Planetary Subsurface: Part I. Calibration and Initial Measurements".

Because this measurement is going to be used as the first calibration for the granite soil sample, enter the time as the "Actual Time Begin" in row 2, column 2, of Table 4 of the DATA SHEET. Enter the microammeter reading obtained with the boiling-water bath in row 5, column 2, of Table 4 of the DATA SHEET. If you are using an analog-to-digital converter to record the data, enter that result in Table 4.

With the zero and gain settings now set, roll the boiling-water bath from under the antenna, roll the ice-water bath into position using the plumb bob, and reread the signal from the ice-water bath. Enter the result in row 4, column 2, of Table 4 of the DATA SHEET. If you are using an analog-to-digital converter to record the data, enter that reading in Table 4.

We now measure the signal from the ambient-temperature water bath, both with and without an overlaid thin sheet of plastic bubble-wrap, in order to determine a correction factor for the emissivity of the similar thin sheet of bubble-wrap plastic that is placed over the boiling-water bath. This water bath should be left to stand overnight to ensure that its temperature reaches room temperature. The result for the correction factor, f_s, that we will calculate later should be very similar to that of Experiment #14, "Thermal Radiation from a Planetary Subsurface: Part I. Calibration and Initial Measurements," but the possibility of a different room temperature and the effect it may have on the emissivity of the plastic material recommends that the calibration be performed here as well.

Roll the ice-water bath from below the antenna and roll the ambient-temperature water bath into position under it. Measure the signal with and without the overlaid plastic sheet. Remember to gently stir the uncovered ambient-temperature water bath to create a rough, less reflective surface. Enter these microammeter readings on the DATA SHEET. If you are using an analog-to-digital converter to record the data, enter those results on the DATA SHEET.

As noted, at first repeat the calibration of the system using the ice-water bath and the boiling-water bath before each observation of the soil samples. As you proceed, you may be able to reduce the frequency of calibrations. In either case, you need not repeat the determination of the emissivity of the thin sheet of plastic bubble-wrap.

During the laboratory session, the boiling water in the boiling-water bath will cool. To keep its temperature as close to 373.2 K as possible, keep it covered with the thin sheet of plastic bubble-wrap and submerge several plugged-in resistive electric coils below the surface when the signal from the boiling-water bath is not being measured.

3. *Heated Soil Sample Measurements*

We now measure the temperatures within the soil samples and the radiation emitted by the soil samples as the soil samples are heated. Some coordination among students and attention to detail is needed to ensure we get good quality data. First, as noted in Experiment #14, "Thermal Radiation from a Planetary Subsurface: Part I. Calibration and Initial Measurements," the microwave radiometer we will use detects only one of the two linear polarizations of radiation. To prevent a bias in your measurements, the material in the sand boxes should be stirred to prevent any clumping of material in a given direction.

One pair of students should perform the soil temperature measurements and a second pair of students should measure the signals. Repeat this cycle of measurements every 15 min, at 15, 30, 45, 60, and 75 min. The roles of the pairs of students can be alternated after the first three cycles have been completed. If you haven't done so during the data taking, share the techniques you have developed with each other at this point. Throughout the experiment, try to keep your hands from under the antenna. Your body emits radiation at the 11 GHz frequency of the experiment.

We do not want the soil samples to significantly cool during the measurement of their temperatures and emissions. When the soil samples are rolled out from under the incandescent light bulbs into position under the antenna, they will begin to cool by radiating energy. To minimize this, the sand boxes should be rolled into position under the antenna quickly so that the temperature and signal measurements can be performed as soon as possible after heating of the soil samples has ceased.

After the soil temperatures and signals from the soil samples have been measured, quickly roll the sand boxes out from under the antenna and back under its set of incandescent light bulbs and turn the lamps back on. With care, the effect will not be great. The heat loss is greatest near the surface, to which measurements of the 2.7 cm-wavelength radiation is not particularly sensitive. In all these

measurements, use the plumb bob suspended from the antenna to ensure that the antenna is positioned directly above the center of the sand boxes. Some loss of heat by conduction through the walls of the sand box will occur.

During the entire sequence of observations, the boiling-water bath should be covered with its thin sheet of plastic bubble-wrap.

We want to prevent spurious signals being received by the radiometer. Consequently, when soil sample measurements are being taken, the water baths should be placed sufficiently distant from the antenna to ensure that no radiation from them enters the main lobe or close side lobes of the antenna. Similarly, when calibration measurements are being taken, the sand boxes of soil samples, whether heated or at room temperature, should be placed sufficiently distant from the antenna. Care should also be taken to position the water baths and soil samples far from the antennae of other groups in the laboratory.

With this preparation, we now measure the signal from each of the sand boxes in turn. Our first measurement, corresponding to a time, $t = 0$, will be of unheated samples. As in Experiment #14, "Thermal Radiation from a Planetary Subsurface: Part I. Calibration and Initial Measurements," all these temperatures should be the same, close to room temperature, about 74°F, equivalent to 23°C or 296 K.

Roll the sand box containing the granite soil sample into position under the antenna. One pair of students should attach the plumb bob to the antenna and adjust the position of the sand box until its center is directly under the plumb bob. Remove the plumb bob. Measure the signal received by the radiometer and enter the result in row 6, column 2, of Table 4 of the DATA SHEET. The second pair of students should pull out the thermometers from each depth, read the temperatures, and enter the temperatures in degrees K in rows 8 through 13, column 2, of Table 4 of the DATA SHEET. After all readings have been entered, enter the "Actual Time End" in row 14, column 2, of Table 4 of the DATA SHEET. Then roll the sand box away from the antenna. Position it under the incandescent light bulbs and turn them on. Rotate the baffles so that the light does not shine on the RTL-11H antenna or receiver.

As we did with the granite soil sample, we now calibrate the radiometer for the first measurement of the sand soil sample. Roll the ice-water bath into position under the antenna, and adjust its position until its center is directly under the plumb bob. Remove the plumb bob. Measure the signal with the microammeter. Enter the time as the "Actual Time Begin" in row 2, column 2, of Table 5 of the DATA SHEET. Enter the microammeter reading in row 4, column 2, of Table 5 of the DATA SHEET. If you are using an analog-to-digital converter to record the data, enter that result in Table 5. Roll the ice-water bath from under the antenna. Remove the heating coils from the boiling-water bath and unplug them. Then roll the boiling-water bath under the antenna, using the plumb bob to ensure it is directly centered under the antenna. Enter the microammeter reading bath in row 5, column 2, of Table 5 of the DATA SHEET.

Roll the boiling-water bath from under the antenna, place the heating coils under its surface, and plug them in. Roll the sand box containing sand under the antenna and position it, as always, using the plumb bob. Remove the plumb bob. Measure the signal received by the radiometer and enter the result in row 6, column 2, of Table 5 of the DATA SHEET. The second pair of students should pull out the

thermometers from each depth and enter the temperatures in rows 8 through 13, column 2, of Table 5 of the DATA SHEET. After all readings have been entered, enter the "Actual Time End" in row 14, column 2, of Table 5 of the DATA SHEET. Then roll the sand box away from under the antenna. Position it under the incandescent light bulbs and turn them on. Rotate the baffles so that the light does not shine on the RTL-11H antenna or receiver.

Repeat the same sequence for the sand box containing sand partially immersed in water. Enter those data in the corresponding rows and columns of Table 6 of the DATA SHEET. After its measurement, enter the "Actual Time End" in row 14, column 2, of Table 6 of the DATA SHEET. Then roll the sand box away from under the antenna. Position it under the incandescent light bulbs and turn them on. Rotate the baffles so that the light does not shine on the RTL-11H antenna or receiver.

Repeat these sequences of calibration and measurement of the soil temperatures and signals from the soil samples at approximately 15 min intervals. In each case, enter the beginning time, calibrate, measure the temperatures and signal from the soil sample, and enter the ending time. All data are entered in Tables 4, 5, and 6 of the DATA SHEET for the granite, sand, and sand partially immersed in water soil samples, respectively.

As you will learn, measurement of microwave signals is an art. To ensure the data are comparable, remember to perform the following operations. Keep the ceiling fluorescent bulbs off as much as possible. When a soil sample has been rolled under the antenna for measurement, turn its incandescent light bulbs off. When it is rolled back under the lamp assembly, turn the lamps back on. When the boiling-water bath is about to be measured, remove and unplug the heating coils. When its measurement is completed, replace and plug the heating coils back in. Keep the boiling-water bath covered with the thin sheet of plastic bubble-wrap. Because you may fall behind in your measurements, you need to record the actual time you begin each measurement cycle and the actual time you complete each measurement cycle. At some time during the laboratory session, sufficient water may have evaporated from the boiling-water bath that it may need to be partially refilled. Try to do this more rather than less frequently so that the small amounts of water are added, allowing the boiling-water bath to stay hot enough to remain boiling.

When you are completed, turn off all the incandescent light bulbs and unplug the heating coils inserted into the boiling-water bath.

D. Calculations and Analysis

1. Calibration and Gain Variation

Determine the correction factor, f_s by dividing the reading from the ambient-temperature water bath without the plastic sheet by the reading from the ambient-temperature water bath with the plastic sheet.

For each of the pairs of calibration observations of the ice-water bath and boiling-water bath, calculate the values of the calibration equation coefficients, a and b, by Eqs. (2) and (3) of Experiment #14, "Thermal Radiation from a Planetary Subsurface: Part I. Calibration and Initial Measurements". Show your calculations on the DATA SHEET. Remember to first multiply the value of the reading from the hot-water bath by the correction factor, f_s, for the emissivity of the plastic sheet. Summarize the results in Table 7 of the DATA SHEET. In column 2 of Table 7 enter the values of "Actual Time Begin" from Tables 4, 5, and 6 corresponding the various calibration experiments.

To see the gain variation more clearly, construct a graph of the values of a and b as a function of the "Actual Time Begin." Use different symbols to distinguish among the three soil samples. Describe the magnitude and trend of the gain variation on the DATA SHEET.

Using the various calibration equations, from Eq. (4) of Experiment #14, "Thermal Radiation from a Planetary Subsurface: Part I. Calibration and Initial Measurements," $T = f_e\,(a + b\,V)$, calculate the calibrated outputs for each soil sample measurement. Enter the results in Table 8 of the DATA SHEET. Enter the "Actual End Time" from Tables 4, 5, and 6 corresponding to the measurement of the soil samples.

2. *Heat Penetration Graphs*

On the graph paper provided on the DATA SHEET or your own sheet of graph paper, construct a graph of the calibrated outputs of the soil samples as a function of time. For the values of time use the "Actual Time End" provided in Table 8. Those are the times closest to the actual times of observation of the emission from the soil samples. Plot the data for all three soil samples on the same graph, thereby producing a family of curves with the soil sample as the parameter. Use different symbols for each of the soil samples.

In Sect. E.3 of Experiment #14, "Thermal Radiation from a Planetary Subsurface: Part I. Calibration and Initial Measurements," you calculated a standard deviation of calibrated outputs, σ_I. On the heat penetration graph, use that value of standard deviation to place error bars on the data. Draw a smooth curve through the six data points for each soil sample. These being experimental data, the line should represent the trend but need not pass directly through all the data points. It should, however, fall within or reasonably close to all the error bars placed on the data points. These three curves show how the radiation changed with the length of time of exposure to the incandescent light bulbs.

Figure 3 shows how this graph should be designed. This should not be taken to indicate the nature of the experimental results you may find.

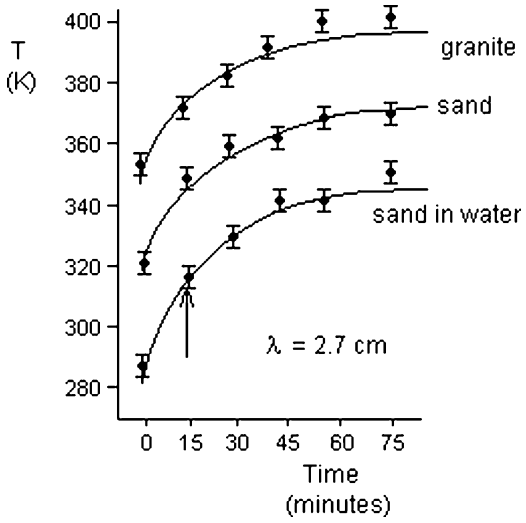

Fig. 3 Example of an "heat penetration graph," calibrated output as a function of time

3. *Temperature Profile Graphs*

On the graph paper provided on the DATA SHEET or your own sheets of graph paper, construct a graph of the temperatures of the soil as a function of depth for each nominal time of measurement. For the values of time use the "Actual Time End" provided in Table 8. Those are the times closest to the actual times of measurement of the temperatures. Plot the data for all three soil samples on the same graph, thereby producing a family of curves with the soil sample as the parameter. If necessary for clarity, use different symbols for the different soil samples, labeled accordingly.

In Sect. E.4 of Experiment #14, "Thermal Radiation from a Planetary Subsurface: Part I. Calibration and Initial Measurements," you calculated a standard deviation of room temperature measurements, $\sigma_{T\text{-}room}$. On the temperature profile graph, use that value of standard deviation to place error bars on the data. Draw a smooth curve through the six data points for each soil sample corresponding to the depth of the thermometers. These being experimental data, the line should represent the trend but need not pass directly through all the data points. It should, however, fall within or reasonably close to all the error bars placed on the data points.

This will produce a total of six graphs, corresponding to the six nominal times of observation. If necessary for clarity, use different symbols for the different soil samples, labeled accordingly. These three curves show how the temperature changed with depth with time of exposure to the incandescent light bulbs.

Figure 4 shows how these graphs should be designed. Again, this should not be taken to indicate the nature of the experimental results you may find.

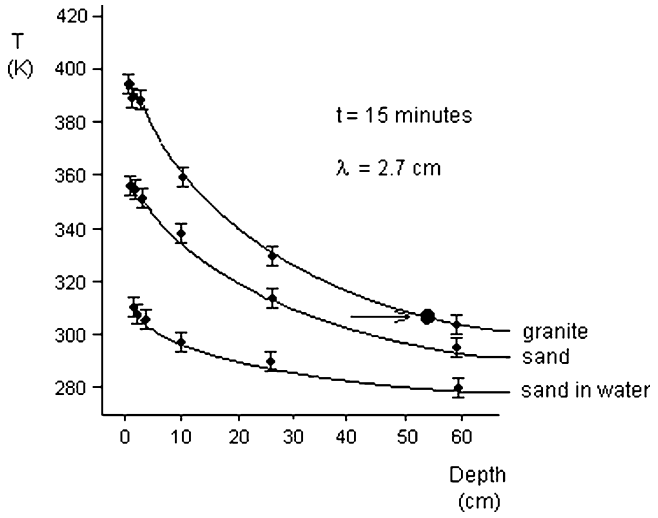

Fig. 4 Example of a "temperature profile graph," thermometer temperature as a function of depth

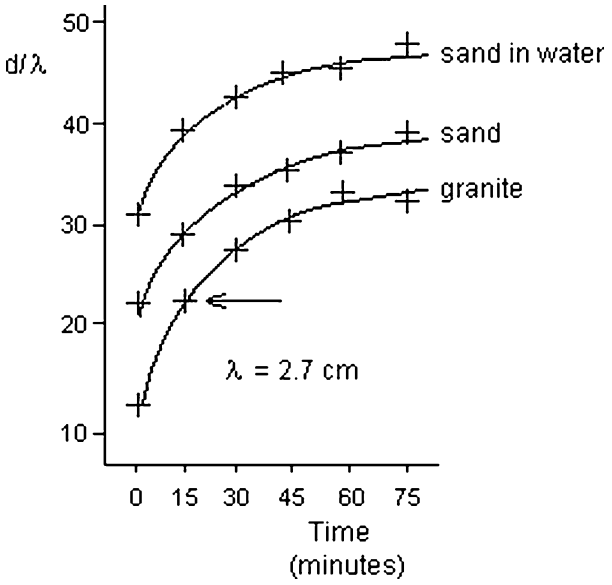

Fig. 5 Example of an "effective depth graph," depth of emission divided by wavelength as a function of time

4. *Effective Depth Graphs*

From the heat penetration graph of each soil sample, read the value of calibrated output from the smooth curve for each of the six nominal times of measurement. On the corresponding six temperature profile graphs, place a circle on the curve of the particular soil sample at the value of temperature which equals that calibrated output. Those circles will correspond to a given depth as read on the abscissa scale. Figure 5 shows how these circles should be placed on the temperature profile graphs.

We recall that the radiative transfer equation, (1), shows that the radiation arises from all depths in the subsurface. The depths at which the subsurface temperature equals the calibrated output can be considered a quasi-"effective" depth from which the radiation is emitted.

In Table 9 of the DATA SHEET, summarize the values of depth, d, at which the subsurface temperatures and calibrated outputs are equal. To adjust the depths according to the wavelength of observation, in the rightmost three columns enter the values of these depths divided by the wavelength, $\lambda = 2.7$ cm, of observation, d/λ.

On the graph paper provided on the DATA SHEET or your own sheet of graph paper, construct a graph using the data of Table 9 of the values of d/λ at which the calibrated output equals the subsurface temperature as a function of the nominal times of observation. Plot the data for all three soil samples on the same graph, thereby producing a family of curves with the soil sample as the parameter. If necessary for clarity, use different symbols for the different soil samples, labeled accordingly.

Draw a smooth curve through the six data points for each soil sample corresponding to the nominal times of observation. These being experimental data, the line should represent the trend but need not pass directly through all the data points.

Connect the points for each soil sample with a smooth curve, but, again, be sure to represent the trend of the data, not any preconceived ideas. Figure 5 shows how these graphs should be designed. Figure 5 should not be taken as indicating the nature of the experimental results you may find.

Figures 3, 4, and 5 illustrate how the graphs should be constructed. The arrows refer to a specific datum, the observation of the intensity of radiation at 2.7-cm-wavelength from the granite soil sample at the nominal time of 15 min. In Fig. 3, at 15 min the calibrated intensity is 317 K. This corresponds in Fig. 4 to a depth of 55 cm. Dividing 55 cm by the wavelength of 2.7 cm gives a value of $d/\lambda = 20$, which is the location of the data point in Fig. 5.

Describe on the DATA SHEET any difference in the graphs between the soil samples, noting in particular the effect of values of emissivity and thermal diffusivity.

5. Diffusion Depths

From the temperature profile graphs for each soil sample for each time, we can estimate the depths to which the energy has reached as a function of time for each soil sample. Estimate the greatest depth at which the temperature has risen above room temperature at each nominal time. Enter those estimates in Table 10 on the DATA SHEET. Construct a graph of those results, plotting the results for all three soil samples on the same graph.

STUDENT'S NAME _____

E. Planetary Subsurface Experiment II Data Sheets

Calibration of thin sheet of plastic bubble-wrap:

Ambient water bath without plastic sheet, V_1 = _____ (millivolts)
Ambient water bath with plastic sheet, V_2 = _____ (millivolts)
$f_s = V_1/V_2$ = _____

Table 4 Measured temperatures and outputs: granite

Nominal Times	t = 0 min	t = 15 min	t = 30 min	t = 45 min	t = 60 min	t = 75 min
Actual time begin						
Output (millivolts)						
Ice-water bath						
Boiling-water bath						
Soil sample						
Temperatures (K)						
0.5 cm						
1 cm						
3 cm						
10 cm						
25 cm						
60 cm						
Actual time end						

STUDENT'S NAME _____

Table 5 Measured temperatures and outputs: sand

Nominal Times	t = 0 min	t = 15 min	t = 30 min	t = 45 min	t = 60 min	t = 75 min
Actual time begin						
Output (millivolts)						
Ice-water bath						
Boiling-water bath						
Soil sample						
Temperatures (K)						
0.5 cm						
1 cm						
3 cm						
10 cm						
25 cm						
60 cm						
Actual time end						

STUDENT'S NAME _____

Table 6 Measured temperatures and outputs: sand immersed in water

Nominal Times	t = 0 min	t = 15 min	t = 30 min	t = 45 min	t = 60 min	t = 75 min
Actual time begin						
Output (millivolts)						
Ice-water bath						
Boiling-water bath						
Soil sample						
Temperatures (K)						
0.5 cm						
1 cm						
3 cm						
10 cm						
25 cm						
60 cm						
Actual time end						

Determination of calibration equations

Show your calculations here. Remember to first multiply the value of the reading from the hot-water bath by the correction, f_s, for the emissivity of the plastic sheet determined above.

Granite:

t = 0 min.

y-intercept, a = _____ slope, b = _____

t = 15 min.

y-intercept, a = _____ slope, b = _____

t = 30 min.

y-intercept, a = _____ slope, b = _____

t = 45 min.

y-intercept, a = _____ slope, b = _____

t = 60 min.

y-intercept, a = _____ slope, b = _____

t = 75 min.

y-intercept, a = _____ slope, b = _____

STUDENT'S NAME _____

Sand:

t = 0 min.

y-intercept, a = _____ slope, b = _____

t = 15 min.

y-intercept, a = _____ slope, b = _____

t = 30 min.

y-intercept, a = _____ slope, b = _____

t = 45 min.

y-intercept, a = _____ slope, b = _____

t = 60 min.

y-intercept, a = _____ slope, b = _____

t = 75 min.

y-intercept, a = _____ slope, b = _____

STUDENT'S NAME _____

Sand partially immersed in water:

t = 0 min.

y-intercept, a = _____ slope, b = _____

t = 15 min.

y-intercept, a = _____ slope, b = _____

t = 30 min.

y-intercept, a = _____ slope, b = _____

t = 45 min.

y-intercept, a = _____ slope, b = _____

t = 60 min.

y-intercept, a = _____ slope, b = _____

t = 75 min.

y-intercept, a = _____ slope, b = _____

STUDENT'S NAME _____

Table 7 Summary of calibration equation parameters

	Sample	Granite		Sand		Sand in water	
Nominal times (min)	Actual time begin	a (K)	b (K/millivolt)	a (K)	b (K/millivolt)	a (K)	b (K/millivolt)
t = 0							
t = 15							
t = 30							
t = 45							
t = 60							
t = 75							

Graph of values of *a* and *b*. Graph the data for *a* using the left-hand ordinate scale and the data for *b* using the right-hand ordinate scale as a function of the "Actual Time Begin." Use different symbols for the different soil samples.

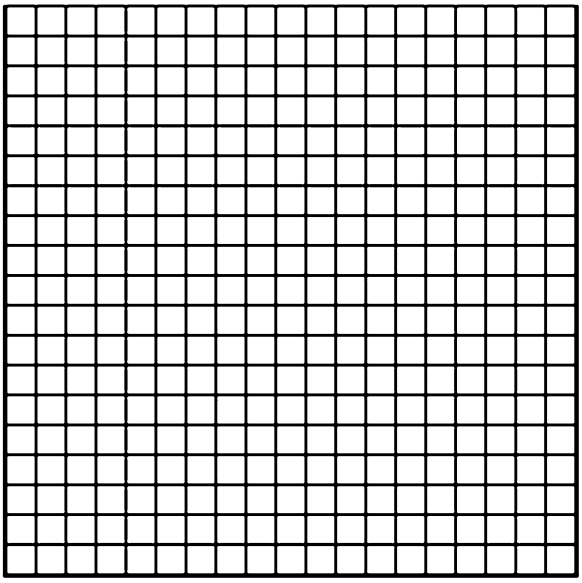

Describe the gain variation you have determined.

STUDENT'S NAME _____

Table 8 Calibrated outputs

Sample	Granite		Sand		Sand in water	
Nominal times (min)	Actual time end	T (K)	Actual time end	T (K)	Actual time end	T (K)
t = 0						
t = 15						
t = 30						
t = 45						
t = 60						
t = 75						

Calculations of the calibrated outputs

Show your calculations of the calibrated outputs calculated from Eq. (4) of Experiment #14, "Thermal Radiation from a Planetary Subsurface: Part I. Calibration and Initial Measurements," $T = f_e\,(a + b\,V)$.

Granite:

Sand:

Sand partially immersed in water:

STUDENT'S NAME _____

Table 9 Depths (cm) at which calibrated radiation output equals subsurface temperature

Soil sample	Granite	Sand	Sand in water	Granite	Sand	Sand in water
	d	d	d	d/λ	d/λ	d/λ
Nominal times (min)						
t = 0						
t = 15						
t = 30						
t = 45						
t = 60						
t = 75						

Heat penetration graph

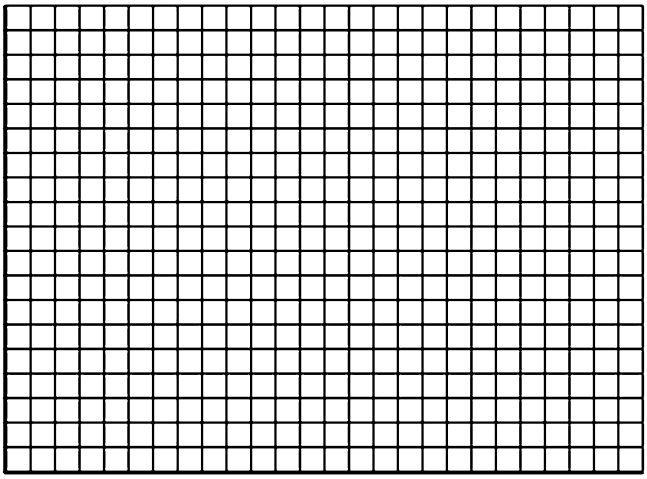

STUDENT'S NAME _____

Construct the "temperature profile" graphs on the page following the next page before constructing the below "effective depth" graph.

Effective depth graph

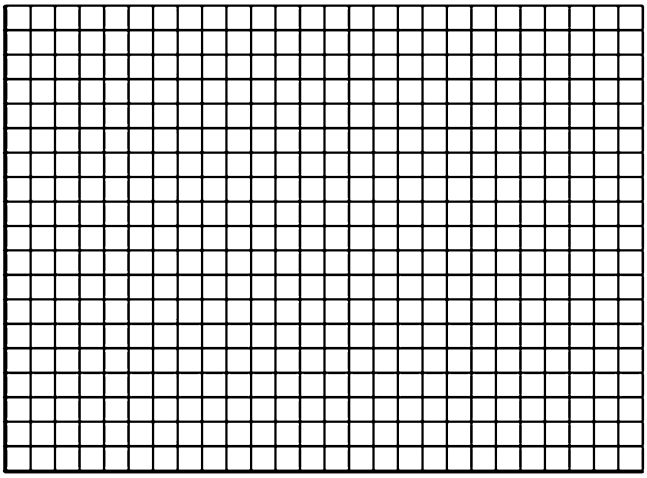

Do the heat penetration graphs, temperature profile graphs, and effective depth graphs differ for the sand partially immersed in water sample soil compared to those for the granite and sand sample soils? Describe any differences.

Can you detect any effect arising from the relative emissivities and thermal diffusivity for granite, sand, and water?

What contribution to such an effect would the void space between the granite rocks provide?

STUDENT'S NAME _____

After a certain amount of time, a steady state should exist in which the amount of heat conducted into the subsurface is balanced by the amount of radiation emitted outwards. It will be manifested by the graph of d/λ as a function of time approaching an asymptote. If this has occurred in any of the soil samples, at about what number of minutes into the heating did it become evident for each?

Temperature profile graphs

Temperature profile graphs

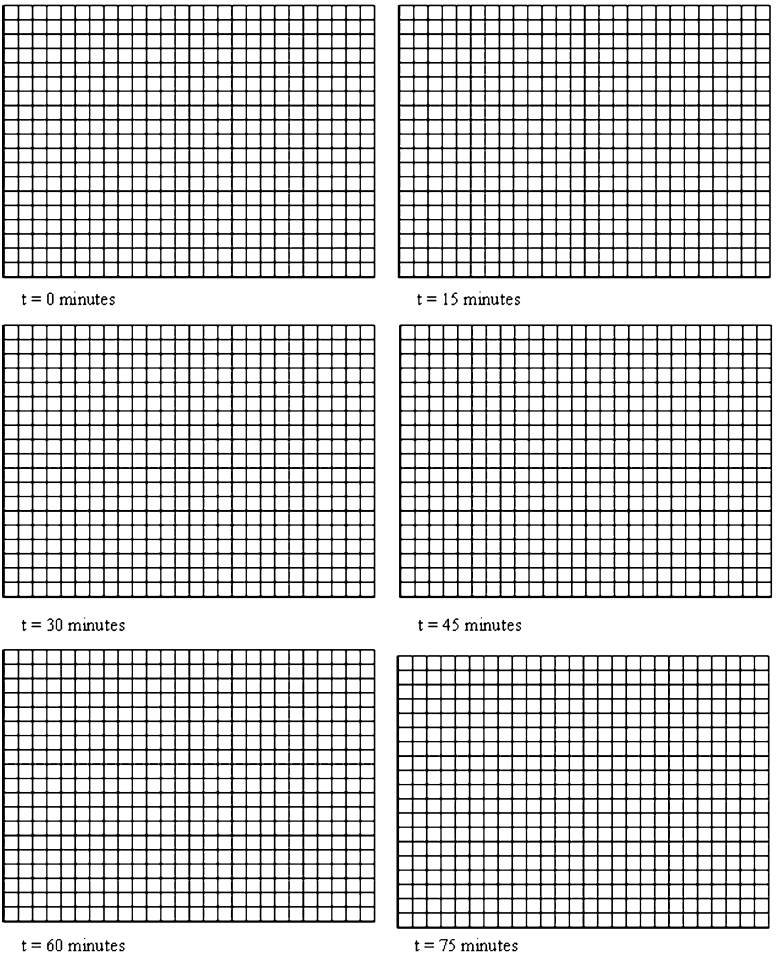

STUDENT'S NAME _____

Table 10 Diffusion Depths (cm)

Soil Sample	Granite	Sand	Sand in water
	D	D	D
Nominal Times			
t = 0 min.			
t = 15 min.			
t = 30 min.			
t = 45 min.			
t = 60 min.			
t = 60 min.			
t = 75 min.			

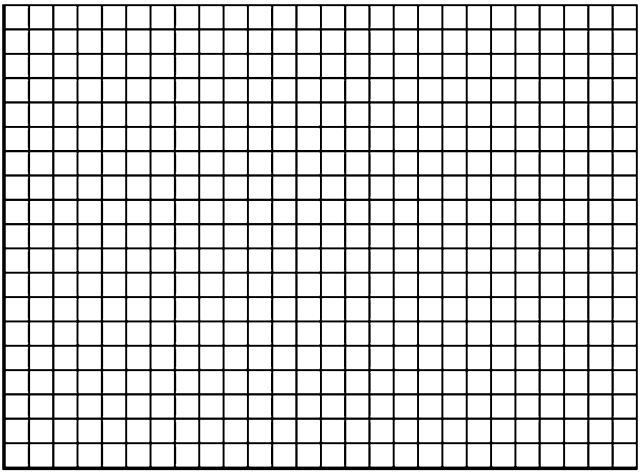

STUDENT'S NAME _____

F. Planetary Subsurface Experiment II Discussion Questions

1. The experiment uses incandescent light bulbs to simulate a star heating the surface of its planets. Why did the experiment not use fluorescent bulbs?

2. Table 10 below provides the average distances of the planets in the solar system from the Sun. Let us say that we have discovered a planetary system about another star and that one of the planets is twice as far from its parent star as the other. Call the near planet "Planet Yxtph" and the far planet "Planet Kqlpr," in a language spoken by a civilization whose location I cannot divulge for reasons of national security and public tranquility.

   a) Which set or sets of two planets in the solar system does this factor of two approximately represent?

   b) The Stefan-Boltzmann Law that you will study in Experiment #17, "Blackbody Radiation," tells us that the total amount of radiation emitted per unit surface area per second of an idealized object known as a blackbody is,

$$F = \sigma T^4, \tag{3}$$

   where T is the surface temperature, expressed in degrees K, and the Stefan-Boltzmann constant $\sigma = 5.67 \times 10^{-8}$ W/m^2-K^4. Assume that all of the radiation incident on these two planetary surfaces is absorbed by, and thereby heats, the surfaces, so that an equilibrium is established between the incoming stellar radiation and the blackbody radiation described by the Stefan-Boltzmann Law. Using the Stefan-Boltzmann Law and Eq. (1) of Experiment #14, "Thermal Radiation from a Planetary Subsurface: Part I. Calibration and Initial Measurements," if the surface temperature at noon on Planet Yxtph is 30°C, what is the surface temperature at noon on Planet Kqlpr? Show your calculations here.

STUDENT'S NAME _____

3. This experiment is performed while we are submersed in the atmosphere of the Earth. How would you expect the results to be changed if the experiment was performed on the surface of an object such as that of Mercury or the Moon, which lack significant atmospheres? How would, in particular, the mechanism of heat conduction be affected?

4. Similarly, how would the mechanism of radiative transport of energy be affected if the experiment were performed on an essentially airless planet?

5. From (1), calculate the amount of time it would take for the temperature to increase from 300 to 320 K in a medium whose density is 1.2 g/cm^3 (1200 kg/m^3), specific heat is 1000 J/kg-K, thermal conductivity is 2 W/m-K and whose value of $\frac{\Delta^2 T}{\Delta x^2}$ is 3 K/cm^2. Show your calculations here.

STUDENT'S NAME _____

6. The specific heat of water is by far the highest of any common substance, Table 3. Helium gas, unknown until it was discovered in the spectrum of the Sun, has a specific heat of the Sun has as specific heat pf 5190 J/kg-K nearly five times larger than of air and 24% larger than that of water. Compare the heat penetrmined temperature profile and effective depth graphs to those determined here for sand to those that might be determined if we observed the microwave radiation from the subsurface of a planet covered with sand that had a pure helium atmosphere. For the sake of this comparison use the temperature profile graph you determined at a nominal time of thirty minutes.

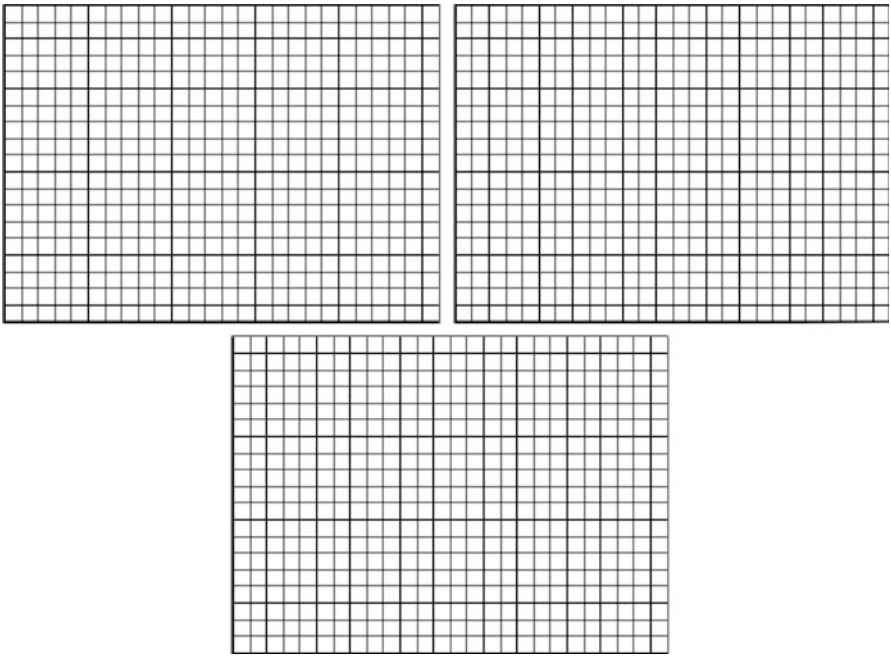

STUDENT'S NAME _____

7. Assuming constant values for the parameters k, ρ, and c_p, the diffusion depth, $D_{(t)}$, varies as the square root of t, equation (2). For a thermal diffusivity of 1.2×10^{-6} m^2/s, the graph of $D_{(t)}$ is shown in Figure 6.

   a) Compare the graph you have constructed for the three soil samples with that of Figure 6. Does each follow the square root dependence?

   b) If they do not, explain the discrepancy between the graph for each soil sample which differs from Figure 6

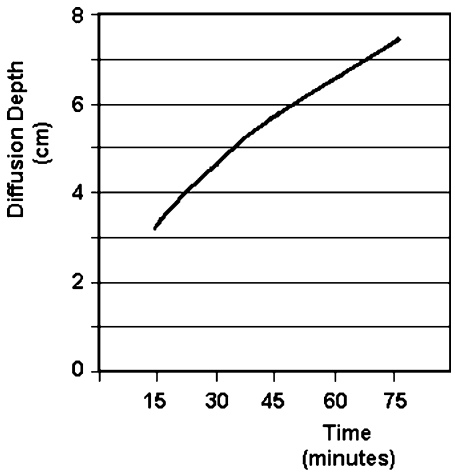

Fig. 6 Diffusion depth as a function of time has a square root dependence for constant values of thermal diffusivity

Removing these DATA SHEETS from the book may damage the binding. You might consider entering the data and performing your calculations in the book, and then photocopying the DATA SHEETS for submission to your instructor for grading.

If you used graph paper other than that provided, attach those graphs to these DATA SHEETS.

STUDENT'S NAME _____

Table 11 Planetary semi-major axes

Planet	Semi-major axis (AU)
Mercury	0.39
Venus	0.72
Earth	1.0
Mars	1.5
Jupiter	5.2
Saturn	9.5
Uranus	19.2
Neptune	30.1
Pluto	39.5

Experiment 16
The Microwave Phase Effect of the Moon

SUMMARY: In this Experiment #16, "The Microwave Phase Effect of the Moon," we connect the receiver of the RTL-11H radio telescope to a communications antenna and observe the Moon over the period of a month. We graph the variation of the 11 GHz emission and the phase angle of the Moon as a function of time and compare the two curves.

LEVEL OF DIFFICULTY: Moderate.

EQUIPMENT NEEDED: Water; ice; 2.5 × 2.5 × 1-ft water containers; Ku-band radiometer with horn antenna; communications antenna; meter stick; thin sheets of plastic bubble-wrap; plumb bob.

MY LEARNING GOALS

1. To be able to predict how the microwave phase effect will change with thermal diffusivity of subsurface soils.
2. To be able to predict how the microwave phase effect will change with the wavelength of observation.
3. To be able to describe the various contributions to the intensity of microwave radiation observed from a "blank" sky.

L.M. Golden, *Laboratory Experiments in Physics for Modern Astronomy: With Comprehensive Development of the Physical Principles*,
DOI 10.1007/978-1-4614-3311-8_16, © Springer Science+Business Media New York 2013

A. Introduction

Radio astronomy had its beginnings in the 1930s in the observations of radio engineers Karl Jansky (1905–1950) at Bell Telephone Laboratories in Holmdel, New Jersey, and Grote Reber (1911–2002) of Wheaton, Illinois. Vigorous observing programs in radio astronomy began following World War II, and although astronomers studied emission from the galaxy and surveyed the entire sky for extragalactic objects they also looked to the nearest objects in the sky for signals.

The Moon was first detected in 1946 and later observations showed that its thermal emission varied with the phases of the Moon. This, of course, was expected. The emission from the Moon in visible wavelengths varies with the phase, the greater the portion of the visible disk illuminated the brighter the Moon. At radio wavelengths, a smaller temperature variation with phase and a phase delay were observed compared to the observations at infrared wavelengths, which emanate from the very surface of the Moon. In addition, a lack of symmetry of the temperatures about the date of the full Moon was observed. These findings indicated that the microwave radiation was being emitted from regions below the lunar surface.

In this experiment, we will use the RTL-11H radio telescope receiver that we used in Experiments #14 and #15, "Thermal Radiation from a Planetary Subsurface: Part I: Calibration and Initial Measurements," and "Thermal Radiation from a Planetary Subsurface: Part II: Soil Sample Measurements," to observe the variation, or *phase effect*, of intensity of the 11 GHz signal from the Moon over a *lunation*, the complete cycle of its phases. If an eclipse occurs during your school semester, it too will be observed.

B. Theory

1. Thermal Diffusivity of the Lunar Subsurface Material

As can be seen from Fig. 1 of Experiment #15, "Thermal Radiation from a Planetary Subsurface: Part II: Soil Sample Measurements," a time delay exists between the heating of the surface of a planet or moon and the flow of that heat to subsurface layers. This makes intuitive sense. The extent of that delay, however, depends upon the values of the thermophysical parameters of the subsurface material such as the heat capacity and thermal conductivity. The heat conduction equation, Eq. (1) of Experiment #15, "Thermal Radiation from a Planetary Subsurface: Part II: Soil Sample Measurements," is parameterized by the thermal diffusivity, thereby explicitly showing this dependence. As discussed there, if the subsurface material possesses large thermal conductivities and small heat capacities the surface heat will be conducted rapidly to the subsurface layers. If, in contrast, the subsurface material possesses small thermal conductivities and large heat capacities the surface heat will be conducted slowly to the subsurface layers.

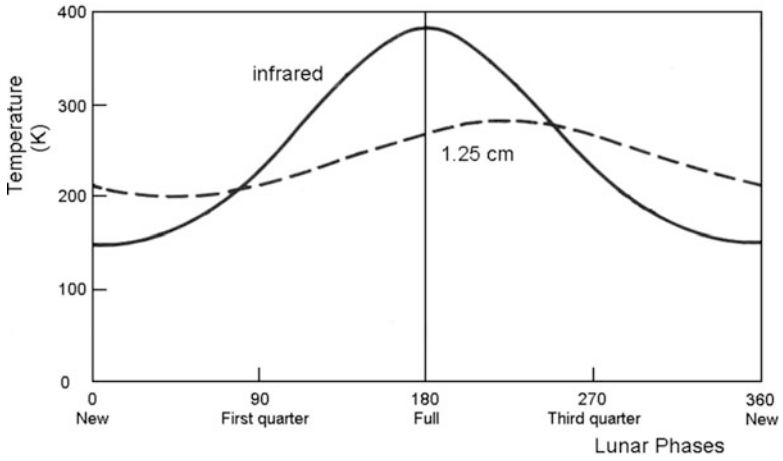

Fig. 1 The microwave phase effect of the Moon. The radiation received from the Moon at 1.25 cm wavelength (24 GHz frequency) lags the phase of the Moon. This indicates that the radiation emanates from the subsurface. The 1.25 cm wavelength observations, made by Australian radiophysicists J. H. Piddington (1910–1997) and H.C. Minnett (1917–2003) in 1949, were the first over the entire lunar phase cycle

In astronomical studies of the surfaces of moons and planets, this enables determination of the nature of the subsurface material. Professional astronomers construct models of the subsurface, including temperature dependences of the thermal conductivity and heat capacity and the depth dependence of the density. Comparing the models calculated for different values of these parameters and the observations, the values of the parameters can be determined. Figure 5 of Experiment #2, "A Review of Graphing Techniques," is an example of this technique applied to the planet Mercury.

2. *Microwave Phase Effect of the Moon*

Here we will utilize a less elaborate means to display the effect of thermal diffusivity in the time lag between heating of the surface of the Moon and the radiation it emits. We measure the amount of heat the surface of the Moon receives by the fraction of its surface that is illuminated by the Sun, the phase of the Moon. We measure the amount of energy the Moon radiates from its subsurface using the radio telescope of Experiments #14 and #15, "Thermal Radiation from a Planetary Subsurface: Part I: Calibration and Initial Measurements," and "Thermal Radiation from a Planetary Subsurface: Part II: Soil Sample Measurements".

Figure 1 shows the microwave phase effect of the Moon at 1.25-cm wavelength compared to the infrared phase effect, which is essentially the radiation from the lunar surface and can be considered as representing the fraction of the surface that is

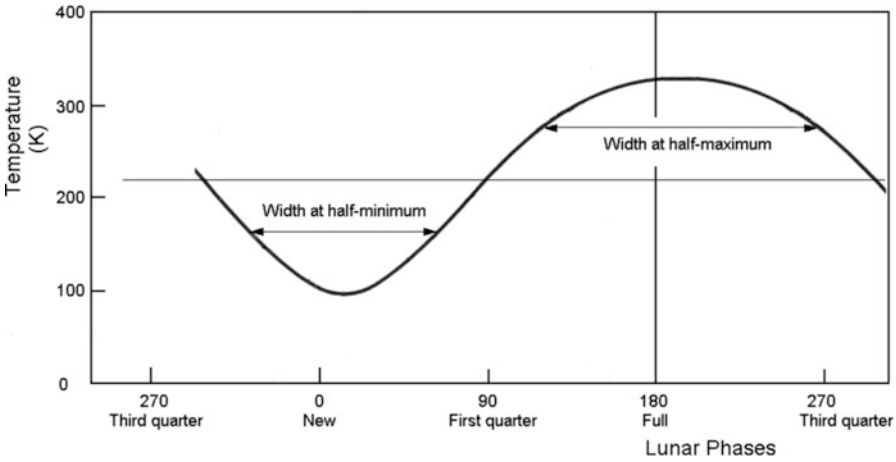

Fig. 2 The asymmetry of the microwave phase curve, a hypothetical example of which is shown, can be quantified by comparing the width of the curve about the maximum and minimum temperatures

illuminated by the Sun. Three effects are seen. A time lag occurs between the phase curve and the thermal radiation detected by the radio telescope. The amplitude of the variation at microwave frequencies is smaller than that at the surface. Finally, unlike the sinusoidal variation of the phase curve, the microwave variation is asymmetric, with a broader maximum about the time of the full Moon than minimum about the time of the new Moon. This can be quantified by comparing the width in time of the curve about a value of temperature equal to half of the maximum temperature to the width in time of the curve about a value of temperature equal to half of the minimum temperature, Fig. 2. All three effects result from values of the thermal diffusivity for real materials being finite.

The Apollo lunar explorations showed that the material of the mountainous highly-cratered highlands regions of the Moon have different composition that than of the dark maria regions. The former are composed mainly of feldspars, a rock rich in aluminum, whereas much of the maria material is composed of basaltic rocks, which have relatively large amounts of iron. The difference in density, color and therefore absorptive and emissive abilities, and thermophysical parameters results in different thermal diffusivities. High-resolution microwave studies of the Moon would demonstrate such differences. Here, observing the entire Moon at one time, the effect will not be detectable.

3. Lunar Eclipses

A total eclipse of the Moon, which can occur from zero to three times a year, provides an excellent opportunity to evaluate the thermal diffusivity of the lunar

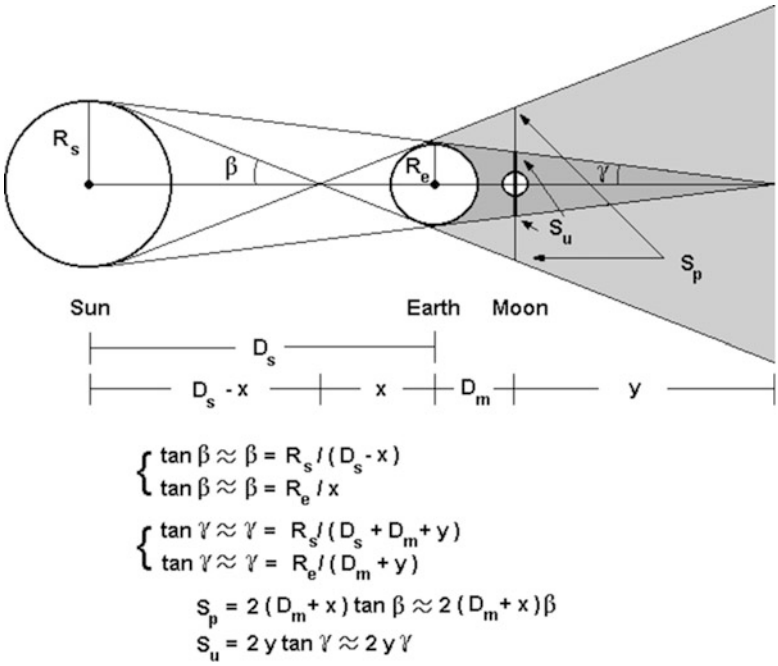

Fig. 3 Using small angle approximations based on the distance from the Earth to the Sun being much greater than the diameter of either object, the physical size of the umbra, s_u, and penumbra, s_p, at the location of the Moon during a total eclipse can be expressed in terms of known quantities. The umbra is found to stretch about 2.7 lunar diameters and the penumbra is found to stretch about 4.8 lunar diameters. The images are not shown to scale

subsurface material over a period of just a few hours. The orbital period of the Moon around the Earth is 27.3 days. Because it traverses 360° in this time interval, it moves 0.55 degrees of arc every hour. Although the angular diameter of the Moon varies from 29.2 to 33.3 minutes of arc depending on the distance of the Moon from the Earth, which varies slightly because of the eccentricity of the lunar orbit, the mean value is 0.52 degrees of arc, or 31.2 minutes of arc. The Moon moves its own angular diameter across the sky in about 1 h.

The geometry of the total lunar eclipse for the case in which the Moon passes directly through the center of the umbra is shown in Fig. 3. From pairs of similar triangles, we have two sets of two equations in two unknowns. As shown in Fig. 3, solving these for x and β, and y and γ, respectively, we can then calculate the physical extent of the umbra, s_u, and penumbra, s_p , at the location of the Moon during a total eclipse. The results are about 2.7 lunar diameters and 4.8 lunar diameters, respectively.

Figure 4 shows the *contact points* for a total lunar eclipse as defined by NASA. *Totality*, the appearance of maximum darkness, is defined as that portion of the eclipse between the events of U2 (umbra-2) and U3, when the Moon is entirely within the umbra. (In fact, viewers of lunar eclipses observe the Moon to have a

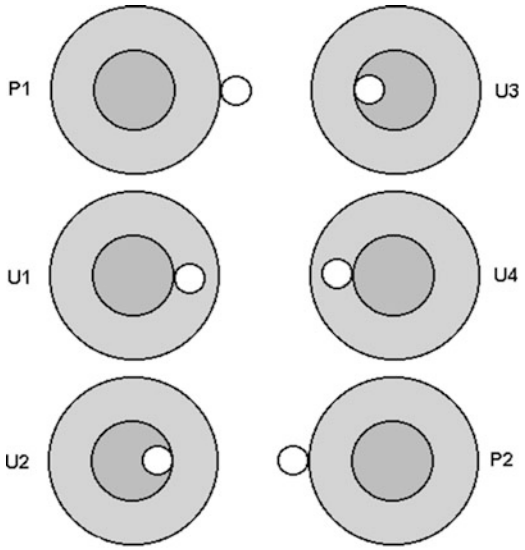

Fig. 4 The contact points of a total lunar eclipse. The *darkly-shaded* region of the shadow is the umbra and the *lightly-shaded* region is the penumbra as in Fig. 3. In the case depicted, the Moon passes directly through the center of the umbra. Totality occurs between portions designated as U2 and U3. The images are not shown to scale

reddish tinge during totality, resulting from the refraction of the rays of the Sun by the atmosphere of the Earth.) Because the umbra extends 2.7 lunar diameters and the Moon moves about one lunar diameter every hour, from the moments of U2 through U3 the Moon will move an additional 1.7 lunar diameters through the umbra.

As a result of the coincidence of the size of the Moon and the angular velocity of the Moon as viewed from the Earth, we accordingly find that the lunar surface experiences totality for about an hour during a total eclipse. Depending on the distance of the Moon from the Earth and the declination of the Moon, which determines its trajectory through the shadow, totality can last as long as about 1.7 h, or about 100 min.

Similarly, it takes approximately an hour for the Moon to first enter the shadow of the Earth, the *ingress* portion of the total eclipse, and an hour for it to exit from the shadow of the Earth, the *egress* portion of the total eclipse. In contrast to Fig. 1, we conclude that the illumination changes rapidly in a total eclipse, Fig. 5.

The parameters of partial and total eclipses umbral eclipses through 2014 are provided in Table 1. Such data are available at various websites, for example, http://www.mreclipse.com/Special/LEprimer.html.

4. Measuring the Temperature of a Celestial Source

The detection of radio emission from celestial objects requires its distinction from other sources of radio noise. At radio wavelengths, the Rayleigh-Jeans approximation to the Planck blackbody curve, discussed in Experiment #17, "Blackbody Radiation," shows that the emission is proportional to the temperature of the object. That is what we want to detect.

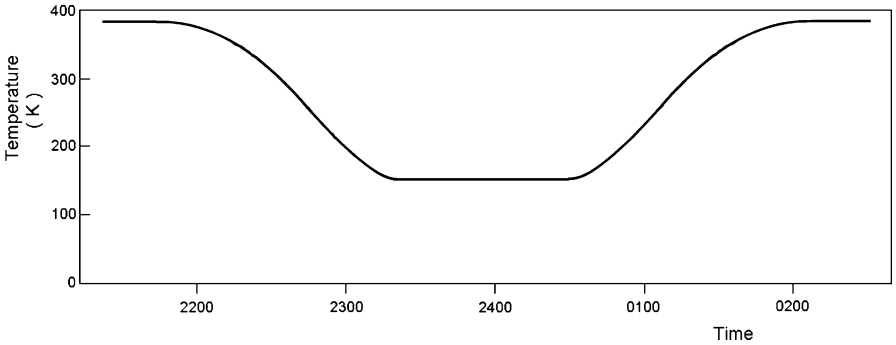

Fig. 5 A total eclipse of the Moon allows determination of the thermal properties of the subsurface material. This idealized light curve of the visible brightness of the Moon illustrates that ingress, totality, and egress are all approximately 1 h in duration. In fact, the different brightnesses between maria and highland regions makes the light curve moderately irregular in shape

Table 1 Partial lunar umbral eclipses and total lunar eclipses through 2014

Date	Appearance	Maximum fraction within umbra	Minimum fraction illuminated	Duration (totality in italics)	Visibility in geographical sequence	Declination of Moon on date
June 4, 2012	Partial	0.370	0.630	2 h 7 min	Asia, Australia, Pacific, Americas	+13.0
April 25, 2013	Partial	0.015	0.985	0 h 27 min	Europe, Africa, Asia, Australia	+3.0[a]
April 15, 2014	Total	1.00	0.00	3 h 35 min *1 h 18 min*	Australia, Pacific, Americas	+2.0[a]
October 8, 2014	Total	1.00	0.00	3 h 20 min *0 h 59 min*	Asia, Australia, Pacific, Americas	+3.0[a]

[a] Because of the low declination of the Moon on these dates, care must be taken to avoid possible interference with emissions from geosynchronous communication satellites

Other sources of radio noise exist. First, the background, including the atmosphere of the Earth, emits radiation, yielding a temperature of the background, T_{back}. This is discussed below. Other sources of background radiation, such as trees, buildings, human bodies, cell phones, and the transmission of communication satellites are a problem, but can be eliminated by careful planning of the observation.

Second, the various components of the radio receiver themselves emit radiation. The noise from radio receivers is well studied by radio engineers. If T_{sys} is the temperature equivalent to the noise generated by the receiver, the *noise figure*, F, is defined as

$$T_{sys} = (F - 1)T_{290},$$

where T_{290} is the ambient temperature, usually taken to be equal to 290 K. Often, the radio engineers quote the noise figure in decibels, $F_{db} = 10\ log(F)$.

The manufacturer has measured the noise figure of the RTL-11H radio telescope as 1.5 dB, which is equivalent to a system noise temperature $T_{sys} = 120$ K.

The temperature that is recorded from a celestial object depends on its brightness and the collecting area of the antenna. It is referred to as the *antenna temperature,* T_a. The total temperature sensed by the radiometer when pointing at a celestial object is accordingly

$$T_{tot} = T_a + T_{sys} + T_{back}.$$

5. *The Brightness of the Sky at 11 GHZ*

Figure 6 shows the contributions of various sources to the brightness of the sky from 100 MHz to 100 GHz in frequency. The minimum of the curve near the 21 cm line of neutral hydrogen and the four lines of the hydroxyl radical (OH), the neutral form of the hydroxyl ion, near 18 cm led Bernard Oliver, one of the early researchers into the possibility of communicative extraterrestrial life, to refer to it as the *water hole,* where species meet. A simplified version of this diagram was first published in *Sky and Telescope* magazine in 1960 by Frank Drake, the first astronomer to mount a radio search (Project Ozma) for extraterrestrial intelligent signals.

The 21 cm line results from the *hyperfine transition,* the change in the energy of the hydrogen atom when the configuration of the magnetic dipole moment of the hydrogen atom being parallel to that of the proton spontaneously changes to a configuration in which the two moments are in opposite directions. This is sometimes referred to as the "spin-flip" transition. This emission provides great information to astronomy, allowing radio astronomers, for example, to map out the spiral arms of the Milky Way galaxy. It was first suggested as a possible mechanism for creation of a spectral line in the radio part of the electro-magnetic spectrum by Dutch astronomer Hendrick van de Hulst (1918–2000) in 1945. The OH lines result from its electric dipole transition.

The contribution from the galaxy noted in Fig. 6 arises from relativistic electrons orbiting stellar and interstellar magnetic field lines. It depends on the distribution of energies of the electrons, but it typically leads to a $v^{-0.7}$ dependence on frequency.

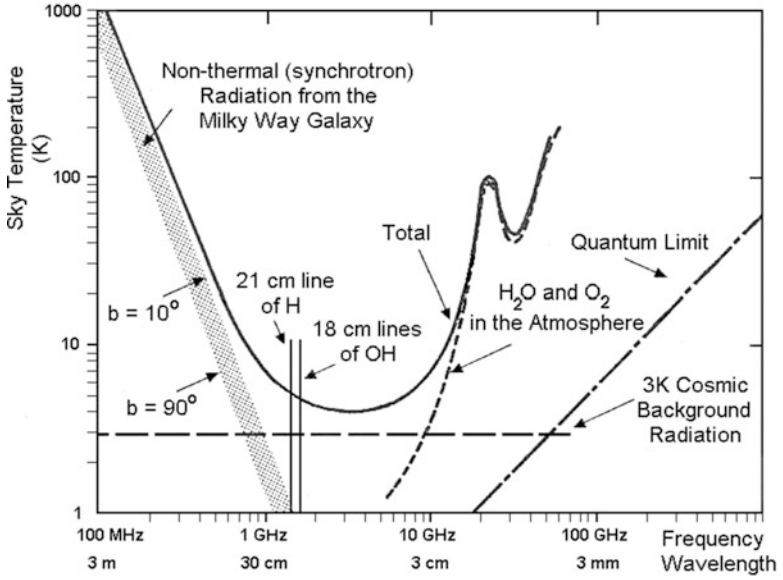

Fig. 6 The radio spectrum has a quiet area near where the constituents of water, hydrogen and OH, have prominent spectral lines. Galactic non-thermal radiation and the emission from water vapor and oxygen in the atmosphere are weak in the so-called "water hole" region. Those who study the possibility of extraterrestrial life consider this to be a likely part of the spectrum for intelligence civilizations to beam signals and to search for signals from other civilizations. The signals from the galaxy are greater than shown here if the galactic plane is viewed and the signals from the atmosphere are greater than shown here if the line of sight is not at the zenith

The quantum limit arising from the receiver itself is proportional to frequency, v. At 11 GHz the major contribution to the emission from the sky is water vapor in the atmosphere.

We should note that this graph, reproduced in one form or another in many publications, is an oversimplification of the true situation. First, the galactic non-thermal contribution varies widely depending on the direction in which you are viewing the galaxy. The minimum non-thermal radiation is viewed if the telescope is pointed out of the galactic plane, toward galactic latitude $b = 90°$. It is significantly greater if the telescope is pointed along the galactic plane, in particular toward the galactic center. Many discussions of the water hole show only the minimum contribution of the non-thermal radiation. Figure 6 shows the difference between the emission viewed at $b = 90°$ and $b = 10°$.

Although the non-thermal radiation is not bright at 11 GHz, at lower frequencies it can dominate observations of planetary objects. Figure 7 shows the correspondence between the celestial coordinate system of right ascension and declination and the galactic coordinate system between declinations of $-10°$ and $10°$. Within $10°$ galactic latitude of the galactic plane, shown by the shaded regions, synchrotron emission is enhanced. If you are not using the RTL-11H radio telescope but rather

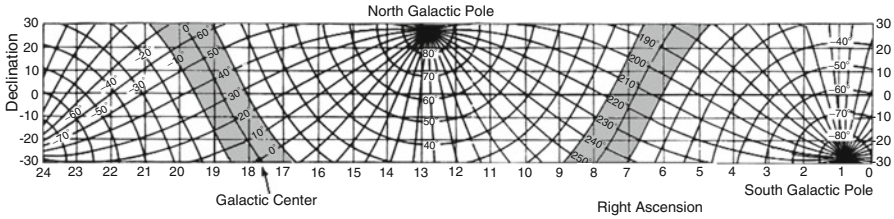

Fig. 7 This graph shows the correspondence between the celestial coordinate system of right ascension and declination and the galactic coordinate system between declinations of $-10°$ and $10°$. Within $10°$ galactic latitude of the galactic plane, shown by the shaded regions, synchrotron emission is enhanced. Although it is not particularly strong at 11 GHz, if you are instead using a receiver operating at frequencies less than about 1 GHz, you should avoid making observations of the Moon if its position is such that its right ascension and declination fall within this band of galactic latitudes

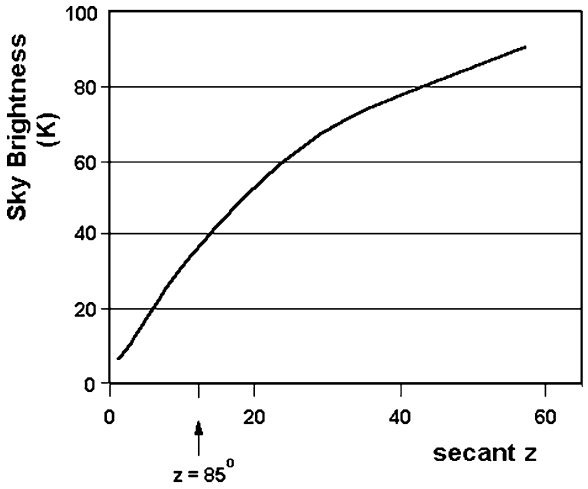

Fig. 8 The brightness of the sky at 11 GHz. As with observations at most wavelengths, it is proportional to the secant of the zenith angle except when observing very close to the horizon

one operating at a frequency less than 1 GHz you should avoid observing the Moon if its position is such that its right ascension and declination fall within this $20°$ band of galactic latitudes.

As a second simplification, the atmospheric contribution varies widely depending on the moisture in the air and the angle of view. The curve in Fig. 6 represents a view to the zenith, resulting in a minimum path length through the atmosphere. Viewing the sky at lower elevations greatly increases the atmospheric contribution by the familiar *sec z* relation, where *z* is the zenith angle. The dependence on the atmospheric contribution at 11 GHz is shown in Fig. 8.

6. *Measuring the Sky Brightness*

The atmosphere poses an additional problem. The radiation from the Moon is absorbed as it passes through the atmosphere and the atmosphere itself emits radiation. This is described by the equation of radiative transfer for radiation passing through a gas, similar to that for the equation of radiative transfer for radiation passing through a soil as described in Fig. 2 and Eq. (3) of Experiment #15, "Thermal Radiation from a Planetary Subsurface: Part II: Soil Sample Measurements". In professional astronomical investigations, our observations would be corrected by consideration of such factors.

Here, however, we will not consider these factors for several reasons. First, we're not interested in the actual temperature of the Moon, only in how it varies with phase. Second, as shown in Figs. 1, 6, and 8, the contribution of the atmosphere in emission will be much less than the contribution of the Moon itself. Finally, we can keep the contributions from the atmosphere relatively constant if we constrain the times of our observations. We should observe only on clear nights, minimizing the amount of water vapor in our line-of-sight to the Moon. If we observe at times when the Moon is as close to overhead as possible, we will minimize the path length in the atmosphere through which the radiation of the Moon must pass in arriving at our telescope. In other words, avoid making observations of the Moon within a few hours of its rising or setting.

C. Procedure and Observations

1. *The Telescope*

In this experiment we will use the receiver of the same RTL-11H telescope that was used in Experiments #14 and #15, "Thermal Radiation from a Planetary Subsurface: Part I: Calibration and Initial Measurements," and "Thermal Radiation from a Planetary Subsurface: Part II: Soil Sample Measurements," but with a larger antenna. This receiver, with the 32-cm diameter parabolic dish antenna of the RTL-11 radio telescope, was designed to measure the emission at 11 GHz from the Sun. This antenna, however, lacks sufficient collecting area to permit the receiver to detect the signals from the Moon, which are approximately 80–100 times weaker at this wavelength than those from the Sun. The small horn antenna of the RTL-11H telescope is even less capable of collecting sufficient signal from the Moon.

A parabolic dish antenna of 8–9 ft in diameter provides sufficient collecting area to detect the Moon above the noise of the RTL-11 receiver. Dishes of this size, fortunately, are commonly used as communication antennas, placed on the grounds or roof-tops of buildings of educational and other institutions. We will accordingly replace the receiver installed on the communications antenna with the receiver of the RTL-11H radio telescope and use it to detect the emission from the Moon.

Depending on the materials out of which they are constructed, these antennas can be fairly massive. If that is the case with the antenna you will be using, and if the antenna cannot be locked down into position, several students should be providing support during the observations. A technician from your school is also encouraged to participate.

Antennas are mounted in either of two ways. In the altitude-azimuth or *alt-azimuth mount*, the antenna is positioned about horizontal and vertical axes, to provide rotation in the altitudinal and azimuthal direction, respectively. In the *polar mount*, the antenna is positioned about an axis pointing to the north pole and an axis perpendicular to that axis, to provide rotation in the directions of right ascension and declination. For our purposes in positioning a potentially massive antenna, the latter mount is preferred. The antenna can be locked in declination position and then simply rotated by hand as the Moon moves.

Because the dish is larger than the aperture of the horn antenna, the beam will be smaller. As discussed in Experiment #15, "Thermal Radiation from a Planetary Subsurface: Part II: Soil Sample Measurements," the HPBW will be approximately λ/D radians. At our wavelength of $\lambda = 2.7$ cm and a value of $D = 96$ in.$\times 2.54$ cm/in. $= 183$ cm, we find $BWHP = 0.63°$. This is only slightly larger than the angular diameter of the Moon.

Such a beam width has two important results. First, we have a good chance of observing the Moon without interference from trees and buildings. Communication satellite signals are sufficiently strong, however, that their reception by the side lobes of the antenna beam may still be a problem. Second, this relatively small beam makes it somewhat difficult to point the telescope at the Moon. As a result, we want to attach a guiding "telescope" to the antenna.

2. *The Optical Guide*

Professional telescopes have accurate guiding mechanisms with which to point the telescope and to track a given object over the period of observation. Many amateur optical telescopes have small guiding telescopes attached to them to enable location of objects within their larger field of view. In radio astronomy, determination of the pointing characteristics of a newly-constructed telescope is performed by a star pointing experiment. In this, as with the amateur optical telescope, an optical telescope is attached to the side of the radio antenna. As the antenna is pointed to different portions of the sky, the difference between the positions provided by the readout of the telescope steering gears and the accurately known position of bright stars are determined. In addition to our inability to "see" objects in radio wavelengths through a radio telescope, this pointing experiment is needed to determine the change of direction of the pointing of massive antennas as they sag under the force of gravity.

In this experiment, because the Moon is so bright, we can simply use a circular piece of plastic pipe as our guide telescope! We only need to be able to attach it

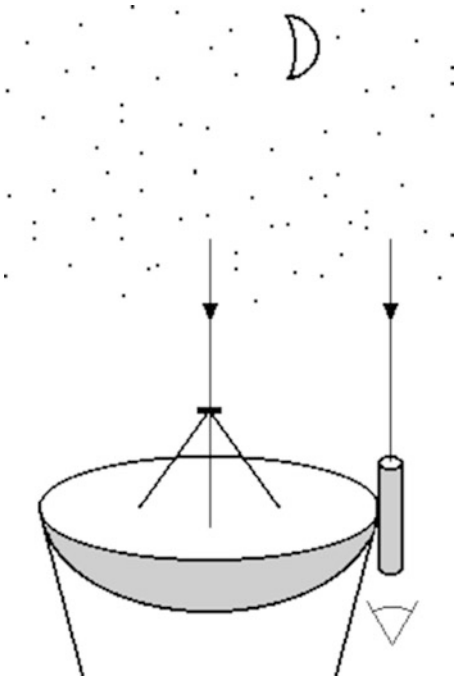

Fig. 9 A hollow plastic pipe can be used as a guide telescope to facilitate pointing of the radio telescope at the Moon

securely to the rim of the communications antenna to enabling our keeping the antenna pointed at the Moon. A circular piece of cardboard such as from a roll of kitchen towels could also be used if it can be secured to the antenna and kept from bending in the wind.

As shown in Fig. 9, we want to align the circular guide "telescope" with the axis of the communications antenna. This is done easily by viewing the Moon with the receiver that is already installed on the antenna. With the assistance of a technician from your school, release the antenna from its locked position. Before moving the antenna, make sure that you have recorded its position so that it can be repositioned to point at the communications satellite after your use. Move the antenna about its two axes so that it points as closely to the direction of the Moon as you can aim. Then move it about that direction until the signal using the receiver in place is greatest, indicating that the Moon lies completely within the beam of the antenna. Now attach the circular guide to the rim of the telescope and orient it so that it looks directly at the center of the Moon and lock it down securely in place. Henceforth, you can use the circular guide to point the antenna to the Moon. Of course, if you prefer you can forego this procedure and simply point the antenna at the Moon and move it about until obtaining the maximum microwave signal.

If the signal from the communications antenna you are using cannot be directly read, use the IF Processor Box from the RTL-11H radiometer for the alignment. Inside the laboratory, disconnect the RTL-11H receiver from the horn antenna. On the RTL-11H radiometer, a cable connects the LNB to the IF Processor Box. Disconnect that

cable from the LNB. Take the cable and its connected to the IF Processor Box outside to the communications antenna. Disconnect the LNB of the communications antenna from its receiver. Now, use the RTL-11H cable to connect the LNB of the communications antenna to the IF Processor Box. You can now use the radiometer to measure the signal of the Moon and thereby align the optical guide. You may require the assistance of a technician from your school to perform this operation.

3. *Avoiding Interfering Signals*

The advantage of observing outdoors is the lack of concern about reflection of microwaves off of walls and radiation from interior wiring. Other sources of interference, however, do exist outdoors.

Figure 5 represents only celestial and atmospheric sources of radiation. At microwave frequencies, trees, buildings, and people also emit significant radiation. These can be somewhat controlled if we are careful to point the antenna away from such objects, that is, far above the horizon. In addition, cellular phones emit signals near the intermediate frequencies of the LNB. No one should be using their cell phones during the observations.

More troublesome is the presence of communication satellites. The LNB of the RTL-11H radio telescope is tuned to the very frequency of these communication satellite transmissions. Because the communication satellites are located in geosynchronous orbits located above the equator, their declinations are all within a few degrees of zero. This implies that the observations with the 11 GHz receiver of the Moon, the orbit of which lies close to the ecliptic plane, should be performed when the Moon is far from the celestial equator, the zero of declination (see Fig. 3 of Experiment #5, "Earth: The Seasons and Local Latitude"). In other words, the observations should be made when the declination of the Moon is close to 23° if you are located in the northern hemisphere or when the declination of the Moon is close to – 23° if you are located in the southern hemisphere. The website http://faculty.physics.tamu.edu/krisciunas/ra_dec_moon.html provides the right ascension and declination of the Moon for all the dates of a given calendar year.

In summary, the best times to observe the Moon with the 11 GHz receiver are when the Moon is at large declinations and when it is distant from the horizon. The former constraint minimizes the chance of interference from communication satellites. The latter constraint will minimize the contribution of the emission from the atmosphere and enable you to avoid possible interference from trees and buildings.

4. *Microwave Phase Effect: Calibration*

We will observe the Moon with the IF Processor Box of the RTL-11H telescope connected to the LNB of the communications antenna on 15–20 clear nights over a

period of at least 1 month at times when the Moon is highest in the sky. Before each observation of the Moon, we will calibrate the telescope inside the laboratory as in Experiments #14 and #15, "Thermal Radiation from a Planetary Subsurface: Part I: Calibration and Initial Measurements," and "Thermal Radiation from a Planetary Subsurface: Part II: Soil Sample Measurements," by observing an ice-water bath and a boiling-water bath covered with a thin sheet of plastic bubble-wrap. On the first day of observation we will determine the emissivity of the thin sheet of plastic bubble-wrap by also measuring emission from an ambient-temperature water bath.

The thin sheet of plastic bubble-wrap covers the boiling water to prevent steam from entering the antenna and to eliminate emission from the water vapor itself. Having a non-smooth surface, it also minimizes reflections of microwave signals from the walls and people in the laboratory into the antenna. Measurements of the ambient-temperature water bath with and without the thin sheet of plastic bubble-wrap will provide a measure of the change of emissivity that results from placing the plastic over the water.

Use different thin sheets of plastic bubble-wrap for the ambient-temperature bath and the boiling-water bath. Remember to gently stir the uncovered ambient-temperature water bath to create a rough, less reflective surface. In all these calibration measurements, use the plumb bob suspended from the antenna to ensure that the antenna is positioned directly above the center of the water containers.

The water containers should have the same areal dimensions as the soil sample box, 2.5 $\times$ 2.5 ft. A depth of 1 ft is sufficient for the calibration. This amounts to about 47 gal of water for each of the three containers. Because of the weight of this amount of water, the three water containers are also seated on a platform mounted on casters for rolling into position under the antenna. One container of water should stand overnight in the laboratory to enable it to reach room temperature.

The zero and gain settings of the microammeter are set as in Experiments #14 and #15, "Thermal Radiation from a Planetary Subsurface: Part I: Calibration and Initial Measurements," and "Thermal Radiation from a Planetary Subsurface: Part II: Soil Sample Measurements". Because all the measured signals will be greater than the signal received from the ice-water bath, we use an observation of the ice-water bath to establish the zero of the microammeter. Attach the plumb bob to the antenna and roll the ice-water bath into position below the antenna. Adjust the position of the water container until its center is directly under the plumb bob. Remove the plumb bob. Read the signal from this bath and set the zero of the microammeter to read about one-fifth of the total scale. This is a reading of 10 divisions if the microammeter scale has a total of 50 divisions. Enter the position of this zero setting on the DATA SHEET.

We now use the signal received from the boiling-water bath to set the gain of the microammeter. Roll the ice-water bath from below the antenna and roll the boiling-water bath into position under it, again using the plumb bob to center it under the antenna. The boiling-water bath should be covered by a thin sheet of plastic bubble-wrap. Read the signal from the boiling-water bath, and adjust the gain of the microammeter so that it reads about three-quarters of the microammeter scale.

Enter the position of this gain setting on the DATA SHEET. For consistency between observations, use the same zero and gain settings in all future observations.

Also enter the microammeter reading obtained with the boiling-water bath in column 5 of Table 2 of the DATA SHEET. If you are using an analog-to-digital converter to record the data, enter that result in Table 2.

With the zero and gain settings now set, roll the boiling-water bath from under the antenna, roll the ice-water bath into position using the plumb bob, and reread the signal from the ice-water bath. Enter the result in column 4 of Table 2 of the DATA SHEET. If you are using an analog-to-digital converter to record the data, enter that reading in Table 2.

On the first day of observation, read the signals from the ambient-temperature water bath both with and without the overlaid thin sheet of plastic bubble-wrap, in order to determine a correction factor for the emissivity of the plastic sheet. Use different thin sheets of bubble-wrap plastic for the ambient-temperature water bath and the hot-water bath measurements. Roll the ice-water bath from below the antenna and roll the ambient-temperature water bath into position under it. Remember to gently stir the uncovered ambient-temperature water bath to create a rough, less reflective surface. Enter these readings on the DATA SHEET. If you are using an analog-to-digital converter to record the data, enter those readings on the DATA SHEET.

5. *Microwave Phase Effect: Observations of the Moon*

If you have not already done so in aligning the optical guide to the communications antenna, disconnect its LNB from its receiver. Before moving the antenna to facilitate your doing this, make sure that you have recorded its position so that it can be repositioned to point at the communications satellite after your use. Your school may require the assistance of a technician to perform these operations.

We now repeat the procedure of connecting the IF Processor Box of the RTL-11H telescope to the LNB of the communications antenna. Inside the laboratory, disconnect the RTL-11H receiver from the horn antenna. On the RTL-11H receiver, a cable connects the LNB to the IF Processor Box. Disconnect that cable from the LNB. Take the cable and its connected IF Processor Box outside to the communications antenna. Now, use the RTL-11H cable to connect the LNB of the communications antenna to the IF Processor Box. You can now use the radiometer to measure the signal of the Moon and thereby align the optical guide. You may require the assistance of a technician from your school to perform this operation.

To ensure that all the connections are secure, point the telescope at your classmates or at a nearby building. Their microwave emissions should lead to an increase in the microammeter reading.

The signals from the Moon and dark sky will be appreciably smaller than those received in the laboratory from the water calibration samples. The water samples

provide a strong signal at 273.2–373.2 K. Including the 120 K system noise temperature, the total measured temperatures vary from 393 to 493 K, a range of a factor of 1.3. The gain setting can be relatively small. In the observations of the dark sky and Moon, the signals and therefore antennas temperatures are significantly smaller. As a result, the gain setting should be greater to allow sufficient precision in the reading of the microammeter scale.

We now determine the zero and gain settings for the observations of the Moon. Because all the measured signals will be greater than the signal received from the dark sky, we use an observation of the dark sky to establish the zero of the microammeter. With the optical guide as an aid, point the telescope at a portion of the dark sky one or two Moon diameters from the Moon. If a large signal is read on the microammeter, you may be looking near a communications satellite. Move the antenna until you observe a small signal. Now adjust the zero of the microammeter to read about one-fifth of the total scale, a reading of 10 divisions if the microammeter has a total of 50 divisions.

We use the signal received from the Moon to set the gain of the microammeter. With the optical guide as an aid, point the antenna directly at the center of the Moon. Adjust the gain setting on the microammeter so that it reads about three-quarters of the microammeter scale. If you are observing a crescent phase of the Moon, the gain setting should be set so that it reads about one-half of the microammeter scale. We anticipate that gibbous and full phases of the Moon will be associated with larger amounts of microwave emission. Enter the microammeter output in column 9 of Table 3 of the DATA SHEET. If you are using an analog-to-digital converter to record the data, enter those results in Table 3. Enter the date and time of your observation in columns 2 and 3, respectively, of Table 3 of the DATA SHEET.

For consistency between observations on all observing nights, enter the position of these zero and gain settings on the DATA SHEET and use the same zero and gain settings in all future observations.

As described above, the beam of the antenna will be appreciably smaller than that of the horn antenna. Depending on the size of your antenna, it may be approximately the size of the lunar disk itself. If you have not installed the optical guide on the antenna, you should move the antenna manually both upwards and downwards and to the sides about the position of the Moon until you obtain the maximum output. As with guided observations, adjust the gain setting on the microammeter until a sizable reading above the zero level is read and enter the microammeter output in column 9 of Table 3 of the DATA SHEET.

We will now examine the area around the Moon to ensure that no communication satellites are present whose transmissions are entering the side lobes of the antenna. Move the antenna off of the Moon one or two Moon diameters to the north and obtain an output reading. Enter it in column 5 of Table 3 of the DATA SHEET. Similarly, move the antenna one or two Moon diameters to the south, east, and west of the Moon and obtain an output reading. Enter those values in columns 6, 7, and 8 of Table 3 of the DATA SHEET.

From Fig. 8, we see that the temperature of the sky at 11 GHz should not be greater than 10 or 20 K. If you observe substantially larger temperatures on a clear night in any of the off-Moon observations, you most likely are receiving emission from trees, buildings, people, or a satellite, or significant thin clouds are in the atmosphere. We will treat the results from the Moon for that particular night with suspicion when analyzing the data later.

Your school will probably have only one communications antenna available for use for this experiment. As a result, the various laboratory teams should calibrate their RTL-11H receivers in the laboratory and then in turn walk outside, connect their receiver, perform the measurements of the Moon and dark sky, and then disconnect their receiver to make room for that of the next team. Note that as the night progresses, some teams may find interference by communication satellites which were not experienced by other teams. That simply results from the Moon changing its position over the sky with time. Varying meteorological conditions will also affect the brightness of the dark sky.

The final team making measurements of the Moon should disconnect their RF Processor Box from the LNB of the communications antenna, reconnect the receiver of the communications antenna, and reposition the antenna to look at the communications satellite. You may require the aid of a technician to perform these operations.

6. *Lunar Eclipses*

If you are fortunate to have a significant partial lunar eclipse or a total lunar eclipse occurring during your school semester, observations can be made of the event over a period of several hours. The observations should span the time interval from before the Moon enters the shadow of the Earth to after the Moon emerges from the shadow. Observations should be made during the ingress, totality, or near maximum obscuration if the eclipse is partial, and egress portions of the eclipse.

Perform the same procedure as you did in observing the microwave phase effect. If you have not aligned an optical guide to the communications antenna, do so following the steps in section "The Optical Guide" above. Using the same zero and gain settings for calibration as you used in observing the phase effect of the Moon, perform the calibration inside the laboratory using the water baths. Enter the results in Table 5 on the DATA SHEET. Then disconnect the IF Processor Box from the LNB of the RTL-11H telescope and connect it to the LNB of the communications antenna.

To make sure that all the connections are secure, point the telescope at your classmates or at a nearby building. Their microwave emissions should lead to an increase in the microammeter reading.

Some time before the eclipse is scheduled to begin, and using the same zero and gain settings for observations of the eclipse as you used in observing the phase effect of the Moon, observe the sky near the Moon to ensure that no spurious signals

are being received from communication satellites or nearby trees and buildings. If the values are significantly higher than those predicted by Fig. 6, move the antenna to a nearby position and observe again. Enter the time of the calibration and the output of the receiver in columns 2 and 3 of Table 6 of the DATA SHEET.

As the eclipse begins, try to keep the antenna pointed at the Moon as it moves over the sky with the rotation of the Earth. You may want to have your laboratory partners alternate holding the antenna in position while another reads the output. You want to make sure that the reading is significantly larger than what you obtained with the blank sky, indicating that you are indeed pointing the antenna at the Moon. If the signal suddenly increases substantially, a communications satellite may have entered one of the side lobes of the antenna. Making at least 10 observations will enable determination of the amount of uncertainty in the observations. Enter the time of the observations and the microammeter reading in columns 2 and 3 of Table 6 of the DATA SHEET. If you are using an analog-to-digital converter to record the data, enter those results in Table 6.

After the eclipse has ended, disconnect the RF Processor Box from the LNB of the communications antenna, reconnect the receiver of the communications antenna, and reposition the antenna to look at the communications satellite. You may require the aid of a technician to perform these operations.

D. Data Reduction and Analysis

1. Radiometer Calibration

We first calibrate the radiometer as in Experiments #14 and #15, "Thermal Radiation from a Planetary Subsurface: Part I: Calibration and Initial Measurements," and "Thermal Radiation from a Planetary Subsurface: Part II: Soil Sample Measurements". Divide the output of the radiometer received from the "Ambient-temperature Water Bath Without Plastic Sheet" as entered on the DATA SHEET by the output received from the "Ambient-temperature Water Bath With Plastic Sheet" to obtain the value of the correction factor, f_s. Enter the result on the DATA SHEET. Because this factor corrects for the emissivity of the plastic sheet, it will not change over the span of your observations and need only be determined once. We are assuming that the emissivity of the plastic material is not temperature-dependent so that the value determined with the ambient water bath is the same as the value when placed on the boiling-water bath. If the plastic bubble-wrap degrades from repeated usage with the boiling-water bath, then the material should be replaced.

Multiply the values of the boiling-water bath output in column 5 of Table 2 of the DATA SHEET by the correction factor, f_s. Enter the result in column 6 of Table 2. This is now the value of the boiling water bath output corrected for the emissivity of the plastic sheet to be used in calculation of the calibration equation.

As in Experiments #14 and #15, "Thermal Radiation from a Planetary Subsurface: Part I: Calibration and Initial Measurements," and "Thermal Radiation from a Planetary Subsurface: Part II: Soil Sample Measurements," we now determine the calibration equation for each observation, which will allow us to convert the microammeter reading from the radiometer to temperatures,

$$T = a + bV.$$

Here V is the microammeter reading and T is the temperature of the Moon at 11 GHz. For each observation, calculate the coefficients a and b of the calibration equation, using

$$T_i = a + b\ V_i$$
$$T_b = a + b\ V_b,$$

where the temperature of the ice-water bath is $T_i = 273.2$ K, the temperature of the boiling-water bath is $T_b = 373.2$ K, and V_i and V_b are the microammeter readings when observing the ice-water bath and (corrected) boiling-water bath, respectively. The solution of these two equations in two unknowns is easily shown to be

$$a = T_b - (T_b - T_i)/(V_b - V_i)V_b$$

$$b = (T_b - T_i)/(V_b - V_i).$$

Two corrections must be made to these data. First, as in Experiments #14 and #15, "Thermal Radiation from a Planetary Subsurface: Part I: Calibration and Initial Measurements," and "Thermal Radiation from a Planetary Subsurface: Part II: Soil Sample Measurements," we must correct for the non-unity value of the emissivity of water. To correct for a representative value of emissivity of 0.97, you can show that we must multiply the values of a and b, and therefore the calibrated temperatures, by an additional factor $f_e = 1.03$. Second, we have used a different gain of the microammeter for the calibration and actual Moon observations. The temperatures must therefore similarly be multiplied by the ratio, r_g, of the gain used for the Moon observations to the gain used for the calibration. With the corrected calibration equation,

$$T = f_e r_g (a + bV), \tag{1}$$

convert the value of lunar output for each observation from column 9 of Table 3 of the DATA SHEET to calibrated lunar output. Enter those values in column 10 of Table 3. Show all your calculations on the DATA SHEET.

Construct a graph of the values of a and b as a function of time to determine the variation of gain during the period of the observations. If any value of pairs of values differs significantly from the trend, treat the result for the temperature of the Moon on that date with suspicion.

2. *Graph of the Microwave Phase Effect*

The U.S. Naval Observatory web site, http://www.usno.navy.mil/USNO/astronomical-applications/data-services/frac-Moon-ill, provides the fraction of the lunar surface illuminated at noon or midnight on any date in a given time zone. The values are provided in tabular form. Provide your local time zone at the website and then read the value for the fraction of lunar surface illuminated on the date of observation from the table generated. Enter that value in the final column of Table 3 of the DATA SHEET.

The fraction of the lunar surface illuminated may vary by as much as 25% on successive days near first and last quarter phases. This is a significant variation. The U.S. Naval Observatory website, however, provides these data for your local time so that no iteration between the tabulated values for successive dates is needed. Even if your observations occur as much as 4 h before or after midnight your error will be no more than $4/24 \times 25\% = 4\%$.

Convert the calendar date of observation to the Julian date using the tables of Appendix III and enter the result in column 3 of Table 3 of the DATA SHEET. Using your own graph paper or the graph paper provided on the DATA SHEET, construct a graph of the fraction of lunar surface illuminated and the calibrated output of the radiometer as a function of Julian date. Draw a smooth curve through the points. If you found evidence for the presence of communication satellite transmissions in your observations, do not consider those points when drawing the smooth curve.

Three indices can be calculated from this graph to represent the effect of finite values of the thermal diffusivity. Using this graph, determine both the time lag between the maximum of the illuminated surface curve and the 11 GHz variation, and the amplitude of the 11 GHz variation. In order to determine a measure of the asymmetry in the variation, first draw a horizontal line at the value of temperature $T = 1/2\,(T_{max} - T_{min})$, where T_{max} is the maximum temperature observed, and T_{min} is the minimum temperature observed. Then determine the width of the variation in time to half of the maximum value and to half of the minimum value, as shown in Fig. 2. Show these calculations on the DATA SHEET and enter your results in Table 4 of the DATA SHEET.

Figure 1 is reproduced on the DATA SHEET, with grid lines, to facilitate measuring. Determine the time lag between the 1.25-cm wavelength phase curve and the infrared phase curve, the amplitude of the 1.25-cm wavelength variation, and the width of the variation in time to half of the maximum value, Δ_2, and to half of the minimum value, Δ_1. Calculate the ratio Δ_2/Δ_1. In Experiment #15, "Thermal Radiation from a Planetary Subsurface: Part II: Soil Sample Measurements," we determined the effective depth of the emitted radiation as a function of time for various soil samples. The fragmented granite is most similarly to lunar material. Enter the value for d/λ for the granite after the maximum amount of time of heating, perhaps 75 min, in column 7 of Table 4 of the DATA SHEET. Multiply that value by the two wavelengths for which we have data, 1.25 and 2.7 cm, to determine the

effective depth from which radiation from those depths is emitted. Enter your results in the final two columns of Table 4 of the DATA SHEET.

Using your own graph paper or the graph paper provided on the DATA SHEET, construct a graph of the time lag and ratio Δ_2/Δ_1 using the left ordinate scale, and the amplitude in degrees K using the right ordinate scale, all as a function of the effective depth. Clearly distinguish the points being graphed by using different symbols.

3. *Graph of the Lunar Eclipse*

As in section "Radiometer Calibration" above, determine the values of a and b of the calibration equation and then correct them for the emissivity of water used in the calibration, f_e and the ratio of the gains, r_g. With the corrected calibration equation, (1), convert the values of lunar output from column 3 of Table 6 of the DATA SHEET to calibrated lunar output. Enter those values in column 4 of Table 6. Show all your calculations on the DATA SHEET.

We will compare the variation of the microwave signal with the light curve of the eclipse, the fraction of the surface illuminated as a function of the time elapsed from the beginning of the eclipse. The minimum fraction of the lunar disk illuminated, as tabulated in Table 1, and the beginning and ending times of ingress, totality, and egress provide the data needed to draw the light curve. Websites such as http://eclipse.gsfc.nasa.gov/eclipse.html or http://www.spacedex.com/lunar-eclipse/ provide the Universal Times, that is, the local time at Greenwich, England, of those events. Your local time depends on the time zone in which you are located. Note that the visibility of the Moon depends on your location. Depending on the latitude and longitude of your location, only portions of the duration of the eclipse may be visible. As the Earth rotates, different parts of the Moon are visible from different parts of the Earth.

Those websites or others may also provide the fraction of the lunar disk illuminated during the eclipse. If those data are available, enter them in column 7 of Table 6 of the DATA SHEET.

Using your own graph paper or the graph paper provided on the DATA SHEET, draw a smooth curve through the points defined by the times of beginning and end of ingress, egress, and totality. In the case of a partial eclipse, use the time of the minimum fraction of the disk illuminated. If you have more detailed data available, entered in column 7 of Table 6, use that. Note that the ingress and egress portions of the eclipse are part of a sine wave, but that the portion of totality will be a flat line. The result is the light curve of the eclipse. On the same graph paper, construct a graph of the calibrated output of the radiometer.

STUDENT'S NAME _____

E. Data Sheet

1. Microwave Phase Effect

Zero setting of the microammeter for calibration: _____
Gain setting of the microammeter for calibration, g_c: _____

Ambient-temperature water bath without plastic sheet, V_1 = _____
Ambient-temperature water bath with plastic sheet, V_2 = _____

$f_s = V_1/V_2$ = _____

Zero setting of the microammeter for Moon observations: _____
Gain setting of the microammeter for Moon observations, g_m: _____

$r_g = g_m/g_c$ = _____

STUDENT'S NAME _____

Table 2 Calibration measurements

Observation	Calendar date	Time	Ice-water bath output, V_i (millivolts)	Boiling-water bath output, V'_b (millivolts)	Corrected boiling-water bath output, $V_b = f_s V'_b$ (millivolts)
1.					
2.					
3.					
4.					
5.					
6.					
7.					
8.					
9.					
10.					
11.					
12.					
13.					
14.					
15.					
16.					
17.					
18.					
19.					
20.					
21.					
22.					
23.					
24.					
25.					

STUDENT'S NAME _____

Table 3 Lunar microwave phase effect observations

Obs.	Calendar date	Time of Moon observation	Julian date	Dark sky north observation (millivolts)	Dark sky south observation (millivolts)	Dark sky east observation (millivolts)	Dark sky west observation (millivolts)	Lunar output (millivolts)	Calibrated lunar output (K)	Fraction of Moon illuminated
1.										
2.										
3.										
4.										
5.										
6.										
7.										
8.										
9.										
10.										
11.										
12.										
13.										
14.										
15.										

(continued)

Table 3 (continued)

Obs.	Calendar date	Time of Moon observation	Julian date	Dark sky north observation (millivolts)	Dark sky south observation (millivolts)	Dark sky east observation (millivolts)	Dark sky west observation (millivolts)	Lunar output (millivolts)	Calibrated lunar output (K)	Fraction of Moon illuminated
16.										
17.										
18.										
19.										
20.										
21.										
22.										
23.										
24.										
25.										

STUDENT'S NAME _____

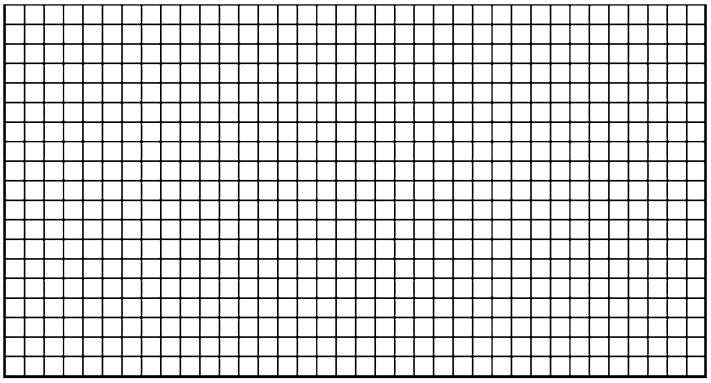

Graph of the values of a and b as a function of time. Use the left ordinate scale for a and the right ordinate scale for b.

STUDENT'S NAME _____

Determination of the calibration equation and calibrated lunar outputs

Show your calculations of the calibrated lunar outputs calculated from (1), $T = f_e\, r_g\, (a + b\, V)$.

Observation 1:

y-intercept, a = _____ slope, b = _____
Calibrated lunar output = _____

Observation 2:

y-intercept, a = _____ slope, b = _____
Calibrated lunar output = _____

Observation 3:

y-intercept, a = _____ slope, b = _____
Calibrated lunar output = _____

Observation 4:

y-intercept, a = _____ slope, b = _____
Calibrated lunar output = _____

Observation 5:

y-intercept, a = _____ slope, b = _____
Calibrated lunar output = _____

Observation 6:

y-intercept, a = _____ slope, b = _____
Calibrated lunar output = _____

STUDENT'S NAME _____

Observation 7:

y-intercept, a = _____ slope, b = _____
Calibrated lunar output = _____

Observation 8:

y-intercept, a = _____ slope, b = _____
Calibrated lunar output = _____

Observation 9

y-intercept, a = _____ slope, b = _____
Calibrated lunar output = _____

Observation 10:

y-intercept, a = _____ slope, b = _____
Calibrated lunar output = _____

Observation 11:

y-intercept, a = _____ slope, b = _____
Calibrated lunar output = _____

Observation 12:

y-intercept, a = _____ slope, b = _____
Calibrated lunar output = _____

STUDENT'S NAME _____

Observation 13:

y-intercept, a = _____ slope, b = _____
Calibrated lunar output = _____

Observation 14:

y-intercept, a = _____ slope, b = _____
Calibrated lunar output = _____

Observation 15:

y-intercept, a = _____ slope, b = _____
Calibrated lunar output = _____

Observation 16:

y-intercept, a = _____ slope, b = _____
Calibrated lunar output = _____

Observation 17:

y-intercept, a = _____ slope, b = _____
Calibrated lunar output = _____

Observation 18:

y-intercept, a = _____ slope, b = _____
Calibrated lunar output = _____

STUDENT'S NAME _____

Observation 19:

y-intercept, a = _____ slope, b = _____
Calibrated lunar output = _____

Observation 20:

y-intercept, a = _____ slope, b = _____
Calibrated lunar output = _____

Observation 21:

y-intercept, a = _____ slope, b = _____
Calibrated lunar output = _____

Observation 22:

y-intercept, a = _____ slope, b = _____
Calibrated lunar output = _____

STUDENT'S NAME _____

Observation 23:

y-intercept, a = _____ slope, b = _____
Calibrated lunar output = _____

Observation 24:

y-intercept, a = _____ slope, b = _____
Calibrated lunar output = _____

Observation 25:

y-intercept, a = _____ slope, b = _____
Calibrated lunar output = _____

STUDENT'S NAME _____

Graph of the fraction of the lunar surface illuminated and the calibrated output of the 11 GHz radiometer as a function of Julian date.

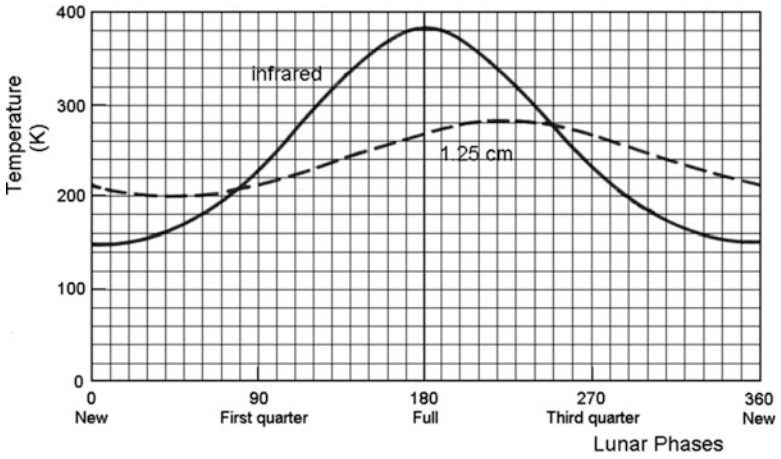

Table 4 Analysis of microwave phase curves

Wavelength of curve, λ (cm)	Time lag (days)	Amplitude (K)	Width at maximum, Δ_2 (days)	Width at minimum, Δ_1 (days)	Δ_2/Δ_1	$(d/\lambda)_{granite}$	Effective Depth = $(d/\lambda)_{granite}$ x λ (cm)
1.25							
2.7							

STUDENT'S NAME _____

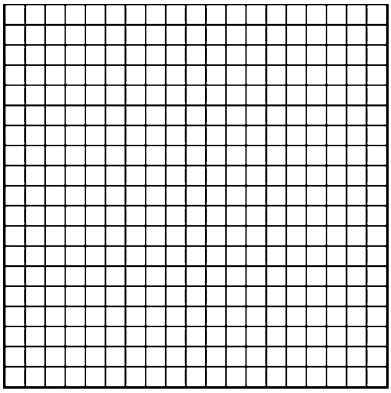

Graph of the time lag and ratio Δ_2/Δ_1 using the left ordinate scale, and the amplitude in degrees K using the right ordinate scale, as a function of effective depth. Clearly distinguish the points being graphed by using different symbols

2. *LUNAR ECLIPSE*

This section is only relevant if an eclipsed was observed during your school semester.

Zero setting of the microammeter for calibration: _____

Gain setting of the microammeter for calibration, $g_c =$ _____

Zero setting of the microammeter for Moon observations: _____

Gain setting of the microammeter for Moon observations, $g_m =$ _____

$r_g = g_m/g_c =$ _____

Table 5 Calibration of receiver for eclipse measurements

Target	Output (millivolts)	Temperature (K)
Ambient water bath without plastic, V_1		
Ambient water bath with plastic, V_2		
$f_s = V_1/V_2$		
Ice-water bath output, V_i		273.2
Boiling-water bath output, V'_b		373.2
Corrected boiling output, $V_b = f_s V'_b$		373.2

STUDENT'S NAME _____

Determination of the calibration equation for each observation. Perform all your calculations here.

y-intercept, a = _____
slope, b = _____

STUDENT'S NAME _____

Table 6 Eclipse data

Observation	Time	Output (millivolts)	Calibrated output (K)	Decimal time	Disk fraction within umbra[a]
Prior to eclipse					
Dark sky					
Moon					
During ingress					
1.					
2.					
3.					
4.					
5.					
6.					
7.					
8.					
9.					
10.					
During egress					
11.					
12.					
13.					
14.					
15.					
16.					
17.					
18.					
19.					
20.					
After eclipse					
Dark sky					
Moon					

[a] If the data are available

STUDENT'S NAME _____

Calibrated lunar output during eclipse. Show your calculations of the calibrated lunar outputs calculated from (1), $T = f_e\, r_g\, (a + b\, V)$.

Observation 1:

Observation 2:

Observation 3:

Observation 4:

Observation 5:

Observation 6:

Observation 7:

Observation 8:

Observation 9:

STUDENT'S NAME _____

Observation 10:

Observation 11:

Observation 12:

Observation 13:

Observation 14:

Observation 15:

Observation 16:

Observation 17:

Observation 18:

Observation 19:

Observation 20:

STUDENT'S NAME _____

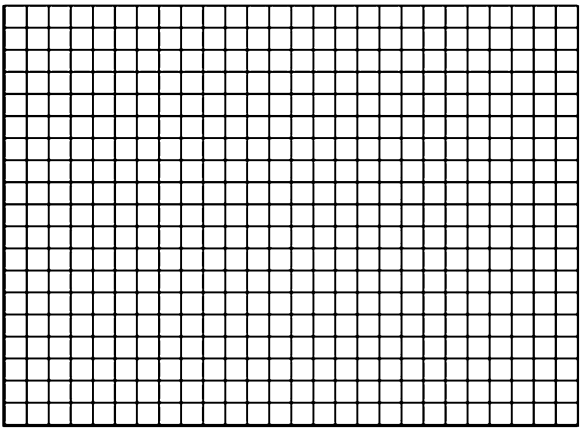

Graph of light curve and 11 GHz temperature results from Table 6.

STUDENT'S NAME _____

F. Discussion Questions for Microwave Phase Effect of the Moon

1. Describe the difference of the time lag, the ratio Δ_2/Δ_1 of widths, and the effective depth of origin of the emissions at the wavelengths of 1.25 cm and 2.7 cm. At which wavelengths of observation are each of the three effects the greatest or the least?

2. Below are two series of hypothetical graphs of the variation of temperature with depth in a planetary or moon subsurface at three times, assuming the same insolation as a function of time. The two graphs represent material of different thermal diffusivity.

   Which of the sets of graphs represent material with the greater thermal diffusivity? Explain your answer in terms of the heat conduction equation, Eq. (2) of Experiment #15, "Thermal Radiation from a Planetary Subsurface: Part II: Soil Sample Measurements". Provide qualitative estimates of the values of dT/dt and the curvature of the $T(x)$ curves, that is, the change with depth of the gradient, $d^2T/dx^2 = d/dx\ (dT/dx)$.

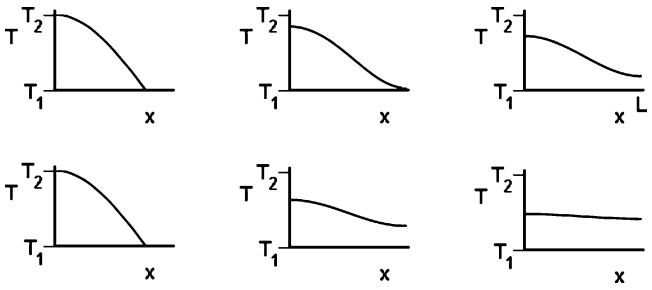

STUDENT'S NAME _____

3. If you observed an eclipse as part of the experiment, the microwave emission from the Moon would be found to be nearly flat as a function of time during the eclipse whereas the fraction of the lunar surface illuminated varied from 100% to 0% and back to 100%. Explain this in terms of the depth from which the microwave radiation was emitted and the thermal diffusivity of the subsurface material.

4. Let us say that an eclipse is observed of a moon of unknown origin and composition, and that the microwave emission varied proportionally to the fraction of the lunar surface illuminated.

   a. What can you deduce about the value of the thermal diffusivity of the subsurface material? Explain your answer.

   b. From Table 1 of Experiment #15, "Thermal Radiation from a Planetary Subsurface: Part II: Soil Sample Measurements," which substance would be most similar to the material of which this hypothetical moon is composed?

5. Because the antenna used in this experiment has a BWHP of size about equal to the angular diameter of the Moon, it receives emission from the entire visible disk. Using a larger telescope could resolve the disk. Referring to the heat conduction equation, Eq. (1) of Experiment #15, "Thermal Radiation from a Planetary Subsurface: Part II: Soil Sample Measurements," and Table 1 of Experiment #15, "Thermal Radiation from a Planetary Subsurface: Part II: Soil Sample Measurements," as the eclipse proceeds what part or parts of the lunar disk, if any, would provide the most useful information about the nature of the subsurface material? Assume that the ingress, totality, and egress portions of the eclipse are of equal duration. Explain your answer.

6. Shown below are the microwave phase curves for four different hypothetical moons, all revolving about the same planet so that they receive the same amount of insolation from the parent star. Observations were made at either 2-cm wavelength or 5-cm wavelength. Which of the following describes which of the observations and the moon being observed? Provide the best answer for each question.

STUDENT'S NAME _____

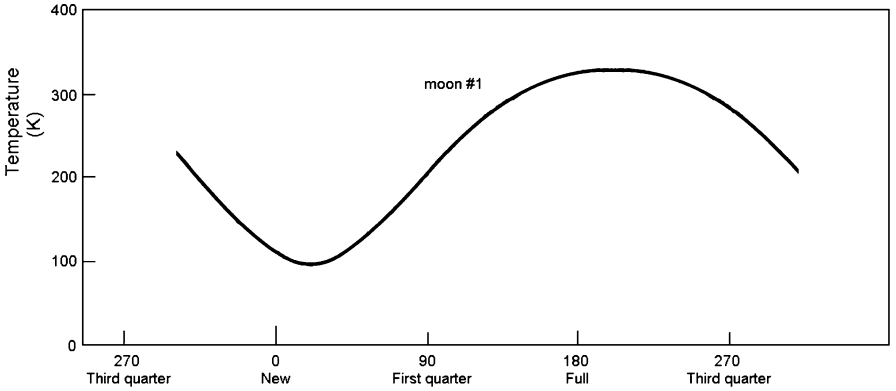

a. Which moon most likely has a subsurface composed largely of volcanic material rich in iron and nickel? Explain your answer.

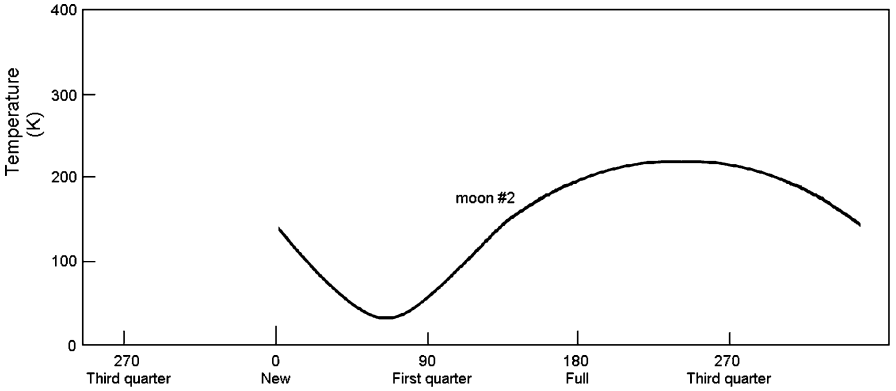

b. Which moon most likely has a subsurface composed largely of sand of fragmented and powdered silicate rocks? Explain your answer.

STUDENT'S NAME _____

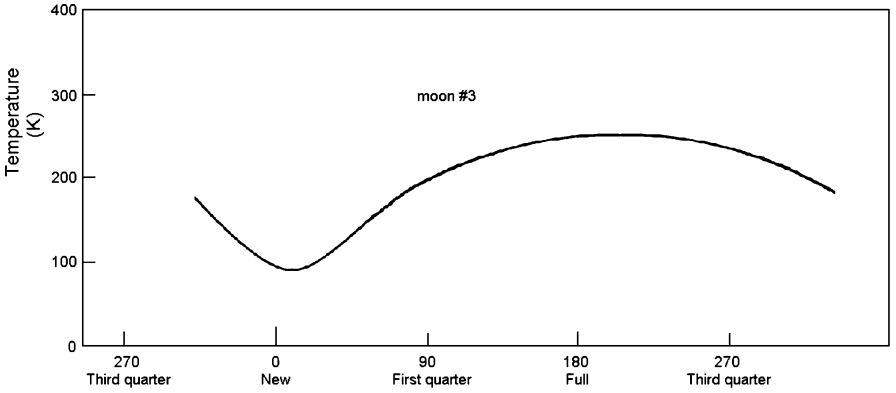

c. Two of the moons have subsurfaces that are known to be identical in composition. Which was observed at 2-cm wavelength? Explain your answer.

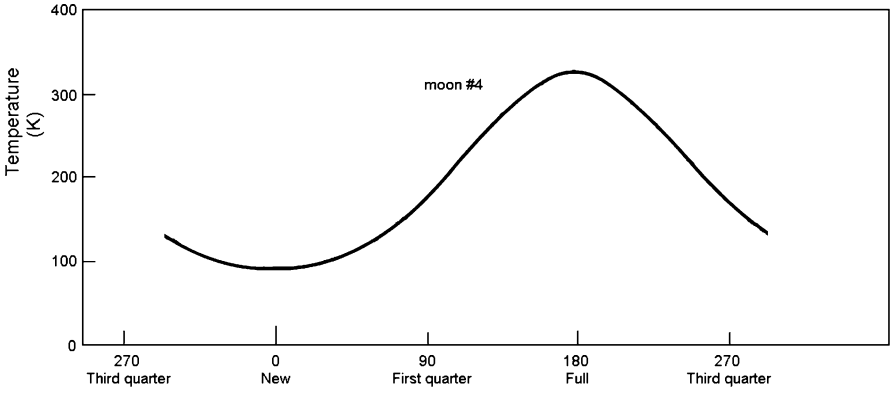

d. Two of the moons have subsurfaces that are known to be identical in composition. Which was observed at 5-cm wavelength? Explain your answer.

e. Which moon would be most likely as the habitat for a primitive form of life? Explain your answer.

STUDENT'S NAME _____

7. Some investigators believe that UFO's can be explained as alien spacecraft. Some of those also believe that the Moon is composed of green cheese. Food engineers have measured the thermal diffusivity of cheese and find it to be approximately equal to that of water, roughly independent of water, fat, and protein content, and age. Based on a value of thermal diffusivity for water as given in Table 2 of Experiment #15, "Thermal Radiation from a Planetary Subsurface: Part II: Soil Sample Measurements," draw a representation of the microwave phase curve for such a moon. So that your observational results of our Moon at 11 GHz can be used as a guide, imagine that such a moon is also observed at 11 GHz.

Removing these DATA SHEETS from the book may damage the binding. You might consider entering the data and performing your calculations in the book, and then photocopying the DATA SHEETS for submission to your instructor for grading.

If you used graph paper other than that provided, attach those graphs to these DATA SHEETS.

Part III
Measuring the Stars and Beyond

Introduction

The ability to observe and analyze the electro-magnetic radiation from objects in space in order to determine their physical and chemical nature stands among the greatest intellectual achievements of mankind. In this section, we introduce two major types of radiation, blackbody radiation and discrete spectral radiation. The energy output of the Sun, which is, as with most stars, a good approximation to a blackbody, is studied. The knowledge of blackbody radiation and spectral radiation is combined in a study of the powerful Kirchhoff's Laws.

Go and catch a falling star
—John Donne (1573–1631)

Experiment 17
Blackbody Radiation

SUMMARY: In Experiment #17, "Blackbody Radiation," we study blackbody radiation by passing a known amount of electrical current through a light bulb and then measuring the amount of radiation emitted by a photometer. The total amount of radiation emitted at all wavelengths and the wavelength at which the radiation is maximum are also measured.

LEVEL OF DIFFICULTY: Moderate

EQUIPMENT NEEDED: 100-Watt incandescent bulb; variable power supply; ammeter; color filters; photometer; ruler.

MY LEARNING GOALS

1. To be able to describe the mathematical dependence of intensity as a function of wavelength of a heated object on its temperature.
2. To be able to apply the Wien displacement law to predict the surface temperature of a star from its color.
3. To be able to describe the mathematical dependence of the total intensity emitted by a heated object such as a lightbulb on its temperature.

L.M. Golden, *Laboratory Experiments in Physics for Modern Astronomy: With Comprehensive Development of the Physical Principles*,
DOI 10.1007/978-1-4614-3311-8_17,

A. Introduction

In 1918 physicist Max Planck (1858–1947) applied the new theory of quantum mechanics to explain the radiation observed from warm objects. He derived the formula for the intensity of radiation produced by an idealized object at a given temperature as a function of frequency. He assumed that electromagnetic energy is carried by particles, *photons*, whose energy is quantized in little quantities according to $E = h\nu$, where ν is the frequency of the electromagnetic radiation and h is *Planck's constant*, $h = 6.63 \times 10^{-27}$ erg-s (or cm^2-gm/s). Planck then derived the following formula for the intensity of radiation produced per volume in a frequency interval centered at ν by an idealized object at temperature T,

$$B(\nu, T) = \left[\frac{8\pi h}{c^3}\right] \frac{\nu^3}{e^{h\nu/kT} - 1}, \tag{1}$$

where the frequency of radiation ν is related to the wavelength of the radiation λ by

$$\nu = \frac{c}{\lambda},$$

c is the speed of light in a vacuum, $c = 3.0 \times 10^{10}$ cm/s, and k is *Boltzmann's constant* (Ludwig Boltzmann, 1844–1906), $k = 1.38 \times 10^{-16}$ erg-s/K (or cm^2-gm/s^2- K).

This formula is derived assuming the object absorbs all the radiation that impinges upon it, reflecting none. Accordingly, it is referred to as a *blackbody*, the radiation is referred to as *blackbody radiation*, and the formula is known as *Planck's Blackbody Radiation Law*, or simply *Planck's Law*. Because no object in nature absorbs all radiation impinging on it, this law is an idealization and the equation describes what is referred to as an "ideal" blackbody.

Although no real material follows this formula exactly, the radiation produced by many objects in nature closely approximates it. One of the closest is a box whose interior is painted black and which is enclosed except for a small opening from which to observe the radiation. In nature, the radiation from stars, the surfaces of planets, bricks, incandescent light bulbs, and innumerable other objects closely follow the formula. This includes the universe itself, cooling as it has expanded following its creation in the big bang of 12–15 billion years ago.

Two limiting cases exist depending on the relative values of $h\nu$ and kT. For wavelengths sufficiently long so that $h\nu << kT$, (1) becomes the *Rayleigh-Jeans Approximation* (James Jeans, 1877–1946),

$$B(\nu, T) = \frac{8\pi\nu^2}{c^3} kT.$$

At Earthlike temperatures of 300 K, the approximation is very good for $\lambda > 2.5$ mm. At the microwave wavelength of 2.7 cm used in Experiments #14 and #15,

"Thermal Radiation from a Planetary Subsurface: Part I: Calibration and Initial Measurements," and "Thermal Radiation from a Planetary Subsurface: Part II: Soil Sample Measurements", and "The Microwave Phase Effect of the Moon," the approximation is excellent.

For wavelengths sufficiently short so that $hv \gg kT$, (1) becomes the *Wien Radiation Law* (Wilhelm Wien, 1864–1928),

$$B(v,T) = \left[\frac{8\pi hv^3}{c^3}\right] e^{-\frac{hv}{kT}}.$$

In this experiment we will examine the radiation coming from both the Sun and an incandescent light bulb. We will determine the effective temperature of the Sun. We will compare the energy sent to the filaments of the light bulb through a simple electric circuit with the energy that it radiates.

B. Theory

1. Blackbody Relationships

Some important mathematical relationships can be derived from Planck's law using the methods of calculus. By integrating the formula over all wavelengths, we find that the total amount of radiation emitted per second per unit area of the radiating surface is proportional to T^4. This, the *Stefan-Boltzmann Law* (Josef Stefan, 1835–1893), is a strong dependence indeed, indicating, for example, that doubling the temperature of a body increases the amount of radiation it produces by a factor of 16.

By differentiating the law with respect to the wavelength, λ, we find that the maximum of the radiation occurs at a wavelength proportional to $1/T$. This, *Wien's displacement law*, often referred to simply as Wien's law, tells us that a correspondence exists between the color of a star and the temperature of the region from which the radiation of the star reaches us, typically the *photosphere*.

For example, a star that appears to be red (a relatively large wavelength) has a smaller "surface" temperature, about 2000–4000 K, and a star that appears to be blue (a relatively small wavelength) has a larger "surface" temperature, about 10,000–20,000 K. In this way, by observing their colors, we determine the temperature of the visible surfaces of stars. Table 1 provides colors, corresponding surface temperatures, and the nomenclature for the familiar stellar classification of *main sequence* stars on the *Hertzsprung-Russell diagram*.

These relationships were in fact known by experimenters in the 19th century before Planck's law was discovered. The precise mathematical relationships thus derived from Planck's law are, first, the total amount of radiation over all

Table 1 Characteristics of main sequence stars

Spectral type	Surface temperature (K)	Color of star
O	>28,000	Blue to violet
B	10,000–28,000	White to blue
A	7500–10,000	White
F	6000–7500	Yellow to white
G	5000–6000	Orange to yellow
K	3500–5000	Red to orange
M	2000–3500	Red

wavelengths emitted by a blackbody per second per unit surface area of the blackbody, or *energy flux*,

$$F = \sigma T^4, \tag{2}$$

where the *Stefan-Boltzmann constant* $\sigma = 5.67 \times 10^{-8}$ W/m^2- K ^{4} if the radiation is measured in Joules and the surface area is measured in square meters.

Wien's displacement law is

$$\lambda_{\max} = \frac{\kappa}{T}, \tag{3}$$

where the constant,

$$\kappa = 2.9 \times 10^7 \overset{o}{A} - K.$$

This relationship is informative. It tells us that the wavelength at which the intensity of radiation is maximum for objects of temperatures 3,000–10,000 K, such as stars, is in the visible portion of the electro-magnetic spectrum; that the wavelength at which the intensity of radiation is maximum for dust particles in interstellar space, with temperatures about 3–10 K, is in the infrared, about 1 mm wavelength; and that the wavelength at which the intensity of radiation is maximum for gases heated to millions of degrees, such as near black holes, is in the x-ray portion of the spectrum, about 30 Å. Indeed, to learn all we would like to know about the universe we must study it in all parts of the electro-magnetic spectrum.

In general, the Rayleigh-Jeans Approximation represents Planck's Law well for wavelengths of the blackbody spectrum much greater than the wavelength of maximum radiation and the Wien Radiation Law represents Planck's Law well for wavelengths of the blackbody spectrum much less than the wavelength of maximum radiation.

We can use (1) to construct graphs of the intensity of blackbody radiation as a function of wavelength λ for any temperature. Figure 1 displays the blackbody curves for an ideal blackbody at various temperatures. These have the characteristic appearance of a Planck radiation curve, a steeply rising portion, a maximum, and a

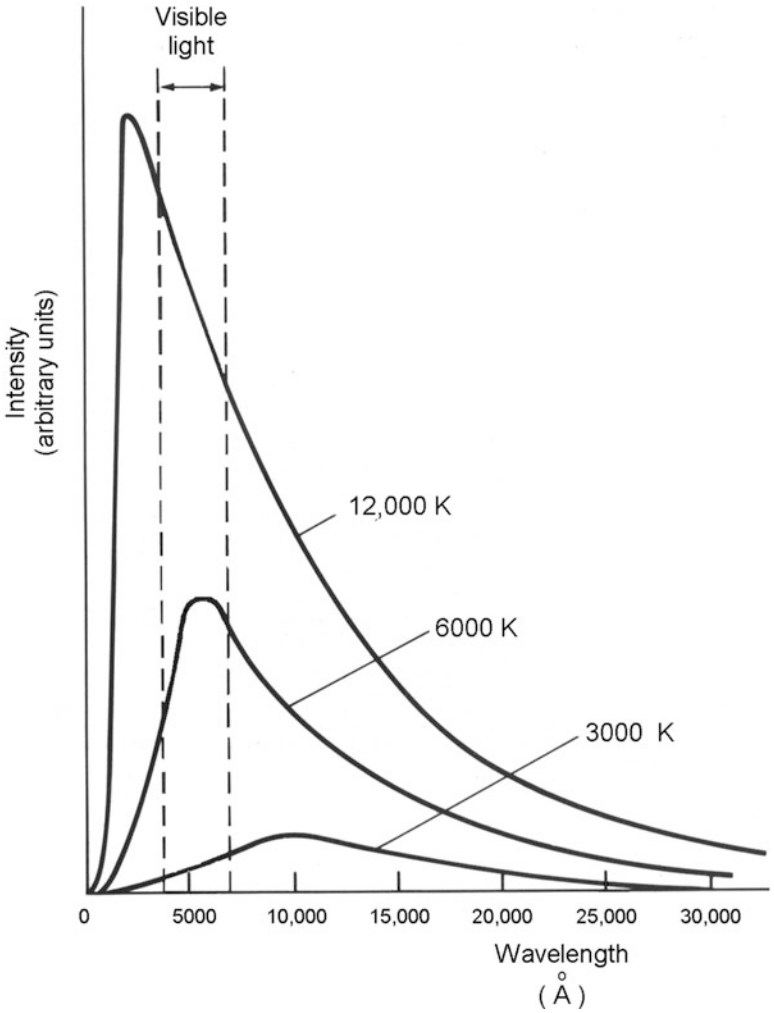

Fig. 1 Blackbody curves provide the intensity of radiation for all frequencies (or wavelengths). The curves depend only on the temperature of the blackbody and that dependence, as can be seen, is marked. For the blackbody curve at 6000 K, the approximate surface temperature of the Sun, the maximum radiation occurs in the visual region of the electromagnetic spectrum. Blackbody curves can be expressed either as a function of frequency or as a function of wavelength

long tail to large frequencies. Note that the total amount of radiation, the area under the curve, increases markedly with increasing T, as shown by (2), and that the frequency at which the radiation is maximum increases with increasing frequency, as shown by (3).

In this experiment we shall test these relationships for an incandescent light bulb and by observations of the Sun.

2. *Ohm's Law*

An incandescent bulb glows because it is radiating energy at wavelengths visible to the eye. We can consider the filament of the bulb as simply a resistor through which current passes. The energy per second, or power, produced in it is then given by $P = V\,I$, where V is the voltage across the resistor and I is the current passing through the resistor. These are related by the well-known *Ohm's law* of electricity, $V = I\,R$, where R is the resistance of the filament, a characteristic of its dimensions and composition. Except for a small amount of energy absorbed by the glass and base of the light bulb, all the electrical energy that passes through the filament is converted into energy that is radiated outwards.

3. *Color Filters*

Astronomers employ various auxiliary equipment attached to telescopes to learn about the objects they are seeing. The first, of course, was the naked eye. These include photographic plates, although now hardly used except for instructional purposes and by amateur astronomers, color filters, such as those you might use with your camera, photometers, similar to those on your camera, and the modern charge coupled detectors or CCD's. To spread out the spectra to see the details of absorption and emission lines, scientists and astronomers, beginning with the famous experiment on the nature of light by Sir Isaac Newton, used, first, prisms, and now spectrographs. In this experiment we shall use color filters to analyze the light.

Historically, the temperatures of the visible surfaces of stars were determined by the technique we will use for the light bulb and the Sun, by using color filters and comparing the amount of radiation passing through the filters to the photometer. In modern times, spectra of stars give more precise values.

A color filter is simply a piece of plastic or glass which allows transmission of a particular color of light. In reality, it is impossible to create a color filter which allows only a single or very small wavelength interval, and, because such a filter would transmit only a small amount of light, making analysis difficult, this would not be useful. In fact, color filters have a finite *bandpass*, a term borrowed from electronics to signify an interval of wavelengths. Figure 2 shows bandpasses for some standard filters. Table 2 provides the effective wavelength of those filters and a measure of the width of the bandpass, its "full-width at half-maximum." This term refers to the difference in the wavelengths at which the light transmitted through the filter is half as large as the maximum amount of transmitted light.

Using (1), we can also calculate the relative intensities of blackbody radiation at different wavelengths for an object at a given temperature. Some of these results are provided in Table 3. For example, for the radiation from the 4000 K object, we see that the ratio of the intensities of the radiation at the wavelength of $\lambda = 5500$ Å, corresponding to yellow, to that at 4400 Å, corresponding to blue, is 2.78. In general

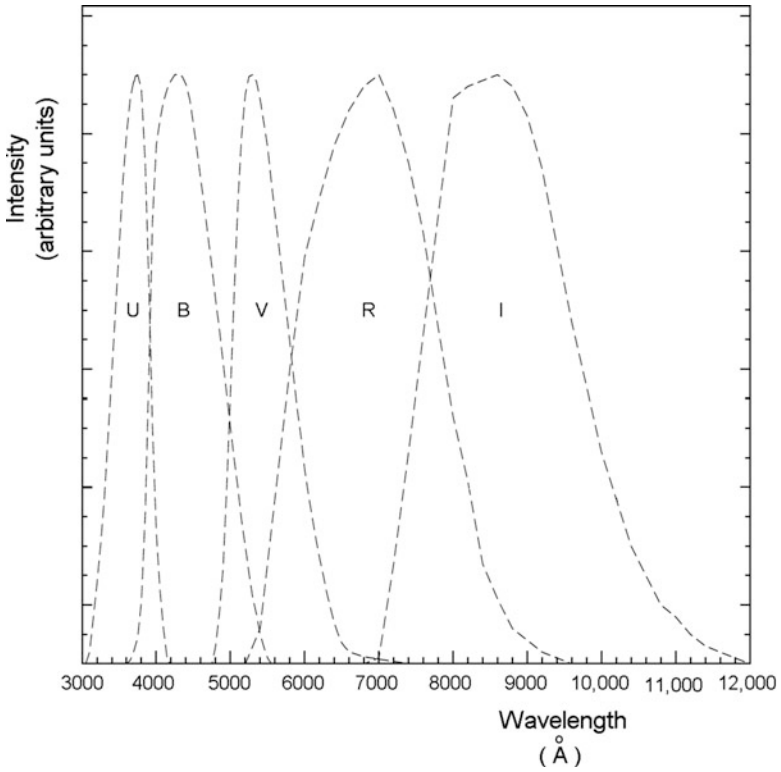

Fig. 2 Color filters were historically used to analyze the light from stars. As with all filters, the ultraviolet, blue, visible, red, and infrared filters, the most commonly used, allow transmission of a range of wavelengths referred to as their bandpass

Table 2 Color filter characteristics

Filter	Effective wavelength (Å)	Full-width at half maximum (Å)
U (ultra-violet)	3735	485
B (blue)	4443	831
V (visible; that is, green-yellow)	5483	827
R (red)	6855	1742
I (infrared)	8637	1970

by measuring these intensities and comparing them to numbers such as those provided in Table 3, we can determine the temperature of the object. Historically, astronomers referred to the filter that passes the light centered near 5500 Å as *V* for "visual." That color is green-yellow, and we will refer to it by the letter "*Y*" to avoid possible student's confusion with the color violet and to prevent confusion with *V* which we will use for voltage.

Table 3 Y/B colors for blackbody temperatures

Intensity ratio yellow/blue filters	Temperature of blackbody (K)	Color
0.775	20,000	Blue
1.00	10,000	White
1.19	8000	Yellow-white
1.67	6000	Yellow
2.78	4000	Orange
6.25	2000	Red

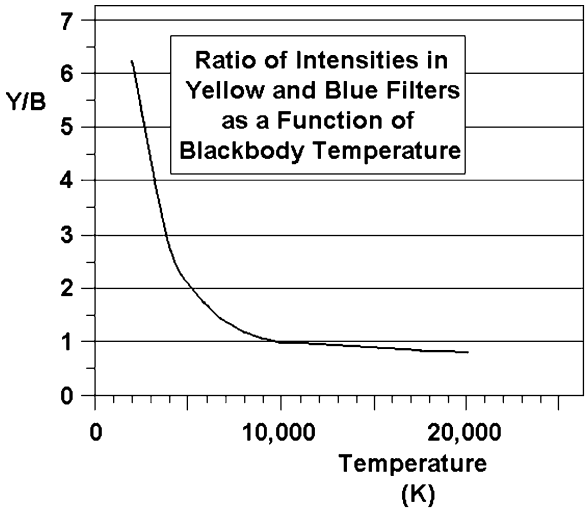

Fig. 3 A graph of the data of Table 3. If the yellow and blue filters available in your laboratory do not have the same characteristics as those of Table 3, you will construct a similar graph for use in the experiment

Figure 3 presents a graph of the data of Table 3 with a smooth curve drawn through the data. Because these are theoretically-determined values rather than experimental data, the curve is constructed to pass through all the data of Table 3. Although relatively standard, the yellow and blue filters that you may use may not have the same characteristics as those from which the ratios of Table 3 and Fig. 3 were determined. In this case, use the corresponding figure determined from the filters available in your laboratory. (In professional astronomical work, the comparison of the intensity measured through the two filters is expressed in terms of the stellar magnitudes observed at the two colors. The ratio of the intensity in the two colors is then related to the difference of the logarithms. In this way, the *color index* is defined as $B-V = 2.5\ log\ (I_V\ /I_B)$, where here B and V are in stellar magnitudes and we adhere to the historical usage of V for the measurement through the visual filter. Because other color indices can also be defined, this is also referred to as the B-V color.)

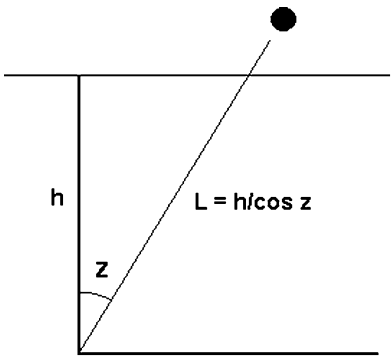

Fig. 4 The path length of rays from the Sun through an atmosphere of thickness *h* to the observer on the ground is proportional to *sec z*

4. The Effective Temperature of the Sun

The rising and setting Sun on a cloudless day appears red, a result of the wavelength-dependent *Rayleigh scattering* (Lord Rayleigh, 1842–1919) of the radiation from the Sun out of the line-of-sight by molecules and fine particles of dust in the atmosphere. The blue rays get scattered by the atmosphere leaving the red rays to reach us. The longer is the path through which the rays of the Sun travel, the greater is the effect, Fig. 4. That path length is proportional to the secant of the zenith angle. The amount of scattering also depends on meteorological conditions, in particular the amount of dust in the atmosphere.

Note that even if you view the Sun directly overhead, some of its blue rays have been scattered, making it appear more yellow than it would appear if viewed in space by astronauts or lunar colonists, we should ever be so lucky. In this experiment, we will observe the color of the Sun at different zenith angles to quantify this effect. Because the intensity of the sunlight at all wavelengths is diminished because of its passage through the atmosphere, we must deal with the ratio of the intensities observed in two colors at a given time rather than the actual value of the intensities.

C. Procedure and Observations

1. The Sun

We will examine the change in the effective color of the Sun as it passes through the sky. At the very beginning of the laboratory session, on a cloudless day, take the photometer outside. Put the photometer directly in sunlight, as perpendicular to the rays of the Sun as possible, and in turn place the filters over the photometer.

To ensure that the photometer window is perpendicular to the rays, simply rotate it slowly until the maximum reading is obtained.

Enter the readings in Table 4 of the DATA SHEET. Enter the time of day of your observations (standard time, not Daylight Savings Time) in Table 4 in military time.

Repeat this at a time near the middle of the laboratory session and also at the very end of the laboratory session, when your measurements of the incandescent light bulb have all been concluded. A three-hour long laboratory session provides approximately a factor of three in *sec z* in the spring months and a factor of four in *sec z* in the fall months, providing sufficient discrimination in path length of the rays of the Sun through the atmosphere for our data reduction and graphical purposes.

2. *Incandescent Light Bulb*

We will use a standard 100-W household incandescent bulb, a variable power supply connected to the light bulb, an ammeter to measure the amount of current going into the light bulb, color filters, and a photometer to measure the intensity of the radiation coming from the light bulb and through the color filters. We will determine the amount of energy that the power supply delivers to the light bulb and compare it to the amount of radiation that the light bulb produces.

Variable power supplies provide a DC voltage. Some also have adjustable currents. If the power supplies in your laboratory lack the adjustable current feature, then your lab technician can construct a simple circuit with a rheostat to provide the variable current.

The light bulb is connected to the variable power supply. Turn it on and rotate the rheostat on the variable power supply to provide only a small amount of current to the light bulb. Increase the current so that the color of the light bulb is moderately dull red. Enter the voltage delivered by the power supply, the amount of current in the circuit, as read on the ammeter, and describe the color of the light bulb in Table 6 of the DATA SHEET.

Place your hand near the light bulb and in column 5 of Table 6 of the DATA SHEET describe the sensation of heat you feel, if any. We want to try to quantify this amount of heat. In Table 6 ascribe the number "1" to it. Similarly, enter a number "1" to describe the brightness of the light bulb in column 6 of Table 6. These will be reference values for our later observations.

Move the photometer to a distance from the light bulb so that the intensity reads toward the lower end of the photometer scale. In all the following measurements, keep the photometer at the same distance from the light bulb. Measure that distance and enter it on the DATA SHEET.

Because the photometer will receive radiation from the ambient light in the room, we need to turn off all the lights before making our measurements. Now place the yellow and blue filters in turn over the light bulb. Enter the readings of the

photometer resulting from the light passing through each filter in columns 7 and 8, respectively, of row 1 of Table 6 of the DATA SHEET.

Remove the blue filter from in front of the light bulb. Increase the amount of voltage being delivered by the power supply so that the light bulb brightens to a reddish-yellow color. In row 2 of Table 6 of the DATA SHEET, enter the voltage and current readings. Describe the color of the light bulb and describe the sensation of heat you feel with the brighter light by ascribing a number to it. Is it, for example, twice or three times as warm? Similarly, enter a number providing the relative brightness of the light bulb. With the ambient light in the room off, place the yellow and blue filters in turn over the light bulb. Enter the readings of the photometer resulting from the light passing through each filter in columns 7 and 8, respectively, of row 2 of Table 6 of the DATA SHEET.

Increase the amount of voltage once again so that the color of the light bulb is white. Repeat the observations and enter your result in Table 6. If the photometer readings have pegged the meter, perform these observations again with a smaller voltage setting on the power supply.

Increase the amount of voltage once again so that the color of the light bulb is whitish-blue. Repeat the observations and enter your result in Table 6. If the photometer readings have pegged the meter, perform these observations again with a smaller voltage setting on the power supply.

D. Analysis and Calculations

1. The Sun

On the DATA SHEET, calculate the ratio, Y/B, of photometer readings through the yellow and blue filters for your three observations of the Sun. As above, from Table 3 find the corresponding color of the Sun. From Fig. 3, find the apparent surface temperature of the Sun corresponding to the values of Y/B. If the Y and B filters you are using do not have the same characteristics as those represented in Table 3, use the graph you have correspondingly prepared. From (3), calculate the wavelength for which the radiation from the Sun is the maximum. Enter the results in Table 4 of the DATA SHEET. Perform your calculations on the DATA SHEET.

To analyze the changing color of the Sun as it travels across the sky as a function of the layer of atmosphere through which the radiation passes, we need to calculate its zenith angle at the three times we observed from Eq. (1) of Experiment #5, "Earth: The Seasons and Local Latitude". To do that, we need the right ascension, declination, and hour angle of the Sun at these times. To calculate the hour angle, we need the *local sidereal time*, or LST.

From internet websites, for example, http://faculty.physics.tamu.edu/krisciunas/ra_dec_sun.html, or a printed Ephemeris of the Sun, find the right ascension, RA, and declination, δ, of the Sun on your date of observation. The right ascension is

provided in hours, minutes, and seconds of time. Convert that to hours and decimal fraction of hours. The declination is given in degrees, minutes, and seconds of arc. Convert that to degrees and fraction of a degree. Perform those calculations on the DATA SHEET and enter the results in Table 5.

From internet websites, for examples, http://tycho.usno.navy.mil/sidereal.html or http://www.jgiesen.de/astro/astroJS/siderealClock/, or a printed Ephemeris or almanac, find the local sidereal time, LST, corresponding to your longitude and the three local times of your observations of the Sun. The former website is simple to use, but will provide the LST only at the time you access the site. The latter website is more complex to use, but also provides data for international cities and you can enter any local standard time. It also provides the declination of the Sun at the time you provide. As with the right ascension, convert the LST to hours and decimal fraction of hours and enter the result in Table 5.

With LST and RA known, we find the values of the hour angles, HA, at which the Sun was observed from the standard astronomical relationship,

$$\mathrm{HA} = \mathrm{LST} - \mathrm{RA}.$$

You can then calculate the hour angle, HA, of your observations in the unit of hours. Enter the result for the hour angle in Table 5.

Convert the hour angle from hours to degrees by the conversion factor, 1 h of time $= 15^{o}$ of arc. (The Earth rotates 360^{o} in 24 h.) Enter that result in Table 5 of the DATA SHEET.

From the zenith angle equation, using the values of the declination of the Sun on the date of your observation and the hour angles at the three times of your observations, calculate the values of $\cos z$ of the Sun at the three times. Recall that we used the letter h for hour angle in the zenith angle equation. Then calculate and enter $\sec z = 1/\cos z$ in Table 5 of the DATA SHEET. Show all your calculations on the DATA SHEET.

Using the axes provided on the DATA SHEET, construct a graph of both Y/B and the corresponding apparent temperature of the Sun as derived from Fig. 3 and entered in Table 4 as a function of $\sec z$. Provide the scale for Y/B on the left ordinate line and the scale for the temperature on the right ordinate line. For reference, draw a line at the known 5800 K temperature of the surface of the Sun on the right ordinate scale.

Draw a smooth curve through the points and extrapolate the curve to a a value of $\sec z = 1$, a zenith angle of zero degrees, corresponding to a view directly overhead. Provide the corresponding values of Y/B and apparent temperature on the DATA SHEET.

Although it makes no trigonometric sense to extrapolate the curve to smaller values of $\sec z$ itself, remembering Fig. 4 we see that the path length of the rays of the Sun is $h \sec z$. Extrapolating the curve to a value of "$\sec z = 0$," is therefore equivalent to extrapolating to the case of no atmosphere. Read the values of Y/B and the corresponding apparent temperature of the surface of the Sun from that extrapolation and enter the results on the DATA SHEET.

2. *Incandescent Light Bulb*

On the DATA SHEET, calculate the value of the power provided by the variable power supply, $P = VI$. Calculate the ratio of photometer readings, Y/B, through the yellow and blue filters for each setting of the variable power supply. Dividing will cause the various constants, such as the collecting area of the photometer, to cancel. Enter those results in Table 7 of the DATA SHEET. Show all your calculations on the DATA SHEET.

For each of the values of Y/B, interpolate using Fig. 3 (or the corresponding curve if the filters in your laboratory have characteristics different from those of Tables 2 and 3) to determine the temperature of the light bulb filament for each setting of the variable power supply. Enter the results in Table 7 of the DATA SHEET.

Equation 2 provides the energy flux, the total amount of radiation over all wavelengths emitted by a blackbody per unit surface area of the blackbody. Using the temperatures you have found, calculate that amount on the DATA SHEET. Equation 3 provides the wavelength, λ_{max}, at which the radiation from a blackbody of a given temperature is maximum. Using the temperatures you found, calculate that value for each setting of the variable power supply. Enter the results for both in columns 5 and 7, respectively, of Table 7 of the DATA SHEET.

If we assume that the total amount of electrical power provided to the light bulb is converted into radiation, we can use (2) to calculate the surface area of the light bulb filament. For each setting of the variable power supply, determine the surface area of the light bulb filament by dividing the power delivered by the variable power supply, entered in column 2 of Table 7, by the energy flux, entered in column 5 of Table 7. Enter the results in column 6 of Table 7. These values for the light bulb surface area should be about the same. Find the average value of the four surface area calculations. If one of the values differs widely from the others, do not include it in this calculation. Perform all your calculations on the DATA SHEET.

STUDENT'S NAME _____

E. Blackbody Radiation Experiment Data Sheet

1. The Sun

Show all your calculations here.

Table 4 Yellow and blue filter readings of the Sun

Observation	Photometer reading yellow filter	Photometer reading blue filter	Local time	Y/B	Color of the Sun	Apparent surface temperature of the Sun (K)	λ_{max} (Å)
Initial							
Middle							
Final							

Calculation of wavelength of maximum emission, λ_{max}

Observation 1:

Observation 2:

Observation 3:

STUDENT'S NAME _____

Table 5 Zenith angle calculations of the Sun

Observation	Local time	LST (hours)	RA (hours)	HA (hours)	HA (degrees)	δ (degrees)	cos z	sec z
Initial								
Middle								
Final								

Conversion of RA from Hours, Minutes, Seconds to Hours

Observation 1:

Observation 2:

Observation 3:

Conversion of δ from Degrees, Minutes, and Seconds of arc to Degrees

Observation 1:

Observation 2:

Observation 3:

STUDENT'S NAME _____

Conversion of LST from Hours, Minutes, Seconds to Hours

Observation 1:

Observation 2:

Observation 3:

Calculation of Hour Angle

Calculation of hour angle by HA = LST – RA.

Observation 1:

Observation 2:

Observation 3:

Conversion of hour angle from hours to degrees by the conversion factor, 1 h of time = 15^{o}

Observation 1:

Observation 2:

Observation 3:

STUDENT'S NAME _____

Calculation of the values of cos z and sec z of the Sun.

The latitude of your city: _____

Calculation of sec z

Observation 1:

.Observation 2:

Observation 3:

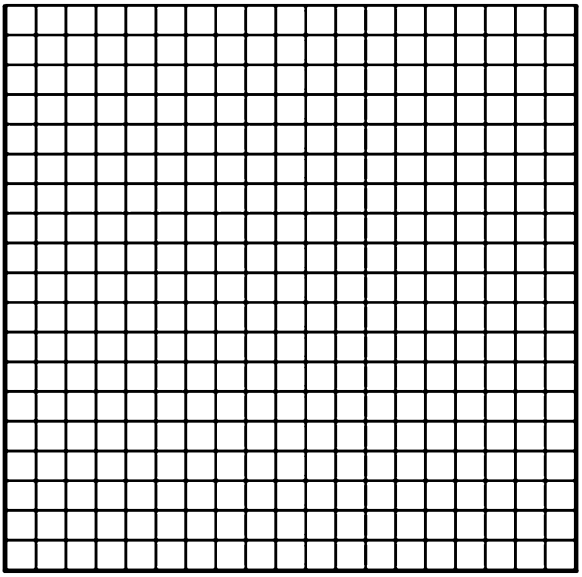

Graph of both *V*/*B* and the corresponding apparent temperature of the Sun as a function of *sec z*.

Y/*B* for *sec z* = 1: _____
Corresponding surface temperature for *sec z* =1: _____ K

STUDENT'S NAME _____

Y/*B* for "no atmosphere": _____
Corresponding surface temperature: _____ K

2. *Incandescent Light Bulb*

Distance of light bulb from photometer: _____

Table 6 Power supply and light bulb data

Power supply setting	Voltage reading, V (volts)	Ammeter reading, I (amperes)	Subjective color	Subjective heat level	Subjective brightness	Photometer reading yellow filter	Photometer reading blue filter
#1							
#2							
#3							
#4							

STUDENT'S NAME _____

Table 7 Light bulb analysis

Power supply setting	$P = V \times I$ (W)	Y/B	Corresponding temperature, T (K)	$F = \sigma T^4$ (W/m^2)	Filament area = P/F (m^2)	λ_{max} (Å)
#1						
#2						
#3						
#4						

Show your calculations here.

Variable Power Supply Setting #1

Power delivered = V × I = _____ Watts

Ratio of Y/B = _____

Interpolated value of light bulb temperature from Figure 3: T = _____ K

Energy per second radiated per unit surface area of filament:

$F = \sigma T^4$ = _____ Watts/m^2

P/F = _____ m^2

$\lambda_{max} = 2.9 \times 10^7/T$ = _____ Å

Variable Power Supply Setting #2

Power delivered = V × I = _____ Watts

Ratio of Y/B = _____

Interpolated value of light bulb temperature from Figure 3: T = _____K

Energy per second radiated per unit surface area of filament:

$F = \sigma T^4$ = _____ Watts/m^2

P/F = _____ m^2

$\lambda_{max} = 2.9 \times 10^7/T$ = _____ Å

STUDENT'S NAME _____

Variable Power Supply Setting #3

Power delivered = V x I = _____ Watts

Ratio of Y/B = _____

Interpolated value of light bulb temperature from Figure 3: T = _____ K

Energy per second radiated per unit surface area of filament:

$F = \sigma T^4 =$ _____ Watts/m^2
$P/F =$ _____ m^2
$\lambda_{max} = 2.9 \times 10^7/T =$ _____ Å

Variable Power Supply Setting #4

Power delivered = V x I = _____ Watts

Ratio of Y/B = _____

Interpolated value of light bulb temperature from Figure 3: T = _____ K

Energy per second radiated per unit surface area of filament:

$F = \sigma T^4 =$ _____ Watts/m^2
$P/F =$ _____ m^2
$\lambda_{max} = 2.9 \times 10^7/T =$ _____ Å

Calculation of the average value of the three surface area calculations

If one of the values differs widely from the others, do not include it in this calculation.

Average area = _____ m^2

STUDENT'S NAME _____

F. Blackbody Radiation Experiment Discussion Questions

1. Figure 1 presents the blackbody spectrum for an object at three different temperatures. Calculate the product of the estimated wavelength at which each curve attains a maximum and the temperature represented by that curve. They should all equal, to uncertainties in your estimate, $\kappa = 2.9 \times 10^7$ Å-K, demonstrating Wien's displacement law.

2. The radius of the Sun is 6.96×10^{10} cm. Using (2), calculate the total amount of radiation emitted by the Sun from its entire surface, its *luminosity*, based on an effective surface temperature of 5800 K.

3. Table 3 presents the colors of blackbodies corresponding to their temperatures. Using the temperatures you found from Fig. 3 for the light bulb filament, how do the corresponding colors of Table 3 compare to the colors you described for the light bulb as its filament was heated?

4. In the last part of the light bulb part of the experiment, you determined a surface area for the light bulb filament. In fact, typical surface areas for the filaments of incandescent light bulbs are about 80 mm^2, or 8.0×10^{-5} m^2.

   a. How does this compare to the average area you determined?

   b. What is the origin of the discrepancy, if any?

STUDENT'S NAME _____

5. Your subjective descriptions of the brightnesses of the light bulb were entered in Table 6 of the DATA SHEET.

   a. How do those descriptions compare with the calculation of the energy emitted by the light bulb in Table 7?

   b. Discuss any bias that might have been introduced by your use of an arithmetic scale for your description of the brightness.

6. If you touch the light bulb after it has been turned off, it is hot to the touch. It should be radiating energy. Why can't you see that shut-off light bulb glow?

7. As you increase the power going into the light bulb, your hand felt an increased warmth. In which part of the electro-magnetic spectrum is that "warmth" radiated?

8. From the measurements of the radiation from the light bulb, you calculated the values of λ_{max} for each setting of the power supply. Compare the color corresponding to that wavelength from Table 3 to the subjective color you entered in Table 6 of the DATA SHEET. Do they agree? If not, how can you explain the discrepancy in the color your eye and brain detects from those colors provided in Table 3?

STUDENT'S NAME _____

9. If you observed the Sun low in the sky, the blue rays would have been scattered by the atmosphere and the Sun will appear more yellow than if viewed overhead. Indeed, as we all have observed, the Sun appears reddish if viewed near the horizon. Even if you view the Sun directly overhead, some of its blue rays have been scattered, making it appear more yellow than it would appear if viewed in space by astronauts or lunar colonists. It might be green. The temperature of the apparent surface of the Sun is known to be 5800 K. Calculate the percentage difference between this value and that which you determined for the Sun being directly overhead.

10. This difference in the temperature you determined for the Sun without the presence of an atmosphere, that is, the "$sec\ z = 0$" temperature, and 5800 K may surprise you.

    a. What in the experimental method, including the time of day, may have caused the difference in the values? Explain your answer.

    b. What observing technique is used to more precisely determine the color of the Sun, one that is not affected by such factors?

11. Some stars are known to pulsate, actually changing their size. At the same time, the outer atmosphere of a star behaves like an ideal gas, and cools as it expands. The pulsating star, then, experiences both a change in its size and in the temperature of its visible surface. At what part of its pulsation cycle would you expect the luminosity of the star, which we observe, to be greatest, when it is large or when it is small? Why? What equation can you use to show this?

STUDENT'S NAME _____

12. Most diurnal, as opposed to nocturnal, creatures on the Earth have evolved eyes which are most sensitive to yellow. Why is this the case?

13. Let us say that you meet a being that is visiting from a planet whose parent star has an apparent surface temperature of one-half that of the Sun.

    a. To what color would you expect that being's eyes to be most sensitive? Why? Refer to an appropriate equation in providing your answer.

    Similarly, let us say that you meet a being that is visiting from a planet whose parent star has a visible surface temperature that is twice that of the Sun.

    b. To what color would you expect that being's eyes to be most sensitive? Why? Refer to an appropriate equation in providing your answer.

14. An ordinary flame is a composite blackbody. The emission originates from hot microscopic-sized pieces of carbon. The part of the flame closest to the ignited material is blue, then with increasing distance it becomes yellow and then red.

    a. Can you explain the changes in color? Refer to an appropriate equation in providing your answer.

    b. If you put a white sheet of paper a few inches above the flame, it will get tarnished with soot. This tells us that the material simply didn't "vanish into thin air." Rather, above the red flame, the soot is still present, but not visible. Describe the radiation it is emitting?

STUDENT'S NAME _____

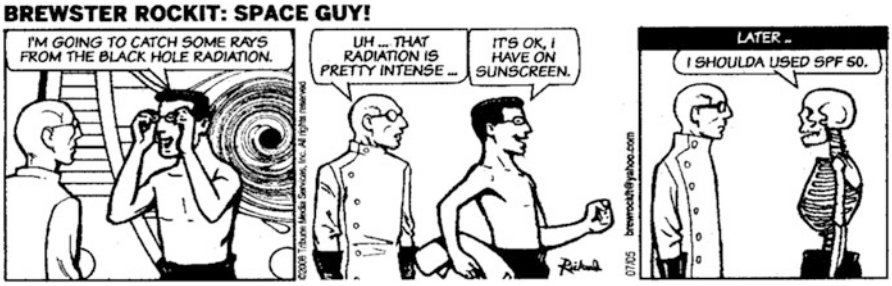

15. The effective blackbody temperature of the hot gas circling about some large black holes is about three million degrees Kelvin.

    a) At what wavelength will the maximum radiation from this so-called "accretion disk" occur? Show all calculations here.

    b) In what portion of the electro-magnetic spectrum, such visible or infrared, is this wavelength located?

    c) Compare the total amount of radiation emitted by a unit volume of a blackbody at this temperature to the total amount of radiation emitted by a unit volume of the photosphere of the Sun, at a temperature of about 5800 K.

    d) Assume that we have a black hole with an accretion disk of the same size as the Sun located at the same distance as the Sun. If it takes 30 min to get a sunburn, how long would it take to get a "black hole burn" of the same severity? Assume that the sunburn and black hole burn result from radiation of all wavelengths.

STUDENT'S NAME _____

e) This entire comic strip was suggested by the author to the cartoonist, nearly verbatim. How much should the author have been paid for his writing?

Removing these DATA SHEETS from the book may damage the binding. You might consider entering the data and performing your calculations in the book, and then photocopying the DATA SHEETS for submission to your instructor for grading.

If you used graph paper other than that provided, attach those graphs to these DATA SHEETS.

Experiment 18
The Surface Temperature and Energy Output of the Sun

SUMMARY: In Experiment #18, "The Surface Temperature and Energy Output of the Sun," we observe solar radiation raising the temperature of a jar of water. Determining the time needed for the temperature to rise a given amount is a measure of the energy received from at the Earth from the Sun and, knowing our distance from the Sun, its rate of energy output. We also measure the solar radiation using a solar cell.

LEVEL OF DIFFICULTY: Moderate

EQUIPMENT NEEDED: Glass jar of regular shape, cylindrical or square; water; cork stopper; digital thermometer; black ink; meter stick; solar cell; light baffles.

MY LEARNING GOALS

1. To be able to predict mathematically the expected lifetime of a star from its observed energy output and mass.
2. To be able to describe mathematically the strong dependence of the luminosity of a star on its surface temperature.
3. To be able to describe how the heat capacity of water enables us to mathematically determine the energy in sunlight reaching the Earth.

L.M. Golden, *Laboratory Experiments in Physics for Modern Astronomy: With Comprehensive Development of the Physical Principles*,
DOI 10.1007/978-1-4614-3311-8_18,

A. Introduction

The Sun is a fairly typical star. With a mass of 1.99×10^{33} g and a radius of 6.96×10^{10} cm, it has existed for five billion years, most spent converting hydrogen into helium in its core regions by nuclear fusion. Its surface temperature and energy output locate it on the main sequence region of the Hertzsprung-Russell diagram and it will exist there for another five billion years until that nuclear fuel is spent. The heat generated by these fusion reactions propagates upwards through the Sun by two modes of heat transfer, radiation and convection, until it reaches the visible surface, about 170,000 years after it was created. From there we receive the energy that sustains most life on Earth. (Some deep ocean life is now known to be sustained by radioactivity-generated geothermal energy and nutrients emanating from undersea vents.)

The amount of energy per second that the Sun emits over all wavelengths, its *luminosity*, L_o, is well studied. Indeed, it is known that the luminosity varies slightly. The amount of energy reaching the mean distance of the Earth from the Sun per second per unit surface area is referred to as the *solar constant*, S_o.

Actually, the solar constant isn't really constant. The output of the Sun varies randomly, has cycles, and as the Sun evolves on the main sequence over hundreds of millions of years its output increases slightly. Furthermore, the distance of the Earth from the Sun changes as the Earth revolves about the Sun in its orbit. We should also remember that the solar constant is defined as the amount of energy per second impinging upon a unit area at the mean distance of the Earth from the Sun, but some of that energy is absorbed by the atmosphere of the Earth or reflected back into space. Not all of it actually reaches the surface of the Earth, where we will be measuring its strength.

The concept of the solar constant is crucial in the study of the possibility of the existence of extraterrestrial life. The further one travels outwards from a star, the greater is the decrease in the intensity of the starlight. Eventually, your exploratory spacecraft reaches a distance where any water would freeze. On the other hand, as you approach the star, eventually you will reach a distance at which any water would boil. Only in the intermediate region could water-based life evolve and exist on the surface. This region is referred to as the *zone of habitability* or *habitable zone*. It is also referred to as the *ecosphere*. (Note, however, that advanced colonizing species might have the technology to modify their environment and survive on planets outside of the habitable zone.) One renowned AstroComedian refers to it as the "Goldilocks Zone," because it's neither too hot nor too cold, but "just right."

Numerous methods of measuring the solar constant exist. They vary from the simplest, observing the warming of a glass of water, to measurement by microwave radiometers, solar cells, and high-precision thermoelectric devices. In this experiment we will use two methods, warming of a glass of water and direct measurement by solar cells.

B. Theory

1. Solar Energy Output and Lifetime

As with any fuel source, such as coal or the wood in a fireplace, once we know the mass of an object and its rate of fuel consumption, we can determine its expected lifetime. Although the luminosity of the Sun measures the energy per second coming from its visible surface, that energy ultimately is derived from nuclear reactions in its center. We can therefore estimate the expected lifetime of the Sun by the simple equation

$$\tau = f\frac{M_o}{r}, \tag{1}$$

where τ is the expected lifetime, M_o is the mass of the fuel available to the Sun, f is the fraction of that mass which is converted into energy through the process of nuclear fusion, and r is the rate at which its mass is consumed. If M is given in grams and r is given in grams per second, then τ is given in seconds.

We have to distinguish the mass of the fuel from the total mass of the Sun. Only that material in the core of the Sun, which is sufficiently hot and dense to undergo nuclear fusion, creates the luminosity of the Sun. This is about 10% of the total solar mass of 1.99×10^{33} g. That is, in (1), f is about 0.10. The value of r is determined from the luminosity of the Sun.

Study of the nuclear reactions converting hydrogen into helium shows that only about 0.04% of the matter is actually converted. Although this seems inefficient, it is about ten times more efficient than the process of nuclear fission and about 10^9 times more efficient than consumption by combustion (fire).

We cannot directly measure the luminosity of the Sun, that requiring us to actually sit on its surface. Instead, we do so by employing the inverse square law of radiation intensity, as illustrated in Fig. 1, together with R_o, our known distance from the Sun, and the solar constant,

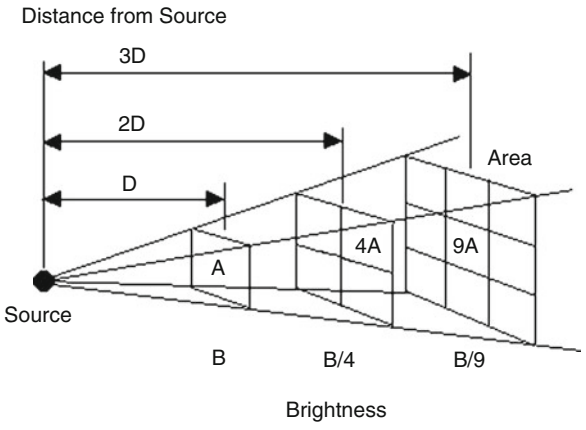

Fig. 1 The brightness of radiation decreases as the inverse square of the distance of the observer from the source of radiation. The radiation spreads out in space

$$S_o = \frac{L_o}{4\pi {R_o}^2}, \tag{2}$$

where $R_o = 1$ A.U. You'll recognize $4\pi r^2$ as the surface area of a sphere. Here, that sphere is an imaginary one with its center at the center of the Sun and its radius equal to the mean distance of the Earth from the Sun.

By measuring the solar constant, we can then calculate the luminosity of the Sun by, rewriting (2),

$$L_o = 4\pi {R_o}^2 S_o. \tag{3}$$

Combining (1) and (3), and recognizing that in fact $r = L_o$, we then can find the expected lifetime of the Sun from our measurement of the solar constant,

$$\tau = f\frac{M_o}{L_o}. \tag{4}$$

To explicitly show the value of S_o in this result, we can also write, using (3),

$$\tau = f\frac{M_o}{4\pi {R_o}^2 S_o}. \tag{5}$$

2. *Relationship Between Surface Temperature and Luminosity of a Star*

Knowing the total energy output of the Sun, that is, its luminosity, and assuming the Sun radiates like a blackbody, we can use the Stefan-Boltzmann Law, Eq. 2 of Experiment #17, "Blackbody Radiation," to calculate the temperature of its visible surface. The total amount of radiation emitted over all wavelengths per second per unit surface area of a blackbody, or energy flux, is

$$F = \sigma T^4, \tag{6}$$

where the Stefan-Boltzmann constant $\sigma = 5.67 \times 10^{-8}$ W/m^2- K^4. The luminosity is simply the amount of radiation emitted by the entire surface,

$$L = 4\pi R^2 F,$$

where R is the radius of the body, assumed spherical, an excellent approximation for most stars. Substituting (6),

$$L = 4\pi R^2 \sigma T^4.$$

Solving this equation for T then allows us to find the temperature of the visible surface from the luminosity of the star,

$$T = \left[\frac{L}{4\pi R^2 \sigma}\right]^{\frac{1}{4}}. \tag{7}$$

The weak dependence of T upon L is striking. Compare two stars of the same radius, but differing in luminosity by, for example, a factor of 100. The surface temperatures differ only by a factor of $100^{1/4} = 3.2$. In other words, we can get a good estimate of the surface temperature of the Sun even if our value for the solar constant is appreciably inaccurate.

3. *Specific Heat Capacity*

The *specific heat capacity* or simply *specific heat* of a substance measures the temperature response of a unit mass of that substance to the introduction of heat. This manifests a property of all matter, that a finite amount of heat is required to increase its temperature. The formal definition of specific heat is the heat absorbed to raise one unit mass of a substance by 1°, and is designated by the letter c,

$$\Delta Q = mc\Delta T. \tag{8}$$

This heat can be transferred by any of the three modes of transfer, radiation, conduction, or convection.

The term has a meaning similar to that in colloquial English. As we speak of someone with a high capacity for pain, for example, as one who can experience a large amount of it without reaction, so a substance with a high specific heat is one that can absorb a large amount of heat without having its temperature significantly increase.

Equation 8 also applies to cooling. If a warm body is placed into a cool environment, then the specific heat describes the decrease in temperature that the warm body experiences as it loses heat.

We will use the heat-absorbing ability of water as a measuring device. We measure the increase in temperature of a container of water placed in sunlight over a given period of time, and knowing the specific heat of water we can use (8) to determine the amount of heat absorbed. Dividing by the time needed for the absorption and the effective area of the container of water, we get a close approximation to the amount of energy per unit time per unit area delivered by the Sun at the surface of the Earth, the solar constant.

If the mass of water so warmed is m and the temperature is measured to have increased by ΔT, then by the definition of specific heat the amount of heat absorbed by the water from the Sun through its radiation is, from (8) above,

$$\Delta Q = mc_w \Delta T, \tag{9}$$

where the subscript w indicates the use of water.

Let Δt be the amount of time we wait for the water to absorb an amount of heat ΔQ from the sunlight before we measure the increased temperature. Then, dividing by Δt to explicitly show the increase in temperature per second, the heat absorbed per second is

$$\frac{\Delta Q}{\Delta t} = mc_w \frac{\Delta T}{\Delta t}.$$

The solar constant is measured in energy per unit area per unit time,

$$S_o = \frac{\Delta Q}{\Delta t A_{bottle}}. \tag{10}$$

where we identify the Sun as the source of the heat warming the water and the area in our case is A_{bottle} , the area of the side of the bottle facing the Sun.

As a result, once we have measured ΔT we can calculate our value for the solar constant from

$$S_o = f_s \, m \, c_w \frac{\Delta T}{\Delta t} \frac{1}{A_{bottle}}. \tag{11}$$

where we have now included a factor f_s to correct for the slanted rays of the Sun, discussed in the next section.

A shortcoming of this technique results form the high specific heat of water, as shown in Table 3 of Experiment #15, "Thermal Radiation from a Planetary Subsurface: Part II: Soil Sample Measurements,". This means that a large amount of heat must be absorbed to raise the temperature of water only 1°. Our experiment would be more sensitive to the heat input if another substance were used, such as a metal, gas, or sand. These, however, present their own problems in either measuring the temperature increase and/or accounting for loss of heat by radiation and heat conduction.

4. *Sun Elevation Correction*

Either by using heating of water or solar cells, a complication exists with orienting our "sensor." As we examined in Experiment #5, "Earth: The Seasons and Local Latitude," the rays of the Sun do not generally strike the surface of the Earth directly. To measure the brightness of the Sun accurately, we need to orient the surface of the water or solar cell exactly perpendicular to the rays of the Sun.

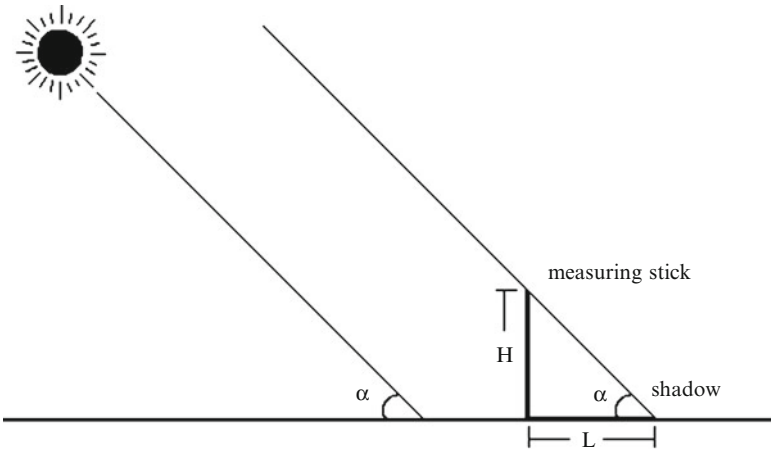

Fig. 2 The energy of the Sun reaching the ground is reduced by a number of effects. The atmosphere reflects and absorbs some energy, and the energy delivered by the rays reaching the ground is reduced in intensity depending on their slant. Correction for the former can be partially made knowing the angle of elevation of the Sun, α. Correction for the latter can be made completely with this information. The angle α can be determined by comparing the length of a measuring stick to the length of its shadow

A second problem arises from the absorption of energy by the atmosphere, its molecules, dust, and man-made pollutants, as the light rays pass through the atmosphere. Corrections for both can be performed by rotating the sensor by eye so that the rays are impinging upon it directly, but error will certainly be introduced.

Instead, the geometry of Fig. 2, similar to that of Fig. 2b of Experiment #5, "Earth: The Seasons and Local Latitude," can be used. We can correct our measurements by dividing by *sin* α, where α is the angle between the ground and the direction to the Sun. As in Experiment #5, "Earth: The Seasons and Local Latitude," we place a meter stick or other measuring device perpendicular to the ground. Measuring the length of the shadow, L, we can determine the tangent of the angle,

$$\tan\alpha = \frac{H}{L}. \tag{12}$$

From this, we can correct our measurement by calculating and then dividing by *sin* α. You can show that the following is a trigonometric identity,

$$\sin^2\alpha = \frac{\tan^2\alpha}{\tan^2\alpha + 1},$$

so that we can calculate *sin* α directly, using equation (12), as

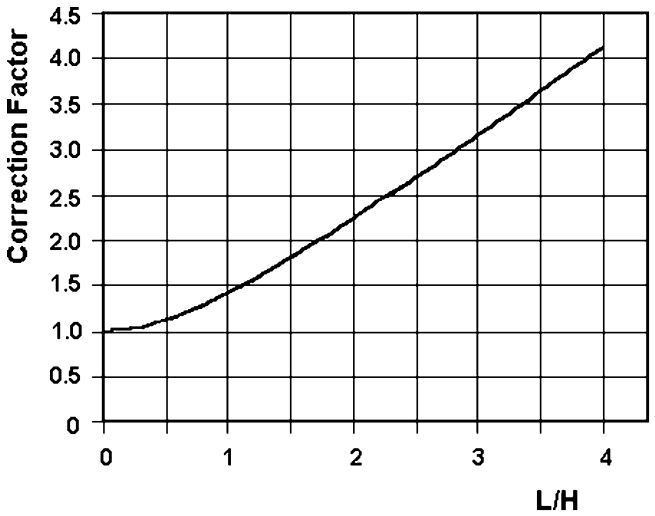

Fig. 3 Correction factor for the Sun angle as a function of the shadow length divided by the height of the measuring stick

$$\sin^2\alpha = \frac{H^2}{H^2 + L^2}.$$

The correction factor for the Sun angle is then

$$f_s = \frac{1}{\sin\alpha} = \sqrt{\frac{H^2 + L^2}{H^2}}.$$

Note, for the Sun directly overhead, $\alpha = 90^o$, $L = 0$, and $sin\ \alpha = 1$, yielding no correction, as should be the case. Similarly, for the Sun near the horizon, α is small, L is large, and $sin\ \alpha$ is small, so that dividing by $sin\ \alpha$ leads to a large correction, again as should be the case.

We can divide all the terms under the square root sign by H to simplify the calculation,

$$f_s = \frac{1}{\sin\alpha} = \sqrt{1 + \left(\frac{L}{H}\right)^2} \tag{13}$$

A graph of this correction factor is provided in Fig. 3. In determining the correction, you can use either (13) or this graph.

C. Procedure and Observations

1. Measurement by Heating of Water

We will be using a bottle of either square or rectangular cross-section. If you are using a bottle of rectangular cross-section, use the larger of the sides. Measure the dimensions of the surface of the side of the bottle, h and l, and enter that information in Table 1 of the DATA SHEET. Calculate the area of that side. Weigh the empty bottle and enter its mass in Table 1 of the DATA SHEET.

Carefully measure 100–200 ml, that is, 100–200 cm^3, of water and pour it into the bottle. Weigh the bottle now and enter the total mass of bottle plus water in Table 1 of the DATA SHEET. Place a few drops of black ink into the water to increase its ability to absorb the sunlight. Put a cork or other insulating stopper in which a hole has been drilled to accept a thermometer and insert it into the bottle top. So that the sunlight will be incident upon the bottle only on one face, the other sides of the bottle should be shielded from the Sun by cardboard or other material once you allow the sunlight to fall upon the bottle.

Take the assembly outside and let it sit in the shade until the temperature of the water in the bottle no longer increases. If your laboratory is at room temperature, and the outside temperature is hot, this may take a half an hour. Because glass has a low thermal conductivity of 1.1 W/m-K, which can be compared to other substances as seen in Table 3 of Experiment #15, "Thermal Radiation from a Planetary Subsurface: Part II: Soil Sample Measurements," the heat takes a while to pass from the air to the water.

Once the temperature of the water has stabilized, move the assembly into the sunlight and orient it so that the face whose dimensions you have measured faces the Sun. Enter the value of the stabilized water temperature and the time in Table 3 of the DATA SHEET. Measure the length L of shadow cast by your meter stick or other measuring device of height H to enable calculation of the correction factor, f_s. Enter the values of H and L in Table 2 of the DATA SHEET.

Allow the water to increase in temperature by 3° or 4°, and when you can read a convenient number from the thermometer note the time. Depending on the time of day, this may take 15 min to half an hour. Enter both the increased temperature and the time in Table 3 of the DATA SHEET. Measure the length of the shadow cast by your measuring device again at this time. Enter that datum in Table 2 of the DATA SHEET.

Remove the bottle from the sunlight, pour cool water over it to reduce its temperature and repeat the measurement cycle. Alternatively, if you have more than one such bottle available, you can allow all three to sit in the sunlight together and measure the temperature of the first after, say, 15 min, the second after 30 min, and the third after 45 min.

2. *Measurement by Solar Cells*

Solar cells are rated by the amount of electrical power they produce given an amount of solar energy they receive. Place the solar cell array flat on the ground. Measure the power output. Repeat the measurement of the power output at least one more time. Enter the results in Table 4 of the DATA SHEET.

Because we are interested in the amount of solar energy reaching the ground per unit time and per unit area, we must measure the area of the solar cells and then multiply by the total number of solar cells in the array. Note that the solar cells have a boundary area which does not receive the sunlight. It is, therefore, best to measure the area of an individual solar cell rather than the size of the array and then, as stated, multiply by the number of cells in the array.

Enter the area of the individual cells, A_{cell} , and the number of cells in the array, N, in Table 4 of the DATA SHEET. Measure the length of the shadow cast by the Sun, L, and the length of the measuring stick, H, and enter both results in Table 4 of the DATA SHEET.

D. Calculations and Analysis

1. *Measurement by Heating of Water*

For each measurement cycle, calculate the amount of water in the bottle by subtracting the masses of the empty and full bottles. Enter the results in the final column of Table 1 of the DATA SHEET. Similarly, calculate the mean values of L for each measurement cycle, divide it by H to obtain L_{mean}/H, and calculate the correction factor, f_s, by (13) or read it from Fig. 3. Enter all values in Table 2 of the DATA SHEET.

For each measurement cycle, calculate the interval of time during which the water received sunlight, Δt, and the temperature increase, ΔT. Then calculate $\Delta T/\Delta t$. Enter those results in Table 3 of the DATA SHEET.

To enable comparison of your calculation of the solar constant with its accepted value in Watts per square meter, convert the masses of water from grams to kilograms and convert the area of the side of the bottle facing the Sun from square centimeters to square meters.

Perform all your calculations on the DATA SHEET.

2. *Measurement by Solar Cells*

Average the results for the output of the solar cell array and enter the result, P_{cell}, in Table 4 of the DATA SHEET. Calculate the total collecting area, A_{Total} , by

multiplying the size of the individual solar cells in square meters, A_{cell}, by the number of cells in the array, N. Enter the result in Table 4 of the DATA SHEET. With the values of L and H entered in Table 4, calculate the correction factor, f_s, using (13) or read it from Fig. 3. Multiply your result for the mean power output of the solar cell array by the correction factor and divide by the area of the array. Enter the result in Table 4 of the DATA SHEET. Then calculate the value for the solar constant as $S_o = f_s P_{cell}/A_{Total}$. Show all your calculations on the DATA SHEET.

3. *Experimental Errors*

The accepted value for the solar constant is 1367.7 W/m. On the DATA SHEET, calculate the percentage error between this value and the values you determined by the two methods used in this experiment.

STUDENT'S NAME _____

E. Energy Output of the Sun Experiment Data Sheets

1. Water Heating

Table 1 Preliminary data: water bottle size and water mass

Bottle	H (cm)	w (cm)	Area A_{bottle} (cm^2)	Mass of empty bottle (g)	Mass of full bottle (g)	Difference = water mass (g)
#1						
#2						
#3						

Calculation of mass of water in bottle

Table 2 Correction factor measurements

Bottle	H (cm)	Start L (cm)	Final L (cm)	Mean value of L , L_{mean}	L_{mean}/H	f_s
#1						
#2						
#3						

Calculation of the mean value of L, L_{mean}/H, and the correction factor. f_s

If you are using the same bottle for each of the three groups of measurements, you need measure only once the area of the side onto which the sunlight will fall. Show your calculations of L_{mean} and the correction factor, f_s, using (13), unless you are using Fig. 3 to determine the correction factor, here.

Table 3 Temperature increase measurements

Bottle	Start time	End time	Δt (s)	Start temp. (°C)	End temp. (°C)	ΔT (°C)	ΔT/Δt (°C/s)
#1							
#2							
#3							

STUDENT'S NAME _____

Calculation of the mean value of the three determinations of $\Delta T/\Delta t$

$$\left(\frac{\Delta T}{\Delta t}\right)_{mean} = \_\_\_\_\_ \ (^{o}\text{C/s.})$$

Convert the values for m from grams to kilograms and the value for A_{bottle} from cm^2 to m^2. Show your calculations here.

m = _____ kg

A_{bottle} = _____ m^2.

From (11),

$$S_o = f_s m\, c_w \left(\frac{\Delta T}{\Delta t}\right)_{mean} \frac{1}{A_{bottle}}.$$

Using $c_w = 4186$ J/kg-°C and the values for m, A_{bottle}, and $\left(\frac{\Delta T}{\Delta t}\right)_{mean}$ you have determined above, calculate S_o.

S_o = _____ Joules/ m^2-s.

STUDENT'S NAME _____

2. Solar Cell

First measurement of output of solar cell, P_{cell}: _____ W

Second measurement of output of solar cell, P_{cell}: _____ W

Mean value of solar cell output: _____ W

Table 4 Solar cell measurements

Average output, P_{cell}	A_{cell}	N	A_{Total} = N x A_{cell}	Shadow length, L	Length of measuring stick, H	f_s	S_o = f_s P_{cell}/ A_{Total}

Show your calculations here.

Total collecting area = _____ m^2

Correction Factor, f_s = _____

Value for Solar Constant = f_s P_{cell}/A_{Total} = _____ W/m^2

3. Experimental Errors

The accepted value for the solar constant is 1367.7 W/m. Calculate the percentage error between this value and the values you determined by the two methods used in this experiment.

a. Heating of water measurement

b. Solar cell measurement

STUDENT'S NAME _____

F. Energy Output of the Sun Experiment Discussion Questions

1. Using the accepted value for the solar constant of 1367.7 W/m^2, use (3) to calculate the luminosity of the Sun, its total energy output in Joules per second.

2. Using (4), calculate the lifetime of the Sun in billions of years that results from the Sun expending its fuel at the rate given by the luminosity you have calculated.

3. Knowing the luminosity of the Sun, its total energy output per second, and assuming the Sun radiates like a blackbody, we can use the Stefan-Boltzmann Law, Eq. (2) of Experiment #17, "Blackbody Radiation," to calculate the temperature of its visible surface. The radius of the Sun is 6.96×10^8 m. Calculate this temperature.

4. In the determination of the solar constant by the heating of water, we placed a stopper on the water bottle. Besides allowing us to insert the thermometer, why was this necessary?

5. Using (2) and the Stefan-Boltzmann Law, Eq. (2) Experiment #17, "Blackbody Radiation," find the distances from the Sun outwards into the solar system that define the "zone of habitability." Recall that the Stefan-Boltzmann Law provides the amount of energy per second emitted by a blackbody per unit surface area. The inner boundary of the "zone of habitability" is the distance at which water would boil from the heat of the Sun, and its outer boundary is the distance at which water would freeze. To simplify your calculations, use the solar constant leading to a temperature on Earth of 288 K to create a proportion To actually determine the temperature on the surface of a planet, one must account for many effects such as reflection of sunlight by clouds, absorption of solar energy in the atmosphere, reflection of sunlight at the surface, the emissivity of the surface material, and conduction of heat into the subsurface. This manner of calculating the boundaries of the zone of habitability is defined by assuming perfect blackbodies are located in space so that all the energy in the sunlight is heating the surface. Show your calculations here.

STUDENT'S NAME _____

6. Referring to Table 11 of Experiment #15, "Thermal Radiation from a Planetary Subsurface: Part II: Soil Sample Measurements," which planets of the solar system lie within the zone of habitability of the Sun that you have defined in question #5?

7. The value you have derived for the solar constant will be less than the accepted value. One problem for which we have corrected is the slanting angle of the rays of the Sun. What are other problems with measuring the solar constant (a) on the surface of the Earth and, (b) in particular, by using a water bottle to perform the measurement?

8. Using the accepted value of the solar constant, calculate the total amount of solar energy incident on a hemisphere of the Earth per second. The equatorial radius of the Earth is 6378 km. Compare this to the power generated by a large municipal power plant, 1 GW, or 1×10^9 W.

STUDENT'S NAME _____

9. If we did not know the value of the distance from the Earth to the Sun, the A.U., from other methods, we could calculate it from the value of the solar constant and a value for the temperature of the visible surface of the Sun determined, for example, from its blackbody curve or spectrum. From (3),

$$R_o = \left[\frac{L_o}{4\pi S_o}\right]^{1/2},$$

where L_o is given by the Stefan-Boltzmann law, Eq. 2 of Experiment #17, "Blackbody Radiation". Calculate the value of the A.U. in kilometers using the accepted value of the solar constant and a value for the luminosity of the Sun of 3.83×10^{26} J/s.

10. The zone of habitability can be calculated by the distance from the parent star and its luminosity. This, however, does not directly predict the surface temperature of a planet. For example, planetary atmospheres can increase the temperature of a planetary surface by effectively providing insulation. In the extreme, as on Venus, a greenhouse effect makes the surface temperature high enough to melt lead, although Venus may in fact be in the zone of habitability of the Sun (see your answer to question #5). For extra credit, what do you think are the odds that the destruction of urban forests for developments such as parking lots and soccer fields, the annihilation of the rain forest for agriculture, mining, lumber, or housing—trees being the natural cooling infrastructure of the Earth, and the injection of carbon dioxide into the atmosphere by vehicles will increase global warming during your lifetime and lead to a greenhouse effect so severe that life will no longer be sustainable on Earth?

Removing these DATA SHEETS from the book may damage the binding. You might consider entering the data and performing your calculations in the book, and then photocopying the DATA SHEETS for submission to your instructor for grading.

Experiment 19
The Theory of Atomic Spectra

SUMMARY: In Experiment #19, "The Theory of Atomic Spectra," we study the emission lines from the hydrogen atom in terms of the Bohr theory of the atom. The light coming from a hydrogen discharge tube is spread into its constituent wavelengths by a diffraction grating. Determination of the angular positions of those lines yields a value for the Rydberg constant.

LEVEL OF DIFFICULTY: Moderate

EQUIPMENT NEEDED: Hydrogen discharge tube; diffraction grating spectrometer.

MY LEARNING GOALS

1. To recognize that every chemical element and their ions produce a distinctive spectrum which is described by the laws of quantum mechanics.
2. To be able to describe how such spectra allow astronomers to identify the composition of astronomical objects such as stars.
3. To be able to describe the Bohr model of the hydrogen atom and how emission and absorption lines are created.
4. To be able to describe how the process of interference in a diffraction grating disperses light into its constituent wavelengths.

L.M. Golden, *Laboratory Experiments in Physics for Modern Astronomy: With Comprehensive Development of the Physical Principles*,
DOI 10.1007/978-1-4614-3311-8_19,

A. Introduction

That electrons, when bound to a nucleus in an atom, can be found possessing only discrete values of energy and are located only in corresponding discrete *energy levels* is one of the major elements of *quantum mechanics*. The twentieth century understanding of the various aspects of this field revolutionized how we view matter and its interaction with radiation. Among its many ramifications for science and technology, it provides astronomers with the ability to identify the substances present in celestial objects simply by analyzing the radiation we receive from them.

Indeed, observations of the electro-magnetic radiation from celestial objects, along with the mathematical modeling of the processes that produces it, provides an understanding of such characteristics as their composition, structure, motion, and temperature, their very nature. It is the major way we learn about them. In this experiment, we will study one model, the Bohr model of hydrogen and its prediction of the nature of the visible light we receive from hydrogen atoms.

B. Theory

1. Atomic Spectra

The atoms of every element, be it hydrogen, oxygen, or calcium, for example, are distinguished by the number of protons and neutrons in their nuclei, and by the number of electrons surrounding those nuclei. If the atom is electrically neutral, then the number of protons and number of electrons are equal. If the atom is ionized by losing one or more electrons, then these numbers differ. In either case, the electrons can be found in only select discrete energy levels. When the electrons move between these energy levels, they may absorb or emit photons of a corresponding wavelength. Because each atom or ion is distinct, the pattern of these wavelengths is distinct. Laboratory studies provide these *spectra* for the elements. Just as fingerprints and to an extent cursive signatures are unique among individuals, so these spectral "fingerprints" or "signatures" are unique among the chemical elements. Figure 1, for example, shows the spectrum of the carbon atom in the visible portion of the electro-magnetic spectrum.

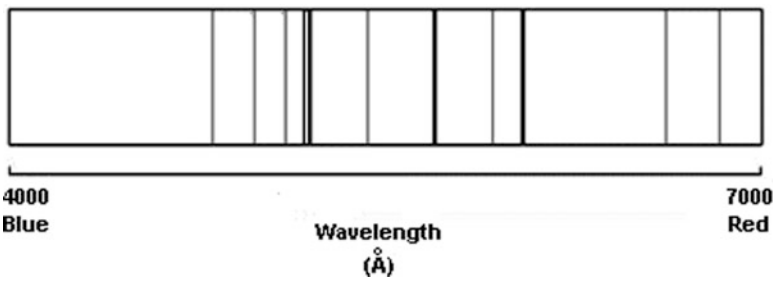

Fig. 1 The spectrum of the carbon atom in the visual

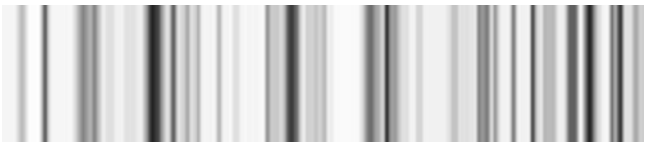

Fig. 2 A portion of the solar spectrum centered at 4700 Å. Such spectra are created by passing sunlight through a dispersive device such as a prism or diffraction grating. Atoms in the solar atmosphere remove light of characteristic wavelengths, resulting in the pattern of darkened absorption lines. Comparison to spectra of atoms obtained in the laboratory allows astronomers to determine which elements are present in the atmosphere of the Sun, as well as in those of other stars

This and similar spectra for other chemical elements are created by passing light from an incandescent lamp through a chamber of, in this case, carbon gas and then focusing that light onto a piece of metal through which a thin slit has been cut. The light coming out of the slit is then passed through a prism which disperses the light into its constituent wavelengths. The result is an image of that slit for the various wavelengths. Because the image of a slit is a straight line, the image of the slit corresponding to a given wavelength is called a *spectral line*.

We also use the term spectrum to refer to the pattern of radiation that we observe from celestial objects. In this case, however, the individual spectra of many atoms may be present. Figure 2 is a portion of the spectrum, for example, of the Sun. Astronomers perform a detective job when they examine the spectrum of a celestial object such as a star and then determine which elements are present by comparing that spectrum with those observed in the laboratory for the chemical elements suspected of being present in that object.

2. *The Bohr Atom*

The simplest element, hydrogen, is composed of a single electron surrounding a single proton. We expect, and find, that its spectrum is the simplest of all the elements. The nature of that spectrum was explained by (Niels Bohr, 1885–1962) in work that gained for him the Nobel Prize in 1922, at the age of 37!

According to the Bohr model of the hydrogen atom electrons can be found only in definite orbits about the atomic nucleus. These orbits are designated by a *quantum number* $n = 1, 2, 3, 4, \ldots$ and are characterized by the energy that the electrons in the orbits possess. The difference in the energy or *energy levels* between two orbits n and m is given by

$$\Delta E_{mn} = R\,h\,c\left(\frac{1}{m^2} - \frac{1}{n^2}\right), n > m, \tag{1}$$

where the Rydberg constant (Johannes Rydberg, 1854–1919),

$$R = 1.097 \times 10^5 \text{ cm}^{-1},$$

Planck's constant (Max Planck, 1858–1947),

$$h = 6.625 \times 10^{-27} \text{ erg-s},$$

and the speed of light (G-d, -∞ to + ∞),

$$c = 3.0 \times 10^{10} \text{ cm/s}.$$

As a result of the wave-particle duality of light, the energy E of a photon ("particle-like" description) is related to the wavelength ("wave-like" description) of the associated radiation by

$$E = \frac{hc}{\lambda}. \tag{2}$$

Using the universal wave equation, Eq. (1) of Experiment #9, "Determination of the Rotation Rate of Planets and Asteroids by Radar: Part I. Observations of Mercury," this can also be written as

$$E = hf,$$

where f is the frequency of the radiation corresponding the wavelength λ.

Electrons in atoms and molecules move between energy levels by changes referred to as *transitions*. When a beam of light hits a hydrogen atom, for example, a photon whose energy corresponds to a given interval between Bohr energy levels will be absorbed if the electron of the hydrogen atom is in the lower energy level. For example, if the electron in a hydrogen atom is in energy level 1 and a photon of energy $E = hc/\lambda = E_{13}$ hits that hydrogen atom, then the electron will be given enough energy to kick it up to energy level 3. Similarly, if the electron in a hydrogen atom is in energy level 3 and a photon of energy $E = hc/\lambda = E_{37}$ hits the atom, then the electron will be given enough energy to kick it up to energy level 7. This particular process is in general called *photo-excitation*.

Collisions between hydrogen atoms or between other atoms or molecules and hydrogen atoms can also "excite" the hydrogen atom by kicking its electron up to higher energy states, by way of *collisional excitation*.

As with all physical systems, atoms and molecules are most stable in their "unexcited" or *ground* states. A hydrogen atom which has been photo-excited or collisionally excited will return to its unexcited state, on its own accord, by having its electron fall to the $m = 1$ energy level either by one or a series of energy level jumps. This process is called *photo-deexcitation* or *spontaneous emission*. Deexcitation can also occur by c*ollisional deexcitation*, in which the electron gives up its energy to the other colliding particle.

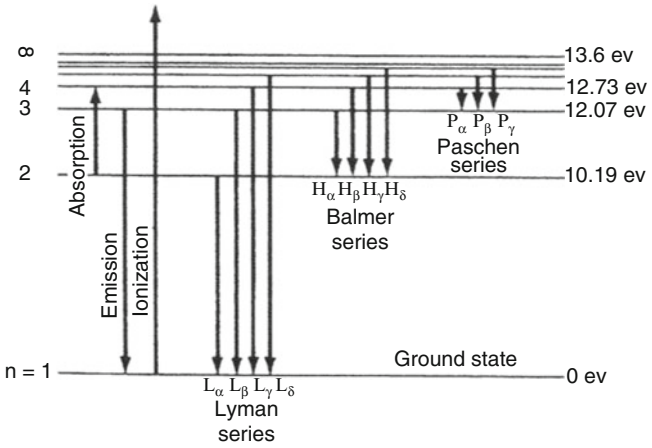

Fig. 3 The energy-level diagram of hydrogen. The Lyman, Balmer, and Paschen series in emission are created by photons being released by the atom and its electron falling to a lower energy level, designated by $n = 1$, 2, and 3, respectively. The energy unit of eV, or electron volts, is convenient to describe the energy levels of electrons in atoms

3. *Hydrogen Energy-Level Diagram*

Such processes can be described by an *energy-level diagram*, such as that of Fig. 3 for the hydrogen atom. In absorption, the atom absorbs the energy of a photon, and the electron jumps up to a higher energy level, indicated by an upward-pointing arrow. In emission, the atom releases a photon and the electron falls down to a lower energy level, indicated by a downward-pointing arrow. Series of such absorptions or emissions are distinguished by their common lower energy level. The quantum nature of matter ensures that all such transitions occur between specific energy levels, guaranteeing that the energies of photons absorbed or emitted have specific values. (In addition, in the process of *ionization*, an electron absorbs sufficient energy to completely free it from the atom.)

Combining (1) and (2) yields the wavelength of radiation corresponding to a jump between two energy levels, m to n, in the hydrogen atom,

$$\frac{1}{\lambda} = R\left(\frac{1}{m^2} - \frac{1}{n^2}\right), n > m. \tag{3}$$

As can be seen from this equation, the greater the difference between m and n, the greater the difference between $1/m^2$ and $1/n^2$, and the smaller the wavelength of the photon absorbed or emitted by the hydrogen atom. This is consistent with larger jumps in Fig. 3 corresponding to larger energies $E = hc/\lambda$.

For example, when the electron in the hydrogen atom performs downward energy level jumps by spontaneous emission, the hydrogen atom releases photons. The energy, and therefore wavelength, of these photons corresponds to the two energy levels of the jump, described by (3).

As the hydrogen atom deexcites by spontaneous emission, some jumps occur down to energy level $m = 1$. The relatively small wavelengths of these jumps correspond to ultraviolet light and are referred to as the *Lyman series*. These are seen in the spectra of highly red-shifted objects such as quasars.

Other jumps occur down to energy level 2. The wavelengths of these jumps correspond to visible light, were described by Balmer (Johann Balmer, 1825–1898) in 1885, and are accordingly called the *Balmer series*. From (3), the wavelengths are given by

$$\frac{1}{\lambda} = R\left(\frac{1}{4} - \frac{1}{n^2}\right). \tag{4}$$

These emissions, referred to as Hα, Hβ, Hγ, and so on, are seen in the spectra of stars, and are the emissions that will be studied in this experiment. You will observe several of the energy level jumps of hydrogen in the Balmer series and determine the value of the Rydberg constant, R.

Note that these relationships of quantum mechanics govern only emission and absorption by atoms. As can be seen by (3) or (4) for the hydrogen atom, as the energy levels n to which the electron is excited or from which it is deexcited increases, the differences between $1/\lambda$ corresponding to adjacent values of n becomes small. For example, the wavelength difference in the Balmer series between interactions with energy levels 3 and 4 can be calculated from (4) to be 1702 Å whereas that between energy levels 50 and 51 is only 0.02 Å. Instead of the emissions or absorptions being widely separated in wavelength, they become nearly adjacent in wavelength and the radiations become less and less distinct, forming a continuous spread of wavelengths.

This is what we would expect. When electrons are flying about freely in space, not bound to atoms, they emit or absorb energy following classical as opposed to quantum mechanics. They produce a *continuum* of radiation, not radiation that is quantized. As the electron gets farther and farther from the nucleus, its behavior becomes more and more like electrons that are free.

C. Procedure and Observations

1. Equipment

To perform the experiment we require a source of excited hydrogen and an instrument which will take this light and spread it out into its constituent wavelengths. The source of excited hydrogen is a familiar hydrogen discharge tube, similar to neon or other fluorescent lights. The hydrogen discharge tube contains hydrogen molecules under low pressure. When a high voltage is applied, typically of the order of 5000 volts, the electrical force strips electrons off of some of the hydrogen molecules. Although these voltages far exceed those needed to ionize the atoms, the electrons

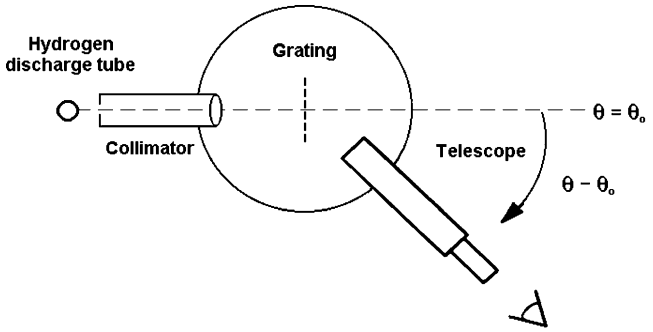

Fig. 4 In this schematic drawing, a diffraction grating spectrometer is shown observing the emission lines from a hydrogen discharge tube. The collimator ensures that the rays of light incident on the grating are parallel

are thereby able to attain sufficient speeds that their impact with the molecules dissociates many into their constituent atoms. The collisions also impart kinetic energy to the atoms and, most important for the emission of photons, excites the atoms into higher energy levels. The result is a gas containing many collisionally-excited hydrogen atoms. The resulting photo-deexcitation produces emission lines not only in the visible but also in the infrared and ultra-violet.

A non-excited hydrogen discharge tube would not produce the desired results. Far from having its electrons in familiar Bohr orbits, the two electrons in the hydrogen atom are shared by both atoms and as they move about the nuclei of the two constituent atoms their paths resemble large ovals and figure eights. The energy levels, in short, are not described by (1).

The instrument is a transmission diffraction grating spectroscope, Fig. 4. A diffraction grating is a piece of glass or transparent plastic onto which has been cut a large number of fine parallel, evenly spaced grooves. The space between each pair of grooves acts as a slit and the light passing through each "slit" experiences diffraction. When parallel light rays are incident upon the grating, the rays of a given wavelength that have been diffracted from the various slits interfere with each other. The nature of the interference for each distinct wavelength, λ, depends on λ/D, where D is the space between grooves. At most angles, the interference is destructive and very little light appears.

At certain angles, however, the waves interfere constructively and a maximum intensity of light appears, symmetrically to the left and to the right of the axis of the diffraction grating in very narrow beams. These angles correspond to differences in the paths of the light of one, two, and so on number of wavelengths, and give rise to "first order," "second order," and so on spectra, at successively larger angles from the axis of the diffraction grating. The first order spectra are by far the brightest and will be those studied in this experiment.

The rays of each different wavelength present in the incident light constructively interfere at a different angle; each color of light reaches a maximum intensity at a different angle. This enables us to associate each particular wavelength of light present in the incident beam with a particular angle of bending.

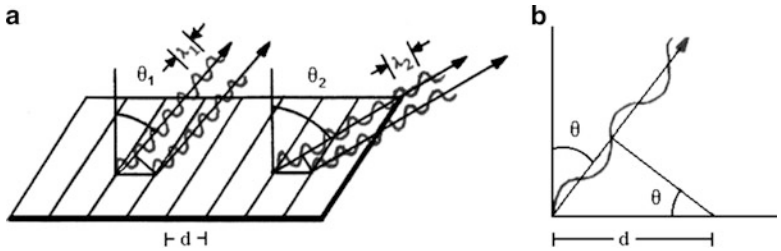

Fig. 5 (**a**) Constructive interference of rays from a diffraction grating. (**b**) Closeup of the geometry

As can be seen from Fig. 5, the longer the wavelength the greater the angle at which the waves will constructively interfere. From Fig. 5b, we can determine the wavelength corresponding to a given angle of observation,

$$\sin\theta = \frac{\lambda}{d}, \tag{5}$$

so that

$$\lambda = d\ \sin\theta. \tag{6}$$

This explicitly shows that light of comparatively longer wavelengths will constructively interfere at comparatively larger angles. Equations (5) and (6) represent the first order spectra. In general, constructive interference will occur at angles given by

$$\sin\theta = \frac{N\lambda}{d}, \tag{7}$$

where the angles for the Nth order maxima are found for values of $N = 1, 2, 3, \ldots$.

In the transmission diffraction grating spectroscope, light is beamed onto the grating. The light from the light source passes through a *collimator*, producing parallel rays incident upon the grating as is needed to achieve constructive interference. A telescope, which can be rotated about the grating, focuses and observes the light coming from the grating at any angle. A common diffraction grating has 600 grooves or lines per millimeter, which corresponds to a distance between each of the 600 lines of $d = 1.667 \times 10^{-4}$ cm, as shown in Fig. 5. If the grating you are using differs, your value of d will be different.

2. *Observations*

The jumps from energy levels 5, 4, and 3 to energy level 2 are identified by their distinctive wavelengths, corresponding to the colors dark blue, cyan, and red,

respectively. Cyan is a light blue/green color, familiar perhaps as one of the four inks used most commonly in color printing. It is similar to turquoise. We want to measure the angles through which each color is bent, and then determine the wavelengths of those colors by the geometry of the diffraction grating.

The reference for our angular position measurements is the axis of the diffraction grating, θ_0. As can be seen from Fig. 4, at this position the light rays are not deflected. The intensity of light will be greatest.

To establish this reference configuration, move the telescope of the spectroscope close to the source and point the telescope directly at it. Then slide the telescope of the spectroscope along its track so that its axis is aligned, as well as you can position it, along the axis of the diffraction grating. Slide the telescope carefully along its track until you see the bright red line in the center of the field of view of the telescope corresponding to no deflection. Enter the value for this angular position of the telescope as θ° in column 2 of Table 1 of the DATA SHEET. For many instruments it will be close to 180°. Enter the angular position as indicated on the scale; do not simply write "180." Note that the vernier scale on many spectroscopes enables measurement of angles to 0.05° if denominated in degrees or $1'$ if denominated in minutes of arc. Make certain you understand the scale on the vernier scale you are using.

Several techniques will aid in ensuring the accuracy of your measurements. First, make sure that the telescope points directly at the bulb to get as bright of images as possible. Second, rotate your telescope so that the slit and cross-hairs in the telescope are parallel to the hydrogen discharge tube. Otherwise the lines viewed through the telescope will be at an angle to the cross-hairs and an unambiguous determination of the position angle of the lines will be difficult to obtain. Again, when trying to locate the various lines, it is useful to open the slit wide, thus allowing a large amount of light into the spectroscope. Then close the slit until the line is thin to enable a precise measurement of the angular position of the telescope. Failure to close the slit can lead to errors of 5–10 minutes of arc. Also, position your apparatus to prevent stray light from the hydrogen discharge tubes and lamps of other experimenters from entering into your telescope. These stray lights may confuse your measurements and make it difficult to see dim lines.

Now move the telescope along its track to the right until the dark blue line is in the center of the field of view of the telescope. Enter the value of the angle, θ_1, in column 3 of Table 1 of the DATA SHEET. Move the telescope to the left, passing over the bright line corresponding to no deflection, until you see a second dark blue line. Measure the angle when that dark blue line is in the center of the field of view of the telescope, θ_2, and enter its value in column 5 of Table 1 of the DATA SHEET. You may see another, fainter dark blue line as you move the telescope. That corresponds to the jump from energy level 6 to energy level 2, but because of its faintness will not be used in the experiment.

Repeat this procedure to get the values of θ_1 and θ_2 for the cyan and red lines. Enter the respective values in columns 3 and 5 of Table 1 of the DATA SHEET. Move the telescope further along its track to determine if you can in fact see the second order diffraction spectra.

D. Calculations and Analysis

1. *Determination of the Wavelength from the Angular Displacements*

Because we are only interested in values of the angle θ relative to the axis of the diffraction grating, we next calculate the differences between θ_1 and θ_0, and between θ_2 and θ_0. We must be careful, however, to calculate the absolute value of the differences, $|\theta_1 - \theta_0|$ and $|\theta_2 - \theta_0|$. If we did not do this, when we averaged values of the differences we would always get close to zero.

Calculate the values of $|\theta_1 - \theta_0|$ and $|\theta_2 - \theta_0|$ for each line and enter the results in columns 4 and 6 of Table 1 of the DATA SHEET. Then average the pairs of values to obtain the value of $|\theta - \theta_0|_{av}$ for the each line and enter the results in column 7 of Table 1 of the DATA SHEET.

Substituting each value of $|\theta - \theta_0|_{av}$ for θ in (6), we can then calculate the wavelength using the particular value of d, for example, 1.667×10^{-4} cm, corresponding to the number of lines per millimeter of the diffraction grating of your spectroscope. Enter your result for λ, both in centimeters and angstroms, the more commonly employed unit for optical wavelengths (remember that $1\ \text{Å} = 10^{-8}$ cm) in columns 8 and 9, respectively, of Table 1 of the DATA SHEET. Show your calculations on the DATA SHEET. Calculate the values of $1/\lambda$ in cm^{-1} and enter them in column 10 of Table 1.

Remembering that dark blue, cyan, and red are the colors of light resulting from jumps from energy levels $n = 5, 4, 3$ to energy level 2, respectively, enter the respective values of n and n^2 in columns 11 and 12 of Table 1.

2. *The Value of the Rydberg Constant*

We can now determine the value of R graphically. Plot the values of $1/\lambda$ in units of cm^{-1} as ordinate as a function of the values of $1/n^2$ as abscissa.

From (4), the value of the slope of the line should be $(-R)$. Determine the value of R by finding the slope of the line using two widely separated points on the graph and dividing the difference between their ordinates by the difference in their abscissas. Show your calculations on the DATA SHEET.

A second determination of R can be made from the value of the y-intercept. We can rewrite equation (4) as,

$$\frac{1}{\lambda} = \frac{R}{4} - R\left(\frac{1}{n^2}\right).$$

Therefore, when $1/n^2 = 0$, the value of $1/\lambda$ is $R/4$. From the graph, estimate the value of the y-intercept and equate it to $R/4$. This allows a second determination of R. Enter its value on the DATA SHEET. We thus have two determinations of the value of R. Average them to get your best value and enter this value on the DATA SHEET.

STUDENT'S NAME _____

E. Atomic Spectra Experiment Data Sheets

Table 1 Angular displacements and wavelengths

Line	θ_0	θ_1	$\lvert\theta_1-\theta_0\rvert$	θ_2	$\lvert\theta_2-\theta_0\rvert$	$\lvert\theta-\theta_0\rvert_{av}$	λ (cm)	λ (Å)	$1/\lambda$ (cm^{-1})	n	$1/n^2$
Dark blue											
Cyan											
Red											

Show your calculations here.

Dark Blue Line:

Cyan Line:

Red Line:

STUDENT'S NAME _____

Graph of $1/\lambda$ as a function of $1/n^2$

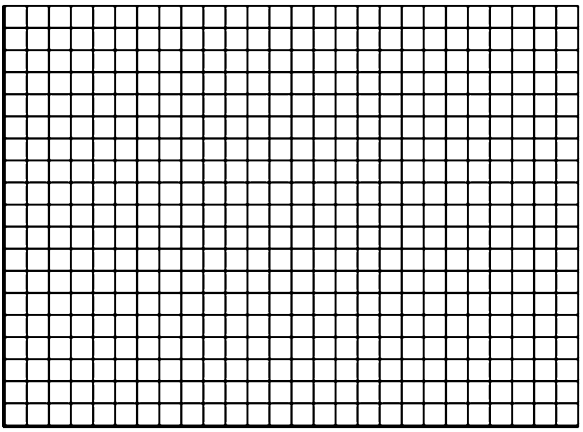

Calculation of slope:

Corresponding value of R: _____

Value of *y*-intercept = _____

Corresponding value of R: _____

Average value of R: _____

Error Analysis

Calculate the percentage error between the average value of R compared to the accepted value, $R = 1.096 \times 10^5\ \text{cm}^{-1}$.

Discuss the sources of error in your determination of R.

STUDENT'S NAME _____

F. Atomic Spectrum Experiment Discussion Questions

1. Compare your values for the wavelengths of dark blue, cyan, and red light with the actual range of values as given in Table 2.

Table 2 Colors of the visible spectrum

Color	Wavelength range (Å)	Your wavelength, λ (Å)
Red	6300–7000	
Orange	5900–6300	
Yellow	5700–5900	
Green	5000–5700	
Blue	4500–5000	
Violet	4000–4500	

If agreement is not found, provide possible explanation for the discrepancy.

2. From (7), calculate the angles of $\theta_{dark\ blue}$, θ_{cyan}, and θ_{red} at which the second order diffraction maxima should appear. If your values of wavelength in Table 2 agree with the actual values, use your values; if not, use a typical value for the wavelengths of these colors from Table 2.

Dark Blue Line:

Cyan Line:

Red Line:

STUDENT'S NAME _____

3. In 1963, astronomer Marteen Schmidt (born 1929) noted that the strange spectrum observed from the starlike object 3C273 was in fact the familiar pattern of the Balmer lines from hydrogen displaced in wavelength to the red. The formula for the redshift of an object with a velocity, v, in the line of sight is ((6) of Experiment #9, "Determination of the Rotation Rate of Planets and Asteroids by Radar: Part I. Observations of Mercury,")

$$z = \frac{\Delta\lambda}{\lambda}$$

$$= \frac{v}{c},$$

where $\Delta\lambda$ is the Doppler shift of light of wavelength λ observed from the object and the speed of light $c = 3.00 \times 10^{10}$ cm/s. Schmidt calculated the implied redshift and discovered that this starlike object was not in our galaxy, but at a great distance.

Using the actual spectrum taken by Schmidt, we will determine the redshift of 3C273. Note that the wavelengths associated with Hδ, Hγ, and Hβ are those provided below the comparison spectrum obtained in the laboratory (at, of course, a velocity $v = 0$ cm/s).

a) Determine the scale factor for the spectrum in angstroms per millimeter. Note that the spectrum of 3C273 and the comparison spectrum have the same scale.

b) Calculate $\Delta\lambda/\lambda$ for each of the three redshifted lines Hδ, Hγ, and Hβ and average the three results.

c) Using that average, what is the implied velocity with which 3C273 is moving away from us? Show all your calculations here.

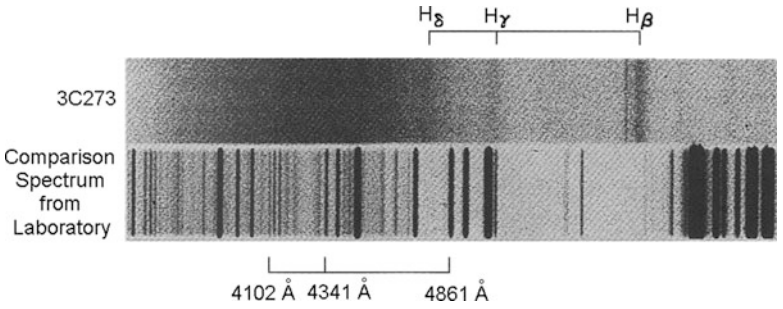

STUDENT'S NAME _____

4. Typical hydrogen discharge tubes operate by the application of 5000 V to the gas of molecular hydrogen. Based on an understanding of Fig. 1, why wouldn't a much larger voltage be suitable for everyday use as well as for this experiment?

5. Although hydrogen is the simplest atom and has the simplest spectrum, some elements have spectra similar to hydrogen.

   a. Draw a schematic diagram of each atom or ion, referring if necessary to the Periodic Table of the Elements.
      1) The calcium atom, Ca

      2) The helium atom, He.

      3) Singly-ionized helium, He^{+}

      4) Doubly-ionized helium, He^{++}.

      5) The lithium atom, Li.

      6) Singly-ionized lithium, Li^{+}.

      7) Doubly-ionized lithium, Li^{++}.

   b. Which of these would you expect to have spectra similar to hydrogen? Why?

6. The spectrum of the calcium atom in the visible, Fig. 1, is reproduced below. Draw the absorption lines corresponding to the Hα, Hβ, and Hγ lines at their approximate appropriate wavelengths on this spectrum.

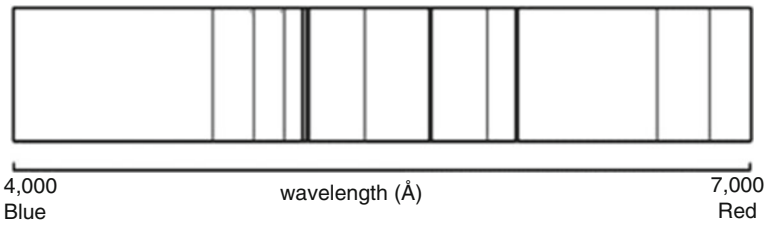

   a. Calculate the scale factor of the spectrum as shown in angstroms per centimeter.

STUDENT'S NAME _____

b. Calculate the position of the Hα line from the left-hand margin of 4000 Å and then draw the corresponding spectral line.

c. Calculate the position of the Hβ line from the left-hand margin of 4000 Å and the draw the corresponding spectral line.

d. Calculate the position of the Hγ line from the left-hand margin of 4000 Å and then draw the corresponding spectral line.

7. The diffraction grating spectrometer used in the experiment had 600 grooves or lines per millimeter, which corresponds to a distance between each of the 600 lines of $d = 1.667 \times 10^{-4}$ cm. What would be the angular displacement at which the Hα, Hβ, and Hγ lines would be observed using a diffraction grating spectrometer having 900 grooves per millimeter, corresponding to a distance between grooves of $d = 1.111 \times 10^{-4}$ cm? Show your calculations here.

   Hα:

   Hβ:

   Hγ:

Removing these DATA SHEETS from the book may damage the binding. You might consider entering the data and performing your calculations in the book, and then photocopying the DATA SHEETS for submission to your instructor for grading.

If you used graph paper other than that provided, attach that graph to these DATA SHEETS.

Experiment 20
Discovering the Nature of Objects in Space: Kirchhoff's Laws of Radiation

SUMMARY: In Experiment #20, "Discovering the Nature of Objects in Space: Kirchhoff's Laws of Radiation," we investigate the important Kirchhoff's Laws, which enable astronomers to determine some of the physical and chemical conditions characterizing celestial objects. Using a light source similar to the hydrogen discharge tube of Experiment #19, "The Theory of Atomic Spectra," and an incandescent light bulb, you will investigate the creation of emission and absorption lines in simulated clouds of interstellar gas or stellar atmospheres.

LEVEL OF DIFFICULTY: Moderate

EQUIPMENT NEEDED: Optical bench; mercury discharge tube or helium discharge tube; light baffles; diffraction grating spectrometer; frosted light bulb and light socket; photometer; rheostat.

MY LEARNING GOALS

1. To be able to describe Kirchhoff's Laws of Radiation.
2. To be able to describe how systems of emission and absorption lines are created in the atmospheres of stars.
3. To be able to describe how the temperature and relative velocity of gas clouds relative to distant objects are determined by analysis of systems of absorption and emission lines..

L.M. Golden, *Laboratory Experiments in Physics for Modern Astronomy: With Comprehensive Development of the Physical Principles*,
DOI 10.1007/978-1-4614-3311-8_20,

A. Introduction

In the preceding experiments, we have studied how astronomers gather data, some of the methods used to analyze data, and then studied some of the physical laws behind motion and the radiation we receive from various types of objects. In two of the latter experiments, we dealt with laboratory equipment that simulated idealized astronomical objects, emission line radiation from a hot gas and blackbody radiation from a heated solid object. The radiation from actual astronomical objects may approach those idealizations, but in general the radiation we receive from them is more complex.

To enable interpretation of the radiation we receive from those objects, we need to understand what produces the actual spectra we receive. Stars, for example, are hot objects producing radiation whose spectra are similar to those of a blackbody at the same temperature, but which have in addition, depending on the star, absorption lines, emission lines, or both. Planets with atmospheres also produce such composite spectra. Depending on the particular situation, the radiation from gas clouds in interstellar space exhibit emission lines, absorption lines, or both.

B. Theory

Gustav Kirchhoff (1824–1887) provided the description of the conditions which produce spectra from astronomical objects. Although they are referred to as Kirchhoff's Laws, they do not have the stature of laws of nature such as Newton's Laws or the Universal Law of Gravitation, but rather summarize what we know about spectral lines and blackbody radiation. This is not to diminish their importance. Without them, the complex radiation we receive from astronomical objects would be largely undecipherable.

I. A hot solid, liquid, or sufficiently dense gas radiates a continuous blackbody emission spectrum in which all wavelengths are present.

II. A low-density, hot gas produces a bright line or emission line spectra, the wavelengths of which are characteristic of the chemical composition of the gas.

III. A low-density, cool gas seen in front of a hotter solid, liquid, or sufficiently dense gas produces an absorption line spectrum, the wavelengths of which are characteristic of the chemical composition of the gas, superimposed on the blackbody emission spectrum of the hotter object.

We studied the idealization of Kirchhoff's first law in Experiment #17, "Blackbody Radiation". We studied the idealization of Kirchhoff's second law in Experiment #19, "The Theory of Atomic Spectra". In this experiment, we will study Kirchhoff's third law.

We should note an implication of Kirchhoff's Laws. Given a low-density gas of a given composition, the wavelengths of the radiation seen in emission if the gas is heated (second law) are exactly the same wavelengths absorbed if the gas is seen in front of a hot background object (third law). It follows that a given cloud of

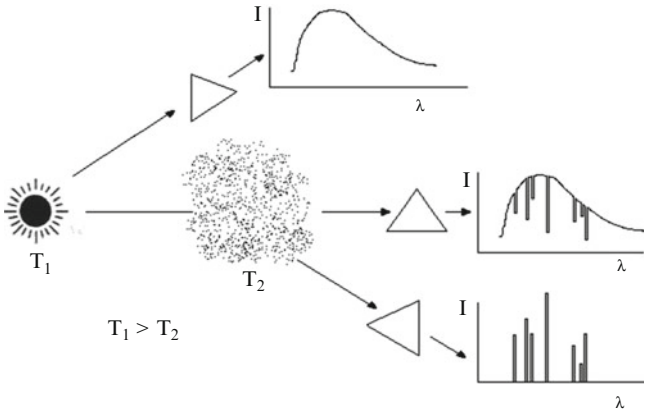

Fig. 1 Kirchhoff's Laws of radiation. The wavelengths of radiation absorbed by a gas cooler than a background object are exactly the same as those emitted by a hot gas of the same chemical composition

low-density gas will produce an emission line spectrum if viewed alone, but will produce an absorption line spectra if viewed in front of a hot solid, liquid, or sufficiently dense gas. Nothing about the gas cloud has changed, only whether or not it is viewed in front of another object. That is the basis of the experiment we will be performing.

These various scenarios of Kirchhoff's Laws are shown in Fig. 1. As we learned in Experiment #19, "The Theory of Atomic Spectra," each chemical element has its own characteristic spectrum. Kirchhoff's Laws, then, enable us to determine the chemical composition of a cloud of gas and its temperature relative to a background object from examination of its spectra.

Close examination of Fig. 1, however, shows that study of spectra can tell us more than the chemical composition of the gas and its temperature relative to a background object. First, the depths of the absorption lines or the height of the emission lines, as the case may be, tell us the amount of such gas presence, its *chemical abundance*. To the extent that the gas is composed of more than one material, we can determine the relative abundances of those constituents. Second, just as examination of the blackbody curve can tell us its temperature, so the depths of the absorption lines or the height of the emission lines, as the case may be, among the various lines of a given gas tell us its temperature. (This requires knowledge of the branch of physics called *quantum mechanics*.) Third, although Fig. 1 does not display this explicitly, the width of the absorption or emission lines, as the case may be, tell us the density of the gas and the rotational speed of the gas, and is an additional measure of the temperature of the gas. Fourth, the extent to which the wavelengths of the absorption lines or the emission lines, as the case may be, are displaced from those wavelengths known for the substance from laboratory measurements or theory, the relative velocity of the gas with respect to us can be determined. Such analyses are the subject of *spectroscopy*.

Although this is not one of Kirchhoff's Laws, one additional scenario exists.

> "IV." A low-density, hot gas seen in front of a cooler solid, liquid, or sufficiently dense gas produces an emission line spectrum, the wavelengths of which are characteristic of the chemical composition of the gas, superimposed on the blackbody emission spectrum of the hotter object.

Many astronomical objects show both emission lines and absorption lines in their spectra. The Sun, for example, has many absorption lines produced near its visible surface as well as emission lines produced in the extremely hot outer regions of the *corona*.

C. Procedure and Observations

We will utilize equipment similar to that which we have used in previous experiments. This includes an optical bench, incandescent light bulb, diffraction grating spectroscope, photometer, and rheostat. Instead of a hydrogen discharge tube we will use either a mercury discharge tube or a helium discharge tube. Both elements exist at room temperature as single atoms. The prominent lines of these two elements in the visible are summarized in Tables 1 and 2. Mercury has eight prominent lines in the visible, but because mercury also emits lines in the ultraviolet any large mercury discharge tubes must be used with care. Baffles may be advisable if your lab uses this source.

Other light sources that your laboratory may have available are not as suitable for our purposes. Sodium has seven prominent lines in the visible, but the pairs of

Table 1 Prominent visible lines of mercury

Color	Relative intensity
Violet	3.0
Violet	1.5
Blue	5.0
Blue-green	0.5
Green	20
Yellow	2.0
Yellow	10
Red	1.3

Table 2 Prominent visible lines of helium

Color	Relative intensity
Blue	2.9
Blue	2.1
Aqua	1.9
Green	2.6
Yellow	3.8
Red	2.9
Blue	2.9

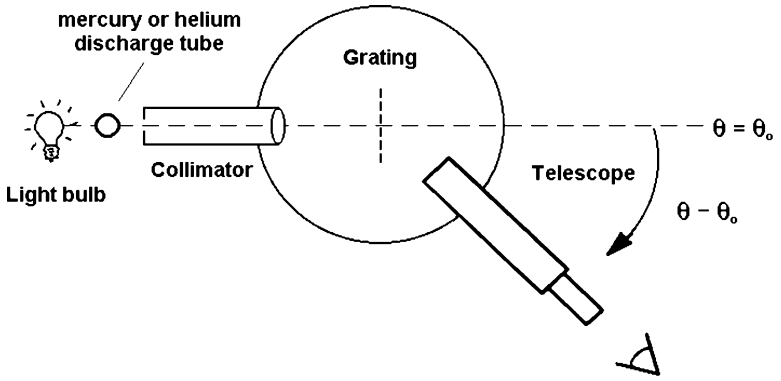

Fig. 2 A socket for placement of an incandescent light bulb is added to the experimental set-up of Experiment #19, "The Theory of Atomic Spectra". The current to the light bulb socket can be varied using a rheostat

green, yellow-orange, and orange lines are separated in wavelength by only a few angstroms and may not be easily distinguished. More importantly, the *sodium D-lines* of yellow-orange color far exceed the other lines in intensity. The multiplicity of lines in the visible spectrum of both argon and neon create unnecessary complexity for analysis. In addition, the lines of neon are concentrated in the yellow to red region. Your choice of light source will depend on the equipment available in your particular laboratory.

The equipment set-up is a slight modification of that used in Experiment #19, "The Theory of Atomic Spectra," (see its Fig. 4). Place the socket for the light bulb on the optical bench. The spectral line light source, either the mercury discharge tube or the helium discharge tube, will be located on the optical bench on the near side of the light bulb. Both positions are aligned with a collimator, Fig. 2. If you cannot physically place the light bulb socket and the spectral line light source on the optical bench, employ it as a straight edge to align these light sources. The current going into the light bulb socket can be varied by a rheostat. As in Experiment #19, "The Theory of Atomic Spectra," we will move the telescope along its track and observe the angular displacement of the spectral lines that appear. We will also observe the blackbody emission from the light bulb.

1. *Continuous Blackbody Spectrum: Kirchhoff's First Law*

We must first align the axis of the diffraction grating with the optical bench. Turn on the spectral line light source. As in Experiment #19, "The Theory of Atomic Spectra," move the telescope of the spectroscope close to the source and point the telescope directly at it. Then slide the telescope of the spectroscope along its track so that its axis is aligned, as well as you can position it, along the axis of the

diffraction grating. Slide the telescope carefully along its track until you see the bright line in the center of the field of view of the telescope corresponding to no deflection. On the DATA SHEET, enter the value for this angular position of the telescope as θ°. For many instruments it will be close to 180°.

Enter the angular position as indicated on the scale; do not simply write "180." Note that the vernier scale on the spectroscope enables measurement of angles to 0.05° if denominated in degrees or 1′ if denominated in minutes of arc.

Turn off the spectral line light source. Place the light bulb in the socket and turn it on. Increase the voltage from the rheostat until the light is a moderately bright white color. Call this intensity I_b. Enter the setting of the rheostat on the DATA SHEET. Move the telescope along its track to the right and, with the photometer placed up against the telescope eyepiece, measure the intensity of the light using every 2° from the reference angle of $\theta^\circ + 2$ to an angle of $\theta^\circ + 32^\circ$. To prevent stray light from entering the photometer, place light baffle material such as tin foil or a dark cloth around the photometer input. Enter those values of intensity in Table 3 of the DATA SHEET.

Turn the light bulb off. When the light bulb has cooled, remove it from the socket.

2. *Emission Line Spectrum: Kirchhoff's Second Law*

We will now repeat the first part of Experiment #19, "The Theory of Atomic Spectra," with our spectral line light source of choice. Move the telescope back to its axis position, the angle of θ_0. Turn on the spectral line light source. Adjust the rheostat so that the light emitted is bright. Enter the reading on the rheostat as V_1 on the DATA SHEET. As in Experiment #19, "The Theory of Atomic Spectra," move the telescope along its track to the right until a spectral line is in the center of the field of view of the telescope. Enter the value of the angle as θ_1 in Table 4 of the DATA SHEET. Move the telescope to the left, passing over the bright line corresponding to no deflection, until you see a second spectral line of the same color. Measure the angle when that line is in the center of the field of view of the telescope. Enter the value of the angle as θ_2 in Table 4 of the DATA SHEET.

Estimate the brightness of the emission line by a number from 1 to 5, with 5 being the brightest. Enter this value in Table 4 of the DATA SHEET.

Repeat this procedure for the other lines described in Table 1 or Table 2, depending on your choice of spectral line light source.

3. *Absorption Line Spectrum: Kirchhoff's Third Law*

To observe the absorption line spectrum, we simply leave the spectral line light source off. Move the telescope to the θ_0 position, the axis of the spectrometer. Turn on the light bulb. We want the setting of the rheostat to be the same as that which

resulted in an intensity of I_b in part 1 above. To ensure this, measure the intensity of the light at the θ_0 on-axis position and compare it to the intensity entry in Table 3. If the photometer reading is not the same, change the setting of the rheostat until the readings agree.

Because this color is white, the temperature of the gas is greater than that of the gas in the spectral line light source, which is of course at room temperature.

We now repeat the measurements of part 2 above. Now, however, you will not be seeing the spikes of intensity from the emission lines, but rather a dimming of the intensity. These absorption lines are more difficult to observe than the spikes of emission, as you might imagine, but you can use as a guide the angular displacements that you entered in Table 4. Enter in Table 5 of the DATA SHEET the angular displacements of the absorption lines and the photometer readings of their brightness.

D. Calculations and Analysis

1. Continuous Blackbody Spectrum: Kirchhoff's First Law

To determine the wavelengths corresponding to these angles of observation, substitute each value of $|\theta - \theta_0|$ for θ into Eq. (6) of Experiment #19, "The Theory of Atomic Spectra," recalling that $d = 1.667 \times 10^{-4}$ cm. As in Experiment #19, "The Theory of Atomic Spectra," if the grating you are using differs from that with 600 lines per millimeter, your value of d will be different. Enter your results for λ in the right-hand column of Table 3 of the DATA SHEET both in centimeters and angstroms. Show your calculations on the DATA SHEET.

Construct a graph of those data, intensity as a function of angle. Draw a smooth line through the data points. This is the continuous spectrum emitted by the light bulb. Your observations will span a significant portion of the visible electromagnetic spectrum and, as a result, the familiar shape of the blackbody curve should be apparent, as shown in Fig. 1 of Experiment #17, "Blackbody Radiation".

2. Emission Line Spectrum: Kirchhoff's Second Law

Calculate the values of the absolute differences between θ_1 and θ_0, and between θ_2 and θ_0. Average the values of $|\theta_1 - \theta_0|$ and $|\theta_2 - \theta_0|$ to obtain the value of $|\theta - \theta_0|_{av}$ for the dark blue, cyan, and red lines and enter their values in Table 4 of the DATA SHEET.

To determine the wavelengths corresponding to the three angles of observation, substitute each value of $|\theta - \theta_0|_{av}$ for θ in Eq. (6) of Experiment #19, "The Theory

of Atomic Spectra". Enter your results for λ in Table 4 of the DATA SHEET both in centimeters and angstroms. Show all your calculations on the DATA SHEET.

Construct a graph of the emission line spectrum, brightness as a function of wavelength using your estimated brightness values as the ordinate. Use the same abscissa scale that you used in constructing the blackbody spectrum graph.

This is the emission line spectrum.

3. *Absorption Line Spectrum: Kirchhoff's Third Law*

Find the mean values, $|\theta - \theta_0|_{av}$, of the angular displacements to the right and to the left of the θ_0 on-axis position, and the mean values, I_{av}, of the corresponding photometer readings. Calculate the wavelengths corresponding to the mean angular displacements. Enter your results in Table 5 of the DATA SHEET. Show all your calculations on the DATA SHEET.

On the graph you constructed in part 1 above, draw lines representing the decreased intensities at the wavelength locations of the absorption lines. As in Fig. 1, so that they are easily seen, draw the lines with some small finite width. This is the absorption line spectrum superimposed on the continuum arising from the light bulb.

We have created two graphs, one of the emission line spectrum and one of the absorption line spectrum. Both the height of the lines in the former and the depth of the lines in the latter indicate the number of atoms emitting or absorbing, respectively, the particular line from your spectral line light source. Construct a third graph, the strength of the absorption lines as a function of the strength of the emission lines. The graph will have only four to seven points, depending on which spectral line light source you used and whether you were able to distinguish the closely-spaced lines of sodium if you used the sodium vapor lamp. Note on the graph which data point refers to which line. Because your emission line brightnesses were only estimates, provide error bars which represent the precision you would ascribe to your subjective estimate.

STUDENT'S NAME _____

E. Kirchhoff's Law Experiment Data Sheets

1. Continuous Blackbody Spectrum: Kirchhoff's First Law

$\theta_0 =$ _____

Voltage setting on rheostat to obtain moderately bright white light intensity of I_b: _____

Show your calculations of the wavelengths here.

Table 3 Continuum spectrum

$\lvert\theta - \theta_0\rvert$ (degrees)	I	λ (cm)	λ ()	$\lvert\theta - \theta_0\rvert$ (degrees)	I	λ (cm)	λ (Å)
2				18			
4				20			
6				22			
8				24			
10				26			
12				28			
14				30			
16				32			

STUDENT'S NAME _____

Graph of the continuous spectrum

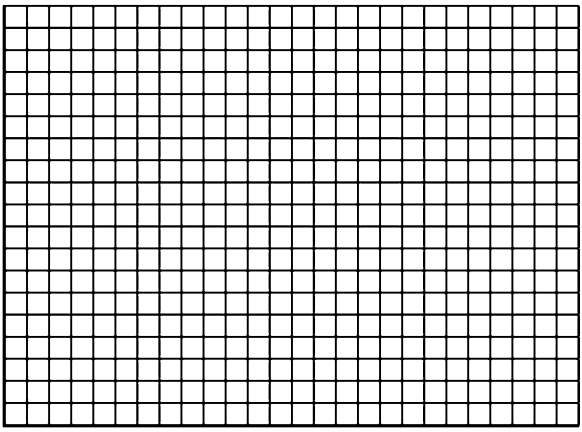

2. *Emission Line Spectrum: Kirchhoff's Second Law*

Table 4 Emission line spectrum

Line (color)	θ_0	θ_1	$\lvert\theta_1 - \theta_0\rvert$	θ_2	$\lvert\theta_2 - \theta_0\rvert$	$\lvert\theta - \theta_0\rvert_{av}$	λ (cm)	λ (Å)	Brightness

Setting of rheostat to obtain bright emission V_1 = _____
Show your calculations of $\lvert\theta - \theta_0\rvert_{av}$ and λ here for each line

STUDENT'S NAME _____

Graph of the absorption line spectrum

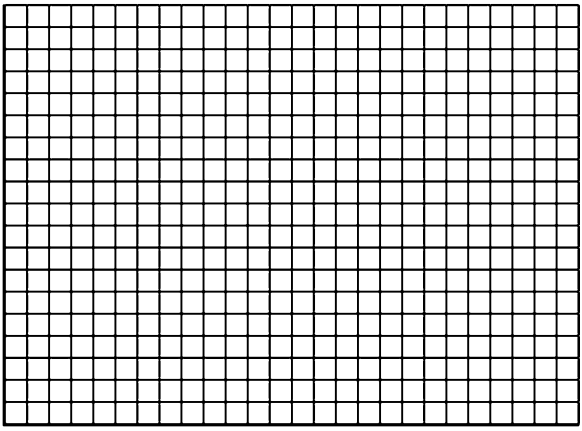

3. *Absorption Line Spectrum: Kirchhoff's Third Law*

Table 5 Absorption line spectrum

Line (color)	θ_0	θ_1	$\lvert\theta_1 - \theta_0\rvert$	I_1	θ_2	$\lvert\theta_2 - \theta_0\rvert$	I_2	$\lvert\theta - \theta_0\rvert_{av}$	I_{av}	λ (cm)	λ (Å)

Show your calculations of $\lvert\theta - \theta_0\rvert_{av}$, I_{av}, and λ here for each line.

STUDENT'S NAME _____

Graph of the absorption line spectrum

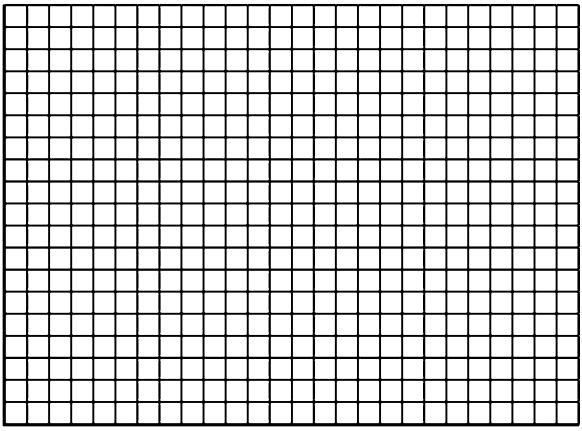

Graph of the strength of the absorption lines as a function of the strength of the emission lines

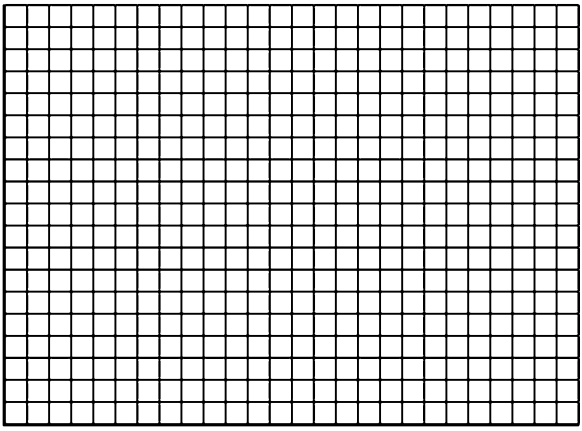

STUDENT'S NAME _____

F. Kirchhoff's Law Experiment Discussion Questions

1. In this experiment we used either a mercury discharge tube or a helium discharge tube. Why did we not choose to use the same hydrogen discharge tube that we used in Experiment #19, "The Theory of Atomic Spectra"?

2. The graph of absorption line strength as a function of emission line strength has some uncertainty resulting from the subjective estimate of the emission line strength, in contrast to the measurements of the intensity of the continuous emission and the absorption lines using the photometer.

   a. Nonetheless, do you detect a pattern? Is the line, for example, a monotonically increasing straight line?

   b. Do you expect it to be? Why or why not?

3. We noted that a low-density, hot gas seen in front of a cooler solid, liquid, or sufficiently dense gas produces an emission line spectrum superimposed on the blackbody emission spectrum of the hotter object. Following Fig. 1, draw a sketch of the appearance of such a spectrum.

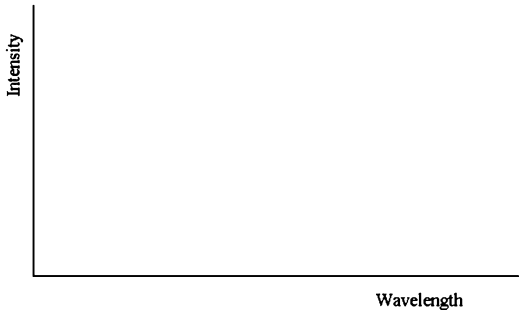

STUDENT'S NAME _____

4. A spectrum is observed to be a blackbody continuum with both absorption and emission lines present. Following Fig. 1, draw a schematic sketch of the object from which this radiation might be received. As in Fig. 1, show the relative temperature of the components of the object.

5. Question #31 of Experiment #1, "A Review of Mathematical Concepts and Tools," discussed the redshift of quasars. Draw a sketch of what the spectrum of a very distant quasar, between which and the Earth are located two clouds of cool intergalactic gas, might look like. Assume that one of the clouds is closer to the quasar than to our Milky Way galaxy, so that it has a redshift which, although smaller than that of the quasar, is still large. Assume that the second cloud is closer to the Milky Way galaxy than the first but still sufficiently far to have a sizeable redshift. Clearly note which lines are from which cloud.

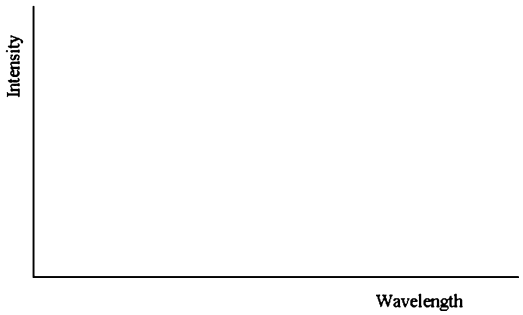

6. You constructed a graph of the blackbody curve of the light bulb as part of the analysis of the continuous blackbody spectrum. Compare its shape to the various blackbody curves of Fig. 1 of Experiment #17, "Blackbody Radiation". What is your estimate of the temperature of the light bulb filament on the basis of that comparison? Make your estimate based on the shape of the curve and Wien's displacement law. Describe the basis for your estimate.

STUDENT'S NAME _____

7. Knowing that absorption lines are created by a relatively cool gas in the atmosphere of its associated star, astronomers study those absorption lines to discover properties of the star. In particular, by observing the width of the absorption lines they can determine its rotation rate. Just as we observed in Experiments #9 and #10, "Determination of the Rotation Rate of Planets and Asteroids by Radar: Part I: Observations of Mercury," and "Determination of the Rotation Rate of Planets and Asteroids by Radar: Part II: Observations of Simulated Planets," with radar observations of the planets, the Doppler effect tells us that the more rapidly rotating the star the broader the absorption lines, a phenomenon referred to as *rotational broadening*. In this context, the different terminologies, "bandwidth" in microwaves and spectral line "width" in visible waves, refer to the same phenomena but in different parts of the electromagnetic spectrum.

   Here are idealized small portions of the spectra of two stars. One represents the spectrum of Vega, an A0-type star and the brightest summer nighttime star in the northern hemisphere (see Table 1 of Experiment #11, "The Orbit of Venus"). The other represents the spectrum of the Sun, which rotates at the equator once every 27 days. With a radius of 7×10^5 km, this corresponds to a velocity at its surface of 1.9 km/s. (Because of the relative temperatures of these two stars, the spectrum for the Sun is sloping upwards at these wavelengths whereas that for Vega is sloping downwards, as explained by Wien's displacement law.)

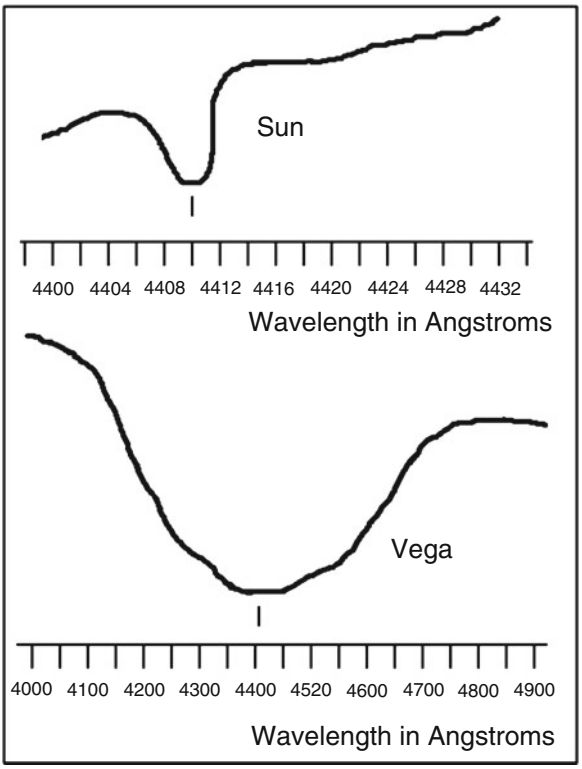

STUDENT'S NAME _____

a) Determine the scale factor of the two spectra. Show your calculations here and enter the results in Table 6.

Vega scale factor : _____ Å/mm

Sun scale factor : _____ Å/mm

b) Measure the widths of the indicated absorption lines of Vega and the Sun centered at 4410 Å. As you will quickly learn, an art exists in determining the widths of spectral lines. For consistency among student groups, use one-half the depth of the line as the reference point at which to determine the spectral line width. Enter the results in Table 6.

c) Calculate the surface velocity of Vega using a proportion based on the modified Doppler shift formula, $\Delta\lambda/\lambda = 2\ v/c$. Because one edge of the star approaches us at the velocity v while the other edge recedes from us at the velocity v, the rotational-broadened line has twice the width provided by the Doppler shift formula, (6) of Experiment #9, "Determination of the Rotation Rate of Planets and Asteroids by Radar: Part I: Observations of Mercury". Show your calculations here.

Table 6 Rotational broadening

Star	Scale factor	Δλ (mm)	Δλ (Å)
Vega			
Sun			

STUDENT'S NAME _____

d) That velocity is related to the rotation period by $v = 2\pi R/P$, where R is the radius of the star and P is the rotation period. Based on new observations using *optical interferometry*, the estimate of the equatorial radius of Vega was updated in 2006 to be equal to about 2.7 solar radii. Derive an equation providing the rotation period of Vega in terms of the rotation period of the Sun and the width of the absorption lines of the two stars.

e) Calculate the rotation period of Vega in days using that equation. Can you think of any other celestial object that has a similar rotation period?

f) Isn't nature wondrous? Aren't mathematics and reason fabulous tools with which to discover and marvel at the workings of nature? (Your final grade in this course may depend on the answer to these two questions.)

Removing these DATA SHEETS from the book may damage the binding. You might consider entering the data and performing your calculations in the book, and then photocopying the DATA SHEETS for submission to your instructor for grading.

If you used graph paper other than that provided, attach those graphs to these DATA SHEETS.

Appendix I
Physical Constants and Astronomical Measurements

Speed of light in a vacuum, $c = 3.00 \times 10^5$ km/s $= 3.00 \times 10^{10}$ cm/s
Acceleration due to gravity, $g = 9.8$ m/s^2 $= 980$ cm/s^2
Gravitational constant, $G = 6.67 \times 10^{-11}$ N-m^2/kg^2 $= 6.67 \times 10^{-8}$ dyne-cm^2/g^2
Boltzmann's constant, $k = 1.38 \times 10^{-23}$ J/K $= 1.38 \times 10^{-16}$ erg/K
Stefan-Boltzmann constant, $\sigma = 5.67 \times 10^{-8}$ W/m^2-K^4 $= 5.67 \times 10^{-5}$ erg/s-cm^2-K^4
Planck's constant, $h = 6.63 \times 10^{-34}$ J-s $= 6.63 \times 10^{-27}$ erg-s

Astronomical Unit, 1 A.U. $= 1.496 \times 10^8$ km
Light year, 1 ly $= 9.46 \times 10^{12}$ km
Parsec, 1 pc $= 3.09 \times 10^{13}$ km (= 3.26 ly = 206,265 A.U.)

Equatorial radius of the Earth = 6378 km
Mass of the Earth $= 5.97 \times 10^{24}$ kg
Radius of the Moon = 1738 km
Mass of the Moon $= 7.35 \times 10^{22}$ kg
Equatorial radius of the Sun $= 6.96 \times 10^5$ km
Mass of the Sun $= 1.99 \times 10^{30}$ kg
Luminosity of the Sun $= 3.83 \times 10^{26}$ W
Effective temperature of the Sun = 5780 K

World human population in 1500 = 450 million
World human population in 2012 = 7000 million

L.M. Golden, *Laboratory Experiments in Physics for Modern Astronomy: With Comprehensive Development of the Physical Principles*,
DOI 10.1007/978-1-4614-3311-8,

Appendix II
Julian Dates

Julian Days, abbreviated J.D., is the time reckoning used by astronomers. This table provides the Julian dates for given calendar dates at 0 hours universal time, the time at Greenwich. For simplicity, we have deleted both the leading two digits, 24, and the 0.5 fraction of a day. The result is the so-called Modified Julian data, MJD = JD −2400000.5. We have chosen to begin the table on January 11, 2012, so that one Julian date is provided for each month, except for the final entry. The interval between entries is 30 days.

TABLE OF JULIAN DATES (January 11, 2012 through December 31, 2013)

Modified Julian Date	Year	Month	Day	Days from 1/11/2012
55937	2012	1	11	0
55967	2012	2	10	30
55997	2012	3	11	60
56027	2012	4	10	90
56057	2012	5	10	120
56087	2012	6	9	150
56117	2012	7	9	180
56147	2012	8	8	210
56177	2012	9	7	240
56207	2012	10	7	270
56237	2012	11	6	300
56267	2012	12	6	330
56297	2013	1	5	360
56327	2013	2	4	390
56357	2013	3	6	420
56387	2013	4	5	450
56417	2013	5	5	480
56447	2013	6	4	510
56477	2013	7	4	540

(continued)

L.M. Golden, *Laboratory Experiments in Physics for Modern Astronomy: With Comprehensive Development of the Physical Principles*,
DOI 10.1007/978-1-4614-3311-8,

(continued)

Modified Julian Date	Year	Month	Day	Days from 1/11/2012
56507	2013	8	3	570
56537	2013	9	2	600
56567	2013	10	2	630
56597	2013	11	1	660
56627	2013	12	1	690
56657	2014	12	31	720

Appendix III
Day-of-the-Year Tables

For convenience, you might want to refer to a table of the days of the year. These provide the ordinal number of each calendar date. For example, January 1 is the first day of the year and December 4 is the 338th day of the year (in a non-leap year). Note that some refer, incorrectly, to days-of-the-year as the Julian date. Many desk calendars also provide the number.

Day-of-the-year (Non-leap years)

Date	Jan	Feb	Mar	Apr	May	Jun	Jul	Aug	Sep	Oct	Nov	Dec
1	1	32	60	91	121	152	182	213	244	274	305	335
2	2	33	61	92	122	153	183	214	245	275	306	336
3	3	34	62	93	123	154	184	215	246	276	307	337
4	4	35	63	94	124	155	185	216	247	277	308	338
5	5	36	64	95	125	156	186	217	248	278	309	339
6	6	37	65	96	126	157	187	218	249	279	310	340
7	7	38	66	97	127	158	188	219	250	280	311	341
8	8	39	67	98	128	159	189	220	251	281	312	342
9	9	40	68	99	129	160	190	221	252	282	313	343
10	10	41	69	100	130	161	191	222	253	283	314	344
11	11	42	70	101	131	162	192	223	254	284	315	345
12	12	43	71	102	132	163	193	224	255	285	316	346
13	13	44	72	103	133	164	194	225	256	286	317	347
14	14	45	73	104	134	165	195	226	257	287	318	348
15	15	46	74	105	135	166	196	227	258	288	319	349
16	16	47	75	106	136	167	197	228	259	289	320	350
17	17	48	76	107	137	168	198	229	260	290	321	351
18	18	49	77	108	138	169	199	230	261	291	322	352
19	19	50	78	109	139	170	200	231	262	292	323	353
20	20	51	79	110	140	171	201	232	263	293	324	354
21	21	52	80	111	141	172	202	233	264	294	325	355
22	22	53	81	112	142	173	203	234	265	295	326	356
23	23	54	82	113	143	174	204	235	266	296	327	357

(continued)

L.M. Golden, *Laboratory Experiments in Physics for Modern Astronomy: With Comprehensive Development of the Physical Principles*,
DOI 10.1007/978-1-4614-3311-8,

(continued)

Date	Jan	Feb	Mar	Apr	May	Jun	Jul	Aug	Sep	Oct	Nov	Dec
24	24	55	83	114	144	175	205	236	267	297	328	358
25	25	56	84	115	145	176	206	237	268	298	329	359
26	26	57	85	116	146	177	207	238	269	299	330	360
27	27	58	86	117	147	178	208	239	270	300	331	361
28	28	59	87	118	148	179	209	240	271	301	332	362
29	29		88	119	149	180	210	241	272	302	333	363
30	30		89	120	150	181	211	242	273	303	334	364
31	31		90		151		212	243		304		365

Day-of-the-year (Leap years)

Date	Jan	Feb	Mar	Apr	May	Jun	Jul	Aug	Sep	Oct	Nov	Dec
1	1	32	61	92	122	153	183	214	245	275	306	336
2	2	33	62	93	123	154	184	215	246	276	307	337
3	3	34	63	94	124	155	185	216	247	277	308	338
4	4	35	64	95	125	156	186	217	248	278	309	339
5	5	36	65	96	126	157	187	218	249	279	310	340
6	6	37	66	97	127	158	188	219	250	280	311	341
7	7	38	67	98	128	159	189	220	251	281	312	342
8	8	39	68	99	129	160	190	221	252	282	313	343
9	9	40	69	100	130	161	191	222	253	283	314	344
10	10	41	70	101	131	162	192	223	254	284	315	345
11	11	42	71	102	132	163	193	224	255	285	316	346
12	12	43	72	103	133	164	194	225	256	286	317	347
13	13	44	73	104	134	165	195	226	257	287	318	348
14	14	45	74	105	135	166	196	227	258	288	319	349
15	15	46	75	106	136	167	197	228	259	289	320	350
16	16	47	76	107	137	168	198	229	260	290	321	351
17	17	48	77	108	138	169	199	230	261	291	322	352
18	18	49	78	109	139	170	200	231	262	292	323	353
19	19	50	79	110	140	171	201	232	263	293	324	354
20	20	51	80	111	141	172	202	233	264	294	325	355
21	21	52	81	112	142	173	203	234	265	295	326	356
22	22	53	82	113	143	174	204	235	266	296	327	357
23	23	54	83	114	144	175	205	236	267	297	328	358
24	24	55	84	115	145	176	206	237	268	298	329	359
25	25	56	85	116	146	177	207	238	269	299	330	360
26	26	57	86	117	147	178	208	239	270	300	331	361
27	27	58	87	118	148	179	209	240	271	301	332	362
28	28	59	88	119	149	180	210	241	272	302	333	363
29	29	60	89	120	150	181	211	242	273	303	334	364
30	30		90	121	151	182	212	243	274	304	335	365
31	31		91		152		213	244		305		366

Appendix IV
Fast Fourier Transform Spectrum Analyzer Software

Spectrum analyzer software allows us to display the intensity of the echo signal as a linear function of frequency without using spectrum analyzer hardware. A brief explanation of how it works will enable you to understand the display of the echo signal you will be observing on the computer screen.

Such software calculates the familiar Fourier transform of a signal of finite time duration, in our case the radar echo. The actual computations utilize the *fast Fourier transform* (FFT), a Fourier transform algorithm which greatly reduces the number of computations, and therefore the time, required to achieve the Fourier transform. Although FFTs were first discussed in 1965, the genius mathematician and physicist Carl Friedrich Gauss (1777–1855) had described the critical concept by 1805.

The range of frequencies you can detect (f_1, f_2) and the frequency resolution Δf you can obtain with FFT spectrum analyzer software depend on two characteristics of the experimental setup. These are the sampling rate, r, of the sound card in your computer and the length of time, T, the signal is detected by the spectrum analyzer software.

Typical computer sound cards have a sampling rate of 44.1 kHz. This means that they can detect frequencies of up to 22 kHz. To understand this, imagine a signal of 1 Hz observed for 1 s, as in Fig. 1. Only if the signal is sampled at least twice during this period, a sampling rate of 2 Hz, will it be identifiable as a 1 Hz signal. We can generalize this finding to the statement that the maximum frequency, f_2, detectable will be one-half of the sampling rate. Audio frequencies, those detectable by the human ear, range from 20 Hz to 20 kHz. This choice of a 44.1 kHz sampling rate for the sound card is therefore common because it enables the computer to detect the very highest frequencies that we can hear.

At the other end of the frequency bandwidth, the minimum frequency you can detect, f_1, and therefore the frequency resolution, $\Delta f = f_1$, is equal to $1/T$, where T is the length of time you are observing the signal. This also makes sense. If you observe a signal for 5 s, say, then the longest wave that would have gone through one complete cycle, and is therefore detectable, has a frequency of once every 5 s, as in Fig. 2. Any longer wave, of smaller frequency, will not have completed a complete cycle and would therefore not be unambiguously detectable. The corresponding minimum detectable frequency is 0.2 Hz, that is, $1/T$.

L.M. Golden, *Laboratory Experiments in Physics for Modern Astronomy: With Comprehensive Development of the Physical Principles*,
DOI 10.1007/978-1-4614-3311-8,

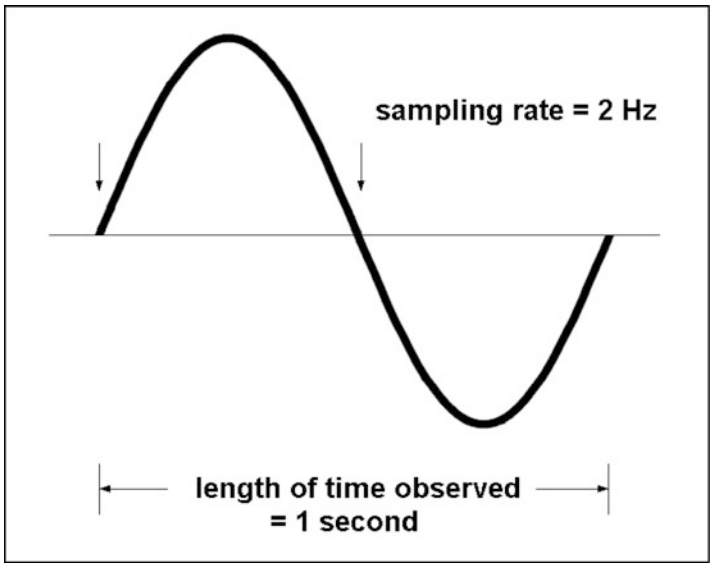

Fig. 1 The maximum frequency detectable by FFT spectrum analyzer software is one-half of the sampling rate

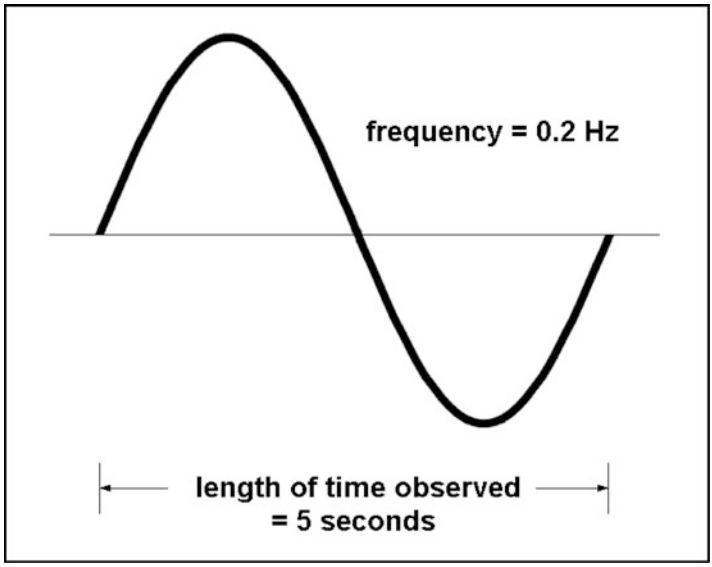

Fig. 2 The minimum frequency detectable by FFT spectrum analyzer software is $1/T$, where T is the length of time observed. This is also the frequency resolution available

In summary, the frequency interval will be $(1/T, r/2)$. The frequency resolution will be $\Delta f = 1/T$. A signal of 1 s length would result in a frequency resolution of 1 Hz.

Sound engineers and software developers often refer to the "block length" of the signal processed rather than the length of time. The block length is defined as the number of samples processed at the given sampling rate. If B is the block length, then we have trivially $T = B/r$ and the frequency interval would be expressed as $(r/B, r/2)$. With this notation, the frequency resolution would be expressed as $\Delta f = r/B$.

Our spheres will be rotating on the turntable at 33 1/3 rpm and 78 rpm, corresponding to 0.55 and 1.3 revolutions per second. As a result, a complete rotation occurs in 1.8 and 0.77 s, respectively. We need only observe the rotating spheres these lengths of time. The corresponding frequency resolutions, given as $1/T$, are therefore 0.55 and 1.3 Hz. Observing the echoes a greater length of time would, by the principle of the Fourier transform, seem to provide information of smaller frequency resolution, but in fact this information would not be physically meaningful because the same echo would repeat itself as the spheres rotate.

Nonetheless, we will observe for greater lengths of time. This will enable the software to average out spurious signals such as those generated by other students moving about in the laboratory.

About the Author

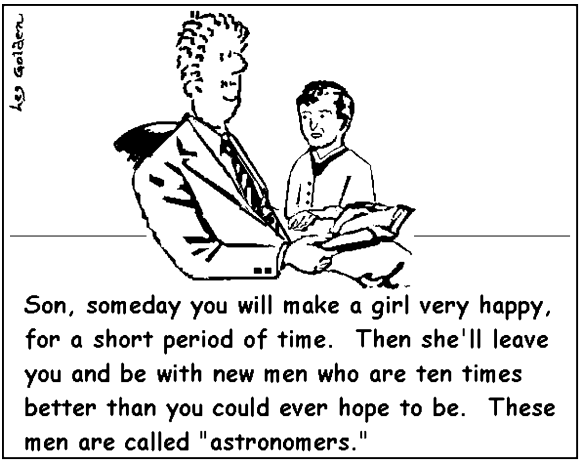

Leslie Morris Golden received the B.A. with Distinction and Masters in Engineering Physics from Cornell University, where he performed his masters' thesis on erosion of lunar craters by micrometeorite impacts under Bruce Hapke and studied radio astronomy with Frank Drake. He was the award-winning editor-in-chief of the *Cornell Engineer* magazine. He received the M.A. and Ph.D in astronomy from the University of California, Berkeley, where he worked with Leland Cunningham on the software for calculations of comet orbits, Carl Heiles on the HI map of the galaxy, Harold Weaver on selection effects in the study of the evolution of quasars, and W.H. McCrea on isotropy of radio source counts with position over the sky. He performed his dissertation, a microwave interferometric study of the subsurface of the planet Mercury, under William J. ("Jack") Welch. He obtained a National Research Council Resident Research Associateship grant to continue studies of Mercury at the Jet Propulsion Laboratory under Michael Janssen

L.M. Golden, *Laboratory Experiments in Physics for Modern Astronomy: With Comprehensive Development of the Physical Principles*,
DOI 10.1007/978-1-4614-3311-8,

The author (*left*) and his devoted and loyal pal, Cicero (*ball in mouth*). Rescued from the streets, my beautiful, athletic, intelligent, spirited, protective, obedient, always wanting to please, and bonded best friend

and studied the time variability of quasars with E.E. Epstein at the Aerospace Corporation before obtaining his academic appointment at the University of Illinois at Chicago, where he became affiliated with both the physics department and the Honors College.

In 1986 Dr. Golden was selected by Royal Cruise Lines to be their on-board lecturer on the high seas during the 1986 apparition of Halley's Comet and in 1996 he was a visiting professor on the University of Pittsburgh's Semester at Sea program. Among his many public speaking appearances, he presented a lecture series on extraterrestrial life to the Field Museum of Natural History and was the featured speaker on the occasion of the dedication of the new wing of Chicago's Adler Planetarium. Dr. Golden's research and scholarly interests are planetary radio astronomy, observational selection effects, cosmology, and the history of astronomy. Dr. Golden is one of a handful of individuals who is a member of both Tau Beta Pi, the engineering honorary society, and Phi Beta Kappa, the arts and sciences honorary society. He was also elected to Pi Delta Epsilon, the honorary journalism society.

Dr. Golden has additional careers as a professional trumpet player, stand-up comedian, and professional actor. He has over 100 stage, screen, radio, television, and commercial credits. At the University of California, he was a jazz disk jockey, the play-by-play announcer for California Golden Bears basketball, and one of the founders, a trumpet player and vocalist, and the emcee for the University of California Jazz Ensembles. He also applies probability and statistics to popular casino games as a columnist for four London-based gambling magazines. He is a passionate animal welfare advocate and fervent environmentalist and shares his home with his rescued canine friends.

Index

L.M. Golden, *Laboratory Experiments in Physics for Modern Astronomy: With Comprehensive Development of the Physical Principles*,
DOI 10.1007/978-1-4614-3311-8, © Springer Science+Business Media New York 2013